UCID- 19638

UCID--19638

DE83 008737

FISSION-SUPPRESSED HYBRID REACTOR - THE FUSION BREEDER

D. H. Berwald, R. W. Moir, J. D. Lee,
J. M. Beeston, G. E. Benedict, R. B. Campbell,
E. T. Cheng, M. S. Coops, R. L. Creedon,
J. H. DeVan, B. Flanders, F. J. Fulton,
J. K. Garner, N. Ghoniem, N. J. Hoffman,
P. Y. S. Hsu, J. S. Karbowski, I Maya,
L. G. Miller, W. S. Neef, Jr., J. Ogren,
V. H. Pierce, R. P. Rose, Y. Saito,
K. R. Schultz, A. Slomovik, J. B. Strand,
P. Torterelli, R. H. Whitley

December 1982

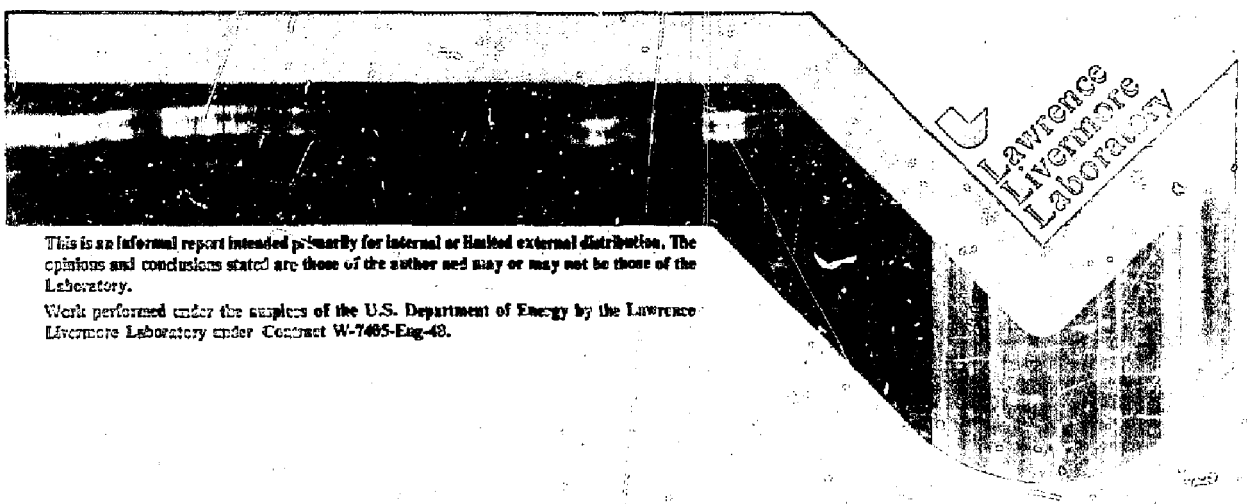

FISSION-SUPPRESSED HYBRID REACTOR: THE FUSION BREEDER

R. W. Moir, J. D. Lee, M. S. Coops,
F. J. Fulton, W. S. Neef, Jr.
Lawrence Livermore National Laboratory
Livermore, CA 94550

D. H. Berwald, R. B. Campbell, B. Flanders,
J. K. Garner, N. Ghoniem (Consultant, UCLA),
J. Ogren, Y. Saito, A. Slomovik, R. H. Whitley,
TRW, Inc.
Redondo Beach, CA 90278

K. R. Schultz, G. E. Benedict, E. T. Cheng
R. L. Creedon, I. Maya, V. H. Pierce, J. B. Strand
GA Technologies, Inc.
San Diego, CA 92138

R. P. Rose, J. S. Karbowski
Westinghouse Electric Corp.
Pittsburgh, PA 15236

J. H. DeVan, P. Torterelli
Oak Ridge National Laboratory
Oak Ridge, TN 37830

L. G. Miller, P. Y. S. Hsu, J. M. Beeston
Idaho National Engineering Laboratory (INEL-EG&G)
Idaho Falls, ID 83401

N. J. Hoffman
Energy Technology Engineering Center
Canoga Park, CA 91304

December 1982

TANDEM MIRROR FUSION BREEDER BLANKET

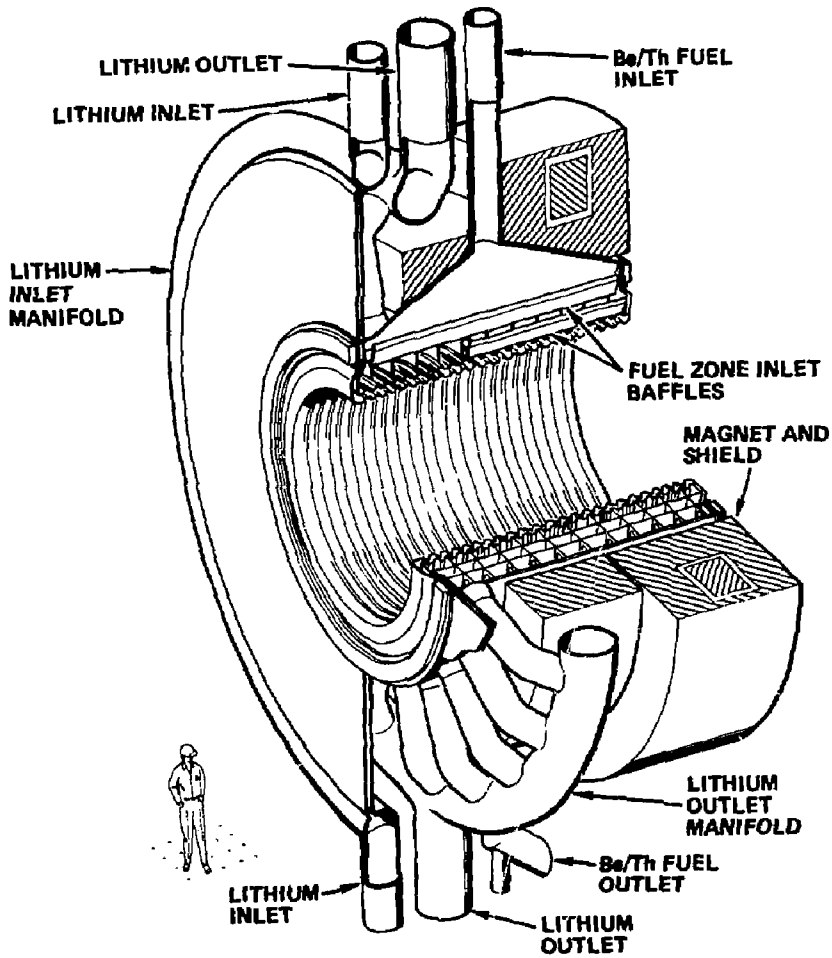

TABLE OF CONTENTS

		Page
SECTION i	ABSTRACT	i-1
SECTION ii	EXECUTIVE SUMMARY	ii-1
I.	Introduction	ii-1
	I.A. Project Goals and Organization	ii-2
	I.B. Fusion Driver Design Basis	ii-4
II.	Reference Blanket	ii-5
	II.A. Design Overview	ii-5
	II.B. Blanket Design and Performance Overview	ii-9
	II.C. Overview of Blanket Design Issues	ii-9
III.	Materials and Lifetime Issues	ii-20
	III.A. Chemical Compatibility Issues	ii-20
	III.B. Blanket Structure and Lifetime Analysis	ii-22
	III.C. Beryllium Fuel Form and Lifetime	ii-25
IV.	Fuel Management Systems and Analysis	ii-32
	IV.A. Fuel Management Mode Selection	ii-32
	IV.B. Isotope Generation	ii-35
	IV.C. Fuel Handling System Design	ii-35
V.	Safety Systems and Analysis	ii-40
VI.	Fusion Breeder Plant Concept	ii-44
	VI.A. Central Cell Layout and Power Conversion	ii-44
	VI.B. Integrated Power Flow	ii-47
	VI.C. Cost Summary	ii-47
VII.	Fuel Cycle Technologies	ii-56
	VII.A. Overview of Fuel Cycles	ii-56
	VII.B. Beryllium Fabrication Technology	ii-60
	VII.C. Reprocessing Technologies	ii-62
VIII.	Systems and Economics Analysis	ii-69
	VIII.A. Introduction and Overview	ii-69
	VIII.B. Economics Analysis for Reference Fusion Breeder	ii-70
	VIII.C. Development of an Optimized Case	ii-76

		Page
	VIII.D. Sensitivity Studies and Comparison with Fusion Electric	ii-81
CHAPTER I	INTRODUCTION AND FUSION BASELINE	1-1
A.	Project Goals and Organization	1-1
A.1	Role and Motivation	1-1
A.2	Project Goals	1-2
A.3	Organization	1-4
B.	Background	1-8
B.1	History of Suppressed Fission Blanket Designs	1-8
B.2	Summary of FY82 Scoping Phase	1-13
B.3	Selection of a Reference Blanket Concept	1-17
C.	Fusion Driver Design Basis	1-21
C.1	Plasma Engineering Basis	1-21
C.2	Driver Technologies	1-27
CHAPTER II	REFERENCE BLANKET DESIGN	2-1
A.	Reference Blanket Overview	2-1
A.1	Design Overview	2-1
A.2	Blanket Design and Performance Overview	2-5
A.3	Overview of Blanket Design Issues	2-5
A.3.a	Design Issues Which Directly Impact Feasibility	2-11
A.3.b	Design Issues Which Strongly Affect Blanket Performance	2-12
A.3.c	Design Issues Which Require Hardware Development and/or Testing	2-13
B.	Mechanical Design	2-17
B.1	Mechanical Design Overview	2-17
B.1.a	Reference Concept Selection	2-17
B.1.b	Design Guidelines	2-17
B.1.c	General Module Arrangement	2-18
B.2	Selection of Structural Materials	2-23

			Page
	B.3	First Wall Design	2-26
	B.4	Inlet/Outlet Piping Considerations	2-28
	B.5	Fuel Zone Design	2-34
	B.6	Mechanical Support of Blanket/Shield/Magnets	2-37
	B.7	Inter-Module Seal Arrangement	2-39
	B.8	Alternate Structural Concept	2-43
	B.9	Summary and Design Issues	2-45
C.	Nuclear Design, Analysis and Performance		2-48
	C.1	Introduction	2-48
	C.2	Cylindrical (1-D) Model	2-49
	C.3	Axial Heterogeneous Effects	2-55
	C.4	Packed Bed Heterogeneous Effects	2-55
	C.5	Criticality	2-60
	C.6	Finite Heterogeneous/Homogeneous Model	2-60
	C.7	End Plug Effects	2-66
	C.8	Estimate of Effective Breeding Ratio, Net ^{233}U Production Rate and Blanket Energy Multiplication	2-66
D.	Fluid Dynamics and Heat Transfer		2-71
	D.1	Introduction	2-71
	D.2	Liquid Metal Blanket Pressure Drop Models and Results	2-72
		D.2.a Channel Flow Liquid Metal Pressure Drops	2-73
		D.2.b Pressure Drops from Turns, Contractions, and Expansions	2-75
		D.2.c Packed Bed MHD Pressure Drop	2-76
		D.2.d First-Wall Pressure Drop	2-85
		D.2.e Pressure Drop Results and Conclusions	2-85
	D.3	Liquid Metal Blanket Heat Transfer Models and Results	2-88
	D.4	Summary of Design Issues	2-93
E.	Operation and Maintenance		2-95
	E.1	Overview	2-95
	E.2	Operation and Maintenance (O&M) Sequence	2-95
		E.2.a Initial Assembly	2-95

			Page
		E.2.b Central Cell Operating Procedure for Reactor Start-Up	2-96
		E.2.c Maintenance - Disassembly/Assembly	2-98
	E.3	O&M Facilities	2-100
CHAPTER III		MATERIALS AND LIFETIME ISSUES	3-1
A.		Materials Compatibility Issues	3-1
	A.1	Overview	3-1
	A.2	Solid-Solid Interactions	3-2
	A.3	Liquid Metal Corrosion/Mass Transfer	3-5
	A.4	Impurity Effects	3-8
	A.5	Results of Li-Be Compatibility Experiments	3-9(a)
	A.6	Summary of Issues	3-12
B.		Analysis of Blanket Structure Lifetime	3-16
	B.1	Overivew	3-16
	B.2	Development of Design Equations	3-17
	B.3	Periodic Annealing for Miligation of Embrittlement	3-21
	B.4	Structural Design Considerations of Blanket Lifetime	3-25
	B.5	Summary of Lifetime Analysis	3-29
C.		Beryllium/Thorium Fuel Forms and Lifetime Considerations	3-35
	C.1	Fuel Form Candidates and Considerations	3-35
	C.2	Reference Fuel Form Selection	3-42
	C.3	Lifetime Analysis of Beryllium Pebbles	3-45
		C.3.a Beryllium Data Base	3-48
		C.3.b Stress Analysis on Beryllium Pebbles	3-55
		C.3.c Lifetime Estimates of Beryllium Pebbles	3-64
		C.3.d Considerations for Increased Lifetime	3-66
CHAPTER IV		FUEL MANAGEMENT SYSTEMS AND ANALYSIS	4-1
A.		Baseline Cycle	4-1

		Page
A.1	Fuel Management Mode Selection	4-1
A.2	Baseline Fuel Management Trade Studies	4-10
A.3	Fuel Management/Safety Interface	4-11
A.4	Fuel Management/Availability Interface	4-21
B.	Fuel Handling Systems	4-23
B.1	Purpose	4-23
B.2	Description	4-23
B.3	System Operation	4-29
C.	Development of an Improved Fuel Cycle	4-33
D.	Optimal Fuel Cycle and Reactor Configuration	4-41
CHAPTER V	REACTOR SAFETY SYSTEMS AND ANALYSIS	5-1
A.	Introduction and Overview	5-1
A.1	Safety Systems and Analysis Goals	5-1
A.2	Safety Criteria Development	5-1
A.3	Safety Systems Overview	5-2
A.4	Safety Analysis Overview	5-4
B.	Safety Criteria Development	5-7
C.	Selection of Reference Safety Systems	5-19
C.1	Approach	5-19
C.2	Reference Safety Systems	5-20
D.	Safety Analysis of Reference System	5-29
D.1	Failure Mode and Effects Analysis	5-29
D.2	Thermal Analysis	5-38
	D.2.a Description of Thermal Model	5-39
	D.2.b Thermal Modeling Results	5-41
D.3	Passive Safety Systems	5-49
CHAPTER VI	FUSION BREEDER PLANT CONCEPT	6-1
A.	Introduction	6-1
B.	Central Cell Layout and Power Conversion	6-3
B.1	Thermal Power Conversion	6-3
	B.1.a Design Approach	6-3

		Page
	B.1.b Thermal Power Conversion System Design	6-9
B.2	Central Cell Layout	6-13
B.3	Key Central Cell Cost Components	6-19
	B.3.a Central Cell Magnet Costs	6-19
	B.3.b Blanket/Shield Costs	6-19
	B.3.c Reactor Building Costs	6-21
C.	End Cell Configuration and Component Subsystem Description	6-22
C.1	End Cell Layout	6-22
C.2	Cost Performance Basis for Key End Cell Components	6-24
	C.2.a Plasma Heating Systems	6-25
	C.2.b End Cell Magnets	6-28
	C.2.c Direct Converter and Beam Dump Systems	6-30
D.	Integrated Power Flow	6-32
E.	Plant Cost Summary	6-35
E.1	Direct Cost Summary	6-35
E.2	Plant Annual Operating Costs	6-35
	E.2.a Fuel Cycle Costs	6-35
	E.2.b Miscellaneous Operation and Maintenance Charges	6-39
	E.2.c Blanket Structure Replacement Costs	6-40
	E.2.d Summary of Plant Annual Operating Costs	6-40
CHAPTER VII	FUEL CYCLE TECHNOLOGIES	7-1
A.	Overview of Fuel Cycles	7-1
A.1	Introduction	7-1
A.2	Fuel Cycle Options and Issues	7-2
	A.2.a Overview of Fusion Breeder Fuel Cycles and Issues	7-4
	A.2.b Overview of LWR Fuel Cycles and Issues	7-7
A.3	Fuel Cycle Summary for Reference Fusion Breeder	7-10
	A.3.a Fusion Breeder Plant Fuel Cycle Summary	7-10
	A.3.b Symbiotic Electricity Generation Systems	7-12

		Page
B.	Beryllium Pebble Fabrication Technologies	7-18
	B.1 Requirements	7-18
	B.2 Beryllium Availability	7-18
	B.3 Fabrication Process	7-20
	B.4 Process Cost Estimate	7-22
	B.5 Development Issues	7-23
C.	Uranium Reprocessing Plant	7-25
	C.1 Reprocessing Plant Design Basis	7-25
	C.1.a Battery Limits	7-25
	C.1.b Reference Plant and Flowsheet	7-28
	C.1.c Operation and Maintenance	7-28
	C.1.d Plant Description	7-31
	C.1.e Process Equipment and Facilities	7-36
	C.2 Cost	7-41
	C.3 Development Requirements	7-41
	C.4 Comparisons with Thorium Blanket Reprocessing	7-44
	C.5 Isotope Considerations	7-45
D.	Pyrochemical Reprocessing	7-48
	D.1 Introduction	7-48
	D.2 Magnesium Precipitation Process	7-53
	D.3 Shielded Containment Facility	7-55
	D.4 Salt Transport Alternative Process	7-56
E.	Comparison of Reprocessing Costs	7-64
F.	Tritium Processing	7-69
	F.1 Overview and Material Choice	7-69
	F.2 Tritium Processing and Inventory Analysis	7-69
CHAPTER VIII	SYSTEMS AND ECONOMIC ANALYSIS	8-1
A.	Introduction and Overview	8-1
	A.1 Introduction	8-1
	A.2 Overview	8-3
B.	An Economics Method for Symbiotic Fusion-Fission Electricity Generation Systems	8-5
	B.1 Introduction	8-5

			Page
	B.2	Defining the Model	8-6
	B.3	Expanding the Fixed and Variable Cost Terms	8-8
	B.4	Inventory Charges	8-11
	B.5	Year-by-Year Fissile and Electricity Costs	8-13
	B.6	Average Present Value of Fissile and Electricity Costs	8-14
	B.7	Cost of Electricity for Same Converter Using Mined Uranium	8-15
C.	Baseline Economics Analysis		8-19
	C.1	Overview of Baseline Analysis	8-19
	C.2	Reference Fusion Breeder Description	8-19
		C.2.a Reference Fusion Breeder Performance Parameters	8-19
		C.2.b Reference Fusion Breeder Cost Parameters	8-21
		C.2.c LWR Performance and Cost Characteristics	8-25
	C.3	Results of Baseline Analysis	8-27
D.	Development of An Optimized Case		8-36
	D.1	Overview	8-36
	D.2	Driver/Fuel Cycle Optimization	8-36
	D.3	Pyrochemical Reprocessing Economics	8-37
	D.4	Denatured Uranium Fuel Cycle Economics	8-39
E.	Sensitivity Studies and Comparison with Fusion Electric		8-42

FISSION-SUPPRESSED HYBRID REACTOR - THE FUSION BREEDER

ABSTRACT

Results of a conceptual design study of a ^{233}U-producing fusion breeder are presented. The majority of the study was devoted to conceptual design and evaluation of a fission-suppressed blanket and to fuel cycle issues such as fuel reprocessing, fuel handling, and fuel management. Studies in the areas of fusion engineering, reactor safety, and economics were also performed.

The blanket structural material is HT-9 ferritic steel. The neutron multiplier consists of a region, 40-cm thick, of a packed bed of beryllium balls 3 cm in diameter which is filled with lithium depleted in ^{6}Li. The fertile material is thorium metal in the form of a snap-ring placed in a small groove around each ball. The blanket is cooled by flowing liquid lithium which also serves as the tritium breeding material. The ^{6}Li to ^{7}Li isotopic ratio is adjusted to give a net tritium breeding just equal to the tritium consumed. Fissioning is suppressed by keeping the thorium atoms dilute (called fertile dilution) so that fast neutrons will collide mostly with beryllium and lithium rather than with thorium, thus suppressing fast fissioning. The ^{233}U is kept dilute by processing at low concentrations ($^{233}U/Th$ ratio $\sim$ 1%) so that thermal fissioning is also suppressed. Fission suppression results in low afterheat and low fission product buildup, thus contributing to safety by largely mitigating loss-of-cooling accidents and their consequences. One reactor sized at 3000 MW of fusion power produces 5700 kg of ^{233}U annually. This is enough to fuel about 17 GWe of light water reactors which use ^{238}U plus ^{233}U, assuming the Pu is recycled (and over 21 LWRs on a thorium cycle). The aqueous reprocessing technology (THOREX) can be used, but our use of metal fuel naturally suggests using pyrochemical processing. Pyro processing should lower the processing cost by several-fold and the basic steps are well founded in laboratory-scale tests.

This large number of supported fission reactors (12 LWRs of equal nuclear power or 17 GWe) means fusion breeders can have an earlier impact than one might think. The fusion breeder technology, which is symbiotic with its client LWRs, can produce electricity for about 10% above the present cost of electricity generation using the LWR technology, and could be demonstrated by about the year 2000. Such a demonstration would provide insurance against the possibility that U_3O_8 prices rise too high (much above $100/pound) and the LMFBR remains too expensive (much over 1.2 times the LWR). The fusion driver for these fusion breeders is a 3000-MW axicell tandem mirror operating in the thermal barrier mode with 20 T barrier coils.

SECTION ii

EXECUTIVE SUMMARY

ii.I. INTRODUCTION

A uranium shortfall is a very real possibility in the future if nuclear fission takes its logical place in the U.S. and world's energy mix. Fusion could alleviate this shortfall by producing fissile fuels.

Fusion will be a prolific source of high energy neutrons (D + T fusion → He (3.5 MeV) + n(14 MeV). In addition to producing heat and the required tritium, fusion neutrons could be used to produce fissile materials by the transmutation of abundant fertile materials such as ^{238}U and ^{232}Th. We are calling this concept the Fusion Breeder. It has also been called the Fusion (Fission) Hybrid and the Fusion (Fission) Fuel Factory.

The ratio of fissile material to energy production in the Fusion Breeder can be widely varied. When optimized to emphasize fissile production, the fusion breeder would replace the uranium mining and enrichment segments of the fission fuel cycle, but would enable the continued use of fission converter reactors such as those currently in use. The nuclear utilities could continue to purchase their fuel much like they do today for their current generation of reactors. Fusion breeders can provide fissile fuel to support over 10 times as much power as they themselves produce and could be owned and/or operated by a separate entity like the enrichment plants are today. Relatively few fusion breeders would be needed to support a rather large nuclear fission capacity.

The basic motivation for the fusion breeder is the need for an assured supply of fissile fuel so fission can grow unencumbered by the threat of mined uranium resource limitations, cartels, etc. The fusion breeder could be considered an insurance policy to protect the nation's (and indeed the world's) financial and technical investment in fission, insurance against the dual possibilities of U_3O_8 prices rising much above $100 per pound and LWFBR costs exceeding LWR costs by much more than 20%.

While the fusion breeder can help make fission a large-scale, long-term energy source, it can also help in the development of fusion by providing a near-term application for fusion before fusion alone would be economically viable. Our studies indicate that the marriage of fusion and fission by the fusion breeder will result in a superior energy source, in terms of both cost

and deployment, than either can on their own.

ii.I.A. Project Goals and Organization

The ultimate goal of the Fusion Breeder Program is to develop and demonstrate the breeder specific technology such that it can be available when both uranium becomes expensive and fusion development results in a practical neutron source. The technologies that complement fusion technology for fissile production are the breeder blanket and fuel cycle technologies. Fuel cycle technologies include the separation of fissile and fertile materials, fuel handling and fabrication, and waste management. The majority of the technology needed for the fusion breeder has been or is being developed by the fusion and fission programs.

Our objectives, at this early stage of the program, are to study and develop blanket conceptual designs to improve our understanding of the technology. A modest effort on design studies and small-scale generic experiments now should save much time and money later when large-scale hardware development is undertaken. By eliminating many of the technological "blind alleys" on paper, it will be possible to provide a lower risk development path.

The major results from the fusion breeder program's FY82 work are reported here.* The blanket, coupled with a tandem mirror fusion driver, results in what we call the FY82 Reference Fusion Breeder. An economic analysis of this fusion breeder and its client fission reactors (LWRs in this case) was made to help quantify its potential and help compare it to other designs developed during previous studies. The cost of electricity from this fusion/fission system and its ability to deploy rapidly (i.e., time to significantly enter the market) are the relevant figures of merit.

The blanket for the FY82 reference fusion breeder is of the fission-suppressed class in which non-fission nuclear reactions [Be(n,2n) and ^{7}Li(n,n'T)] are used to generate the excess neutron multiplication needed for net breeding. We are concentrating on this class of blankets because the decay afterheat is much lower and the fissile fuel production per unit of thermal energy generated in the blanket is much higher than that of the fast fission

*Initial work on a blanket adapted to a tokamak are presented in another report.

class of blankets that use ^{238}U or ^{232}Th fissions (induced by 14 MeV neutrons) to generate the excess neutrons. The lower afterheat should lead to simpler, less risky designs, while the higher specific fuel production should result in more attractive deployment scenarios because fuel becomes the principle product of the fusion breeder, not electricity. The fission-suppressed, fusion breeder can fuel (support) 12-15 LWRs of equal thermal power, where a uranium fast fission, fusion breeder supports only about 5 LWRs. The fission-suppressed fusion breeder will also require higher fusion power drivers (approaching the power level of fusion electric applications) to be competitive. There is an unresolved debate about which class of blanket is best: fission-suppressed or fissioning blanket. More detailed design studies, which include reactor safety considerations, are needed before a definitive comparison can be made and this debate resolved.

Our FY82 blanket design is based, as much as possible, on conventional or near-term materials and process technologies; namely LMFBR liquid metal technologies and THOREX aqueous fuel processing (although we are pursuing a simple form of pyrochemical processing which could cut the reprocessing cost by several-fold.) In terms of performance, technological development requirements and risk, this design could be classified as "moderate technology". For comparison a "low technology" blanket could be a low temperature ($\sim$ 100 ^{o}C) water-cooled design using low stressed, well understood materials producing fuel but no power, while a "high technology" case might be based on Molten Salt Breeder Reactor technology in which a fertile molten salt is used for on-line fueling and processing as well as cooling.

Emphasis of the study is placed upon blanket engineering in the context of a tandem mirror fusion neutron source. A blanket concept for a tokamak neutron source will be selected and studied during FY83.

Fusion breeder design has progressed to a level of conceptual detail which requires a multidisciplinary team approach. The present study includes the participation of the following organizations.

Organization	Principal Roles
Lawrence Livermore National Laboratory	Program Manager, Tandem Mirror Physics and Technology, Nuclear Design
TRW, Inc.	Technical Integration, Tandem Mirror Plasma Engineering, Reactor Systems Modeling, Design Support

GA Technologies, Inc.	Fluid Mechanics and Heat Transfer, Fuel Management Systems, Reactor Safety Systems, Fuel Reprocessing
Westinghouse Electric Company	Mechanical Design, Operation and Maintenance, Reactor System Layout
Oak Ridge National Laboratory	Chemical Engineering and Materials
Princeton Plasma Physics Laboratory	Tokamak Plasma Engineering and Technology
Idaho National Engineering Laboratory	Reactor Neutron Testing

In addition, investigators from the University of California, Los Angeles (ferritic steel irradiation damage), and the Energy Technology Engineering Center (liquid metals and materials) are participating in the study.

ii.I.B. Fusion Driver Design Basis

The fusion driver for the FY82 reference fusion breeder is a tandem mirror with thermal barriers in the end plugs and is similar to that being developed for a reference fusion electric reactor in the ongoing MARS study (MARS stands for Mirror Advanced Reactor Study). For the breeder application, the level of fusion technology is somewhat, but not significally, lower than that called for by MARS. The plasma energy gain, Q, is 19 compared to 35 for MARS. The cost of bred fuel doesn't increase significantly until Q drops below about 6. The B fields and plasma power density are also lower.

ii.II REFERENCE BLANKET

ii.II.A Design Overview

After an extensive scoping phase, a reference blanket concept based upon the use of a liquid lithium coolant flowing radially through a two zone packed bed of composite beryllium/thorium pebbles was selected. The design shown in Figure ii.II.1, uses a ferritic steel (i.e., HT-9 or similar) structure and operates in the 350-500°C temperature range. In this concept, the coolant flow resembles that of a conventional oil filter. Specifically, the coolant flows to the first wall plenum through a thin coolant annulus and is distributed to the packed bed through perforations in a corrugated intermediate wall which, in combination with a corrugated first wall and radial stiffeners (tied to the back of the blanket), provides structural support.

The coolant flows radially outward through two fuel zones (separated by another perforated wall), exits the bed through a third perforated wall outside of the second fuel zone, and exits the blanket through 20 large outlet pipes. The composite fuel pebbles (beryllium pebbles with thorium snap-rings) are loaded into the top of the blanket and discharged at the bottom in a frequent batch process (i.e., fuel residence time ~ 3-6 months).

The reference blanket concept offers several potentially attractive design and performance features:

- high breeding performance per unit of thermal power production
- low decay afterheat and excellent provision for cooling in the event of a loss of coolant or coolant flow accident
- a beryllium multiplier form which can be easily fabricated and readily recycled, and
- the extensive use of conventional materials and coolant technologies.

These features are described in more detail below.

The breeding performance is excellent for two reasons. First, the design features a high volume fraction of high efficiency neutron multipliers. The bed volume fractions in Figure ii.II.1 include about 55% beryllium, 40% lithium, and 3% thorium -- all excellent neutron multipliers. The remainder of the fuel region following the two corrugated walls is less than 2% steel. Second, the design effectively suppresses the fissioning in the blanket

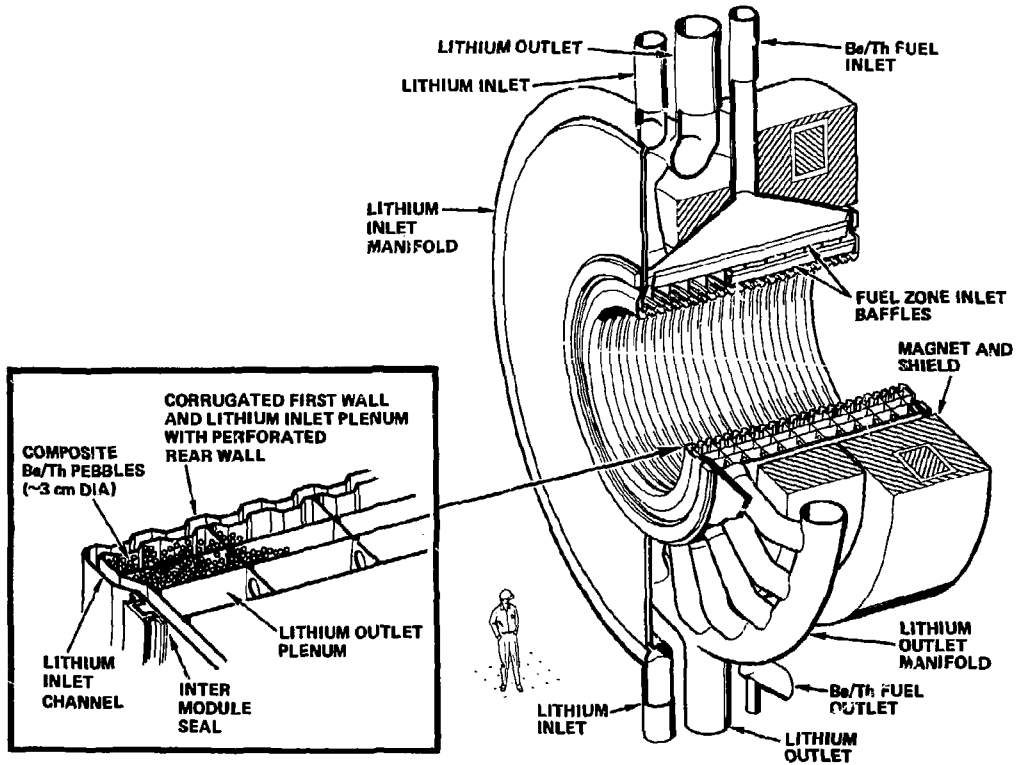

Figure ii.II.1 Reference Tandem Mirror Fusion Breeder Blanket

(< 0.04 fission per fusion neutron at 0.5% ^{233}U concentration in thorium). Fast fissions are suppressed due to neutron moderation in the beryllium and low thorium volume fraction. Thermal and epithermal fissions in the bed ^{233}U are suppressed due to fuel discharge at low concentration ($\lesssim$1%) in the small volume of thorium as well as thermal neutron depletion due to the large 1/V neutron absorption cross section of the ^{6}Li in the liquid lithium coolant.

As a result of the low fission rate, the fission product inventories and decay afterheat levels in the fuel are very low. In fact, the fission product decay afterheat is a relatively minor contribution to the total afterheat and the afterheat associated with actinide decay through the chain

$$n + {}^{232}Th \rightarrow {}^{233}Th \xrightarrow[23\ m]{\beta^-} {}^{233}Pa \xrightarrow[27\ d]{\beta^-} {}^{233}U$$

dominates the overall afterheat level. Typical fission product levels in the discharge fuel are only about 1000 ppm in thorium, or roughly 1/60 that of LWR discharge fuel. These advantages are uniquely associated with fission suppressed blankets since fast fission blankets, with blanket energy multiplications of 6-10, increase the fission rate by factors of 10-20.

Additional reactor safety benefits for the reference design result from the use of a mobile fuel form (i.e., the composite beryllium/thorium pebbles) with provision to discharge the fuel to an independently cooled dump tank should the need arise. In addition to the primary coolant loop and the dump tank loop, the fuel handling sytem piping and valving provides a coolant flow sufficient to remove the decay afterheat. Therefore, double redunancy of the cooling systems is provided in the event of a loss of coolant or loss of coolant flow accident.

The composite beryllium/thorium pebble fuel form employed in the reference design provides several advantages in comparison with previous designs. First, this form provides a relatively simple method to achieve uniform mixing of the beryllium and thorium throughout the blanket - an advantage with respect to the thermal and nuclear breeding performance. Second, the design is relatively insensitive to the high rate of volumetric swelling in beryllium since the beryllium is discharged frequently and the packing density of the bed, although high, is low enough to accommodate some growth (typically 0.2% linear growth occurs over a 90 day irradiation). Finally, the small size of the pebbles (1.5 cm radius) limits the thermal and

differential swelling induced stress levels in the beryllium - key lifetime determinates. Our results indicate that an average beryllium in-core lifetime in excess of two years should be easily achievable, but that more materials data and more accurate models are required before a more definitive lifetime estimate will be possible. The reference blanket provides a flexible design which can accommodate a wide variation in the irradiated properties of beryllium without imposing a substantial penalty on the overall level of performance.

Finally the reference design utilizes conventional and well known materials and coolant technologies. Our selection of ferritic steels was based upon their irradiated and un-irradiated materials properties (e.g., high strength, high thermal conductivity, low neutron swelling, excellent liquid metal compatability) as well as the extensive industrial experience in the fabrication of components from ferritics (principally 2-1/4 Cr-1Mo) and the current interest of the nuclear materials community in these alloys.

Our choice of liquid lithium as the blanket coolant primarily derived from nuclear, heat transfer, and tritium extraction advantages, but also considered the operational and safety implications of liquid lithium versus the obvious alternative, $Li_{17}Pb_{83}$. It is our considered opinion that liquid lithium systems can be designed to operate more economically and more reliably than lead-lithium systems and will have the advantage of lower normal tritium releases. An acceptable level of lithium safety appears to be achievable based upon the development of liquid sodium coolant safety systems in the LMFBR program. The recognition that fusion breeder reactors would not, most likely, be sited near population centers (but, rather, in remote safeguarded fuel cycle centers) provides additional confidence in the choice of a liquid lithium coolant.

Our choice of thorium metal as a fertile fuel form rather than thorium dioxide (thoria) or another thorium form is primarily based upon fuel cycle considerations. Although thorium oxide would provide fewer compatability concerns, thorium metal is less expensive to reprocess (Either aqueous or pyrochemical) and is more amenable to the selected fuel form. There is considerable experience in the use of thorium metal in fission reactors.

ii.II.B Blanket Design and Performance Overview

Table ii.II.1 is an overview of several key design and performance parameters for the reference fusion breeder blanket.

ii.II.C Overview of Blanket Design Issues

The reference blanket performance is attractive and our analysis indicate overall feasibility. Nevertheless, during the course of the study, several issues require additional analysis, experimental data acquisition and/or component development and testing were identified. These issues are listed in Table ii.II.2. Although the actual impact of the resolution of any issue is, to a large extent, unknown prior to the resolution of that issue, an attempt has been made to prioritize the issues in decreasing importance as they relate to design feasibility, blanket performance, and development/testing requirements. These issues are briefly described below.

Design Issues Which Directly Impact Feasibility

Any compatibility assessment of the present fusion breeder blanket design concept is complicated by the number of blanket components. To address these issues, a large matrix of materials compatibility concerns were considered during the course of the study. In several cases capsule experiments were performed. Among the possible interactions, solid-solid interactions include self-welding of the thorium and beryllium (in the presence of lithium), the inter-alloying of thorium and beryllium, and the inter-alloying of beryllium and the structural steel. Of highest priority are the self-welding reactions, because they will determine whether barrier coatings must be applied to the pebbles to guarantee their removability. Possible coatings for the thorium metal are ThO_2, ThC, or TiC. Possible coatings for the beryllium metal are $Be_{12}Fe$, or $Be_{12}Cr$, or $Be_{12}Mo$. Next in priority are the possible reactions of beryllium with thorium. The same coating candidates listed above could also be used to reduce the extent of the latter reaction. Last in priority are the reactions between beryllium and HT-9, which preliminary experiments have shown to be slow at 450°C.

TABLE ii.II.1. Key Design and Performance Parameters for the Reference Blanket

Central Cell Parameters	
Central Cell Fusion Power[a]	3000 MW
Central Cell Fusion Neutron Power[b]	2400 MW
Maximum Central Cell Thermal Power[c]	4728 MW
Average Central Cell Thermal Power[d]	3864 MW
^{233}U Fuel Production[e]	5625 Kg/yr
Central Cell Length[f]	200 m
Number of Blanket Modules	50
Number of Central Cell Coils	50
Central Cell Coil B Field Strength on Axis	4.2 T
Blanket Module Mechnical Design	
Structural Material[g]	HT-9 Ferritic Steel
Module Length	4 m
Inter-module vacuum seal arrangement	metal omega seal
Fraction of module length used for multiplier/ fuel zones[h]	~ 95%
First Wall Radius	1.5 m
Number of Multiplier/Fuel Zones	Two
Multiplier/Fuel Zone Volume Fractions[i]	
Beryllium	55%
Lithium (0.2 a/o ^{6}Li)	40%
Thorium (incl. bred fissile)	3%
Ferritic Steel	2%
Thickness of Each Fuel Zone[j]	20 cm
Lithium Reflector Thickness[k]	30 cm
Blanket Outer Radius	2.34 m
Shield Thickness	75 cm
Magnet Inner Bore	6.7 m
Magnet Pitch	4 m
Number of Coolant Outlet Pipes	20 each

Table ii.II.1 (Continued)

Heat Transfer, Power Flow, and Thermal Design Parameters	
Neutron Wall Loading	1.27 MW/m^2
Coolant[l]	liquid lithium
Maximum Thermal Power Per Blanket Module	94 MW
Coolant Inlet Temperature[m]	340°C
Coolant Outlet Temperature[n]	490°C
Lithium Flow Rate	0.31 m^3/sec
Lithium Pressure Drop[o]	~ 2 MPa (~300 PSI)
Lithium Pump Power (all modules)	~ 35 MW
First Wall Pressure[o]	~ 1.7 MPa (~250 PSI)
Minimum First Wall Temperature[p]	361°C
Maximum First Wall Temperature[q]	409°C
Maximum Structure Temperature[r]	490°C
Maximum Beryllium Surface Temperature[s]	475°C
Maximum Beryllium Internal Temperature[s]	< 483°C
Maximum Beryllium ΔT[s]	< 38°C
Nuclear Design Parameters	
Net Fissile Breeding Ratio[t]	0.62
Net Tritium Breeding Ratio[u]	1.06
Minimum Blanket Energy Multiplication[v]	1.25
Maximum Blanket Energy Multiplication[w]	1.97
Maximum Thorium Power Density[w]	182 $/cm^3$
Maximum Beryllium Power Density[w]	5.4 w/cm^3
Maximum Lithium Power Density[w]	3.3 w/cm^3
Maximum Average Power Density[w]	7.7 w/cm^3
Zone 1 Fuel Residence Time[j]	78.3 days
Zone 1 Uranium Discharge Concentration	.856%
Zone 1 Protactinium Discharge Concentration	.532%
Zone 2 Fuel Residence Time[x]	156.6 days
Zone 2 Uranium Discharge Concentration	.739%
Zone 2 Protactinium Discharge Concentration	.195%
Average Fission Rate Per Fusion[x]	~ 0.04
Average Fission burnup at Fuel Discharge[w]	~ 500 MWD/MT

Table ii.II.1 (Continued)

a) all quantities normalized to central cell fusion power (3000 MW). End cell fusion power = 140 MW.

b) Charged particle and radiation power (~ 850 MW) primarily deposited in end cells on direct converter and electron dump, but ~ 40 MW of radiation surface heat load appears on first wall (0.018 MW/m^2).

c) Corresponds to maximum blanket energy multiplication of 1.97.

d) Corresponds to average over-cycle blanket energy multiplication of 1.61.

e) At 70% plant average capacity factor and fissile breeding ratio = 0.62 per fusion.

f) Shorter central cells also possible as discussed in Chapters IV and VIII.

g) Or similar low nickel ferritic (e.g., 2-1/4 Cr-1Mo). Design stress ~ 16 KSI.

h) Remaining ~ 5% used for module side walls and inlet coolant duct.

i) Assumes 59% packing of beryllium/thorium pebbles in the 98% of volume not occupied by structure.

j) Zone 1 recycled twice as often as Zone 2.

k) Reflector is also the lithium outlet annulus.

l) 0.2% a/o ^6Li.

Table ii.II.1 (Continued)

m) Lowest temperature to avoid loss of ductility (DBTT) during irradiation.

n) Highest temperature to provide confidence in corrosion/ compatability characteristics.

o) Approximate values based upon existing modeling capability.

p) Coolant interface at left side first wall inlet.

q) Plasma inside interface at right side of first wall.

r) At rear of blanket

s) Estimate requires more detailed model

t) Adjusted for multidimensional and heterogenious effects

u) This quantity is net for the blanket. The reactor net tritium breeding is 1.01 after correcting for tritium to sustain the additional 140 MW of fusion in the end plugs (no blanket).

v) Beginning of cycle - no fissile material

w) End of cycle- prior to Zone 1 and Zone 2 fuel discharge.

x) Average over time and blanket volume

TABLE ii.II.2 Reference Blanket Design Feasibility, Performance, and Development/Testing Issues

Issues Which Directly Impact Blanket Design Feasibility

- Blanket Material Compatibility
- Beryllium Pebble Lifetime

Issues Which Strongly Effect Blanket Performance

- Liquid Metal (MHD) Pressure Drop
- Beryllium Neutron Multiplication
- First Wall Lifetime
- Heterogenious Nuclear Effects

Issues Which Require Hardware Development and/or Testing and have Significant Impact on Performance and/or Cost

- Beryllium/Thorium Composite Pebble Fabrication
- Composite Pebble and Thorium Fuel Handling Systems
- HT-9 Fabrication and Heat Treatment
- Electrically Insulated Coolant Duct Development
- Pyrochemical Thorium Metal Fuel Reprocessing
- Lithium Safety Systems Development and Integration
- Molten Salt Extraction Process for Tritium Removal from Liquid Lithium
- Tritium Permeation Control Technologies
- Remote Maintenance and Inter-module Seal Technologies

In order of priority, the most critical liquid-solid compatibility issue is the rate of thermal gradient mass transfer of HT-9 and beryllium in lithium at the reference reactor operating temperatures. Tests are currently underway to evaluate this potential problem, although, in the case of beryllium, truly definitive studies will not be possible until it is determined what, if any, coatings will be applied to the beryllium. These tests will also define the potential for carbon transport by the lithium.

The beryllium pebble lifetime is determined by the thermal and irradiation swelling induced stress levels in the beryllium and the irradiation time required to degrade the mechanical properties of the beryllium such that the yield stress would be exceeded. Although this problem is considered a several year average lifetime is predicted, improved analysis of the stress levels in the beryllium is required. Such an analysis should consider the differential swelling stress, the thermal stress (a multi- dimensional problem), the bearing stress exerted by adjacent pebbles, and any transient stress due to pebble dropping, etc. In addition, the mechanical properties of the sintered beryllium product require further definition, especially in the flux/temperature environment of the reference blanket. An optimization to achieve the maximum lifetime will ultimately be required.

Design Issues Which Strongly Effect Blanket Performance

The pressure drop associated with pumping liquid lithium through the packed bed and complex flow path associated with the reference blanket is quite uncertain. In particular, an adequate model of the magnetic field induced (MHD) pressure drop for packed bed flow (as well as turns, baffles, orifices, etc.) does not currently exist. We believe that our estimate of an ~ 250 PSI pressure at the first wall is reasonable (and possibly conservative), but a smaller scale experimental verification is required. The MHD interaction impacts the overall design in several ways. Most importantly, by determining the structure fraction in the blanket, the MHD pressure drop directly affects the fissile fuel breeding performance and limits the neutron wall loading (i.e., the pressure drop is directly proportional to the coolant velocity which, in turn, is proportional to the wall loading).

Although beryllium is clearly the best non-fissioning neutron multiplier, reported integral experiments and comparisons with neutron transport calculations have cast some doubt on the adequacy of current nuclear data and

calculational methods. A specific concern is the angular and energy distribution of secondary (n,2n) neutrons as modeled in the evaluated nuclear data files and utilized in discrete ordinates and Monte Carlo transportation codes. Our most recent consideration of this issue indicates that the ENDL data file and the TARTNP Monte Carlo code used in our analysis provide an ~ 10% uncertainty in fissile breeding. Despite this encouraging result, more work (and possibly an experiment) is required to reduce and/or confirm the breeding uncertainty.

Another nuclear issue concerns the effects of spatial heterogenity in the blanket. Our preliminary modeling indicates a loss of ~ 5% in total breeding (i.e., tritium plus fissile) and a gain of ~ 25% in the end-of-cycle blanket energy production. These effects are particularly difficult to model in the complex source driver geometry of the fusion breeder blanket. An explicity finite model of the blanket including the first wall/intermediate wall zone followed by a packed bed of individual beryllium/thorium pebbles is currently under development.

An adequate prediction of the lifetime of the blanket structure (and specifically the first wall) requires the integration of detailed stress and thermal models with consideration of many non-nuclear and irradiation dependent materials effects:

- neutron swelling
- irradiation creep
- irradiation induced embrittlement
- thermal creep
- alloy manufacturing control
- temperature/time/fluence related metalurgical phase transitions

The problem is complicated by the complex configuration of the blanket structure (requiring multi-dimensional stress and thermal models) and by the time dependent nature of the problem. Specifically, the properties of the materials vary in time with irradiation (as well as the amount of thermal and mechanical cycling) and the stress levels also evolve as a function of time due to deformations which occur during previous intervals. Since failure is likely to occur in a weld (or possibly due to grain boundary attack by

corrosive products) any modeling of the structural evolution must be subject to an experimental confirmation which models the real environment as closely as possible.

In the reference design we have selected a strong, low swelling structural material (HT-9) and a low wall loading (~ 1.3 MW/m^2). An integrated lifetime of about ten calendar years (~ 10 MW-yr/m^2) seems reasonable based upon our initial calculations. More detailed analysis is desirable in the absence of integrated testing.

Design Issues Which Require Hardware Development and/or Testing

Several important reactor and fuel cycle technologies which are required and/or desirable for economical and reliable operation of the reference blanket require significant development.

One such technology is the remoted and automated manufacturing line for the beryllium pebbles. The proposed process utilizes cold press, vacuum sinter, hot forge, and vacuum anneal steps to produce pebbles in a manner similar to a process used to manufacture aircraft brake parts. The two key development items are the development of a free flowing beryllium powder (to further automate the process) and the development of a remotely maintained and shielded facility (to remanufacture irradiated beryllium pebbles). Due to the toxicity of beryllium, manufacturing operations are already high remoted and automated.

Another required technology is the remoted and automated machine which retrieves the irradiated beryllium/thorium pebbles from the blanket, removes the thorium snap ring, replaces it with a new ring, and returns the pebble to the blanket (or returns the beryllium part to the remanufacturing line). Such a machine was conceived, and is similar to many machines which are routinely used in industry (e.g., an apple coring machine). Again, the developmental emphasis would be in the area of remote maintenance.

Although HT-9 was selected as the reference design structural material, industrial experience in the fabrication of this ferritic is quite limited. If HT-9 fabrication, impurity control, or heat treatment, etc., proves excessively difficult, the reference design would specify 2-1/4 Cr-1Mo as a second choice. The latter is a very common alloy in pressure vessel use, but

is somewhat weaker than HT-9 in the 500°C range. Other ferritics currently under development (e.g., 3Cr-1.5Mo) potentially offer both the strength of HT-9 and the fabricability of 2-1/4 Cr-1Mo.

A preliminary design of an electrically insulated coolant duct to limit the MHD pressure drop in straight pipe sections (e.g., I/O piping) was proposed as part of our FY81 study. Electrically insulated ducts could significantly decrease the MHD pressure at the first wall and this technology is an attractive, but not critical, candidate for development.

Aqueous fuel reprocessing technologies for thorium metal fuels (such as THOREX), are reasonably well established, but the estimated cost of THOREX reprocessing is both high (i.e., ~ 300 $/Kg HM) and uncertain. In contrast, pyrochemical reprocessing technologies for thorium metal based fuels offer the potential of an order of magnitude cost reduction due to a dramatic reduction in the size of the plant and number of components. The proposed magnesium dissolution process is simple, straightforward, and well suited to the fusion breeder fuel (e.g., fission product separation from the very low burnup breeder fuel not necessarily implemented). Nevertheless, a substantial development effort would be required to commercialize the pyrochemical option.

The use of liquid lithium coolants in fusion applications raises concern regrading the liquid metal safety. Nevertheless, liquid lithium has unique properties, which help to maximize breeding in the reference blanket. Liquid lithium safety is addressed and many candidate liquid metal safety systems are identified. LMFBR experience provides us additional confidence in the ability to engineer safety into liquid lithium systems, but development and integration of such systems is required.

A molten salt tritium extraction process for liquid lithium has been developed through the proof-of-principle stage, but the development of a fully closed process has not been demonstrated. The molten salt tritium extraction process should keep the inventory to less than 1 Kg in the entire lithium loop and requires equipment of minimal size, electrical requirements and cost. Therefore, the developmental risk is expected to be minimal.

Tritium permeation control technologies for the reference lithium cooled blanket have not been evaluated in the context of the present study. However, the high tritium solubility of the liquid lithium is expected to minimize this concern. The largest tritium escape path is eliminated in the reference

design by use of a cold trapped sodium intermediate loop. However, technologies related to tritium diffusion barriers, double walled pipes, and gettering systems may require additional development.

The intermodule seal (metal omega seal) is expected to be a difficult and high risk technology due to the large seal perimeter (~ 16 m), the probability of local faults, and the amount of pressure required to make the seal. It is quite possible that a differential vacuum pumping may be required to further increase the vacuum impedance and seal effectiveness. If this concept fails, we would revert to a remotely formed and inspected welded seal. The primary impact relates to a possible loss in availability due to increased remote operations.

ii.III MATERIALS AND LIFETIME ISSUES

Several materials and lifetime issues have been addressed in the context of the reference blanket design. Most importantly, issues related to chemical compatibility of the blanket constituents (i.e., HT-9 ferritic steel, lithium, beryllium, thorium) were addressed in some detail, and in some cases, experimentally. Other lifetime issues which were considered in detail include the expected lifetimes of the blanket structure and the beryllium pebble fuel.

ii.III.A Chemical Compatibility Issues

The reference blanket presents a complicated compatibility/mass transfer matrix with possibilities for both solid-solid and liquid metal-solid interactions. This matrix has been examined to identify possible reactions under relevant operating conditions and their effects on blanket integrity and performance. The materials compatibility effort utilized thermodynamic and existing compatibility data to consider the severity of the expected reactions. Also, experimental reaction couples consisting of beryllium, static lithium, and stainless steel were fabricated and exposed at 350, 450, and 550°C.

The results of the compatibility assessment are shown in Table ii.III.1. The interaction of highest concern is self welding of the beryllium pebbles since an assurance of free flow of the pebbles is key to the safe and reliable operation of the blanket. This interaction has not been shown to be intolerable without coatings, but a need for beryllium coatings might be indicated. Some candidate coatings which would not introduce a new elemental constituent into the blanket include $Be_{12}Fe$, $Be_{12}Cr$, and $Be_{12}Mo$. Other concerns relate to thorium self welding and Th-Be interactions which could affect the fuel removal and beryllium recycle, respectively. Again, the possibility of coatings is suggested, but the real extent of such interactions during the relatively short fuel residence time (~ 1/2 year) requires further characterization.

Among the liquid-solid interactions which could lead to temperature gradient mass transfer and flow channel plugging, the highest priority is beryllium mass transfer in lithium complicated by nitrogen impurities in the lithium. The later can lead to Be_3N_2 formation at typical impurity levels. The presence of nitrogen in lithium has also been observed to accelerate, and

Table ii.III.1 Possible Materials Compatability and Mass Transfer Concerns

INTERACTION	CONCERN	RESOLUTION PRIORITY	COMMENT
Be-Be	Self welding during ~ 1/2 year blanket residence time could affect fuel removal	highest	Possible need for coatings. Candidates include $Be_{12}Fe$, $Be_{12}Cr$, $Be_{12}Mo$. A perfect coating would not be required.
Th-Th	Self welding during ~ 1/2 year blanket residence time could affect fuel removal	high	Less Th-Th contact than Be-Be contact. Possible need for coatings. Candidates include ThO_2, ThC, TiC. Perfect coating not required.
Th-Be	Inter-alloying during ~ 1/2 year blanket residence time could affect throium snap-ring removal and/or beryllium pebble recycle	medium	Possible need for Th coating and/or Be coating. Some possibilities as above.
Be-HT9	Loss of integrity of ferritic steel surface over 5-10 year structure life	low	Preliminary experiments indicate that this reaction will be slow for low nickel alloys (i.e., ferritics) at the proposed operating temperature
Li-HT9	Temperature gradient mass transfer of iron and/or chromium leading to plugging. De-carburization of HT-9 leading to degradation of HT-9 surface integrity.	medium	Low temperature (<500°C) and choice of a low nickel alloy should relax these concerns. Decarburization is slow for HT-9, but Be and Th are both strong carbide formers. Nitrogen impurity effects could be important.
Li-Be	Temperature gradient mass transfer of Be leading to plugging	high	Complicated by nitrogen impurities leading to Be_3N_2 formation. Possible need for coatings. Same candidates as above.

possibly change, the corrosion reactions of steel with lithium. Consequently, despite the favorable operating temperature and the choice of a low nickel alloy, HT-9 mass transfer is also a concern.

Finally, the Be-HT9 solid-solid interaction, a high priority for resolution at the beginning of the study, does not appear to be a critical concern if a low nickel, low chrome alloy is used and is operated in the range of 450°C.

ii.III.B Blanket Structure and Lifetime Analysis

As is the case with any proposed blanket for reasonably high fluence fusion applications, the lifetime limiting failure mechanism for the reference fusion breeder is difficult to predict. In particular, an acceptable blanket lifetime prediction would involve a detailed, time dependent, stress map to track the interaction between applied stresses (such as thermal and hydraulic stresses), inelastic deformations (such as swelling and creep), and the degradation of material properties with irradiation (e.g., welds). Such a non-linear analysis would require complex analytical tools (e.g., 3-D time dependent stress modeling), and the result would not, in any case, be definitive since: (1) the materials data base for fusion irradiation is insufficient to support such an analysis, and (2) no comparable benchmark calculation exists.

Instead, the reference fusion breeder blanket is, to the greatest extent possible, based upon the use of a conservative design utilizing the following features:

- a low wall loading of 1.3 MW/m^2 which accumulates only 9.1 $MW\text{-}yr/m^2$ of fusion fluence over a ten year lifetime (70% capacity factor included)
- a very low swelling, high strength alloy, HT-9, is selected for use below 500°C to minimize the overall extent of inelastic deformations while allowing for an acceptable design stress of 20 ksi.
- a minimum structure temperature of 365°C provides a margin of safety against neutron embrittlement during operation.
- moderate shifts in the ductile-to-brittle transition temperature (DBTT) are eliminated by a 450°C anneal for ~ 50 hours during annual scheduled maintenance periods.

Detailed analyses were performed to determine the extent of inelastic deformations and to predict the DBTT shift with irradiation and subject to post-irradiation annealing. During the course of this analysis, a set of design equations was developed (and/or adopted) to predict the swelling, thermal creep, irradiation creep, DBTT shift, and the post-irradiation annealing characteristics of ferritic steels.

The issue of embrittlement is of particular interest since, with neutron irradiation, the DBTT of the reference blanket (defined more precisely as the temperature at which the fracture stress equals the yield stress) can shift from a pre-irradiation DBTT of -18°C to a saturation DBTT above 135°C. The design equation developed for the DBTT shift is given below:

$$\Delta DBTT = \frac{18,700}{(T-238)} \{1 - \exp [- (\frac{4T-350}{T}) \delta^{1/2}]\}$$

where T is the operating temperature in °C and δ is the displacement dose in dpa (10 dpa/FPY). This equation indicates that the majority of the shift occurs within about one week to one month after startup. The implication of large upward shifts in the DBTT is that, should the module cool below the DBTT, failure due to brittle fracture under dynamic loads would be possible. For operating temperatures below 300°C, the DBTT would quickly increase above the operating temperature.

Although fracture mechanics approaches based upon the fracture toughness parameter, K_{IC}, and a maximum surface crack size indicate that operation in the brittle regime need not be catastrophic, we have selected a design philosophy whereby the minimum temperature of 365°C is well above that required to prevent the DBTT from rising into the operating temperature. Also, we would lower the DBTT periodically by annealing. The fraction of the DBTT shift, $\Delta DBTT$, which can be recovered by annealing is given by:

$$f_{DBTT} = 1 - exp [- 3.885 \cdot 10^5 \, t \, exp(- 1.002/K_b T)]$$

where T is the annealing temperature (°K) and t is the annealing time (hours). The results of our analysis, shown in Figure ii.III.1, indicate that a 50-60 hour annual anneal at 450°C can reduce the DBTT to below room temperature.

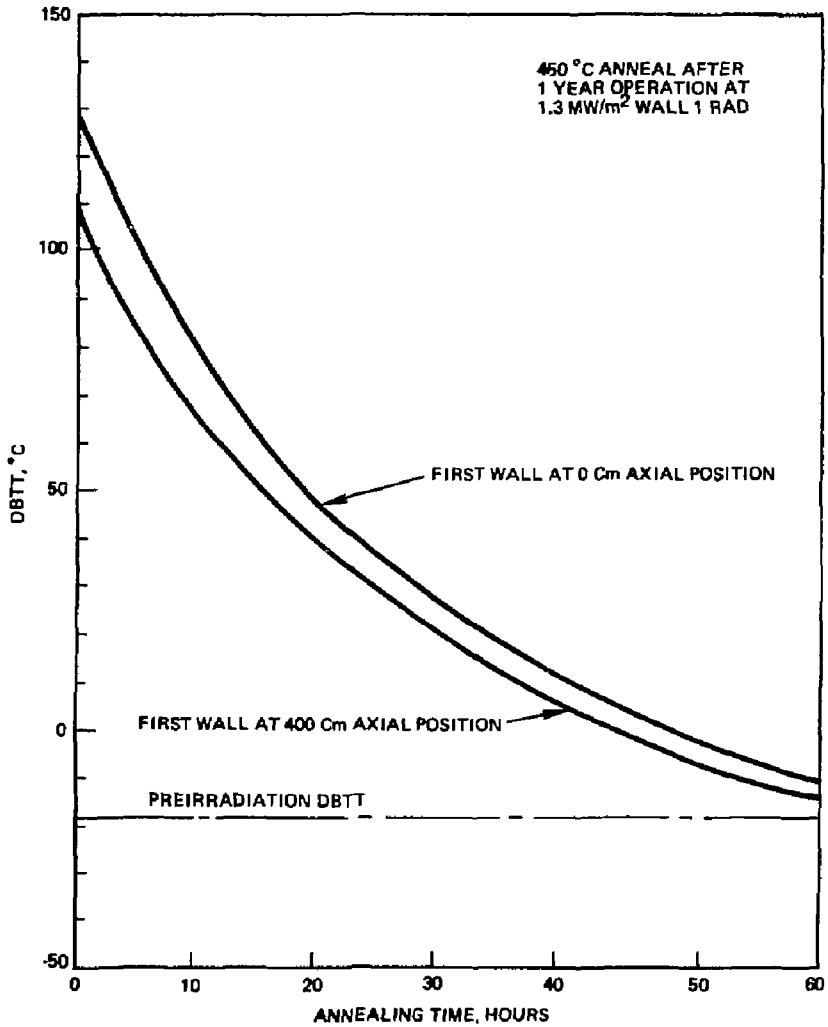

Fig. ii.III.1 First Wall DBTT vs. Post Irradiation Annealing Time at 450°C

To estimate the blanket lifetime, inelastic deformations in the radial and axial blanket directions were calculated as a function of time. Assuming a wall loading of 1.3 MW/m^2 and a design stress of 20 ksi, the maximum swelling, thermal creep, and irradiation creep induced linear strains are 0.12%/FPY, 0.20%/FPY, and 0.07%/FPY, respectively. The cumulative strain is greatest at the first wall and is room temperature dependent as shown in Figure ii.III.2.

Considering first the radial direction, we have observed that the swelling and creep strains are oriented in opposite directions and should, for the most part, cancel. In the axial direction, an average linear growth rate of 0.32%/FPY is equivalent to an axial growth of 1.28 cm/FPY (0.90 cm/CY) over the 4 m module length. The module lifetime will, to first order, be limited by out-of-plane deflection stresses introduced at the end caps of the module by this axial growth. Assuming that a 9 cm deflection is tolerable, a ten year blanket life can be achieved. Although a more detailed analysis is desirable, we note that the accumulated damage is only about 100 dpa at end of life.

ii.III.C Beryllium Fuel Form and Lifetime

Several considerations bear upon the selection of a composite beryllium/throium fuel form for the reference blanket:

- the fabrication and recycle cost
- the impact on breeding, thermal, and fluid flow characteristics
- chemical compatibility between beryllium and thorium with other blanket constituents
- the impact on fuel management and fuel handling operations
- the expected lifetime as affected by the thermal, irradiation damage, and chemical environment in the blanket.

In practice, the selected fuel form will provide a compromise between goals relating to the above considerations. In this section we discuss the selection of a fuel form and lifetime considerations. The behavior of beryllium pebbles in the blanket was discussed in Section ii.II while fuel management handling and fabrication/recycle are discussed in Sections ii.IV and ii.VII, respectively.

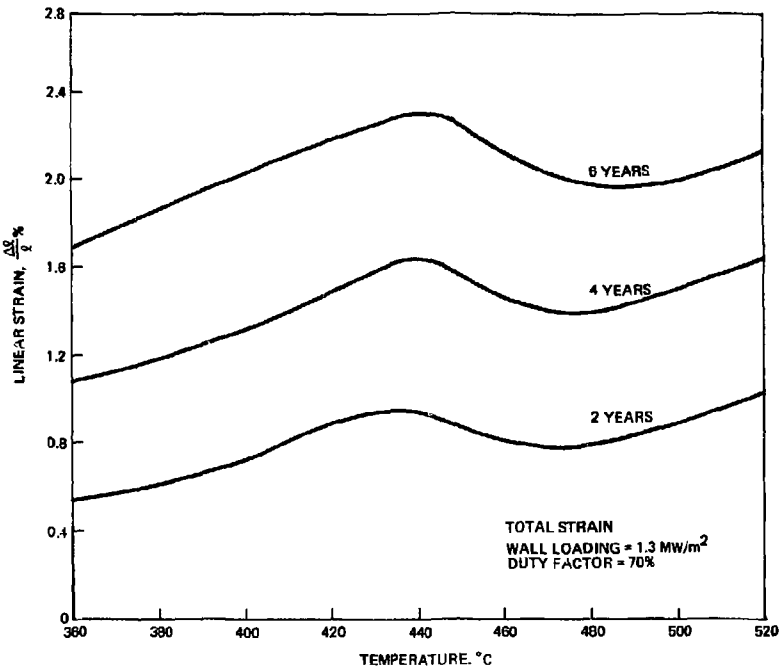

Fig. ii.III.2 Accumulated Axial Strain in First Wall vs. Temperature and Time

During the reference phase of the study, three generic composite fuel forms were considered: 1) beryllium pebbles with drilled and reamed cylindrical holes in the center and thorium pin inserts held in place by alloy steel spring clips; 2) beryllium pebbles with cylindrical holes in the center and scroll-pin (or spiral wound dowel) inserts held in place by their own spring forces, and 3) solid beryllium pebbles with shallow grooves at the equator which hold C-shaped thorium metal snap-rings which conform to the groove. These three options are illustrated in Figure ii.III.3.

The beryllium pebbles would, in each case, be fabricated into a low tolerance, sintered form with minimal machining required. The thorium would be fabricated as metal. Each of the three fuel forms would have approximately the same outer dimension (3 cm O.D.) and thorium to beryllium ratio. There are approximately 35 million fuel pebbles in the 50 blanket modules of the fusion breeder.

A comparison between the three fuel forms is shown in Table ii.III.2. The cylindrical pins with steel clips provide better chemical compatibility characteristics because the thorium pin does not contact the beryllium or other thorium pins. However, this fuel form has drawbacks in other areas. For example, the metal pins and clips are expected to be more difficult to handle and manufacture than the more simple scroll pin option. More importantly, both internal pin designs introduce heterogenious effects into the blanket which can act to reduce fissile breeding and limmit the beryllium lifetime. The snap-ring fuel design, which was selected as the reference fuel form, can increase breeding relative to the pin designs and also increases the expected beryllium lifetime by lowering the thermal gradient from the inside to the outside of the beryllium pebble (see later discussion).

Our analysis of the expected lifetime of the beryllium pebbles considered two failure modes: 1) fracture due to contact loading caused by the weight of the pebbles and the hydraulic pressure of the coolant, and 2) failure due to internal thermal and differential swelling stresses which can ultimately exceed the yield stress.

Considering first the contact loading, it was calculated that a force of up to 150 lb (670 N) could be applied to each pebble, causing it to deform at the point of contact. If the pebble retains ~ 3% ductility, it would deform a small amount without fracture so that a contact radius of 0.04 in (0.102 cm)

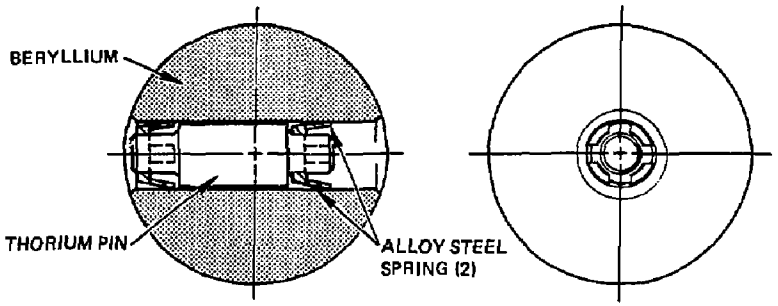

(A) SOLID PIN WITH STEEL SPRINGS

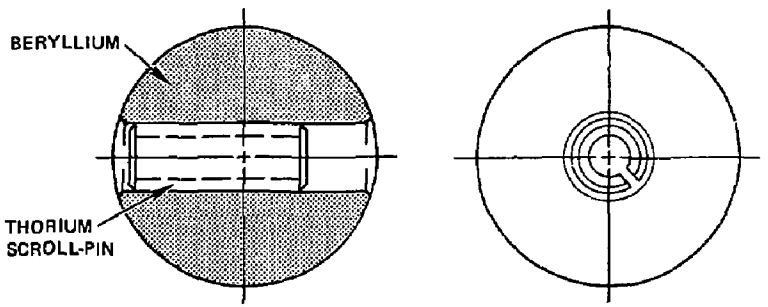

(B) SCROLL PIN

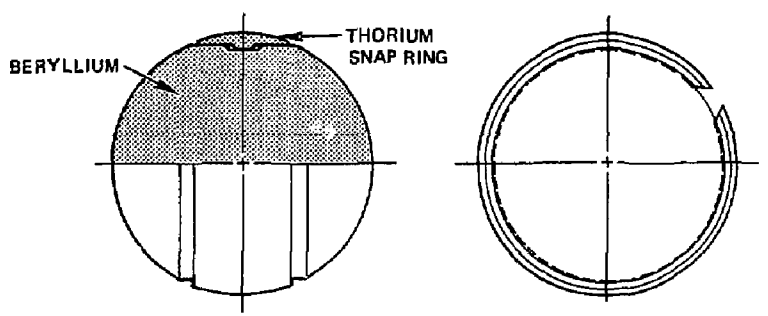

(C) SOLID SPHERE WITH SNAP-RING

Fig. ii.III.3 Beryllium/Thorium Composition Fuel Form Options

Table ii.III.2 Summary of Fuel Form Preferences As Related to Various Considerations

Key: +1 - Preferred 0 - neutral -1 - possibly undesirable	Fuel Form		
	Cylindrical pins with steel clips (2)	cylindrical scroll or dowel pins	C-shaped snap-ring
Beryllium Fabrication	0	0	0
Thorium Fabrication	0	+1	0
Lifetime (thermal stress)	-1	-1	0
Breeding Performance	0	0	+1
Chemical Compatability	+1	0	0
Fuel Handling Operations	0	+1	+1

is determined by the beryllium yield stress (40 ksi or 276 MPa in this analysis). In this case, the maximum tensile stress near the contact point would be 12.7 ksi (87.5 MPa) and, assuming a fracture toughness of 11.1 $ksi \cdot in^{1/2}$ (12.0 $MPa \cdot m^{1/2}$), a surface crack less than 0.24 in (0.62 cm) would be stable. This encouraging result appears to be conservative because the 150 lb loading is, most likely, an upper bound.

The internal stress within the pebble is given by the sum of the thermal stress caused by the temperature gradient into the pebble and the swelling stress caused by differential swelling on the inside versus outside of the pebble. The latter effect is caused, in part, by the fast flux attenuation across the blanket, but is determined to a larger extent by the fact that beryllium swelling is a strong function of temperature and a small temperature difference across the pebble leads to a large differential stress.

The internal stress/lifetime calculation for the beryllium pebbles is summarized in Table ii.III.3. Note that the annual differential swelling stress contribution is five times as great as the thermal stress contribution. Together, they predict a minimum estimated lifetime of 1.75 years (average lifetime about 3.2 years). It should also be noted that this calculation is conservative because it was performed for the pin fuel design. The reference snap-ring fuel form will have a much lower thermal gradient and both stress contributions will be greatly reduced.

Our economics analysis assumes a two year beryllium lifetime prior to recycle and refabrication.

Table ii.III.3 Internal Stresses for Hollow Pebble for One Year Irradiation and Estimated Lifetime

Position In Blanket	Thermal Stress (ksi)	Swelling Stress Per Year (ksi)	Total Stress Assumulation in 1 Year (ksi)	Estimated Lifetime (70% Capacity Factor)
Near First Wall	5.6	28.1	33.7	1.75 year
Near Center	3.4	24.9	28.3	2.10 year
Near Back Wall	1.1	6.0	7.1	9.3 year

ii.IV FUEL MANAGEMENT SYSTEMS AND ANALYSIS

The fusion breeder fuel management system must function efficiently to remove bred fuel from the blanket, load fresh fuel (including recycled beryllium pebbles), provide a safety dump capability, and agitate the beryllium multiplier to prevent the possibility of jamming due to accumulated swelling strains. In this section we describe both the fuel management mode and the fuel handling systems which were considered during the study.

ii.IV.A Fuel Management Mode Selection

Several operational modes of the reference blanket design are possible. For example, the fusion power (i.e., wall loading) can be held constant or can be varied to maintain a constant blanket thermal power. In the first case, the thermal power of the plant increases over the irradiation period as the ^{233}U concentration increases. In the second case, the thermal power is constant, but the fusion power decreases.

Another option involves the use of "axial zoning" by module. If the blanket modules are operated such that, at any given time, alternating modules are at alternating stages of "enrichment maturity" then all of the blanket modules are never at maximum (or minimum) power generation at one time. As a result, the thermal power swing can be reduced relative to all 50 modules at a single enrichment maturity.

A third option involves the number of radial blanket zones employed and the irradiation period for each zone. Although a one zone design is mechanically simpler, multiple zone designs can achieve higher average enrichments if irradiated for different periods of time.

The reference fuel cycle employs the following features:

- Single axial enrichment maturity
- Constant fusion power operation
- Two radial zones with the front zone reaching maturity twice as often as the rear zone.

Although the concept of axial zoning was seriously considered, it was discarded due to several perceived operational difficulties. Most importantly, it was recognized that the achievement of an efficient equilibrium fuel cycle would be difficult because, in the event of a scheduled outage lasting more than a few weeks (such as an annual maintenance period to remove and replace irradiated blanket modules), the majority of ^{233}Pa in the system would decay to ^{233}U ($T^{1/2}$ = 27 d). As a result of increased ^{233}U fissioning, the blanket power density at re-start would be substantially higher than at shutdown. Consequently, to maintain a given design maximum power level at end-of-cycle, the fuel would have to be discharged earlier, at a lower fissile concentration (i.e., ^{233}U plus ^{233}Pa) in the irradiation periods immediately following such an outage. Since our analysis indicated that the period between annual maintenance outages would be, at most, only a few irradiation periods, the axial zoning option was not adopted. The single axial enrichment scheme has the further safety and operational advantages that all of the modules have identical thermal behavior at any given time and that all are discharged prior to each major maintenance outage.

Our decision to maintain constant fusion power derived from three observations: (1) the cost of the fusion plant dominates the overall plant cost (see Section ii.VI), (2) the fissile fuel production rate in the suppressed fission blanket is directly proportional to the fusion power, and (3) the increased power conversion system cost implied by the larger thermal power swing for constant fusion power is, for the most part, compensated by increased electrical production. Consequently, we would utilize the full fusion power capabilities of the fusion breeder and pay a slightly higher capital cost due to the power swing.

The choice of two radial zones was made to optimize the maximum fissile enrichment. Since the breeding rate in the front 20 cm zone is about twice that of the rear zone, two radial zones with a two-to-one reprocessing frequency can achieve high enrichment without introducing unacceptable complexity into the design.

As shown in Figure ii.IV.1, the front zone would be irradiated for 82.5 days and the rear zone would be irradiated for 165 days. Such a fuel management scheme can achieve a 70% average availability with a 43 day

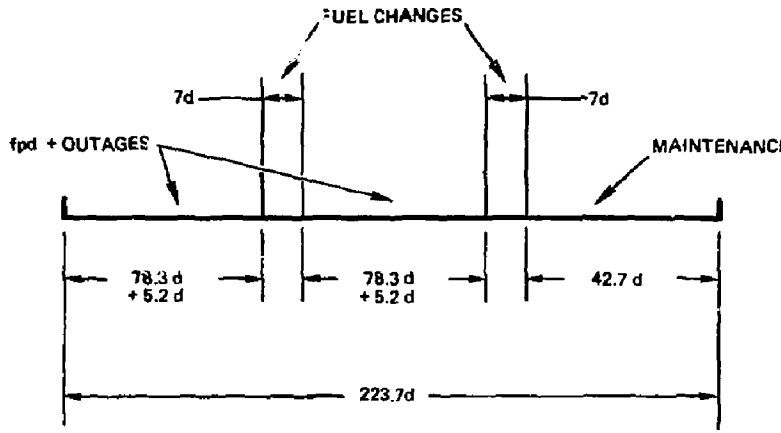

1)	78.3	fpd
	5.2	UNSCHEDULED OUTAGE DAYS
2)	7	SCHEDULED FUEL CHANGE
3)	78.3	fpd
	5.2	UNSCHEDULED OUTAGE DAYS
4)	7	SCHEDULED FUEL CHANGE
5)	42.7	SCHEDULED MAINTENANCE
	223.7	FUEL CYCLE PERIOD

UNAVAILABILITY = 0.30 = (2 x (5.2 + 7) + 42.7)/223.7

Figure ii.IV.1 Baseline Availability Budget

scheduled maintenance outage each 224 days and two 7 day shutdown periods for fuel changeout/recycle. During each 82.5 day operating period, 5.2 days are allotted for unscheduled outages.

ii.IV.B Isotope Generation

The fuel cycle has impacts on reactor safety; both because the fuel contains hazardous fission products and actinides and because the afterheat generated in the fuel must be removed during accident (e.g., loss of coolant or coolant flow) situations. The hazard sources and afterheat sources were predicted using the TRW ISOGEN code.

The fuel management scheme described above achieves an average fissile discharge concentration (^{233}U plus ^{233}Pa) of 1.23% in thorium. As shown in Table ii.VII.1, the ^{233}Pa concentration is about one-third of the total fissile mass at discharge. In fact, the ^{233}Pa concentration exceeds the ^{233}U concentration during the first two months of irradiation.

The principal fuel afterheat sources result from fission product decay and the beta decay of ^{233}Th and ^{233}Pa. The beta decay energies of ^{233}Th and ^{233}Pa are 0.43 and 0.23 MeV, respectively. These quantities are reduced relative to the Q value of the reactions because some appreciable fraction (approximately two-thirds) of the total energy is carried away by neutrinos. An LWR fission product decay energy expression was used in our analysis (see Section ii.V) and is expected to be adequate in comparison with other uncertainties.

Figure ii.IV.2 shows the relative afterheat power density as a function of time after shutdown. Importantly, either the ^{233}Th afterheat source or the ^{233}Pa afterheat source exceeds the fission product afterheat source for all reactor safety relevant times. This is considered to be an important feature of the suppressed fission blanket technology.

ii.IV.C Fuel Handling System Design

The fuel handling system design is shown schematically in Figure ii.IV.3. This design was developed for the internal pin fuel form, but can be adopted to the reference snap-ring design (which was selected later in the study).

Table ii.IV.1

Fuel Handling System Characteristics

Maximum Batch Size: 50 modules x 2 zones x 8 m^3 per zone = 800 m^3

Beryllium pebble quantity: 50 x 2 x 360,000 pebbles per zone = $36 \cdot 10^6$

Process time: ~ 1 week

Rate for full batch: 59 pebbles/second

Pin cooling time before reprocessing: 180 days

Pin initial thermal deposition : 0.3 w/cc (0.678 cc each)

Mode of pebble extraction from blanket: coolant flow diversion and flushing

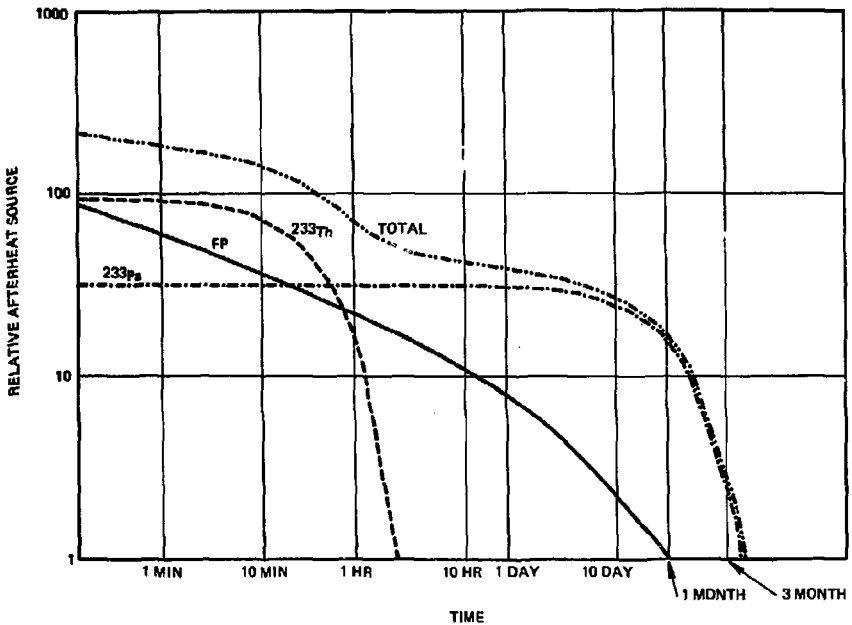

Figure ii.IV.2 Relative afterheat sources for the reference blanket

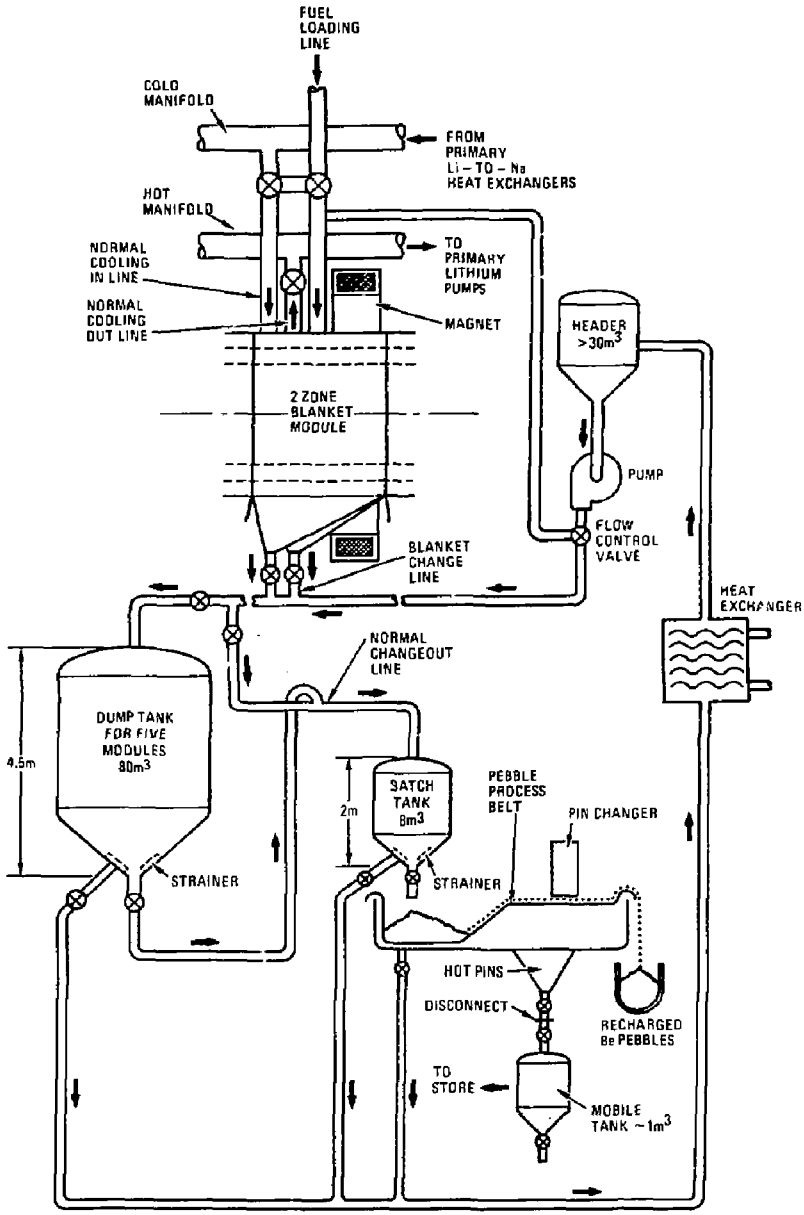

Figure ii.IV.3 Pebble handling circuit and module safety coolant system.

As shown in the figure, each radial fuel zone, of which there are 100, has a valved connection to a liquid metal circuit. This circuit includes a dump tank sufficient to accommodate the blanket volume of five modules (80 m^3), a batch tank of 8 m^3, a pump, a header, and a heat exchanger which will be specific to this circuit (for safety reasons). Under the batch tank is a liquid metal bath through which a metal link belt is driven. The batch tank can be emptied into this bath, the fluid being pumped back to the header and the pebbles being transported out on the metal belt. The belt passes over a separately pumped area where a few kilo pascals pressure is introduced beneath the belt. The pebbles, which ride in circular depressions in the metal links, orient themselves uniformly with the pin in a vertical position. This occurs due to the un-balanced center of gravity which is provided by inserting the thorium pin in an offset position relative to the center of the pebble. As they continue along the belt, they pass under a device which punches out the thorium pin and replaces it with a fresh pin in one operation. The punched pins sink into a small (< 1 m^3) tank connected to the bottom of the machine. These pins are taken to storage after the tank is filled and disconnected. A new tank replaces it for continued operation. The pebble processing machine has a inert atmosphere (e.g., argon) above its free surfaces at a nominal overpressure. The 8 m^3 batch tank and the enriched pin tanks, both of which can be emptied in one operation, will be back-filled with inert gas. Both the batch tank and the dump tank have fluid circulation cooling. The major system characteristics are listed in Table ii.IV.1.

ii.V SAFETY SYSTEMS AND ANALYSIS

A major feature of the fission-suppressed blanket concept is the reduction of fission product and transuranic nuclide inventories and their attendant problems of radionuclide containment and decay heat removal. These reductions translate into significant, quantifiable advantages from the viewpoints of engineering design and public safety.

The Biological Hazard Potential (BHP), the decay heat rate, and structural material temperature safety limits were evaluated in this study with the intent of quantifying the safety connotations of the term "fission-suppressed." Fission-suppressed and fast fission blankets were compared. The safety distinction between the two blanket types can be attributed to the contribution of the fission products to the BHP and the decay heat rate level. The results showed that the actinide hazard reaches an equilibrium condition at low enrichment levels, whereas the fission product hazard is proportional to the overall fission rate and continuously increases with enrichment. The isotopic distribution and temporal behavior of the hazard after shutdown was also evaluated. The decay power density increases significantly with enrichment and the increase can be directly attributed to the fission products. The actinide BHP was found to dominate the biological hazard, independent of the enrichment or irradiation time.

A preliminary evaluation of the time to creep-rupture failure at the stress levels of the present blanket was performed for HT-9 and 2-1/4Cr-1Mo. From the analysis, a safe HT-9 temperature limit of 750°C was established as the maximum temperature that could be experienced by the module for significant periods of time and still permit module reuse. An HT-9 temperature limit of 900°C was established as the maximum temperature above which failure could be presumed to occur within a short (1/2 hour) time. These results were combined with the thermal analysis in establishing acceptable safety system performance.

The safety systems addressed in this study focus on those systems which would have significant impact at the conceptual design stage due to their requirements of special design effort, impact on parallel systems designs,

or cost. Specifically addressed herein are the primary coolant and decay afterheat removal systems, the module safety coolant systems, and the safety dump system.

The primary coolant system serves as the first level of safety and also serves as the decay afterheat removal system during normal shutdown. Its principal components, shown in Fig. ii.IV.1, are five lithium coolant pumps, six Li-to-Na heat exchangers, a cold inlet manifold to the modules, a hot outlet manifold from the modules, a heat exchanger common plenum, and associated piping and valving. The parallel arrangement of the components, redundancy, and over-capacity designed into the system can accommodate the outage due to failure or maintenance of a number of components and still permit full power operation. Under shutdown conditions, this system also serves as the decay afterheat removal system.

In the event of a malfunction of the primary coolant system, the fuel handling system provides the redundant and diverse circuit required to maintain adequate module cooling. This system consists of its own auxiliary pumps and heat exchangers, and provides the coolant flow necessary for shutdown afterheat removal. The fuel handling system is shown in Figure ii.IV.3 This system also contains the fuel dump circuit. The fuel dump is initiated for failures which prevent adequate cooling from reaching any of the 50 individual modules. The dump tank was sized to contain the fuel volume of five modules on the basis of isolating the failed module and preventing the propagation of a failure to adjacent modules.

A Failure Modes and Effects Analysis (FMEA) was performed at the component level of the systems described above. Failures considered include active component malfunctions, primary coolant outer boundary and first wall structural failures, and failures of interface systems such as the power supply and secondary heat removal.

The failure modes were divided into three categories related to their effects on the system. Thermal analyses were then performed to determine the course of action required subsequent to the initial failure. Although some of the results of the thermal analyses were sensitive to the assumed parameters governing the heat transfer, failure of the blanket module was

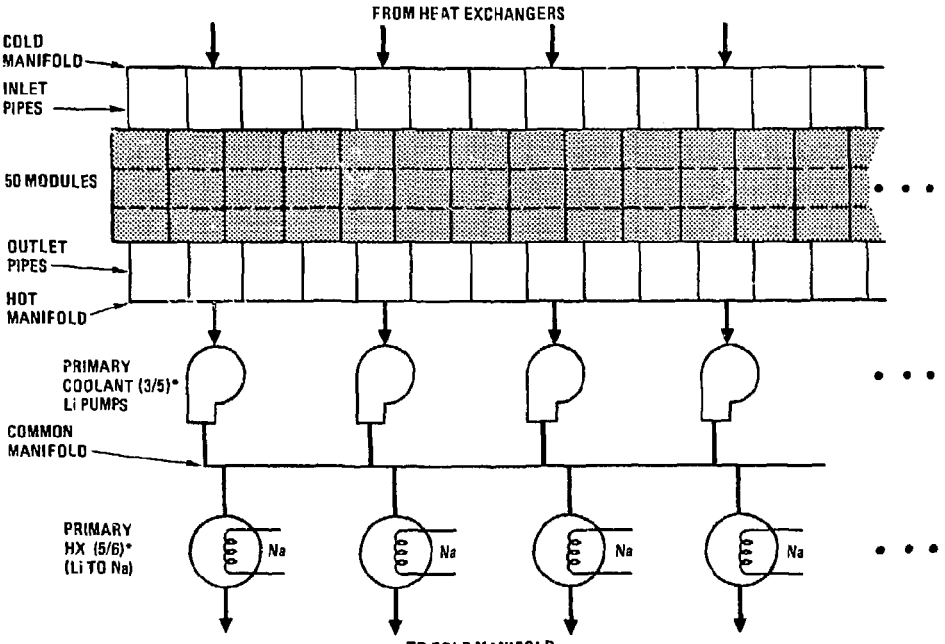

*(REQUIRED NUMBER OF COMPONENT/NUMBER OF COMPONENT AVAILABLE)

Fig. ii.V.1 Primary coolant and decay afterheat removal system.

identified only for initiating events which lead to partial or complete loss of lithium to the fertile fuel pellets. This dictated the scenarios requiring fuel dumping. The allowed time to dump prior to structural failure was estimated.

The initiating events which would lead to uncovered fuel were determined to be rupture or leakage of the piping leading to or from the first wall, and mechanistic failure of the first wall. These events require dumping, since a short-circuit path may occur which would preclude coolant from reaching the fuel. Failure to dump the fuel would then lead to loss of the module. Although the probability of such a sequence of events is thought to be low, it is recommended that the adjacent modules be dumped to limit failure propagation and minimize accident consequences. Subsequent to the fuel dump, the temperature of the isolated, radiating first wall will remain below the limit established for HT-9 structural failure. Uncertainties in the first wall emissivity and afterheat levels warrant more data and analysis in future evaluations of this important accident scenario.

The effectiveness of natural circulation of the lithium in removing first wall afterheat after a fuel dump was evaluated. The results show that with the proper design of the coolant heights and orientation, natural circulation will be sufficient to remove the afterheat from the first wall and maintain its temperature below 750°C without any operating, active components in the absence of a magnetic field. In the presence of a magnetic field, natural circulation is not adequate.

In conclusion, the redundancy and diversity of the reference safety systems provide adequate protection of the reactor against loss-of-coolant accidents. To further optimize the safety systems, an integrated analysis of overall system and reactor reliability/availability/maintainability/safety/economics should be performed. More detailed calculations of the first wall decay afterheat rates are recommended for future thermal analyses efforts. Experiments should be carried out to determine the emissivities of metal surfaces exposed to flowing liquid metals. There are relatively simple experiments which can be performed on existing liquid metal loops and would address one of the major safety issues of the fusion breeder.

ii.VI FUSION BREEDER PLANT CONCEPT

Although the fusion breeder program has emphasized the design of breeding blankets and associated technologies, there has also been an attempt to describe and cost the entire power plant. There are three reasons why such as exercise is useful:

- A more complete definition of the surrounding plant provides additional confidence in the reference blanket concept by demonstrating its reasonableness in the overall plant context.
- A format is provided whereby plant related issues which are not directly associated with the blanket design can be considered.
- An integrated description of the plant cost and performance can be used to generate trade and optimization studies and to provide a best estimate of the ultimate commercial merit of the fusion breeder application.

The plant design information developed in this chapter is used to generate the systems and economics analysis described in Section ii.VIII.

ii.VI.A Central Cell Layout and Power Conversion

The main reactor building will contain the 200 m long central cell and will terminate at the walls adjoining the end plug regions. The central cell, containing 50 blanket modules, and a typical section with its piping are shown in Figure ii.VI.1. The piping arrangement for one of five groups of ten modules is shown in Figure ii.VI.2.

As shown, the lithium coolant is discharged from each module outlet torus to a common outlet header. Effectively, the flow from all ten modules enters a single 85,000 GPM lithium pump which discharges into a common header and feeds an intermediate heat exchanger (IHX). Each pump and IHX can be connected to other pumps and IHX's via a common circuit so that any module (or set of modules) can be serviced by any pump and/or IHX. In all, there are five pumps (two redundant) and six IHX's (one redundant). Normally all are operated at about 60% of their full rated capacity. To minimize the blanket pressure, the lithium pumps are located on the hot leg near the blanket outlet. The area to the left of the module is reserved for module changeout.

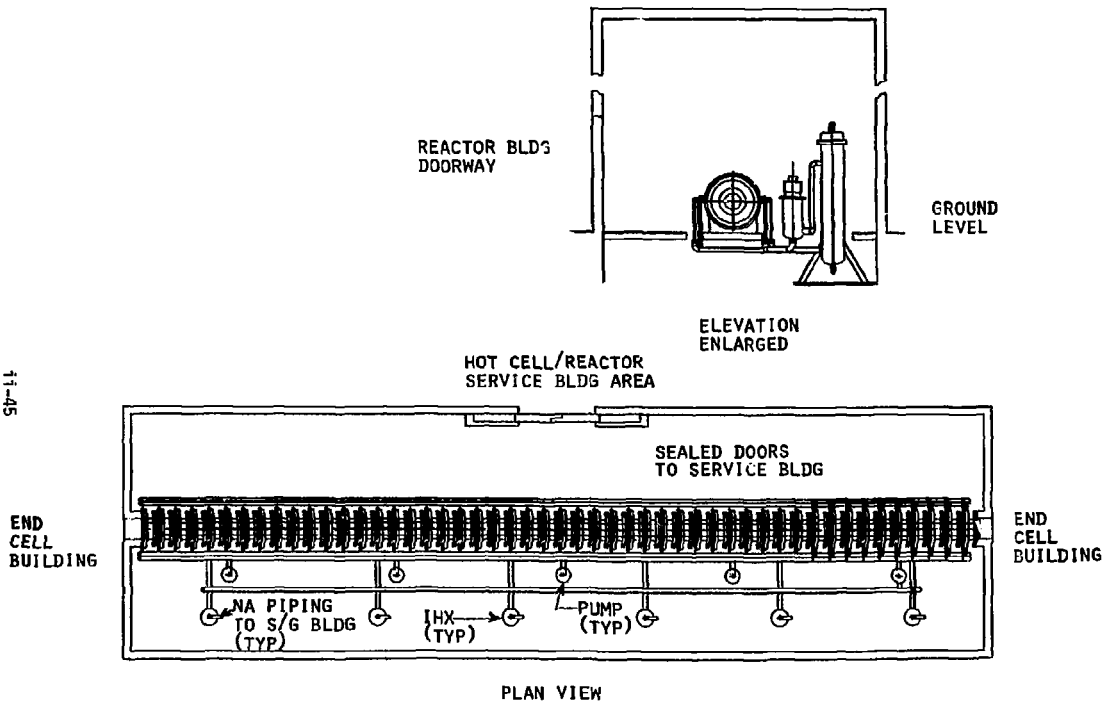

Figure ii.VI.1 Fusion Breeder Reactor reactor building showing central cell, piping and component arrangement.

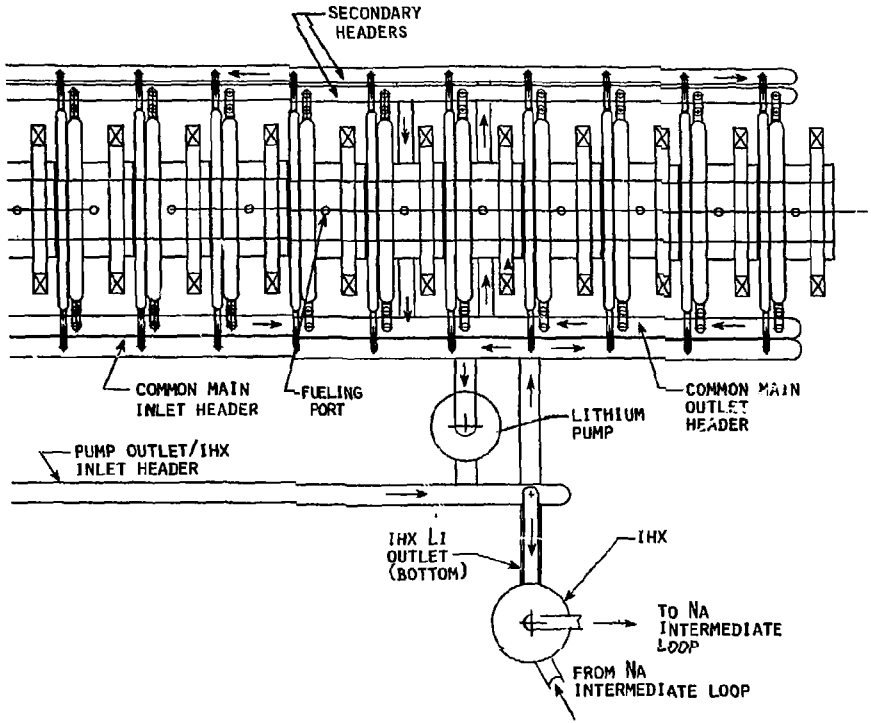

FIG. ii.VI.2 Typical 10 module group of Fusion Breeder Reactor central cell assembly.

A schematic of the thermal power conversion cycle is shown in Figure ii.VI.3. As shown, a sodium intermediate loop is employed to isolate the radioactive primary from the steam side of the system. The intermediate loop also provides an effective trap for tritium so that it should be possible to minimize its release to the environment. The intermediate loop requires 8 pumps (2 redundant) and 15 hockey stick design steam generators similar to those being developed for the Clinch River Breeder Reactor Project.

The performance of the power conversion system is summarized in Table ii.VI.1. Note that the values indicated refer to end-of-cycle operation when the power level is highest.

ii.VI.B Integrated Power Flow

The integrated power flow of a tandem mirror fusion breeder includes the direct converter and particle dumps, each plasma heating system, and auxillary system power flows in addition to the thermal conversion system described above. An integrated power flow diagram for end-of-cycle conditions, is shown in Figure ii.VI.4. As shown, 18% of the 2381 MW gross electric power is produced by direct conversion. The total recirculating power of 719 MWe is dominated by the plasma heating systems (64%). In all, 1662 MWe of net electricity are produced. The net nuclear-to-electric efficiency is $1662/(3000\ (0.8 \times 1.97 + 0.2)) = 31.1\%$.

In fact, the power level of the fusion breeder swings ± 26% from beginning-of-cycle to end-of-cycle conditions as shown in Table ii.VI.2. The average net electrical power output is 1317 MWe and the average net electrical efficiency is 29.5%.

ii.VI.C Cost Summary

To support the economics analysis, rough estimates of the direct and annual operating costs of the fusion breeder plant were developed. Many of the direct costs, shown in Table ii.VI.3, were estimated using the algorithms developed in conjunction with a tandem mirror reactor design code which is maintained by TRW. Other costs (e.g., the THOREX reprocessing plant cost) were developed based upon design studies which were performed in support of the fusion breeder program. Finally, some costs (e.g., remote maintenance equipment) were based upon little or no detailed design information.

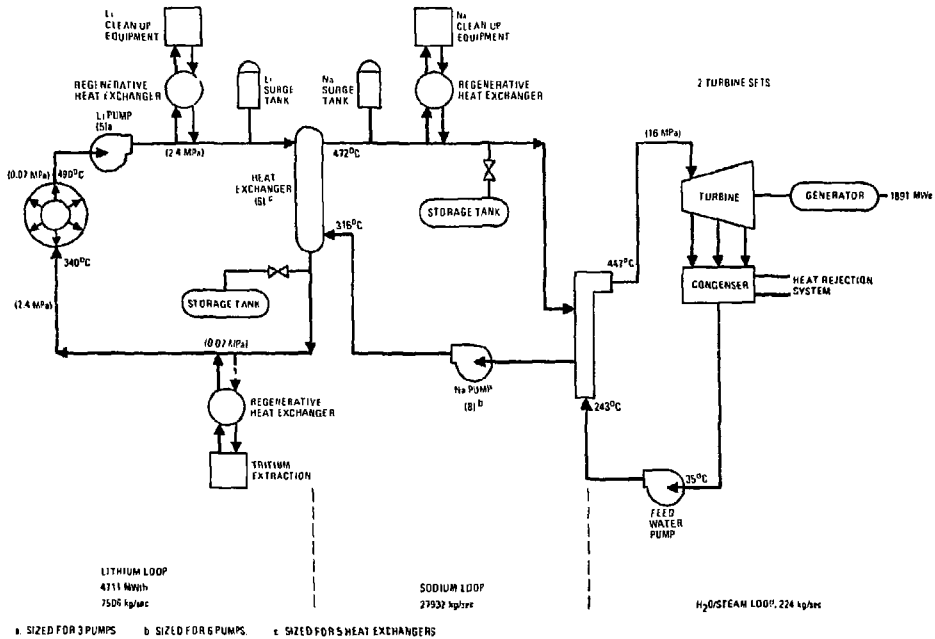

Fig. ii.VI.3 Power conversion cycle schematic

Table ii.VI.1 Power Conversion System Summary

Reactor thermal power, maximum	4711 MW
Gross power conversion efficiency	40%
Electrical power	1881 MW
Auxiliary electrical power[a]	154 MW
Net blanket power conversion efficiency	36.7%

[a]The auxiliary electrical power requirement includes all pumping and clean-up equipment for the primary loop, all heat and tritium removal machinery, and miscellaneous in-plant equipment.

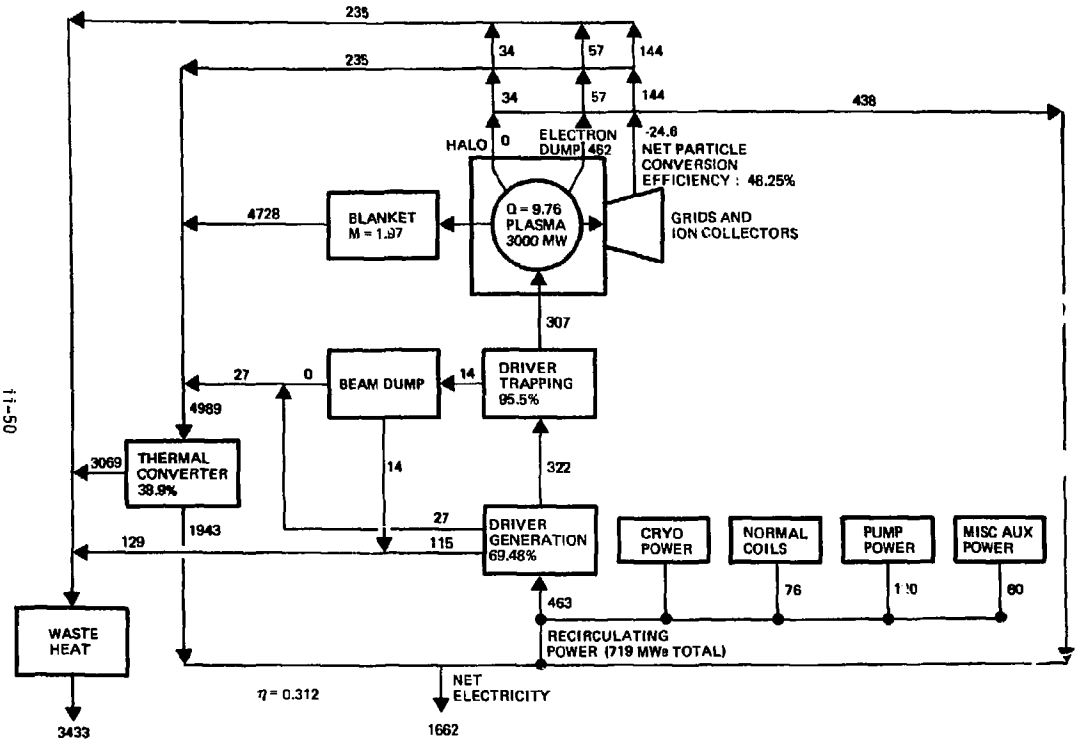

Fig. ii.VI.4 Integrated Power Flow for Reference Fusion Breeder

Table ii.VI.2 Power Swing Summary

	BOC	AVERAGE	EOC
Blanket M	1.25	1.61	1.97
Blanket Thermal Power	3000 MW_t	3864 MW_t	4728 MW_t
Electricity from Blanket Thermal[a]	1200 MWe	1546 MWe	1891 MWe
Electricity from Other Thermal[a]	52 MWe	52 MWe	52 MWe
Electricity from Direct Conversion	438 MWe	438 MWe	438 MWe
Gross Electricity	1690 MWe	2036 MWe	2381 MWe
Recirculating Power Requirement	719 MWe	719 MWe	719 MWe
Net Electrical Output	971 MWe	1317 MWe	1662 MWe
Relative Power Swing	- 26%	0	+ 26%
Net Electrical Efficiency[b]	0.269	0.295	0.311

a) low grade heat converted to electricity at 20% efficiency

b) defined as (net electrical output)/(fusion power x [0.8 x blanket energy multiplication + 0.2]).

Table ii.VI.3 Reference Fusion Breeding Direct Cost Breakout by Cost Account Number

ACCOUNT NUMBER	ACCOUNT TITLE	DIRECT COST $M
20	Land and land rights	6
21	Buildings and structures	569
21.1	Site improvements and facilities	14
21.2	Reactor containment building	171
21.3	Turbine generator building	56
21.4	Cooling system structure	9
21.5	Other plant buildings	319
21.6.1	Reactor auxiliary building, R	68
21.6.2	Reactor auxiliary building, NR	16
21.6.3	Reactor service building	62
21.6.4	Steam generator building	51
21.6.5	Control building	23
21.6.6	End cell buildings	85
21.6.7	Misc. structures	14
22	Reactor plant equipment	2694
22.1	Fusion reactor equipment	1942
22.1.1	Blanket/shield	492
22.1.2	Remote maintenance equipment	75
22.1.3	Magnets	674
22.1.3.1	End cell magnets	140
22.1.3.2	Central cell magnets	554
22.1.4	Plasma heating systems	429
22.1.4.1	Neutral beams	273
22.1.4.2	RF heating	156
22.1.5	Direct converter and beam dump	131
22.1.6	Vacuum vessels	15
22.1.7	Cryogenics plant	35
22.1.8	Intermodule Structure	5
22.2	Reactor plant and fuel cycle equipment	752
22.2.1	Heat transport system	390
22.2.2	Fuel management equipment	15
22.2.3	Dump tank and coolant	40
22.2.4	Beryllium Fabrication Plant	50
22.2.5	Thorium Fabrication Plant	15
22.2.6	THOREX Reprocessing Plant	307

(Continued)

Table ii.VI.3 (CONTINUED)

23		*Turbine plant equipment*	304
	23.1	Turbine generators	158
	23.2	Main steam system	14
	23.3	Heat rejection system	41
	23.4	Condensing system	29
	23.5	Feed heating system	39
	23.6	Other equipment	23
24		Electric Plant Equipment	157
	24.1-24.3	*Switch gear and related equipment*	8
	24.4	Protective equipment	3
	24.5-24.6	Electrical bulks	140
	24.7	Electrical lighting	6
25		*Misc. plant equipment*	14
90	TOTAL PLANT DIRECT CAPITAL COST		3744

As shown in the table, the total fusion breeder direct cost estimate is 3774 $M. Of this, 16% can be attributed to conventional buildings and structures, 72% to reactor plant equipment, 8% to turbine plant equipment, and 4% can be attributeds to electrical plant equipment. Of the reactor plant equipment, 51% is fusion plant equipment and 49% is nuclear and fuel cycle equipment.

The total capital cost of the plant (including the direct cost plus indirect cost and the time value of money during construction) is estimated to be 8.15 $B. This cost, on a unit nuclear power basis, is about 3.3 times the cost of an LWR. As discussed in Section ii.VII, each fusion breeder provides enough fissile fuel to support over 20 LWRs.

The annual operating costs are summarized in Table ii.VI.4. As shown, about 40% of the operating cost is associated with the fuel cycle, while only about 1% is associated with the cost to replace the blanket structure. The latter cost is better represented in terms of lost availability due to maintenance and blanket changeout. A 70% average capacity factor is believed to allow adequate time for blanket changeout.

Table ii.VI.4 Summary of Plant Annual Operating Costs

• Fuel Cycle Costs:	
• Fuel Reprocessing Plant Operating Cost	42 $M/yr
• Thorium Fabrication Plant Operating Cost	19 $M/yr
• Beryllium Fabrication Plant Operating Cost	4.5 $M/yr
• Beryllium Material Losses	10 $M/yr
• Product and Waste Transfer	9 $M/yr
• Blanket Structure Replacement Cost	2 $M/yr
• Miscellaneous Operation and Maintenance Cost	137 $M/yr
Total	223 $M/yr

ii.VII FUEL CYCLE TECHNOLOGIES

ii.VII.A Overview of Fuel Cycles

The principal role of the fusion breeder reactor is to provide an external source of fissile fuel to support a fission power reactor economy composed of light water reactors (LWRs) or other fission reactors. In this role, the fusion breeder is operationally similar to a fissile enrichment plant which requires no fissile feed stream and is an electricity producer rather than a consumer. In contrast with fission breeder reactors (i.e., liquid metal fast breeder reactor (LMRBR) and light water breeder reactor (LWBR)), the neutron rich fusion breeder is a subcritical assembly, produces an order of magnitude more net excess fuel per unit of thermal power, and is not subject to the neutron balance constraints of conventional fission reactors. As a result, a wide variety of fuel cycles and fuel forms are possible. In general, the fusion breeders may produce either ^{233}U or ^{239}Pu using metal, oxide, carbide, molten salt or other fertile fuel forms.

After the bred fissile material is recovered from the fertile fuel, it may be used to provide initial inventories or fissile makeup to fuel conventional light water reactor (LWR) clients operating on one of several possible fuel cycles. Alternatively, the bred fuel could be used to fuel advanced fission converter reactors such as the high temperature gas cooled reactor (HTGR) or the Canadian heavy water reactor (CANDU). If desired, the fusion breeder might also breed fuel to provide initial fissile inventories for liquid metal breeder reactors (LMFBR).

Fuel cycle related issues will, in general, depend upon the particular breeding blanket design, the choice of fertile fuel form, and the choices of a client reactor type and its associated fuel cycle. These issues can have a potentially large impact on the cost of bred fuel, the cost of electricity generation, and overall feasibility of the fusion breeder.

A summary of the fuel cycle data for the reference fusion breeder is shown in Table ii.VII.1. The reference fusion breeder operates in a batch fuel reprocessing mode in which the first fuel zone is discharged at relatively frequent intervals after about 80 days of exposure when the combined (^{233}U plus ^{233}Pa) fissile concentration in thorium reaches about 1.4%. The second, or rear, zone is irradiated for twice this period such that its

Table ii.VII.1 Fuel Cycle Summary for the Reference Fusion Breeder Plant

Thorium Inventory, MT	293
Fissile Inventories, Kg	
^{233}U + ^{233}Pa In-core[a]	1032
^{233}U + ^{233}Pa Ex-core[b]	2784
Fuel Management Mode[c]	Batch
Zone 1 Fuel Residence Time[c], yr	0.21
Zone 2 Fuel Residence Time[c], yr	0.42
Net Fissile Production[d], kg/yr ^{233}U	5646
Average Blanket Discharge Concentrations in Thorium[a], atom %	
^{233}U	0.81
^{233}Pa	0.42
Fission Products	0.081
^{228}Th	$2.92 \cdot 10^{-7}$
^{232}U	$3.21 \cdot 10^{-4}$
Reprocessing Plant Thorium Throughput[d], MT/yr	604
Reprocessing Plant Discharge Product Concentrations[b], atom %	
^{232}U in ^{233}U	0.026
^{228}Th in Thorium	$1.7 \cdot 10^{-6}$
Beryllium Inventory, MT	885
Number of Be Pebbles	$36 \cdot 10^{6}$
Estimated Pebble Lifetime[d], yr	2
Estimated Pebble Throughput, yr^{-1}	$18 \cdot 10^{6}$
Required Be Makeup[e], MT/yr	29

a) average over fuel cycle and fuel zones
b) 0.5 yr ^{233}Pa decay to ^{233}U included
c) see Chapter IV for details
d) 70% average plant capacity factor included
e) 7% loss assumed

combined fissile concentration at discharge is 0.93%. Considering both zones together, the net average fissile discharge concentration is (2 x 1.4 + 0.93)/3 = 1.24 atoms percent in the thorium.

As discussed earlier, 5464 Kg/yr of fissile fuel is produced annually if the plant capacity factor is 70%. The average total fissile inventory is 3816 Kg and the annual thorium throughput is 604 Kg/yr. This throughput is less than half that of typical commercial fuel reprocessing plant designs, but is equivalent to the heavy metal throughput rate of about twenty 1 GWe LWRs. Such comparisons illustrate the importance of reprocessing technologies for suppressed fission hybrid blanket concepts.

It is of interest to define the minimum size and characterisitics of a fuel cycle center which contain fusion breeders, their fuel cycle facilities and the fuel cycle facilities associated with a self-consistent number of client LWRs. The size of such a fuel cycle center will be determined by two constraints:

- All fuel cycle facilities should be large enough to benefit from economies of scale
- The total number of fuel cycle centers should be small (perhaps 5-10 in the U.S.)

In Figure ii.VII.1, a fuel cycle center concept for the reference fusion breeder with LWR denatured thorium (and plutonium) fuel cycle clients is shown. In this configuration, three fusion breeders supply 16,900 Kg/yr of ^{233}U (70% capacity factor) to support sixty-four 1 GWe LWR clients for a total electrical output of 68 GWe. The plutonium produced by 56 of the LWRs is sufficient to support an additional eight 1 GWe LWRs (or, alternatively, it could be stockpiled for LMFBR inventories). The fusion breeders each have a dedicated beryllium recycle plant and, together share a single fuel reprocessing plant of 1812 MT/yr capacity. The mixed oxide LWR reprocessing/-fabrication throughput is about 1300 MT/yr. Of this, about 70 MT/yr is associated with the plutonium burners (i.e., PUREX aqueous reprocessing) and about 1200 MT/yr is associated with the ^{233}U burners (i.e., THOREX aqueous reprocessing).

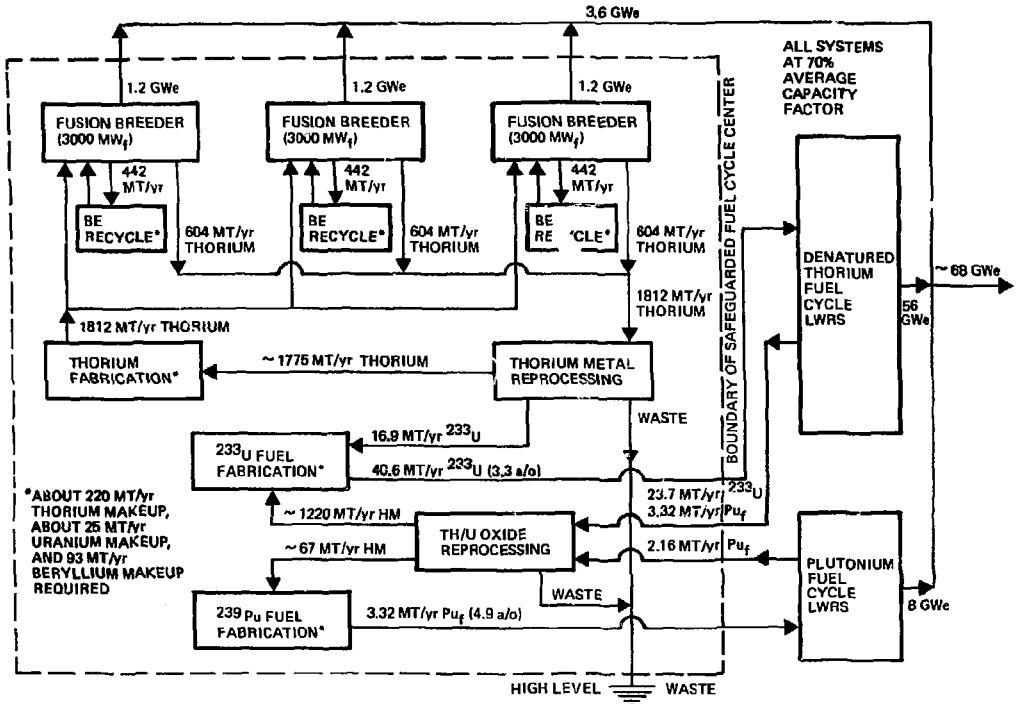

Figure ii.VII.1 Symbiotic Electricity Generation System Based Upon Reference Fusion Breeder Denatured Thorium Fuel Cycle

A similar fuel cycle center concept, where LWR denatured uranium fuel cycle clients are utilized instead of denatured thorium fuel cycle clients, has also been considered and is shown in Figure ii.VII.2. In this case, a smaller total of about 54 LWRs can be supported (including about 14 plutonium burners), but since none of the LWR fuel is thorium oxide based, the need for THOREX reprocessing of LWR fuel is eliminated and PUREX reprocessing (1350 MT/yr uranium) can be used exclusively for these fuels. In comparison with THOREX, the PUREX process is considered to be closer to commercial viability and less expensive. The net electrical output for this three fusion breeder driven system would be 57 GWe.

ii.VII.B Beryllium Fabrication Technology

The beryllium pebble inventory in the reference blanket is 885 MT (ρ = 1.84 g/cm^3), or $36 \cdot 10^6$ pebbles. This quantity represents about 1.2% of the total estimated beryllium resource in the United States (~ 0.2% of the world wide resource). Therefore, in the U.S., it might be reasonable to assume that about 50 fusion breeders could ultimately be built. These could provide fissile makeup to support about 1000 LWRs on the denatured thorium fuel cycle.

If the beryllium lifetime is two calendar years, $18 \cdot 10^6$ pebbles/yr would have to be refabricated in a hot beryllium refabrication plant. Assuming a 7% loss rate in this process, the net makeup would be about 31 MT/yr.

Currently, the only source of beryllium in the free world is Brush Wellman. They produce about 270 MT of beryllium per year. Of this, about 10% is beryllium metal. Thus, the beryllium industry would have to expand considerably to produce the initial inventory of even one fusion breeder, but the overall resource does not appear to be limited for this application.

The selected pebble fabrication process involves the development of an automated line which will cold press pebbles, vacuum sinter them, hot forge them to full density, and vacuum anneal them. Brush currently uses the first three steps of this process to produce aircraft brake segments - the only difference is that the process is manually operated because current Be powder is not free flowing and is not amenable to automated operations. In order to automate this process, a free flowing Be powder is required.

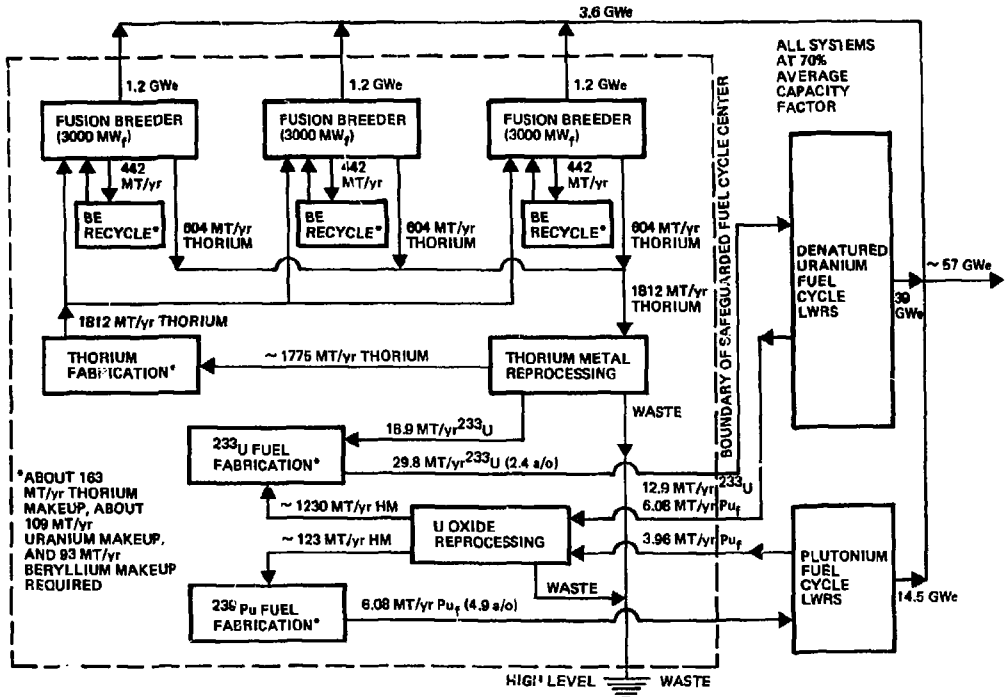

Figure ii.VII.2 Symbiotic Electricity Generation System Based Upon Reference Fusion Breeder and Denatured Uranium Fuel Cycle

The equipment needed for production is simple: mechanical presses and powder feeders to make cold pressed compacts, automated vacuum sintering furnaces for pressureless sintering, mechanical presses for hot sizing the sintered compacts, an automated vacuum furnace for annealing the forged compact, and an automated mill to machine the fuel snap ring groove to final dimensions.

For fabrication of pebbles too damaged to reinsert into the blanket after an irradiation period, we would vacuum melt the hot pebbles and use an automated atomization process (modeled after the Brush Wellman process) to first re-manufacture the beryllium powder prior to the cold press step. The entire process will require provision for shielding and remote maintainability. Given a two year beryllium lifetime, and assuming an automated plant which operates 24 hours/day, 7 days/week, and is operating 85% of the time with no rejects, the production rate will be 240 balls per minute. While this is a very high production rate for Be parts, it is very low for some powder metal industries (e.g., capacitor manufacturers produce thousands of parts/minute).

The total cost of such a facility (i.e., direct + indirect + cost of money during construction) is estimated to be about 70 $M. The annual operating cost (@ 25¢/pebble) is estimated to be 4.5 $M. The cost of fine commercial grade beryllium is estimated to be 330 $/Kg (292 $M for the initial inventory and 10 $M/yr for makeup).

ii.VII.C Reprocessing Technologies

During the past three years, the following four studies of reprocessing plant technologies have been conducted to estimate the cost to recover fuel produced in a fusion breeder:

- a pre-conceptual design and cost estimate for a PUREX fuel reprocessing plant for uranium-plutonium fuels.
- a pre-conceptual design and cost estimate for a THOREX fuel reprocessing plant for thorium-uranium fuels.
- a conceptual design description and rough cost estimate for a pyrochemical fuel reprocessing plant for thorium metal fuels.
- a pre-conceptual design and cost estimate for a molten salt fuel reprocessing plant for molten thorium-uranium fluoride salt fuels.

The PUREX and pyro-chemical reprocessing plant studies were performed as part of the FY82 fusion breeder program. The THOREX study was performed in 1980 by Bechtel and was updated for use in economic studies associated with the current program. The molten salt reprocessing plant study (performed in 1981 by ORNL) demonstrated the inexpensive nature of molten salt reprocessing, but was not applied to the reference blanket.

Although the reference blanket utilizes a thorium metal fuel form to breed ^{233}U, this design could be modified to breed ^{239}Pu from uranium carbide. As such, we have investigated the implications of such a choice with concentration on the most important fuel cycle technology -- breeder fuel reprocessing. In the PUREX assessment, the design basis plant was sized to allow processing of 1030 metric tons per year of uranium, in the form of carbide, at an instantaneous rate of 4 MT/day. The economic scaling factor for larger and smaller plants was also estimated. The fusion breeder reactor, reprocessing plant, and uranium carbide fabrication plant were assumed to be colocated on-site. A schematic of the PUREX plant layout is shown in Figure ii.VII.3. The cost of this facility is shown in Table ii.VII.2.

Importantly, the PUREX study also provided a critical review of the THOREX cost estimate and the later was revised upwards. A comparison of the cost of reprocessing using the PUREX, THOREX, and pyro-chemical reprocessing technologies is shown in Table ii.VII.3. As shown, the unit costs for the aqueous reprocessing technologies are similar, but our preliminary assessment indicates that pyro-chemical reprocessing might offer a four-fold cost advantage.

It should be noted that the unit reprocessing costs shown are lower than those obtained in our previous studies due to the higher discharge enrichment which is achieved in the present design. Since the overall cost of bred fissile fuel is expected to be about 195 $/g during the first year of operation, the impact of aqueous reprocessing would only be about 11%. Also, it should be noted that the above THOREX cost relates to thorium metal reprocessing rather than thorium oxide (thoria). The cost to reprocess the later has been suggested to be substantially higher.

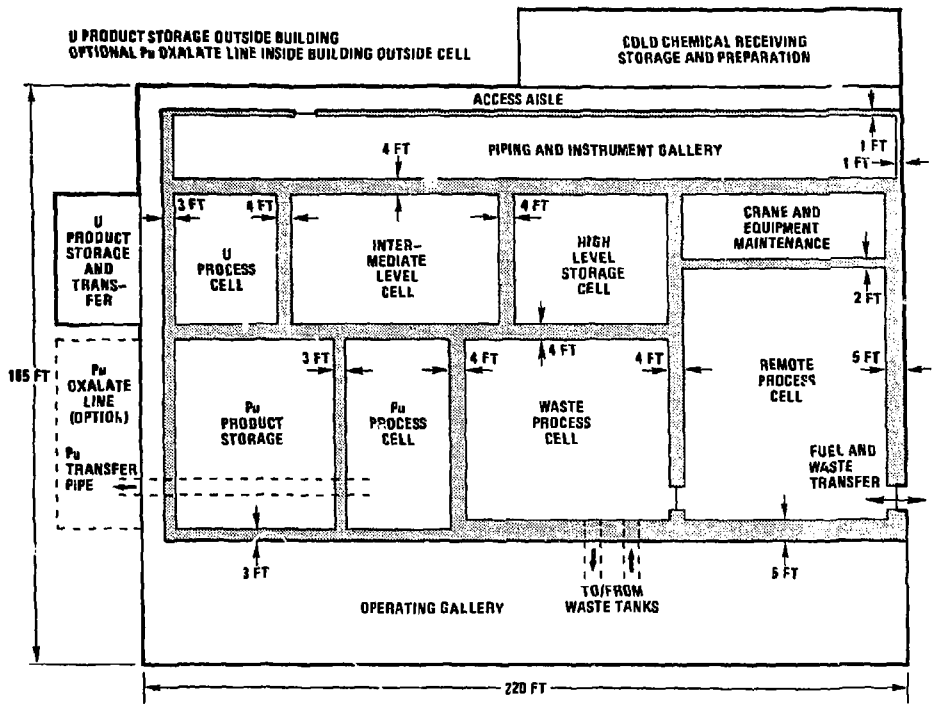

Figure ii.VII.3 PUREX Facility Layout

Table ii.VII.2 Uranium Carbide Blanket Reprocessing Plant Equipment and Facility Cost (1030 MTHM/year)

Equipment Section	Cost 1982 Dollars (Millions)[a]
Receiving and storage	84
Uranium carbide oxidizers and off-gas	70
Dissolvers and centrifuge (includes feed storage)	56
Solvent extraction (includes solvent washing and intercycle uranium concentration	50
Acid and water recovery	20
High-level waste treatment, storage, and shipping capability	120
Uranium product concentration and storage	11
Plutonium product concentration and storage	14
A plutonium product oxide conversion (optional)	35
Balance-of-plant	280
Total equipment and facility	740[b]

[a]End of first quarter

[b]Equipment facility total for 515 MTHM/year plant = 475

1545 MTHM/year plant = 960

or (size factor) $^{0.64}$ = cost factor.

Table ii.VII.3 Reprocessing Cost Comparison

PROCESS	THOREX	PUREX	PUREX	PYRO-CHEMICAL
Fuel Type	thorium metal	uranium carbide	uranium metal or oxide	thorium metal
Throughput,[a] MTHM/yr	604	604	604	604
Fissile Discharge Assay,[a] atom %	1.24	1.24	1.24	1.2%
Plant Capital Cost, $M	685	641	602	150
Cost of Capital,[b] $M/yr	124	115	109	27.1
Plant Operating Cost, $M/yr	42	42	39	10
Total Annual Cost, $M/yr	166	157	148	37.1
Reprocessing Cost,[c] $/KgHM	274	260	245	61.4
Unit Cost,[c] $/g fissile	22.2	21.0	19.8	4.95

a) based upon reference fuel cycle as described in Section VII.A.

b) 18.04% carrying charge (see Chapter VIII)

c) Current dollar cost referenced to 1982 dollars

The reduced cost for pyro-chemical reprocessing, shown in the table, is a rough estimate, but derives from an expected order-of-magnitude reduction in the size of the facility relative to that required for the aqueous process (i.e., ~ 2700 ft^2 versus 36,000 ft^2 for PUREX). Several pyro-chemical process options were considered, but our first choice for uranium recovery is a process that exploits the high solubility of thorium, and the low solubility of uranium, in molten magnesium. Uranium metal is essentially insoluble in both pure magnesium and magnesium-thorium alloys while thorium is quite soluble (see Table ii.VII.4).

We propose to utilize thorium metal (which may contain from 0.5 to 1.5% uranium-233 plus a small quantity of fission products) directly from the blanket and dissolve it in a bath of molten magnesium. The uranium contained in the original blanket will be essentially insoluble in the melt at 677°C and exists as β-uranium metal. The solubility of uranium in 33 wt% Th-67 wt% Mg alloy is 1.6×10^{-5} moles/mole solvent, or 0.032 wt% of the thorium in the solvent. If we assume 0.94 wt% ^{233}U build-up in the alloy, the uranium remaining dissolved in the solvent would be 3.4% of the initial uranium present. Essentially all of this ^{233}U can be recovered by scavenging the solvent alloy with an equal mass of ^{238}U, thereby diluting the isotopic purity to 50% ^{233}U. As safeguard regulations will probably require isotopic dilution prior to shipment of recovered ^{233}U, it is possible to protect the product in process by diluting the ^{233}U by a factor of five with ^{238}U at dissolution with elimination of the scavenging step after initial precipitation.

The thorium is recovered from the magnesium alloy by simply distilling the volatile magnesium fraction away from the residual thorium and fission products. This distillation can be easily performed under about one torr vacuum. The recovered magnesium will be used for dissolution of the next batch of blanket feed. The residual thorium and FP fraction can be refabricated into suitable metallic shapes for return to the breeder blanket assembly. Most of the fission products will remain in the thorium metal and decay away during the next irradiation sequence. After many blanket cycles, the stable fission produce concentrations may require removal, or alternatively the thorium (about 280 MT) could be replaced. The highly contaminated thorium blanket can simply be treated as fission product waste.

Table ii.VII.4 Solubility of Uranium in Pure Magnesium and Mg-33 wt % Th between 600 and 850°C

Temperature		U solubility (atom fraction in indicated solvent	
°C	$10^4/T(°K)$	Mg	Mg-33 wt % Th
600	11.45	—	7.1×10^{-6}
650	10.83	5.9×10^{-6}	1.3×10^{-5}
700	10.28	1.1×10^{-5}	—
750	9.78	1.68×10^{-5}	2.75×10^{-5}
800	9.32	2.73×10^{-5}	4.22×10^{-5}
850	8.90	4.04×10^{-5}	5.07×10^{-5}

Reference: Unpublished Work by Fred J. Smith, October 6, 1982, Oak Ridge National Laboratory. Sponsored by Division of Chemical Sciences, Office of Basic Energy Sciences, D.O.E.

ii.VIII SYSTEMS AND ECONOMICS ANALYSIS

ii.VIII.A Introduction and Overview

The economic incentives for a fusion breeder reactor can be best understood and evaluated in the context of a symbiotic fusion fuel factor-fission burner electricity generation system whose sole product is electricity. In this concept, the fusion fuel factory is typically incorporated into a remotely sited and safeguarded fuel cycle complex along with fuel reprocessing plants, fuel fabrication facilities and possibly a waste disposal facility. Typical fuel cycle complex configurations were discussed in Section ii.VII. Four such fuel cycle complexes, containing three fusion breeders each, could provide makeup fissile material to support about 250 GWe of LWR capacity. Only about 15 GWe would be produced by the fusion breeders themselves (~ 1250 MWe per fusion breeder).

The basic analytical capability used to generate the results presented in this chapter is provided by three computer codes developed over the course of the past several years and implemented on the Magnetic Fusion Computing Network: the LLNL Tandem Mirror Physics Code (TMPC), the Tandem Mirror Reactor Design Code (TMRDC), and the TRW economics analysis code (PERFEC). Each of these codes has a distinct function. TMPC is used to estimate plasma engineering parameters associated with the fusion driver configuration and power flow. TMRDC is used to integrate these quantities into a reactor design and estimate the net TMHR power flow, fissile production, and direct cost. PERFEC combines the TMRDC output with fission reactor, fission fuel cycle, and financial accounting data to estimate the economic performance of the entire symbiotic electricity generation system. In performing the systems and economics analysis, the capital and operating costs of the entire symbiotic electricity genration system are used to estimate the costs of the production in one net product, electricity.

This section is broken into three principal subsections. In Section ii.VIII.B, the economics analysis for the reference fusion breeder described in the previous sections is summarized. A summary of the global cost, performance and fuel cycle data which is required to develop the economics analysis is provided first. The economics results, focusing upon the cost of

electricity for the symbiotic system as compared with the electricity generation cost for a conventionally fueled LWR (mined U_3O_8 at 55 $/Kg with full reprocessing and recycle), are presented next.

Section ii.VIII.C describes optimizations of the fusion breeder about the reference case which can provide a lower symbiotic cost of electricity. Three cases are considered. In the first case, an improved fusion driver and fuel management operating point is developed. In the second case, we consider the cost advantages associated with the use of pyro-chemical reprocessing instead of aqueous (THOREX) reprocessing. In the third case, we consider the economics of switching from the denatured thorium to denatured uranium fuel cycle on the LWR burner side of the system.

Section ii.VIII.D addresses the sensitivity of the system electricity cost to plant component cost and performance uncertainties. In particular, electricity cost sensitivities to power flow and cost uncertainties are considered. The cost of electricity as a function of achievable plasma energy gain (i.e., Q_p) is compared with consistently derived results for a fusion electric plant.

ii.VIII.B Economics Analysis for Reference Fusion Breeder

Estimates of the following quantities for both the fusion breeder and the client fission burners were required to develop a consistent estimate of the symbiotic cost of electricity:

- Fixed capital costs
- Variable operating costs
- Fissile fuel production and consumption
- Fissile fuel inventories
- Net thermal-to-electric conversion efficiencies

Given the above data, the PERFEC computer code may be used to estimate the year-by-year costs of electricity and the bred fissile fuel over the fixed operating lifetime of the fusion breeder and its fission reactor clients. These year-by-year costs may be combined to provide average present value costs of electricity and fuel as

$$S_{PV} = \frac{1}{N} \sum_{n=0}^{N-1} \frac{S_n}{(1+i)^n}$$

and

$$C_{fiss,PV} = \frac{1}{N} \sum_{n=0}^{N-1} \frac{C_{fiss,n}}{(1+i)^n}$$

where N is the reactor operating lifetime (30 years in this analysis), S_n is the symbiotic cost of electricity in year n dollars, i is the general inflation rate, S_{pv} is the average present value cost of electricity, $C_{fiss,n}$ is the cost of bred fuel in year n dollars, and $C_{fiss,PV}$ is the average present value cost of bred fuel. If S_0 and $C_{fiss,0}$ are referenced to 1982 dollars (as they are in this analysis), then S_{pv} and $C_{fiss,PV}$ are also referenced to 1982 dollars. Note that, in practice, the conditions

$$S_{pv} < S_n \qquad n=0,1, \text{---}, N-1$$
$$C_{fiss,PV} < C_{fiss,n} \qquad n=0,1, \text{---}, N-1$$

usually hold since the total annual cost of plant operation (i.e., capital cost plus operating cost plus inventory cost) is not expected to rise as quickly as inflation. This is especially true of highly capitalized facilities such as nuclear plants where the effective cost of power generation to the public decreases over the life of the plant.

Summaries of the reference fusion breeder performance and cost data, as input to the economics analysis are provided in Tables ii.VIII.1, ii.VIII.2, and ii.VIII.3. Many of the parameters shown in these tables are normalized to the nuclear power of the fusion breeder. This convenient quantity, which is similar to the thermal power of reactors which do not utilize direct conversion of charged particle power into electricity, is calculated as

$$P_n = P_f\ (0.8\ M + 0.2) = 4464\ MW_n$$

where P_f = 3000 MW is the fusion power and M = 1.61 is the blanket energy multiplication. The nuclear power of a 1 GWe LWR is taken to be the same as the thermal power, or 3000 MW_t.

Referring to Table ii.VIII.1, we see that the net nuclear-to-electric conversion efficiency of 0.295 is comparable to that of an LWR (typically about 33%). The breeders net specific fissile fuel production rate of 1.81

TABLE ii.VIII.1 Reference Fusion Breeder Performance Parameters

Fusion Power, MW_f	3000
Average Blanket Energy Multiplication, (M)[a]	1.61
Average Total Nuclear Power, MW_n[a]	4464
Average Net Electrical Power, MW_e[a]	1317
Average Net Nuclear-to-Electrical Efficiency[a]	0.295
Net Fissile Fuel Production Rate, Kg/yr[b]	5646
Net Specific Fissile Fuel Production Rate, Kg/MW_n-yr[c]	1.81
In-Core Fissile Inventory, Kg	1032
Ex-Core Fissile Inventory, Kg[b]	2874
Total Fissile Inventory, Kg[b]	3816
Specific Fissile Inventory, Kg/MW_n	0.854
Average Fissile Discharge Enrichment, %[a]	1.24
Heavy Metal Throughput, MT/yr thorium[b]	604
Average Plant Capacity Factor, %	70

a) Average over blanket operation
b) At 70% capacity factor
c) Value for full power operation

Table ii.VIII.2 Summary of Fusion Breeder Fixed (Indirect) Charges

Direct Cost, $M	3744
Indirect Cost, $M	3179
Time-related cost, $M	1232
Total Capital Cost, $M (1982 $)	8155
Specific Cost, $/kW$_n$	1826
Total Annual Charge at 18.04%/yr $/kW$_n$-yr	329

Table ii.VIII.3 Summary of Fusion Breeder Variable (Direct) Charges in Year Zero

Fuel Cycle Operating Cost, $M/yr[a]	89
Blanket Structure Replacement Cost, $M/yr	2
Miscellaneous Operation and Maintenance cost, $M/yr	132
Total Variable (Direct) Charge in Year Zero, $M/yr	223
Specific Variable (Direct) Charge in Year Zero, $/KW$_n$-yr	50.0

a) see further breakdown in Section VI.E.

Kg/MW_n-yr is 14.4 times the net specific fissile consumption rate of its client LWRs (denatured thorium fuel cycle). However, since the fusion breeder nuclear power is higher (4464 MW_n versus 3000 MW_n for the LWR), over 21 LWRs can be supported by a single fusion breeder.

In Table ii.VIII.2 we develop the total capital cost of the fusion breeder from the direct cost estimate shown earlier by including indirect and time related costs based upon LWR construction experience. The ratio of the total to the direct cost of 2.18 is larger than usually used in fusion studies, so comparisons with other fusion plants on this basis alone are discouraged. An LWR, when costed consistently, has a specific capital cost of 540 \$/KW_n, so the fusion breeder cost of 1826 \$/KW_n is 3.4 times the LWR cost on this basis.

Interestingly, these fusion breeder versus LWR comparisons can be lumped to a simple and convenient figure-of-merit for the symbiotic system. This figure of merit, the average capital cost of electricity generation relative to the LWR is defined as

$$C^{Ave.} = \frac{C^B + R}{\eta_{rel} + R}$$

where C^B (3.4 in the above analysis) is the breeder capital cost relative to the LWR cost per unit nuclear power, R (14.4 in the above analysis) is the nuclear support ratio, and η_{rel} is the electrical efficiency of the breeder relative to an LWR (0.295/0.33 = 0.89 in the above analysis). So, in the reference case, an average capital cost of

$$C^{Ave.} = \frac{3.4 + 14.4}{.89 + 14.4} = 1.16$$

is obtained.

In the more detailed analysis, summarized in Table ii.VIII.4, the average present value of the cost of electricity for the symbiotic system is 38.7 mil/KWeH (1982 dollars). When compared to a consistent calculation for the cost of electricity from an LWR that is fueled with conventionally mined uranium costing 55 \$/Kg in the first year (with 3% real escalation above

Table ii.VIII.4 Summary of Results for Baseline Economics Analysis

Year Zero Bred Fissile Fuel Cost[a]	198 $/g
Ave. Present Value of Bred Fissile Fuel	93 $/g
Year Zero Symbiotic Electricity Cost	76.3 mil/KW_eH
Ave. Present Value of Symbiotic Electricity Cost	38.7 mil/KW_eH
Year Zero Conventional Electricity Cost	61.8
Ave. Present Value of Conventional Electricity Cost	34.8
Symbiotic/Conventional Cost of Electricity[b]	1.11

a) All costs in 1982 dollars

b) Basis: average present value

inflation in each of the succeeding years), the symbiotic cost of electricity is only 11% higher. In the case of the conventional LWR, full reprocessing and fissile recycle of uranium and plutonium was assumed.

This result indicates that fusion breeders, introduced into the nuclear economy, could preserve the economic viability of the LWR indefinitely.

ii.VIII.C Development of an Optimized Case

The baseline fusion breeder economics discussed in Section ii.VIII.B relate to the reference fusion breeder as designed and described in the previous sections. However, we have also identified variations about the reference fusion driver design and fuel management mode which lead to a lower symbiotic cost of electricity and the definition of an optimized fusion breeder. In this section we review and summarize an optimized case, and also consider two alternative paths which have not yet been factored into the analysis. The first is substitution of the less expensive pyro-chemical reprocessing technology for THOREX reprocessing of the fusion breeder discharge fuel. The second alternate path is the use of the denatured uranium LWR fuel cycle instead of the denatured thorium fuel cycle. In the later case, fuel cycle and inventory charges are reduced, but the number of LWRs which are supported by the fusion breeder is also reduced.

The reference driver and fuel cycle were reconfigured and optimized subject to several constraints:

- fixed central cell fusion power of 3000 MW
- fixed end-of-cycle MHD pressure drop obtained by requiring that the product of the neutron wall loading, maximum blanket energy multiplication, and the square of center cell field strength is the same as the reference case (i.e., $\Gamma MB^2 = \Gamma_0 M_0 B_0^2 = 1.27 \times 1.97 \times 4.2^2 = 44.1$ in all cases).
- fixed wall loading over the entire fuel cycle period such that the fusion power is constant and the blanket thermal power increases with time
- maximum central cell length of 200 m and minimum neutron wall loading of 1.27
- fixed first wall radius of 1.5 m

- no axial variation of blanket module maturity (i.e., enrichment)
- two radial fuel zones with an inner-to-outer reprocessing frequency of two-to-one
- maximum axicell magnet field strength of 20 tesla

The motivating rationale for these constraints is related to a desire to limit the overall facility size and power level while maintaining relevancy of the blanket design point, maximizing the use of the expensive fusion driver, and simplifying the impact of fuel management on plant operations.

In Table ii.VIII.5 we summarize important differences in the optimized and reference cases as they relate to the fusion breeder design, cost, and the resulting symbiotic electricity generation system results. Importantly, the optimized plant, which costs about 2.7 times as much as an LWR on a per unit nuclear power basis, provides about the same fissile fuel production and about 30% higher average electricity production at a capital cost which is about 8% lower than that of the reference system. This results in a 26% decrease in the cost of fissile fuel and a 6% decrease in the symbiotic cost of electricity (to only about 5% above the cost of electricity for a conventionally fueled LWR).

In Section ii.VIII, pyrochemical reprocessing s suggested as a less expensive alternative to aqueous THOREX reprocessing. In this section we consider the economic effect of its use in the context of a further improvement to the optimized case presented above.

In general, the cost of a pyrochemical reprocessing plant is expected to be about 1/4 the cost of an aqueous plant of the same capacity. Therefore, we estimate that the total cost of a facility to reprocess the discharge fuel in the optimized case (674 MT/yr) would be on the order of 1/4 x 600 = 150 $/M. The operating cost for such a facility is e timated to be on the order of 5-10 $M/yr.

Our analysis indicates that, for the optimized case, a switch to pyrochemical reprocessing would be equivalent to an overall capital cost savings of about 951 $/M (or 13%) and could decrease the symbiotic electricity cost by about 0.55 mil/KWe (about 1.5%).

Table ii.VIII.5 Comparison of Reference and Optimized Fusion Breeders

	Reference System	Optimized System
Fusion Power, MW	3000	3000
Maximum End Cell B Field, Tesla	15	20
Central Cell Length, m	200	193
Central Cell B Field, Tesla	4.20	3.66
Fusion Power Gain $(N_{trap}Q)^a$	14.6	16.6
Neutron Wall Loading, MW/m^2	1.27	1.32
BOC Blanket Energy Multiplication	1.25	1.25
EOC Blanket Energy Multiplication	1.97	2.50
Average Blanket Energy Multiplication	1.61	1.885
EOC Net Electrical Production, MW	1662	2256
Average Net Electricity Production, MW	1317	1720
Annual Fissile Fuel Production,[b] Kg	5646	5590
Discharge Fissile Enrichment, %	1.24	1.10
Direct Capital Cost, $	3744	3439
Average Present Value Cost of Electricity, mil/KWeH	38.7	36.5
Average present Value Cost of Fissile Fuel, $/g	92.7	68.7
Cost of Electricity Relative to LWR with Reprocessing and 55 $/Kg Mined U_3O_8	1.11	1.05

a) $N_{trap}Q$ is the ratio of fusion power to injected power

b) at 70% capacity factor

Although the cost of electricity would decrease only marginally, the average present value of the cost of reprocessing fissile fuel would decrease by about 14 $/g to 55 $/g (20% decrease). This comparison is summarized in Table ii.VIII.6.

It is important to note that the sensitivity to reprocessing costs would be much larger were the fissile discharge concentration lower than the optimized value (1.1% ^{233}U plus ^{233}Pa in thorium metal). Earlier suppressed fission blankets which were designed to about 0.6% discharge concentration are about twice as sensitive to the cost of reprocessing such that a ~ 30 $/g impact of pyroprocessing would be implied.

The economic effect of operating on the denature uranium fuel cycle instead of the denatured thorium fuel cycle was also considered. The latter fuel cycle provides a 21% larger number of LWR clients, but the fissile inventory cost and fuel reprocessing cost are lower for the depleted uranium fuel cycle. As a result, the calculated difference in the electricity cost (a decrease of 0.15 mil/KWe-H) is insignificant and the two fuel cycle are equally attractive from an economics perspective. A choice between these must derive from non-economic considerations such as the larger LWR support and a smaller fraction of plutonium burners for the denatured thorium fuel cycle. The denatured uranium fuel cycle preserves PUREX reprocessing on the LWR side of the system and minimizes the LWR fissile inventory per unit electrical power generation.

Table ii.VIII.6 Economic Impact of Pyrochemical Reprocessing

	THOREX	PYRO
Throughput, MTHM/yr	674	674
Total Reprocessing Plant Capital Cost, $M	600	150
Annual Operating Cost, $M/yr	45	5
Symbiotic Cost of Electricity,[a,b] mil/KWeH	36.45	35.20
Cost of Fissile Fuel,[a] $/g	69	55

a) average present value of 30 year operation

b) based upon equivalent capital cost savings of 450 + ([45-5]/0.1804) x 2.26 = 951 $M where 0.1804 is the fixed charge rate (yr^{-1}) and the weighting factor 2.25 is the conversion from the average present value of a dollar of operating cost to the average present value of a dollar of fixed charge.

ii.VIII.D. Sensitivity Studies and Comparison with Fusion Electric

In this section we present sensitivity studies which indicate the change in the present value of the symbiotic cost of electricity as a function of the uncertainties in the cost of the fusion breeder, the recirculating power requirement, and the fuson power gain (Q). In all cases we have selected the optimized design described in Section ii.VIII.C as the reference point.

In Figure ii.VIII.1, the sensitivity in the electricity cost is plotted as a function of the plant direct capital cost. The reference point, 3.44 $B corresponds to a fusion breeder which costs 2.7 times as much as an LWR on a unit thermal basis. The figure shows that a ± 50% change in the capital cost of the breeder corresponds to a ± 13.6% change in the system cost of electricity, or a low sensitivity coefficient of 0.27 (i.e., 13.6%/50%).

This sensitivity is compared in the same figure with a similar analysis for a pure fusion electric tandem mirror which was modeled consistently using the same physics, design, and economics codes. In the latter case, a 50% change in the capital cost corresponds to a 49% change in the cost of electricity, or a high sensitivity coefficient of 1.0. Therefore, the fusion electric case is at a disadvantage with respect to both the reference cost of electricity (71% higher than the symbiotic system) and its sensitivity to cost uncertainties.

Interestingly, if the cost of the fusion breeder decreased to about 500 $/KW$_t$ (~ 2 times the LWR cost), then the 30 year average present value of the cost of symbiotic electricity would be similar to that of the conventionally fueled LWR with the current (55 $/Kg) U_3O_8 cost. The fusion electric direct capital cost would have to decrease to about 300 $/KW$_t$ (~ 1.2 times the LWR cost) to achieve the same breakeven.

In Figure ii.VIII.2, we show similar sensitivities to uncertainties in the recirculating power requirement of the fusion breeder. Our optimized case, with a fusion gain of 16.6, assumes that a very efficient fusion plant will be available. This result is consistent with current theoretical projections, but any number of factors could increase the recirculating power. The figure indicates that, on a power flow basis alone, such uncertainties are not

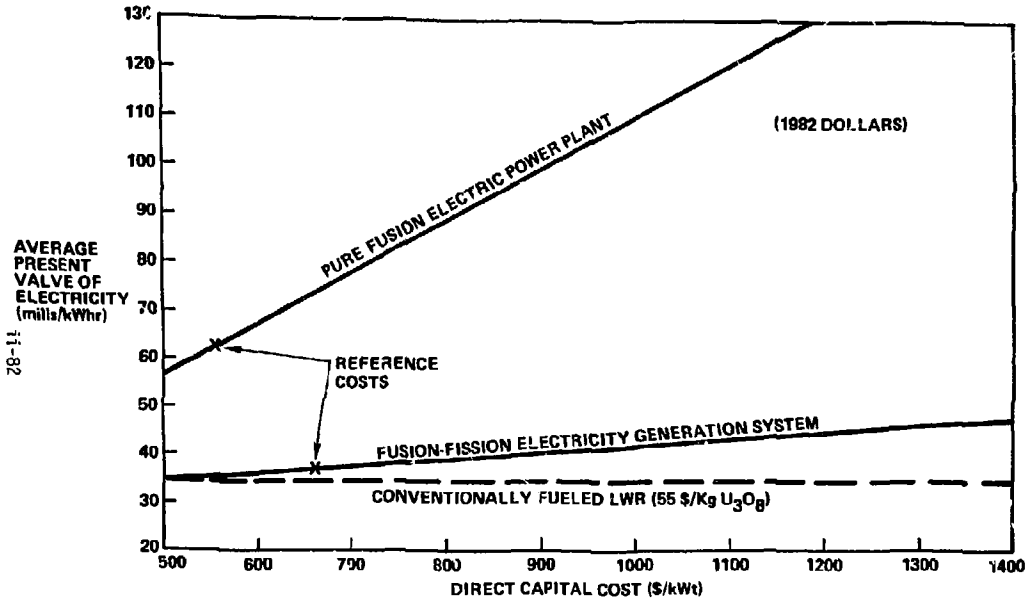

Figure ii.VIII.1 The Cost of Electricity for Fusion-Fission Electricity Generation and Fusion Electric Versus the Capital Cost of the Plant

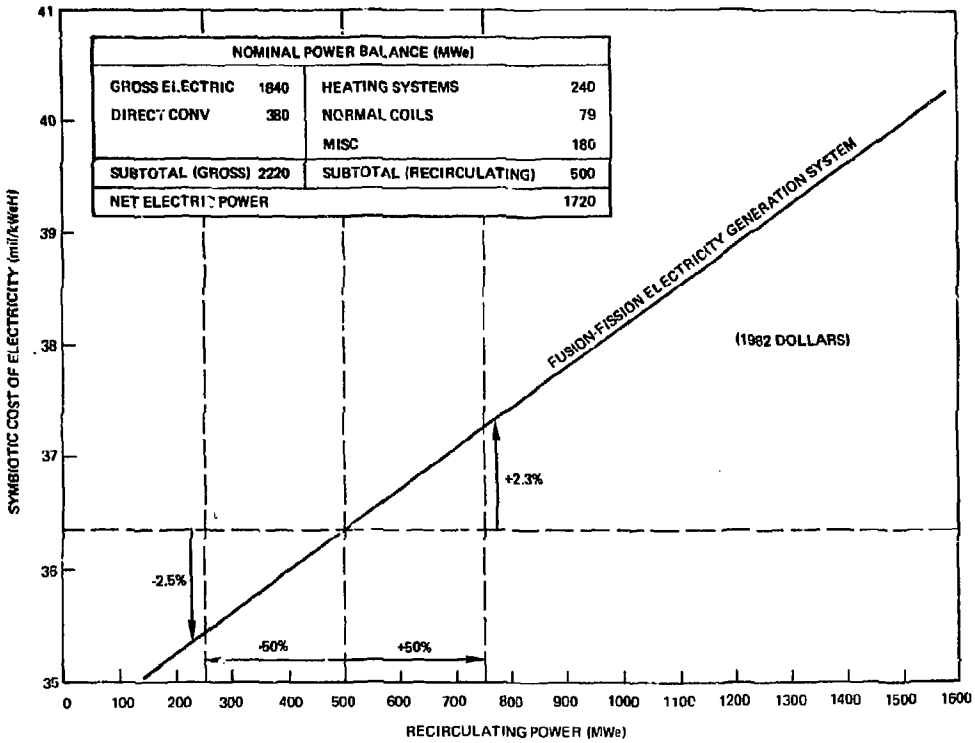

Figure ii.VIII.2 Cost of Symbiotic Electricity as a Function of Total Recirculating Power for the Optimized Fusion Breeder Case

highly important for this application. In particular, a 50% increase in the recirculating power from 500 to 750 MWe results in only a 2.3% increase of the cost of symbiotic electricity.

In fact, the largest uncertainty, the fusion gain ($\tau_{trap}Q$) does not affect the recirculating power requirement alone, but also affects the size and cost of the plasma heating systems. In Figure ii.VIII.3, we show the affect of fusion gain uncertainties for both the fusion breeder and fusion electric cases.* As shown, the symbiotic cost of electricity is insensitive to fusion gains below about 10 and does not increase significantly until the gain falls to about 5 - threefold below the predicted value. Conversely, for fusion electric generation, the range of insensitivity is about 30 and very substantial increases in the cost of electricity occur for gains below about 15.

* It is important to note that the cases shown in Figure ii.VIII.3 do not represent optimized plant costs versus plasma gain, but are developed by assuming that the heating system cost and recirculating power are each inversely proportional to the plasma gain.

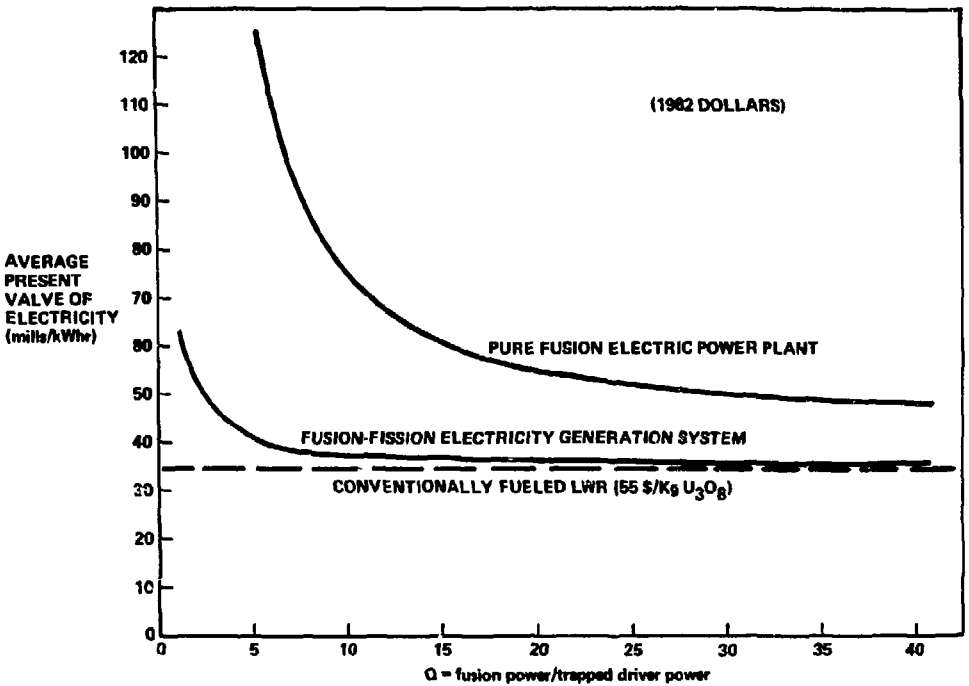

Figure ii.VIII.3 The Cost of Electricity for Fusion-Fission Electricity Generation and Fusion Electric Versus the Fusion Gain

CHAPTER I

INTRODUCTION AND FUSION BASELINE

I.A. PROJECT GOALS AND ORGANIZATION

I.A.1 Role and Motivation

Relatively low-cost fossil fuels and nuclear fuel cycle resources dependent upon the naturally occurring isotope (i.e., ^{235}U) will, most likely, run out in the next century. Regardless of long-range energy projections, only a few energy sources can be considered inexhaustible in a practical sense. These include solar energy, nuclear fusion energy, and nuclear fission energy with a technology to convert abundant resources of naturally occurring fertile isotopes (i.e., ^{232}Th and ^{238}U) to fissile isotopes that can be used to fuel conventional fission reactors. The fusion breeder combines the last two options by using nuclear fusion to produce fissile fuel for fission reactors such as the light water reactor (LWR). Results show that fusion breeders, especially those using suppressed fission blankets, can produce unprecedented quantities of fissile fuel per unit of nuclear power.

Research in the area of fusion-fission hybrid reactor concepts began more than 25 years ago[1,2] and progress in the controlled nuclear fusion experimental program and recent innovations in hybrid blanket designs have raised renewed interest in the attractive potential for this technology.[3-5] Since 1979, projections from fusion experimental programs indicate that the fusion plasma physics performance needed to economically breed fissile fuel are expected to be verified within the next decade. Fusion breeder blanket designs considered during the past four years (namely suppressed fission blankets) can double the fissile fuel production per unit of thermal (or nuclear energy.[5,6] Several studies affirm the general conclusion that the fusion breeder is a superior option when viewed from the joint perspectives of cost of electricity, potential to displace expected fossil fuel shortfalls, and ability to provide real energy growth during the first half of the next century.[7,8]

Because each fusion breeder can produce enough fissile fuel to support about 20 relatively inexpensive LWRs, this application raises nuclear fusion to an economically attractive level of performance, even if the cost of the

fusion breeder is several times that of a fission plant of comparable power.[7] Similarly, by producing fuel for existing fission reactors, fusion can rapidly help meet our energy needs while preserving the utility industry's investments in conventional LWR reactor systems.

As a new source of fissile fuel, the fusion breeder can compete with mined and enriched uranium for LWR consumption, and will begin displacing conventional sources of LWR fuel as reserves and resources become depleted during the first decades of the next century. Effectively, this competition can place a ceiling on the escalating price of mined U_3O_8.[8]

The fusion breeder can also help accelerate the commercial development of fusion power plants because the need for fusion breeders will be an acceptable motive for introducing them with lower fusion performance and higher fusion component costs than would be acceptable for fusion electric power plants. The early commercialization of fusion breeders will give the industrial sector experience relevant to the development, operation, and improvement of fusion component technologies.

I.A.2 Project Goals

The ultimate goal of the Fusion Breeder Program is to develop and demonstrate the breeder specific technology so that the fusion process can be used to produce commercial fissile fuels when both uranium becomes expensive and fusion development results in an economical neutron source. The technologies that complement fusion technology for fissile production are the breeder blanket and fuel cycle technologies. In the blanket fusion produced neutrons transmute fertile materials (^{232}Th and/or ^{238}U) into fissile materials (^{233}U and/or ^{239}Pu) and breed tritium from lithium. Fuel cycle technologies include the separation of fissile and fertile materials, fuel handling and fabrication, and waste management. Most of the technologies for the fusion breeder are developed or are being developed by either the fusion or fission programs.

Our objectives at this early stage of the program are to study a few blanket conceptual designs in order to improve our understanding and to expose pitfalls on paper as the designs evolve. A modest effort now on design studies and small-scale generic experiments will eliminate many technological "blind alleys" and should save much time and money later when large-scale hardware development is undertaken.

The major results from the fusion breeder program's FY82 work evolved from the work in FY81[5] and are reported here. The blanket, coupled with a tandem mirror fusion driver, results in what we call the FY82 Reference Fusion Breeder. An economic analysis of this fusion breeder and its fueled fission reactors (LWRs in this case) was made to help quantify its potential and help compare it to other designs. The cost of electricity from this fusion/fission system and its ability to deploy rapidly (i.e., time to significantly enter the market) are the relevant figures of merit. The FY82 study was performed in the context of the following goals, all of which were proposed at the start of the program:

1. Develop fission suppressed blanket concepts which, together with their fuel cycles, result in superior safety characteristics and the greatest impact on fission reactor fuel supply. The development time, cost, and risk were to be reasonable for this application.
2. Consider the advantages and disadvantages of ^{233}U and Pu to determine which is the better fuel to breed in the above context.
3. Find ways to use Be as the nonfissioning neutron multiplier such that fabrication costs and radiation damage effects are minimized.
4. Plan a development program which includes early testing in fission reactors and which seeks to minimize:
   (a) the cost of development,
   (b) risk of not being successful in developing the technology, and
   (c) the time from demonstration of fusion to introduction of commercial fusion breeders. The focus of the development plan was to include construction of a demo in 1995 and the operation of a commercial-scale prototype plant in 2015. Due to reduced funding, the development plan work was greatly reduced.
5. Safety - Show that loss of coolant type accidents can be noncatastrophic (even economically noncatastrophic). The use of passive cooling and dump tanks for pebble or other mobile fuel was to be considered.

The resulting blanket for the FY82 reference fusion breeder is of the fission- suppressed class in which non-fission nuclear reactions [Be(n,2n) and $^{7}Li(n,n'T)$] are used to generate the excess neutron multiplication needed for net breeding. We are concentrating on this class of blankets because the decay afterheat is much lower and the fissile fuel production per unit of

thermal energy generated in the blanket is much higher than that of fast fission blankets that use ^{238}U or ^{232}Th fissions (induced by 14 MeV neutrons) to generate the excess neutrons. The lower afterheat should lead to simpler, less risky designs, while the higher specific fuel production should result in more attractive deployment scenarios because fuel becomes the principle product of the fusion breeder, not electricity. The fission-suppressed, fusion breeder can fuel (support) 12-15 LWRs of equal thermal power, where a uranium fast fission, fusion breeder supports only about 5 LWRs. The fission-suppressed fusion breeder will also require higher fusion power drivers (approaching the power level of fusion electric applications) to be competitive. There is a lively debate about which class of blanket is best. More detailed design studies, which include reactor safety considerations, are needed before a definitive comparison can be made and this debate resolved.

Our FY82 blanket design is based, as much as possible, on conventional or near-term materials and process technologies; namely LMFBR liquid metal technologies and THOREX aqueous fuel reprocessing (although we are pursuing a simple form of pyrochemical processing which could cut the reprocessing cost several-fold). In terms of performance, technological development requirements and risk, this design could be classified as "moderate technology". For comparison a "low technology" blanket could be a low temperature ($\sim$ 100 ^{o}C) water-cooled design using low stressed, well understood materials producing fuel but no power, while a "high technology" case might be based on Molten Salt Breeder Reactor technology in which a fertile molten salt is used for on-line fueling and processing as well as cooling.

Emphasis of the study is placed upon blanket engineering in the context of a tandem mirror fusion neutron source. A blanket concept for a tokamak neutron source will be selected and studied during FY83.

I.A.3 Organization

Fusion breeder design has progressed to a level of conceptual detail which requires a multidisciplinary team approach. The present study includes the participation of the following organizations with the further work breakdown by discipline as shown in Fig. I.A.1.

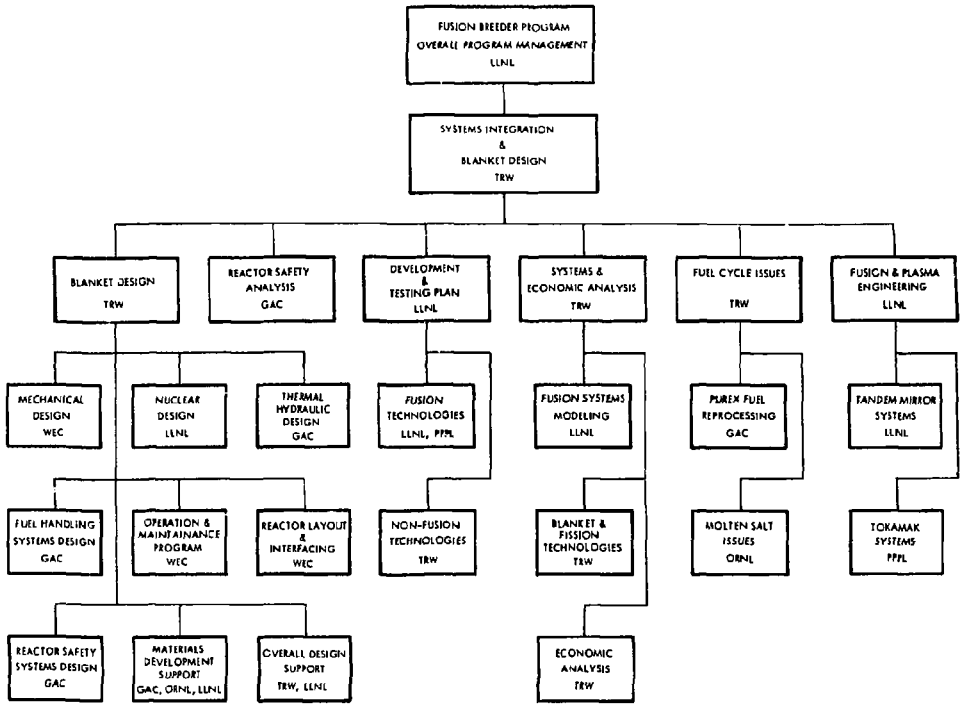

FIGURE I.A-1 Fusion Breeder Program Organization

Organization	Principal Roles
Lawrence Livermore National Laboratory	Program Manager, Tandem Mirror Physics and Technology, Nuclear Design
TRW, Inc.	Technical Integration, Tandem Mirror Plasma Engineering, Reactor Systems Modeling, Design Support
GA Technologies, Inc. General Atomic Company	Fluid Mechanics and Heat Transfer, Fuel Management Systems, Reactor Safety Systems, Fuel Reprocessing
Westinghouse Electric Company	Mechanical Design, Operation and Maintenance, Reactor System Layout
Oak Ridge National Laboratory	Chemical Engineering and Materials
Princeton Plasma Physics Laboratory	Tokamak Plasma Engineering and Technology
Idaho National Engineering Laboratory	Reactor Neutron Testing

In addition, investigators from the University of California, Los Angeles (radiation damage), and the Energy Technology Engineering Center (liquid metals and materials) are participating in the study.

References, Section I.A

1. J. D. Lee, et al., "Feasibility Study of the Fission Suppressed Tandem Mirror Hybrid Reactor," Lawrence Livermore National Laboratory, UCID-19327 (1982).

2. D. H. Imhoff, et al., "A Driven Thermonuclear Power Breeder," California Research and Development Corporation, CR-6 (1954).

3. B. R. Leonard, Jr., "A Review of Fusion-Fission (Hybrid) Concepts," Nucl. Tech., 20, 161 (1973).

4. Proc. DCTR Fusion/Fission Energy Systems Review Mtgs., Germantown, Maryland, December 3-4, 1974, ERDA-4, U.S. Energy Research and Development Administration (1974).

5. D. L. Jassby, Ed., Proc. 3rd US/USSR Symp. Fusion-Fission Reactors, Princeton, NJ (1979).

6. R. W. Moir, Ed., "Tandem Mirror Hybrid Reactor Design Study," Lawrence Livermore National Laboratory, UCID-18808 (1980).

7. J. A. Maniscalco, et al., "Recent Progress in Fusion-Fission Hybrid Reactor Design Studies," Nuclear Technology/Fusion, 1, 4, 419 (1981).

8. D. L. Chapin, et al., "Preliminary Feasibility Assessment of Fusion-Fission Hybrids," Westinghouse Fusion Power Systems Department, WFPS TME-81-003 (1980).

I.B BACKGROUND

I.B.1 History of Suppressed Fission Blanket Designs

During the past four years, the suppressed fission blanket has emerged as a possibly superior path towards achieving a hybrid which maximizes the number of client fission reactors (e.g., LWR) which can be supported by a single hybrid.[1] The fission-suppressed blanket option (also known as the fusion breeder reactor) is a challenging technological goal but, in comparison with fast fission hybrids, the fusion breeder has superior reactor safety and institutional characteristics.[2] Reactor safety advantages result due to its low fission rate (< 0.05 per fusion) and institutional advantages result because a high support ratio fusion breeder would fuel about 15 1-GWe-client LWRs while producing only about 1 GWe locally. In this sense, fuel cycle centers consisting of fusion breeders and the fuel cycle activities associated with the fusion breeders and their LWR clients could replace present day uranium mining and uranium enrichment plants.

Economics and deployment studies have shown that the fusion breeder/LWR option can provide electricity inexpensively (less than 15% above the cost of electricity for current technology LWRs) and could rapidly expand during the next century to satisfy a substantial fraction of our electrical demand.[1] Despite a projected commercial introduction date of ~ 2015, the fusion breeder can impact electricity generation requirements more quickly than other advanced technologies (e.g., LMFBR, fusion electric). As natural uranium resources become depleted, the current plan (without an external source of fissile fuel) would wind down the rate of commitment to new LWR construction. Once the feasibility of fusion breeder technology is demonstrated (perhaps ~ 2005), LWR operators will have an assured future fissile fuel supply and LWR electricity generation capacity can expand without interruption.

The design of a fission-suppressed blanket was first addressed in a 1979 study performed by Lawrence Livermore National Laboratory (LLNL) with the General Atomic Company (GAC), the General Electric Company (GE), and Bechtel National, Inc.[3,4] As a result of this study, a fission-suppressed blanket concept based upon beryllium neutron multiplication and a lithium/thorium bearing molten salt coolant was developed. Although the Be/MS blanket performance was excellent, materials problems associated with the use of beryllium and a high temperature salt (> 550 ^{o}C) in the fusion environment

led to the pursuit of other blanket concepts. Nevertheless, due to the superior operational and fuel cycle characteristics of Be/MS blankets, modified versions of the original blanket are being considered at a low level of effort.

Two suppressed fission blanket designs were studied in detail as part of a 1981 study performed by LLNL with TRW, GAC, Westinghouse Electric Corp. (WEC), and Oak Ridge National Laboratory (ORNL).[5]

The first of these blankets featured a one-zone design with beryllium as a neutron multiplier, helium as a coolant, and a liquid suspension of thorium oxide particles in lead-lithium (i.e., $Li_{17}Pb_{83}$) as a fertile fuel, tritium breeding material, and heat transfer medium. In this design, as in other suppressed fission blanket designs, a mobile fuel with on-line reprocessing is necessary to keep fissile content low and suppress fission of the ^{233}U. To obtain maximum irradiation life from the structural material, ferritic steel (HT-9) with a low pressure corrugated box sub-module design was specified. Thorium oxide was chosen as the fertile material form to be circulated through the blanket because its density is a close match to that of $Li_{17}Pb_{83}$. Cooling is accomplished by helium flowing in reentrant thimble tubes. Neutron multiplication occurs in triangular-shaped prismatic blocks of hot pressed beryllium. The beryllium blocks are essentially unconstrained to accommodate irradiation-induced swelling. Thermal contact between the beryllium blocks and the cooling tubes is maintained by liquid Pb-Li.

The suspension of ThO_2 microspheres in the mixture of Pb-Li is slowly circulated to allow reprocessing to remove bred fuel. Because of the small concentration of Th, a 0.6% concentration of ^{233}Pa plus ^{233}U in thorium is reached in less than 2 months of exposure. The fissile discharge concentration results from a trade-off between fission suppression at low concentration and economical reprocessing at high concentration. The ^{233}U content is only about 0.25% at discharge (i.e., $\sim$ 0.35% ^{233}Pa). The concept of using low thorium concentration to achieve rapid breeding rates is called "fertile dilution." Following the beryllium region is a silicon carbide reflector region which substantially reduces the beryllium requirements. The net breeding of ^{233}U per fusion reaction is quite good (F = 0.73).

Although the gas-cooled Be/ThO_2 blanket resulted in excellent breeding performance and afterheat safety characteristics, a number of design issues including concerns relating to design complexity ($\sim$ 800 pressure tubes/m^2), beryllium irradiation damage and recycling, and chemical compatibility

motivated a search for an alternate concept.

The second blanket featured ^{6}Li-depleted lithium as a coolant and as an effective neutron multiplier (i.e., the ^{7}Li(n,n'α) reaction produces tritium without the loss of a neutron). In this two-zone configuration, shown in Fig. I.B.1, a 50-cm-thick liquid lithium zone is followed by a flowing molten salt zone. The molten salt contains thorium and also serves as a coolant for the outer zone. Stainless steel was used as the structural material and corrosion is greatly retarded by maintaining a frozen layer of the thorium-bearing salt on the steel. However, the steel might last many years without this protective layer. Also, Hastelloy (which is used for the outer wall of the blanket as well as the piping and heat exchangers) might be used with several years of service before radiation damage effects cause end of life. The MHD pressure drop was found to be manageable (∿ 100 psi pressure at the first wall) due to the low magnetic field (∿ 3 T).

The Li/MS blanket resulted in lower breeding performance than the Be/ThO_2 blanket (0.49 vs. 0.73 fissile atoms per source neutron) due to less effective neutron multiplication in lithium as compared with beryllium. However, the reprocessing cost was estimated to be exceptionally low for molten salt and expensive for ThO_2 (2-4 vs. ∿ 40 \$/g ^{233}U recovered).

The following observations result from these two blanket studies:

- Beryllium is markedly better as a neutron multiplier than ^{7}Li;
- One-region designs performed better than two-region designs;
- Molten salt (pyrochemical) reprocessing results in much lower cost than aqueous reprocessing if all other aspects are similar;
- Liquid metals have potential to provide less mechanical complexity for suppressed fission blankets.

A third blanket concept, identified during the latter part of the FY81 study, was a preliminary attempt to combine the attractive features of beryllium neutron multiplication with the design simplicity associated with the liquid metal coolants. A schematic diagram of an internal pipe-cooled beryllium/thorium pebbles blanket option is shown in Fig. I.B.2 and the design is more fully discussed in Ref. 5. This option featured only one neutronic zone and utilized beryllium pebbles as the neutron multiplier. In this design, nonreactive lead-lithium could be substituted for liquid lithium as the primary coolant since the neutron multiplication occurs primarily in the beryllium spheres and liquid lithium is not required for neutronic reasons alone. The blanket coolant enters the module on one side, flows through

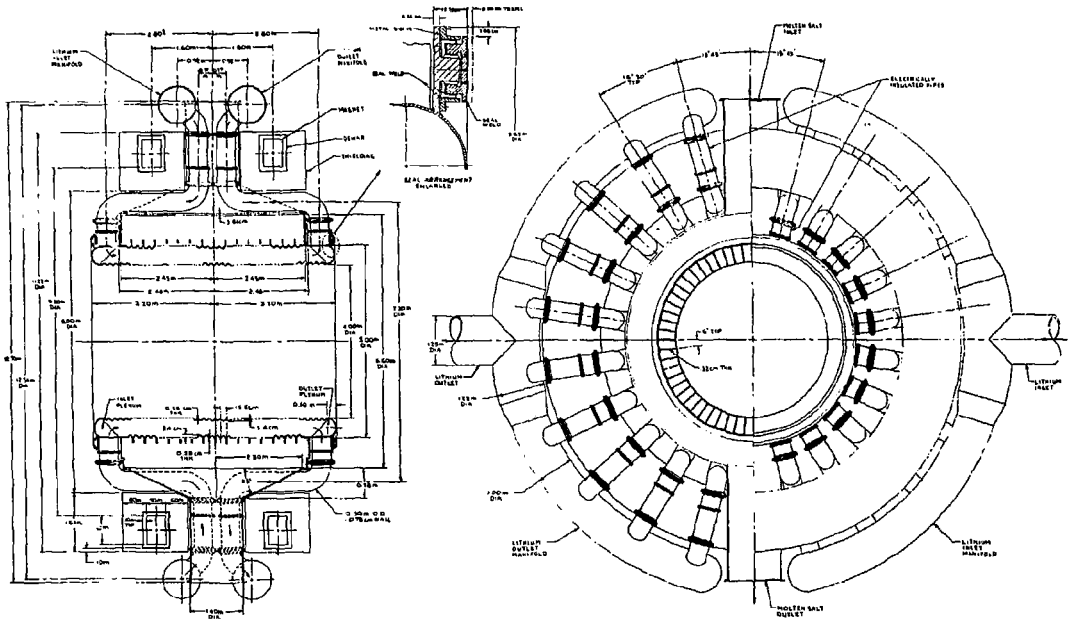

FIGURE I.B-1 Component arrangement and dimensions for the reference TMHR liquid metal-cooled blanket module assembly

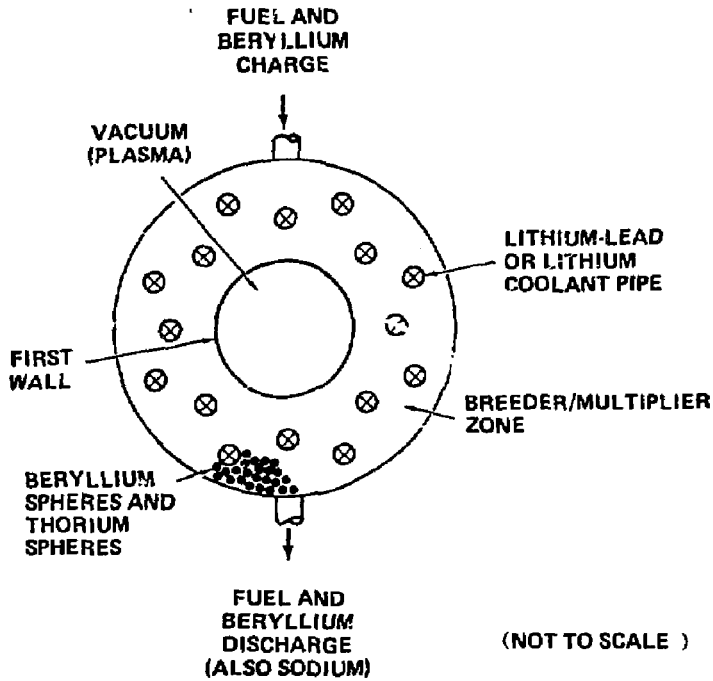

FIGURE I.B-2 Beryllium/thorium pebble blanket option, module and view

axially oriented pipes (i.e., parallel to the central cell B-field) which are embedded within the pebble bed. Heat is conducted from the bed to the coolant. In addition, the first wall would be cooled by axial lithium flow along the wall. The fertile fuel form in the design is metallic thorium pebbles randomly packed between larger beryllium pebbles. The remaining voids in the bed would be filled with the liquid metal (e.g., sodium) to improve heat transfer.

This internal pipe-cooled beryllium/thorium metal design option offered several potentially attractive features:

1. Excellent fissile breeding performance;
2. Conventional liquid-metal technologies;
3. Possibility for nonreactive primary coolant;
4. Continuous recycling of both beryllium and thorium;
5. Excellent heat transfer capabilities;
6. Fuel cycle flexibility (i.e., fertile pebbles can be thorium metal, thorium oxide, or uranium oxide);
7. Separation of fissile and tritium breeding;
8. Structural temperatures below 400 ^{o}C insure long life.

This blanket concept was chosen as a starting point for our FY82 reference blanket design work.

I.B.2 Summary of FY82 Scoping Phase

Although the third FY81 design described above has several attractive features and was chosen as a starting point for the present study, the design concept was not subjected to the same level of design detail during FY81 as its precursors. At the start of the FY82 program, four variations of this design concept were considered in an effort to select a single concept for further development as the FY82 reference blanket design. The four scoping options are shown below:

	Option Number			
	1	2	3	4
Fertile fuel form	Th	UO_2	Th	UC (U-Nb)
Primary coolant	Li (Pb-Li)	Li (Pb-Li)	Li (Pb-Li)	Li (Pb-Li)
Coolant configuration	Pipes	Pipes	Direct	Direct
Heat transfer fluid	Na	Na	Li	Li
Structural material	SS (FS)	SS (FS)	FS (SS)	FS (SS)
Max. structural temperature	360	360	< 500	< 500
Max. bed temperature	500	500	< 500	< 500
Surfaces requiring coatings	(SS) (BeO) (ThO_2)	(SS) (BeO)	(FS)	(FS)

(NOTE: Parenthesis indicate design alternatives which are not necessarily required)

This section provides a brief overview relating to our selection of a reference design concept from these options. The reader is referred to our FY82 interim report for the details of studies performed during the scoping phase of the program which begin to address the design issues associated with the four scoping phase concepts.[6]

In comparison with the FY81 design, the internal pipe-cooled options (options 1 and 2), provide the closest resemblance. These differ from one another only with respect to the fertile fuel form. A preliminary choice of lithium over Li-Pb as the coolant was based upon several factors: a general consensus that liquid lithium safety can be engineered into the design of suppressed fission blanket fusion breeders (especially considering siting in remote fuel cycle centers), better known liquid metal compatibility characteristics, a more established technology base (e.g., impurity control), better tritium retention, lower static loading and better heat transfer characteristics. The advantages of Pb-Li over Li include the following: less chemical reactivity in accident situations, better compatibility with some materials (e.g., SiC, C, ThO_2) and a lower characteristic MHD pump power (due to lower electrical conductivity). An investigation of the safety implications of this choice concluded that Li-Pb is preferred over Li but both can be handled safely.

Issues relating to options 1 and 2 which were considered at the start of the study included the choice of an austenitic stainless or ferritic steel,

pebble packing and flow characteristics for beryllium and thorium spheres, and various materials compatibility issues (including the selection of a 500 ^{0}C maximum temperature for the blanket).[7] It was the consensus that all of these issues can be amenable to engineering solutions, but further study was recommended.

The choice of stainless steel for the blanket structure was made with consideration of several comparisons (see Sections II.B and III.B). In particular, ferritic steels are expected to have superior radiation damage characteristics in most respects (e.g., void swelling, helium embrittlement), but the ductile-to-brittle transition temperature (DBTT) could rise to the blanket operating temperature for operation below about 400 ^{0}C.[8] Considering the time to reach this point (i.e., weeks) and our assessment of operation of a blanket in the brittle regime, the low DBTT was considered to be unacceptable for options 1 and 2. Ti-modified 316 stainless steel (PCA) will be acceptable, but has lower strength and thermal conductivity than HT-9 or 2-1/4 Cr-1 Mo ferritic steels. Also, there is reason to believe that improved 316 stainless steels will swell at a faster rate than low nickel ferritic steels. Tritium diffusion will be less for stainless steels than for ferritic steels. Chromium requirements for some ferritic alloys (e.g., HT-9) may become an issue, but are relaxed for others (e.g., 2-1/4 Cr-1 Mo).

Concerns related to pebble packing primarily involve three issues: packing fraction, beryllium/thorium distribution, and pebble flow. It was originally anticipated that the pebbles would be batch processed and loaded by layering. Since maintaining the required beryllium/thorium distribution could prove to be excessively difficult, a directed thorium flow in wire mesh pipes was suggested, but the reactor safety implications of such a design fix were unknown. Because segregation of separate Be and Th pebbles was predicted in LLNL experiments, a composite Be/Th pebble was chosen for further study (see Section III.C).

The key materials compatibility issues for all four options are given in Table I.B.1. Although materials experts involved in the study predict reasonable confidence of compatibility without coatings at the suggested operating temperatures, beryllium/steel and beryllium self-welding issues were considered to be sufficiently important that experimental verification of their extent was undertaken (see Section III.A). If compatibility issues are judged to be sufficiently important, coating one or more of the steel structures, beryllium pebbles, or thorium pebbles would be considered.

Table I.B.1 Key materials compatibility issues investigated during the scoping phase

	Issue	Applicable Blanket Options	Specifications*
1.	Extent of steel/beryllium reactions (both solid-solid and beryllium transport in sodium and lithium)	1,2,3,4	With and without oxide coatings. Ferritic and stainless steels
2.	Self welding of beryllium pebbles in lithium and sodium	1,2,3,4	With and without oxide coatings
3.	Extent of beryllium/thorium reactions ($Th + Be \rightarrow Th_xBe_y$)	1,3	Consider oxides
4.	Same as 3 for beryllium/UO_2 ($UO_2 + 15\ Be \rightarrow UBe_{13} + 2\ BeO$)	2	
5.	Same as 3 for beryllium/UC	4	
6.	Ability of oxides to exist in liquid lithium	3,4	Consider BeO, ThO_2, UO_2
7.	Tritium/thorium reactions and diffusion	3,4	Consider ThO_2 depending upon results of 6
8.	Beryllium recoil into steel		Same as 1 above

*Temperature range is 360-530 ^{o}C in all cases.

Proposed coatings include aluminides, oxides, carbides, nitrides, and metals such as molybdenum, niobium, and zirconium. Coating techniques could include plasma spraying, ion implantation, magnetron sputtering, and the use of sacrificial layers.

Comparing direct-cooled options 3 and 4 with options 1 and 2, the principal difference relates to the coolant flow. Instead of cooling via internal pipes, options 3 and 4, the "direct cooling" options, feature a possibly simpler scheme in which coolant flows directly through the bed. For example, the configuration which was studied routes the coolant from the inlet duct to a first-wall cooling plenum, through an inner radial flow baffle into the bed, out of the bed and into an exit plenum through an outer radial flow baffle, and out the exit pipes. This type of design, which in some respects resembles an automotive oil filter, could allow larger pebbles than the internal pipe design since piping within the bed is eliminated. Considering the direct-cooled options, the following issues arise:

- MHD-induced effects on heat transfer and pressure drop through a packed bed of larger beryllium and thorium pebbles
- Lithium replacement of sodium as the packed bed heat transfer fluid with consequent impacts on compatibility and coupling to the heat exchanger
- Tritium is introduced into the fertile breeding region

Despite the new concerns, these concepts have potential to provide a less complex design and improved breeding performance due to reduced structure (provided that the MHD pressure drop through the bed is not prohibitive). Several issues for the direct-cooled designs are similar to those for the pipe-cooled designs. These include: lithium vs. lead-lithium, $\sim 500\ ^{o}C$ temperature limit, stainless vs. ferritic steel, pebble packing and flow, and materials compatibility issues. During the scoping phase MHD and compatibility were emphasized as key feasibility issues. To address the MHD effects, a conservative analytical model is required. Information regarding the two key compatibility issues which are unique to options 3 and 4 (i.e., tritium/thorium interactions and the ability of BeO and ThO_2 to survive in lithium) was sought.

I.B.4 Selection of a Reference Blanket Concept

The reference blanket concept chosen was the cooling concept with thorium

metal fuel (option 3). To arrive at this choice, two key decisions were made independently. The first concerns the choice of a uranium or thorium fuel form. This choice primarily resulted from systems and economics trade studies which considered breeding performance, the LWR client performance and fuel cycle cost, technology development requirements, and institutional issues.[11] Other secondary issues which factored into this decision were compatibility issues and issues relating to afterheat safety. In particular, the 2.3-day decay half-life associated with ^{239}Np decay to ^{239}Pu is a possible advantage relative to the 27-day half-life associated with ^{233}Pa decay to ^{233}U.

The second key decision involved the coolant configuration: internal pipes or direct cooling? The comparative evaluation of the pipe and direct cooling alternatives is summarized in Table I.B.2, however, it is clear that all areas should not be equally weighted. Among all of the areas of consideration, three stand out:

- Design flexibility
- Overall confidence in the design
- Projected performance

In all probability, the projected performance for both blankets would be adequate and similar. Therefore, no choice was made on this basis.

The materials compatibility issues, MHD pressure drop for direct cooling, and pebble flow and packing for pipe cooling represented the largest unknowns for the two cooling alternatives. These issues were not resolved prior to our choice of a reference concept, but there is considerable confidence that the materials and MHD issues can be favorably resolved. Since the direct cooling alternative provided more flexibility with respect to operating temperatures and is amenable to the development of a large, low density or composite pebble, direct cooling was recommended for further study during the reference blanket design phase.

Pending a resolution of the fuel management and compatibility issues for pipe cooling, this option was deselected for the FY82 study. However, if future results indicate that a viable fuel management option providing adequate thorium/beryllium mixing is identified, the pipe cooling option would be favored because its materials compatibility characteristics are considered to be more favorable. A modest experimental program is required to resolve these issues.

Table I.B.2 Summary of Comparative Evaluations

Key Area	Preferences		
	Pipes	Indifferent	Direct
Fluid mechanics/heat transfer			X
Mechanical design and maintenance		X	
Fuel management/fuel cycle			X
Material compatibility		X	
Irradiation damage		X	
Nuclear performance		X	
Tritium control and processing	X		
BOP and availability	X		
Safety	X		

References, Section I.B

1. J. A. Maniscalco, et al., "Recent Progress in Fusion-Fission Hybrid Reactor Design Studies," Nuclear Technology/Fusion, 1, 4, 419 (1981).

2. I. Maya, et al., "Safety Evaluation of Hybrid Blanket Concepts," General Atomic Company, GA-A160101 (1980).

3. J. D. Lee, "The Beryllium/Molten Salt Blanket," Lawrence Livermore National Laboratory, UCRL-82663 (1979); also published in Proc. of 3rd US/USSR Symp. on Fusion-Fission, Princeton, NJ (Jan. 1979).

4. R. W. Moir, Ed., "Tandem Mirror Hybrid Reactor Design Study," Lawrence Livermore National Laboratory, UCID-18808 (1980).

5. J. D. Lee, Ed., "Feasibility Study of a Fission Suppressed Tandem Mirror Hybrid Reactor," Lawrence Livermore National Laboratory, UCID-19327 (1982).

6. R. W. Moir, et al., "Fusion Breeder Program Interim Report, December 1981 - February 1982," Lawrence Livermore National Laboratory, UCID-19406-1 (June 1982).

7. J. DeVan, Oak Ridge National Laboratory, personal communication (1981).

8. N. Ghoniem and R. Conn, "Assessment of Ferritic Steels for Steady State Fusion Reactors," Proc. IAEA Tech. Comm. Meeting on Fusion Tech., Tokyo, Japan (1981); also published as UCLA Rept. PPG-587 (1981).

I.C. FUSION DRIVER DESIGN BASIS

I.C.1 Plasma Engineering Basis

The fusion driver for the 1982 Tandem Mirror Hybrid Reactor (TMHR) is the tandem mirror utilizing electron thermal barriers, and the "axicell" end plug configuration. Figure I.C.1 shows an isometric view of the end cell.

The thermal barriers for electrons are created with the electron cyclotron resonance heating (ECRH or ECH) launched by the quasi-optical microwave system, the potential peak which confines central cell ions is produced by the ECRH launching system further outboard in the barrier region. Neutral beams which fuel the sloshing ions are injected just outboard of the inner peak of the yin-yang. These sloshing ions provide microstability of the yin-yang plasma, which in turn provides pressure in regions of good curvature to make the entire system MHD stable. To keep the potential and density low in the transition region between the axicell and the yin-yang, a neutral beam which is intended to remove trapped particles by charge exchange is injected. The high density axicell plasma is produced by neutral beams*, and serves the purpose of attenuating the central cell ions passing into the transition and thermal barrier regions. The power to produce this axicell plasma plus the extra copper coil power is less than the power it saves by reducing the end cell density, thereby making it worthwhile to have an axicell.

The magnetic field strengths produced by the axicell are high. The outer mirror of the axicell needs to produce an on-axis field strength of 15-20 T, the field produced by the inner mirror is only slightly lower. Attaining these field strengths is accomplished by coils which are multilayered, consisting of NbTi, Nb_3Sn, and normal conducting copper. The copper comprises the innermost layers and provides fields above 12 T, the B-field limit for a Nb_3Sn conductor conservatively cooled by HeI**. The design of 24 T coils similar to these is being pursued as part of the Mirror Advanced Reactor Study (MARS)[1] by General Dynamics. The lower fields needed for the

*There is currently interest to replace the neutral beams with ICRH heating, as shown in the figure.

**Using superfluid HeII, the maximum conductor field strength that can be produced with Nb_3Sn is about 15 T.

FIGURE I.C-1 **FUSION BREEDER AXI-CELL CONFIGURATION**

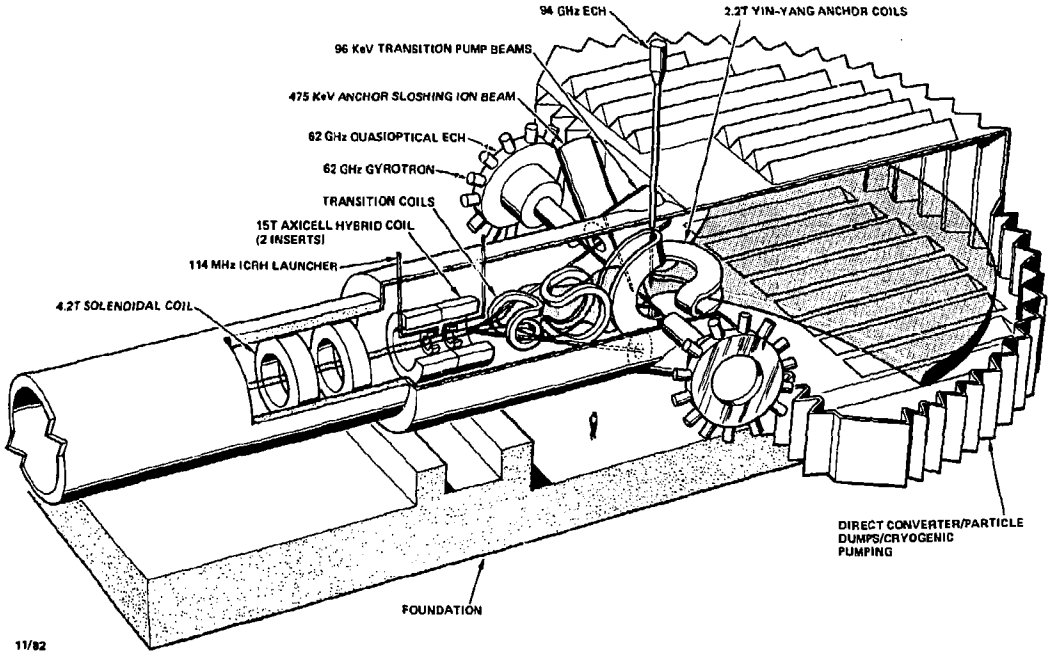

11/82

the fusion breeder axicell represent a relaxation of technological requirements compared to fusion applications. The lower fields are acceptable because lower Q at the same wall loading is acceptable for the hybrid. The low wall loading for the hybrid ($\sim$ 1.3 MW/m^2) can result in a higher Q than that of MARS, even with the lower magnet technology. The area in which the hybrid may suffer compared to MARS is that the end cell and central cell coil sets have to be larger and more costly (but of lower technology).

Table I.C.1 lists the physical characteristics of an optimized (20 T) fusion breeder configuration (see Chapters IV and VIII for comparison with the 15 T baseline). The end cell has changed somewhat in basic configuration from that described in earlier studies. The change was in response to the discovery[2] that an instability with a large growth rate will occur unless a minimum fraction of ions can pass freely into the yin-yang "anchor" region where they can sample "good curvature." This type of instability is classified a "trapped particle mode". The resulting stability criterion requires us to move the ion confining potential peak from the axicell out to the yin-yang. This minimum fraction of passing density for stability directly opposes the desirability to increase Q because lower passing ion density translates to higher Q operation. The lowest minimum passing density fraction occurs at small central cell plasma radius, high central cell magnetic field, and high central cell plasma density. In comparison with our 1981 study, the central cell magnetic field went up from last year's 3T to 3.66T, the plasma radius decreased from 1.04 meters to 0.58 meters and the density increased from 1.6 x 10^{14} cm^{-3} to 2.5 x 10^{14} cm^{-3}. The increased central cell magnetic field makes blanket design more difficult because the increased MHD pressure (which scales as B^2) which is induced by the liquid metal flowing across field lines can decrease breeding performance. Elsewhere in this report the reference central cell magnetic field is quoted as 4.2T. This number was based on a physics case which had a large margin of safety in the stability of trapped particle modes, as well as an under-utilization of the 1.5 meter radius vacuum chamber. The blanket design, based on 4.2T, is preserved in the case on Table I.C.1 by keeping the product of blanket energy multiplication, wall loading, and the square of the central cell magnetic field constant. The specific central cell field strength and length was chosen to satisfy this constraint along with the trapped particle constraint. The details of this process is outlined in Chapter IV.

Higher plasma pressure in the transition region requires that we use a

Table I.C.1 Parameters for the Baseline TMHR Case

Parameter	Value
Central Cell	
Fraction of thermalized alpha particles, $C_\alpha = n_\alpha/n_c$	0.1
DT Ion Density, n_c (cm^{-3})	2.5×10^{14}
Ion Temperature, T_c (keV)	35
Electron Temperature, T_{ec} (keV)	29
Plasma Radius, r_{cc} (cm)	57.7
Vacuum Magnetic Field, $B_{c,vac}$ (T)	3.66
Beta, β_c	0.7
Floating Potential, ϕ_e (keV)	205
Cold Fueling Current, I_c (k amps)	1.37
Ion Confinement Parameter, $(n\tau)_i$ (sec cm^{-3})	5.67×10^{14}
Electron Confinement Parameter, $(n\tau)_e$ (sec cm^{-3})	6.67×10^{14}
First Wall Radius (cm)	150
Central Cell Length (m)	193
Axicell	
ICRH Heated Species	T
Total Density (cm^{-3})	7.84×10^{14}
Hot Ion Density (cm^{-3})	6.65×10^{14}
Hot Ion Energy (keV)	300
Plasma Radius, r_x (cm)	27
Axicell Length, L_x (m)	2
Axicell beta, β_x	0.4
Hot Ion Confinement $(n\tau)_H$ (cm^3/sec)	7.8×10^{13}

Table I.C.1 (Continued)

Parameter	Value
Potential Bump Height, $\Delta\phi_{pc}$ (keV)	27.7
Inner Mirror, B_{x1} (T)	17.5
Midplane Vacuum Field, B_{x2} (T)	14.42
Outer Mirror, B_{x3} (T)	20
Transition Region	
Length, L_t (m)	12
Vacuum Field at Midplane, $B_{vac,t}$ (T)	1.6
β_t	0.103
MEPB Injection Energy, E_{pump} (keV)	84
Pump Beam Injection Angle, $\theta_{MEPB,(deg)}$	25
Passing DT Density at Midplane, $n_{pass,t}$ (cm^{-3})	3.6×10^{12}
Plug/Barrier/Anchor	
Vacuum Field at Barrier Midplane, $B_{vac,b}$ (T)	2.27
β_b	0.65
Passing DT Density at Midplane, $n_{pass,b}$ (cm^{-3})	2.65×10^{12}
Hot Electron Energy, E_{eh} (keV)	737
Warm Electron Temperature, T_{ew} (keV)	75
Cold Electron Density Fraction, F_{ec}	7.7×10^{-3}
Mirror to Mirror Length, L_b (m)	7
Inner Yin-Yang Mirror, B_{Ai} (T)	6
Outer Yin-Yang Mirror, B_{Ao} (T)	6
Sloshing Ion Injection Energy, $E_{inj,A}$ (keV)	475
ECRH Frequency at pt. "b" (hot electrons) (GHz)	75
ECRH Frequency at pt. "a" (warm electrons) (GHz)	74
Barrier Potential Dip, ϕ_b (keV)	211
Ion Confining Potential, ϕ_c (keV)	151

Table I.C.1 (Continued)

Plasma Power Balance	Value		
	Trapped		Incident
Axicell ICRH Power, $P_{nb,x}$ (MW)	33.6		39.53
Anchor Sloshing Beam Power, P_{slosh} (MW)	11.3		29
ECRH Power to Hot Electrons, $P_{ech,b}$ (MW)	47 9		47.9
ECRH Power to Warm Electrons, $P_{ech,a}$ (MW)	0.62		0.62
Pumping Power in Transition and Barrier, P_{pump} (MW)	63.7		64.1
Fusion Power, P_{fus} (MW)		3000	
End Cell Fusion Power (MW)		130	
Neutron Wall Loading (MW/m^2)		1.31	
Plasma Q (P_{fus}/P_{inj})	19.1		16.6
η^*Q		8.3	

* The power generation efficiency, η, is taken to be 50% in all cases.

charge exchange pump beam to help keep the trapped contribution to this pressure at as low a level as possible. The extra power which is required to do this tends to degrade performance.

Table I.C.2 summarizes the power, energy, and frequency requirements for this year's optimized driver design and compares them to what was required last year. The power flow bottom line, Q, is actually higher than last year, although we are taking a penalty in a lower wall loading (1.3 versus 2) longer central all length (193 m versus 130 m.) This illustrates that adherence to the trapped particle stability criterion does indeed reduce the performance, but not prohibitively so. Indeed, for the case with the same wall loading as last year the Q was found to be 11. The power and technology requirements for that case are shown on the third column of Table I.C.2. Note, from Table I.C.2, that the distribution of the powers, particularly between beams and ECRH, is quite different in this year's case compared to last year's. This is a result of upgrading the formulae used to compute the separate powers to reflect the latest information gleaned from Fokker-Planck codes.

The beam energies, especially that of the sloshing beam, have increased since last year. For the sloshing beam, the larger energy (475 keV versus 150-250 keV) is required because its injection point has been shifted from the outer turning point of the sloshing ions to the inner turning point. In order for a sloshing ion to be confined at its outer turning point, where the plasma potential is higher, its injection energy must be greater than the desired energy for confinement at the outer turning point (by the potential difference between these two points). This amounts to around 200 keV for the optimized case. This makes a 250 keV injected ion from last year's design have about the same confinement properties as a 475 keV ion this year. The ECRH frequencies have also increased since last year by roughly 30% but are still within the frequency ranges outlined in the Fusion Component Development Plan.[3]

I.C.2 Driver Technologies

As was the case last year, the TMHR will require high energy neutral beams, ECRH power in megawatt tube sizes, superconducting magnets, layered superconductor/copper "hybrid" magnets, direct conversion technology, and vacuum pumping technology. Each of these technologies (except the hybrid magnets) at the required level of sophistication, will be available in the required timeframe, according to the Fusion Component Development Plan.[3] A

Table I.C.2

Power* and Technology Requirements for Three Fusion Breeder Drivers

	'81 Driver	'82 Driver	'82 TMHR with '81 wall loading
Axicell Sloshing Power (MW)	17 @ 250 keV	N.A.	N.A.
Anchor Sloshing Power (MW)	6.4 @ 150 keV	11 @ 475 keV @ 152 MHz	14.3 @ 475 keV @ 152 MHz
Axicell ICRH/Beam Power (MW)	N.A.	33.6 or @ 300 keV	33.9 or @ 300 keV
Charge Exchange Pump Power (MW)	120 @ 120 keV	63.7 @ 96 keV	148 @ 97 keV
ECRH Power Applied to Barrier (MW)	27 @ 62 GHz	48 @ 75 GHz	72.4 @ 75 GHz
ECRH Power Applied to Potential Peak (MW)	26 @ 57 Ghz	0.6 @ 74 GHz	2.04 @ 74 GHz
Plasma Q value (= $P_{fus}/P_{inj,abs}$)	15.3	19.1	11.0
Neutron Wall Loading (MW/m^2)	2 @ 1.5 m	1.32 @ 1.5 m	2 @ 1.5 m
Maximum Magnetic Field Strength (T)	20	20	20

*Powers shown are those absorbed in plasma.

development plan is necessary to develop the high field hybrid magnets. The driver technologies for the TMHR were described in more detail in Chapter III of last year's study.[4] The interested reader is urged to consult this chapter for more detail.

References, Section I.C.

1. "Mirror Advanced Reactor Study (MARS) Interim Design Report," Lawrence Livermore National Laboratory, UCRL-53333 (1982).

2. M. N. Rosenbluth, H. L. Berk, D. E. Baldwin, H. V. Wong and T. M. Antonsen, "Fast Growing Trapped Particle Modes in Tandem Mirrors," paper 3A2, Sherwood Theory Meeting, Santa Fe, NM, April 1982.

3. "Fusion Engineering Development Plan," prepared by Division of Development and Technology, Office of Fusion Energy, U.S. Department of Energy (1982).

4. J. D. Lee, et al., "Feasibility Study of a Fission-Suppressed Tandem Mirror Hybrid Reactor," Lawrence Livermore National Laboratory, UCID-19327 (1982).

CHAPTER II

REFERENCE BLANKET DESIGN

II.A. REFERENCE BLANKET OVERVIEW

The reference fusion breeder blanket design is presented in this chapter. Section II.A provides a design overivew while sections II.B through II.E describe the design of mechanical, nuclear, thermal-hydraulic, and maintenance systems. Other design information relating to the reference blanket may be found in Chapters III through V.

II.A.1 Design Overview

After an extensive scoping phase(1), a reference blanket concept based upon the use of a liquid lithium coolant flowing radially through a two zone packed bed of composite beryllium/thorium pebbles was selected. The design shown in Figure II.A.1, uses a ferritic steel (i.e., HT-9 or similar) structure and operates in the 350-500°C temperature range. In this concept, the coolant flow resembles that of a conventional oil filter. Specifically, the coolant flows to the first wall plenum through a thin coolant annulus and is distributed to the packed bed through perforations in a corrugated intermediate wall which, in combination with a corrugated first wall and radial stiffeners (tied to the back of the blanket), provides structural support.

The coolant flows radially outward through two fuel zones (separated by another perforated wall), exits the bed through a third perforated wall outside of the second fuel zone, and exits the blanket through 20 large outlet pipes. The composite fuel pebbles (beryllium pebbles with thorium snap-rings) are loaded into the top of the blanket and discharged at the bottom in a frequent batch process (i.e., fuel residence time ~ 3-6 months as described in Section IV.A).

The reference blanket concept offers several potentially attractive design and performance features:

- high breeding performance per unit of thermal power production
- low decay afterheat and excellent provision for cooling in the event of a loss of coolant or coolant flow accident

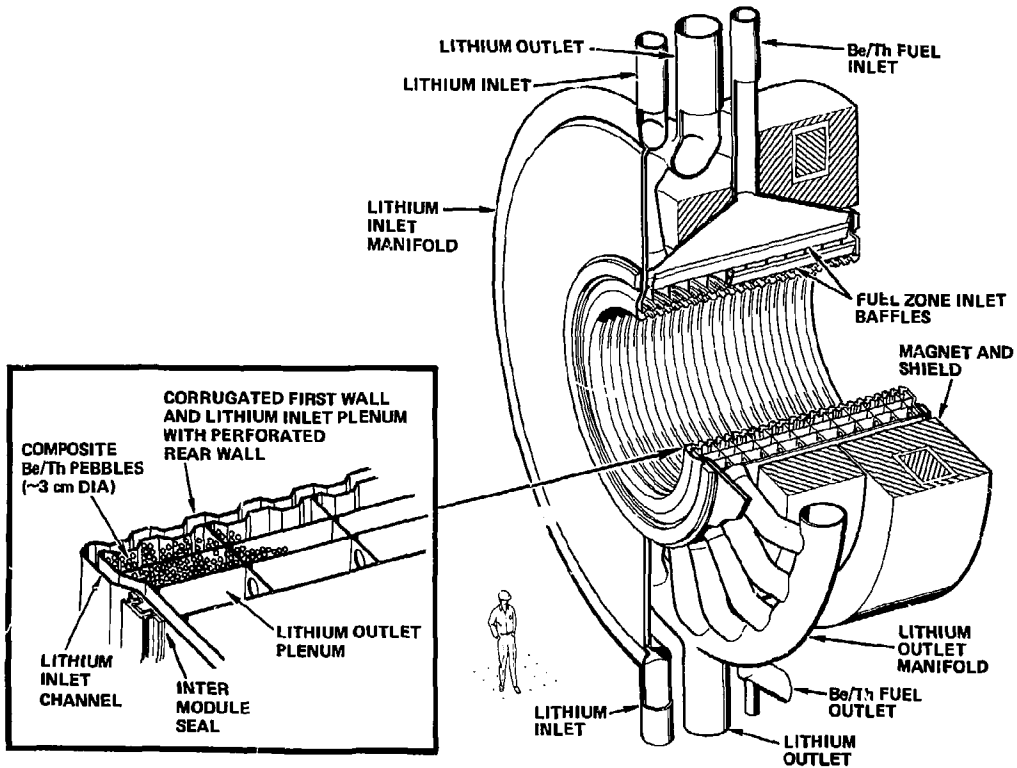

Figure II.A.1 Reference Tandem Mirror Fusion Breeder Blanket

- a beryllium multiplier form which can be easily fabricated and readily recycled, and
- the extensive use of conventional materials and coolant technologies.

These features are described in more detail below.

The breeding performance is excellent for two reasons. First, the design features a high volume fraction of high efficiency neutron multipliers. The bed volume fractions in Figure II.A.1 include about 55% beryllium, 40% lithium, and 3% thorium -- all excellent neutron multipliers. The remainder of the fuel region following the two corrugated walls is less than 2% steel. Second, the design effectively suppresses the fissioning in the blanket (< 0.04 fission per fusion neutron at 0.5% ^{233}U concentration in thorium). Fast fissions are suppressed due to neutron moderation in the beryllium and low thorium volume fraction. Thermal and epithermal fissions in the bed ^{233}U are suppressed due to fuel discharge at low concentration ($\lesssim$1%) in the small volume of thorium as well as thermal neutron depletion due to the large 1/V neutron absorption cross section of the ^{6}Li in the liquid lithium coolant.

As a result of the low fission rate, the fission product inventories and decay afterheat levels in the fuel are very low. In fact, the fission product decay afterheat is a relatively minor contribution to the total afterheat and the afterheat associated with actinide decay through the chain

$$n + {}^{232}Th \rightarrow {}^{233}Th \xrightarrow[23\ m]{\beta^-} {}^{233}Pa \xrightarrow[27\ d]{\beta^-} {}^{233}U$$

dominates the overall afterheat level. Typical fission product levels in the discharge fuel are only about 1000 ppm in thorium, or roughly 1/60 that of LWR discharge fuel. These advantages are uniquely associated with fission suppressed blankets since fast fission blankets, with blanket energy multiplications of 6-10, increase the fission rate by factors of 10-20.

Additional reactor safety benefits for the reference design result from the use of a mobile fuel form (i.e., the composite beryllium/thorium pebbles) with provision to discharge the fuel to an independently cooled dump tank should the need arise. In addition to the primary coolant loop and the dump tank loop, the fuel handling sytem piping and valving provides a coolant flow

sufficient to remove the decay afterheat. Therefore, double redundancy of the cooling systems is provided in the event of a loss of coolant or loss of coolant flow accident.

The composite beryllium/thorium pebble fuel form employed in the reference design provides several advantages in comparison with previous designs(1,2,3). First, this form provides a relatively simple method to achieve uniform mixing of the beryllium and thorium throughout the blanket - an advantage with respect to the thermal and nuclear breeding performance. Second, the design is relatively insensitive to the high rate of volumetric swelling in beryllium since the beryllium is discharged frequently and the packing density of the bed, although high, is low enough to accommodate some growth (typically 0.2% linear growth occurs over a 90 day irradiation). Finally, the small size of the pebbles (1.5 cm radius) limits the thermal and differential swelling induced stress levels in the beryllium - key lifetime determinates (see Section III.C). Our results indicate that an average beryllium in-core lifetime in excess of two years should be easily achievable, but that more materials data and more accurate models are required before a more definitive lifetime estimate will be possible. The reference blanket provides a flexible design which can accommodate a wide variation in the irradiated properties of beryllium without imposing a substantial penalty on the overall level of performance.

Finally the reference design utilizes conventional and well known materials and coolant technologies. Our selection of ferritic steels was based upon their irradiated and un-irradiated materials properties (e.g., high strength, high thermal conductivity, low neutron swelling, excellent liquid metal compatability) as well as the extensive industrial experience in the fabrication of components from ferritics (principally 2-1/4 Cr-1Mo) and the current interest of the nuclear materials community in these alloys(4,5).

Our choice of liquid lithium as the blanket coolant primarily derived from nuclear, heat transfer, and tritium extraction advantages(6,7,8), but also considered the operational and safety implications of liquid lithium versus the obvious alternative, $Li_{.7}Pb_{83}$ (1). It is our considered opinion that liquid lithium systems can be designed to operate more economically and more reliably than lead-lithium systems and will have the advantage of lower normal tritium releases. An acceptable level of lithium safety appears to be achievable based upon the development of liquid sodium coolant safety systems in the

LMFBR program. The recognition that fusion breeder reactors would not, most likely, be sited near population centers (but, rather, in remote safeguarded fuel cycle centers) provides additional confidence in the choice of a liquid lithium coolant.

Our choice of thorium metal as a fertile fuel form rather than thorium dioxide (thoria) or another thorium form is primarily based upon fuel cycle considerations. Although thorium oxide would provide fewer compatability concerns, thorium metal is less expensive to reprocess (Either aqueous or pyrochemical) and is more amenable to the selected fuel form (Section III.C). There is considerable experience in the use of thorium metal in fission reactors(9).

A list of reference design parameters is provided in Section II.A.2 and a discussion of outstanding blanket design issues is presented in Section II.A.2.

II.A.2 Blanket Design and Performance Overview

Table II.A.1 is an overview of several key design and performance parameters for the reference fusion breeder blanket. These parameters are discussed in more detail throughout this chapter. Additional information relating to the reference fusion breeder is presented elsewhere in this report.

II.A.3 Overview of Blanket Design Issues

The reference blanket performance is attractive and our analysis indicate overall feasibility. Nevertheless, during the course of the study, several issues require additional analysis, experimental data acquisition and/or component development and testing were identified. These issues are listed in Table II.A.2. Although the actual impact of the resolution of any issue is, to a large extent, unknown prior to the resolution of that issue, an attempt has been made to prioritize the issues in decreasing importance as they relate to design feasibility, blanket performance, and development/testing requirements. These issues are briefly described below.

TABLE II.A.1. Key Design and Performance Parameters for the Reference Blanket

Central Cell Parameters	
Central Cell Fusion Power[a]	3000 MW
Central Cell Fusion Neutron Power[b]	2400 MW
Maximum Central Cell Thermal Power[c]	4728 MW
Average Central Cell Thermal Power[d]	3864 MW
^{233}U Fuel Production[e]	5625 Kg/yr
Central Cell Length[f]	200 m
Number of Blanket Modules	50
Number of Central Cell Coils	50
Central Cell Coil B Field Strength on Axis	4.2 T
Blanket Module Mechnical Design	
Structural Material[g]	HT-9 Ferritic Steel
Module Length	4 m
Inter-module vacuum seal arrangement	metal omega seal
Fraction of module length used for multiplier/ fuel zones[h]	~ 95%
First Wall Radius	1.5 m
Number of Multiplier/Fuel Zones	Two
Multiplier/Fuel Zone Volume Fractions[i]	
Beryllium	55%
Lithium (0.2 a/o ^{6}Li)	40%
Thorium (incl. bred fissile)	3%
Ferritic Steel	2%
Thickness of Each Fuel Zone[j]	20 cm
Lithium Reflector Thickness[k]	30 cm
Blanket Outer Radius	2.34 m
Shield Thickness	75 cm
Magnet Inner Bore	6.7 m
Magnet Pitch	4 m
Number of Coolant Outlet Pipes	20 each

Table II.A.1 (Continued)

Heat Transfer, Power Flow, and Thermal Design Parameters	
Neutron Wall Loading	1.27 MW/m^2
Coolant[l]	liquid lithium
Maximum Thermal Power Per Blanket Module	94 MW
Coolant Inlet Temperature[m]	340°C
Coolant Outlet Temperature[n]	490°C
Lithium Flow Rate	0.31 m^3/sec
Lithium Pressure Drop[o]	~ 2 MPa (~300 PSI)
Lithium Pump Power (all modules)	~ 35 MW
First Wall Pressure[o]	~ 1.7 MPa (~250 PSI)
Minimum First Wall Temperature[p]	361°C
Maximum First Wall Temperature[q]	409°C
Maximum Structure Temperature[r]	490°C
Maximum Beryllium Surface Temperature[s]	475°C
Maximum Beryllium Internal Temperature[s]	< 483°C
Maximum Beryllium ΔT[s]	< 38°C

Nuclear Design Parameters	
Net Fissile Breeding Ratio[t]	0.62
Net Tritium Breeding Ratio[u]	1.06
Minimum Blanket Energy Multiplication[v]	1.25
Maximum Blanket Energy Multiplication[w]	1.97
Maximum Thorium Power Density[w]	182 $/cm^3$
Maximum Beryllium Power Density[w]	5.4 w/cm^3
Maximum Lithium Power Density[w]	3.3 w/cm^3
Maximum Average Power Density[w]	7.7 w/cm^3
Zone 1 Fuel Residence Time[j]	78.3 days
Zone 1 Uranium Discharge Concentration	.856%
Zone 1 Protactinium Discharge Concentration	.532%
Zone 2 Fuel Residence Time[x]	156.6 days
Zone 2 Uranium Discharge Concentration	.739%
Zone 2 Protactinium Discharge Concentration	.195%
Average Fission Rate Per Fusion[x]	~ 0.04
Average Fission burnup at Fuel Discharge[w]	~ 500 MWD/MT

Table II.A.1 (Continued)

a) all quantities normalized to central cell fusion power (3000 MW). End cell fusion power = 140 MW.

b) Charged particle and radiation power (~ 850 MW) primarily deposited in end cells on direct converter and electron dump, but ~ 40 MW of radiation surface heat load appears on first wall ($0.018\ MW/m^2$).

c) Corresponds to maximum blanket energy multiplication of 1.97.

d) Corresponds to average over-cycle blanket energy multiplication of 1.61.

e) At 70% plant average capacity factor and fissile breeding ratio = 0.62 per fusion.

f) Shorter central cells also possible as discussed in Chapters IV and VIII.

g) Or similar low nickel ferritic (e.g., 2-1/4 Cr-1Mo). Design stress ~ 16 KSI.

h) Remaining ~ 5% used for module side walls and inlet coolant duct.

i) Assumes 59% packing of beryllium/thorium pebbles in the 98% of volume not occupied by structure.

j) Zone 1 recycled twice as often as Zone 2.

k) Reflector is also the lithium outlet annulus.

l) 0.2% a/o ^6Li.

Table II.A.1 (Continued)

m) Lowest temperature to avoid loss of ductility (DBTT) during irradiation.

n) Highest temperature to provide confidence in corrosion/ compatability characteristics.

o) Approximate values based upon existing modeling capability.

p) Coolant interface at left side first wall inlet.

q) Plasma inside interface at right side of first wall.

r) At rear of blanket

s) Estimate requires more detailed model

t) Adjusted for multidimensional and heterogenious effects

u) This quantity is net for the blanket. The reactor net tritium breeding is 1.01 after correcting for tritium to sustain the additional 140 MW of fusion in the end plugs (no blanket).

v) Beginning of cycle - no fissile material

w) End of cycle- prior to Zone 1 and Zone 2 fuel discharge.

x) Average over time and blanket volume

TABLE II.A.2 Reference Blanket Design Feasibility, Performance, and Development/Testing Issues

Issues Which Directly Impact Blanket Design Feasibility

- Blanket Material Compatibility
- Beryllium Pebble Lifetime

Issues Which Strongly Effect Blanket Performance

- Liquid Metal (MHD) Pressure Drop
- Beryllium Neutron Multiplication
- First Wall Lifetime
- Heterogenious Nuclear Effects

Issues Which Require Hardware Development and/or Testing and have Significant Impact on Performance and/or Cost

- Beryllium/Thorium Composite Pebble Fabrication
- Composite Pebble and Thorium Fuel Handling Systems
- HT-9 Fabrication and Heat Treatment
- Electrically Insulated Coolant Duct Development
- Pyrochemical Thorium Metal Fuel Reprocessing
- Lithium Safety Systems Development and Integration
- Molten Salt Extraction Process for Tritium Removal from Liquid Lithium
- Tritium Permeation Control Technologies
- Remote Maintenance and Inter-module Seal Technologies

II.A.3.a Design Issues Which Directly Impact Feasibility

Any compatibility assessment of the present fusion breeder blanket design concept is complicated by the number of blanket components. To address these issues, a large matrix of materials compatibility concerns were considered during the course of the study (see Section III.B). In several cases capsule experiments were performed (see Section III.A). Among the possible interactions, solid-solid interactions include self-welding of the thorium and beryllium (in the presence of lithium), the inter-alloying of thorium and beryllium, and the inter-alloying of beryllium and the structural steel. Of highest priority are the self-welding reactions, because they will determine whether barrier coatings must be applied to the pebbles to guarantee their removability. Possible coatings for the thorium metal are ThO_2, ThC, or TiC. Possible coatings for the beryllium metal are $Be_{12}Fe$, or $Be_{12}Cr$, or $Be_{12}Mo$. Next in priority are the possible reactions of beryllium with thorium. The same coating candidates listed above could also be used to reduce the extent of the latter reaction. Last in priority are the reactions between beryllium and HT-9, which preliminary experiments have shown to be slow at 450°C.

In order of priority, the most critical liquid-solid compatibility issue is the rate of thermal gradient mass transfer of HT-9 and beryllium in lithium at the reference reactor operating temperatures. Tests are currently underway to evaluate this potential problem, although, in the case of beryllium, truly definitive studies will not be possible until it is determined what, if any, coatings will be applied to the beryllium. These tests will also define the potential for carbon transport by the lithium.

The beryllium pebble lifetime is determined by the thermal and irradiation swelling induced stress levels in the beryllium and the irradiation time required to degrade the mechanical properties of the beryllium such that the yield stress would be exceeded. Although this problem is considered in Section III.C, and a several year average lifetime is predicted, improved analysis of the stress levels in the beryllium is required. Such an analysis should consider the differential swelling stress, the thermal stress (a multi-dimensional problem), the bearing stress exerted by adjacent pebbles, and any transient stress due to pebble dropping, etc. In addition, the mechanical properties of the sintered beryllium product require further definition,

especially in the flux/temperature environment of the reference blanket (see Section III.C for experimental data from EBR-II irradiation). An optimization to achieve the maximum lifetime will ultimately be required.

II.A.3.b Design Issues Which Strongly Affect Blanket Performance

The pressure drop associated with pumping liquid lithium through the packed bed and complex flow path associated with the reference blanket is quite uncertain (see Section II.D). In particular, an adequate model of the magnetic field induced (MHD) pressure drop for packed bed flow (as well as turns, baffles, orifices, etc.) does not currently exist. We believe that our estimate of an ~ 250 PSI pressure at the first wall is reasonable (and possibly conservative), but a smaller scale experimental verification is required. The MHD interaction impacts the overall design in several ways. Most importantly, by determining the structure fraction in the blanket, the MHD pressure drop directly affects the fissile fuel breeding performance and limits the neutron wall loading (i.e., the pressure drop is directly proportional to the coolant velocity which, in turn, is proportional to the wall loading).

Although beryllium is clearly the best non-fissioning neutron multiplier, reported integral experiments and comparisons with neutron transport calculations(2,10,11) have cast some doubt on the adequacy of current nuclear data and calculational methods. A specific concern is the angular and energy distribution of secondary (n,2n) neutrons as modeled in the evaluated nuclear data files and utilized in discrete ordinates and Monte Carlo transportation codes. Our most recent consideration of this issue(11) indicates that the ENDL data file(12) and the TARTNP Monte Carlo code(13) used in our analysis provide an ~ 10% uncertainty in fissile breeding. Despite this encouraging result, more work (and possibly an experiment) is required to reduce and/or confirm the breeding uncertainty.

Another nuclear issue concerns the effects of spatial heterogenity in the blanket (see Section II.C). Our preliminary modeling indicates a loss of ~ 5% in total breeding (i.e., tritium plus fissile) and a gain of ~ 25% in the end-of-cycle blanket energy production. These effects are particularly difficult to model in the complex source driver geometry of the fusion breeder blanket.

An explicity finite model of the blanket including the first wall/intermediate wall zone followed by a packed bed of individual beryllium/thorium pebbles is currently under development.

An adequate prediction of the lifetime of the blanket structure (and specifically the first wall) requires the integration of detailed stress and thermal models with consideration of many non-nuclear and irradiation dependent materials effects:

- neutron swelling
- irradiation creep
- irradiation induced embrittlement
- thermal creep
- alloy manufacturing control
- temperature/time/fluence related metalurgical phase transitions

The problem is complicated by the complex configuration of the blanket structure (requiring multi-dimensional stress and thermal models) and by the time dependent nature of the problem. Specifically, the properties of the materials vary in time with irradiation (as well as the amount of thermal and mechanical cycling) and the stress levels also evolve as a function of time due to deformations which occur during previous intervals. Since failure is likely to occur in a weld (or possibly due to grain boundary attack by corrosive products) any modeling of the structural evolution must be subject to an experimental confirmation which models the real environment as closely as possible.

In the reference design we have selected a strong, low swelling structural material (HT-9) and a low wall loading (~ 1.3 MW/m^2). An integrated lifetime of about ten calendar years (~ 10 MW-yr/m^2) seems reasonable based upon our initial calculations (see Section III.B). More detailed analysis is desirable in the absence of integrated testing.

II.A.3.c Design Issues Which Require Hardware Development and/or Testing

Several important reactor and fuel cycle technologies which are required and/or desirable for economical and reliable operation of the reference blanket require significant development.

One such technology is the remoted and automated manufacturing line for the beryllium pebbles. The proposed process (see Section VII.B) utilizes cold press, vacuum sinter, hot forge, and vacuum anneal steps to produce pebbles in a manner similar to a process used to manufacture aircraft brake parts. The two key development items are the development of a free flowing beryllium powder (to further automate the process) and the development of a remotely maintained and shielded facility (to remanufacture irradiated beryllium pebbles). Due to the toxicity of beryllium, manufacturing operations are already high remoted and automated.

Another required technology is the remoted and automated machine which retrieves the irradiated beryllium/thorium pebbles from the blanket, removes the thorium snap ring, replaces it with a new ring, and returns the pebble to the blanket (or returns the beryllium part to the remanufacturing line). Such a machine is described in Chapter IV, and is similar to many machines which are routinely used in industry (e.g., an apple coring machine). Again, the developmental emphasis would be in the area of remote maintenance.

Although HT-9 was selected as the reference design structural material, industrial experience in the fabrication of this ferritic is quite limited. If HT-9 fabrication, impurity control, or heat treatment, etc., proves excessively difficult, the reference design would specify 2-1/4 Cr-1Mo as a second choice. The latter is a very common alloy in pressure vessel use, but is somewhat weaker than HT-9 in the 500°C range (see Section II.B). Other ferritics currently under development (e.g., 3Cr-1.5Mo) potentially offer both the strength of HT-9 and the fabricability of 2-1/4 Cr-1Mo(1).

A preliminary design of an electrically insulated coolant duct to limit the MHD pressure drop in straight pipe sections (e.g., I/O piping) was proposed as part of our FY81 study(2). Electrically insulated ducts could significantly decrease the MHD pressure at the first wall and this technology is an attractive, but not critical, candidate for development.

Aqueous fuel reprocessing technologies for thorium metal fuels (such as THOREX), are reasonably well established, but the estimated cost of THOREX reprocessing is both high (i.e., ~ 300 $/Kg HM) and uncertain (see Chapter VII). In contrast, pyrochemical reprocessing technologies for thorium metal based fuels offer the potential of an order of magnitude cost reduction due to a dramatic reduction in the size of the plant and number of components. The proposed magnesium dissolution process, also described in Chapter VII, is

simple, straightforward, and well suited to the fusion breeder fuel (e.g., fission product separation from the very low burnup breeder fuel not necessarily implemented). Nevertheless, a substantial development effort would be required to commercialize the pyrochemical option.

The use of liquid lithium coolants in fusion applications raises concern regrading the liquid metal safety(14). Nevertheless, liquid lithium has unique properties, which help to maximize breeding in the reference blanket(1). In Chapter V, liquid lithium safety is addressed and many candidate liquid metal safety systems are identified. LMFBR experience provides us additional confidence in the ability to engineer safety into liquid lithium systems, but development and integration of such systems is required.

A molten salt tritium extraction process for liquid lithium has been developed through the proof-of-principle stage(8), but the development of a fully closed process has not been demonstrated. The molten salt tritium extraction process should keep the inventory to less than 1 Kg in the entire lithium loop and requires equipment of minimal size, electrical requirements and cost(2,8). Therefore, the developmental risk is expected to be minimal.

Tritium permeation control technologies for the reference lithium cooled blanket have not been evaluated in the context of the present study. However, the high tritium solubility of the liquid lithium is expected to minimize this concern. The largest tritium escape path is eliminated in the reference design by use of a cold trapped sodium intermediate loop. However, technologies related to tritium diffusion barriers, double walled pipes, and gettering systems may require additional development.

The intermodule seal (metal omega seal) described in Section II.E is expected to be a difficult and high risk technology due to the large seal perimeter (~ 15 m), the probability of local faults, and the amount of pressure required to make the seal. It is quite possible that a differential vacuum pumping may be required to further increase the vacuum impedance and seal effectiveness. If this concept fails, we would revert to a remotely formed and inspected welded seal. The primary impact relates to a possible loss in availability due to increased remote operations.

Section II.C References

1) R.W Moir, et.al., "Fusion Breeder Program Interim Report, December 1981 - February 1982", UCID-19406-1, Lawrence Livermore National Laboratory (1982).

2) J.D. Lee, et.al., "Feasibility Study of a Fission Suppressed Tandem Mirror Hybrid Reactor", UCID-19327, Lawrence Livermore National Laboratory (1982).

3) R.W. Moir, et.al., "Tandem Mirror Hybrid Reactor Design - Final Report", UCID-18808, Lawrence Livermore National Laboratory (1980).

4) N.M. Ghoniem and R.W. Conn, "Assessment of Ferritic Steels for Steady State Fusion Reactors", Proc. Technical Committee Meeting and Workshop on Fusion Reactor Design and Technology, Tokyo, (1981). Also as UCLA report.

5) E.A. Little, and D.A. Stow, J. Nucl. Mater. 87, 25 (1979).

6) W.R. Meier and J.A. Maniscalco, "Liquid Metal Requirements for Inertial Confinement Fusion", UCRL-80424, Lawrence Livermore National Laboratory (1977).

7) J.A. Maniscalco, et.al., "Laser Fusion Driver Breeder Design Study - Final Report:, DOE Contract DE-AC08-79DP40-111, TRW (1980).

8) W.F. Calloway, "Electrochemical Extraction of Hydrogen from Molten LiF-LiCl-LiBr and Its Application to Liquid Lithium Fusion Reactor Blanket Processing, Nucl. Tech., 39, 63 (1978).

9) L.R. Weissert and G. Schileo, Fabrication of Thorium Fuel Elements, American Nuclear Society Monograph (1968).

10) T.K. Basu, et.al., "Neutron Multiplication Studies in Beryllium for Fusion Reactor Blankets", Nucl. Sci. Engr., 70, 3 (1979).

11) J. Doyle, "Asssessment of the Neutron Mutliplication Uncertainties in Beryllium", or similar title, draft report to be published by LLNL (1982).

12) J. Howerton, et.al., "An Integrated System for the Production of Neutronics and Photonics Calculational Constants", UCRL-50400, Lawrence Livermore National Laboratory (1972-82).

13) E. Plechaty and J. Kimlinger, "TARTNP: A Coupled Neutron - Photon Monte Carlo Code", UCRL-50400, Vol. 14, Lawrence Livermore National Laboratory (1976).

14) M.S. Kazimi and R.W. Sawdye, "Radiological Aspects of Fusion Reactor Safety: Risk Constraints in Severe Accidents", J. Fusion Energy, 1, 1 (1981).

II.B MECHANICAL DESIGN

II.B.1 Mechanical Design Overview

II.B.1.a Reference Concept Selection. Design studies and supporting thermal/hydraulic, neutronic, material compatability studies, etc., led to the selection of the direct cooled concept as the reference blanket concept. The concept selection process and basis for the decision are documented in Reference 1. Except for the replacement of the graphite reflector with a lithium reflector and changes in some basic dimensions and parameter values the reference concept discussed here is essentially a more advanced design of the direct cooled concept selected in the above referenced document.

II.B.1.b Design Guidelines. The reference blanket concept was developed in accordance with the design guidelines developed during the study. These are presented in Table II.B.1. In addition, other guidelines such as designing for reliability and ease of remote maintenance and service, consistent with attaining adequate thermal and neutronic performance were considered. The arrangement of, and extent of, component redundancy (in particular the pumps and intermediate heat exchangers (IHX)) were important considerations with respect to reliability, safety and maintenance.

TABLE II.B.1 Key design guidelines and design parameters of the reference direct cooled metal cooled blanket.

Design and Performance Guidelines	
Central Cell Fusion Power	3000 MW
First Wall Neutron Loading	<1.5 MW/m^2
First Wall Surface Heat Load	~0.02 MW/m^2
First Wall Radius	1.5 m
Magnet Pitch	4 m
Magnetic Field on Axis	4.2 Tesla

TABLE II.B.1 (Continued)

Blanket Structure	Ferritic Steel
Minimum Structural Temperature	350°C
Maximum Structural Temperature	500°C
Coolant	Liquid Metal
Fuel Form	Composite Be/Th Pebbles (Spheres)
Sphere Diameter	3 cm
Fuel Processing	On Line, Continuous or Batch
Blanket Lifetime	>5 years
Plant Duty Factor	∿.7
Shield Thickness	75 cm
Coolant Pressure at the First Wall	250 psi

II.B.1.c General Module Arrangement. A layout of the Fusion Breeder Program (FBP) tandem mirror reactor blanket module concept is shown in Figure II.B.1, Sheet 1 and 2.

Liquid lithium coolant enters the toroidal inlet manifold and flows radially into the inner first wall region of the blanket through a 10 cm wide plenum between two circular plates connected to the left hand side of the module. After exiting the flat plate plenum, the coolant is turned 90° and flows axially through an annulus composed of the first wall and an intermediate wall behind the first wall. This intermediate wall separates the multiplier/breeder regions of the blanket from the first wall lithium coolant annulus. Coolant flow through the annulus accomplishes two functions. First, the lithium cools the first wall. Second, as the coolant traverses through the annulus axially toward the right hand side of the module, portions of the flow are uniformly bled through holes in the perforated intermediate wall. Thus, the lithium first wall coolant annulus serves as an inlet plenum for supplying the coolant to the outer regions of the blanket. A small fraction of the coolant at the extreme right end of the module enters a narrow double walled flat plate plenum (similar to the inlet plenum) and cools the right hand end of the module.

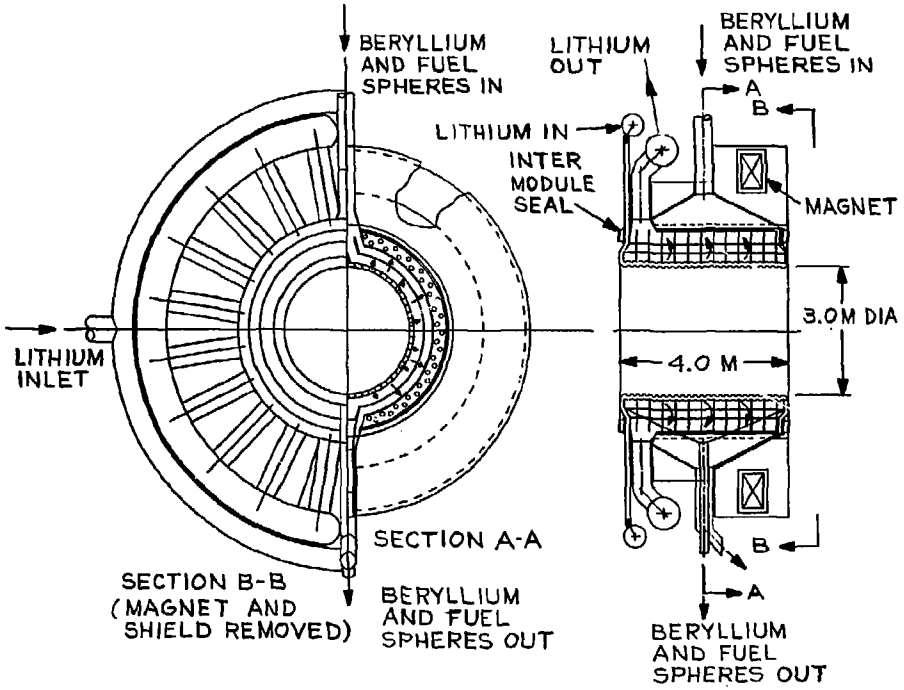

FIG. II.B.1. Component arrangement and dimenisons for the Fusion Breeder Reactor reference liquid metal direct cooled blanket module assembly - sheet 1.

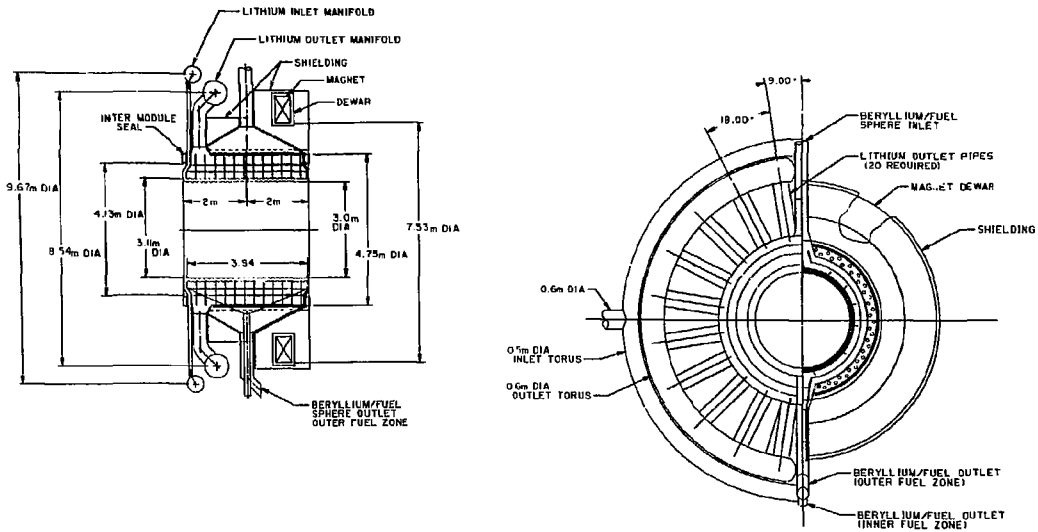

FIG. II.B.1. Component arrangements and dimensions of the Fusion Breeder Reactor reference liquid metal direct cooled module assembly - sheet 2.

The coolant which is bled through the intermediate wall flows radially outward to directly cool the beryllium/thorium spheres in the fertile fueled regions of the blanket. After flowing through the multiplier/breeder region, the coolant is collected in an outer lithium reflector plenum where it is directed axially back toward the left hand side of the outer region of the blanket. Finally the coolant flows outward through 20 radial pipes, 50 cm in diameter, and is directed into the toroidal outlet manifold. The coolant finally leaves the magnetic field through the outlet plenum discharge pipes. Because of the proximity of the inlet and outlets (a common wall exists between the inlet coolant and hotter coolant in the blanket) thermal insulation is provided at the boundary to avoid excessive thermal stresses.

The beryllium/thorium pebbles are loaded through a pipe at the top of the module (detail shown in later section) and flow circumferentially through the fueled zone between the intermediate wall and the outer lithium plenum/reflector until the zones are filled. For reprocessing the fuel is discharged through a set of concentric pipes located at the bottom center of the module. The beryllium/thorium sphere inlet and outlet pipes are sized to permit movement of the spheres during refueling/reshuffling without jamming or bridging.

The selection of liquid metal as a coolant had a major influence on the magnet and piping design configuration. Relatively large pipes are required to minimize the MHD induced pressure drop which results from pumping the coolant through the magnetic field. The space required for piping, plus the shielding around the magnets were instrumental in establishing a magnet pitch of 4m axial spacing between centerlines. This pitch allowed for .5m of shielding between the magnet and the piping into and out of the module. The central cell magnet geometry is shown in Figure II.B.2. A 4m length module with a single magnet per module and the coolant and fuel inlet and outlet piping located on only one side of the magnet was selected for the reference blanket module. The key advantages resulting from this magnet/piping configuration choice are the following:

- Remote reassembly of the blanket/shield/magnet assembly is improved because the magnet can be replaced on the module without remotely welding and inspecting the 20 coolant outlet pipes between the blanket and the main coolant outlet torus.
- Fissile breeding is enhanced since the space required for piping the coolant occupies only about 5% of the module length. A fertile fueled region which is about 95% of the total module length is provided.

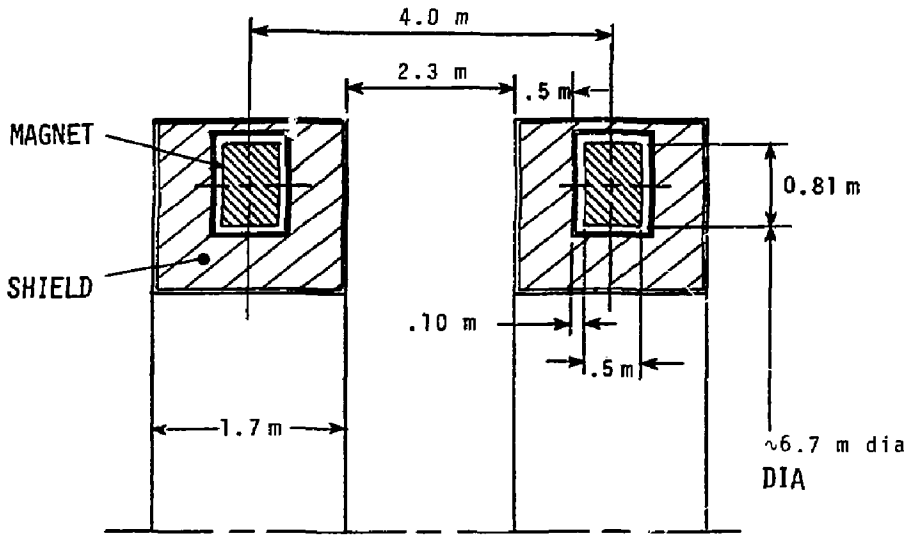

MAGNET BUILD	
- WIDTH	0.5 M
- RADIAL DEPTH	0.81 M
DEWAR ALLOWANCE	0.10 M
SHIELD THICKNESS (SIDES)	0.50 M
SHIELD THICKNESS (INNER BORE)	0.75 M
MAGNET PITCH	4.0 M
CLEARANCE BETWEEN MAGNETS (INCL. SHIELD)	2.3 M
MAGNET INNER BORE DIAMETER	6.7 M

FIG. II.B.2. Tandem mirror reactor magnet geometry for the reference liquid metal cooled blanket.

- The module is not excessively large or heavy so that handling of the module during assembly and/or replacement is practical.

These advantages are further discussed in the sections which follow. Because a common lithium coolant is used to cool both the first wall and the fertile fueled region, tritium breeding occurs in both the first wall and fertile fueled regions.

II.B.2 Selection of Structural Materials

The first wall of TMHR will be subjected to elevated temperatures in an irradiation environment which can affect the dimensional stability and degrade the mechanical properties of the structural material. Although a thorough understanding and data base relating to the radiation effects on the material properties is not complete at this time, it is clear that major differences exist between steel alloy classes considered for the reference blanket, alloys within a class, impurities contents, temperatures required, heat treatments, etc. The material selection therefore, involves design trade-offs. In any selection, however, t is essential to fix a reference design and operating conditions. The following conditions were considered:

Operating temperature	500°C Max
Fusion Neutron Wall Loading	1.27 Mw/m^2
Annual Neutron Fluence	2.0×10^{22} n/cm^2 (11 dpa)
Total Neutron Fluence*	2.0×10^{23} n/cm^2 (E > 0.1 MeV)

*10 year lifetime, 0.7 availability

Of the number of alloy classes presently under consideration in Alloy Development for Irradiation Performance (ADIP) program of the Office of Fusion Energy, the two that are emphasized most are Austenitics (based on AISI 316 Stainless Steels) and Ferritic/Martensitic Steels based on Fe-Cr-Mo alloys (e.g., HT-9, 2-1/4 Cr-1 Mo). The choice between AISI 316 Stainless Steel and Ferritic/Martensitic (HT-9, 2-1/4 Cr-1 Mo) alloys was based on the following considerations:

- Swelling/Dimensional Stability: Ferritic/martensitic alloys swell substantially less than austenitic alloys over a wide range of temperatures. For example, in EBR-II irradiation tests at 500°C and a projected fluence of 2 x 10^{23} (E > 0.1 Mev) HT-9 shows a factor of 1-2 orders of magnitude less swelling than CW 316 SS (see Figure II.B.3) (1). In fusion reactor conditions, which indicate a higher helium/dpa ratio (especially for 316 stainless), these trends are expected to continue and HT-9 is expected to swell substantially less than CW 316 SS. Titanium modified 316 SS (e.g. PCA) alloy may show improved swelling resistance over 316 SS, however, sufficient data base have not been developed to make a good assessment.

- Thermal Stresses: The thermal stresses induced during operation are an important consideration, especially in pulse mode operation. The thermal stresses are significantly less in ferritic/martensitic alloys (e.g. HT-9) than CW 316 SS because of the former's high thermal conductivity and lower thermal expansion coefficient (2). The thermal fatigue lifetime of HT-9 will be substantially better than 316 SS.

- Mechanical Properties:

(1) The post-irradiation tensile strength of HT-9 is $\leq$20% better than CW 316 SS.

(2) Ductility of HT-9 is far superior to that of CW 316 SS. This is especially true in off-normal conditions. High temperature helium embrittlement (in transient conditions) is not expected to occur in HT-9.

(3) Ferritic alloys (including HT-9) are more irradiation creep resistant than CW 316 SS.

(4) Ferritic/martensitic alloys, however, undergo elevation in the Ductile-to-Brittle Transition Temperature (DBTT) with irradiation (2). The DBTT elevation appears to saturate with fluence to temperatures less than the operating temperature (about 350°C). DBTT is a function of impurity content and thermomechanical treatment. By improved chemistry, melt practice and heat treatments, it is possible to lower the DBTT. Also, it seems reasonably possible to alleviate this concern by periodic annealing of the structure (see Section III.B for detailed discussion of irradiation effects on HT-9).

- Corrosion: Ferritic/martensitic steels show significantly better corrosion resistance in lithium than CW 316 SS (3). A temperature of 450°C is

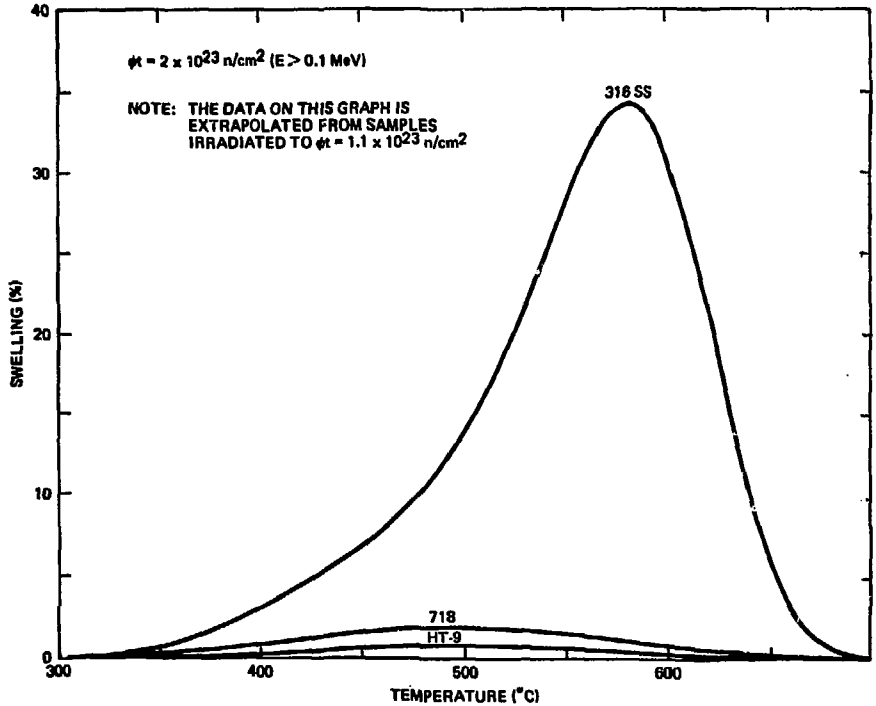

FIG. II.B.3. Swelling of candidate CTR materials during neutron irradiation (from Reference 1)

considered a reasonable upper limit for CW 316 SS, whereas HT-9 may be used to a higher temperature. HT-9 therefore provides a greater temperature margin of operation.

- Fabrication and Experience: Austenitic 316 SS and some ferritics (e.g., 2 1/4 Cr-1 Mo) enjoy a vast experience and ease of welding and structural fabrication technology. Fabrication of thick members of HT-9 steels is more difficult and may require warm working. Post-weld heat treatment may also be required for good corrosion performance(1).
- Neutronics: Ferritic/martensitic alloys, in general, contain elements with lower neutron absorption coefficients, therefore their neutronic properties are better than austenitics. The principal advantage results from thinner sections due to higher strength.
- Post Shut-Down Radioactivity: Substantial advantages in long-term post shutdown radioactivity inventories are realized in ferritic/martensitic over austenitics, due to their lower nickel and molybdenum contents(5). Isotopic tailoring can further enhance this advantage.

The above discussion shows that ferritic/martensitic materials (especially HT-9) will outperform austenitic CW 316 SS in a number of ways. The limitations of ferritic alloys appear to be surmountable. Therefore HT-9 was selected as the first wall blanket material for this study. A choice between different ferritic/martensitic steels, for example: HT-9 versus 2-1/4 Cr-1 Mo is difficult at this time. Note: 2 1/4 Cr should be better due to lower Cr. A preliminary comparison, based on elevated temperature mechanical properties, however favors the choice of HT-9(6).

II.B.3 First Wall Design

In order to achieve attractive neutronic performance in a fission suppressed blanket, a first wall, as structurally thin as possible is a prerequisite design requirement. For example, a 5% loss in fissile breeding for a 3000 MW fusion driver corresponds to roughly 300 Kg/yr ^{233}U. The latter quantity is roughly equivalent to $45 million/year in revenue at (150 $/g) or $300 million in capital cost (at 15%/year capital cost).

In order to withstand the compressive buckling pressure, the first wall is connected to a thicker intermediate wall which separates the first wall coolant annulus from the fertile fueled region. The connections between these two walls consist of 90 radial ribs equally spaced around the first wall/intermediate wall assembly and extending the full length of the module. By corrugating the first wall circumferentially, the wall thickness of 0.36 cm is capable of withstanding the bending stresses. The intermediate wall is also corrugated to increase the stiffness against buckling since the compressive stress is transmitted to the intermediate wall by the radial ribs and both act structurally as a unit to withstand the 250 psi coolant pressure. In addition, it is still necessary to connect this double shell assembly to the thick outer wall of the module via several radial support sheets extending from the intermediate wall through the fertile fueled regions and outer lithium plenum to the outer wall of the module. The radial support sheets are similar to tubesheets in a heat exchanger. The radial support sheets are spaced axially at ~30 cm intervals to provide additional radial support to sustain the coolant pressure compressive load on the first wall/intermediate wall assembly. The spacing between radial supports is consistent with maintaining adequate space for the fuel pebbles to flow freely.

The first wall/intermediate wall corrugated assembly and the remainder of the blanket structure are fabricated from HT-9 ferritic steel. The first wall/intermediate wall sizing and radial rib stiffness arrangement for the intermediate wall are shown in Figure II.B.4 and II.B.5 respectively. Figure II.B.5 shows the structural dimensions from the first wall to the module outer wall. The radial support sheets are indicated in Figure II.B.6. The design features for the blanket module are summarized in Table II.B.2.

TABLE II.B.2 Design features for the FBR direct cooled blanket concept.

Total Module Length	4 m
Length of Fertile Region	~3.8 m
- Fraction of Blanket Length	90-95%

TABLE II.B.2 (Continued)

Fertile Fueled Region Thickness	0.4 m
- Inner Zone	0.2 m
- Outer Zone	0.2 m
Beryllium/Thorium Sphere Diameter	3 cm
Lithium Coolant First Wall Annulus Thickness	~5.3 cm
Lithium Outer Plenum/Reflector Thickness	0.3 m
Corrugated First Wall Thickness	0.36 cm (0.14 in.)
- Allowable Pressure Across First Wall	250 psi
Corrugated Intermediate Wall Thickness (Perforated*)	0.64 cm (0.25 in.)
Clear Opening Between Shells (First & Intermediate Walls)	3 cm
Fuel Zone Separator Thickness (Perforated*)	1.2 cm (0.47 in.)
Fueled Region/Outer Plenum Boundary Thickness (Perforated*)	1.8 cm (0.71 in.)
Module Outer Wall Thickness	~5 cm (1.97 in.)
Inlet Coolant Plenum Width	10 cm
Outlet Coolant Pipes Required	20 each
- Coolant Pipe Diameter	~0.5 m
Magnet Inner Bore Diameter	~6.7 m
Number of Modules	50
Central Cell Length	200 m

*Perforations = 20% of area, maximum

II.B.4 Inlet/Outlet Piping Considerations

Several key items must be considered in determining the coolant piping design and arrangement. These considerations include the following:

- MHD induced pressure drop
- Availability of space for the blanket fertile fueled region
- Impact on remote maintenance

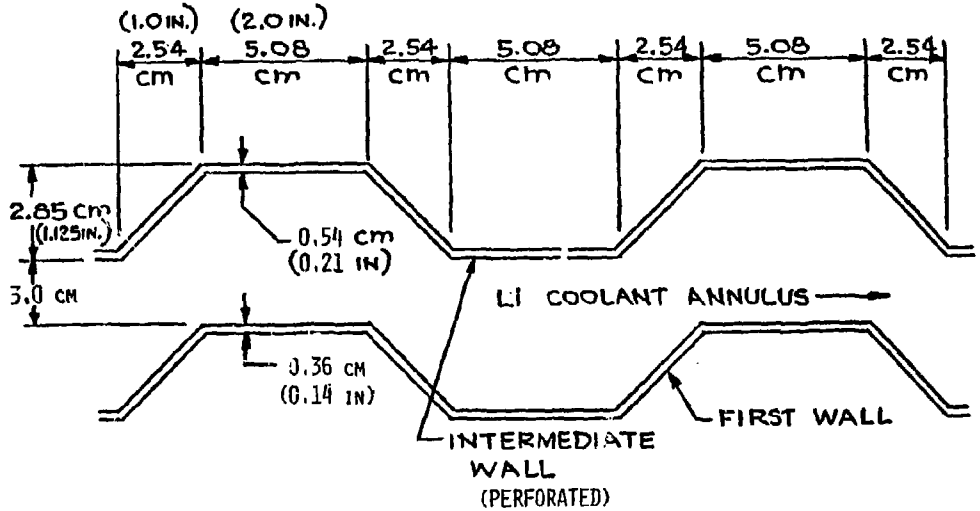

FIG. II.B.4. Structural dimensions for the Fusion Breeder Reactor blanket module corrugated wall assembly (not to scale).

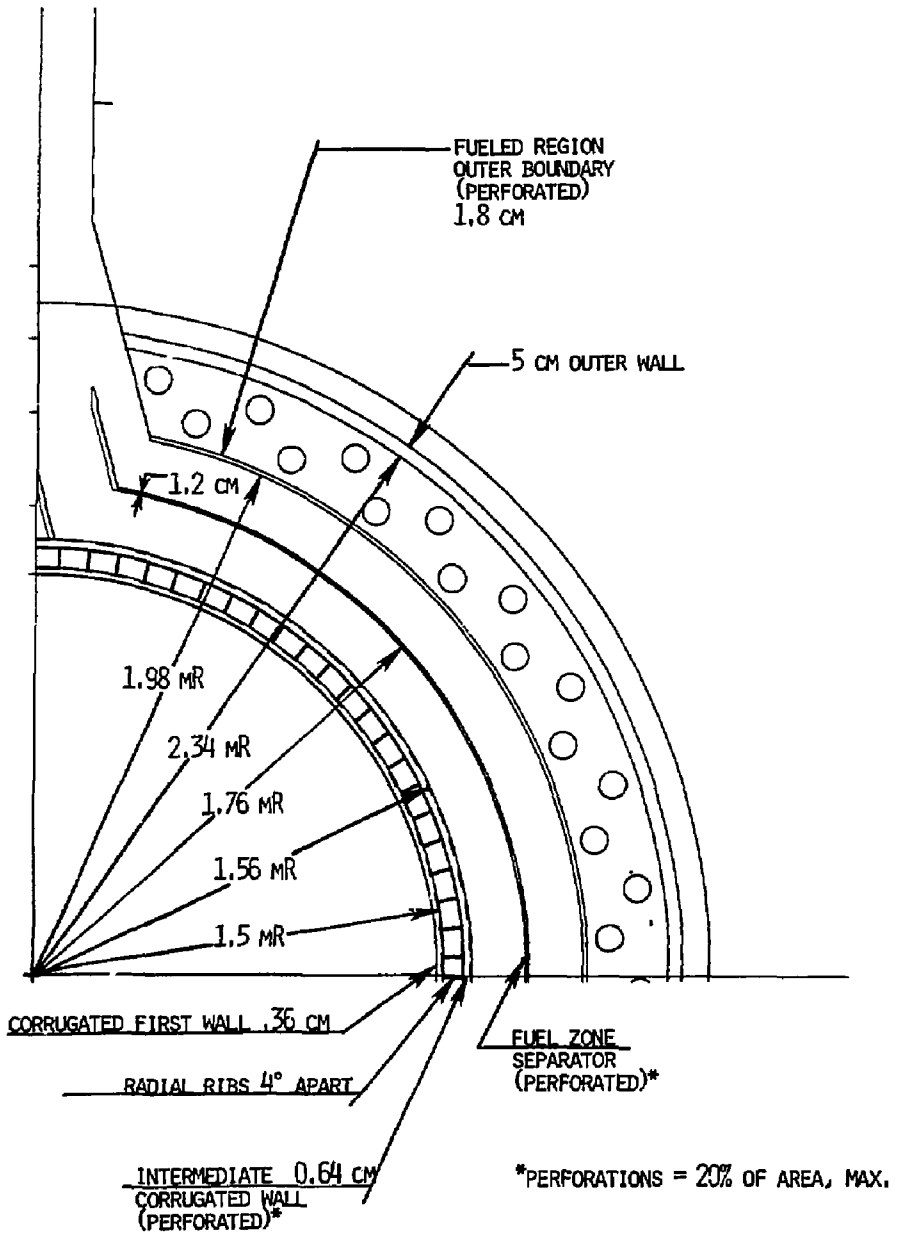

FIG. II.B.5. Structural dimensions for the Fusion Breeder Reactor direct cooled reference blanket concept (not to scale).

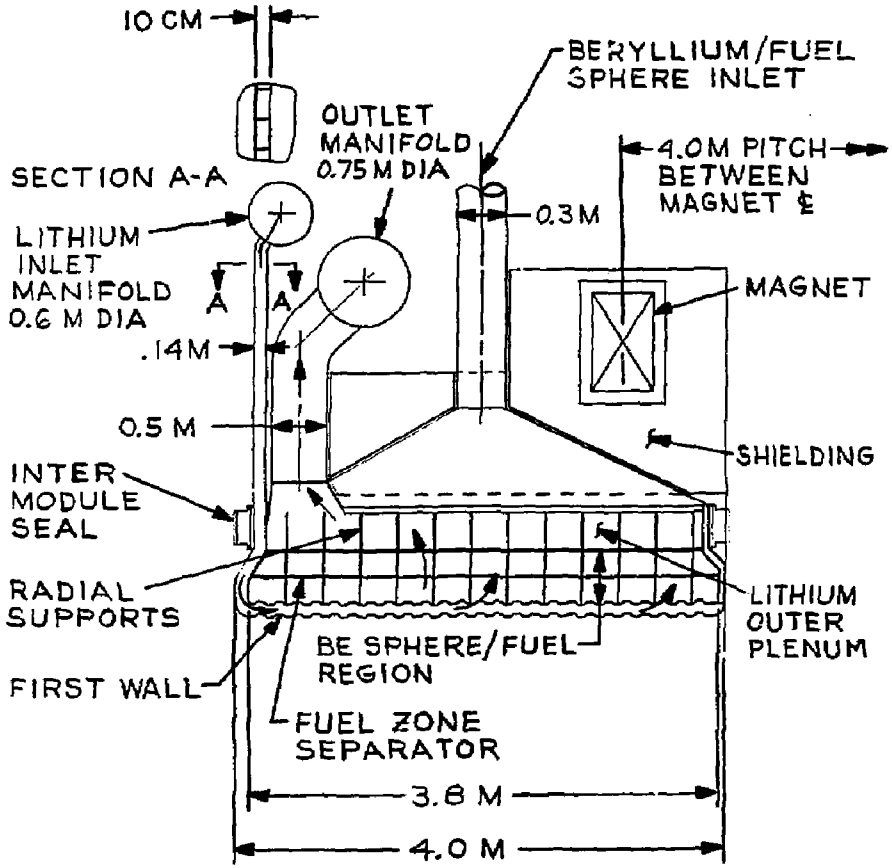

FIG. II.B.6. Reference Fusion Breeder Reactor direct cooled blanket module concept cross section - top portion of module.

The lithium coolant piping arrangement selected is shown in Figure II.B.6; an elevation view cross section of the upper half of a blanket module. Although coolant velocities up to 30 ft/sec (~9 m/s) are permitted in liquid Na piping in plants such as the Clinch River Breeder Reactor, this velocity is not tolerable in the magnetic field of the reference blanket. Consequently, the blanket design dictates that piping sizes as large as practical and coolant velocities as low as possible be utilized within the magnetic field to provide a reasonable pressure across the blanket first wall. Specific pressure drop calculational results are discussed in Section II.D.

In order to maintain the first wall design pressure, the outlet piping is rather large in size while the inlet duct is narrow. This design philosophy recognizes that only the coolant flow through the packed bed and the outlet piping has a direct impact on the first wall pressure. Although, coolant pressures in the inlet duct are higher, these do not impact the nuclear performance. Twenty outlet pipes, each one a half meter in diameter, are used. Similarly, a correspondingly sized outlet toroidal manifold to collect the pipe flow is used. Since the piping leaving the outlet torus is outside the magnetic field higher coolant velocities can be tolerated and the piping diameters can be reduced appreciably.

The two main coolant feed pipes entering and leaving the inlet torus are located at each side of the inlet torus at the horizontal centerline, as are the outlet pipes from the outlet torus of each blanket module. Later, concern for venting trapped gases and drainage considerations led to locating the inlet/outlet pipes on top and bottom of the torus as shown previously in Figure II.A.1.

The coolant inlet configuration consists of a set of parallel circular plates separated by a 10 cm gap (Section A-A of Figure II.B.6) which forms the inlet plenum from a toroidal manifold surrounding the outer diameter of the circular plates. The plates are connected together by radial ribs spread ~10 to 15 cm apart since they converge as they extend from the outer diameter of the plenum at the toroidal inlet manifold to the inlet to the first wall annulus. The flow area similarly converges from approximately 2.9 m^2 at the outer diameter to 0.9 m^2 (for an average inlet area of 1.9 m^2) where it joins the first wall coolant annulus. The inlet flow area is thus approximately one half of the 3.9 m^2 area of the twenty outlet coolant pipes. Because of the reduced area of the inlet, the pressure drop is

higher than that in the exit pipes. As mentioned above, the higher pressure drop should occur before the coolant reaches the first wall since the wall thickness required to withstand this pressure must be as thin as possible to provide attractive neutronic performance.

The use of electrically insulated pipe sections had been investigated in previous studies (7) as a possibility for reducing the MHD induced pressure drop. Insulated concepts were proposed for circular pipes. The reference concept at this time considers insulation only for the coolant outlet piping.

As can be seen in Figure II.B.6, there is additional incentive for keeping the size of the inlet coolant inlet pipes and ducts to a minimum. The inlet piping competes directly for the volume required for the beryllium/thorium fueled region of the blanket since the coolant must feed the first wall coolant annulus. On the other hand the exit pipes receive coolant from the lithium outer plenum outside of the fueled region and there is less restriction on size. If inlet pipes were used instead of the double wall flat plate annulus inlet, the fraction of fertile fueled region would be reduced from the 90-95% in the current concept.

As in the case of most liquid metal systems, the piping (and other external structure of the module) will utilize heat tracing and electrical heaters on the outside surfaces to assure that the lithium remains molten during fill and standby conditions. Since it is not practical to provide electrical heating inside the blanket, provision to preheat the blanket with hot argon or helium will be included. Similarly, insulation will be required on the outer surfaces to prevent excessive heat loss. Neither the heaters or insulation are shown in the blanket concept.

The piping configuration, in addition was influenced, by remote maintenance considerations. Since it is acceptable from field ripple considerations to require only one magnet per module, the magnet can be located at the right end of the module. Locating the coolant inlet and outlets at the left side of the module permits magnet removal without cutting the piping between the inlet or outlet manifolds and the module. This arrangement will facilitate initial assembly and subsequent remote disassembly/maintenance of the blanket.

A more detailed perspective of the piping and its interfacing relationship with the modules and other components of the primary heat transport system is presented in Section VI.C and shown in Figure VI.C.3.

The inlet and outlet piping are located close to each other. In fact, they have a common boundary between the inlet plenum and the inside of the blanket where the coolant progresses radially outward along the left side. Appropriate thermal insulation is provided in this region to minimize thermal gradients.

II.B.5 Fuel Zone Design

The fuel zone of the blanket in the reference concept is configured to meet the requirement for automated refueling/reshuffling without the removal of the blanket module. In order to allow a longer residence time for fuel in the back of the blanket to achieve a higher average fissile enrichment and more economical reprocessing, two radial zones are incorporated into the concept. The first fuel zone of the blanket (Figures II.B.5 and 6) begins at the perforated intermediate wall through which the lithium coolant flows. The two 20 cm zones extend radially ~40 cm outward to a metal shell which acts as the boundary between the fueled region and the lithium outer plenum (which also serves as a reflector).

The blanket is zoned by incorporating a perforated wall or separator which divides the region into two 20 cm radial thick fuel zones. The fuel zone separator (Figures II.B.7 and 8) extends around the blanket and connects to a funnel shaped discharge section through which the beryllium/thorium pebbles can be channeled into a separate outlet pipe for the inner zone. In similar fashion the fuel in the outer region between the zone separator and fuel/lithium plenum boundary can be removed separately. The outer zone boundary is connected to a funnel arrangement at the bottom of the module and the pebbles are collected in the funnel region between the zone separator and the outer funnel. The outer zone discharge pipe surrounds the inner zone discharge pipe in a concentric fashion and the spheres flow out through the concentric annulus between pipes. The pipes are sized to provide space for at least 10 sphere diameters in the central pipe and 5 diameters in the annular region between pipes to preclude sphere bridging or jamming during removal. The rectangular shaped regions formed by the zone boundaries and radial supports are 20 cm x 30 cm allowing for at least 6-10 sphere diameters to permit the spheres to flow circumferentially through the blanket without flow

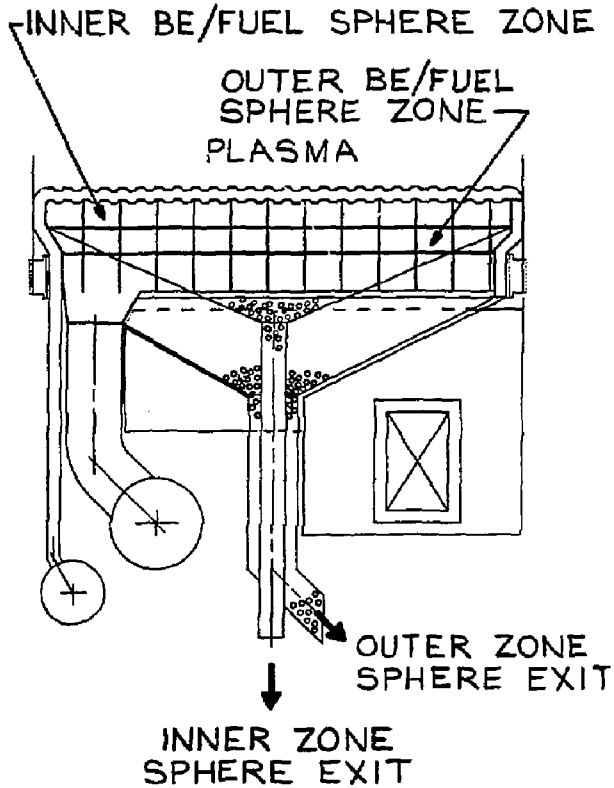

FIG. II.B.7. Reference direct cooled blanket module concept cross section - bottom portion of module (not to scale).

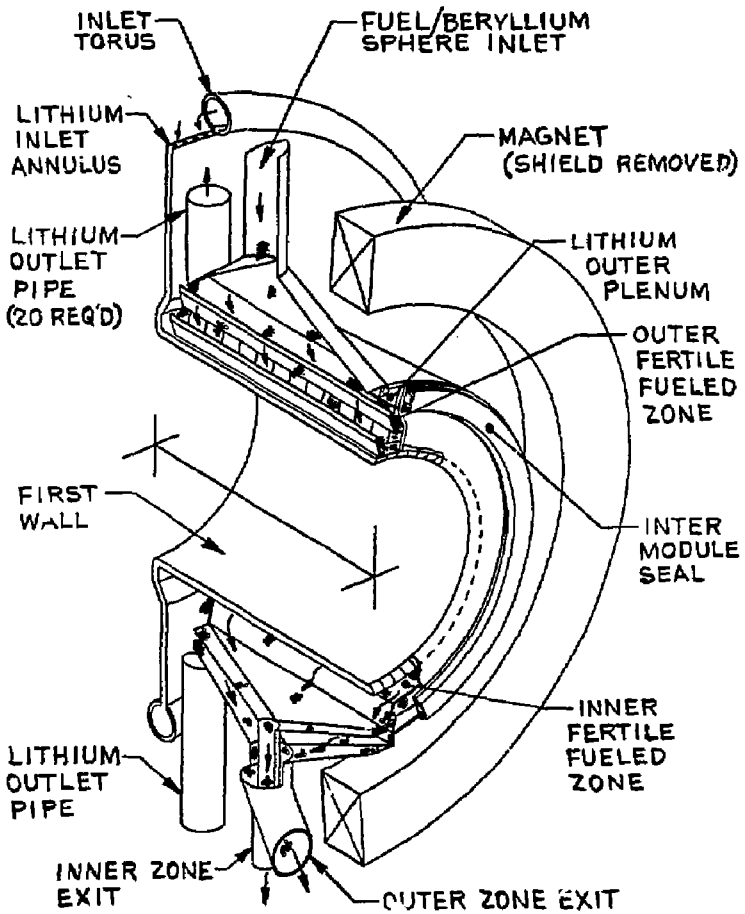

FIG. II.8.8. Trimetric of Fusion Breeder Reactor direct cooled blanket module concept showing radial zoning and fuel sphere movement through the blanket.

interruption due to bridging, etc. Since fuel removal is regulated through the bottom, only a single beryllium/thorium sphere inlet pipe is required at the top of the module.

Zone Separator and Fuel Zone/Lithium Boundaries. There is only a small hydraulic pressure drop across each of these boundaries. However, the zone separator will feel a hoop stress from the total force of the spheres due to the integrated pressure drop through each successive row of spheres as the coolant progresses radially through the blanket. The fuel zone separator is 1.2 cm in thickness. It extends to and is connected to the module end walls (plates) and helps carry the axial force on the plates due to the resulting force from the pressure on the spheres. The pressure acting radially outward on the separator is on the order of 125 psi which is about one half of the pres ure drop through the module. Similarly the wall or boundary between the fuel zone and the lithium outer plenum can be postulated to transmit the full pressure drop through the blanket. If the spheres in the two zones are well packed, some of the sphere pressure from the inner zone can be transmitted to the outer zone spheres. This fuel zone/lithium plenum boundary also is connected to the module side walls to help carry the thrust on the walls. The relatively high force of contact between the spheres and walls raises a design issue with respect to the sphere contact stresses. This issue is discussed later in section III.C. The enlarged view of the trimetric drawing (Figure II.B.9) more clearly shows the common inlet to the two fueled zones at the top of the module. Illustrated also are fuel zone separators, the boundary between the fueled zone and lithium outer plenum. The tube sheets are shown with appropriate flow holes in the outer plenum to permit the coolant to flow from the outer periphery of the blanket, then toward the left to the outlet pipes.

II.B.6 Mechanical Support of Blanket/Shield/Magnets

The design of the magnets, shielding or their associated cooling systems were not addressed during this study. However, the magnet size and amount of shielding required (see Section II.B.1, Figure II.B.2) were furnished in the design guidelines for this study and their sizing was considered and factored into the module and blanket piping coolant system design. The large bulk

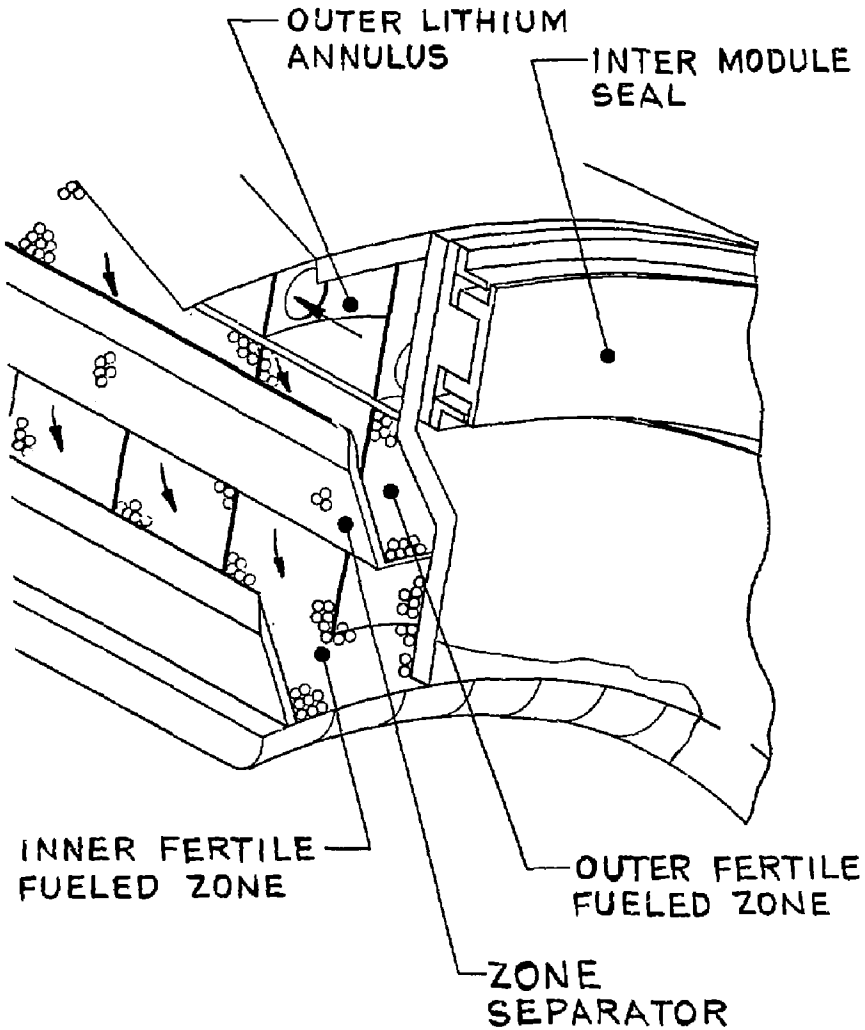

FIG. II.B.9. Enlarged view of upper portion of FIG. II.B.8 in vicinity of the fuel zone inlet and outer lithium plenum.

weight of the shield (~400 tons) compared to the blanket within it (~130 tons with fuel) and magnet (~80 tons) dictates that the shield requires its own support system. In addition it should be made in sections for removal since it surrounds the magnet and should be removed separately. A further reason for separate supports for the shield, magnet, and module are the relatively large differences in thermal expansion between these components during operation after assembly at room temperature. In particular the contraction of the magnet operating at cryogenic temperatures and the blanket module operating at ~500°C will have the largest relative dimensional change. The module growth will be in the order of 2.5 cm (1 inch) in the axial direction. For this reason it should be supported at the center so that the growth at each end is only one half of this value. The module interface sealing considerations and impact of the design on the central cell assembly are discussed in more detail in the following section. It is anticipated that the magnets will be supported from insulated pedestals set beneath each magnet and extending to the floor of the reactor building. Handling of these components comprising the complete blanket assembly are discussed in Section II.E.

II.B.7 Inter-Module Seal Arrangement

The method to be employed for sealing the vacuum boundary at the plane of contact between the modules is a key design issue for at least three important reasons:

- Maintenance of the vacuum boundary over an ~15 m length is required.
- Accommodation of some thermal growth of the modules during operation after initial assembly is needed.
- There is an impact on availability due to the time required to install and change/service modules.

First, a large circumferential length, representing the circumference of the module at the plane of the intermodule seal must be effectively sealed. It is desirable to achieve a seal without welding to minimize remote removal of the module which would require time consuming cutting and rewelding of the joint. A mechanical seal is therefore required which can be readily activated on released to minimize down time and improve availability.

With respect to the second item, a module installed at room temperature will grow due to thermal expansion by approximately 2.5 cm (1.0 inch). This requires that a seal must deflect this amount at operating temperature or one half that amount if similar flexible seals are incorporated at each end of the module. Additional amounts of deflection may be necessary if irradiation induced axial swelling is anticipated.

Seals with appreciable flexibility have been proposed by LLNL for such use in previous studies(8-9). The proposed reference concept is shown in greater detail in Figure II.B.10. The sealing is accomplished by pressurizing the chamber omega seal to deflect until it contacts the mating surface, exerting uniform interface pressure (as opposed to bolting) on the adjacent module (which has an identical type seal). In addition, LLNL is currently investigating a surface seal (10) design similar to the optional flexible rolling seal strip shown in Figure II.B.10.

In the alternate arrangement, the omega seals are replaced by a "rolling strip" seal. To prevent leakage from the pressure chamber very thin, a "U" type, annular flexible "rolling" seal strip is used. In applications such as this (steady operation with few shutdown cycles), it appears possible to maintain leak integrity even though the flexible seal strip may deform plastically. In principle, the annular seal strips could replace the omega type flexible seals shown, although they have been commonly used to seal against components with relative motion. If more effective sealing is required, the face of the seal could be fitted with raised knife edges which would embed in the surface of a soft material in the mating seal face. This alternate is also shown in the figure. Further sealing effectiveness can be achieved by evacuating the volume between the knife edges. Finally, the mating surfaces could be seal-welded; however, this approach would entail a penalty in the time required for cutting and welding the seals and should be used only as a last resort. Future design efforts should focus on designing and testing concepts which have the potential for a practical seal design without welding. The inter-module seal arrangement is shown in Figure II.B.11 for a group of eight modules of the central cell. This arrangement assumes each module is centrally supported and free to expand from its center axially toward the ends. This prevents accumulation of 50 module deflections which would have to allow for a sealing arrangement capable of accommodating ~130 cm (in excess of four feet) of central cell and movement.

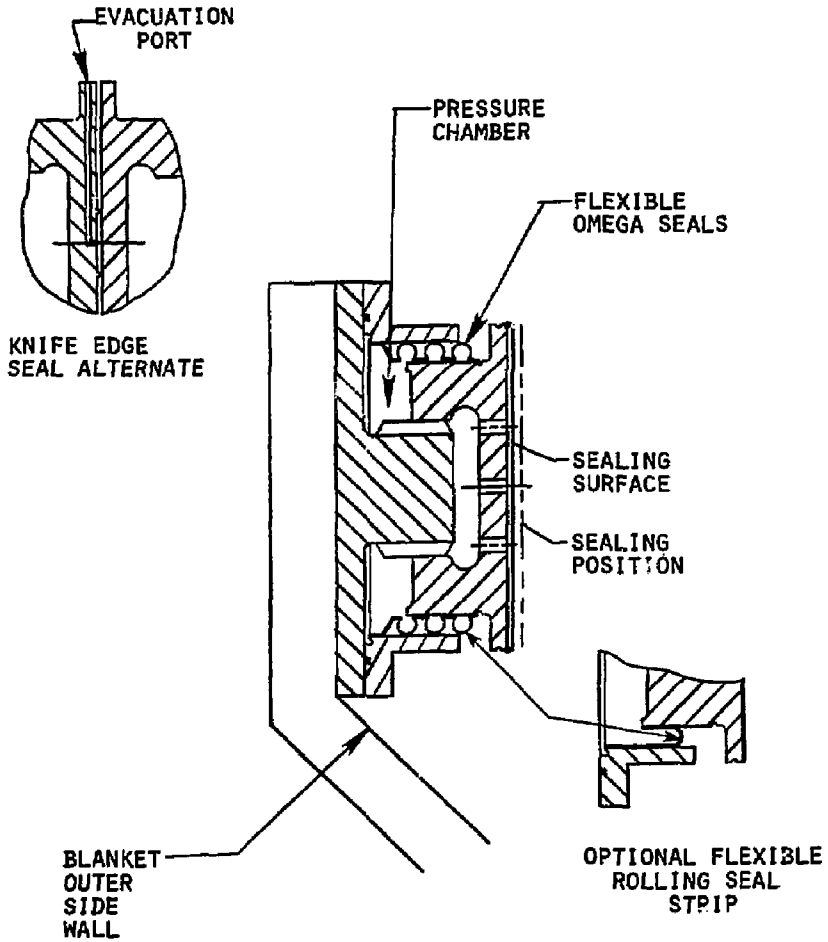

FIG. II.B.10. Module interface sealing concept for the Fusion Breeder Reactor reference blanket module concept-enlarged (see Figure II.B.11).

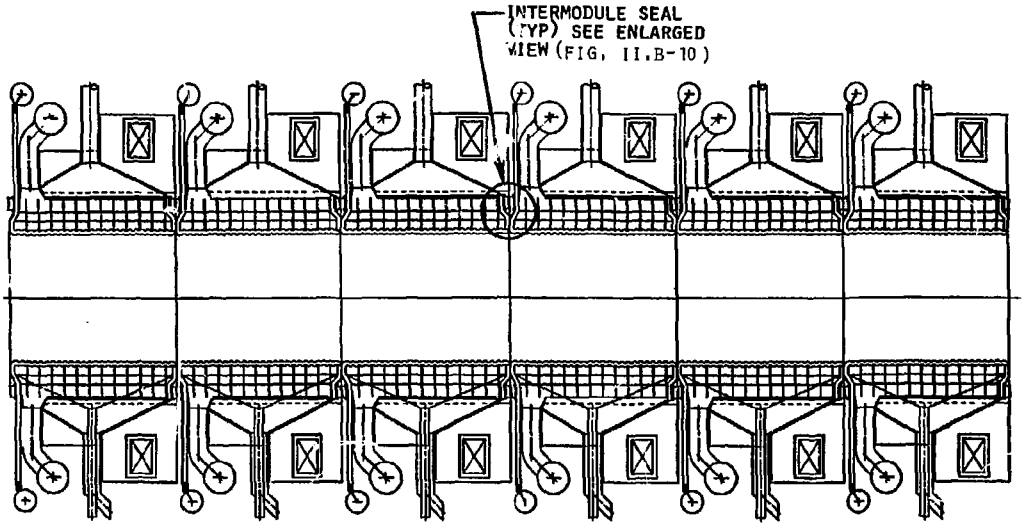

FIG. II.B.11. Fusion Breeder Reactor blanket module cross section arrangement for a position of the central cell showing intermodule seal location and relationship with adjacent modules.

Recognizing the seal design impact on availability and remote maintenance an intermediate vacuum outside of the vacuum boundary should be considered. If an intermediate vacuum (10^{-3} - 10^{-4} torr) is maintained outside the vacuum vessel as has been proposed(11,12) in other reactor studies, then a perfect seal may not be required. With this arrangement, the impedence to flow at the module-to-module interface could be tolerable with the pumping capability of the high capacity vacuum vessel pumps and the pumping action of the halo plasma.

II.B.8 Alternate Structural Concept

One of the design issues raised relative to the reference first wall design is its sensitivity to irradiation induced swelling if swelling should become excessive. If the first wall were to swell and move radially outward and/or tube sheets were to swell and move radially inward, the radial support required to prevent the circumferential buckling of the first wall/intermediate wall assembly would be reduced. If sufficiently reduced, buckling of the assembly could be postulated.

An alternate concept was investigated briefly but not analyzed in sufficient depth to determine its structural adequacy. However, the concept appears to be worthy of further investigation. The concept is shown in Figure II.B.12. As shown, the double wall, circumferentially corrugated in the reference case and axially corrugated in this case still relies on the radial supports in the current concept to furnish additional strength. Since the first wall is now essentially buckled in a circumferential direction, load carrying capability as obtained by resistance to bending of the axial corrugations in the span between radial supports. If swelling occurs and tries to decrease the inner radius of the assembly, the corrugations can deflect circumferentially to accommodate this motion. As shown, the coolant flows axially through the annulus formed by the trapezoided openings at the top of the corrugation and an additional gap between the corrugation and the flow baffle. The flow baffle extends between radial supports and rests on standoffs provided at the top of the corrugation. The flow baffle, which is perforated with a series of holes, acts as a plenum to feed the fueled zone of the blanket. If the flow baffle swells and lifts off the standoffs (thereby reducing its radial support) it could be replaced by a flow baffle corrugated

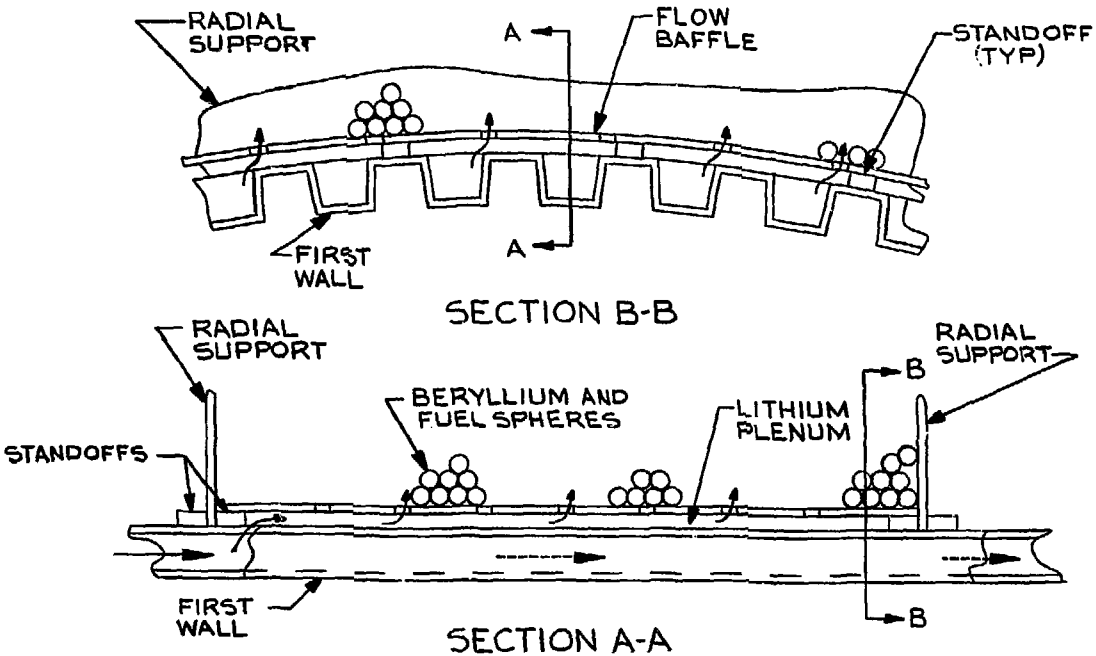

FIG. II.B.12. Axial corrugation first wall concept for the Fusion Breeder Reactor blanket module.

axially. The outer grooves could be covered with a thin circular shell arcs of metal in contact with the baffle and spanning one or more grooves in the corrugation. The circular arcs could overlap as shingles to form a relatively smooth circumference for the spheres to move along the surface during refueling/reshuffling of the spheres.

In summary, the concept appears to offer relief from circumferential swelling but axial swelling will have to be accommodated by leaving an as assembled clearance between adjacent modules. Both the first wall and flow baffle need to be sized and the neutronic performance evaluated. Design of the inlet and outlet ends of the corrugations was not considered and should be pursued if the neutronic performance is encouraging.

II.B.9 Summary and Design Issues

The reference blanket proposed has several attractive mechanical design features. The design is simplified by the use of a single coolant. The piping arrangement achieves a high percentage of the total blanket lengths (90-95%) devoted to the fertile fueled region. The design is complicated by incorporating fuel region zoning but this appears feasible and could be omitted if necessary. The lithium cooled blanket design pressure is low compared to a helium or a high temperature water cooled design. Uncertainties in MHD induced pressure drops through the spherical fueled zones may be causing an unnecessary neutronic penalty because of the structural metal thickness (in particular the first wall and intermediate wall) necessary to withstand the postulated pressure. Component tests should be initiated to simulate the fuel region to determine the degree of conservatism in the 250 psi design pressure. In addition, the pressure drop through the spheres generates high contact forces between the spheres and at contact points with walls which are subjected to these forces. The effects of contact stresses need to be assessed.

Welding of HT-9 is not as easily accomplished as it is in the case of austenitic stainless steels, but is felt to be achievable and the more easily fabricated 2 1/4 Cr-1 Mo ferritic is also available. However, better data are required on radiation induced swelling to properly assess the lifetime of the design. The ductile to brittle transition temperature is higher than desired

but below the normal operating temperature. Periodic annealing of the structure is being considered to minimize this problem.

Scoping structural analysis performed was not in enough detail or depth to predict the stress levels and amount of creep and/or swelling which might occur as a result of extended operation over the contemplated number of startup and shutdown cycles. More detailed stress and lifetime models are required to predict the lifetime resulting from evolutionary stress levels which may accumulate over the design life of the structure.

Intermodule sealing with relatively large motions between modules is a problem which is generic to many blanket designs. Candidate seal concepts therefore should be developed and tested. Location of the intermediate vacuum boundary will probably have to be made based on both design and economic considerations.

The reference liquid metal cooled blanket appears to be attractive enough to warrant further design effort. However, key design issues such as blanket design pressure, and intermodule sealing should receive a high priority. The MHD induced pressure drop through the blanket should be accurately assessed by simulated component testing. Seal development and testing should be aggressively pursued. Finally, a detailed structural analysis should be performed which is in sufficient depth to account for the cumulative effect of the imposed stress on blanket lifetime.

References, Section II.B

1) R. W. Moir, J. D. Lee, W. Neef, et al., "Fusion Breeder Interim Report," UCID-19406-1, June 1982.

2) S. N. Rosenwasser, P. Miller, J. A. Dalessandro, et al., "The Application of Martensitic Stainless Steels in Long Lifetime Fusion First Wall/Blankets," J. Nucl. Mater., 85,86 (1979), pp. 177-182 (1979).

3) F. A. Smidt, J. R. Hawthorne, and V. Provenzano, "Fracture Resistance of HT-9 After Irradiation at Elevated Temperature," in Effects of Radiation Materials ASTM-STP, pp. 269-284, American Society for Testing Materials, Philadelphia, 1981.

4) Personal Communication, R. Bajaj with C. Bagnall and S. Shiels, Westinghouse Electric Corporation.

5) R. W. Conn and K. Okula, "Minimizing Radioactivity and other Features of Elemental and Isotopic Tailoring of Materials for Fusion Reactors," Nuc. Technol., 41, pp. 389-400 (1978).

6) Personal Communication, J. S. Karbowski and R. Bajaj, Westinghouse Electric Corporation, with D. H. Berwald, TRW, June 3, 1982.

7) J. D. Lee, R. W. Moir, W. L. Barr, et al., "Feasibility Study of a Fission--Suppressed Tandem Mirror Hybrid Reactor," UCID-19327, April 1982.

8) R. W. Moir, B. M. Boghosian, R. S. Devoto, et al., "Tandem Mirror Hybrid Reactor Design Study Final Report," UCID-18808, September 1980.

9) G. A. Carlson, B. Arfin, W. L. Barr, et al., "Tandem Mirror Reactor with Thermal Barriers," Lawrence Livermore National Laboratory Report UCRL-52836, September 1979.

10) Private Communications, June 1981, Discussions between J. S. Karbowski of Westinghouse Fusion Power Systems Department and W. S. Neef, Jr., of Lawrence Livermore National Laboratory.

11) R. W. Werner, "ORNL Fusion Power Demonstration Study: Arguments for a Vacuum Building in Which to Enclose a Fusion Reactor," ORNL/TM-5664, December 1976.

12) "Recent Development in INTOR 1 Design," in Proceedings of the 9th Symposium on Fusion Technology, Garmisch-Partenkirchen, Germany, June 14-18, 1976, pp. 375-380, Pergamon Press, New York, 1976.

II.C. NUCLEAR DESIGN, ANALYSIS AND PERFORMANCE

II.C.1. Introduction

Tritium and ^{233}U breeding, energy multiplication, power density, fissile buildup, and other isotopics are nuclear parameters important in the design and evaluation of blankets for fusion breeders. The basic nuclear objective of a fission-suppressed blanket is to maximize fissile breeding while breaking even in tritium ($T \sim 1.0$) and suppressing fission of both the fertile and bred fissile materials. In addition to the nuclear objectives, blanket structure, heat transfer, and fuel handling requirements must be met. Thus an interactive and iterative design process is required.

If nuclear performance was the only requirement, the blanket would consist of beryllium (Be) plus a few atom percent ^{6}Li and ^{232}Th, and its breeding ratio (T + F) would be about 2.7.(1) Thus the potential nuclear performance of the Be blanket is high. To estimate how much of this potential performance can be achieved when structure, heat transfer, and other blanket engineering requirements are met, the blanket nuclear performance must be analyzed with appropriate models and methods.

The principal method used for nuclear analysis of the blanket is TARTNP, a coupled neutron-photon, 3-D Monte Carlo transport code, and 175 group constants generated from ENDL, the Livermore evaluated nuclear data library.(2,3)

Four types of geometric models were developed and employed to predict the blanket's nuclear performance. The first is a radial-zoned cylinder, the second a radial- and axial-zoned cylinder, the third a radial-zoned spherical unit cell, and the fourth a cylindrical segment containing unit fuel cells imbedded within homogenized fuel zones. These models evolved during the course of the study as the mechanical design and our understanding of the nucleonics evolved.

The first model is most easily constructed and is used to predict the integral performance of the blanket. The additional models were developed to examine effects the basic model could not address. Results generated using these models were used to modify results from the basic model to arrive at a more accurate estimate of performance.

Each model will now be described and the results discussed.

II.C.2. Cylindrical (1-D) Model

The basic model used to analyze the blanket is a nested set of concentric cylindrical shells surrounding a cylindrical source of 14-MeV neutrons. The geometry and composition of the blanket shells for the base case are shown in Fig. II.C.1. Starting at the left in the figure is the first wall, consisting of 2 Fe zones separated by a 5.3-cm coolant plenum containing Li + 2.5 v/o Fe. The 2.5 v/o Fe accounts for the stiffening ribs. Following the first wall are two 20-cm packed beds composed of Be/Th spheres, Li coolant and Fe structure. Each bed consists of Li (40 v/o), Be (57 v/o), thorium (3 v/o) plus 2 v/o Fe superimposed to account for the radial stiffeners. The Be and Th are 98% of theoretical density. The two beds are separated by a 1-cm Fe wall and are followed by 1.3 cm of Fe, 30 cm of Li + 2.5 v/o Fe, 2 cm Fe and finally 10 cm of graphite. The outer graphite surface is a radial leakage boundary while the ends (axial) are reflecting boundaries. Making the ends reflecting boundaries is considered reasonable because in the reactor the plasma extends beyond the blanket; therefore, the net axial leakage should be about 0. Each of the two packed beds are divided into two 10-cm zones to get better resolution of the spatial reaction rates and heating in the beds.

Performance parameters calculated with this base model are given in Tables II.C.1 through II.C.4. Table II.C.1 lists reactions and resulting breeding ratios at three enrichments (% ^{233}U in Th) 0, 0.25 and 1.0. Net breeding is 1.33, 1.88, and 1.83 and M is 1.39, 1.66, and 2.14 for these three calculations. Statistical accuracy is within about 5%. Note that ^{233}U fission as well as ^{233}U n,gamma reactions are, effectively, directly proportional to ^{233}U concentration, at least up to 1.0 a/o. It is also interesting to point out that the capture reactions of benefit, in ^{6}Li and ^{232}Th, account for 87% of the total captures. The Fe structure accounts for 6% of the captures. When compared with the theoretical value of 2.7, this blanket model achieves 70% of theoretical breeding. The difference is the result of moderation by materials other than Be and a relatively thin blanket, thus reducing Be (n,2n) reactions and allowing more leakage. Table II.C.2 gives more details of the fission reactions in the blanket. Table II.C.3 lists other heavy metal reactions that affect isotopics and reactions in the Fe structure. Table II.C.4 gives power densities in each zone for a 1 MW/m^2 source neutron wall loading and a 1% ^{233}U concentration in Th. The maximum volumetric heating is in the first wall (7.3 w/cc). The calculated maximum and minimum heating in the homogenized

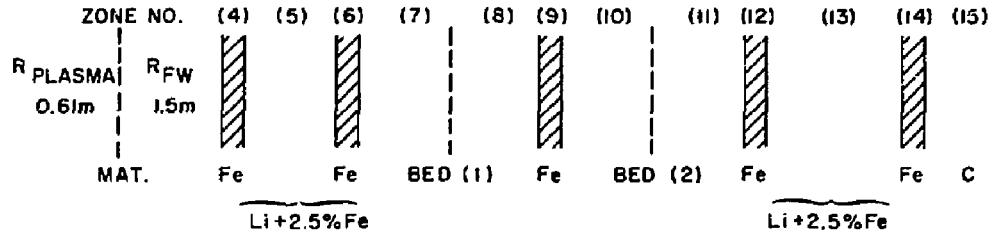

BED MATERIAL VOLUME FRACTIONS

MATERIAL	VF
Th+U-233	.03x.98=.029
Be	.57x.98=.55
Li	.40 (1% Li 6)
Fe	.02

NOTE:
(Li=0.2% Li6 IN ZONES 5 & 13)

72-331-0

Fig. II.C.1 Cylindrical Model - Geometry and Composition

Table II.C.1. Cylindrical Model - Results per D-T Neutron at 0, 0.25, and 1.0 a/o ^{233}U

Zone #	T^6	T^7	$^{232}Th(n,\gamma)$	^{233}U (n,fiss)	$^{233}U(n,\gamma)$
5	.055/.059/.056	.136/.130/.133			
7	.283/.303/.287	.061/.061/.059	.298/.315/.310	0/.0054/.0209	0/.00084/.00327
8	.252/.253/.248	.029/.029/.028	.225/.234/.237	0/.0043/.0170	0/.00068/.00268
10	.144/.154/.147	.011/.011/.011	.125/.132/.133	0/.0025/.0101	0/.00040/.00161
11	.081/.089/.090	.005/.005/.005	.068/.073/.079	0/.0014/.0060	0/.00023/.00096
13	.049/.039/.055	.011/.011/.011			
Totals	.814/.897/.883	.253/.247/.247	.716/.754/.759	0/.0136/.0540	0/.00215/.0085

Bottom Line:

T = 1.12/1.14/1.13, T + F = 1.83/1.90/1.89, T + F_{net}* = 1.83/1.88/1.83

M = 1.39/1.66/2.14

* $F_{net} = {}^{232}Th(n,\gamma) - {}^{233}U(n,fiss) - {}^{233}U(n,\gamma)$

** Includes equilibrium decay of activation and fission products in the beds.

Totals include structural zones.

Zone #	Energy (MeV)/ Source 14.1 MeV Neutron**
5	2.35/2.28/2.35
7	6.78/8.31/10.77
8	4.44/5.45/7.72
10	2.24/2.84/4.26
11	1.23/1.51/2.47
13	0.58/0.41/0.65
Totals	19.5/23.3/30.1

Table II.C.2. Fission Reactions Per Source Neutron in Cylindrical Model

Zone	^{232}Th	^{233}U	Total
	(at 0.25 a/o ^{233}U)		
7	.0036	.0054	.0090
8	.0018	.0043	.0061
10	.0007	.0025	.0032
11	.0003	.0014	.0018
Total	.0064	.0136	.0200
	(at 1.0 a/o ^{233}U)		
7	.0036	.0209	.0245
8	.0017	.0170	.0188
10	.0007	.0101	.0108
11	.0003	.0060	.0063
Total	.0063	.0540	.0603

Table II.C.3. Other Metal Reactions

Reactions in Heavy Metals in Zone 7

(Per Source Neutron)

Reaction	^{232}Th	^{233}U (@ 0.25 a/a)
n,2n	.0109	9.68 E-6
n,3n	.00295	4.44 E-7

Reactions in Fe in Zone 5 (Per Source Neutron)

n,2n = .00460	n,a = .00039
n,p = .00214	n,g = .00505

Table II.C.4. Radial Power Density (n + γ)

(1 a/o ^{233}U in Th Case)

$$PD = \frac{E}{V} \cdot \frac{1}{14.06} \cdot A_{FW} \cdot \Gamma$$

Zone	ΔR(cm)	E(MeV)	$Vx10^{-6}$cc	PD(w/cc at Γ = 1.0 MW/m^2)
4	.41	.421	.155	7.28
5	5.3	2.35	2.08	3.03
6	.60	.574	.244	6.32
7	10.	10.77	4.20	6.88
8	10.	7.72	4.45	4.65
9	1.0	.462	.459	2.70
10	10.	4.26	4.72	2.42
11	10.	2.47	4.98	1.33
12	1.3	.141	.511	.735
13	30.	.646	15.75	.110
14	2.	.090	.539	.448
15	10.	.038	5.81	.018

packed beds are 6.9 and 1.3 w/cc. The energy deposition (E) and power densities (PD) listed include decay of reaction products such as ^{233}Th, ^{233}Pa and fission products. These are slightly conservative since they assume decay equilibrium (requires several months operation) and local deposition of the decay gammas. To estimate power densities at other ^{233}U concentrations, scale ^{233}U fission in zones 7, 8, 10 and 11 with concentration and use 190 MeV/fission.

II.C.3. Axial Heterogeneous Effects

The 1-D cylindrical model does not account for the lithium inlet and slipstream plena at the ends of each module. To estimate their effect, a 21-cm-long axial section at the end of the 4-m blanket module is replaced by a zone containing 90 v/o Li (0.2 a/o ^{6}Li) and 10 v/o Fe. By symmetry the model used is 1/2 the module length and is shown schematically in Fig. II.C.2. The effect is a 2.9% drop in net breeding and a 2% drop in M.

A similar model was also used to examine the effect of homogenizing the radial stiffeners. This was done by removing the 2% Fe from the beds and the lithium plena and putting it into a 0.61-cm axial zone on the end of a 30.5-cm blanket segment. There was no detectable effect. Therefore, no correction is used to account for homogenizing the radial stiffeners.

II.C.4. Packed Bed Heterogeneous Effects

The basic 1-D cylindrical blanket model treats the packed beds as homogeneous mixtures of Li, Be, Th/U and Fe. To determine if there are heterogeneous effects in the beds, two models were developed. Breeding ratio, energy multiplication, energy partitioning in the bed materials, and isotopic composition of the Li required to give the correct tritium breeding ratio (T) are all nuclear performance parameters that could be affected by heterogeneous effects.

The first model developed to appraise these heterogeneous effects is a spherical unit cell consisting of a Th (+ U) sphere surrounded by a Be annulus which in turn is surrounded by a Li annulus as shown in Fig. II.C.3. Volume fractions of these materials in the unit cell are Th (3%), Be (57%), and Li (40%). The Be contains 0.1 a/o Fe impurity. An isotopic point source of 14 MeV neutrons is located in the outer Li zone. The outer surface of the cell

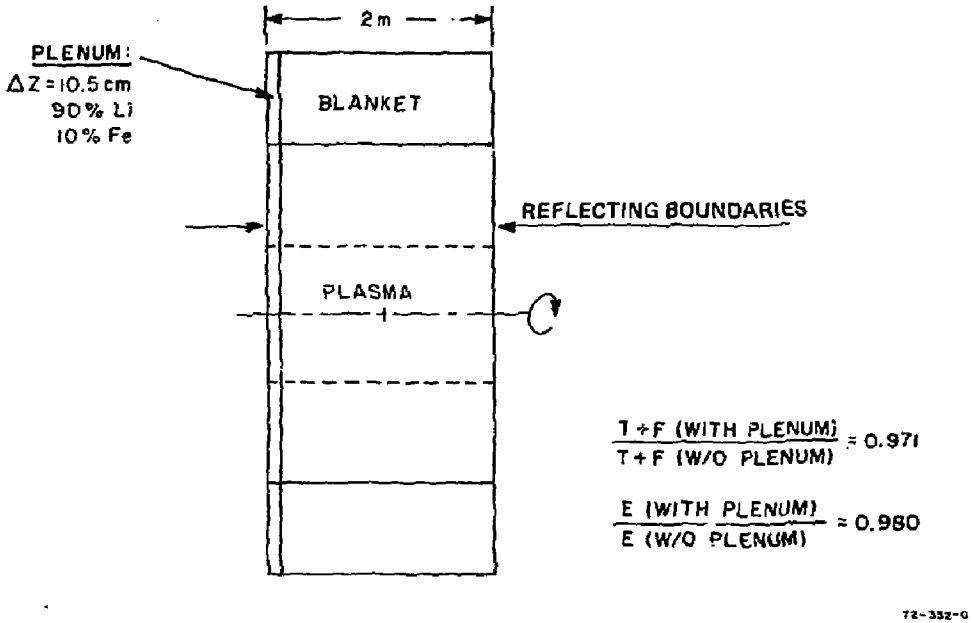

Fig. II.C.2 Module End Plena Effects - Model and Results

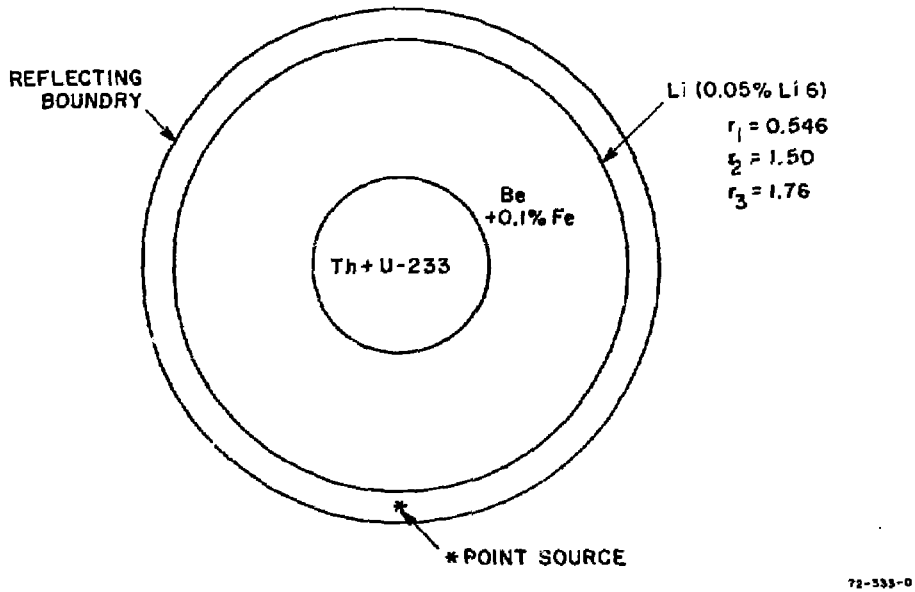

Fig. II.C.3 Spherical Unit Cell Model

is a reflecting boundary making the cell an infinite array of unit cells.

By comparing the nuclear parameters calculated with this unit cell to those calculated with a homogenized version of the same cell, an estimate of the heterogeneous effect can be made. Results at two sets of ^{6}Li concentrations 0.05 a/o (het.)/0.2 a/o (hom.) and 0.2 a/o (het.)/1.0 a/o (hom.) and two ^{233}U concentrations, 0 and 0.25 a/o in the Th, are given in Table II.C.5. The factor of 5 difference in ^{6}Li concentration between the het. and homo. cases is needed to keep the tritium breeding ratio (T) approximately equal. These results indicate that heterogeneous effects in the pebble beds could be significant. For these cases the net breeding ratio ($T + F_{net}$) dropped between 5.5 and 7.7% and the change in M ranged between 5% lower to 54% higher than their homogeneous counterparts. Energy (heating) partitioning is also significant with 20 to 65% of the energy being deposited in the Th (+ U) slug. This model is pessimistic in that it must overpredict ^{233}U fission due to its infinite geometry and lack of structure. Results with this model really only tell us that bed heterogeneous effects could be important and must be investigated further.

A number of other variations were also examined with this model. For example, with the ^{6}Li concentrations fixed at 0.2% (het.)/1.0% (hom.) and the ^{233}U concentration fixed at 0.25%, the following observations are made compared to the fourth case on Table II.C.5:

1. Changing the Th/U sphere to a 3-cm-long cylinder with the same volume reduced the drop in the net breeding ratio, from 7.7% to 5%, while further increasing M from 33% to between 34 and 64% depending on the source-slug orientation.

2. Doubling the Th/U sphere volume reduced the drop in breeding ratio to 5% while further increasing M to 44%.

3. Moving the Th/U to the outside of the Be sphere reduced the reduction in breeding to 5.7% (from 7.7%) and reduced the increase in M to 26% (from 33%). Energy partitioning in this case is 26% Be, 47% Th/U and 27% Li. This type of fuel was selected for the reference case and thus further analysis is required.

Table II.C.5. Spherical Unit Cell Sample Results

	T	F	T + F_{net}	M	E_{Th}	E_{Be}	E_{Li}
With 0.05 a/o ^{6}Li (Heterogeneous) and 0.2 a/o ^{6}Li (Homogeneous)							
With 0 a/o ^{233}U							
Het.	1.09	1.14	2.23	1.49	26%	37%	37%
Homo.	1.16	1.27	2.40	1.57			
Het/Homo.			.929	.949			
With .25 a/o ^{233}U							
Het.	1.15	1.10	2.25	3.45	65%	18%	17%
Homo.	1.19	1.27	2.39	2.24			
Het/Homo.			.941	1.54			
With 0.2 a/o ^{6}Li (Heterogeneous) and 1.0 a/o ^{6}Li (Homogeneous)							
With 0 a/o ^{233}U							
Het.	1.53	0.77	2.30	1.48	20%	33%	47%
Hom.	1.38	1.05	2.43	1.56			
Het/Homo.			0.945	0.949			
With 0.25 a/o ^{233}U							
Het.	1.54	0.81	2.27	2.47	50%	21%	29%
Hom.	1.41	1.08	2.46	1.86			
Het/Homo.			0.923	1.33			
With Th + 0.25 a/o ^{233}U moved to outside of Be pebble							
Het.	1.28	1.11	2.32	2.32	47%	26%	27%
Hom.	1.41	1.08	2.46	1.86			
Het/Homo			0.943	1.26			

II.C.5. Criticality

The spherical unit cell model was also used to calculate the ^{233}U concentration which results in $K_\infty = 1.0$. Since we want k to be less than 1.0 under all potential conditions, k_∞ with and without Li vs ^{233}U concentration was calculated and plotted in Fig. II.C.4. As expected, the case without Li was found to be the most restrictive with $k_\infty \approx 1.0$ occurring at a ^{233}U concentration of 1.6 a/o compared to 9 a/o with Li. Based on this analysis it is required that the maximum concentration of $^{233}U + ^{233}Pa$ in Th in either bed be limited to less than 1.6 a/o.

II.C.6. Finite Heterogeneous/Homogeneous Model

The spherical unit cell model used to estimate heterogeneous effects is an infinite-integral model, and as such cannot show spatial effects on energy partitioning. To see if spatial effects are important, a fourth model was developed. This model (shown in Fig. II.C.5), called the Finite Heterogeneous/Homogeneous Model, is a pie-shaped segment of the blanket with reflecting sides and homogenized pebble beds, plus unit cells at the inner and outer radii of the two bed zones. The source is an isotropic point source located at the center of the first wall. Results, at an estimated example end-of-cycle ^{233}U concentration profile, are listed in Table II.C.6. The average ^{233}U concentrations in Th are 0.86% in the inner bed and 0.75% in the outer bed. Concentrations for the unit cells are listed in the table. As shown, energy partitioning is a function of position as well as ^{233}U concentration. The maximum fraction in the Th/U is 67%, occurring at the inner radius of the outer bed. At the most critical location, the inner radius of the inner bed, the Th/U fraction is 55 percent, resulting in a power density of 143 W/cc in the Th/U at 1 MW/m^2 wall loading (not including decay heat which is about a 5% addition). The average PD in that innermost cell is 7.71 W/cc. An approximate profile of the average power density across the bed is shown in Fig. II.C.6. The power density profile from the basic model (at 1.0% ^{233}U) is also plotted for comparison. The principal difference between the two is due to differences in ^{233}U concentration (significantly lower for the heterogeneous case).

The reactions of interest for breeding, calculated with this model, are listed in Table II.C.7. Net breeding is 1.80, and M is 1.94.

Note that the power densities and blanket M apply to this model only and

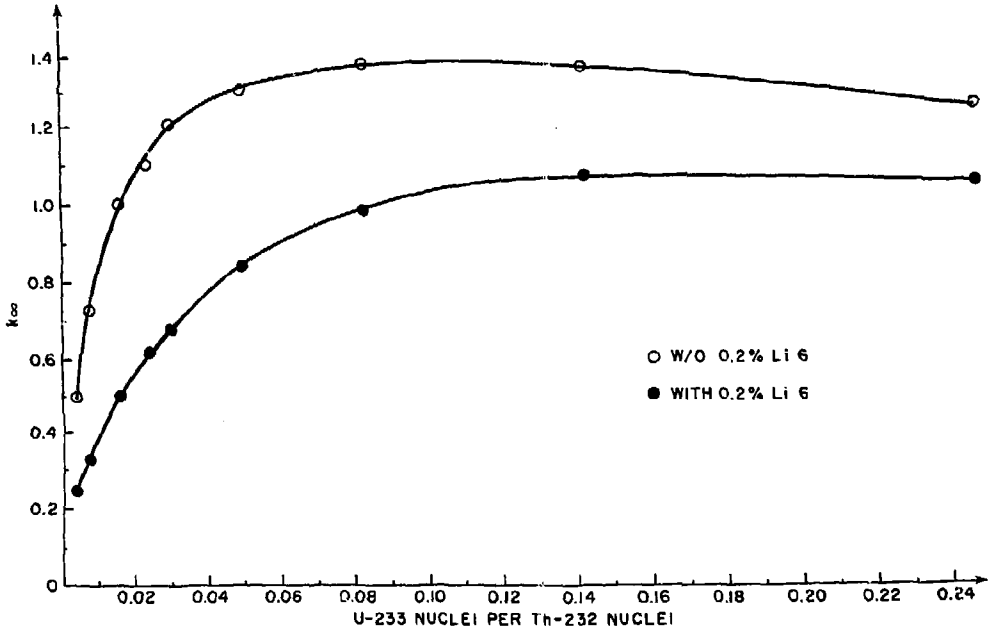

Fig. II.C.4 k_∞ vs Concentration of ^{233}U in ^{232}Th

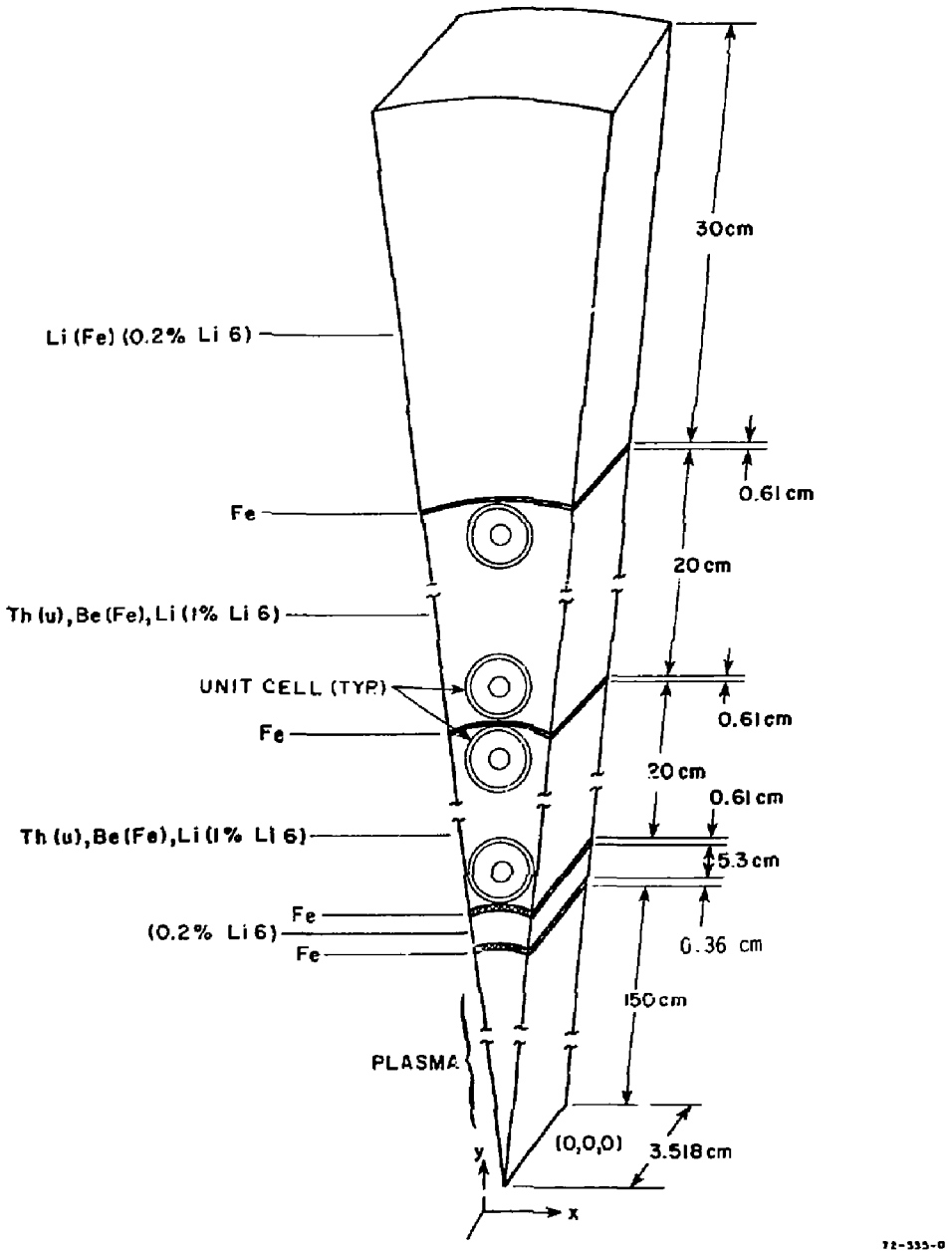

Fig. II.C.5 Finite Heterogeneous/Homogeneous Model

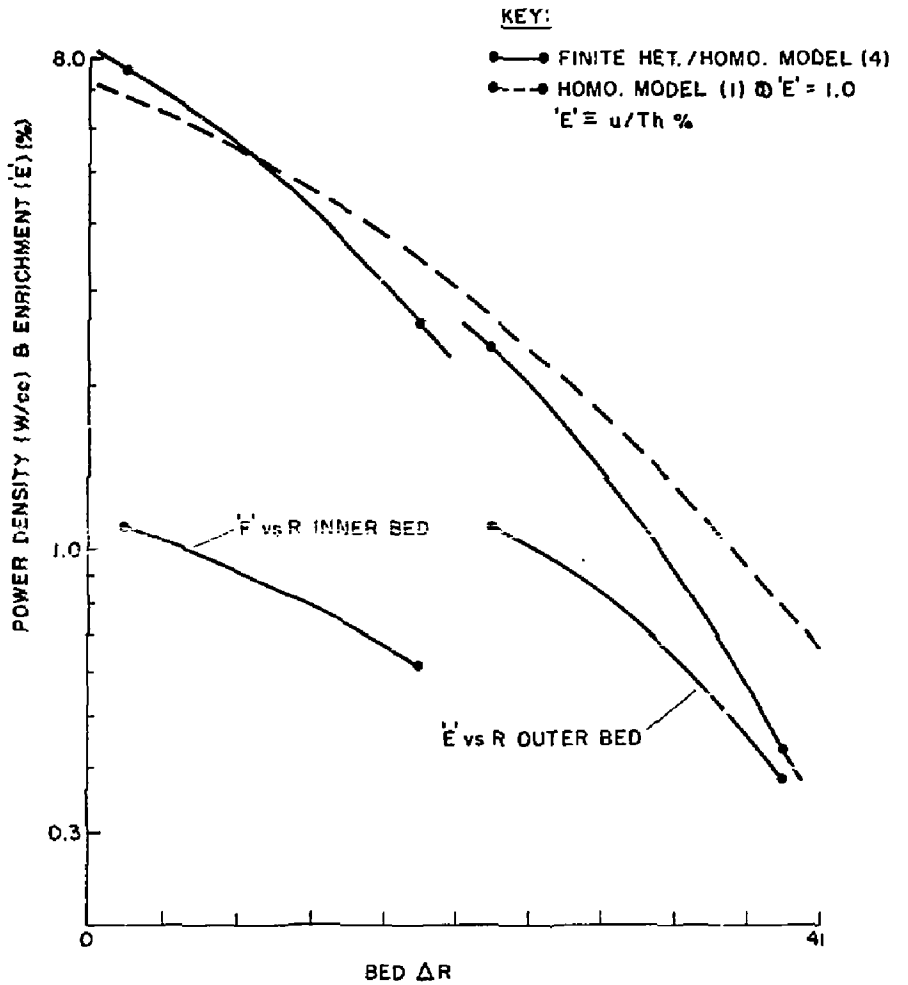

72-336-0

Fig. II.C.6 Bed Power Density and "Enrichment" Profiles (Models 4 and 1)

Table II.C.6. Energy Partitioning, Power and Power Density in the Unit Cells of the Finite Heterogeneous/Homogeneous Model

Cell #	Material	V(cc)	E(MeV)*	E(%)	P(w)**	PD(w/cc)**
1	Th + 1.1 a/o U	.682	1.18	(55)	97.4	143
	Be	13.5	.688	(32)	56.8	4.22
	Li	8.66	.270	(13)	22.3	2.57
	Total	22.8	2.13	(100)	176	7.71(ave)
2	Th + .62 a/o U		.403	(56)	33.2	48.8
	Be		.211	(30)	17.4	1.29
	Li		.101	(14)	8.33	.962
	Total		.715	(100)	59.0	2.59(ave)
3	Th + 1.1 a/o U		.441	(67)	36.4	53.4
	Be		.146	(22)	12.0	.895
	Li		.070	(11)	5.78	.667
	Total		.657	(100)	54.2	2.38(ave)
4	Th + .38 a/o U		.056	(47)	4.62	6.78
	Be		.044	(37)	3.63	.270
			.019	(16)	1.57	.181
	Total		.119	(100)	9.82	.431(ave)

* Per source neutron

** @ 1 MW/m^2 wall loading

Table II.C.7. Reactions in the Finite Heterogeneous/Homogeneous Model (per DT Neutron)

Zone	T^6	T^7	$^{232}Th(n,\gamma)$	$^{233}U(n,fiss)$	$^{233}U(n,\gamma)$	$^{232}Th(n,fiss)$
Pebble No. 1	0.0118	0.0122	0.0362	0.00534	0.00083	.00083
Inner Bed	0.530	0.0602	0.461	0.0296	0.0046	0.0037
Pebble No. 2	0.0085	0.0024	0.0150	0.00176	0.00026	0.00017
Pebble No. 3	0.0064	0.0014	0.0114	0.00221	0.00036	0.00011
Outer Bed	0.200	0.0087	0.148	0.0091	0.0014	0.0006
Pebble No. 4	0.0015	0.0003	0.0032	0.00019	0.00003	0.00002
Inner Li Plenem	0.0670	0.136				
Outer Li Plenem	0.0202	0.0076	———	———	———	———
Totals	1.104		0.682	0.0482	0.0075	
					(Radial leakage = 0.098)	

Bottomline: $T + F_{net}$ + (leakage - 0.029) = 1.73 + 0.069 = 1.80, M = 1.94.

do not include heterogeneous effects of the whole bed, which the spherical unit cell indicated could be significant. A finite heterogeneous model that is intended to address this question is under development. Although a ^{233}U concentration significantly less than 1.0 may well be needed to limit fissioning to an acceptable level, the effective fissile concentration can be higher because of undecayed ^{233}Pa in the fuel (see Section IV.A).

II.C.7. End Plug Effects

Fusion reactions take place in end plugs (and transition regions) that are not covered by a blanket. Not only are fusion neutrons lost, but tritium consumed must be made up by the blanket as well. Analysis has not been done to see what happens at the blanket-transition region interfaces. The assumption made is that the net leakage at these interfaces is zero. This assumption is based on the fact that the plasma extends beyond the interface, thus leakage into the blanket will occur. For this case, total fusion power is 3140 MW, 3000 of which occurs "under" the blanket. Therefore this 3140-MW fusion reactor requires a net blanket tritium breeding ratio that is

$$\frac{3140}{3000} = 1.047$$

times higher than the reactor requires to satisfy the tritium requirements of both the central cell and the end plugs.

II.C.8. Estimate of Effective Breeding Ratio, Net ^{233}U Production Rate and Blanket Energy Multiplication

Using the results calculated with the models described, the following nuclear performance estimates are made:

For the Case with Thorium Inside Each Beryllium Pebble

Blanket breeding ratio, fusile plus net fissile:

$(T + F_{net})_{blk} = (T + F_{net})_{Model\ 1}$ x plena correction x heterogeneous correction

- $(T + F_{net})_{Model\ 1} = 1.13 + 0.70 = 1.83$
- The value of $T + F_{net}$ appears to be insensitive to ^{233}U content ("ε") and therefore is assumed to be independent of "ε."
- Plena correction (from Model 2) = 0.971.
- Heterogeneous correction (Model 3) = 0.923. This correction is sensitive to "ε"; the value used was calculated at "ε" = 0.25%, and is taken to be the average value.

$\therefore (T + F_{net})_{blk} = 1.83 \times 0.971 \times 0.923$

$= 1.83 \times 0.896 = \underline{1.64}$

Net fissile breeding ratio (F_{net}):

$(F_{net})_{blk} = (T + F_{net})_{blk} - T_{blk}$

$\therefore (F_{net})_{blk} = 1.64 - 1.06 = \underline{0.58}$

where a blanket tritium breeding ratio (T) of

$$T_{blk} = T_{reactor} \times \frac{P_{f\text{-}reactor}}{P_{f\text{-}blk}} = 1.01 \times 1.05 = 1.06$$

is needed to sustain the reactor.

Fissile production rate (G):

$G = 4.32\ (kg/MW_fY) \times P_f\ (MW) \times (F_{net})_{blk}$

$\therefore G = 4.32 \times 3000 \times 0.58 = \underline{7517\ kg\ ^{233}U/full\ power\ year}$

Blanket energy multiplication, M:

$M = M_{model\ 1}$ x plena correction x heterogeneous correction.

At start of cycle ($^{233}U = 0$), $M = 1.39 \times 0.98 \times 0.95 = \underline{1.29}$.

At a ^{233}U concentration of 0.25%, $M = 1.66 \times 0.98 \times 1.165 = \underline{1.90}$.

For the New Reference Case (Thorium Around the Outside of the Beryllium Pebbles)

Blanket breeding ratio, fusile plus net fissile:

$(T + F_{net})_{blanket} = (T + F_{net})_{Model\ 1}$ x plena correction x heterogeneous correction

- $(T + F_{net})_{Model\ 1} = 1.13 + 0.70 = 1.83$
- The value of $T + F_{net}$ appears to be insensitive to ^{233}U content ("ε") and therefore is assumed to be independent of "ε".
- Plena correction (from Model 2) = 0.971.
- Heterogeneous correction (Model 3) = 0.943. This correction is sensitive to "ε"; the value used was calculated at "ε" = 0.25%, and is taken to be the average value.

$\therefore (T + F_{net})_{blanket} = 1.83 \times 0.971 \times 0.943$

$= 1.83 \times 0.916 = 1.68$

Net fissile breeding ratio (F_{net}):

$(F_{net})_{blanket} = (T + F_{net})_{blanket} - T_{blanket}$

$\therefore (F_{net})_{blanket} = 1.68 - 1.06 = 0.62$

where a blanket tritium breeding ratio of

$$T_{blk} = T_{reactor} \times \frac{3140}{3000} = 1.01 \times 1.047 = 1.06$$

is needed to sustain the device.

Fissile production rate (G):

$G = 4.32\ (kg/MW_fY) \times P_f\ (MW) \times (F_{net})_{blanket}$

$\therefore G = 4.32 \times 3000 \times 0.62 = 8035$ kg ^{233}U/full power year

Blanket energy multiplication, M:

$M = M_{model\ 1}$ x plena correction x heterogeneous correction.

At start of cycle ($^{233}U = 0$), M not yet calculated; assume same as base case (1.30).

At a ^{233}U concentration of 0.25%, M = 1.66 x 0.98 x 1.13 = 1.84.

The heterogeneous corrections for M are taken to be 1/2 that calculated because of the infinite nature and lack of structure in the model (No. 3) from which they came. A finite, heterogeneous model is under development to better determine this correction. Preliminary results suggest that an average ^{233}U concentration of 0.5% will give a blanket M of about 2.0 and power densities like those listed in Table II.C.6.

Blanket performance is quite sensitive to structural content, especially in the first wall, as previously shown in Fig. II.C.2 of the Interim Report.[4] Based on this sensitivity, it is estimated that if the first wall structure thickness of the present blanket is reduced 29% (from 0.35" to 0.25"), breeding ($\bar{T} + F_{net}$) would increase 3%, thus net fissile breeding would increase 8% (from 0.62 to 0.68). Such a reduction in first wall structure could be achieved if first wall pressure is reduced to 200 psi from 250 psi, as discussed in Section II.B. It is apparent that an optimization that trades off wall loading and maximum ^{233}U content with structural requirements, thus breeding ratio, is needed.

It must be stressed that the nucleonics appraisal of this blanket is not complete and work is continuing in order to improve and expand the estimate of nuclear performance. Major improvement is needed in determining energy generation vs. ^{233}U content.

References, Section II.C

1) J. D. Lee, The Beryllium/Molten Salt Blanket, Lawrence Livermore National Laboratory, Livermore, CA, UCRL-82663 (1979); also published in Proceedings of the 3rd Symp. on Fusion-Fission, Princeton, NJ (1979).

2) TARTNP: A Coupled Neutron-photon Monte Carlo Transport Code, Lawrence Livermore National Laboratory, Livermore, CA, UCRL-50400, Vol. 14 (July 1976).

3) The LLL Evaluated Nuclear Data Library (ENDL): Evaluation Techniques, Graphical Displays and Descriptions of Individual Evaluations, Lawrence Livermore National Laboratory, Livermore, CA, UCRL-50400, Vol. 15 (Sep. 1975).

4) R. W. Moir, et al., Fusion Breeder Program, Interim Report (Dec. 1981 - Feb. 1982).

II.D FLUID DYNAMICS AND HEAT TRANSFER

The fluid dynamics and heat transfer aspects of using liquid lithium as the coolant for a magnetic fusion reactor blanket are of key concern because of the large magnetohydrodynamic (MHD) effects that can occur, the liquid metal flow models are reviewed and further developed when needed in this section, design results are presented, and critical design issues are discussed.

II.D.1 Introduction

The fluid dynamic and heat transfer characteristics of a fusion reactor blanket must be such that the coolant is able to transfer the blanket power to a thermal power conversion system at a temperature adequate to attain reasonable efficiency. At the same time, the blanket temperature distribution has to be acceptable (i.e., within specific limits for different materials) and the pressure drops in the blanket and power conversion loops have to be acceptable, so as not to introduce excessive stress or pumping power requirements. With the selection of lithium as the heat transfer medium, the effects of the interaction of the highly electrically conducting lithium coolant with the relatively high magnetic field of 4.24 T for the reference reactor, and the impact of this interaction on pumping power and heat transfer need to be analyzed. Most importantly, since higher pressures in the blanket translate to a requirement for more structural materials, the MHD pressure drop associated with liquid metal flow can directly affect the breeding performance of the blanket.

During the scoping phase of this study (1), the direct radial flow of lithium through a packed bed blanket configuration was selected as the reference design. The pressure drops and temperature distribution were calculated based upon available analytical and experimental results. Since appropriate methods for calculating the MHD effects on the pressure drop through a packed bed do not exist in the literature, several different MHD

models were developed. A realistic model that gave presumably conservative results was then selected. The pressure drop calculated using this model was then used to obtain the maximum blanket fluid pressure that the mechanical design might be required to accommodate. The objective of the thermal-hydraulic design effort during this phase of the study was to evaluate the feasibility of the blanket concept rather than to develop an optimized design. After the reference design was defined, critical MHD-related issues associated with this design were identified.

II.D.2 Liquid Metal Blanket Pressure Drop Models and Results

In general, liquid metal flow components perpendicular to an applied magnetic field produce eddy currents within the liquid metal that are directed perpendicular to both the field lines and the flow (i.e., $\vec{J} \sim \vec{V} \times \vec{B}$). As a result of such current generation, the following intrinsic interactions between the magnetic field and the liquid metal must be considered:

1. Hartmann flow. With electrically conducting walls, the eddy currents generated as a result of fluid flow through a uniform magnetic field can return through these walls, resulting in a net electromagnetic body force against the flow direction.

2. Magnetic field gradient losses. The eddy currents generated in a fluid moving through a magnetic field gradient (and/or the turning of the fluid through magnetic field) will also generate net electromagnetic body forces that are in the opposite direction to the fluid flow.

3. Turbulence suppression. The inherent generation of electromagnetic body forces in directions against the fluid flow across field-lines will cause fluid turbulence suppression, altering the characteristics of fluid flow heat transfer.

4. Variation of the fluid flow profile. The electrical eddy currents generated in a plane perpendicular to the fluid velocity can cause thinning of the sidewall boundary layer; thus increasing wall friction.

In this section, the applicable equations for pressure drop calculations and their limited forms for the Fusion Breeder Reactor blanket are presented. The relevance of these equations to the reference blanket design is then discussed. The form of the equation used for turning, contraction, and expansion calculations is also presented. To calculate the pressure drop through the packed bed, different models were evaluated and the model that gave conservative and yet realistic answers was selected.

II.0.2.a Channel Flow Liquid Metal Pressure Drops. The exact solution for the pressure gradient of liquid metal flow in parallel plate geometry across perpendicularly oriented magnetic field lines is given by (2,3):

$$\frac{dp}{dx} = -\frac{\mu v}{a^2}\left(\frac{H^2 \tanh H}{H - \tanh H} + \frac{H^2 C}{1 + C}\right) \quad . \ . \ . \qquad (1)$$

where μ = fluid viscosity, (kg/m·sec)
v = mean fluid velocity, (m/sec)
a = flow channel half width, (m)
H = Hartmann number, $Ba\sqrt{\sigma/\mu}$
σ = fluid electrical conductivity, $(\text{ohm-m})^{-1}$
B = magnetic field strength, (Tesla)
C = wall conductance ratio, $\sigma_w t_w/\sigma a$
σ_w = wall electrical conductivity, $(\text{ohm-m})^{-1}$
t_w = wall thickness, (m).

For our reference design, the Hartmann number is given by $H = (4.24)(a)\,[(3.1 \times 10^6)/(0.38 \times 10^{-3})]^{1/2} = 3.8 \times 10^5$ at ~450°C for lithium flowing across a magnetic field strength of 4.24 T. With the range of channel half width of 10^{-2} m < a < 0.5 m, the range of Hartmann number is $3800 < H < 1.9 \times 10^5$. Equation (1) can then be simplified to the following for the reference design,

$$\frac{dp}{dx} \approx -\frac{\mu v}{a^2}\left(H + \frac{H^2 C}{1 + C}\right) \quad . \ . \ . \qquad (2)$$

In a circular geometry, a correction factor can be multiplied to Eq. (2), and one gets,

$$\frac{dp}{dx} = - 1.3 \frac{\mu v}{a^2} \left[H + \frac{H^2 C}{1 + C}\right] \quad . \ . \ . \qquad (3)$$

When the wall is electrically insulated, i.e., when C = 0, Eq. (2) becomes,

$$\frac{dp}{dx} = - \frac{\mu v}{a^2} H = - \frac{vB}{a} \sqrt{\sigma \mu}$$

$$\text{or} \qquad = - vB^2 \frac{\sigma}{H} \quad . \ . \ . \qquad (4)$$

which is the same limiting form as given by Hunt and Hancox (4).

When the wall is electrically conducting, for $H^2C/(1 + C) >> H$, Eq. (2) becomes,

$$\frac{dp}{dx} \simeq - \frac{\mu v}{a^2} \left(\frac{H^2 C}{1 + C}\right) = - \sigma B^2 v \frac{C}{1 + C} \quad . \ . \ . \qquad (5)$$

and when $C \simeq 1$, Eq. (5) becomes

$$\frac{dp}{dx} \simeq - \frac{\sigma B^2 v}{2} \quad . \ . \ . \qquad (6)$$

Comparing Eq. (4) and Eq. (6), one should note that the pressure gradient can be increased by a factor of H/2 in changing from electrically insulated to electrically conducting walls.

For lithium flow parallel to a magnetic field, the main effect from the presence of magnetic field is turbulence suppression. The flow remains laminar if the Reynolds number is less than the transition Reynolds number of $Re_t \simeq 60H_\parallel$ (5), where $H_\parallel$ is the Hartmann number as defined by the parallel magnetic field strength.

It appears that, for the laminarized parallel flow, the ordinary laminar flow and friction factors apply. Thus, the pressure drops for flow parallel to field lines can be calculated with the available laminar flow equations.

II.D.2.b Pressure Drops from Turns, Contractions, and Expansions. Pressure drops of slug flows for change in magnetic fields were also considered by Hoffman and Carlson (5). In general, the pressure drop can be put into the form of:

$$\Delta P = - K\sigma v B^2 b \quad . \ . \ . \qquad (7)$$

where K is the pressure drop coefficient and b is the channel half width perpendicular to the magnetic field direction. The value of K is a function of the wall conductance ratio, the ratio of fringe field length L (distance where the magnetic field strength varies along the fluid flow) to flow channel height b; and the general geometric variation of the magnetic field. To determine the values of K, the following observations can be made from analytical results for a channel configuration with top and bottom conducting walls (5).

At $L/b = 0$

$0.27 < K < 0.54$ for $0 < C < 1$

At $C = 1$

$0.54 > K > 0.14$ for $0 < L/b < 8$

At $C = 0$

$0.25 > K > 0.05$ for $0 < L/b < 8$

Thus one can see that the pressure drops from fringe magnetic fields can differ by an order of magnitude depending upon the wall conductance ratio and magnetic field variation characteristics.

There are limited experimental data on pressure drops on fringe magnetic fields. Wells (6) has performed experiments using mercury in a square channel with electrically insulating walls. A value of K equal to 0.362 was obtained for a range of Reynolds number from 5×10^5 to 2×10^6 and Hartmann number from 320 to 1400. For a lower Reynolds number varying from 1.48×10^5 to 8.39×10^5, the value of K reduces to 0.024 (5). For this study, we used K value of 0.03 for our calculation for the following reasons. The range of Reynolds number for the reference design is relatively low at 10^3 to 10^4, the values of L/b would be > 10 and the walls would be insulated whenever feasible in order to minimize pressure losses. The theoretical maximum value of K = 0.54 was also used for comparison.

There does not appear to be an adequate understanding of the MHD pressure drops for turns in a magnetic field. Because turning of flows from a parallel to a perpendicular orientation with respect to the magnetic field, or vice versa, may be similar to the entrance and exit in effect, we used the above K values for all the calculations of turns, contractions, and expansions. While the precision of this approximation is not known, this will allow us to make a relative comparison of the magnitude of these MHD pressure drops with other pressure drop contributions.

II.D.2.c Packed Bed MHD Pressure Drop. The selected reference blanket design schematic is shown in Fig. II.D.1. It shows the direction of the incoming lithium from one side of the four meter long module as it flows through the corrugated first wall. The lithium then turns and flows radially outward through the packed bed of spherical beryllium pebbles. It then reaches the lithium reflector and flows out of the blanket module through the outlet plenum and the outlet pipes. Although accurate analytical models exist only for well developed flow in the simplist geometries (i.e., square

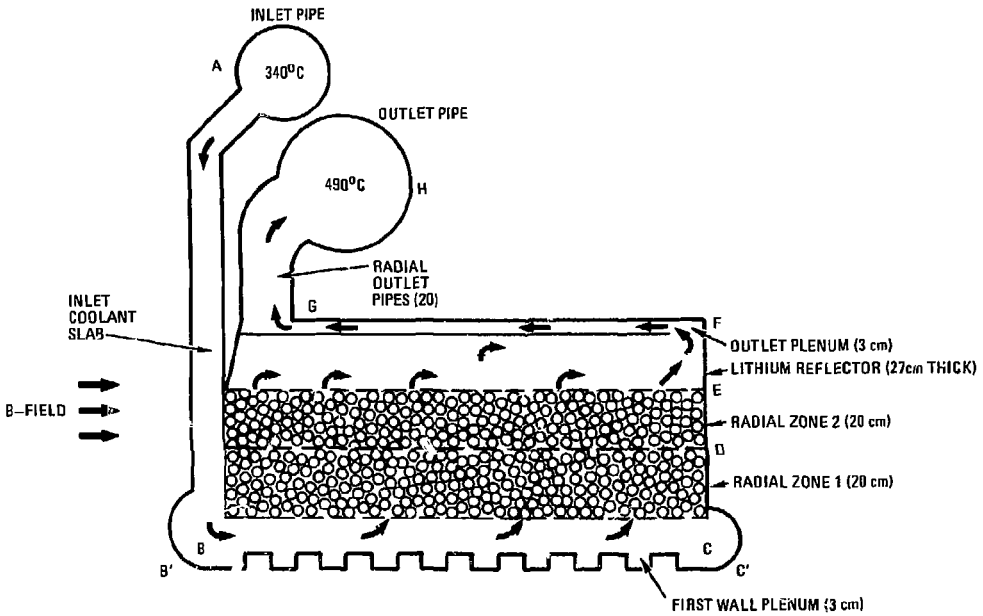

Fig. II.D.1 Packed bed blanket schematic.

or round straight pipes), the MHD pressure drops in flow segments other than the packed bed can be calculated in a straightforward manner.

The key difficulty in the calculation of the pressure drops for liquid metal flow through a packed bed in the presence of a magnetic field is the lack of analytical support from the literature. The coolant paths formed by the close-packed pebbles are very tortuous and coolant flow in and out of magnetic field lines is unavoidable. Because of the relatively high electrical conductivities of lithium, beryllium, and thorium metal, induced currents will be formed inside the blanket, which will in turn generate body forces against the direction of fluid flow. Precise analysis of the aggregate or cancelling effects of these body forces as formed by surrounding coolant paths is impossible because of the 3-D geometric complication and the unspecified packing structure of the pebbles, (which is a function of the method of packing and the packed bed characteristic dimensions). Physically, one can observe that the coolant will flow through the blanket by taking the paths that have the least resistance, which implies paths that would contribute least pressure drop. Because of the difficulties associated with modeling the complex packed bed configuration, simplified assumptions were made in considering the pressure drops through the packed bed. The results can be used as indications of design feasibility. To begin, an order of magnitude determination, comparing the MHD-induced pressure drop to the pressure drops which exist regardless of the magnetic field (i.e., viscous and packed bed momentum transfer), was made by starting from basic principles using the momentum equation. It was shown that at a coolant ΔT of 150°C and a pebble diameter of 3 cm, the MHD pressure drop due to the 4.24 T B-field is at least four orders of magnitude higher than the zero field packed bed and viscous pressure drops. This allowed us to concentrate on the contribution of pressure drop from MHD losses.

For this study, four analytical models were considered. The first model, illustrated in Fig. II.0.2, utilized the following assumptions:

1. For the general flow direction perpendicular to the magnetic field (corresponding to the radial flow portion), the pressure drop through a straight channel formed by the cusp between three pebbles was calculated. The channel wall thickness and electrical conductivity were taken to be those of the pebble radius and of beryllium, respectively. The local maximum fluid velocity through the cusp was used in the calculation.

2. Pressure drops from turning losses due to flow through the packed bed in the presence of a uniform magnetic field were estimated by the entrance and exit loss of liquid metal through a field gradient of $\Delta B = B$, multiplied by the number of turns as defined by the number of pebbles along the flow path. The resulting pressure drop was added to that associated with cusp flow.

This model was selected instead of summing up the total fluid winding paths traversing the B-field, because the Hartmann flow solution as given by equation 1 is only valid for well developed pipe flow, whereas the situation for the flow around packed pebbles is that the fluid flow has short flow paths and is not developed at all. It was found from this model that the pressure drops due to MHD flow effects are independent of pebble sizes.

Based upon the cusp flow concept, a second model was developed by assuming that the cusp wall (formed by the beryllium pebbles) is fully insulated. In this case, the calculated pressure drop is about 3 orders of magnitude lower, at 1.7 kPa (0.25 psi), than with the conducting wall model at ~1.96 MPa (284 psi). This is due to the dominant contribution of the pressure drop when the wall is conducting, which varies with the square of the Hartmann number, whereas the insulated wall pressure drop is directly proportional to the Hartmann number. For the packed bed region, the Hartmann number is equal to 1219. These results indicate the importance of identifying the current return path in calculating the packed bed pressure drop.

The third model was constructed by considering the potential current paths and calculating the pressure drops accordingly. It was noted that at a temperature of 400°C, the electrical conductivity of beryllium metal is

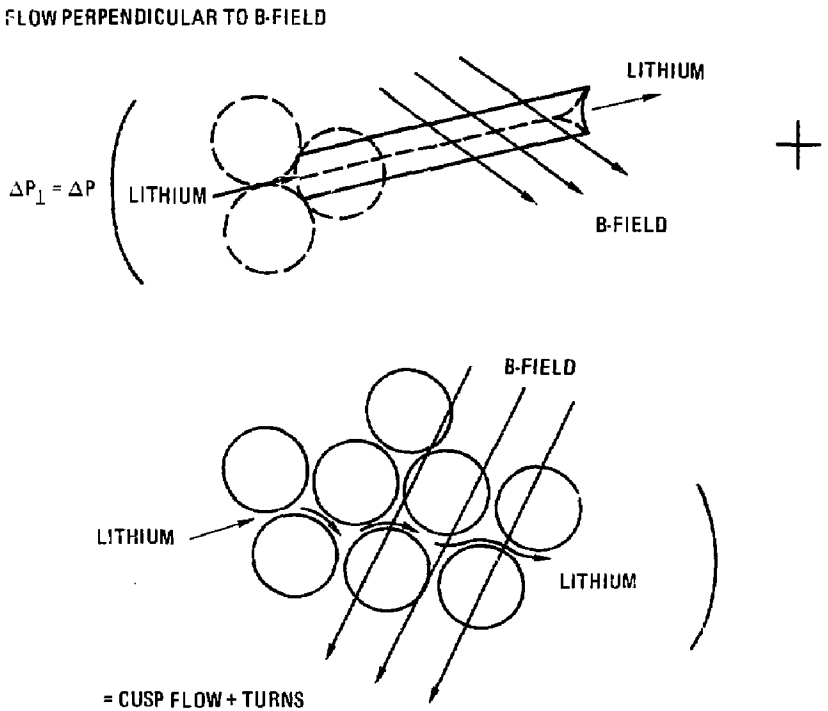

Fig. II.D.2 Packed bed pressure drop model 1.

6.2×10^6 $(\text{ohm-m})^{-1}$, about twice as high as lithium at 3.2×10^6 $(\text{ohm-m})^{-1}$. Assuming perfect electrical contact of the lithium with the beryllium pebbles, the induced currents would flow in both the lithium and in the beryllium pebbles. Considering the radial flow through individual cusp and the configuration and the orientation of the magnetic field, it can be seen that the induced currents, which result from flow among adjacent pebbles, would form a matrix of current flowing among the pebbles. Considering the blanket as a whole as shown in Fig. II.D.3, the local currents in the fluid among the pebbles can form circumferential currents around the blanket.

Based upon the above observation, it is possible to estimate the pressure drop through the bed by starting with the magnetic field contribution to the momentum balance equation:

$$\vec{\nabla}P = \vec{J} \times \vec{B} \tag{8}$$

where $\vec{\nabla}P$ is the pressure gradient vector, $\vec{J}$ is the induced current vector, and $\vec{B}$ is the magnetic field vector. In the above equation, $\vec{J}$ is given by

$$\vec{J} = \sigma \vec{V} \times \vec{B} \tag{9}$$

where σ is the lithium electrical conductivity and $\vec{V}$ is the coolant velocity vector. Considering only the bulk radial flow velocity, the velocity vector is given by:

$$\vec{V} = V_r \vec{r} \tag{10}$$

where

$$V_r = V_0 \frac{R_0}{R} \quad . \tag{11}$$

In the above equation, V_0 is the average radial bulk velocity of the coolant at radius R_0. The bulk radial velocity is determined by the flow area available in the bed i.e., between the pebbles).

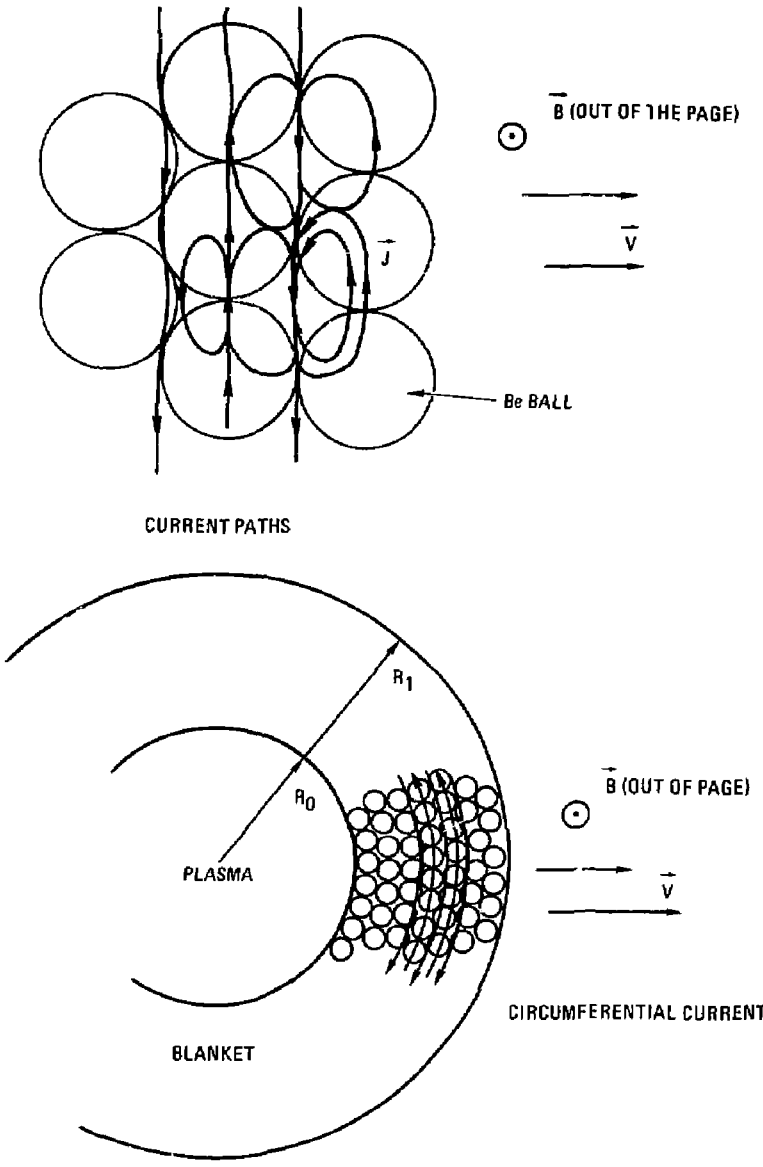

Fig. II.D.3 Current matrix and circumferential current path.

Substituting Eqs. (11), (10), and (9) into Eq. (8) and recognizing that $\vec{B} = B_z\vec{z}$ yields

$$\frac{\partial P}{\partial r} = \sigma V_0 R_0 B^2/R \tag{12}$$

Integrating Eq. (12) over the blanket thickness yields

$$\begin{aligned}\Delta P &= \sigma V_0 R_0 B^2 \int_{R_0}^{R_1} \frac{dr}{R} = \sigma V_0 R_0 B^2 \\ &= \sigma V_0 R_0 B^2 \ln (R_1/R_0) \\ &= \frac{\sigma}{\rho C_p} \left(\frac{\Gamma M B^2}{\Delta T}\right) \frac{R_0}{F} \ln(R_1/R_0)\end{aligned} \tag{13}$$

where ΔP = packed bed MHD pressure drop,
σ = electrical conductivity, (3.2×10^6 ohm-m^{-1}),
ρ = fluid density (486 kg/m^3)
C_p = fluid specific heat, (4184 J/kg),
Γ = neutron wall loading, (1.27 MW/m^2),
M = blanket energy multiplication, (1.97),
B = magnetic field strength, (4.24 T),
ΔT = coolant inlet-outlet temperature differential, (340° to 490°C),
R_0 = packed bed inner radius, (1.587 m),
F = coolant flow cross-sectional area fraction, (0.0931),
R_1 = packed bed outer radius, (1.987 m),
V_0 = fluid velocity at R_0.

V_0 has been substituted by $\frac{\Gamma M}{\rho C_p \Delta T}\left(\frac{1}{F}\right)$, in balancing the power generated in blanket and the power carried away by the coolant.

With lithiuim as the blanket coolant and the blanket operating at the end of life, the calculated pressure drop from this model is 1.81 MPa (262 psi), which is similar to the results from the first model.

With the identification of circumferential current density as the principal cause for the pressure drop, a fourth model was considered by assuming the presence of insulation that can disrupt the current in the fluid, yet allowing the current density $\vec{J}$ to return in the conducting walls, as illustrated in Fig. II.D.4. Considering this as a channel flow problem with ferritic steel (HT-9) as the conducting wall material, the pressure drop was calculated to be only 738 Pa (0.1 psi). This shows the large impact of a highly resistive current return path.

Comparing the four proposed models with consideration of the lithium-filled packed-bed configuration, the circumferential current paths will be very difficult to avoid even if the beryllium pebbles are electrically insulated. Disruption of this circumferential current path, as indicated in the last model, would not be easy to achieve because of the necessity of disrupting the major load path. Even if this can be accomplished, there is a possibility of currents returning through relatively stagnant layers of lithium in the plena regions. Comparing the two models that give high pressure drops, the one that includes the consideration of circumferential currents seems to be more realistic. This model is somewhat conservative because of the use of local maximum fluid velocity in the packed bed geometry for the calculation. The lithium would actually have a varying, and on the average, lower speed as it is passing through openings of varying cross-sectional areas through the packed bed.

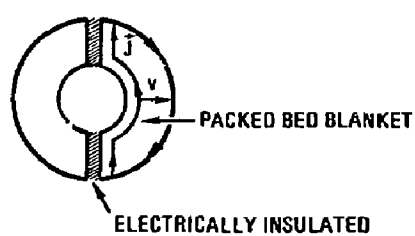

Fig. II.D.4 Current path for packed bed pressure drop model 4.

It is clear from the complexity of the MHD packed bed flow under consideration that there is a need for simple and relevant MHD experiments, in addition to further analytical work in order to understand the MHD effects and to use this understanding to help develop future experiments and improved blanket designs.

II.D.2.d First-Wall Pressure Drop. Figure II.D.5 illustrates the first-wall configuration under consideration. The wall is corrugated for configurational stability, and allows for material swelling under neutron irradiation (see Sections II.B and III.B). A simplified MHD flow model was assumed for the analysis of this flow configuration.

Because of the presence of the strong magnetic field of 4.24 T, the fluid flowing against the field lines will be strongly retarded. Therefore, the coolant lithium was assumed to flow in the 3.0 cm width annulus along the direction of the magnetic field, where the lithium in the "troughs" to each side of the annulus was assumed to be stagnant. The power generated in the metallic structure, in the lithium coolant, and 5 cm into the blanket was conservatively assumed to be carried by the circulating first wall lithium coolant. Based upon this model, the pressure drop of the lithium flowing parallel to the magnetic field lines through the annulus can then be calculated by using the laminar flow equations in the absence of magnetic field.

II.D.2.e Pressure Drop Results and Conclusions. Blanket pressure drops for the primary lithium coolant loop were calculated by using the appropriate equations and approaches discussed in the above sections. The results are summarized in Table II.D.1, with the following input parameters:

First wall radius	1.5 m
Neutron wall loading	1.27 MW/m^2
Module length	4 m
Blanket thickness	0.4 m
Blanket energy multiplication	1.97

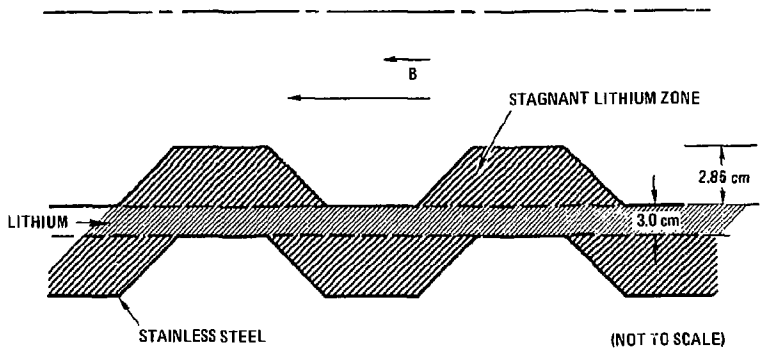

Fig. II.D.5 Corrugated first-wall configurations.

TABLE II.D.1 Blanket Primary Loop Pressure Drops

	Pressure Drops (Pa)	Pressure Drops (Psi)
Inlet plenum[a]	0.26×10^6	38
First wall	392	0.06
Packed bed	1.81×10^6	262
Lithium reflector	0.01×10^6	1.8
Outlet plenum and pipes[a]	0.04×10^6	5.8
Turns, contractions, and expansions[b]	0.107×10^6	15.5
Total	2.2×10^6	323
First wall pressure	1.9×10^6	279
Total blanket pumping power	0.7 MW/ module	0.7 MW/ module
Blanket pumping power/thermal power	0.7%	0.7%

[a]Insulated inlet plenum and outlet pipes [with layer of insulation and 1 mm thick metallic wall (Reference 1)].
[b]Pressure drop coefficient K = 0.03. Note a theoretical and pessimistic upper-bound estimate of K = 0.54 would increase the turning loss to 1.9 MPa (279 psi) with a corresponding increase in first wall pressure and pumping power.

Number of modules	50
Thermal power/module*	94.3 MW
Lithium volumetric flow rate/module*	0.31 m^3/s
Lithium inlet temperature	340°C
Lithium outlet temperature	490°C
Central cell B-field strength	4.24 T

*End of blanket irradiation period.

It can be noted from Table II.D.1 that the packed bed MHD pressure drop dominates the blanket total pressure drop. It was felt that with the conservative assumptions made in the modelling of the packed bed MHD pressure drop, a reduction of the calculated pressure drop will be achieved with further, more accurate, analytical computations. Thus, as a reasonable input to mechanical design, a pressure of 1.7 MPa (250 psi) was selected as the design value for the first wall. At this pressure, it was shown that a reasonable mechanical design can be made with a structural fraction that does not unduely penalize the design. Table II.D.1 also shows that the pumping power required to circulate the coolant is acceptable.

It is obvious that, because of the magnitude of the packed bed pressure drop and the large size of the turning losses if a high theoretical and pessimistic pressure drop coefficient is used, experimental investigation of these MHD effects should be performed for further blanket design evaluations.

It was because of the potentially high blanket pressure drop that the location of the lithium pumps in the power conversion circuit becomes important. As indicated in Section VI.B, the lithium pumps are located at the lithium outlet stream such that the fluid pressure to be experienced by the first wall is at a minimum.

II.D.3 Liquid Metal Blanket Heat Transfer Models and Results

One of the critical effects that high magnetic fields have on liquid metal heat transfer is turbulance suppression. The transition Reynolds

number for flow of conducting fluids in circular pipes in parallel and transverse magnetic fields are (7):

$$Re_{\perp}^{*} = 550\ H_{\perp}$$

and $$Re_{\parallel}^{*} = 60\ H_{\parallel}$$

where $Re_{\perp}^{*}$ and $Re_{\parallel}^{*}$ are the transition Reynolds numbers; and $H_{\perp}$ and $H_{\parallel}$ are the Hartmann numbers for magnetic field orientations perpendicular and parallel to the fluid flow directions.

For the Hartmann number range of 1300 to 7×10^4, the corresponding critical Reynolds number ranges from 6.5×10^5 to 3.5×10^7 for perpendicular flow and from 7.8×10^4 to 4.2×10^6 for parallel flows. For the channel dimensions of the reference design, the Reynolds number range is 3×10^3 to 5×10^4. This indicates that all our flows are well within laminar flow limits.

For liquid metal flow between parallel plates, as for the first wall and inlet annulus models, Nusselt numbers of 12.0 and 10.8 (Ref. 7) can be used for flow direction perpendicular and parallel to the magnetic field lines. For liquid metal flow in smooth round pipes, Nusselt numbers of 7.1 and 6.1 (Ref. 7) can be used for similar flow directions perpendicular and parallel to the magnetic lines. Knowing the applicable Nusselt numbers, the fluid heat coefficients and thus the film drop temperatures can then be calculated.

For the packed bed zone, there is no good heat transfer correlation for liquid metal in this configuration. We have therefore used a conduction model for the temperature drop from the beryllium/thorium pebble to the lithium coolant. Heat is assumed to be uniformly conducted through a spherical shell of lithium of thickness equal to the pebble radius and the resulting temperature drop is used for the effective film drop.

Results of the blanket temperature calculations are illustrated in Fig. II.D.6. The locations in the blanket are those illustrated in Fig. II.D.1. For each location three temperatures are indicated, they are

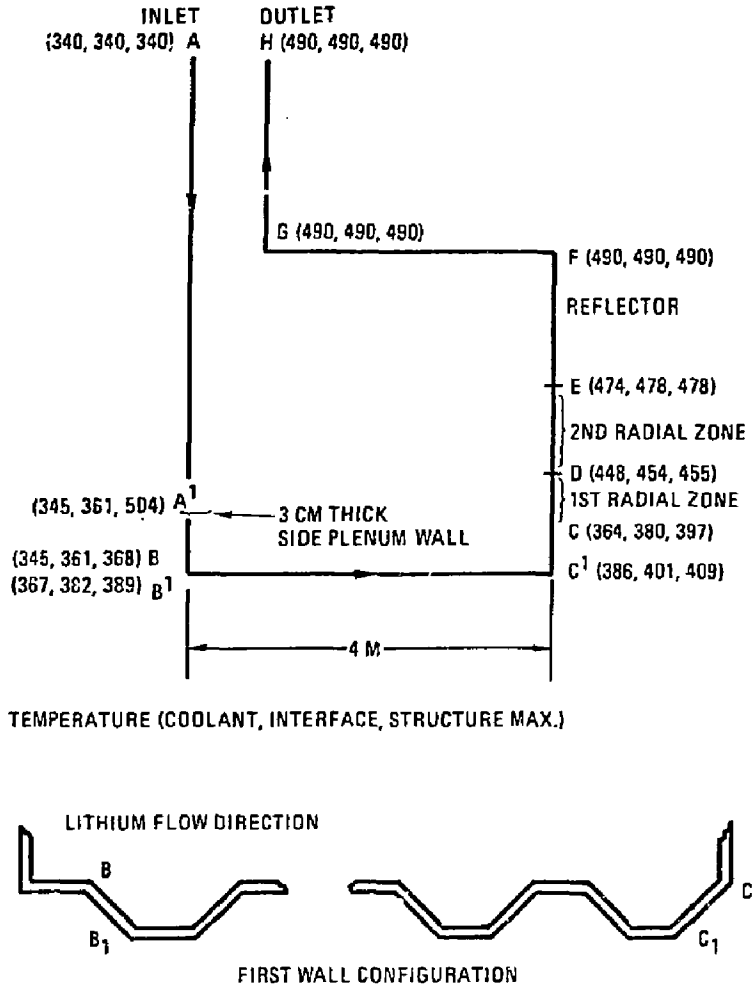

Fig. II.D.6 Blanket temperature distribution.

the coolant temperature, the coolant and steel structure interface temperature, and the maximum structural material temperature, taking into consideration the material thicknesses and volumetric power generation. The lithium coolant temperature was defined by the thermal power carried by the coolant at the particular location, using blanket inlet/outlet temperatures of 340°/490°C.

As noted in Fig. II.D.6, four temperature locations at the first wall are of interest. They are located at the extreme ends of the 4 m long blanket module and on top and bottom of the first wall corrugations as indicated as B, B', C, and C' in the figure. A stagnant layer of lithium thicker than 8 cm at the right side of the first wall can lead to a structural material (HT-9) temperature higher than 546°C. To ensure that the stagnant layer of lithium is not allowed to become thicker than 4 cm at the side of the first wall, a shunt flow of lithium is designed at the location C. As indicated from the above results, the temperature distribution in the blanket is acceptable.

To calculate the temperature distribution in the beryllium pebbles in the packed bed zone, a spherical geometry was used in the calculation. To simulate the thorium pin geometry realistically, the surface heat flux from the thorium pin was calculated from the power generated in the pin divided by the surface area of the cylindrical pin. Table II.D.2 illustrates the temperature distributions in different pebble regions at different locations of the blanket.

Table II.D.2 shows that the temperature distribution in the packed bed is acceptable. A potential problem, however, is the temperature differential across the beryllium metal. This maximum temperature differential of 38°C causes a differential radiation-induced swelling of the material which limits the pebble life to ~1 year. To alleviate this potential difficulty, the reference design was changed by placing a thorium ring around a solid beryllium pebble instead of the thorium pin configuration (see Section III.C). This will reduce the temperature differential through the beryllium metal. Thermal modelling of this design will be developed in the next phase of this work.

TABLE II.D.2 Fertile Fuel Temperature Distribution

SPHERICAL MODEL:

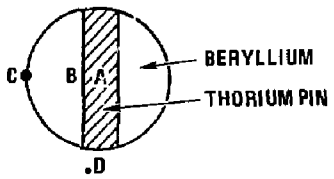

	TEMPERATURE, °C			
	A	B	C	D
BLANKET LOCATION	Th-METAL T_{MAX}	INTERFACE	BALL SURFACE	LITHIUM
FRONT (CLOSE TO FIRST WALL)	422	405	367	364
BACK (NEXT TO OUTLET PLENUM)	487	483	475	474

II.D.4 Summary of Design Issues

The following summarizes the design issues for the fluid dynamics and heat transfer designs for the 1982 Fusion Breeder Reactor Blanket.

- Packed bed MHD pressure drop dominates the blanket design affecting its mechanical design, neutronics performance, power conversion system design, and blanket life-time, further modelling and analysis will be needed for this problem.
- Pressure drops from turns, contractions, and expansions are also areas of uncertainty that need to be further studied.
- The selected reference design first-wall pressure drop of 1.7 MPa (~250 psi) is reasonable.
- Experimental investigation of packed bed, turns, contraction, and expansion pressure drops is recommended for future studies.
- Available heat transfer correlations for MHD calculations are adequate for existing scoping studies.
- Blanket temperature distribution is within acceptable material temperature limits.
- Thermal stress problems for high temperature liquid metal cooled blanket design and power conversion system will need to be addressed in addition to the MHD problems considered in this section.

References, Section II.D

1) R. Moir et al., "Fusion Breeder Program Interim Report," UCID-19406-1, June 1982.
2) E. W. Sutton and A. Sherman, Engineering Magnetohydrodynamics, McGraw-Hill, New York, 1965.
3) G. A. Carlson, "Magnetohydrodynamic Pressure Drop of Lithium Flowing in Conducting Wall Pipe in a Transverse Magnetic Field - Theory and Experiment," Proceedings of the 1st Topical Meeting on the Technology of Controlled Nuclear Fusion, CONF-740402-P1, 1974.

4) J. C. R. Hunt and R. Hancox, "The Use of Liquid Lithium as Coolant in a Toroidal Fusion Reactor, Part 1, Calculation of Pumping Power," Culham Laboratory Report, CLM-R115, 1971.

5) M. A. Hoffman and G. A. Carlson, "Calculation Techniques for Estimating the Pressure Losses for Conducting Fluid Flows in Magnetic Fields," UCRL-51010, 1971.

6) W. M. Wells, "Experiments and Calculations on the Feasibility of Pumping Liquid Lithium in a Thermonuclear Reactor Blanket," Lawrence Radiation Laboratory, Livermore, UCRL-50544, 1969.

7) M. A. Hoffman, "Magnetic Field Effects on the Heat Transfer of Potential Fusion Reactor Coolants," Lawrence Radiation Laboratory Report, UCRL-73993, June 1972.

II.E OPERATION AND MAINTENANCE

II.E.1 Overview

An awareness of the impact of remote maintenance on the operation of a reactor and its components is a key consideration often overloooked in the initial design phases of fusion systems. As discussed elsewhere in this report, the blanket (in particular the first wall) is not expected to survive as long as the shield, magnets, and other reactor hardware. Since the blanket module interfaces with these components as well as the lithium coolant system, the blanket module should be capable of being removed and a new module reassembled with the longer lived shield and magnet.

It is extremely important to minimize the number of connections, both from the standpoint of coolant lines and instrumentation. Mechanical seals and remote quick disconnect joints should be incorporated to facilitate assembly/disassembly. Welded seals or pipe connections should be avoided to the maximum extent possible since they have a great impact on the assembly/disassembly/replacement time. This additional time affects plant availability which directly impacts the overall plant economics. This remote maintenance aspect has been factored into the design as previously mentioned in Section II.B and discussed to some extent in Section VI.B.2.

Further considerations of operation and maintenance are addressed in the remainder of this chapter.

II.E.2 Operation and Maintenance (O&M) Sequence

II.E.2.a Initial Assembly. A complete blanket module assembly (which consists of the blanket assembly, shield assembly, and magnet) is positioned into its station. There are fifty stations equally spaced along the central cell region of the reactor building. Each module is located at the center of the station and aligned with the axis of the central cell. The blanket assembly is fixed at the center to prevent axial motion of the center during subsequent heat up of the central cell assembly. When properly positioned at room temperature there will be approximately 2.5 cm (1 inch) of clearance between adjacent modules (see Section II.B.7) and their intermodule seal

faces. The shield blanket, and magnet assemblies are supported separately so that each assembly, operating at its own temperature, can move independently due to thermal expansions/contractions between initial assembly and operating conditions.

The blanket, shield, and magnet coolant line connections as well as the electrical and instrumentation connections are completed. The pressure lines are connected to the intermodule seals and pressure applied to deflect the seals (Figure II.E.1) until their mating faces contact to seal off the clearance gap between modules. After all electrical and fluid piping connections are checked the modules are ready for start-up preparation.

II.E.2.b Central Cell Operating Procedure for Reactor Start-Up. Auxiliary heating and heat tracing systems are installed on all liquid lithium piping in order to assure that the lithium remains molten at all times. This technique for maintaining coolant in the molten state has been satisfactorily addressed in LMFBR and liquid metal loop designs. These are also well insulated to prevent excessive heat losses. Since the blanket internals are complex, these are heated by means of a hot argon cover gas which is circulated through the blanket and part of the primary loop prior to start-up. After sufficient magnet cooldown, the loop and cover gas heaters are turned on until the temperature of the structure is in excess of the 180°C lithium melting temperature. The liquid lithium will be stored at a higher temperature (250-300°C) to assure that freeze up will not occur during the filling operation should local cooler spots exist in the loop.

The coolant loop is then filled with molten lithium and the hot gas is evacuated from the loop. After the loop is filled the pumps can be turned on and the loop heated further by the pump work required to circulate the coolant. During the above procedure, the major portion of the axial module expansion occurs and the gap between modules in the vicinity of the intermediate seals will be substantially reduced. The cental cell region is then ready for vacuum pump down and reactor start up. The beryllium/thorium fuel spheres are loaded by the fuel handling system immediately prior to start-up (Section IV.C).

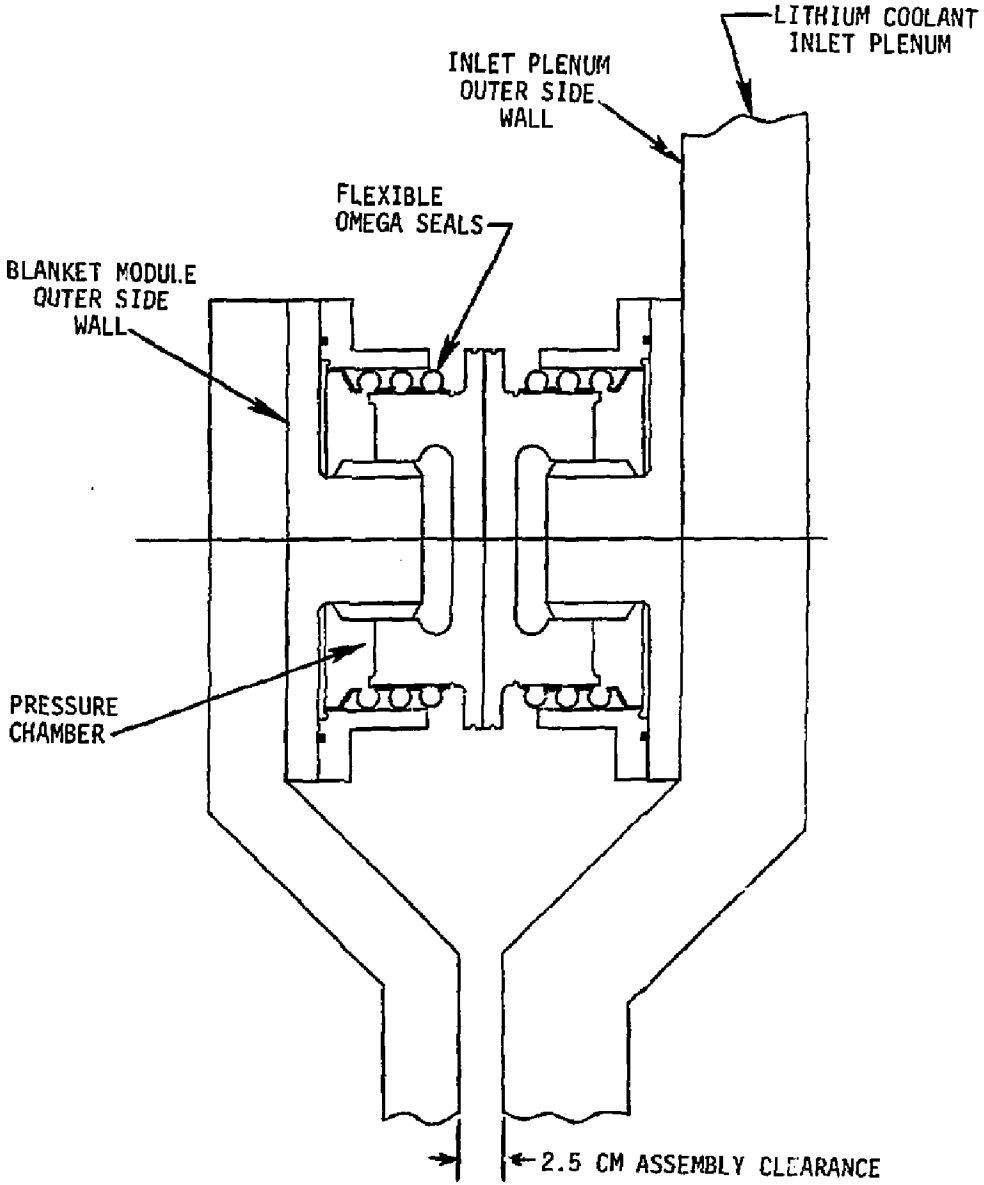

FIG. II.E.1. Intermodule seal arrangement showing relationship of seal and modules during initial assembly after seal pressurization.

II.E.2.c Maintenance - Disassembly/Assembly. During the evaluation of the design concept for the blanket module, remote maintenance was a key consideration. Although the shield and magnets for the module were not designed except to the extent that size and envelope constraints were established, it is important that attention be given to their design. The following sequence describes the blanket module removal/replacement procedure.

At the appropriate time (either for scheduled maintenance or unscheduled maintenance in the event of some malfunction requiring blanket replacement), the reactor is shutdown. The shutdown consists of turning off the plasma, reducing the coolant flow and de-energizing the magnets. After isolating the module by appropriate valving, the fuel is removed by the fuel handling system, but the lithium coolant level and some flow is maintained to remove structural afterheat (see Chapter V Safety Analysis). After ~2-4 days the lithium coolant is drained into its storage tank and the module is completely drained. The shield and magnet coolant lines are disconnected and all electrical joints are disconnected. An auxiliary cryogenic system is connected to the magnet to maintain it at low temperature to reduce cooldown after re-assembly prior to startup. Finally, after the plasma chamber (e.g., cryopanels) is adequately evacuated of tritium, the intermodule seals are depressurized and retracted to provide clearance for withdrawal of the module.

A transporter vehicle is proposed for module removal and transport of the module after removal. Alternate methods are the use of high capacity roller assemblies or oil or air pad bearings to carry the weight while the module is being moved. The reference module/blanket/shield assembly is estimated to weigh from 600-800 tons. Reference 1 suggests the use of a wheeled transporter for removing and transporting a tokamak module approximately the same size and weight as the reference design module.

The transport vehicle is positioned under the module, and automatic jacks are activated to transfer the load from the floor to the transporter. The fuel inlet and outlet pipes at the top of the module are disengaged similar to the coolant lines described below. Next the two 180° elbows behind the module (Figure II.E.2) (which are fitted with quick disconnect joints and connected to the inlet/outlet torii) are released and lifted away. Quick disconnect joints which are either motor or hydraulically actuated will need to be developed, or else the joints will have to be remotely cut and rewelded. The corresponding inlet/outlet "J" shaped pipes on the opposite side of the module

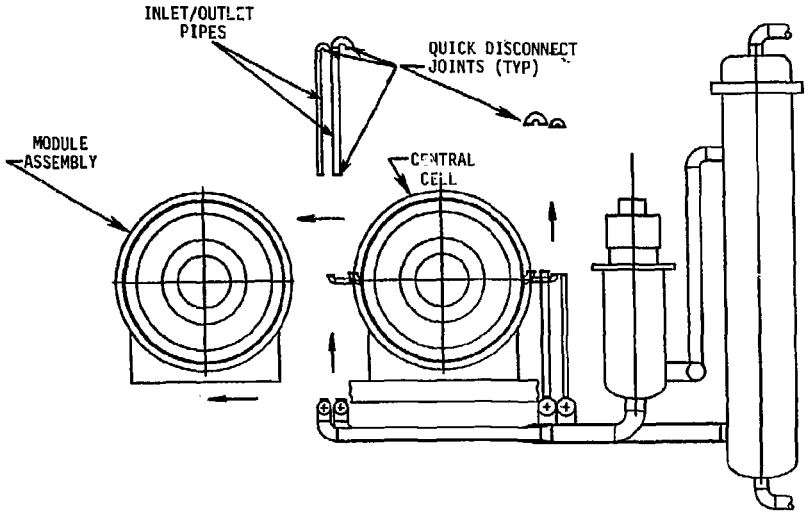

FIG. II.E.2. Sequence of steps for removal of blanket module assembly from the central cell.

torii (left side of the figure) are similarly disconnected and lifted away to clear the module assembly. Since this concept was initially conceived later concerns for evacuating trapped gases, and filling and draining of the module led to changing the location of the main inlet and outlet pipes. The pipes are now located at the top and bottom of the torii (as shown in Figure II.A.1) instead of at the horizontal centerline as shown in Figure II.E.2. The change in location is not expected to have a significant impact on disassembly time. The complete module assembly is then extracted horizontally as indicated.

The complete assembly is then transported to the reactor maintenance building for further disassembly and replacement of the blanket/first wall assembly. In order to permit removal of the blanket/first wall assembly, the shield is split circumferentially at the left hand side of the magnet as shown in Figure II.E.3. This permits the right hand side of the shield to be moved from the assembly and provides access to the magnet so that it can be removed. The remaining left hand portion of the shield is split at the vertical centerline so that it can be removed from the blanket without interfering with the fuel inlet/outlet pipes. A similar procedure for remote removal/replacement of a module assembly has been proposed for MARS (2). (Figure II.E.4 shows the MARS concept which utilizes a blanket module transporter and has the capability for decoupling the module from the magnet). The shield and magnet are installed in reverse order on a new blanket assembly and returned to the reactor building for re-installation into the central cell assembly. A new or refurbished blanket module assembly is re-installed in essentially the reverse order from that required for removal from the central cell as previously described.

II.E.3 O&M Facilities

Since maintenance of the reactor is the key ingredient affecting plant availability, it is imperative that the O&M facilities have the capability for processing and replacing spent modules efficiently. The Hot Cell/Reactor Service building must have sufficient shielded storage area for accommodating many used blanket modules. In addition several work stations must be provided so that more than one module can be processed simultaneously. This is required to achieve the desired .70 plant availability with the central cell area configuration and the requirements defined in Table II.E.1. The remote

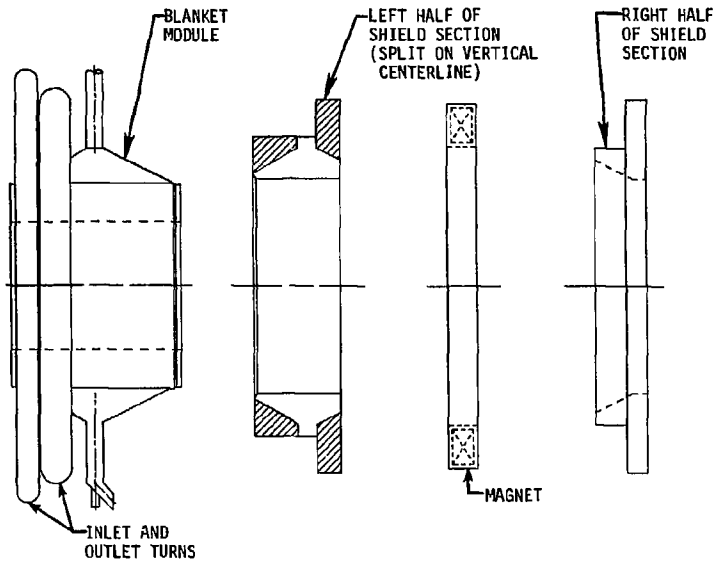

FIG. II.E.3. Blanket, magnet and shield components from the Fusion Breeder Reactor blanket module assembly showing the split shield arrangement.

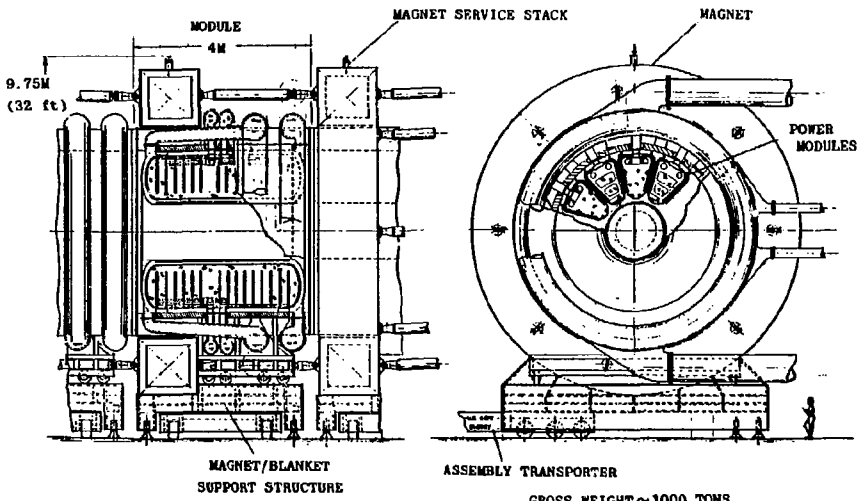

FIG. II.E.4. MARS magnet and module assembly showing the blanket assembly transporter.

maintenance study of Reference 1 showed that it would take approximately two months to remove a sector of a tokamak containing a pair of toroidial field coils, and sections of the vacuum vessel and blanket/shield. However, the procedure considers time required for removal/replacement of a welded vacuum vessel section, poloidal field coils, neutral beams and divertor. If elimination of these steps were factored into maintaining the central cell, the time interval appears to be reduced to approximately 48 days per blanket module removal and replacement. Table II.E.2 gives the breakdown of time intervals required to perform the various operations for the FBR blanket replacement utilizing applicable information from Reference 1.

As shown in Table II.E.1 for a blanket lifetime of 10 years, three modules would be replaced during each full fuel cycle period of 224 days (see fuel management Section IV.B). An availability budget was constructed and the 48 day total changeout time indicates that it is within the budget. For a 5 year life the corresponding number of modules requiring replacement would be six. The interface between fuel cycle operations and module replacement requires further optimization. In addition, the blanket O&M interval for replacement needs to be looked at in more detail in the future to see if some of the time associated with disassembly/assembly operations could be reduced to less than the 48 days estimated.

TABLE II.E.1 Central cell parameters affecting availability and module replacement inerval.

Number of Blanket Modules	50
Life of Blanket Module	5-10 yrs.
Average Number of Modules Replaced per year	5(10)*
Availability	70%
Average Annual Number of Outage Days/Months @ 70% Availability	109/3.6
Number of Days/Months in a full fuel cycle period (Including Maintenance Period)	224/7.4

TABLE II.E.1 (Continued)

Number of Days/Months Available for Maintenance during Fuel Cycle Period (at 70% Availability)	43/1.4
Number of Modules to be Replaced at End of Fuel Cycle Period	3(6)*
Estimate Module Replacement Interval (Month)	1

*Numbers in parenthesis where appropriate based on 5 year life, others applicable to 10 year life predicted in Section III.B.

TABLE II.E.2 Estimated disassembly/reassembly time intervals for the Fusion Breeder Reactor blanket module assembly.

Task Designation	Task Description	Est. Time To Complete (Hrs)
	Disassembly	
1	Shutdown plasma and begin tritium out-gassing	12
2	Dump fuel via fuel handling system	120
3	Provide cooling for decay afterheat	P*
4	Deactivate central cell magnets	P
5	Isolate central cell from end cells	P
6	Drain blanket and shield coolants	12
7	Deactivate intermodule seals	P
8	Disconnect electrical connections	24
9	Cut (or disconnect) blanket/shield I/O piping	48
10	Remove intermodule biological shields	36
11	Remove intermodule mechanical structure	48
12	Connect magnet auxiliary cooling (liquid He)	6

TABLE II.E.2 (Continued)

Task Designation	Task Description	Est. Time To Complete (Hrs)
13	Disconnect primary magnet cooling (liquid He)	6
14	Install module transporter	24
15	Remove module to hot cell	6
16	Remove right shield component	12
17	Remove magnet	6
18	Remove left shield components (2)	12
19	Remove and dispose blanket structure	6
	Assembly	
1	Replace left shield components on new blanket	12
2	Replace magnet on left shield	6
3	Replace right shield component	12
4	Return module to central cell location	6
5	Align module and remove module transporter	24
6	Connect primary magnet cooling	6
7	Disconnect magnet auxiliary cooling	6
8	Install intermodule mechanical structure	48
9	Install intermodule biological shield	36
10	Weld (or connect) blanket/shield I/O piping	168
11	Connect electrical connections	24
12	Preheat blanket and primary loop	24
13	Fill blanket and shield coolants	12
14	Activate central cell magnets	24

TABLE II.E.2 (Continued)

Task Designation	Task Description	Est. Time To Complete (Hrs)
15	Activate intermodule seals	24
16	Load unirradiated fresh fuel	24
17	Perform pre-operational testing	48
18	Remove central cell/end cell isolation	P
19	Startup plasma	264
	TOTAL	1146 hrs (47.75 days)

*P designates a parallel task which should not require additional time.

References, Section II.E

1) M. Sniderman, "Fusion Reactor Remote Maintenance Study, Final Report," Electric Power Research Institute Report EPRI ER-1046 (RP-1044). (April, 1979.)

2) Private Communications, September 1981, Discussions between J.S. Karbowski of Westinghouse Advanced Reactors Division and D. H. Berwald of TRW.

CHAPTER III

MATERIALS AND LIFETIME ISSUES

III.A. MATERIALS COMPATIBILITY ISSUES

III.A.1. Overview

The reference direct cooled blanket design incorporates a cylindrical module with a beryllium multiplier in mobile pebble form, thorium metal snap-ring overlays (possibly coated) on the beryllium pebbles (see Section III.C), and a liquid lithium coolant which is pumped directly through the pebble bed. Such a concept presents a complicated compatibility matrix with the possibilities for both solid-solid and liquid metal-solid interactions. This matrix has been examined to identify possible reactions under relevant operating conditions and their effects on blanket integrity and performance. Solid-solid interactions include the following:

1. Be — structural alloy (currently HT-9)
2. Th — structural alloy
3. Be — Th (plus possible barrier coating)

In addition, self-welding may occur at contact points between the beryllium pebbles (Be-Be) or thorium rings (Th-Th). Liquid metal interactions are those of molten lithium with the thorium, steel, and beryllium. Mass transfer of these materials in lithium under temperature and concentration gradients may be an important problem. Deposition of dissolved species in the cooler regions of the lithium circuit can potentially affect reactor operation. Effects of impurities in the solid and liquid blanket materials (principally O, N, C, and T) on compatibility must also be examined. Although this matrix of potential compatibility concerns is large, the maximum operating temperature in the present reactor concept is relatively conservative ($\leq$500°C) in terms of conventional liquid metal heat transfer systems (for example, fast breeder reactors).

During FY 1982 the materials compatibility effort consisted of examining many of the possible interactions theoretically and/or experimentally. In the former case, thermodynamic and existing compatibility data were used to assess the severity of the expected reactions. Experimentally, compatibility reaction couples of a type described previously (1) were exposed in static lithium at 350, 450, and 550°C. The specific purpose of these experiments has been to examine the reactions between beryllium and stainless steel in direct contact and across a molten lithium gap. Results from this study as well as the compatibility assessments are presented below.

III.A.2. Solid-Solid Interactions

The most significant solid-solid interactions are anticipated to be those involving metallic beryllium. This is because beryllium forms very stable intermetallic compounds (beryllides) with both transition and actinide metals. Furthermore, because the beryllium atom is relatively small, the solid-state diffusion rates that control interfacial reactions with beryllium tend to be correspondingly high.

In the current reference design concept, the beryllium pebbles are overlaid with a thorium ring. The maximum temperature at the contact interface is estimated to be 500°C. There are no experimental data on the interdiffusion of thorium and beryllium; however, thermodynamic data indicate the metals should react to form the compound $Be_{13}Th$. The compound can be expected to form as a uniform layer at the Be-Th interface and to grow at a rate controlled by the diffusion of beryllium through the developing layer (that is, with a half-power time dependence). The mutual solubilities of beryllium and thorium are negligible at 500°C (2) so there should be no interdiffusion effects other than the growth of the intermetallic

compound. The thorium density in the compound is sufficiently low that the build-up of ^{233}U should not constitute a hot spot problem, although the compound could make it difficult to separate the thorium rings after the one-half year residence time. In the latter case it may be necessary to employ a diffusion barrier between the two metals. Possible barriers include CVD-deposited or ion-plated molybdenum, applied to the inside of the thorium ring, or a stable carbide coating (for example, TiC) applied to the exterior of the beryllium pebble. Either approach would require an experimental evaluation.

The reaction of beryllium with the containment alloy, HT-9, constitutes another potential compatibility problem. The absence of nickel as an alloying element in HT-9 should reduce its rate of interalloying with beryllium compared to that for an austenitic stainless steel. Nevertheless, the interdiffusion between iron and beryllium at the proposed operating temperature could limit the containment lifetime. The compatibility of beryllium with structural metals has been addressed in previous reports, and the conclusions have led to testing of diffusion couples of stainless steel and HT-9 with beryllium (discussed in Section III.A.5).

The only solid-state thorium reaction of engineering significance appears to be the beryllium-thorium reaction referred to above. Various fuel irradiation capsules and at least one reactor experiment (SRE) have operated with thorium-metal-matrix fuels in contact with austenitic stainless steel without significant interaction up to 650°C. (3) Of most concern will be the tendency for carbon to be transferred from HT-9 to the thorium, which can dissolve up to 4 at. % C. However, as discussed in Section III.A.3, decarburization of the HT-9 via the lithium coolant will be a more significant problem overall than what accrues from direct contact with thorium.

The extent of self-welding between beryllium-beryllium and thorium-thorium contact points is critical to the removal of beryllium pebbles after the prescribed radiation period. Unfortunately, there is little experimental information by which to gauge any self-welding tendencies. As will be discussed in Section III.A.3, thermodynamic considerations indicate that a thin oxide coating could develop on the thorium surfaces exposed to lithium, but the beryllium surfaces will be oxide free. The growth rate of interfacial attachment areas (necks) between pebbles have been calculated (1) assuming that volume diffusion is the rate-controlling mechanism. On this basis, the attachment of thorium to thorium was predicted to be negligible, and the attachment rate for beryllium was estimated to be $\leq$0.12 mm/y (0.06 mm/irradiation period). Although this is an extremely slow rate in terms of the fraction of the pebble circumference affected, it could nevertheless limit the mobility of the pebbles. Furthermore, other transport processes could operate to permit interfacial attachment, including surface diffusion and a dissolution/deposition process through the lithium melt. Thus, it is important to establish the nature of the external beryllium surface that will exist in the blanket (for example, whether it will develop an intermetallic or carbide layer in contact with lithium, as discussed below).

If beryllium self-welding is shown experimentally to be a potential problem at 500°C, there are various coatings that can be applied to the pebbles to limit the volume and surface diffusion rates of beryllium. One logical approach would be to take advantage of the very stable and refractory intermetallic compounds formed between beryllium and such metals as chromium, iron, and molybdenum. Coatings of the latter metals could be applied in pure form to the beryllium surface and then reacted at about

800°C to produce the beryllide compound. Producing a nitride or carbide coating on the beryllium could also be an effective approach, but achieving chemical stability in the presence of HT-9 and thorium may be more difficult than for a beryllide.

III.A.3. Liquid Metal Corrosion/Mass Transfer

The direct-cooled blanket concept is predicated on the chemical compatibility of beryllium, thorium, and HT-9 with liquid lithium. The compatibility issue here transcends more than just the resistance of these individual materials to lithium at design temperatures. A larger concern is how the presence of any one material in the circuit will affect the corrosion performance of the others. For example, all of the solid-solid interactions discussed above will be fundamentally affected by the presence of lithium.

Lithium corrosion can take several forms: dissolution, alloying, impurity (including carbon) transfer, intergranular penetration, and thermal-gradient and dissimilar metal mass transfer. Each type of corrosion reaction can lead to specific problems. For example, the mass transfer of dissolved species and subsequent deposition of such can cause flow restrictions with attendant hot spots in the pebble bed (although this effect could be mitigated by the one-half year residence time), while in cases where intergranular penetration may occur, the mechanical integrity of the structural alloy could be compromised. Impurity transfer can result in the formation of surface compounds on the solid blanket components or in the carburization/decarburization of a steel. Impurities can also promote intergranular attack in lithium systems.

As noted previously (1), corrosion data for thorium in liquid lithium are not available in the open literature and will be needed for complete

compatibility assessment of the blanket system. However, the excellent compatibility of thorium with sodium (4) indicates reasonable compatibility with lithium. Whether a diffusion barrier is used against the thorium to prevent interalloying with beryllium will obviously impact the lithium compatibility question. Thermodynamic calculations indicate that at 500°C, ThO_2 would not be reduced by lithium containing more than 5 ppm (by weight) of oxygen. Thus, even in the absence of a deliberate barrier, wetted surfaces of thorium metal would probably be covered by a thin oxide that might serve to reduce beryllium interalloying. Carbide coatings have also been suggested as possible diffusion barriers. While such coatings could afford excellent compatibility with lithium (5), it will be difficult to find carbide coatings that are simultaneously compatible with two strong carbide formers, thorium and beryllium, in the same system.

Little is known concerning the compatibility of beryllium with lithium, particularly at the proposed blanket temperature ($\leq$500°C). The corrosion resistance of beryllium in sodium, which is acceptable up to 600°C, may have little bearing on its resistance to lithium, since a surface oxide would normally be present on the beryllium in the case of sodium, but definitely not in the case of lithium. However, no Be-Li compounds have been reported and there appears to be only limited solubility of beryllium in lithium. (6) As discussed in Section III.A.5, the dissolution of beryllium in lithium may be exacerbated by the presence of nickel-bearing alloys in contact with the same lithium. This was demonstrated by the results from diffusion couple experiments in which BeNi formed near the beryllium surface even when type 316 stainless steel and beryllium were separated by lithium. HT-9 should therefore be an improvement over austenitic stainless steels for containment of lithium and beryllium.

Corrosion studies of ferrous alloys in liquid lithium have been ongoing in the U.S. magnetic and inertial confinement programs for several years. (7,8) The fusion breeder effort can therefore draw from this relevant work. Studies to date have indicated the nature and, to a lesser extent, the rate of temperature gradient mass transfer that will occur from the hotter to the cooler regions of iron-based alloy heat transfer circuits containing lithium. While mass transfer rates depend on a number of factors, the rates appear generally acceptable for HT-9 at the projected 500°C maximum with a ΔT of 150°C. In the case of Fe-Ni-Cr steels, nickel and a smaller amount of chromium are preferentially leached from the surface by the lithium until an iron-rich (~85-90 wt %) surface forms. (8) Use of a Fe-Cr (ferritic) steel in lithium would therefore avoid the problem of rapid nickel dissolution during the initial stage of lithium exposure. However, this material selection may not avoid possible initial formation of pure chromium deposits that have been observed in some stainless steel-lithium circuits. (9)

Another important compatibility reaction is that of carbon transfer between the structural alloy and the lithium. (10,11) In many cases, a ferritic steel can decarburize in lithium with an attendant change in its mechanical properties, while an austenitic stainless steel may carburize. The direction and extent of carbon transfer depend on the relative carbon activities in the lithium and steel as they are affected by temperature (including the temperature differential of a system), alloy composition, and heat treatment. (10,11) Microstructural manipulation can aid in minimizing carbon redistribution in lithium systems, and such carbon transfer should be relatively sluggish at the operative temperatures of the present blanket system (<500°C). However, both the thorium and beryllium surfaces in the

lithium circuit are effective sinks for carbon given the initial carbon activity of HT-9.

The rate-controlling step for the release of atoms from the solid to the molten lithium can be in the liquid boundary layer, at the solid/liquid interface, or in the solid. If diffusion in the liquid lithium boundary layer is rate-controlling for the dissolution process (as is often the case), the fusion reactor's magnetic field can affect the mass transfer rate. (12) A transverse magnetic field would act to restrict turbulence such that a thinner effective boundary layer is produced, and a higher corrosion rate would be expected. Magnetic fields may similarly influence deposition rates. There have also been several observations of preferential accumulations of iron and iron-manganese deposits in the areas of electromagnetic pumps in lithium circuits. (13,14) In view of these possible effects, the lower magnetic field strength of a mirror fusion reactor (4.2T), relative to a tokamak, may mitigate this particular problem.

III.A.4. Impurity Effects

The corrosion of beryllium can be exacerbated by its reaction with nitrogen in the lithium to form Be_3N_2, which has been determined to be a stable compound in the Li-Be-O-C-N system at typical impurity levels (6) (see Fig. III.A.1). In addition, results from experimental work (as reviewed in ref. 8) have indicated that higher levels of nitrogen in lithium accelerate, and possibly change, the corrosion reactions of steel with lithium. Because of the lack of thermodynamic data on the Th-N system, we cannot assess the influence of nitrogen on the compatibility of thorium with the other blanket materials.

Thermomechanical calculations involving the Be-Li-C-O-N system (6) have shown that BeO and 2 BeO·Li_2O are not stable under conditions of normal

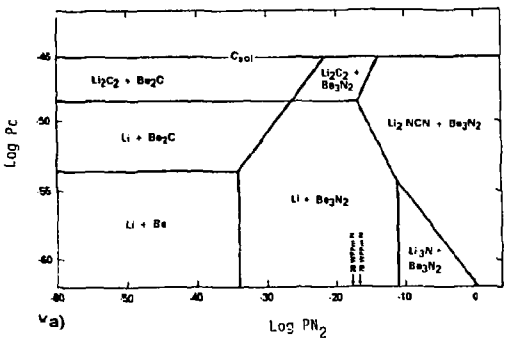

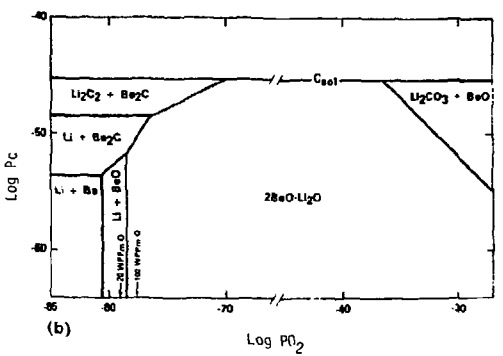

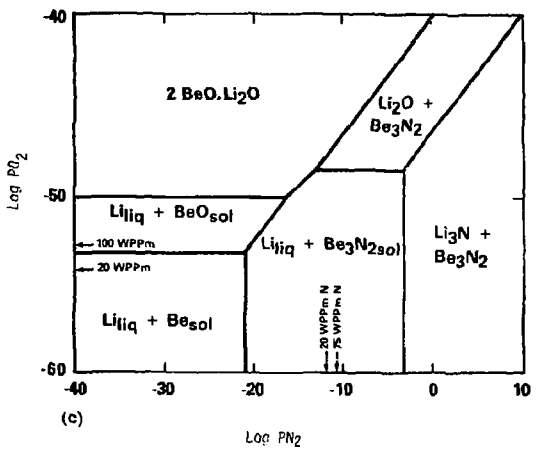

Fig. III.A.1. Thermochemical calculations as published by Migge in ref. 4. Typical impurity levels in lithium are indicated. (a) Li-Be-N-C system, 427°C. (b) Li-B-O-C system, 427°C. (c) Li-Be-N-O system, 727°C.

impurity limits for lithium (see Fig. III.A.1). We thus do not expect any beryllium corrosion problems related to oxygen impurities. However, the surface oxide on the beryllium pebbles exposed to the lithium will dissolve fairly rapidly upon exposure, thereby resulting in a higher than normal oxygen level in the lithium. Although oxygen impurities do not normally affect the dissolution behavior of lithium, concentrations above about 5 ppm would result in oxidation of any uncoated thorium in the system. If these films were as protective as those formed on thorium in air at 500°C, their presence may actually be beneficial.

As discussed above in Section III. A.3, the activities of carbon in lithium and in the structural steel determine whether carburization or decarburization of the steel will occur. Typical steel carbides ($M_{23}C_6$, M_6C) are thermodynamically more stable than stoichiometric thorium carbide and are about as (or possibly less) stable than Be_2C. A carbide coating on the thorium metal (for example, TiC) would be stable in lithium so long as it is also more stable than Be_2C. Thorium carbide is marginal in this respect.

III.A.5. Results of Li-Be Compatibility Experiments

In support of the fusion breeder program, Oak Ridge National Laboratory (ORNL) has tested diffusion couples of type 316 stainless steel against beryllium in static lithium at 350, 450, and 550°C. The design and conditions of the experiments were presented in the interim report. (1) Examination of couples exposed for 1000 h showed significant interalloying between the beryllium and steel at 450 and 550°C, the depth increasing with temperature (Fig. III.A.2). Additionally, as shown in Fig. III.A.3, a layer of BeNi (as identified by x-ray diffraction) was formed within lithium-filled gaps which separated the beryllium and steel at distances of 0.8 and

(THIS PAGE LEFT BLANK INTENTIONALLY)

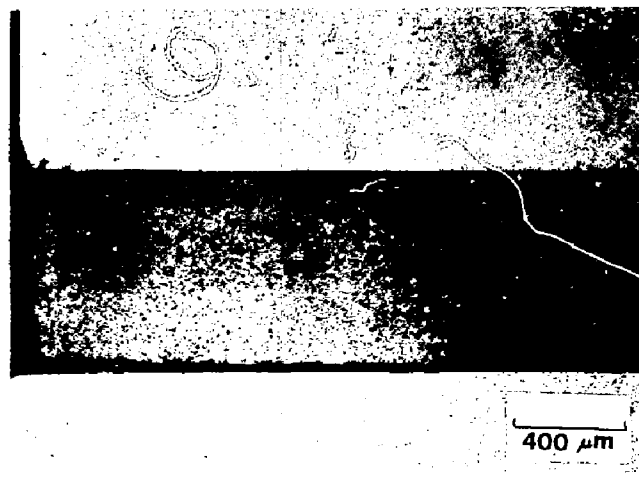

(a)

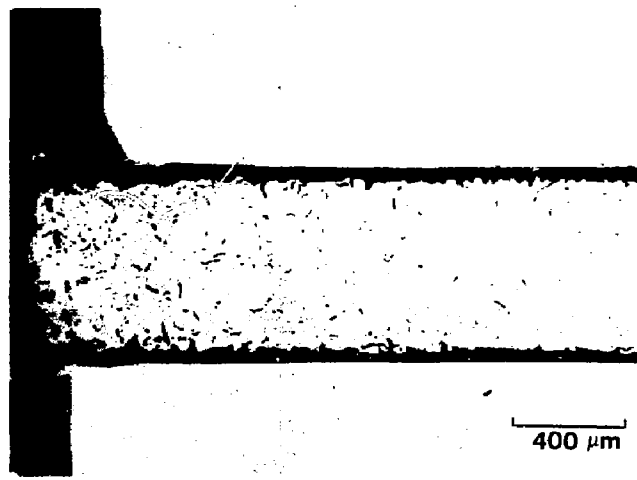

(b)

Fig. III.A.2. Type 316 stainless steel/Be/type 316 stainless steel reaction couples exposed in static lithium for 1000 h. (a) 450°C. (b) 550°C.

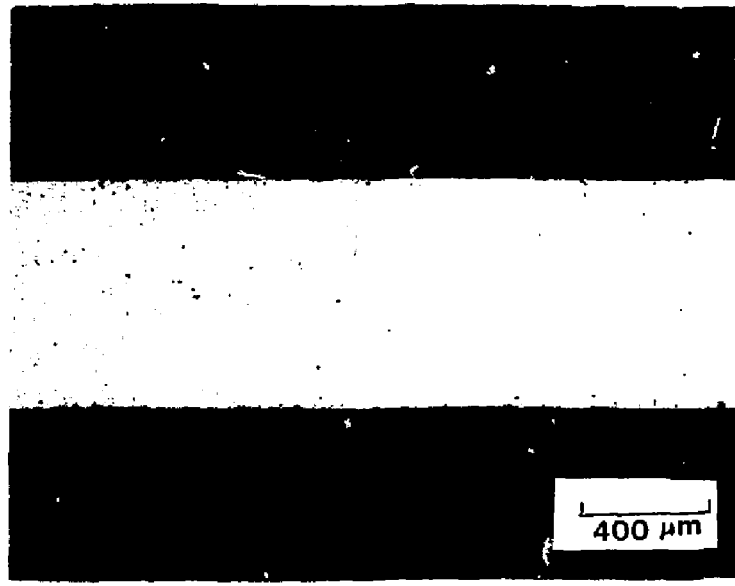

(a)

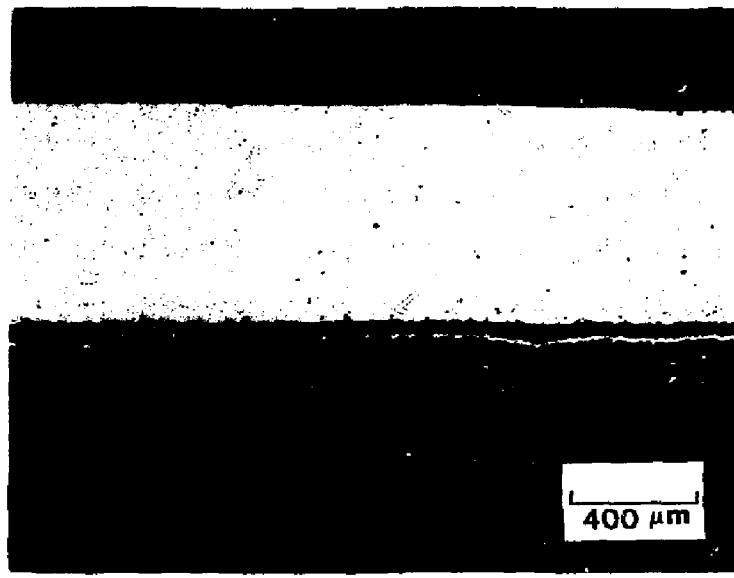

(b)

Fig. III.A.3. Cross-sections of beryllium that have been exposed for 1000 h in static lithium with type 316 stainless steel in close proximity. Detached material is BeNi. (a) 450°C. (b) 550°C.

1.3 mm, respectively. The 350°C diffusion couple showed only a superficial beryllium-nickel reaction layer at points of direct contact. No evidence of beryllium-iron interalloying was found in these tests. Iron-chromium steels would therefore be preferable to those containing nickel. Accordingly, a similar series of tests is being conducted on HT-9/beryllium diffusion couples. In addition, couples of type 316 stainless steel/beryllium tested for 3000 and 5000 h remain to be examined.

III.A.6. Summary of Issues

Any compatibility assessment of the present fusion breeder blanket design concept is complicated by the number of blanket components. Solid-solid interactions include self-welding of the thorium and beryllium (in the presence of lithium), the interalloying of thorium and beryllium, and the interalloying of beryllium and the structural steel. Of highest priority are the self-welding reactions, because these will determine whether barrier coatings must be applied to the pebbles to guarantee their removability. Possible coatings for the thorium metal are ThO_2, ThC, or TiC. Possible coatings for the beryllium metal are $Be_{12}Fe$, $Be_{12}Cr$, or $Be_{12}Mo$. Next in priority are the possible reactions of beryllium with thorium. The same coating candidates listed above could also be used to reduce the extent of the latter reaction. Last in priority are the reactions between beryllium and HT-9, which preliminary experiments have shown to be slow at 450°C.

In the area of liquid-solid interactions, major concerns are (1) temperature gradient mass transfer of the containment alloy (HT-9) and/or breeding materials by lithium with attendant reduction of the blanket fluid passages by chromium, iron, or beryllium deposition and (2) mass transfer of metallic and nonmetallic (impurity) elements among the chemically dissimilar blanket and structural materials. The use of a structural steel of low nickel and chromium activity and the relatively low operating

temperature ($\leq$500°C) will each reduce the severity of mass transfer of the containment material by lithium. The beryllium mass transfer problem can be approached by using the same coating techniques as proposed for reducing solid-state beryllium reactions. Impurities in the lithium, particularly, nitrogen, can adversely affect compatibility by accelerating corrosion of the steel by lithium and promoting the formation of Be_3N_2. Again, a coating on the beryllium could prevent the latter reaction. Another impurity of potential importance is oxygen. Any oxygen present on the as-fabricated beryllium surfaces will be dissolved by the lithium and, at concentrations above 5 ppm in lithium, would react with thorium to form ThO_2. This is not of concern from the standpoint of compatibility, but an oxygen trapping system will probably be required to avoid the deposition of Li_2O in colder regions of the lithium circuit. One additional lithium corrosion reaction of importance to mechanical design concerns carbon transport. Both thorium and beryllium are strong carbide formers and may act to decarburize HT-9 by lowering the carbon activity of the lithium. However, except for relatively thin cross-sections, the decarburization of the HT-9 is sufficiently slow that it should not degrade the properties of the steel over the proposed reactor lifetime.

In order of priority, the most critical liquid-solid compatibility issue is the rate of thermal gradient mass transfer of HT-9 and beryllium in lithium at the reference reactor operating temperatures. Tests are currently underway to evaluate this potential problem, although, in the case of beryllium, truly definitive studies will not be possible until it is determined what, if any, coatings will be applied to the beryllium. These tests will also define the potential for carbon transport by the lithium, but engineering parameters of the system must be defined in detail before the effects of carbon, nitrogen, and oxygen can be assessed quantitatively.

References, Section III.A

1) R. W. Moir et al., "Fusion Breeder Program Interim Report, December 1981–February 1982," Lawrence Livermore National Laboratory report UCID-19406-1, May 1982.

2) R. P. Elliott, Constitution of Binary Alloys, First Supplement, McGraw-Hill, New York, 1965, p. 172.

3) Private communication, H. Pearlman, Atomics International, June 1982.

4) H. Pearlman, "Corrosion of Uranium, Thorium, and Uranium Alloys in Sodium and Organics," pp. 565–87 in Fuel Element Conference, Paris, November 1957, TID-7546.

5) E. E. Hoffman, "Corrosion of Materials by Lithium at Elevated Temperatures," Oak Ridge National Laboratory report ORNL-2674, March 1959.

6) H. Migge, "Thermodynamic Stability of Ceramic Materials in Liquid Metals Illustrated by Beryllium Compounds in Liquid Lithium," J. Nucl Mater. 103&104 (1981) 687–92.

7) Alloy Development for Irradiation Performance Progress Reports, U.S. Department of Energy, DOE/ET-0058/1-7 (March 1978–September 1979) and DOE/ER-0045/1-8 (December 1979–March 1982).

8) P. F. Tortorelli and O. K. Chopra, "Corrosion and Compatibility Considerations of Liquid Metals for Fusion Reactor Applications," J. Nucl. Mater. 103&104 (1981) 621–32.

9) P. F. Tortorelli and J. H. DeVan, "Mass Transfer Deposits in Lithium-Type 316 Stainless Steel Thermal-Convection Loops," Proc. Second Int. Conf. Liquid Metal Technol. in Energy Production, U.S. Department of Energy report CONF-800401-P2 (1980), pp. 13-55–13-63.

10) T. L. Anderson and G. R. Edwards, "The Corrosion Susceptibility of 2 1/4 Cr-1 Mo Steel in Lithium - 17.6 Wt Pct Lead Liquid," J. Mater. Energy Systems 2 (1981) 16–25.

11) P. F. Tortorelli, J. H. DeVan, and R. M. Yonco, "Compatibility of Fe-Cr-Mo Alloys with Static Lithium," J. Mater. Energy Systems 2 (1981) 5–15

12) J. H. DeVan, "Compatibility of Structural Materials with Fusion Reactor Coolant and Breeder Fluids," J. Nucl Mater. 85&86 (1979) 249–56.

13) M. Soenen and J. DeKeyser, "Experimental Facilities at SCK/CEN for Lithium Technology," Proc. Second Int. Conf. Liquid Metal Technology in Energy Production, U.S. Department of Energy report CONF-800401-P1 (1980), pp. 5-11–5-24.

14) V. A. Maroni et al., "Analysis of the October 5, 1979 Lithium Spill and Fire in the Lithium Processing Test Loop," Argonne National Laboratory report ANL-81-25, December 1981.

III.B. ANALYSIS OF BLANKET STRUCTURE LIFETIME

III.B.1. Overview

The lifetime of structural components in the reference blanket is recognized as an important design issue, since the blanket module lifetime impacts both operation costs and system reliability. Furthermore, maintenance considerations and design decisions are influenced by the lifetime analysis. Early fusion reactor studies have based lifetime predictions on gross failure criteria such as a maximum limit on swelling or a minimum value of ductility. Recently, detailed analyses(1,2) have shown the need for more accurate failure criteria together with appropriate design equations for material properties. Progress in this area is hampered by an insufficient data base for material properties, and the complexity of global structural analyses including radiation effects.

The expected radiation resistance of ferritic (or martensitic) alloys is an exciting development. It is generally predicted that ferritic steels offer neutron fluence limits for structural alloys which are significantly higher than those for austenitic steels. With this in mind we have opted for the selection of HT-9, a martensitic steel, as our candidate alloy for the blanket structure (see also Section II.B.). The low chrome ferritic, 2-1/4 Cr-1Mo is also an attractive candidate for this application, but provides a somewhat lower allowable design stress.

In the next section we will discuss the development of design equations for critical material properties. An important consideration in our study has been the embrittling effect of neutrons on ferritic alloys, especially at low temperatures. It will be shown in the next section that a significant elevation of the Ductile-to-Brittle-Transition-Temperature (DBTT) results from exposure to moderate neutron fluences at low temperature. The blanket structure temperature should, therefore, be maintained above 350 ^{o}C during operation. Our choice of coolant conditions and structure temperature achieves this criterion, but a considerable shift in the DBTT is still realized under irradiation. A later section discusses design methods to mitigate this problem. Structural design considerations relating to the blanket lifetime will then follow. Finally, our results and a summary of the lifetime analysis will be presented.

III.B.2 Development of Design Equations

In this section, we present empirical design equations for changes in mechanical properties of ferritic alloys as functions of the irradiation environment. Design equations are developed here for void swelling, the shift in the DBTT, and thermal creep rupture at high temperature.

Recent fast reactor irradiation experiments have shown low swelling for ferritic alloys. The work of Little and Stow (3) considered the swelling behavior of the following categories of ferritic alloys: (a) pure iron and mild steels; (b) binary iron-chromium alloys; (c) commercial ferritic and martensitic steels.

All the binary iron-chromium alloys exhibit well defined swelling peaks following irradiation to 30 dpa at temperatures in the range of 380-400°C (3). The peak swelling temperature was found to be independent of the chromium concentration. The magnitude of the swelling, however, was found to be a function of the chromium concentration, with a minimum around 3-5% chromium. Gelles (4) has also confirmed this conclusion in a more recent report. For commercial alloys at high fluences (on the order of 100-250 dpa), the situation is not clear. The existing data base does not permit definitive conclusions on compositional and heat treatment effects. We have developed the following swelling design equation from the limited available data (3-6):

$$\frac{\Delta V}{V}(\%) = \exp\left\{-\left((T-T_p)/W\right)^2\right\}\{0.036\delta - 0.074\}\{\phi(Cr)\} \qquad (1)$$

$$\Phi(Cr) = \begin{cases} 0.067\ Cr^2 - 0.457\ Cr + 1.0 & (Cr<5\%) \\ 0.037\ Cr + 0.237 & (Cr>5\%) \end{cases} \qquad (2)$$

where Cr = chromium concentration, %.

In equation (1), W = 59°C is the full width of the assumed Gaussian distribution, δ is the displacement dose (dpa), T is the irradiation temperature (°C), and T_p is the peak swelling temperature given by:

$$T_p = 420 + 7.27 \ln\left\{\frac{\dot{P}(dpa/s)}{10^{-6}}\right\} \qquad (3)$$

One of the most serious concerns in our study is the embrittling effect of neutron irradiation becuase it produces brittle fracture even at relatively high temperature. The DBTT can be defined as the intersection of the fractures stress (σ_f) and the yield stress (σ_y) when each is plotted as a function of temperature. At low temperature, the material undergoes brittle fracture before reaching the yield point. Data from the LWR surveillance programs shows a declining trend in the increase in DBTT with integrated fluence(7,8). The data shows that saturation effects are important, and that saturation in DBTT occurs at a lower fluence for a higher temperature. Recent neutron irradiation results on the embrittlement behavior of the high chromium alloy HT-9 show a DBTT shift of 108°C at an irradiation temperature of 419°C.

Composition, heat treatment and type of steel are known to influence the neutron irradiation embrittlement response of steels (7). For the purpose of the present analysis, we will assume that these effects are controllable, and that the dominant influence is due to neutron irradiation. A design equation for the shift in DBTT, that is based on hardening theories (8), can be written in the form:

$$\Delta DBTT = \frac{1.87X10^4}{(T-238)} \left[1-\exp\left[-\left(\frac{4T-350}{T}\right)\delta^{1/2}\right]\right] \qquad (4)$$

where T is the temperature in °C, and δ is the displacement dose in dpa. This equation is approximately valid above an irradiation temperature of 250°C.

The present design philosophy is based on the DBTT analysis, where a margin of safety is required for the operating structure temperature above the DBTT (i.e., to remain in the ductile regime). In contrast, recent fracture mechanics approaches (2), based on the fracture toughness parameter K_{IC}, can also be utilized to demonstrate that operation in the brittle regime may not be catastrophic. However, crack growth rates can be related to Charpy C_v toughness measurements which are performed at a relatively low strain rate, while DBTT measurements are essentially dynamic. Therefore, care must be exercised in using K_{IC} measurements. In the reference design, dynamic loads are a possibility due to operational transients or module handling. A more conservative approach that is based on DBTT analysis is therefore followed.

Figure III.B.1 shows the estimated DBTT's for HT-9 as a function of the axial first wall position, starting at the coolant inlet (i.e.,low temperature) side. DBTT's are shown for the bottom and top portions of the corrugated wall. It is shown that the DBTT saturates after a period of few months of operation.

The small differences between the DBTT of the top and bottom of the corrugated boundary may translate into preferential crack growth during startup/shutdown procedures, or during accident conditions (this is similar to the thermal shock problem of LWR pressure vessels during emergency core cooling). Although the present design achieves the goal of a DBTT that is significantly lower than the operating temperatures as shown in Figure III.B.1, it is advisable to eliminate shifts in the DBTT caused by neutron irradiation. In the next section, we will develop an annealing procedure designed to eliminate the embrittlement problem altogether.

At high temperatures, structural failure results from the slow deformation under creep conditions. At still higher temperatures, the design must be based on creep rupture data. At temperatures roughly below 500°C, creep rupture may not occur and excessive deformation due to both irradiation effects and thermal creep can be life-limiting. Unfortunately, most high-temperature designs require that components have service lives greater than those for which experimental data are available. A great many time-temperature parametric methods have been developed for extrapolation of creep rupture data. As yet, there is no universally accepted "best" procedure. One of the most common parameters in this respect is the Larson-Miller (LM) parameter developed in 1953. Creep rupture data are extrapolated on a plot of log σ versus the LM parameter defined as:

$$T(C + \log t_R) = \text{constant} \qquad (5)$$

where T is the temperature in °K, C is a constant, and t_R is the time to rupture.

Recently, Ghoniem and Conn (9) have suggested an extrapolation scheme suitable for a range of ferritic alloys proposed for fusion applications. The empirical correlations between applied design stress, S_{mt}; the temperature, T; and the time-to-rupture, t_R are given by:

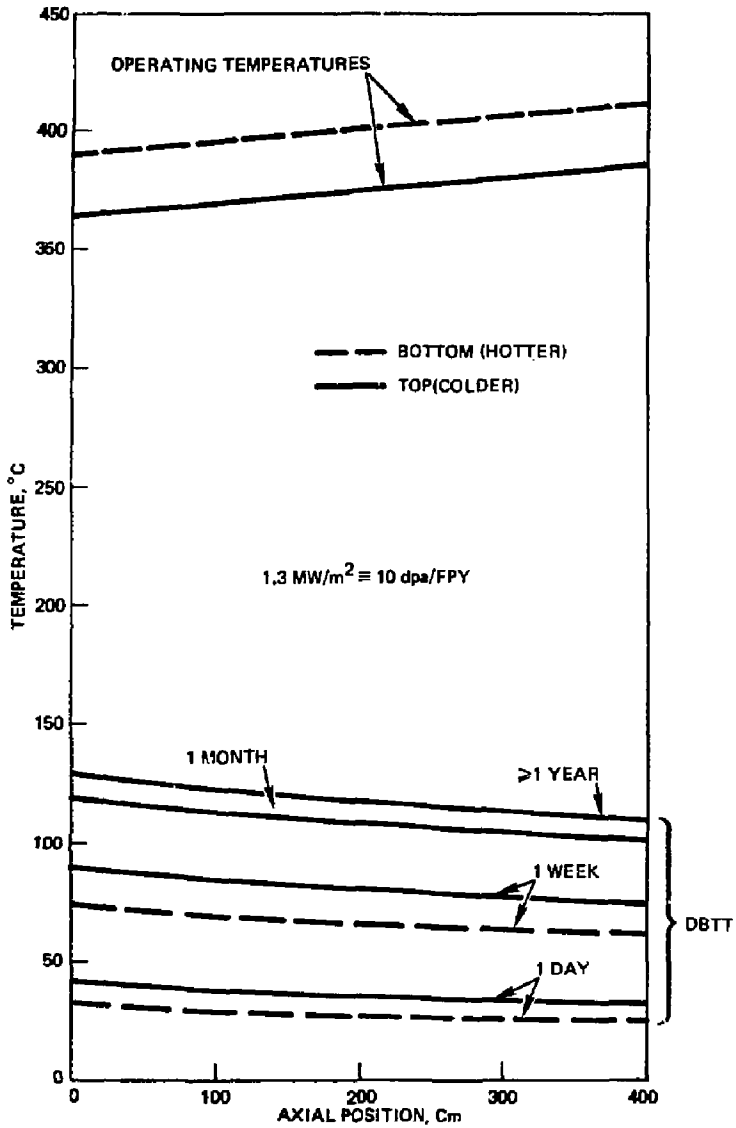

Fig. III.B.1 Reference Blanket First Wall DBTT vs. Axial Position and Irradiation Time

$$t_R = \frac{\exp\{K(T)m(T)\}}{\sigma^{m(T)}} \quad (6)$$

$$K(T) = A_1 + A_2 T + A_3 T^2 \quad (7)$$

$$m(T) = B_1 + \frac{B_2}{T} + \frac{B_3}{T^2} \quad (8)$$

$$\sigma = \frac{3}{2} S_{mt} \quad (9)$$

where σ is the stress-to-rupture. The method together with the constants A and B, for various ferritic alloys, is described in detail in reference (9).

Figure III.B.2 is a comparison between the allowable design stress for both 2-1/4 Cr - 1 Mo and HT-9 for service lives of 3 and 30 years as a function of the operating temperature. Very comfortable allowable stresses are expected in the reference design since the maximum structure temperature at the back side of the blanket is only 490°C. At this temperature, the allowable design stress is calculated to be 23 ksi for HT-9 and a life-time of 30 years. The calculations are based on unirradiated HT-9 data and the extrapolation procedure of reference (9). However, irradiated data (10) on HT-9 show little effect (and possibly an improvement!) of irradiation on rupture properties. Although detailed structural stress analysis has not been performed, it is expected that the stress levels are lower than 20 ksi (a simple static calculation of the axial stress in the back wall where the temperature is greatest yields only 970 Psi). Detailed stress analysis is needed to determine the maximum stress due to pressure loading on the subtended flat plates between the axial ribs and radial support plates.

III.B.3. Periodic Annealing for Miligation of Embrittlement

As pointed out in the previous section, dynamic component loading is a possibility during startup/shutdown and accidental transients. A conservative approach should therefore be followed whereby the moderate shifts in the DBTT are eliminated during scheduled maintenance periods. It is assumed that

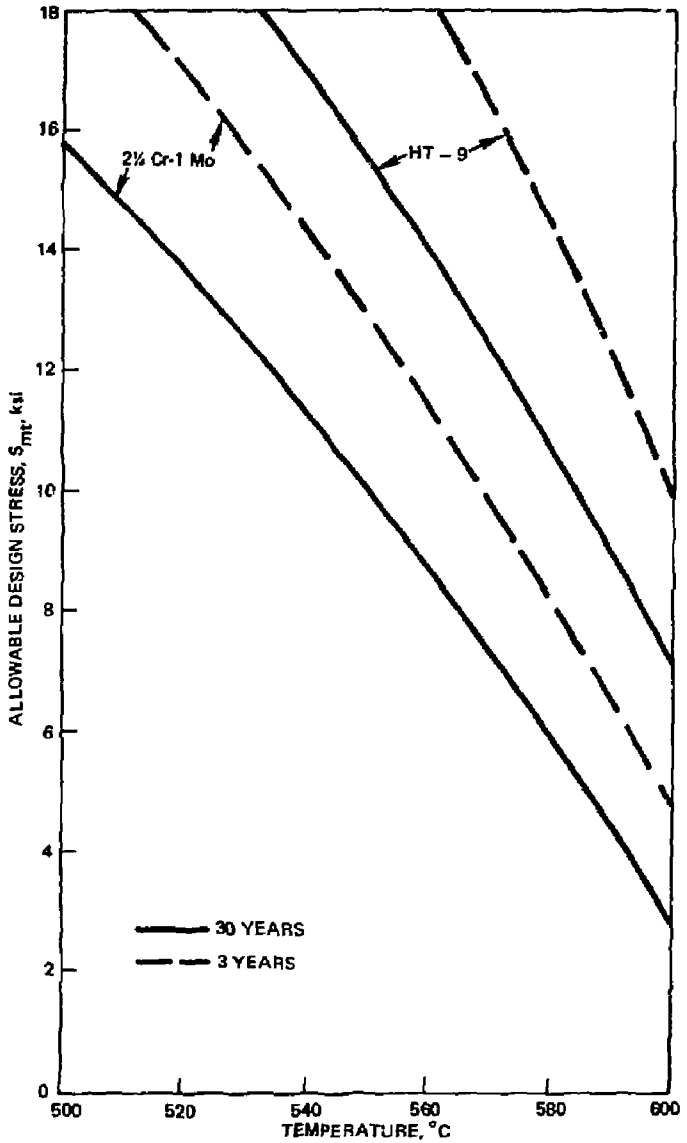

Fig. III.B.2 Allowable Design Stress for Ferritic Steels vs. Temperature and Required Lifetime

scheduled maintenance is planned once every year (see sections II.E and IV.B). During this time, it is recommended that the entire blanket structure temperature is given a 450°C anneal for a reasonably short period of time to lower the DBTT.

A program to develop annealing methodologies for nuclear reactor pressure vessels embrittled by irradiation is being sponsored by the Electric Power Research Institute (EPRI). In particular, the recovery kinetics is being studied to allow the development of a metallurgically-based model for DBTT recovery as function of annealing time and temperature (11). Similar efforts are being conducted at the Naval Research Laboratory (NRL)(12) and in the Federal Republic of Germany (13). Spitznagel and co-workers (11) developed the RANEL annealing model for the recovery kinetics which relates recovery to dissolution of vacancy clusters. Pachur (13) uses a different approach for annealing kinetics, where hardening measurements are used to characterize dissolution activation energies according to the equation

$$H_n = H_{no} \exp\{-\lambda_o\, t \exp(-U_n/kT)\} \qquad (10)$$

where H is the Vicker's hardness, λ is a constant and U_n is an activation energy. Following an approach similar to Pachur's, we have developed the following design equation for the fraction of the ΔDBTT that is recovered upon annealing, f_{DBTT}. This is given by the equation:

$$f_{DBTT} = 1 - \exp\{-3.885X10^5\, t \exp(-1.002/kT)\} \qquad (11)$$

where T is the annealing temperature in °K and t is the annealing time in hours. Results of equation (11) are in reasonable agreement with the RANEL computer model.

Figure III.B.3 shows the predicted annealing characteristics of the DBTT at two axial positions along the reference blanket first wall. The DBTT values corresponding to the axial position at 400 cm from the coolant entrance are lower than at the cooler side of the wall (0 cm axial position). It is shown in the figure that annealing at 450°C for a period of 50-60 hours should be sufficient to eliminate most of the embrittlement accumulated in the structure after 1 year of operation. The pre-irradiation DBTT of HT-9 is -18°C.

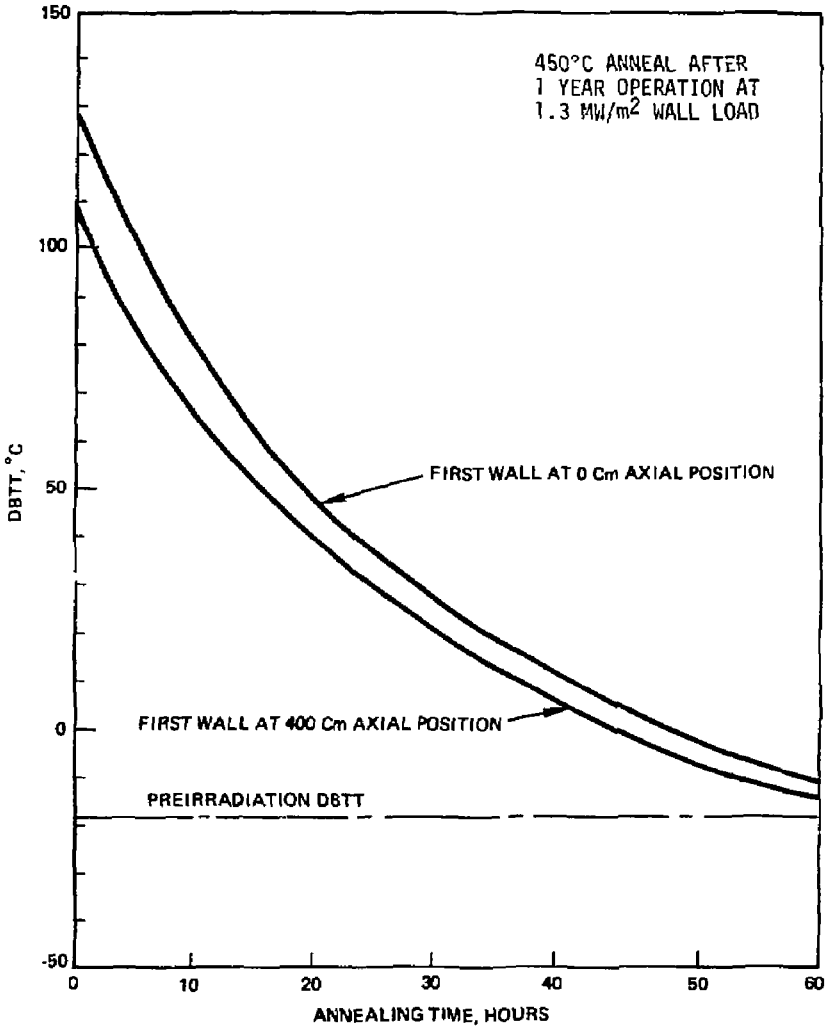

Fig. III.B.3 First Wall DBTT vs. Post Irradiation Annealing Time at 450°C

III.B.4. Structural Design Considerations of Blanket Lifetime

At temperatures below which significant thermal creep occurs, ASME Code Case 1592 specifies that the design stress should be the minimum of 2/3 σ_y, 2/3 $\sigma_{0.2}$, and 1/3 σ_u. Where σ_y is the yield stress, $\sigma_{0.2}$ is the 0.2% offset stress, and σ_u is the ultimate tensite stress. At high temperature, the code specifies that the allowable design stress, S_{mt}, should be a fraction of the rupture stress, σ_R, such that:

$$S_{mt} = \frac{2}{3} \sigma_R \qquad (12)$$

To illustrate the use of our design equations, we have parametrically studied the design lifetime as function of the structure temperature, at various stress levels. Figure III.B.4. shows the predicted thermal creep rupture lifetime at design stresses of 20,24, and 28 ksi. If we assume that at the hottest parts of the blanket structure (490°C) the stress will not exceed 24 ksi, a maximum design lifetime of ~ 14 years is predicted based on the simple creep rupture criteria.

The remaining issue regarding lifetime analysis is the possibility of structural failure due to various inelastic strains. The sources of those inelastic strains can be due to temperature gradients, thermal creep, irradiation creep and swelling. Unfortunately, a very complex global inelastic stress analysis is required in order to determine the weak points in the blanket system and possible failure modes. Without this level of detail, lifetime estimates are subject to great uncertainties. In the following, we analyze the sources of inelastic strains, and apply this analysis to a qualitative assessment of the present blanket structure.

Swelling of HT-9 has not been fully assessed in a neutron environment. Limited data exist up to 20-30dpa of EBR-II irradiation showing insignificant swelling (14). High fluence data is not available, since its use is restricted under the LMFBR Program auspecies. Lacking this data, we have used equations (1) and (2) to derive the linear strain due to swelling of the blanket structure. It can be seen (from Figure III.B.5) that at 410°C (maximum front wall temperature), a maximum linear strain of less than 0.8% will be achieved in 6 years. An average strain of ~ 0.1%/FPY is expected due to swelling of the first wall. This swelling strain is directed in both the axial and in the radial directions. Since the hoop stress is compressive due

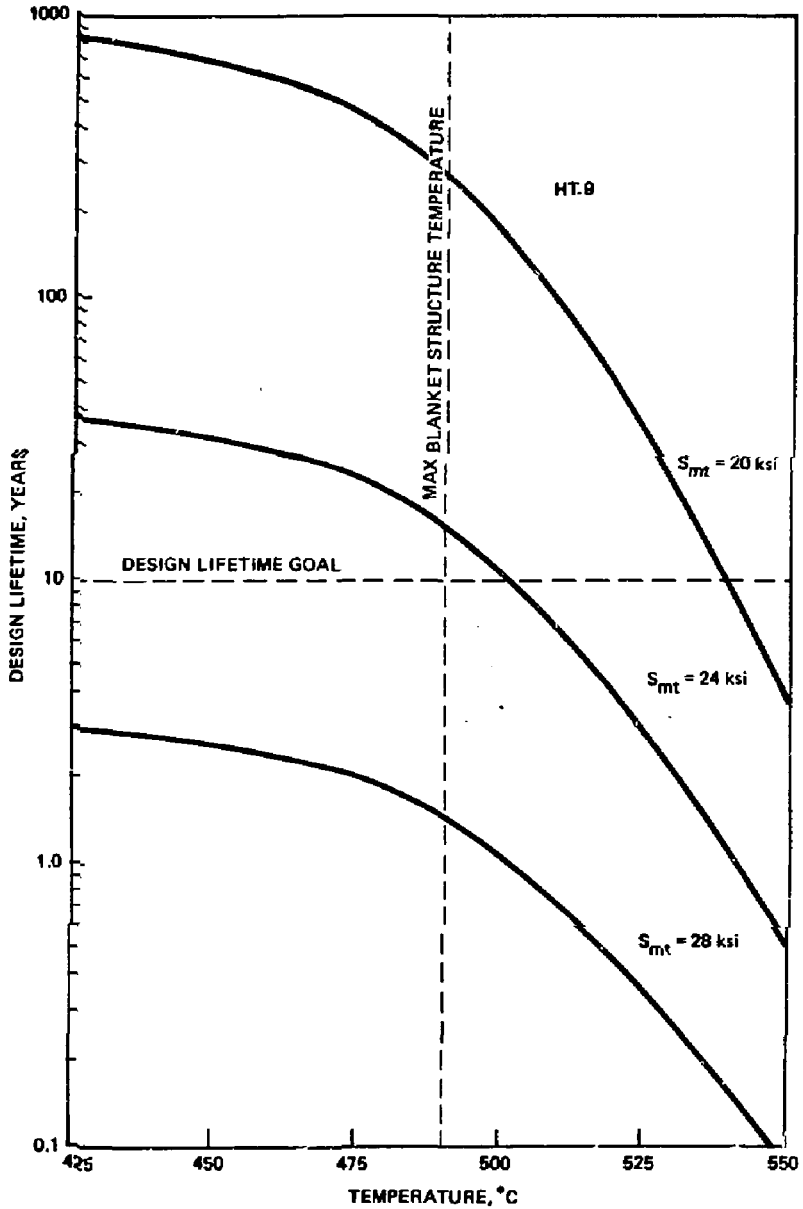

Fig. III.B.4 Thermal Creep Design Life vs. Temperature and Stress Level

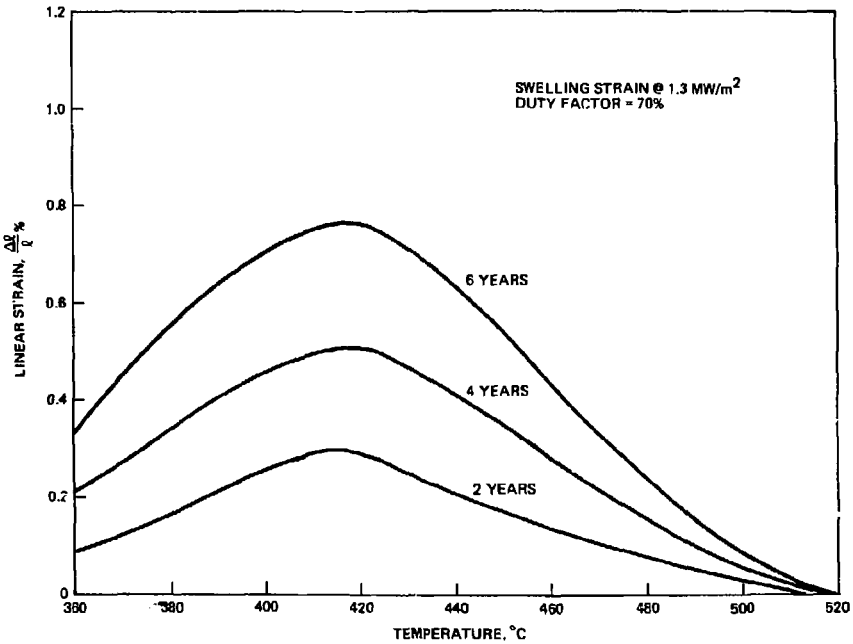

Fig. III.B.5 Swelling Induced Strain vs. Irradiation Temperature and Time for HT-9

to coolant pressure, the radial swelling will be cancelled, in part, by both thermal and irradiation creep. It appears, therefore, that the most critical design consideration is the accomodation of enhanced axial deflections due to inelastic strains. We will therefore devote the remainder of the section to this particular issue.

Irradiation creep data exist for a limited number of ferritic alloys. Odette(15) compiled such information, with a suggested correlation of the form:

$$\varepsilon_c = \left(\frac{\Delta \ell}{\ell}\right)_c = B\ \sigma\ \delta \qquad (13)$$

where B is a constant (creep compliance), σ the applied Von Mises (equivalent) stress, and δ is the irradiation dose. The values of B seem to be temperature dependent, and alloy dependent. Values ranging from 10^{-13} dpa^{-1} Pa^{-1} to 2×10^{-12} dpa^{-1} Pa^{-1} were reported. Paxton, Chin and Gilbert(10) suggested a linear dependence of creep and swelling in the form:

$$B = H + D\dot{S} \qquad (14)$$

where H and D are constants, and $\dot{S}$ is the swelling rate. This implies that the creep coefficient, B, is a function of both irradiation temperature and fluence. To be on the conservative side, we have used a constant value of B of $B = 10^{-12}$ dpa^{-1} Pa^{-1}. For an assumed axial stress of σ = 20 ksi, the calculated irradiation creep strain is on the order of 0.2%/FPY.

Thermal creep rates for HT-9 are not available at the present time, therefore, an approximate method for the solution of thermal creep rates of HT-9 has been developed. The method is based on the approach developed by Goodman and Coworkers(16) for the characterization for design purposes of the creep strain behavior of Cr-Mo steels. The following parametric equation is suggested for HT-9:

$$\sigma_R = 1.367\ \sigma_\varepsilon + \frac{13.03}{\varepsilon} + \frac{0.0696\ \sigma_\varepsilon}{\varepsilon} - \frac{1.67}{\varepsilon^2} \qquad (15)$$

where σ_ε is the stress-to-strain ε, and σ_R is the stress-to-rupture. Eliminating σ_R between equations (6) and (15) results in a unique relationship between time, stress, and strain for HT-9 at any given temperature. This is

given by

$$534.6\ t^{-\frac{1}{m}} = 1.367\ \sigma_\varepsilon + \frac{13.03}{\varepsilon} + \frac{0.0696\ \sigma_\varepsilon}{\varepsilon} - \frac{1.67}{\varepsilon^2} \qquad (16)$$

and

$$m = -367.277 + \frac{5.573 \times 10^5}{T} - \frac{2.024 \times 10^8}{T^2} \qquad (17)$$

where,

t = Time, hours
ε = Strain, %
σ_ε = stress-to-strain, MPa
T = Temperature, ^{o}K.

The results of this analysis are shown on Figure III.B.6 for the relevant temperatures where thermal creep applies (i.e., above 450°C). This mechanism of deformation will only be of concern in the back blanket wall where temperatures can reach 490°C. At 20 ksi, the creep rate at the back wall is predicted to be a maximum of 0.07% per FPY.

An addition of the previous ineleastic strains in the axial direction is illustrated in Figure III.B.7. It is shown that at the maximum front wall temperature of 410°C, the total axial strain after six years will be ~ 2.1%. Averaged over the entire first wall, the strain is roughly 0.32%/FPY.

III.B.5. Summary of Lifetime Analysis

The present blanket design is very conservative as compared to previous studies. The choice of a low-swelling ferritic alloy added great advantages to the present design. To realize such advantages, we have adopted the following design features:

(1) HT-9 is used in a relatively low temperature design (below 500°C) to give an allowable design stress of 24 ksi for a maximum creep rupture lifetime of 14 years.

(2) A minimum structure temperature of 365°C ensures a good margin of safety against neutron embrittlement during operation.

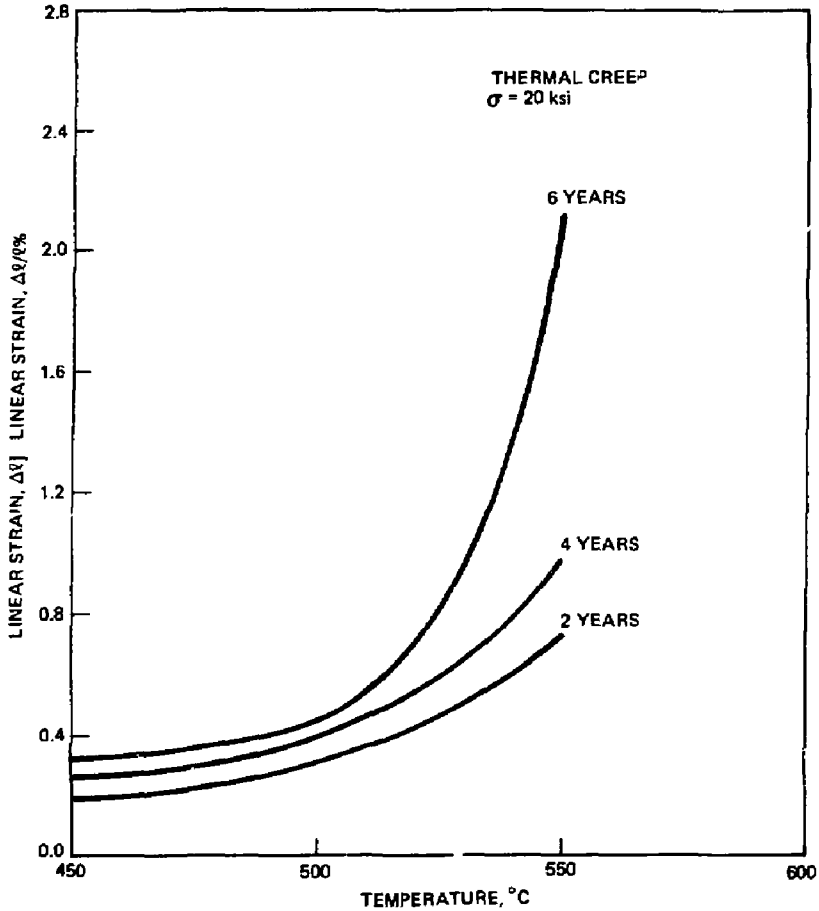

Fig. III.B.6 HT-9 Thermal Creep vs. Temperature at 20 KSI stress

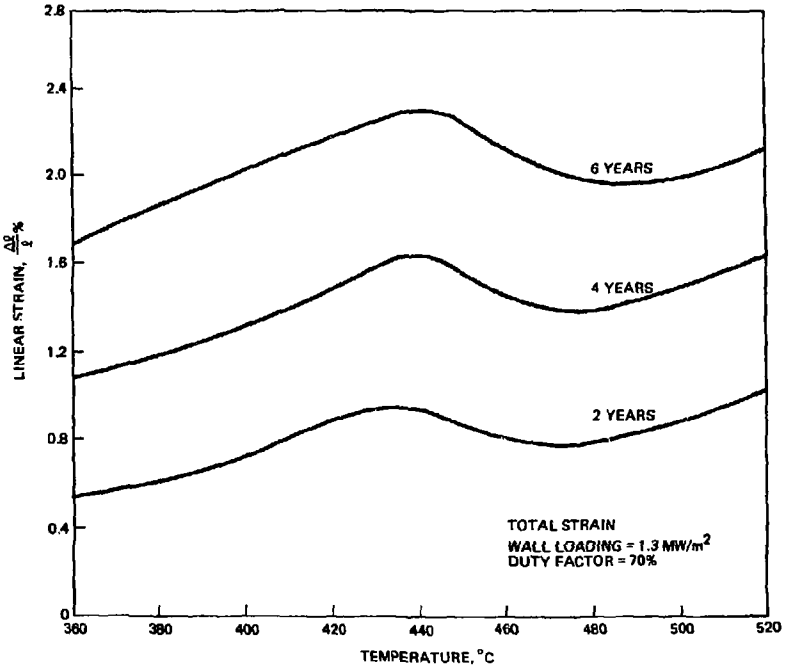

Fig. III.B.7 Accumulated Axial Strain in First Wall vs. Temperature and Time

(3) The moderate shifts in DBTT of the blanket structure are eliminated by a 450°C anneal every scheduled maintenance period for at least 50-60 hours. Higher temperature anneals are not advisable because of the possibility of temper embrittlement(24).

(4) Inelastic radial strains can easily be accomodated.

The most critical design issue is the accomodation of axial expansion due to swelling, irradiation creep and thermal creep. The total average axial displacement rate is estimated as 0.32%/FPY, or 1.28 cm/FPY. With an availability factor of 0.7, this translates to 0.9 cm/year. Out-of-Plane deflection stresses may be introduced at the end caps due to the different expansion rates of the first and back end blanket walls. Also, module-module contact will occur, if clearance is not provided. Assuming a module-to-module axial clearance of 10 cms, a reasonable estimate of the structure lifetime would be 10 years. The analysis should be on the conservative side, since the accumulated damage is only ~ 100 dpa at the end of life. Speculated damage limits of 200-250 dpa are expected for ferritic alloys. The present design can therefore be significantly relaxed without seriously affecting the predicted lifetime.

References, Section III.B.

1) Ghoniem, N.M., Conn, R.W., "Assessment of Ferritic Steels for Steady-State Fusion Reactors", Technical Committee Meeting and Workshop on Fusion Reactor Design and Technology, Tokyo, Japan, October 5-16, (1981).

2) Watson, R.D., Wolfer, W.G., "The Effect of Irradiation Creep, Swelling, Wall Erosion and Embrittlement on the Fatigue Life of Tokamak First Walls", Proc. of the Second Topical Meeting on Fusion Reactor Materials, August 1981, Seattle, WA.

3) Little, E.A., Stow, D.A., Journal of Nucl. Mater., 87 (1979) p25.

4) Gelles, D., "Microstructural Examination of a Series of Commercial Feritic Alloys Irradiated to Moderate Fluence", ADIP Quarterly Report, DOE/ER-0045/6, 1981, p157.

5) Little, E.A., Stow, D.A., Metal Science, (1980).

6) Smidt, F.A., et. al., "Swelling Behavior of Commercial Ferritic Alloys EM-12 and HT-9 as Assessed by Heavy-Ion Bombardment", Proc. of Irradiation Effects on the Microstructure and Properties of Metals, ASTM-STP 611, Amercian Soc. for Testing and Materials, Phil. PA, (1976), p227.

7) Steele, L.E., and Hawthorne, J.R., ATSM-STP 380, American Soc. for Testing and Materials, (1965) p283.

8) Ghoniem, N.M., Alhajji, J.N., and Garner, F.A., "Hardening of Irradiated Alloys due to the Simultaneous Formation of Vacancy and Interstitial Loops", Effects of Radiation on Materials: Eleventh Conference, ASTM-STP 782, H.R. Brager and J.S. Perrin, Eds., American Society for Testing and Materials, 1982.

9) Ghoniem, N.M., Conn, R.W., "High-Temperature Evaluation of Ferritic Steels for Fusion Reactors", ANS Trans, Vol. 41, (1982) p294.

10) Paxton, N.M., Chin, B.A., and Gilbert, E.R., "The In-Reactor Creep of Selected Ferritic, Solid Solution Strengthened and Precipitation Hardened Alloys", Journ. Nucl. Mater. 95 (1980) p185.

11) Mancuso, J.F., Sptiznagel, J.A., Shogan, R.P., Jouris, G.M., "Irradiation and Annealing of Pressure Vessel Steel", ANS Trans. Vol. 38, (1981), p305.

12) Hawthorne, J.R., "The Significance of Selected Residual Elements to the Radiation Sensitivity of A302B Steel", ANS Trans, Vol. 38, p304.

13) Pachur, D., "The Influence of Neutron Fluence and Irradiation Temperature on the Radiation Annealing Mechanisms of Reactor Pressure Vessel Steels", ANS Trans., Vol. 38, (1981) p306.

14) Straalsund, G., Gelles, D., HEDL, Private communications.

15) Odette, G.R., "Property Correlations for Ferritic Steels for Fusion Applications", Damage Analysis and Fundamental Studies Information Meeting, October 2-3, 1980, p384.

16) Goodman, A.M., et. al., "Characterization for Design Purposes of the Creep Strain Behavior of Cr Mo Steels", Proc. of Conf. on Ferritic Steels for Fast Reactor Steam Generators, BNES, London.

III.C. BERYLLIUM/THORIUM FUEL FORMS AND LIFETIME CONSIDERATIONS

The multiplier/breeder zone of the reference liquid metal cooled suppressed fission blanket contains beryllium and thorium in an approximately 20:1 ratio by volume. In addition, the mobile fuel form must be configured such that the packed bed nature of the blanket is preserved and insignificant volumes of non-neutron multiplying material are introduced.

Seperate beryllium and thorium pebbles (which vary by a factor of six in solid density) were considered during the scoping phase of the study (1), but were rejected due to experimentally observed difficulties in the attainment of a uniform mix of pebbles. Hollow thorium pebbles of identical section density to beryllium were also examined, but it was found that the resulting thorium wall thickness is not great enough to withstand the point stresses imparted by the coolant pressure drop across the blanket. Similarly, thorium coated beryllium pebbles were rejected because of chemical compatability concerns and because a chemical seperation of the beryllium and thorium would require an unacceptable (order of magnitude larger) throughput of materials to the head-end of the fuel reprocessing plant.

Instead, it was decided that a composite beryllium thorium fuel form would be adopted for the reference design and that various implications of such a choice would be addressed. Fuel form selection considerations, composite fuel form options, and our analysis of the expected beryllium lifetime are provided in the sections below.

III.C.1 Fuel Form Candidates and Considerations

Several considerations bear upon the selection of a composite fuel form:

- the fabrication and recycle cost
- the impact on breeding, thermal, and fluid flow characteristics
- chemical compatability between beryllium and thorium and with other blanket constituents
- the impact on fuel management and fuel handling operations
- the expected lifetime as affected by the thermal, irradiation damage, and chemical environment in the blanket.

In practice the selected fuel form will provide a compromise between goals relating to the above considerations.

During the reference phase of the study, three generic composite fuel forms were considered: 1) beryllium pebbles with drilled and reamed cylindrical holes in the center and thorium pin inserts held in place by alloy steel spring clips; 2) beryllium pebbles with cylindrical holes in the center and scroll-pin (or spiral wound dowel) inserts held in place by their own spring forces, and 3) solid beryllium pebbles with shallow grooves at the equator which hold C-shaped thorium metal snap-rings which conform to the groove. These three options are illustrated in Figure III.C.1.

The beryllium pebbles would, in each case, be fabricated into a low tolerance, sintered form with minimal machining required. The thorium would be fabricated as metal. Each of the three fuel forms would have approximately the same outer dimension and thorium to beryllium ratio. There are approximately 35 million fuel pebbles in the 40 blanket modules of the fusion breeder.

Considering first the cost of beryllium fabrication, Figure III.C.2 shows the cost of fabricated beryllium as a function of the pebble radius and fabrication cost per pebble. In this figure a raw material cost for fine commercial grade beryllium of 330 $/Kg was used(2). The fabrication costs per pebble which are indicated derive from an attempt to understand the combination of unit cost and pebble radius which results in a beryllium cost which is close to the raw material cost. For example, if pebbles can be fabricated for 40¢ each, then the initial fabrication of any pebble of rating greater than 1.0 cm will not result in a large cost impact above that of the raw material alone. Similarly, the cost of recycling and refabricating pebbles, i.e., no raw material cost will be reasonable. At a fabrication cost of 80¢ each, the pebble size required for a very low cost impact is only about 1.5 cm in radius. The predicted cost of beryllium fabrication by automated pressureless sintering and hot machining techniques is discussed in Section VII.B.

A set of curves, similar to those shown in Figure III.C.2, can be constructed for the allowed cost of fabricating and handling low tolerance thorium pins and/or rings. In this case, the following assumptions are made:

- beryllium : thorium volume ratio = 20:1
- allowed fabrication/handling cost = 10% of ^{233}U value
- ^{233}U value = 150 $/g

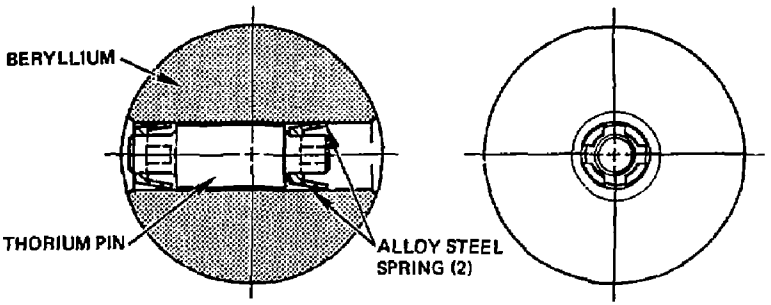

(A) SOLID PIN WITH STEEL SPRINGS

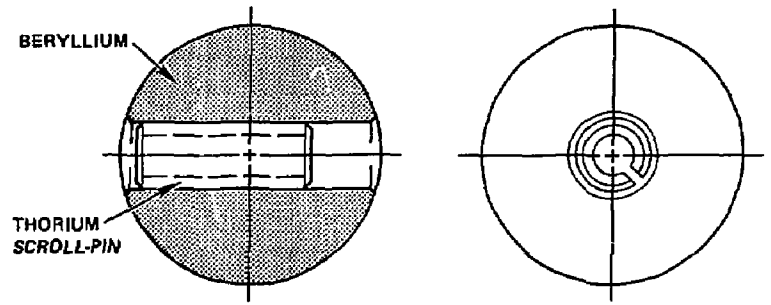

(B) SCROLL PIN

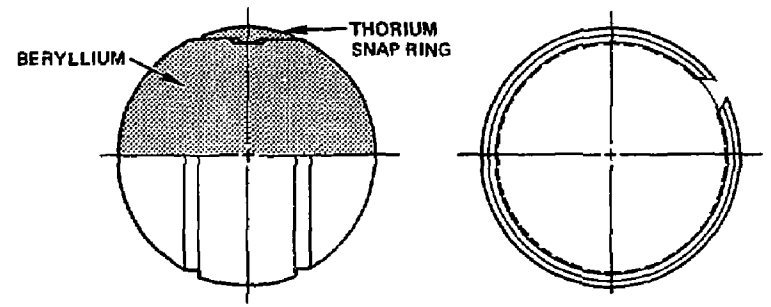

(C) SOLID SPHERE WITH SNAP-RING

Fig. III.C.1 Beryllium/Thorium Composition Fuel Form Options

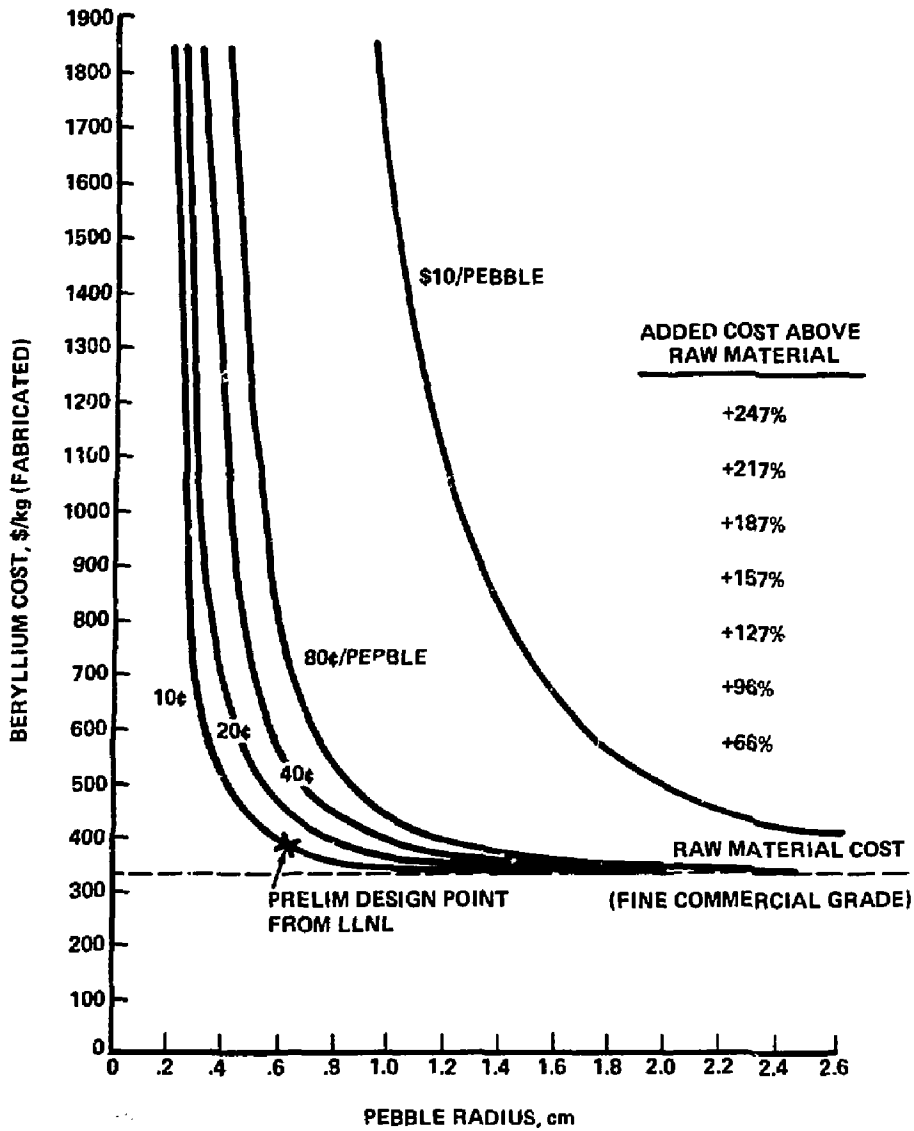

Fig. III.C.2 Cost of Fabricated Beryllium Material

The results shown in Figure III.C.3, indicate that the allowed thorium manufacturing and handling cost exceeds 1 $/pebble for pebble radii above 1.5 cm and fissile discharge concentrations (i.e., ^{233}U plus ^{233}Pa) above 0. It is important to note that the allowed cost scales as the pebble radius cubed for a fixed Be:Th volume ratio.

Based upon the results presented in Figure III.C.2 and III.C.3 a minimum pebble radius of 1.5 cm was selected to provide a margin of safety with respect to the cost of beryllium and thorium manufacture and handling. This pebble size provides a ratio of 6.7 for the fuel zone radial clearance (20 cm) to pebble diameter (3 cm). This ratio is considered to be large enough to prevent bridging of the pebbles in slot flow through the blanket. The minimum inside diameter of the circular pebble charge/discharge pipes is 8 pebble diameters, or 24 cm. For slot flow (such as the blanket and the outer annulus of the fuel discharge pipe discussed in Section II.B.5) the minimum clearance is considered to be 5-6 pebble diameters, or 15-18 cm.

The choice of a fuel form can potentially limit the overall performance of the reference blanket in several ways:

- by affecting the thermal and heat transfer characteristics of normal and off-normal conditions
- by affecting coolant flow
- by affecting the neutron economy

Considering the three fuel forms described earlier, the snap-ring design provides superior thermal performance because heat generated in the thorium ring is not conducted through the beryllium to the coolant as it is in the two inside pin designs. As discussed in Section III.C.4, the thermal stress resulting from thorium heat transfer through the beryllium can be life-limiting for the beryllium pebble and might impact design feasibility.

Our neutronics models (section II.C) also indicate an advantage for the snap-ring fuel design due to a less localized distribution of thorium and increased surface contact with the lithium. This reduction in heterogenious effects (i.e., self-shielding) can result in a significantly higher net fissile breeding ratio.

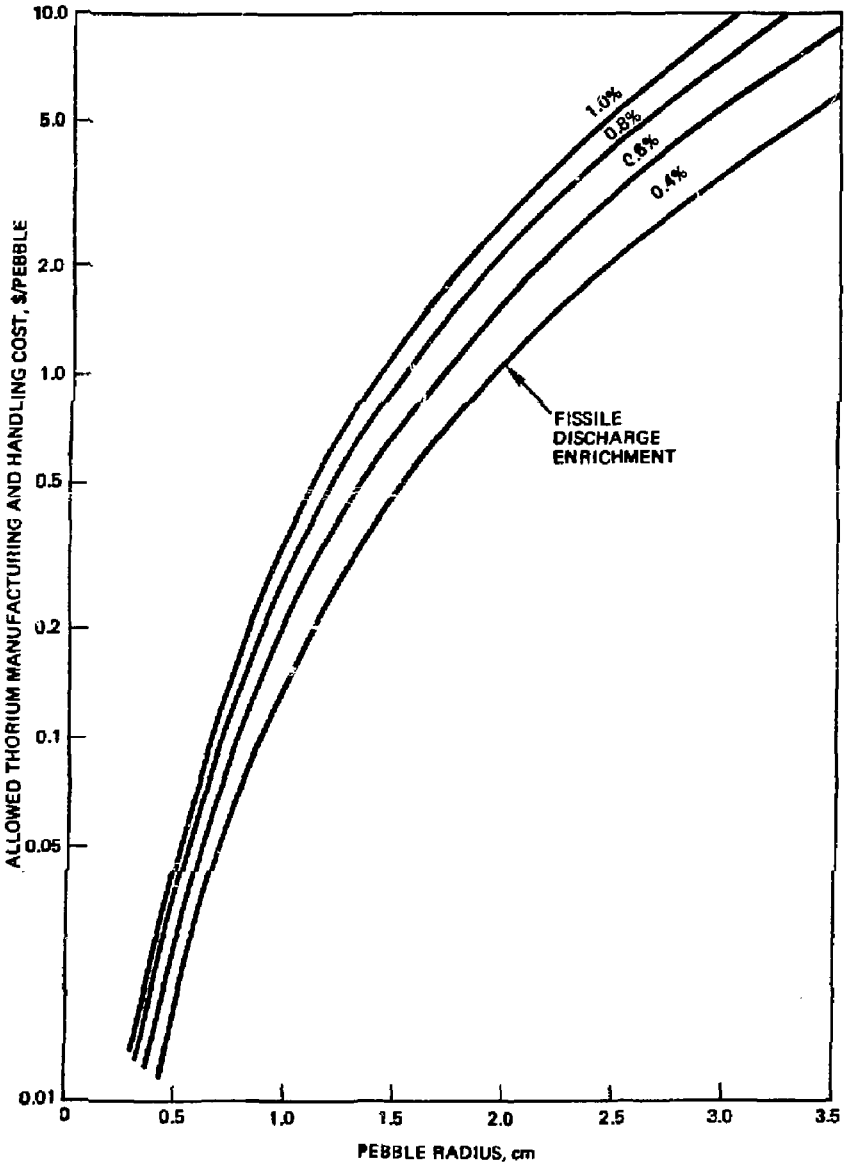

Fig. III.C.3 Allowed Thorium Manufacturing and Handling Costs vs. Pebble Radius

Chemical compatability issues relating to beryllium and thorium as well as beryllium and steel are important concerns which are described in detail in section III.A. Although we are hopeful that these interactions will not have a major impact on the fuel design, such a determination will await further experimental results. In general, the inside pin fuel form with steel clips is preferred in this respect since the thorium and beryllium do not contact one another. However, the extent of this reaction in liquid lithium at 500°C is not known and it is quite possible that the two other fuel forms can survive the effects of such interactions - particularly if the beryllium diffuses into the thorium as expected and bonding between the two surfaces is not excessive over the relatively short (i.e., less than 6 months) fuel residence time. Although coatings are not adopted as a baseline, the scroll-pin and snap-ring fuel forms could utilize a natural or applied coating on the thorium (e.g., ThO_2 or T_iC) to prevent such reaction.

Fuel management and fuel cycle operations will be affected by the volume of material to be managed and the difficulty in seperating the thorium from its beryllium carrier. In this respect the inside scroll-pin fuel form has a slight advantage over the inside pin with steel clips since the two steel clips are avoided and the thorium scroll-pin can be retained in the beryllium pebble with no additional springs, clips, or other fastening devices. The snap-ring fuel form has the same advantage.

All three fuel forms are quite simple in geometry and are ameanable to automated orientation and a single step process to replace the old thorium pin or ring with a new pin or ring. The design of fuel handling systems is addressed in more detail in section IV.C.

The scroll-pin is probably the easiest and least expensive thorium form to manufacture as thorium sheet metal, which is the basic material, is readily fabricable in thicknesses ranging from plate down to foil. The machinability is excellent and welding/brazing, which is rather difficult, is not required. The thorium modulus, which is about one third that of steel, should allow direct fabrication of a conventional steel scroll pin design out of thorium. Pins of this diameter (~7 mm) are in common use.

III.C.2 Reference Fuel Form Selection

Our preferences with respect to various considerations bearing upon the selection of a reference fuel form are summarized in Table III.C.1. The overall assessment favors the C-shaped snap-ring fuel design (see Figure III.C.1) because of lower thermal stress (and hence longer lifetime in the radiation environment as material properties degrade) and superior breeding potential (less heterogenions effect). We have not identified any serious shortcomings for this fuel form relative to the other candidates.

The dimensions and principal characteristics of the reference C-shaped snap-ring fuel form are described below:

- beryllium pebble radius - 1.5 cm
- beryllium volume fraction - 95%
- thorium volume fraction - 5%
- snap-ring width - 1.0 cm
- snap-ring thickness - 0.075 cm

Although we have not postulated the requirement for a coating on the thorium snap-ring, experimental results could lead to the adoption of a coating (probably thorium oxide or titanium carbide). Also, a minor modification of the ring position with a slight flattening of the beryllium pebble surface could be required to provide the correct orientation for indexing the pebbles prior to replacement of the old ring with a new ring by an automated machine. Such a modification is indicated in Figure III.C.4.

Table III.C.1 Summary of Fuel Form Preferences
Related to Various Considerations

Key: +1 - Preferred 0 - neutral -1 - possibly undesirable	Fuel Form		
	Cylindrical pins with steel clips (2)	cylindrical scroll or dowel pins	C-shaped snap-ring
Beryllium Fabrication	0	0	0
Thorium Fabrication	0	+1	0
Lifetime (thermal stress)	-1	-1	0
Breeding Performance	0	0	+1
Chemical Compatability	+1	0	0
Fuel Handling Operations	0	+1	+1

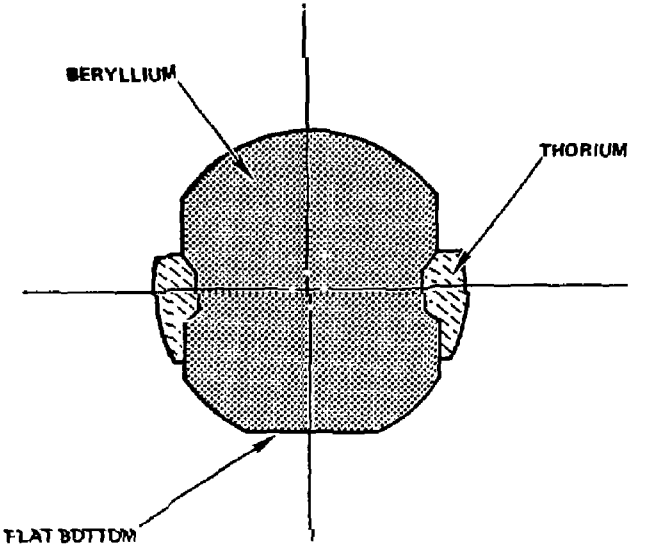

Fig. III.C.4 Modified Reference Fuel Form to Enable Gravitational Indexing

III.C.3 Lifetime Analysis of Beryllium Pebbles

Beryllium's low density, high specific heat, high modulus of elasticity,[a] and relatively high melting point (3) are not properties which limit the lifetime of the beryllium balls used as a neutron multiplier in the reference blanket design. Rather, t limited ability of the metal to undergo plastic deformation, restricting the redistribution of localized stresses, is likely to be responsible.

The ductility (3,4) and fracture toughness (5) properties, which measure the ability of beryllium to plastically deform, are relatively low for a material required to withstand high loading stresses. Before irradiation, the tensile elongation of hot-pressed beryllium is less than 5% at room temperature and the fracture toughness is about 12 $MPa \cdot m^{1/2}$. These properties are sensitive to the physical condition and test temperature of the beryllium: at 400°C the elongation of hot pressed beryllium may be above 14 percent, at 600°C the elongation of "as-extruded" beryllium (3,6) may be above 17 percent, while in the heat treated condition it may be above 42 percent (Figure III.C.5 a and b).

Upon irradiation, the beryllium structure is further restrained from plastic deformation by the defects produced (especially at irradiation temperatures less than 100°C). At higher temperatures, many of the defects agglomerate or anneal out. Since the tensile elongation (Figure III.C.5) and fracture toughness may vary with the type of beryllium (hot pressed or pressureless sintering with various densities, oxide content and purity), and with the irradiation temperature and fluence, the extent of failure of the pebbles by cracking or deformation can vary. The loading stresses on the pebbles are produced from thermal expansion, differential swelling from irradiation, and from external forces [weight, flow (hydraulic) pressure etc].

---

a. Highest modulus to density ratio of any metal

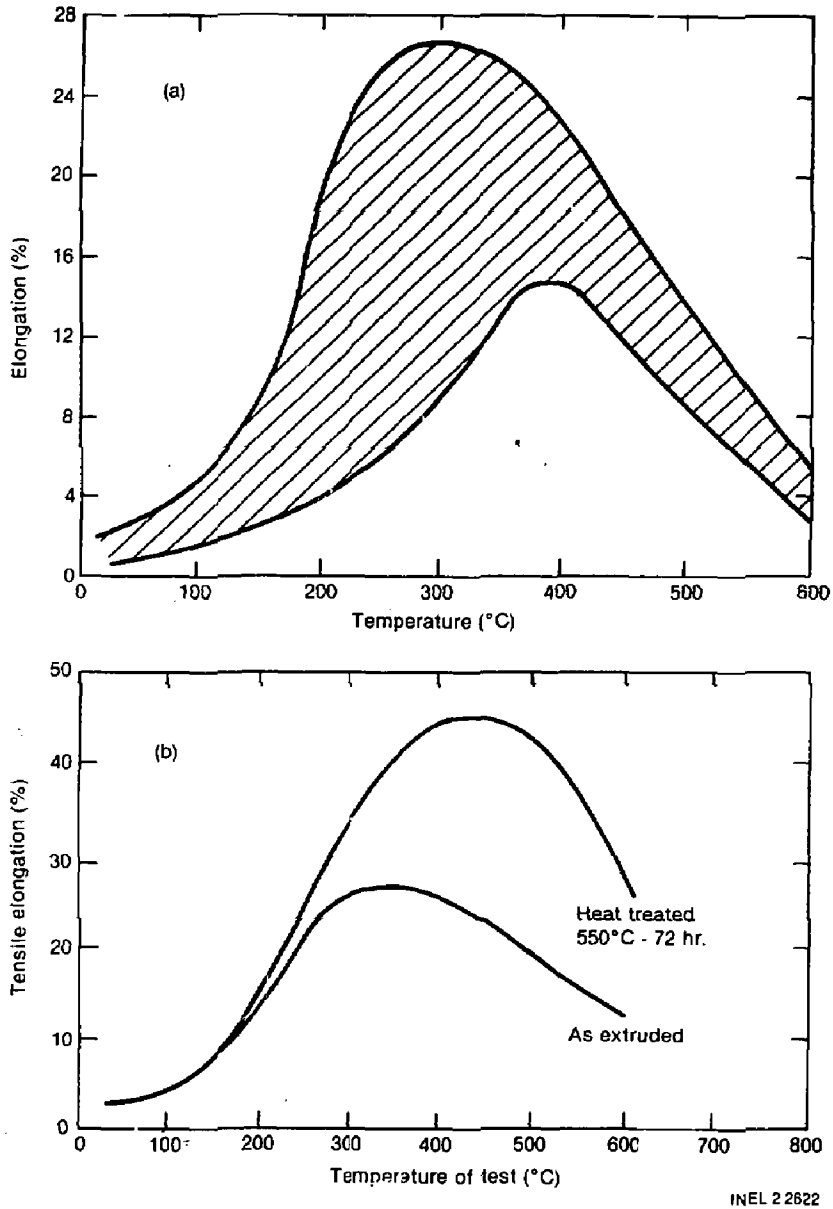

Figure III.C.5 Ductility vs. Temperature for Unirradiated Beryllium

a. Unirradiated ductility scatter - band for hot-pressed--200 mesh berllium powder.

b. Unirradiated tensile elongation vs. temperature of test for as-extruded and heat-treated metal.

The question of failure and lifetime continues to hinge upon the ductility of the irradiated beryllium pebbles, since the irradiated data base is sparse. Indications from postirradiation annealing tests (7) and high temperature irradiation tests (8,9) are that the defects may agglomerate with retention of some ductility. The retention of some ductility is necessary so that the pebbles do not act as indenters with one another, producing Hertzian contact cracking (10) and premature failure. Assuming sufficient ductility, the lifetime of the pebbles is estimated on the basis of the maximum stress theory; wherein failure occurs when one of the principal stresses from loading reaches the minimum yield strength of the irradiated beryllium. However, surface cracks, and defects that may propagate must be stable with respect to the stress intensity and fracture toughness of the irradiated beryllium.

III.C.3.a *Beryllium Data Base*

Yield Strength and Ductility

Irradiation of beryllium at 300 and 400°C produces an increase in yield strength and decrease in ductility.(8) With 400°C irradiation and test, the yield strength was 48 ksi and the ductility of extruded (hot pressed) beryllium was about 10% tensile elongation--less than the 20 percent elongation for the unirradiated material at this temperature [Figure III.C.5(b)]. Upon irradiation and test at 600°C, there was little difference in the tensile yield strength from the unirradiated, but the ductility was only about 3 percent (1/3 of the unirradiated tensile elongation.(8) When irradiated to a fluence of 1.08×10^{21} n/cm^2 (E > 1 MeV) and compression tested at room temperature (9), extruded beryllium gave yield strength values of 334 MPa and plastic strain of 19.6 percent (Table III.C.2). From these tests an estimate of the yield strength for failure analysis of 276 MPa was postulated for irradiation temperatures of 400-500°C. The ductility appears adequate (~3%, hence greater than yield strain) so that some deformation of the pebbles will accommodate the point loading of the pebbles without Hertzian contact cracking.(10)

Irradiation Elongation (Swelling)

An estimate of the elongation (swelling) versus irradiation temperature for calculation of thermal and differential swelling stresses is given in Figure III.C.6. The curve is a composite of a fluence term and a temperature term estimated from postirradiation annealing of beryllium irradiated to a fluence of 3×10^{22} n/cm^2 E > 1 MeV, (7) and is given as

$$\frac{\Delta L}{L} = f_1(\phi) + f_2(T) = 0.00183(\phi)^{1.035} + 2.6 \times 10^{-4} (2.5)^X$$

where ϕ is fluence n/cm^2 E > 1 MeV in units of 10^{22}

TABLE III.C.2. MECHANICAL PROPERTIFS OF COMPRESSION TESTED BERYLLIUM SAMPLES

Material	Yield Strength 0.2%, Offset, ksi *	Ultimate Strength, ksi *	Plastic Strain, %
As-received specimens	44.0	191.7	30.1
Capsule 1, control specimens (600 C, 3432 hr, 105 cycles)	46.4	210.1	30.7
Capsule 2, control specimens (750 C, 1589 hr, 55 cycles)	47.0	212.0	26.5
Capsule 3, control specimens (600 C, 1992 hr, 52 cycles)	51.0	184.5	27.8
Capsule 6, 600 C, 3559 hr (Irradiated to 1.08 x 10^{25} n/m^2)	48.5	147.9	19.6
Capsule 7, 750 C, 1586 hr (Irrdiated to 0.75 x 10^{25} n/m^2)	49.3	147.1	19.9
Capsule 8, 600 C, 1973 hr (Irradiated to 0.88 x 10^{25} n/m^2)	64.9	174.7	25.2

* In compression

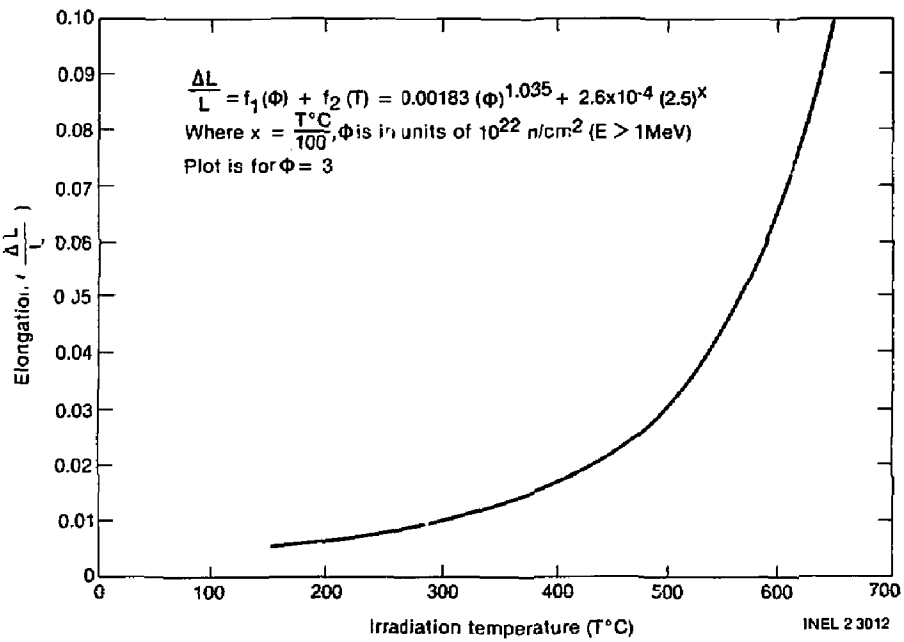

Figure III.C.6. Elongation vs. irradiation temperature

and

$$X = \frac{T°C}{100}$$

For fluences other than 3×10^{22} n/cm^2, the curve will shift up or down a slight amount due to the fluence term. For fluences less than 1×10^{22} n/cm^2 the elongation predicted by the equation is expected to be high. For fluences greater than 5×10^{22} n/cm^2, the equation may predict low elongation values due to the effect of helium. The differing helium content in a fusion reactor from that in a fission reactor is incorporated into the lifetime evaluation by utilization of an equivalent damage fluence. The equivalent damage fluence in a fission reactor is obtained from a ratio of the cross sections for helium production in the two flux spectrums. The assumption is that the point defects anneal out and the damage at 400-500°C is principally due to the helium. The equivalent damage fluence is shown in Table III.C.3. The equivalent damage fluence (11) for the three beryllium positions (near plenum wall, middle and near back wall) were used in the determination of stress and lifetime. Note the first zone beryllium is changed in position every three months which adds a conservatism in this zone.

Fracture Toughness of Irradiated Beryllium

The fracture toughness has been measured (12) for beryllium irradiated at 166°C to fluence of 5×10^{21} n/cm^2 E > 1 MeV and tested at room temperature as 4.8 MPa$\cdot$m$^{1/2}$ (4.4 ksi$\cdot$m$^{1/2}$) for full dense (1.85 g/cm^3) and 4.2 MPa$\cdot$m$^{1/2}$ for 95% dense (1.76 g/cm^3) specimens. For beryllium with a tensile ductility of about 4% elongation, the fracture toughness was 12 MPa$\cdot$m$^{1/2}$ (11.1 ksi$\cdot$in$^{1/2}$).

TABLE III.C.3 HELIUM PRODUCTION AND EQUIVALENT DAMAGE FLUENCE

Reactor	Cross Section (appm He per 10^{22} n/cm^2 E>1 MeV)	Cross Section Ratio[a] Fusion to Fission	Beryllium Zone Fluence (n/cm^2 E>1 MeV per year)	Equivalent Damage Fluence (n/cm^2 E>1 MeV per year)
Fusion Breeder				
Near first zone wall	6700-7000[a]	1.81	0.71×10^{22}	1.28×10^{22}
Near center	5900-6200	1.59	0.24×10^{22}	0.38×10^{22}
Near back wall	5500-5800	1.49	0.038×10^{22}	0.057×10^{22}
ATR (Fission Reactor)	3700-4700[a]	--	--	--

a. Second number assumes complete burnup of Li daughter into helium. First number is used in determination of ratio for conservatism.

Fluence Distribution Through Blanket

The fluence distribution through the blanket is shown in Figure III.C.7. It was obtained by a parabola fit to the three fluences given, namely:

1. near first wall--1.28 x 10^{22} n/cm^2 E > 1 MeV per year.
2. near center--0.38 x 10^{22} n/cm^2 E > 1 MeV per year.
3. near back wall--0.057 x 10^{22} n/cm^2 E > 1 MeV per year.

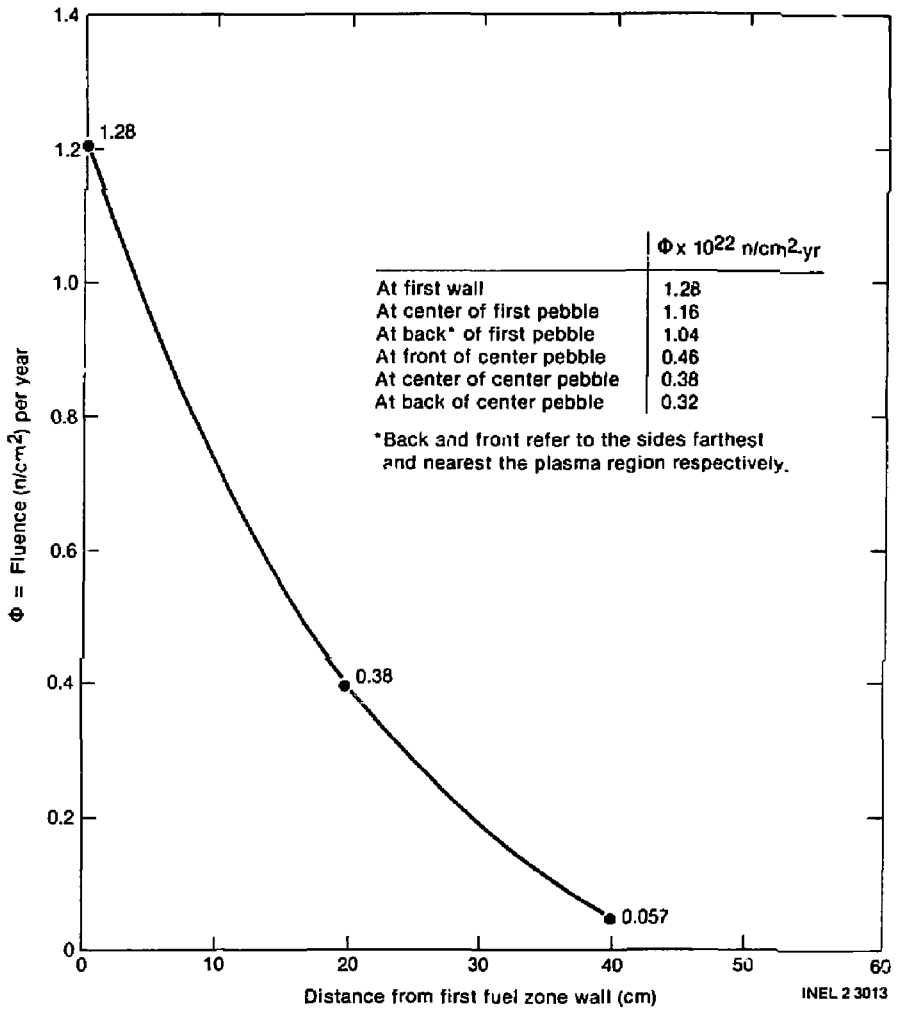

Figure III.C.7 Equivalent Damage Fluence Distribution

III.C.3.b Stress Analysis on Beryllium Pebbles

The Hybrid Reactor blanket fuel zone is 0.40 m thick and is divided into two 0.20 m thick annular zones filled with beryllium pebbles (pebbles) of 0.03 m diameter. A lithium plenum precedes the fuel zones. The stress analysis considers the forces due to lithium flow and pebble stacking height and the internal stresses due to thermal expansion and differential swelling. Although the snap-ring fuel form was selected late in the study as the reference design, this analysis considers the earlier cylindrical pin design (see Section III.C.1). Consequently, the estimated lifetime is considered to be conservative based on early estimates of thermal gradient and neglecting any stress concentration effects.

Stress from Hydraulic Forces

The liquid lithium is dispersed from the inlet header in the radial direction. The hydraulic force due to the MHD pressure drop is opposing the stacking pebble weight at the top of the fueled zone and in the same direction as gravity at the bottom of the fuel zone. The hydraulic force, F, on the pebbles in the annulus is approximated by considering the constraint force on the perforated zone separator sheet as a reaction force transferred through all of the beryllium pebbles. The constraint force on the annulus grid is the pressure drop times the projected area.

$$F = \Delta P \, A$$

The beryllium pebble reaction force is also applied on the projection area. The hydraulic force on each pebble is then,

$$F = 125 \, \pi r^2 = 125 \, \pi \left(\frac{3}{2 \times 2.54} \right)^2 = 137 \text{ lb } (609 \text{ N})$$

Where a 125 psi pressure differential across each zone is assumed (see Section II.D).

The force due to the weight of the pebbles is the density times the volume. Assuming that the volume fraction of beryllium is 0.65 (lithium is

0.35) and that the height of the column above a pebble at the bottom of the blanket is 6 m, then

$$F = \rho A h$$

where

ρ = density

A = projected area of ball

h = height of column.

and

$$F = [0.65\ (1.85) + 0.35\ (0.543)]\ \frac{\pi \left(\frac{3}{2 \times 2.54}\right)^2}{454\ g/lb} \times 600 = 13\ lb\ (58\ N)$$

Thus, the hydraulic force due to the flowing lithium is ten times that of the weight of the pebbles.

To accommodate the point loading the pebble must crush or fracture or deform a small amount to carry the load. We assume the beryllium pebble has sufficient ductility to deform a small amount without fracture so that the contact radius, a, of the pebble on the zone separator sheet is determined by the yield stress of the beryllium. From Section III.C.3, the yield stress at high fluence and 500°C was taken as 276 MPa. The peak compressive stress, σ_o, is given (13) as

$$\sigma_o = \frac{3P}{2\pi a^2}$$

hence for a contact loading, P, of 58 N (13 lb) the contact radius would be

$$a = \left(\frac{3\ P}{2\pi\ \sigma_o}\right)^{1/2} = \left(\frac{3 \times 13}{2\pi \times 40{,}000}\right)^{1/2} = 0.0124 \text{ in. } (0.0314 \text{ cm})$$

The maximum tensile stress near the contact point is

$$\sigma_t = \frac{1-2\nu}{3}\ \sigma_o = \frac{1 - 2 \times 0.024}{3}\ 40{,}000 = 12{,}690 \text{ psi } (87.5 \text{ MPa}).$$

Assuming the fracture toughness is 12.0 $MPa \cdot m^{1/2}$ = 11.1 $ksi \cdot in.^{1/2}$, the depth of a surface crack, c, in the vicinity of the contact point which would be stable (not propagate) can be calculated from

$$K = \sigma\ (\pi c)^{1/2} \text{ or } 11{,}100 = 12{,}690\ (\pi c)^{1/2}$$

whereupon

$$c = 0.245 \text{ in. } (0.62 \text{ cm}).$$

If the fracture toughness drops to 4.4 $ksi \cdot in.^{1/2}$ then the stable surface crack depth decreases to $c = \left(\frac{4.4}{12.69}\right)^2 \frac{1}{\pi} = 0.038$ in. (0.097 cm).

The values of stress and stable surface defect size for a contact loading of 58 N (13 lb) raise the question of whether the hydraulic loading on the pebbles of 609 N (137 lb) can be accommodated without fracture of the pebbles. The deformation that would have to occur would be such as to give a contact radius of

$$a = \left(\frac{3 \times 137}{2\pi \times 40{,}000}\right)^{1/2} = 0.040 \text{ in. } (0.102 \text{ cm}).$$

The maximum tensile stress near point of contact and the stable surface defect size would be as before 87.5 MPa and 0.62 cm, respectively.

However, if the pebbles, because of irradiation hardening, behave elastically the point load between two pebbles (13) would be determined as:

$$a = \sqrt[3]{\frac{3j}{4} P \frac{(k_1 + k_2)}{R_1 + R_2} R_1 R_1}$$

where

$$k_1 = k_2 = \frac{1 - (0.02)^2}{\pi E} \quad \frac{1}{\pi E} \text{ and } k_1 + k_2 \quad \frac{2}{\pi E} ,$$

$$R_1 = R_2 = \frac{3}{2.54} = 1.181 \text{ in.}$$

so that,

$$a = \left(\frac{3\pi}{4} P \frac{2}{\pi E} \frac{R_1 R_2}{R_1 + R_2} \right)^{1/3}$$

$$a = \left[\frac{6}{4} \left(\frac{137}{40 \times 10^6} \right) \frac{(1.181)^2}{(1.181 \times 2)} \right]^{1/3} = 0.014 \text{ in. } (0.0355 \text{ cm})$$

where

P = 137 lb and

E = 40×10^6 lb/in.

The maximum tensile stress is

$$\sigma_t = \left(\frac{1 - 2\nu}{3} \right) \sigma_o = \left(\frac{1 - 2 \times 0.02}{3} \right) \left(\frac{3 \times 137}{2\pi (0.014)^2} \right) = 10b,800 \text{ psi } (736.4 \text{ MPa})$$

and the pebbles will, most likely, fracture since the tensile yield is 276 MPa.

Hollow Sphere Assumptions

The beryllium pebbles considered have a drilled hole 0.007 m diameter in which is inserted a thorium metal slug. The thorium slug is held in place and central in the hole away from the beryllium with a spring clip. At no time will the thorium contact the beryllium. The beryllium is thus not loaded by the thorium slug and hence the stress calculations are based on a hollow sphere.

The fluences and temperatures for the thorium slugs and beryllium pebbles were as follows:

	Temperature; C			
		Beryllium		
	Thorium	Inside	Outside	ΔT
(1) Near first wall; $\phi t = 1.28 \times 10^{22}$ n/cm^2 per year	422	405	367	38
(2) Near blanket center; $\phi t = 0.38 \times 10^{22}$ n/cm^2 per year	455	445	422	23
(3) Near back wall; $\phi t = 0.057 \times 10^{22}$ n/cm^2 per year	488	485	477	8

Normal Stresses

The internal thermal stresses from thermal expansion of a hollow pebble from the temperature difference between the surface and inside of the beryllium assuming steady heat flow (13) is calculated as follows:

The thermal stress, σ_t, a maximum at the outside radius is given as;

$$\sigma_t = \frac{\alpha E T_i}{2(1-\nu)} \frac{(a)(b-a)(2a+b)}{b^3 - a^3}$$

where

α = 17.8×10^{-6} cm/m°C (value at 700 K)

E = 40×10^6 lb/in = 275,800 MPa

a = inside radius = 3.5 mm

b = outside radius = 15 mm

σ_r = stress at surface = 0

and T_i is the difference between the inside and outside surface temperatures. T, the difference between the temperature at radius, r, and the outside surface temperature, is given by

$$T = \frac{T_i\, a}{b-a}\left(\frac{b}{r} - 1\right)$$

Thus, the maximum thermal stress, σ_t, near the first wall is,

$$\sigma_t = \frac{(17.8 \times 10^{-6})(275{,}800)(T_i)}{2(1-0.024)}\left(\frac{3.5 \times (15-3.5)(2 \times 15 + 3.5)}{15^3 - 3.5^3}\right)$$

$$= 1.014\, T_i \text{ MPa}$$

For a pebble near the first wall

T_i = 38°C

hence

$$\sigma_t = 1.014 \times 38 = 38.5 \text{ MPa } (5586 \text{ lb/in.}^2)$$

Values for three annular positions: (1) near the first zone wall, (2) near the center, and (3) near the back wall are tabulated in Table III.C.3. The lifetime is estimated by subtracting the thermal stress from the failure yield strength and dividing by the swelling stress per year and the usage factor, thus, estimated lifetime = $\frac{40 - 5.6}{28.1 \times 0.7} = 1.75$ years. The swelling stresses will be calculated in the next section.

TABLE III.C.3 INTERNAL STRESSES FOR HOLLOW PEBBLE FOR ONE YEAR IRRADIATION AND ESTIMATED LIFETIME

Position in Blanket	Thermal Stress (ksi)	Swelling Stress Per Year (ksi)	Total Stress Accumulation in 1 Year (ksi)	Estimated Lifetime (70% Capacity Factor)
Near First Wall	5.6	28.1	33.7	1.75 year
Near Center	3.4	24.9	28.3	2.10 year
Near Back Wall	1.1	6.0	7.1	9.3 year

Differential Swelling Stresses

The internal stresses from irradiation given as elongation in Figure III.C.6 produced by differential swelling were calculated by the equation for elongation ($\frac{\Delta L}{L}$, Section III.C.3.a),

$$\frac{\Delta L}{L} = 0.00183(\phi)^{1.035} + 2.6 \times 10^{-4}(2.5)^{T/100}$$

The differential swelling stresses were calculated for three positions in the hybrid reactor blanket: (1) near the first fuel zone wall, (2) near the center, and (3) near the back wall of the blanket. The differential swelling stress was calculated for an irradiation time of one year.

The outside surface of the pebble will be in tension and reach the failure stress before the compression on the inside of the pebble, since the irradiated tensile yield strength is less than the irradiated compressive yield strength. The maximum swelling gradient is from the center to the outside of the pebble away from the first zone wall because of the increase in temperature. To calculate the swelling stress, a pseudo temperature is calculated from the relation between the elongation and the thermal expansion, i.e.,

$$T = \frac{\Delta L}{\alpha L}$$

for each position in the pebble.

The procedure for the pebble near the first wall is as follows:

(1) for inside position at $\phi = 1.16 \times 10^{22}\ n/cm^2$ (Figure III.C.7) at temperature of 405°C

$$\frac{\Delta L}{L} = 0.00183(1.16)^{1.035} + 2.6 \times 10^{-4}(2.5)^{4.05} = 0.0128$$

(2) For beryllium at outside of pebble at temperature of 367°C and $\phi = 1.04 \times 10^{22}\ n/cm^2$ (Figure III.C.7)

$$\frac{\Delta L}{L} = 0.00183(1.04)^{1.035} + 2.6 \times 10^{-4}(2.5)^{3.67} = 0.0094$$

So that the pseudo temperatures are

$$T \text{ at inside} = \frac{\Delta L}{\alpha L} = \frac{0.0128}{17.8 \times 10^{-6}} = 719°C$$

and

$$T \text{ at outside} = \frac{0.0094}{17.8 \times 10^{-6}} = 528°C$$

Hence

$T_i = \Delta T = 719 - 528 = 191°C$

and the swelling stress is given by the earlier thermal stress equation

$\sigma_t = 1.014\ T_i = 1.014 \times 191 = 194$ MPa (28,090 lb/in.^{2})

and is given in Table III.C.4 with those for the other two blanket positions.

The depth of a surface defect that would be stable for the internal tensile stress in Table III.C.4, as it reaches the failure stress of 40,000 psi can be estimated from the relation

$$c = \frac{K}{\sigma}^2 \frac{1}{\pi} = \frac{11,100}{40,000}^2 \frac{1}{\pi} = 0.024 \text{ in. } (0.061 \text{ cm}).$$

Thus, providing the surface defects are less than 0.061 cm depth, the lifetime estimate of the beryllium hollow pebbles can be estimated from the maximum stress theory for a yield strength of 276 MPa.

III.C.3.c Lifetime Estimates of Beryllium Pebbles

According to the failure theory stated earlier and the total internal stresses shown in Table III.C.4, the estimated life of the hollow beryllium pebbles near the first wall of the blanket is about 1.6 calendar years, Table III.C.4 providing the surface defects are less than 0.024 in depth. The beryllium pebbles near the center of the blanket have over two years average life and those near the back wall have more than nine years average life. Averaging over the entire blanket, the average beryllium lifetime is estimated to be about 2.6 years. The surface of the pebbles must be free of defects $\geq$0.024 in. deep.

The estimated life is based on the following assumptions:

1. The ductility of the irradiated beryllium is greater than that to accommodate yielding ($\sim$1%).

2. The irradiated yield strength has a minimum value of 276 MPa (40 ksi).

3. The fracture toughness of beryllium irradiated at 400°C is 12 MPa$\cdot$m$^{1/2}$.

4. The stresses may be approximated on the basis of a thick hollow pebble.

5. The irradiation swelling may be approximated from postirradiation measurements.

As indicated in Section III.C.3.b the snap-ring fuel form was selected as the reference design. This analysis which considers the earlier hollow pebble design (see Section III.C.1) is expected to give a shorter beryllium:

Since the temperature gradient, ΔT, through the beryllium is less for the snap-ring fuel form.

It is noted that there are some uncertainties in the data bases, however, preliminary results on beryllium irradiated in EBR-II at 450°C to a fluence of 1.01×10^{22} n/cm^2 E >1 MeV are not inconsistent with the postirradiation results or other data considered in the data bases.

III.C.3.d. CONSIDERATIONS FOR INCREASED LIFETIME

Considerations for increased lifetime of the beryllium pebbles are important to reduce the cost of replacement. There are, however, other conditions which will affect the cost such as automated fabrication and recycling of reconditioned beryllium. Factors which affect the ductility of irradiated beryllium will affect the lifetime. These factors are complex because of the sensitivity of the mechanical properties of the metal beryllium to other properties such as fabrication, anisotropy, grain size, purity, percent BeO, and etc. Generally, beryllium of fully dense low BeO content, fine grain, hot pressed has the best anisotropic ductility. However, preferred orientation by extrusion increases the ductility in the extruded direction, so that considerations of the behavior of the beryllium in the irradiation, stress, and temperature environment may change the ductility assessment.

References, Section III.C.

1) R.W. Moir, et.al., "Fusion Breeder Program Interim Report: December 1981 - February 1982", UCID-19406-1, Lawrence Livermore National Laboratory (1982).

2) Personal Communication, R.Corle (Rockwell, Rocky Flats) to N. Hoffman (Rockwell, Energy Technology Engineering Center), March 17, 1982.

3) J. M. Beeston, Beryllium Metal as a Neutron Moderator and Reflector Material, Nuclear Engineering and Design 14 (1970) pp. 445-474.

4) W. J. Salmen and L. P. Gobble, Tensile Properties of Beryllium from Room Temperature to 1600 F, Proceedings of the ASTM, 62, (1962) pp. 1-12.

5) J. M. Beeston, Fracture Toughness of Irradiated Beryllium, Effects of Radiation on Structural Materials, ASTM STP 683, J. A. Sprague and D. Kramer, Eds, (1979), pp. 309-325.

6) A. Moore, F. Morrow, V. D. Scott, and D. A. Cheer, Precipitation Aging and Improved Mechanical Properties in Commercially Pure Beryllium and Beryllium Alloys, in the Metallurgy of Beryllium, Metals Monograph, Chapman and Hall Ltd. (1963) pp. 112-126.

7) G. E. Korth and J. M. Beeston, Interim Report of Post-Irradiation Results of ATR Beryllium Surveillance Program, IN-1397 May 1970 also in Metallurgy and Materials Science Branch Annual Report Fiscal Year 1970, IN-1437 November 1970 and internal reports.

8) G. P. Walters, Effect of Neutron Irradiation on the Mechanical Properties of Hot-Pressed and Extruded Beryllium, J. Less-Common Metals, 11, 1966, pp. 77-88.

9) J. M. Beeston, Gas-Release and Compression Properties in Beryllium Irradiated at 600 and 750°C, Effects of Radiation on Structural Metals, ASTM STP 426 (1967) pp. 135-148.

10) B. R. Lawn, S. M. Wiederhorn, and H. H. Johnson, Strength Degradation of Brittle Surfaces: Blunt Indenters, J. American Ceramic Society, 54, No. 9-10 September-October 1975, pp. 428-432.

11) E. H. Ottewitte, EG&G Idaho, Inc., private communication, October 27, 1982.

12) J. M. Beeston, Fracture Toughness of Irradiated Beryllium, in Effects of Radiation on Structural Materials, ASTM STP 683, (1979) pp. 309-325.

13) S. Timoshenko and J. N. Goodier, Theory of Elasticity, McGraw Hill, (1951), pp. 372-377.

CHAPTER IV

FUEL MANAGEMENT SYSTEMS AND ANALYSIS

A baseline fuel cycle analysis was carried out early in the program for the purpose of providing a design basis for the fuel handling and safety systems and motivating a plant operation scheme. The work was based on available neutronics data and was, in general, intended to scope out the fuel cycle prior to a more detailed resolution. The baseline fuel cycle analysis and a description of the fuel handling equipment are provided in Section IV.A and IV.B. An improved fuel cycle plan, developed towards the end of the study is presented in IV.C and a comparison with the baseline fuel cycle described below is provided. The fuel cycle studies reported in Section IV.C include more recent neutronics data and describe a more advanced optimization scheme.

IV.A. BASELINE FUEL CYCLE

IV.A.1 Fuel Management Mode Selection

In the development of the baseline fuel cycle, the following issues were considered:

- The Choice Between Several Design and Operational Modes:
  - Single versus Multiple Radial Zones
  - Fuel Irradiation Period and Availability Budget
  - Single versus Multiple Axial Zoning (i.e., by module)
  - Variable versus Constant Wall Load
- The Achievement of Maximum Fissile Fuel Production Subject to Several Goals and Constraints:
  - Maximum Fissile Enrichment and Enrichment Rate
  - Limited Fusion and Overall Power Levels
  - Constant Thermal Hydraulic Performance (i.e., constant product of wall loading and blanket energy multiplication).
  - Limited Central Cell Length

- The Achievement of Attractive Reactor Safety Characterisitics (See Chapter V):
  - Minimum Actinide and Fission Product Production
  - Minimum Afterheat Generation

Early in the study a fuel zone design with two radial zones was chosen. A design with at least two zones is desirable because, otherwise, the fuel irradiation period would be limited by ^{233}U buildup in the first 10 cm of the fertile blanket. With two or more zones, the irradiation periods of the zones can be adjusted so that the front zones are cycled most frequently while the back zones are cycled less often. It was postulated that more than two zones would add undue complexity to fuel handling systems and excessive structure from the standpoint of neutronics performance.

An important choice in determining the operational mode is the relative irradiation period of the front and rear radial zones of the reference blanket module. Based on two radial zones of equal thickness (20 cm), the thorium (n,γ) reaction rate is about 2.7 times greater in the front zone that in the rear zone, but the large fission rate in the front zone (due to greater ^{233}U breeding) decreases net breeding in that zone such that the net breeding in the front zone is about twice that of the back zone. Table IV.A.1 shows the results of a study which examines fuel cycles which achieve the same end of cycle blanket energy multiplication with front to rear zone reprocessing frequency ratios of 1, 2, and 3. For example, in the second case the front zone is cycled each 80 days and the rear is cycled each 160 days. Although an optimized three cycle scheme could be expected to slightly outperform the two cycle case, it appears that a two cycle scheme is close to optimal. This was chosen as the baseline.

In addition to radial zoning, the reactor may be partitioned into separate axial zones (i.e., by module) which can be reprocessed at different times. The advantages of this staggered type of configuration are:

- Reduced load on fuel handling machinery
- Smaller swings in thermal power
- Frequent reprocessing shutdowns which might also allow some routine maintenance

TABLE IV.A.1 SUMMARY OF FUEL CYCLE PARAMETRICS

CYCLE DESCRIPTION	FRONT ZONE IRRADIATION PERIOD	REAR ZONE IRRADIATION PERIOD	MAX M	FISSILE ENRICHMENT
1. One cycle	90 d	90 d	1.80	.982%
2. Two cycle	80 d	160 d	1.81	1.183
3. Three cycle	70 d	210 d	1.80	1.175

Notes:

1) Neutron wall loading = 1.45 MW/m^2
2) Neutronic data as of 06/29/82.
3) Maximum M in fuel zone only.
4) All cases are for two radial zones. Front to rear relative frequencies are 1:1, 2:1, and 3:1.

Considering the fuel changeout process, if the number of modules which are discharged at a single time is small, it might be desirable to provide an intermediate inventory of Be/Th fuel pebbles which could be kept on hand for immediate loading into empty modules. This would reduce downtime, eliminate the requirement that the fuel handling equipment process the entire load of discharged fuel during a short (~ 1 wk) period during which the reactor would be shut down, and allow the pebble handling machinery to operate continuously during breeder operation. As a result, the required process rate (i.e., pebbles/sec) could be greatly reduced. If all modules were to be discharged at once (i.e., a single axial zone), then the cost of an intermediate Be/Tn pebble inventory (~ 150 $M) would most likely become prohibitive in comparison with the cost of additional fuel handling machinery.

In order to further study the impacts of axial zoning, work has been undertaken in two areas:

- Development of an analytic model for blanket power as a function of the number of axial zones.
- Examination of extreme conditions which can affect reactor operation.

In development of the model of reactor performance, several assumptions have been made. First, each module or submodule has been assumed to behave independently of the other submodules. Second, for the modeling of reactor power, the ^{233}U concentration has been assumed to grow linearly with irradiation time. Thus, the average power in a module is simply the initial power at the start of operation with fresh fuel plus one half the power swing over the irradation period. Both of these assumptions have been shown to be reasonable for concentrations less than 1% (see Section II.C).

Consider a two zone problem representing a reactor with two identical axial zones. If the additional energy multiplication due to increased ^{233}U fissions at the end of cycle for both zones is ΔM, then the average overall blanket energy multiplication is $M_0 + \Delta M/2$ and the blanket power swing is ΔM. This method can be applied to the situations illustrated in Figure IV.A.1 which shows two operational schemes: 1) two identical axial zones which are reprocessed simultaneously, and 2) two zones which are reprocessed at staggered intervals. Case one might be two groups of blanket modules which are reprocessed as a single unit. Case two best represents a reactor divided into

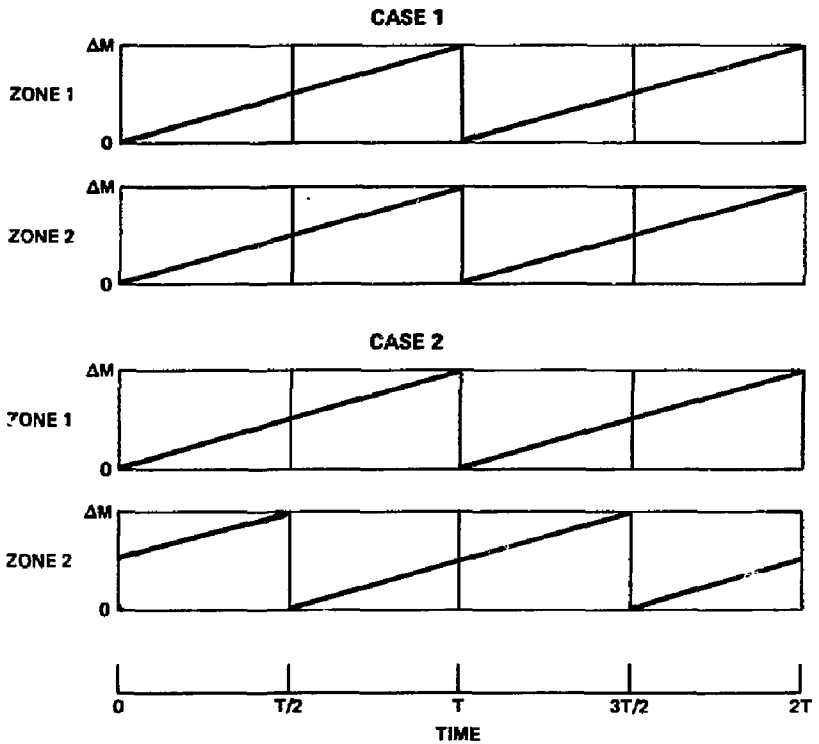

Figure IV.A.1 Axial Zone Energy Multiplication Swing as a Function of Fuel Cycle Time

two axial zones which are reprocessed at alternate shutdown times. Referring again to Figure IV.A.1, a full process cycle takes time T and one half cycle takes T/2. Table IV.A.2 summarizes the zonal blanket energy multiplication at beginning-of-cycle, at mid-cycle, and at end-of-cycle. The overall reactor blanket multiplication swing and the average blanket multiplication are also shown. Of interest is the fact that the average energy is the same for both cases. The time dependent power swing of the two cases is different, however. In comparison with Case 1, Case 2 shows that the power swing can be reduced during operation by axial zoning of the reactor. In particular, for case 2, the overall reactor blanket power swing is reduced by 50%.

The two axial zone case can be easily extended to an arbitrary number of axial zones. If the number of axial zones is denoted by n, the overall reactor blanket swing in energy multiplication is

$$\Delta M_{zone}/n$$

Other simple expressions can be found which represent the beginning-of-cycle and the end-of-cycle energy multiplication:

$$M_{ave}(BOC) = M_0 + \Delta M_{zone}([n-1]/2n)$$

$$M_{ave}(EOC) = M_0 + \Delta M_{zone}([n+1]/n)$$

In general, the effect of axial zoning on reactor power swing is to make it smaller while reducing the maximum multiplication and increasing the minimum energy multiplication. Table IV.A.3 shows how several different schemes compare. Four axial zones in theory reduce the power swing by a factor of four.

There are, however, other important considerations which relate to axial zoning. These include the following:

- Cycle startup procedures
- Operation in a non-equilibrium mode following long shutdown periods
- Unanticipated reactor shutdowns
- Frequent thermal cycling caused by relatively frequent anticipated shutdowns.

Table IV.A.2 TIME DEPENDENT REACTOR BLANKET ENERGY MYLTIPLICATION FOR TWO AXIAL ZONING OPTIONS

		By Zone			Reactor	
		BOC	Mid-Cycle	EOC	M_{swing}	M_{ave}
Case 1	Zone1	M_0	$M_0 + \Delta M/2$	$M_0 + \Delta M$	ΔM	$M_0 + \Delta M/2$
	Zone2	M_0	$M_0 + \Delta M/2$	$M_0 + \Delta M$		
Case 2	Zone1	M_0	$M_0 + \Delta M/2$	$M_0 + \Delta M$	$\Delta M/2$	$M_0 + \Delta M/2$
	Zone2	$M_0 + \Delta M/2$	$M_0 + \Delta M$	$M_0 + \Delta M/2$		

TABLE IV.A.3 ENERGY MULTIPLICATION INCREASES FOR SEVERAL AXIAL ZONE SCHEMES

# Axial Zones	M(BOC)	M(EOC)	M_{swing}	M_{ave}
1	M_0	$M_0 + \Delta M$	ΔM	$M_0 + \Delta M/2$
2	$M_0 + \Delta M/4$	$M_0 + 3/4\Delta M$	$\Delta M/2$	$M_0 + \Delta M/2$
3	$M_0 + \Delta M/3$	$M_0 + 2/3\Delta M$	$\Delta M/3$	$M_0 + \Delta M/2$
4	$M_0 + 3/8\Delta M$	$M_0 + 5/8\Delta M$	$\Delta M/4$	$M_0 + \Delta M/2$

Most importantly, the quantitative expressions shown above apply to a fuel cycle which is in equilibrium (i.e., at a given time, some zones are just beginning their irradiation cycle while others are in the middle or completing theirs). This condition is not easily satisfied by the fusion breeder because, at some initial time, all fuel is fresh. One possible strategy for achieving equilibrium would be to remove some fuel before it had achieved its target enrichment. In this way the proper stagger of enrichment times could be established. However, partially irradiated fuel results in a reprocessing cost penalty. For a blanket with n axial zones, it would take n full cycles before equilibrium would be achieved. Thus, the required time to equilibrium might be greater than the period between longer shutdowns if several axial zones are used. The intervention of longer shutdown periods, either anticipated or un-anticipated, would disrupt the transition from startup to equilibrium or disrupt an established equilibrium cycle since significant ^{233}Pa decay would occur during shutdown.

Even if the number and length of shutdowns is kept to a minimum, the larger the number of axial zones, the higher the number of scheduled reactor shutdowns. Each shutdown will result in some thermal cycling. This cycling will in general degrade the reliability of the reactor. Another effect will result because each group of modules will require a different operational cooling level depending on its state of enrichment and ^{233}U concentration. This requires more careful valving and adds additional complexity to control and monitoring systems.

Although it is possible to analyze these detailed effects and the different reactor operating regimes which might result from both startup procedures and mixes of long and short shutdown periods, the above factors essentially compromise the operability of a multiple axial zone scheme. In our opinion, a qualitative understanding of the concerns associated with the operation of the multiple axial zoned reactors is sufficient to discourage their use without additional analyses. On this somewhat subjective basis we have selected a one axial zone configuration for the baseline.

Finally for a single axial zone, by adjusting the fusion power level, the wall load can be varied. Specifically, the wall load can be adjusted to keep the blanket energy production constant as ^{233}U builds up. The advantage of this scheme is that balance-of-plant systems can be sized for a constant

energy production. The disadvantage of this approach is that fusion systems must be cycled. Since the cost of fusion driver components dominates the plant cost (about 60%) the fuel cycle baseline postulates a constant wall loading.

In summary, multiple axial zoned reactors present operational difficulties which are sufficient to discourage their use. These include the adverse affects of long shutdown periods on thermal limits and discharge enrichment. In addition, equilibrium cycles take longer to achieve for larger numbers of axial zones. The alternative is a single axial zoned reactor which may have two radial zones. As previously mentioned, two radial zones are attractive because they take advantage of the more rapid enrichment that takes place in the first part of the blanket. The fuel cycle baseline operational *mode has the following characteristics:*

- Constant Wall Load Operation
- Single Maturity (no axial zoning)
- Two radial zones with the front zone reaching maturity twice as often as the back zone

IV.A.2 Baseline Fuel Management Trade Studies

Two immediate goals relating to blanket fuel management are the maximization of both the effective discharge fissile enrichment and the enrichment rate. A high discharge enrichment (> 1% ^{233}U in thorium) improves the reprocessing economics. A high enrichment rate minimizes ^{233}Pa decay and, consequently, minimizes ^{233}U fissions. Three somewhat arbitrary constraints which were imposed on the analysis were a maximum blanket thermal power at end of cycle, a fusion power of 3000 MW, and a central cell length of less than 200 meters. The thermal power constraint requires a neutron wall loading times blanket energy multiplication product equal to 2.5. This constraint is imposed by the desire to limit the MHD pressure drop (see Section II.D). The trade studies described below attempt to determine if low wall loading and high end of cycle blanket energy multiplicaton lead to higher discharge fissile enrichment than a higher wall loading coupled with a lower energy multiplication.

The TRW isotope generation and depletion code, ISOGEN, was used for this analysis. ISOGEN solves a set of coupled linear homogeneous first order differential equations using the matrix exponential method as described in Table IV.A.4. Solution of the actinide buildup/decay equations for the thorium/uranium fuel cycle requires the specification of a combined decay/activation matrix describing the isotopic decay and activation that can occur in a neutron environment. Once the magnitude of the neutron flux is specified, the time dependent evolution of a vector of blanket nuclide concentrations can be described.

The constraints on central cell length (200 m) and power (3000 MW_f) discussed above determine the minimum wall load. For any given wall load, the fixed wall loading times energy multiplication product constraint determines the end of cycle blanket energy multiplication. Thus, by specifying the wall loading, ISOGEN can be run and trade studies can be performed to determine which combination of wall loading and corresponding blanket energy multiplication maximizes the discharge enrichment. ISOGEN has the capability of tracking multiple reactor zones at the same time. This feature was used to follow both the front and rear radial zones.

Since length, wall load, and maximum M are all related by the imposed constraints, all trades can be simply shown as in Table IV.A.5. A simple economic comparison was also performed (shown in Table IV.A.6) with the result that the case with the longest central cell, the smallest wall load, and the largest maximum M was selected. The baseline fuel cycle parameters are summarized in Table IV.A.7 and some aspects of the fuel cycle are discussed in the following sections.

IV.A.3 Fuel Management/Safety Interface

The fuel cycle has impacts on reactor safety; both because the fuel contains hazardous fission products and actinides and because the afterheat generated in the fuel must be removed during accident (e.g., loss of coolant or coolant flow) situations. The hazardous sources and afterheat sources can be predicted using ISOGEN. A general discussion of the method and results follows. More detailed results which consider accident paths are contained in Chapter V. The ^{233}U and ^{228}Th levels in the bred fuel are discussed in Chapter VII.

TABLE IV.A.4 DESCRIPTION OF ISOGEN CODE USE

- ISOGEN CODE NUMERICAL METHOD (MATRIX EXPONENTIAL)

Equation: $\frac{d\underline{N}}{dt} = \underline{\underline{\lambda}}\,\underline{N}$

Solution: $\underline{N}(t) = \underline{N}_0 \; e^{\underline{\underline{\lambda}}t}$

Expansion: $e^{\underline{\underline{\lambda}}t} = \underline{\underline{I}} + \underline{\underline{\lambda}}t + \frac{(\underline{\underline{\lambda}}t)^2}{2!} + \frac{(\underline{\underline{\lambda}}t)}{3!} + \cdots = \sum_{m=0}^{\infty} \frac{(\underline{\underline{\lambda}}t)^m}{m!}$

Recursion: $\underline{N}^{n+1} = \underline{N}^n \; e^{\underline{\underline{\lambda}}t}$

where:

- $\underline{N}(t)$ is the nuclide concentration "Vector" and $\underline{\underline{\lambda}}$ is the combined activation/decay exchange matrix.
- Activation data from TARTNP neutronics calculation
- Multiple zoning optional in ISOGEN
- Time dependent flux adjustment optional in ISOGEN

TABLE IV.A.5 LINEAR BEHAVIOR OF BREEDING PERFORMANCE AS A FUNCTION OF REACTOR LENGTH

	Case I	Case II	CaseIII
Fusion Power, MW	3000.	3000.	3000.
Neutron Wall Load, MW/m^2	1.45	1.39	1.27
Central Cell Length, m	175.	184.	200.
First Wall Radius, cm	150.	150.	150.
Lithium Coolant ΔT, °C	150.	150.	150.
BOC Blanket Energy Multiplication (M)	1.06	1.06	1.06
EOC Energy Multiplication (M)	1.72	1.79	1.97
Maximum Blanket Thermal Power	4128.	4296.	4728.
Ave. Fissile Discharge Enrichment (ε),%	.91	1.0	1.23
Fissile Production (F), Kg/yr	5649.	5659.	5686.
Fuel Cycle Period[a]	145.	168.	224.

a) Includes two front zone cycles, one rear zone cycle, and a blanket changeout period (See Figure IV.A.5 for typical breakdown).

TABLE IV.A.6. ECONOMIC IMPACT STUDY

	(Differential Benefit ($M/yr))	
	L_1 = 175 m	L_2 = 200 m
1. Central Cell Cost	27	
2. Heat Transport System Cost	36	
3. Reprocessing Cost		66
4. Electricity Revenue		35
5. Fuel Production Revenue		5
	63	106 (Δ = 43 $M/yr)

1. Central Cell Cost = Δ L (m) x 7.3 ($M/m) x 0.15 yr^{-1}
2. Heat Transport System Cost = Δ P (MW_t) x 0.4 ($M/MW) x 0.15 yr^{-1}
3. Reprocessing Cost = 400 $/kg x ($F_1/\varepsilon_1 - F_2/\varepsilon_2$) (kg/year)
4. Electricity Value = Δ M/2 x 5.15 x 10^9 (kWeH/yr) x 0.055 ($/kWeH)
5. Fuel Value = Δ F (kg/yr) x 1.5 x 10^5 $/kg

TABLE IV.A.7 BASELINE FUEL CYCLE PERFORMANCE SUMMARY

Fusion Power	3000 MW
Wall Loading	1.27 MW/m^2
Central cell Length	200 m
Max. Blanket Thermal Power	4728 MW
Min. Blanket Thermal Power	2544 MW
Fissile Production[a]	5624 kg/yr
Average Fissile Discharge Enrichment	1.23%
Zone 1 Discharge Enrichment	1.39%
Zone 2 Discharge Enrichment	.934%
Fuel Cycle Period	224 d (78,156)
Average Duty Factor	70%

a) at 70% duty factor

Figure IV.A.2 shows the buildup ^{233}U, ^{233}Pa, fission products, and other actinides as a function of irradiation time for the baseline fuel cycle. Included in the other actinides are ^{228}Th, ^{231}Pa, ^{231}Th, ^{232}Pa, ^{232}U, ^{232}Th, ^{233}Th, and ^{234}U. The figure gives a qualitative appreciation for the general way in which the constituent fissile concentrations track in time. Most importantly, we observe that the ^{233}Pa concentration is larger than the ^{233}U concentration for the first ~ 65 days.

Figure IV.A.3 shows the behavior of the sum of ^{233}U and ^{233}Pa as a function of time and fuel region. In general, all actinide concentrations are tracked for each of four separate fuel regions. The first of these two regions make up the first fuel zone, and the last two regions are the second fuel zone. Volume averaged concentrations are plotted in the above two figures and used in all analyses.

The principal fuel afterheat sources are from fission product decay and the beta decay of ^{233}Th and ^{233}Pa. Table IV.A.8 describes how each of these sources was estimated for the baseline fuel cycle. Note that the beta decay energies of ^{233}Th and ^{233}Pa are the average energies deposited locally by the resultant beta particles. These quanitities are reduced relative to the Q value of the reactions because some appreciable fraction (approximately 2/3) of the total energy is carried away by neutrinos. The LWR fission product decay energy expression used here is expected to be adequate in comparison with other uncertainties in the analysis (neutronics data, mechanical configuration, and burnup scheme). Possible corrections to the fission product decay heat source term include a specific tailoring of the source term for the thorium fuel and the reactor spectrum, but these corrections should be relatively small. Figure IV.A.4 shows the relative afterheat power density as a function of time after shutdown.

Fig. IV.A.2 Blanket Average Relative Actinide Fractions

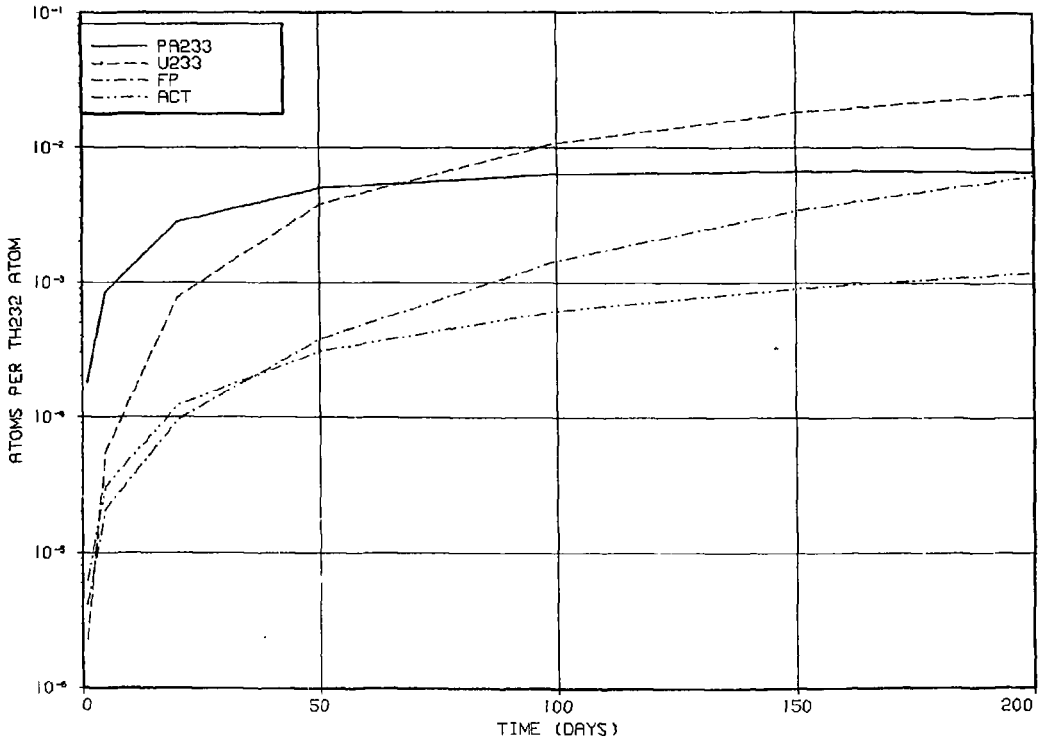

Fig. IV.A.3 Average Concentrations of (PA233 & U233) for Zones 1 and 2

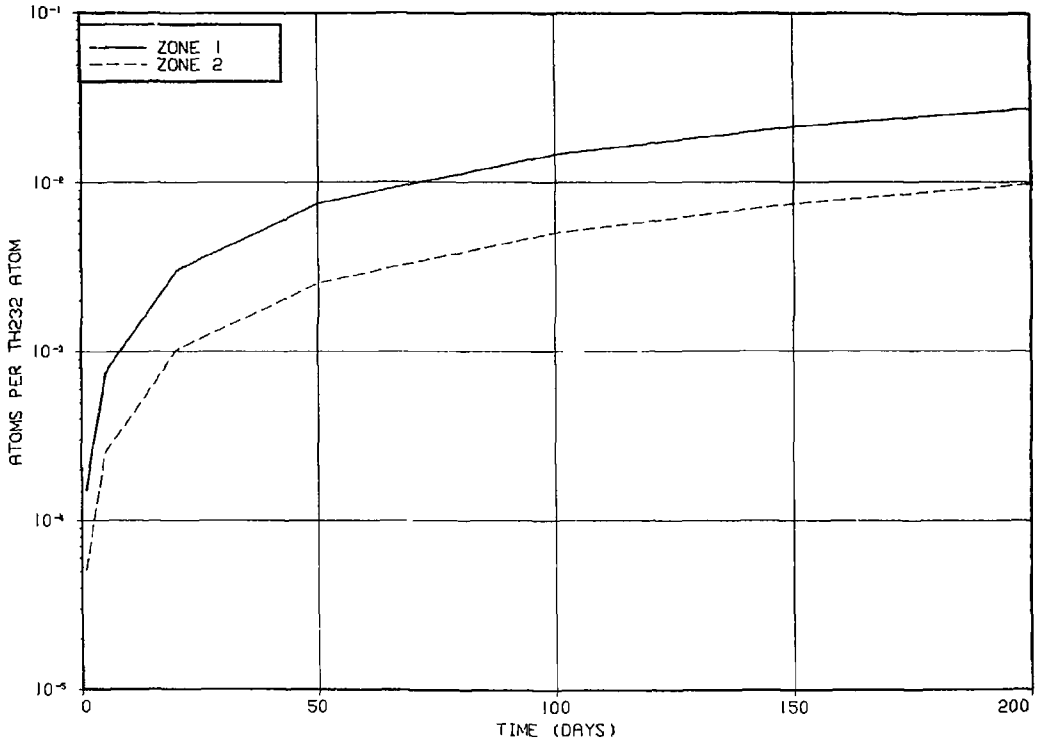

TABLE IV.A.8. AFTERHEAT SOURCE DATA BASE

- Fission Products

$P(t) = P_0 \times 6.5 \times 10^{-2} \times [(t)^{-0.2} - (t + \tau)^{-0.2}]$

t = time after shutdown in sec; τ = reactor operating time in sec

	ZONE 1	ZONE 2
P_0 =	2.38 w/cc	.801 w/cc

- Actinides

Discharge concentrations relative to thorium at $N^{232} = 8.74\ 10^{-4}$ a/b cm Th

		ZONE 1	ZONE 2
^{233}Th	ϵ_T =	3×10^{-6}	1.1×10^{-6}
^{233}Pa	ϵ_P =	5.32×10^{-3}	1.95×10^{-3}

- Beta decay energies

^{233}Th	E_T =	.427 MeV
^{233}Pa	E_T =	.228 MeV

- Decay rates

^{233}Th	λ_T =	$5.25 \times 10^{-4}\ s^{-1}$
^{233}Pa	λ_T =	$2.97 \times 10^{-7} s^{-1}$

- Actinide Power Densities

^{233}Th

$$PD = E_T\ \lambda_T\ N_T\ e^{-\lambda_T t} \times 1.6 \times 10^{-13} \quad W/cc$$

$$N_T = N^{232} \times \epsilon_T \times 10^{24}$$

^{233}Pa

$$PD = E_p\ \lambda_p\ [N_p\ e^{-\lambda_p t} + \frac{\lambda_T}{\lambda_p - \lambda_T} N_T\ (e^{-\lambda_T t} - e^{-\lambda_p t})] \times 1.6 \cdot 10^{-13} \quad W/cc$$

$$N_p = N^{232} \times \epsilon_p \times 10^{24}$$

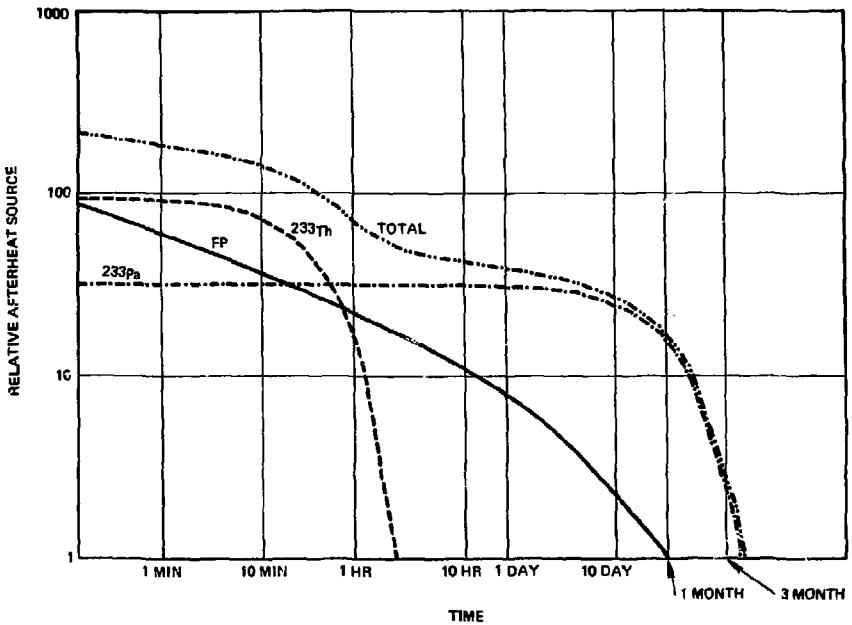

Fig. IV.A.4 Relative afterheat sources for the reference blanket

IV.A.4 Fuel Management/Availability Interface

There were two overall availablity goals observed in constructing the fuel management scheme:

- Ninety percent availability during reactor operation
- Seventy percent availability for entire fuel cycle including operation and shutdown

The operational availability of 90% was established by using a capacity factor of .90 in ISOGEN. After the baseline fuel cycle was found which met the operational mode requirements, fuel cycle goals, and fuel cycle constraints, allowable maintenance periods were established such that the overall availability was 70%. For instance, if d is the maintenance period to be assigned, then d satisfies the following equation where T is the fuel cycle period established in the ISOGEN run using the .90 capacity factor:

$$(.10T + d)/(T + d) = .30$$

The period d can be easily found, and segments of d can be apportioned between the operational periods in a two cycle scheme (where the first fuel region is reprocessed twice as frequently as the second) to allow time to remove, handle, and reload the fuel. Figure IV.A.5 shows how these periods were assigned for the baseline fuel cycle. This schedule provided the basis of the development of the fuel handling machinery presented in Section IV.B and the blanket replacement scheme discussed in Section II.E. It is felt that this fuel cycle represents a good compromise between the factors discussed above and has enough time available for routine and unscheduled maintenance.

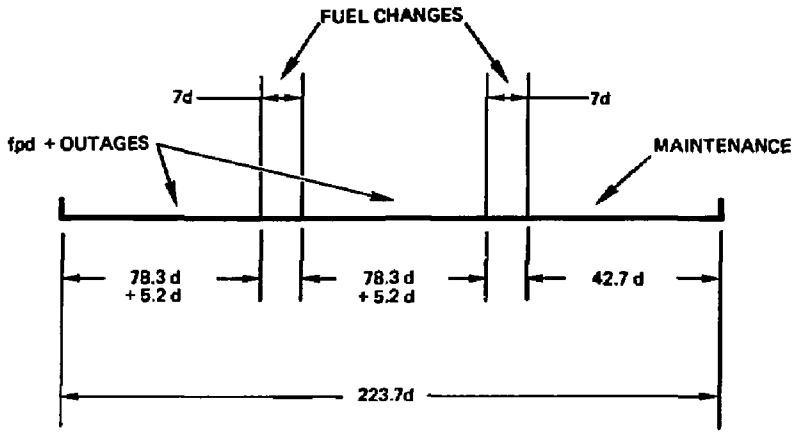

1)	78.3	fpd
	5.2	UNSCHEDULED OUTAGE DAYS
2)	7	SCHEDULED FUEL CHANGE
3)	78.3	fpd
	5.2	UNSCHEDULED OUTAGE DAYS
4)	7	SCHEDULED FUEL CHANGE
5)	42.7	SCHEDULED MAINTENANCE
	223.7	FUEL CYCLE PERIOD

UNAVAILABILITY = 0.30 = (2 x (5.2 + 7) + 42.7)/223.7

Figure IV.A.5 Baseline Availability Budget

IV.B FUEL HANDLING SYSTEMS

IV.B.1 Purpose

There are two purposes ascribed to the fuel handling system: 1) the removal of appropriately enriched thorium from the blanket and its replacement with fresh thorium for continuing operations; and 2) the inspection and agitation of the beryllium neutron multiplying material. The latter function is intended to prevent pebble jamming and fracturing which may occur as a result of radiation-induced swelling of the beryllium.

IV.B.2 Description

The beryllium/thorium fuel form, described in Section III.C, is a 3 cm diameter pebble with a snap-ring which fits over a groove located near the equator of the pebble. As shown in Fig. III.C.1, the offset position of the snap-ring causes the pebble to have an offset center of gravity. Section II.B describes the two radial-zone blanket module design. The central cell of the fusion breeder consists of 50 blanket modules, each 4 m long. Each 0.2 m deep fuel zone has a gross volume of about 8 m^3 and it is this amount which the handling system must accommodate. The perspective view of the dumpout/pebble change system is given in Fig. IV.B.1. Each zone, of which there are 100, has a valved connection to a liquid metal circuit (see Fig. IV.B.2) which includes a dump tank sufficient to accommodate five modules blanket volume (80 m^3), a batch tank of 8 m^3, and a pump, header, and heat exchanger which may be specific to this circuit as shown in Fig. IV.B.1. The last three items can also be part of the main coolant system. The dump and batch tanks are alternative loops of the same transport/cooling system. One dump tank and two batch tanks (one redundant) are provided for the 50 blanket modules.

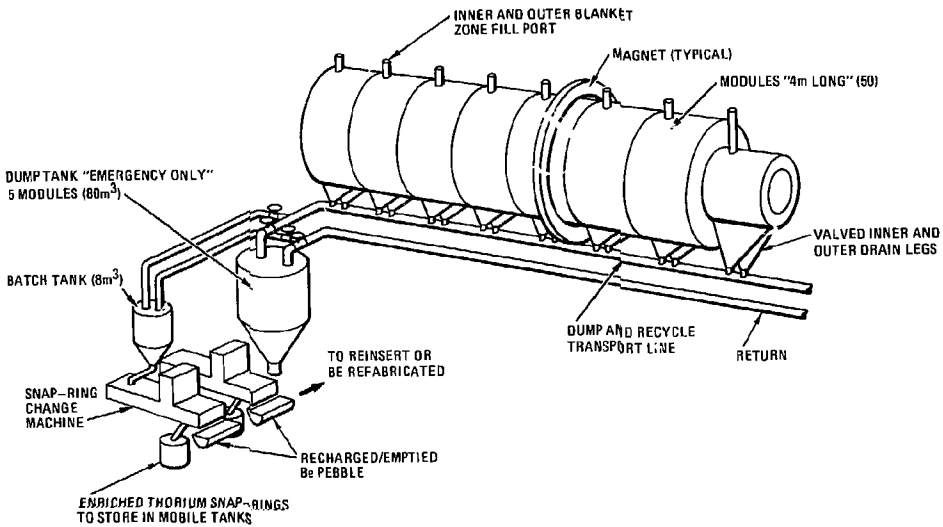

Fig. IV.B.1 Dumpout/pebble change system.

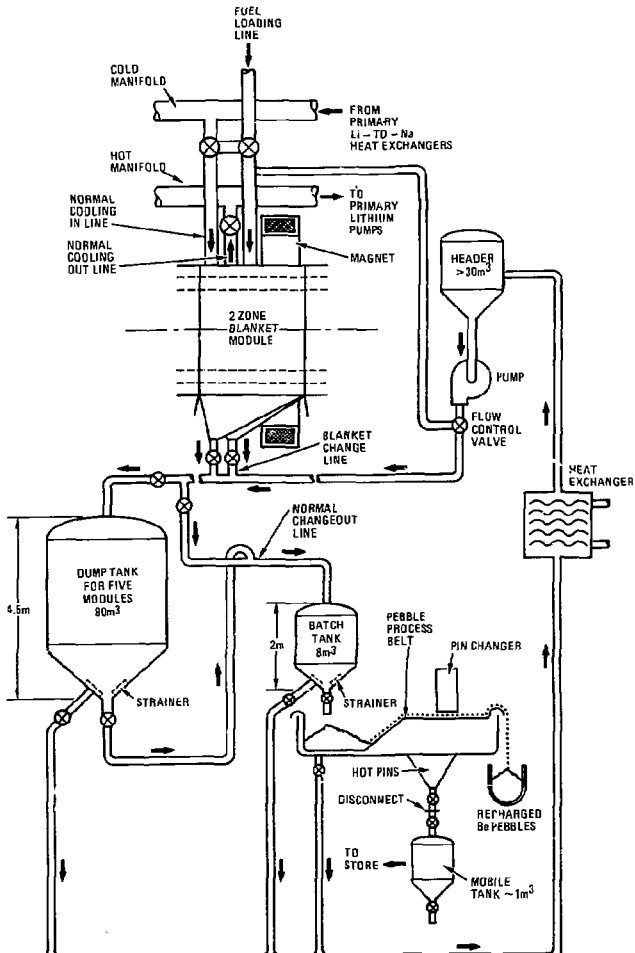

Fig. IV.B.2 Pebble handling circuit and module safety coolant system.

Under the batch tank is a liquid metal bath through which a metal link belt is driven as illustrated in Fig. IV.B.3.* The batch tank can be emptied into this bath, the fluid being pumped back to the header, and the pebbles being transported out on the metal belt. The belt passes over a separately pumped area, placing a few kilo Pascals pressure beneath the belt, thus lifting the pebbles which are caught in perforations in the metal links. This allows them, by virtue of their offset center of gravity, to orient themselves uniformly (see Fig. IV.B.4*). As they continue along on the belt, they pass under a device which punches off the thorium snap-ring and replaces it with a fresh snap-ring in one operation. The punched snap-rings sink into a small (<1 m^3) tank connected to the bottom of the machine. These snap-rings are taken to storage after the tank is filled and disconnected. A new tank replaces it for continuing operation. The pebbles with the fresh snap-rings fall into a dry container and are transported to the full reloading system. The snap-ring punch machine has the capability of working in an alternate mode where the snap-rings are extracted but not replaced, enabling pebbles which have reached the swelling limit to be diverted for refabrication. It is proposed that the small enriched snap-ring tank be of such form that it can be surface-cooled by immersion in a liquid or by free convection in air after storage. The ball processing machine has an inert atmosphere (e.g., argon) above its free surfaces at a nominal overpressure. The 8 m^3 tank and the enriched fuel tanks, both of which can be emptied in operation, will be back-filled with inert gas. The contents of both the 3 m^3 tank and the dump tank are cooled by continuous circulation of liquid lithium through the tank. Major system characteristics are listed below.

*The fuel handling system design was developed when the inside pin fuel forms (see Section III.C) were favored for the reference blanket. The snap-ring fuel form was selected later in the study because it offers advantages with respect to a lower thermal stress in the beryllium (consequently longer life) and superior fissile breeding performance (less heterogeneous effect). We expect that the issues associated with handling the snap-ring fuel form will be similar to those associated with the inside pin fuel forms and that the fuel pin change machine developed for the earlier fuel form (see Figs. IV.B.3 and IV.B.4) can be easily adapted to provide for the required changes.

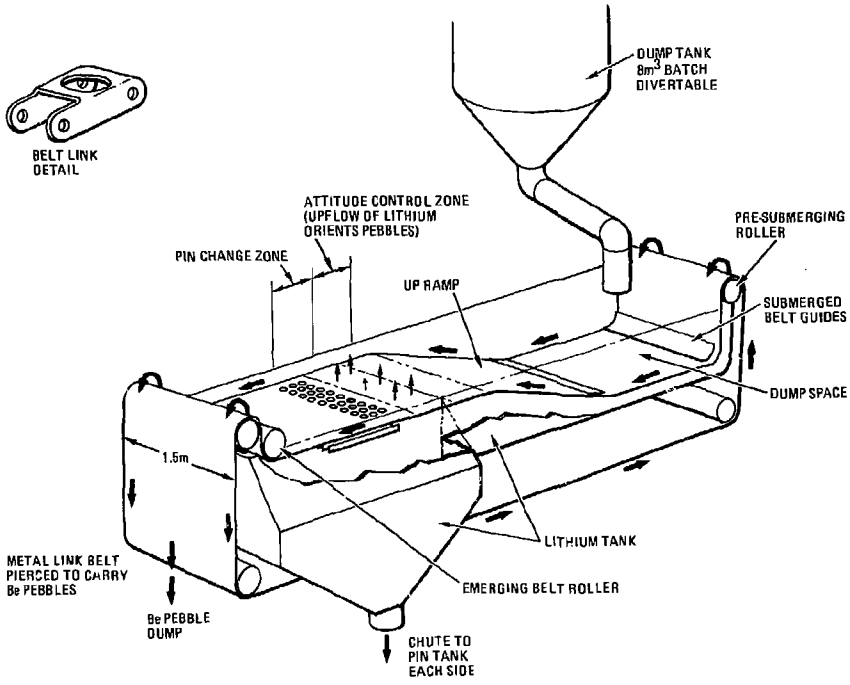

Fig. IV.B.3 Pin change machine.

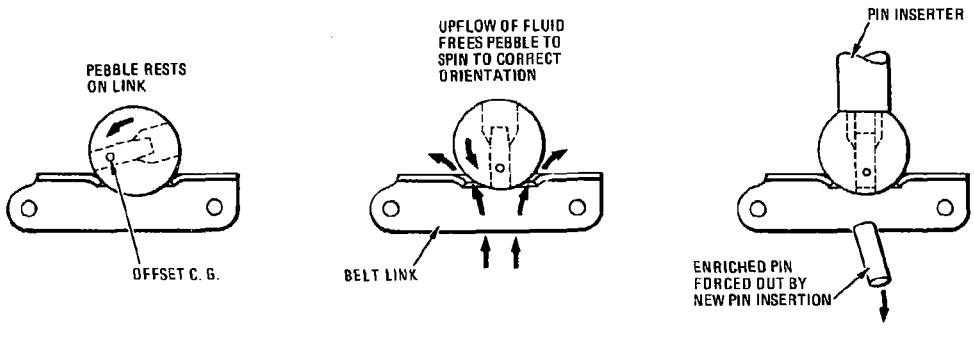

Fig. IV.B.4 Beryllium pebble orientation and thorium pin extraction schematic.

Fuel Handling System Characteristics

Volume of Be/Th fuel zones to be changed per refueling interval:
50 modules × 2 zones × 8 m^3 = 800 m^3
Beryllium pebble quantity: (62% of packed bed module volume);
50 × 2 × 351,000 = 35.1 × 10^6 balls
Process time: 1 week
Rate for full batch: 58 pebbles/second
Snap-ring cooling time before reprocessing: 270 days
Snap-ring initial thermal deposition: 0.3 w/cc* (0.678 cc each)
Pebble extraction from blanket is by coolant flow diversion and flushing

IV.B.3 System Operation

Due to the presence of a magnetic field, its effect on the vertical removal of highly conducting beryllium pebbles by gravity in the bath of lithium has to be considered. This result is then used to guide the design of pebble removal during change/dump-out operations.

Considering the kinetic, potential, and magnetic body forces experienced by the fluid, at a fluid height of h meters, the force per unit area balance equation can be written as:

$$\frac{1}{2}\rho v^2 = \Delta\rho g h - \sigma v B^2 h^{**} \qquad (1)$$

where: ρ = density of beryllium pebbles
v = velocity of beryllium pebbles
$\Delta\rho$ = density difference of beryllium and lithium
g = acceleration of gravity

---

*Average volumetric power generation of the first fuel zone

**The magnetic body force $\vec{J}\times\vec{B}$ generated in the pool of lithium and beryllium is approximated by $\sigma v B^2$.

h = pebble blanket height

σ = electrical conductivity.

Equation (1) is a quadratic equation of velocity v. For a h of 3.65 m and a magnetic field strength of 4.24 T, the ball velocity at the bottom of the module was calculated to be 0.11 mm/sec (0.4 m/hr). This is too low a speed for pebble removal and surely not acceptable for pebble dump operation as may be required by safety considerations.

The available approaches to handle the MHD effect are to turn the magnetic field off or to re-route the main lithium coolant to the pebble removal circuit and actively pump the pebbles outside of the blanket zone. The second option was selected in order to minimize the required down-time to perform the on/off operations for the superconducting magnet. Hence, the handling system first receives pebbles carried in a diverted coolant stream through the open valve. From this point, the separate fuel transport flow takes over, carrying the round pebbles along the 30 cm diameter pipe to the dump tank or the batch tank. The flow speed associated with transporting 56 pebbles/sec along the pipe is not expected to be excessive; we do not expect the pebbles to be truly suspended, but rather, rolled. The blanket dump valves will never be closed onto a solids-bearing stream before the pebbles are emptied, hence a comparatively simple gate valve will suffice. This particular scenario is preserved whenever possible throughout the handling system.

This stream then arrives at its destination tank and is slowed appropriately; the pebbles drop out and the stream is returned through a large area separator grille in the tank bottom (see Fig. IV.B.2).

The dump tank, as discussed in Section V, can accept up to five blanket module contents. The transfer of such an 80 m^3 dump to the separation process is accomplished by pumping lithium through the dump tank. The lithium then emerges as a pebble-bearing stream which is directed to the batch tank. At the batch tank, the pebbles are separated and the fluid recirculated. This scheme requires a valving arrangement which is capable of arresting a solid bearing stream, by first straining the solids against a movable grille arrestor and secondly, shutting off the fluid. This is required

since the process system is only designed for 8 m^3 batches, while the dump tank may receive up to 80 m^3 at one time.

In all accident scenarios including the fuel-handling system, fuel-bearing pebbles are directed to the dump tank. Only the main transfer line from the modules to the dump tank is shown for simplicity. The dump tank is physically situated at the lowest point in the system. In transferring from the dump tank back to the batch tank, the pebbles travel in an upward direction. The question of vertical lift of the pebbles is thus of interest. By balancing the gravitational force with the upward lift force of the pumped lithium, flow speeds of less than 2 m/sec appear adequate for the conveyance of the pebbles in the present system. The proportion of pebbles to fluid could be as low as 1% by volume and will not mandate that the flow be turbulent in order to hold the pebbles in suspension. The power requirement, even for a large system, is unlikely to be large, and this is not seen as a critical issue.

If for any reason, the flow speed is locally insufficient to lift any single pebble, then that pebble will cause an obstruction and a corresponding increase in the flow speed. The flow speed will continue to increase with the arrival of additional pebbles until the speed is sufficient for the lift. The net effect is an increasing pebble concentration with height in the rising pipe. In the limit, the rising pipe will resemble a fluidized bed, but without enough flow to be fluid. This situation is easily avoided by maintaining the lithium flow speed above the aforementioned 2 m/sec. In a practical application, experimental work will be required to determine the best fluid speed in the conveyer piping to carry the pebble load to the batch tank.

When the 8 m^3 tank is full, the entire contents are dropped into the process machine which will adjust its liquid level by returning fluid to the header. The heap of pebbles in the tank is then conveyed on the link belt to the righting and separation steps. A grille is arranged to ensure that the belt leaves the loading region with only a single layer of pebbles and without an overload which would stop the next processes. The punch machine, which replaces the thorium snap-rings, is envisaged as having continuous snap-ring feed from a hopper and a stepping function which allows it to

follow the belt and step back to its original position for the next row. To achieve the necessary reliability, there will in fact be two 8 m^3 tanks delivering to four snap-ring changers and the system will be such that any one of these six components could be inoperative and the design throughput of pebbles can be maintained.

IV.C DEVELOPMENT OF AN IMPROVED FUEL CYCLE

Sections IV.A. and IV.B describe the methods and results of the baseline fusion breeder fuel management analysis. In this section, later work will be presented which uses updated neutronics data (see Section II.C) and reconsiders the basic issues which influence and involve the fuel cycle. In this section we also provide the ability to vary the fusion driver parameters and technologies to achieve an improved operating point which interfaces with fuel cycle and blanket thermal constraints.

Section IV.A.1 discusses the choice of a blanket configuration with two radial zones and one axial zone. Essentially, a two radial zone design allows the first zone to be cycled more frequently which takes advantage of higher front zone breeding rates. The single axial zone provides operational simplicity and maximizes the fissile enrichment, but also results in a large power swing.

Having specified the method of operation and the reactor zoning scheme, several physics and engineering constraints must be considered in the development of an improved fuel management scheme. These constraints essentially specify the reactor configuration (i.e., the central cell length) as a function of the maximum blanket energy multiplication. Two constraining equations were considered:

$$M \Gamma B_c^2 \leq 44.13$$

$$B_c = 1.16 \times \left[\frac{P_f \times B_p}{L_c}\right]^{1/5}$$

The first equation represents a limitation on blanket pumping power where M is the maximum blanket energy multiplication, Γ is the neutron wall loading (MW/m^2), and B_c is the central cell mangetic field strength (tesla). The second equation is a passing ion criteria which reflects plasma stability as affected by trapped particle modes. B_p is the maximum end cell magnetic field (tesla), P_f is the fusion power (MW), and L_c is the central cell length (meters). These equations can be combined to eliminate B_c:

$$L_c = 1.9 \times 10^{-2} \times M^{5/7} \times P_f \times B_p^{2/7} / R_{fw}^{5/7}$$

This relationship parameterizes the central cell length as functions of the end plug axicell field, maximum blanket M, and fusion power and first wall radius. The fusion power and wall radius are fixed at 3000 MW and 1.5 m in this analysis. Given L_c, Γ is calculated as $\Gamma = .8\ P_f/(2\ \pi\ r_{fw}\ L_c)$. Therefore, the central cell field strength, central cell length and wall loading are specified as functions of the end plug axicell field and the maximum blanket multiplication. M also determines the discharge enrichment achievable under the above wall load.

The plasma gain, Q_p, also changes with M and B_p, but this more complex relationship is modeled using the LLNL tandem mirror physics code(1). Table IV.C.1 shows the physics code results for plasma gain as a function of M and B_p.

All of the cases presented in Table IV.C.1 satisfy the known physics and engineering constraints. In order to choose from the parameter space one other constraint was established: A maximum end plug axicell field of 20 Tesla to achieve a plasma Q as high as possible with reasonable technological constraints. It is important to note that the original baseline case utilized an axicell field strength of only 15 Tesla. The 20T cases, represented by fixed B_p, but variable M were analyzed using ISOGEN to see what relative breeding could be achieved. These results are shown in Table IV.C.2 and Figure IV.C.1. The double radial zone results assumed that the first zone is reprocessed twice as frequently as the second.

Using average discharge enrichment as a measure, the largest case (193 m) results in the highest discharge enrichment. This case also has the highest plasma Q.

Some further insights can be gained by rewriting the constraining equation as the function $F(L_c,M)$ where

$$F(L_c,M) = L_c - 100. \times M^{5/7} = 0$$

for Rfw = 1.5 m, P_f = 3000 MW, and B_p = 20 tesla. The variation of this function can be described as

$$\Delta F(L_c,M) = \frac{\partial F}{\partial L_c}\ \Delta L_c + \frac{\partial F}{\partial M}\ \Delta M = 0$$

Table IV.C.1 REACTOR CONFIGURATION PARAMETERS FROM PHYSICS CODE AND CONSTRAINT EQUATION ANALYSIS

	B_p	L_c	B_c	$\eta_t Q$	$\Gamma_{1.5}$
M = 1.5 Cases					
	15	123.6	3.77	5.16	2.06
	17.5	129	3.86	8.25	1.97
	20	134	3.93	11.4	1.90
	22	138	3.98	13.58	1.84
	24	141	4.04	14.85	1.81
M = 1.75					
	15	138	3.69	6.34	1.84
	17.5	144	3.77	9.87	1.76
	20	150	3.85	13.3	1.70
	22	154	3.9	15.4	1.65
	24	158	3.95	16.6	1.61
M = 1.97					
	15	150	3.63	7.4	1.69
	17.5	156	3.71	11.1	1.63
	20	163	3.78	14.8	1.56
	22	167	3.83	16.83	1.52
	24	172	3.88	17.5	1.48
M = 2.25					
	15	165	3.56	8.65	1.54
	17.5	172	3.64	12.75	1.48
	20	179	3.71	16.6	1.42
	22	184	3.76	18.6	1.38
	24	189	3.81	19.7	1.35
M = 2.50					
	15	178	3.51	9.04	1.43
	17.5	186	3.58	13.12	1.37
	20	193	3.66	16.58	1.32
	22	198	3.71	18.20	1.28
	24	203	3.75	18.55	1.25

Notes:

1) $\Gamma_{1.5}$ is at a first wall radius of 1.5 m.

2) η_t is the plasma trapping fraction and $\eta_t Q$ represents the ratio of plasma power to total trapped driver power.

Table IV.C.2 ISOGEN ANALYSES OF 20 TESLA CASES

L	Γ	Blanket M_{max}	$\eta_t Q$	Single Zone $\epsilon,(T)^a$	Double Zone $\epsilon,(T)^a$
134	1.90	1.50	11.4	.3524,(36)	.4129,(31,62)
150	1.70	1.75	13.3	.5266,(61)	.6224,(53,106)
163	1.56	1.97	14.8	.6414,(82)	.7658,(72,144)
179	1.42	2.25	16.6	.7830,(12)	.9405,(99,198)
193	1.32	2.50	16.6	.9064,(142)	1.0848,(125,250)

a) $\epsilon,(T)$: fissile discharge enrichment, full power irradiation period (first zone, second zone)

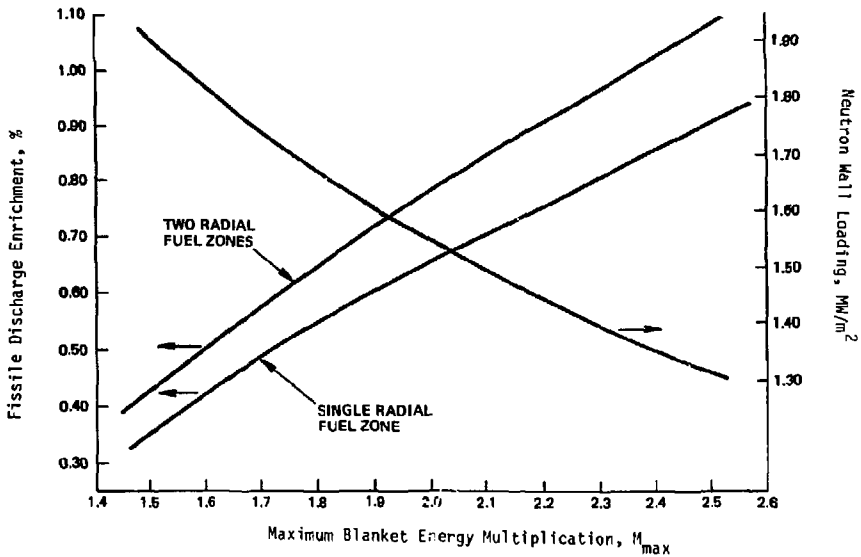

Figure IV.C.1. Discharge Enrichment for Single and Double Radial Zoned Blankets as a Function of Maximum Blanket M

which gives

$$\frac{\Delta L_c}{\Delta M} = 71.74 \times M^{-2/7}$$

This expression can be reconfigured as a function of L_c or Γ using the previous relationships. Figure IV.C.2 shows the variations in L_c and M as a function of M (or L_c). As evident from the figure, for larger M values, given changes in L_c require larger changes in M to preserve all applicable constraints. Thus, if M is a desirable quantity, it is possible to gain increasingly large amounts of M for given, constant changes in L_c at larger values of M or L_c. In our case, higher achievable enrichments can be attained by both higher Γ and higher M. This analysis explains why the larger lengths (lower Γs) are more desirable for high enrichment in spite of the resulting lower wall loads. The gain in M is more than large enough to compensate for the lower wall loads at larger lengths.

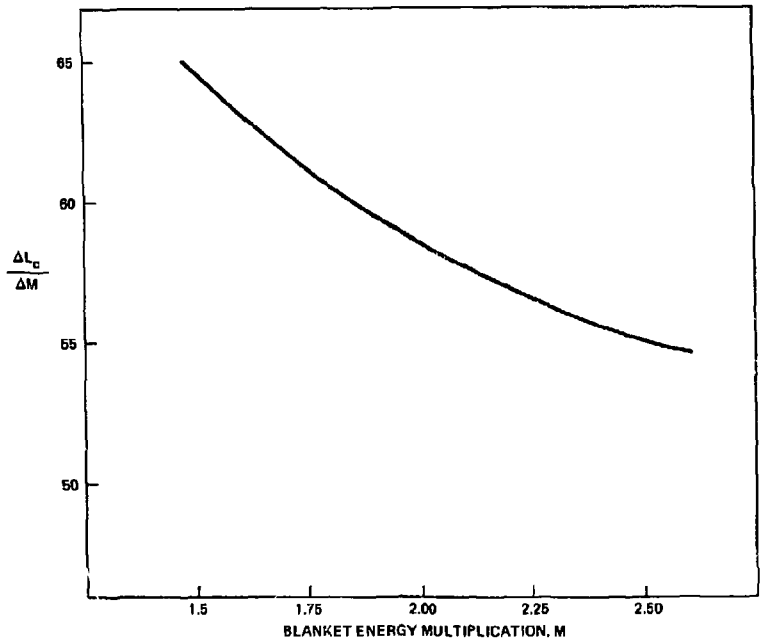

Figure IV.C.2. Sensitivity of M and L_c as a Function of M (or L_c)

References, Section IV.C

1) Original code as described in G.A. Garlson, et al., "Comparative End Plug Study for Tandem Mirror Reactors", UCID-19271, Lawrence Livermore National Laboratory (1981). Current version of the code is maintained at LLNL.

2) Original code as described in D.L. Chapin, et al., "Preliminary Feasibility Assessment of Fusion-Fission Hybrids", WFPS-TME-81-003, Westinghouse Fusion Power Systems Department (1981). Current version of the code is maintained at TRW.

2) Original code as described in D.H. Berwald and J.A. Maniscalco, "An Economics Method for Fusion-Fission Electricity Generation Systems", Nucl. Tech./Fusion, 1, 128 (1981). Current version of the code is maintained at TRW.

IV.D. OPTIMAL FUEL CYCLE AND REACTOR CONFIGURATION

The last case in Table IV.C.2 provides the highest enrichment, but other factors must be considered in choosing the most desirable reactor configuration. This section presents the optimal case and explains the method used to choose among the cases in Table IV.C.2.

Chapter VIII describes the methods and results of the systems and economic analyses which are performed for the tandem mirror hybrid. As described in that chapter (and in Chapter VI), the tandem mirror reactor design code(1) is used to predict the reactor direct capital cost. This cost along with reactor operating and maintenance costs is used in the economics analysis code(2) to predict a cost of electricity for a symbiotic fusion breeder-fission converter electricity generation system. This method was used to choose the optimal fuel cycle. The five cases in Table IV.C.2 were all costed with the optimal case being the one with the lowest resulting cost of electricity. All five cases are shown in Table IV.D.1 with the optimal case being case 5. This case resulted in a cost of electricity of 36.45 mills/kWhr. For comparison, the previous baseline case discussed in Section IV.A gave a system electricity cost of 38.7 mills/kWhr. Therefore, our optimization resulted in a 6% system cost savings relative to the baseline. A detailed comparison, focusing upon fuel management is provided in Table IV.D.2. The improved case is discussed in Chapter VIII.

Note that the choice with the highest M confirms the conclusion of Section IV.C. Essentially the length dependent costs were overshadowed by cost savings in the driver, fuel reprocessing, and thermal systems. The thermal system is relatively cheaper due to economy of scale since the M = 2.5 blanket makes more power.

Figure IV.D.1 shows the availability budget of the improved case. Again, two assumptions were made in the availability budget calculation:

- 90% availability during two irradiation periods and 7 day fuel handling interval
- Overall availability of 70%

Table IV.D.1 FUEL CYCLE SYSTEMS AND ECONOMIC ANALYSIS SUMMARY

	CASE[a]				
	1	2	3	4	5
Maximum Blanket Energy Multiplication	1.50	1.75	1.97	2.25	2.50
Central Cell Length, m	134	150	163	179	193
$\eta_t Q$	11.4	13.3	14.8	16.6	16.6
Net Fusion Breeder Elec. Generation Efficiency	.286	.303	.314	.325	.331
Average Discharge Enrichment, %	.41	.62	.77	.94	1.08
Total Operating Period, T (days)	62	106	144	198	250
Direct Capital Cost, $/kW$_n$	829.	761.	723.	686.	660.
System Elect. Cost, mills/kWh	39.11	37.90	37.27	36.76	36.45

a) All cases for 20 T field strength

Table IV.D.2 FUEL CYCLE OPTIMAL CONFIGURATIONS

	Optimized	Old Baseline
Central Cell Length, m	193	200
Wall Load, MW/m^2	1.32	1.27
$n_t Q$	16.6	14.6
Maximum End Plug Field, Tesla	20	15
Maximum Blanket Energy Multiplication	2.50	1.97
Average Blanket Energy Multiplication	1.885	1.61
Net Fusion Breeder Elect. Generation Efficiency	.336	.295
Maximum Breeder Nuclear Power, MW	6600	5328
Average Breeder Nuclear Power, MW	5124	4484
Maximum breeder Electric Power, MW	2256	1662
Average Breeder Electric Power, MW	1720	1317
Average Discharge Enrichment, %	1.10	1.24
Radial Zone 1 Average Discharge Enrichment, %	1.24	1.39
Radial Zone 2 Average Discharge Enrichment, %	0.81	.93
Volume per radial zone 1 module, cm^3	2.09×10^4	2.09×10^4
Volume per radial zone 2 module, cm^3	2.35×10^4	2.35×10^4
Fuel Cycle Periods		
Radial Zone 1, days	125	78
Radial Zone 2, days	250	156
Direct Capital Cost[a], Million $	3439	3744
Symbiotic System Electricity Cost, mills/kWhr	36.5	38.7

a) Includes fuel reprocessing plant (see Chapter VII).

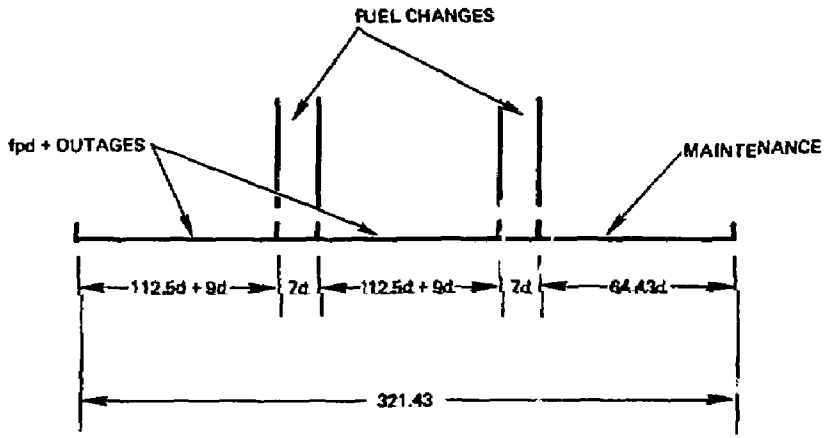

SEQUENCE

1)	112.5	fpd
	9	UNSCHEDULED FUEL OUTAGE DAYS
2)	7	SCHEDULED FUEL CHANGE
3)	112.5	fpd
	9	UNSCHEDULED OUTAGE DAYS
4)	7	SCHEDULED FUEL CHANGE
5)	64.43	SCHEDULED MAINTENANCE
	321.43	FUEL CYCLE PERIOD

UNAVAILABILITY = 0.30 = (2 x (9 + 7) + 64.43/321.43

Figure IV.D.1 Availability Budget for Optimized Case

The overall unavailability is .30. It is related to the fuel cycle period, T = 250 days, (developed from the ISOGEN calculations), and the scheduled downtime d by

$$.30 = (.10\ T + d)/(T + d)$$

which gives

$$d = 2/7 \times T$$

We assume that two fuel changes, each seven days long, are scheduled between the operational phases. One of these seven day periods is included in the .10T = 25 days operational unavailability. Since our full power operational periods are .90T/2 = 112.5 days long, the unscheduled outages during each operational phase are (.10T-7)/2 = 9 days long. Thus, given the ISOGEN periods of (125,250) days, the total scheduled downtime following the two operational periods and one of the seven day fuel change outages is a total of 71.43 days long (71.43 = 7 + 64.43). The total fuel cycle period is 321.43 days long. These periods are all arranged as in the figure.

References, Section IV.C

1) Original code as described in D.L. Chapin, et. al., "Preliminary Feasibility Assessment of Fusion-Fission Hybrids", WFPS-TME-81-003, Westinghouse Fusion Power Systems Department (1981). Current version of the code is maintained at TRW.

2) Original code as described in D.H. Berwald and J.A. Maniscalco, "An Economics Method for Fusion-Fission Electricty Generation Systems", Nucl. Tech./Fusion, 1, 128(1981). Current version of the code is maintained at TRW.

CHAPTER V
REACTOR SAFETY SYSTEMS AND ANALYSIS

V.A INTRODUCTION AND OVERVIEW

V.A.1 Safety Systems and Analysis Goals

A major feature of the fission-suppressed blanket concept is the reduction of fission product and transuranic nuclide inventories and their attendant problems of radionuclide containment and decay heat removal. These reductions translate into significant, quantifiable advantages from the viewpoints of engineering design and public safety. The safety effort presented in this chapter was aimed at ensuring that these safety advantages play a significant role in the evolution of the fusion breeder reactor.

The three goals of the safety systems and analysis effort were as follows:

- Continue the development of safety criteria and quantify the characteristics and safety connotations of the term "fission-suppressed" (Section V.B).
- Define the safety systems and specify the major components pertinent to ensuring the safety associated with the fusion breeder, including the heat removal systems and the fuel dump system (Section V.C).
- Perform the supportive safety analysis to identify the major sources of hazard and the most probable release pathways associated with the reference system, thereby providing additional guidance in the design of the system (Section V.D).

The results are summarized in the remainder of this section and presented in detail in the appropriate subsequent sections.

V.A.2 Safety Criteria Development

The Biological Hazard Potential (BHP), the decay heat rate, and structural material temperature safety limits were evaluated in this study

with the intent of quantifying the safety characteristics of the reference fission-suppressed blanket. This was accomplished by performing a parametric analysis of the BHP and decay heat source for the reference blanket as a function of the fuel enrichment/irradiation time/fuel management scheme. Fission-suppressed and fast fission blankets were then compared. The safety distinction between the two blanket types can be attributed to the contribution of the fission products to the BHP and the decay heat rate level. The results show that the actinide hazard reaches an equilibrium condition at low enrichment levels, whereas the fission product hazard is proportional to the overall fission rate and continuously increases with enrichment. The isotopic distribution and temporal behavior of the hazard after shutdown was also evaluated. The decay power density increases significantly with enrichment and the increase can be directly attributed to the fission products. The actinide BHP was found to dominate the biological hazard, independent of the enrichment or irradiation time.

A preliminary evaluation of the time to creep-rupture failure at the stress levels of the present blanket was performed for HT-9 and 2-1/4Cr-1Mo. From the analysis, a safe HT-9 temperature limit of 750°C was established as the maximum temperature that could be experienced by the module for significant periods of time and still permit module reuse. An HT-9 temperature limit of 900°C was established as the maximum temperature above which failure could be presumed to occur within about (1/2 hours) time. These results were combined with the thermal analysis in establishing acceptable safety system performance.

V.A.3 Safety Systems Overview

The safety systems addressed in this study focus on those systems which would have significant impact at the conceptual design stage due to their requirements of special design effort, impact on parallel systems designs, or cost. Specifically addressed herein are the primary coolant and decay afterheat removal systems, the module safety coolant systems and the fuel dump system.

The primary coolant system serves as the first level of safety and also serves as the decay afterheat removal system during normal shutdown. Its principal components, shown in Figure V.A.1, are described below.

- Primary Coolant Pumps -- There are five main coolant pumps, all operating at 60% of their rated capacity. Only three of these are required for full power operation, so that in the event of a single failure, the remaining pumps can be brought up to 80% of their rated capacity, and normal full power operation can be maintained. Sufficient excess capacity is available that one pump may be down for a limited period of time for repair and the system will still satisfy the single-failure criteria for full power operation. Under shutdown conditions, any single main coolant pump operating at 20% of its rated capacity is sufficient to circulate coolant for afterheat removal and maintain temperatures below those experienced during operation.

- Primary Heat Exchangers -- There are six Li-to-Na heat exchangers, all operating at 83% of their rated capacity. Only five are required for full power operation, and in the event of failure or maintenance of one, the remaining units can maintain full power operation.

- Coolant Manifolds -- These include a cold inlet manifold to the modules, a hot outlet manifold accepting coolant from all the modules, and a heat exchanger common plenum. The arrangement shown in Fig. V.A.1 permits any pump and any heat exchanger to serve any of the blanket modules.

In the event of a malfunction of the primary coolant system, the fuel handling system provides the redundant and diverse circuit required to maintain adequate module cooling. This system consists of its own auxiliary pumps and heat exchangers, and provides the coolant flow necessary for shutdown afterheat removal. The fuel handling system is shown in Fig. IV.B.2 and is more fully described in Chapter IV. This system also contains the fuel dump circuit. The fuel dump is initiated for failures which prevent adequate cooling from reaching an individual module. The dump tank was sized to contain the fuel volume of five modules on the basis of isolating the failed module and preventing the propagation of a failure to adjacent modules.

These systems form the basis for the safety analysis summarized in the next section.

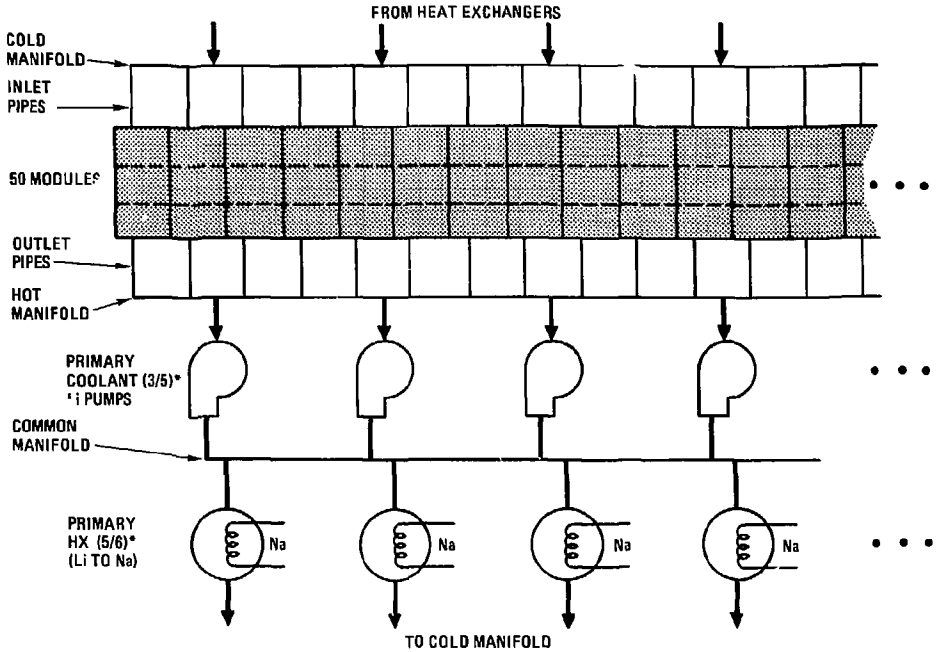

Fig. V.A.1 Primary coolant and decay afterheat removal system.

V.A.4 Safety Analysis Overview

A Failure Modes and Effects Analysis (FMEA) was performed at the component level of the systems described above. Failures considered include active component malfunctions, primary coolant outer boundary and first wall structural failures, and failures of interface systems such as the power supply and secondary heat removal.

The failure modes were divided into three categories related to their effects on the system. Thermal analyses were then performed to determine the course of action required subsequent to the initial failure. Although some of the results of the thermal analyses were sensitive to the assumed parameters governing the heat transfer, failure of the blanket module was identified only for initiating events which lead to partial or complete loss of lithium to the fertile fuel pellets. This dictated the scenarios requiring fuel dumping. The allowed time to dump prior to structural failure was estimated.

The initiating events which would lead to uncovered fuel were determined to be rupture or leakage of the piping leading to or from the first wall, and mechanistic failure of the first wall. These events require dumping since a short-circuit path may occur which would preclude coolant from reaching the fuel. Failure to dump the fuel would then lead to loss of the module. Although the probability of such a sequence of events is thought to be low, it is recommended that the adjacent modules be dumped to limit failure propagation and minimize accident consequences. Subsequent to the fuel dump, the temperature of the isolated, radiating first wall will remain below the limit established for HT-9 structural failure. Uncertainties in the first wall emissivity and afterheat levels warrant more data and analysis in future evaluations of this important accident scenario.

The effectiveness of natural circulation of the lithium in removing first wall afterheat after a fuel dump was evaluated. The results show that with the proper design of the coolant heights and orientation, natural circulation will be sufficient, in the absence of a magnetic field, to remove the afterheat from the first wall and maintain its temperature below 750°C without any operating, active components. In the presence of a magnetic field natural circulation is not adequate.

In conclusion, the redundancy and diversity of the reference safety systems provide adequate protection of the reactor against loss-of-coolant accidents. To further optimize the safety systems, an integrated analysis of overall system and reactor reliability/availability/maintainability/safety/economics should be performed. More detailed calculations of the first wall decay afterheat rates are recommended for future thermal analyses. Experiments should be carried out to determine the emissivities of metal surfaces exposed to flowing liquid metals. These are relatively simple experiments which can be performed on existing liquid metal loops and would address one of the major safety issues of the fusion breeder.

V.B SAFETY CRITERIA DEVELOPMENT

The evaluation of the safety characteristics of fission-suppressed blanket concepts in Refs. 1 and 2 has demonstrated the improvement in safety which is associated with this type of fertile blanket. The improvement has been quantified as a one to two order of magnitude reduction in the Biological Hazard Potential (BHP) over thorium and uranium fast-fission blankets, and a substantial increase in the time-to-melt of structural components, in the event of loss-of-cooling, as a result of reduced afterheat levels. The relative risk (the product of the probability of an event and its consequence) has also been shown to be reduced for fission-suppressed blankets.

Based on the recommendations of Ref. 2, the BHP, decay heat rate, and the structural material temperature to prevent failure were chosen for further study in the present work, with the goal of establishing a quantitative, safety-oriented definition of the term "fission-suppressed." The continued use of relative risk as a safety criteria was deferred until design details of the system hardware and configuration became better defined.

To establish a safety-oriented definition of the term "fission-suppressed," the nature and behavior of the radioactive inventory, BHP, and decay afterheat generation rate were studied by performing parametric analysis of these quantities for the reference blanket as a function of the fuel enrichment/irradiation time/fuel management scheme. The analysis provided information on the major hazard contributors as a function of the operating parameters which determine isotopic content of the fuel. The results of these analyses are presented below. The section concludes with a general discussion of conventional safety criteria and their applicability to the safety systems of the fusion breeder.

The variation of the total BHP, and the decay heat rate as a function of irradiation time and enrichment are shown in Figs. V.B.1 and V.B.2. The figures show that the actinide hazard reaches an equilibrium condition at low enrichment levels whereas the fission product hazard continuously increases. The actinides dominate safety concerns at all enrichment levels relevant to the reference blanket, consistent with past work.

The results presented in Figs. V.B.1 and V.B.2 are average values for the first 10 cm of the front zone of the present blanket design. The significance of this is the higher fast flux level, and its relationship to the enrichment and irradiation time. At a given flux level (or equivalently, wall loading), the total fissile enrichment (i.e., $^{233}U + ^{233}Pa$) is approximately a linear function of the irradiation time. The enrichment rate is also approximately a linear function of the flux, so that the higher the flux level, the shorter the time required to reach a given enrichment. The primary hazard contributors, (^{233}Pa, ^{233}Th, and many of the fission products), have relatively shorter half-lives. Therefore, the concentrations of these in the blanket are not linear functions of time for long irradiation periods, but approach equilibrium conditions at low enrichment values, regardless of the irradiation time to a given enrichment. Though the long-lived fission-products continue to build up in concentration, a net safety advantage can still be realized by operating at a lower flux. Since a longer irradiation time will be needed to achieve the desired enrichment level, this tradeoff requires a quantitative economic evaluation. A quantitative assessment of the safety advantage is presented in Figs. V.B.3 and V.B.4. These figures correspond to a four-zone breakdown of the present blanket design. Although differences exist in the flux spectrum of the four zones, major differences among the four zones are the absolute magnitude of the flux and the neutron energy spectrum (softer toward the rear of the blanket).

In addition to the magnitude of the hazard, which increases with enrichment, the temporal behavior after irradiation of the hazard is also of importance in the design of safety systems and the analysis of accident situations. Figures V.B.5 and V.B.6 provide the temporal behavior and isotopic distribution of the hazard after shutdown for two values of enrichment. The two values chosen correspond approximately to a very low enrichment blanket (similar to those of Ref. 1), and an enrichment slightly higher than that of the reference blanket.

Figure V.B.5 shows that the BHP after shutdown of both fuel-producing blankets is dominated by the actinides. This statement is expected to be true even for fast-fission blankets. Though the fission-product BHP of fast-fission blankets at shutdown is significant, their initially rapid

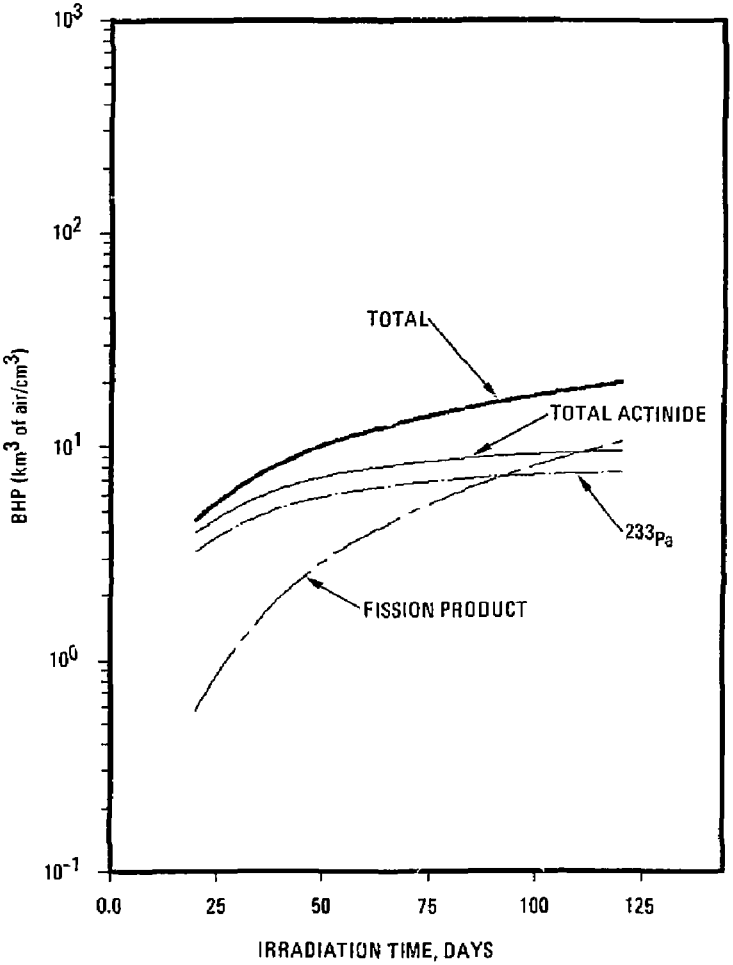

Fig. V.B.1 Biological Hazard Potential versus irradiation tine and enrichment.

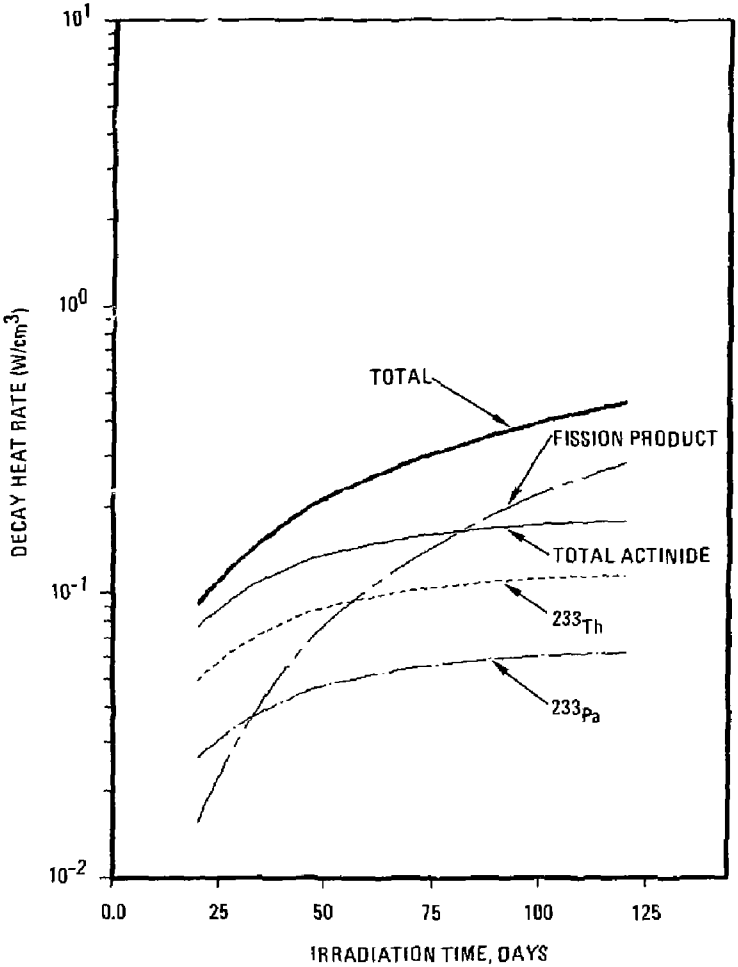

Fig. V.B.2 Decay heat rate level versus irradiation time and enrichment.

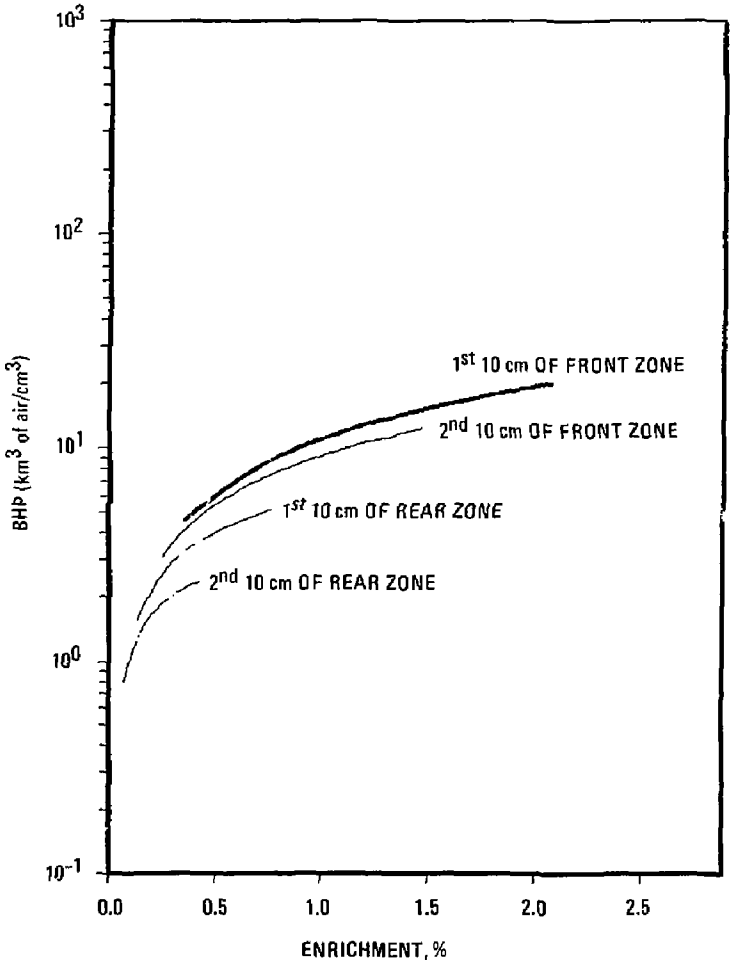

Fig. V.B.3 Total BHP versus enrichment for four zones of the present blanket. All curves span a 120 day irradiation period.

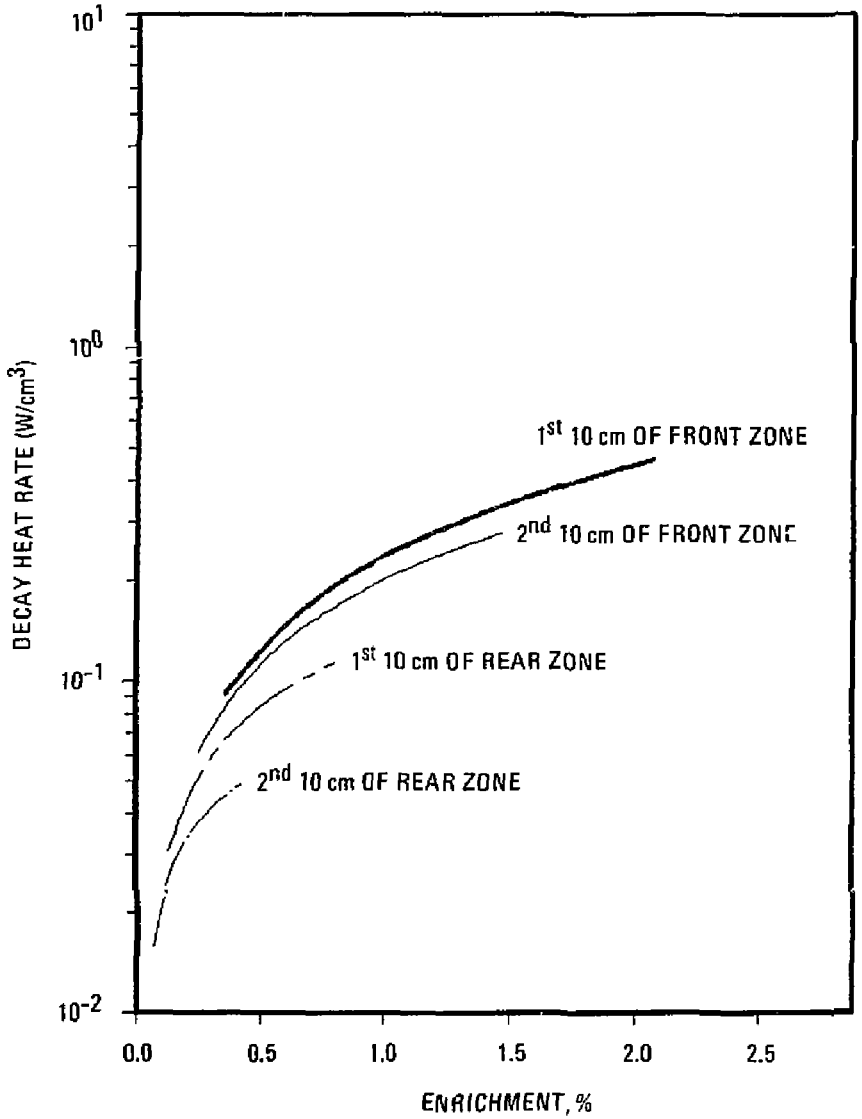

Fig. V.B.4 Total decay heat rate versus enrichment for four zones of the present blanket. All curves span a 120 day irradiation period.

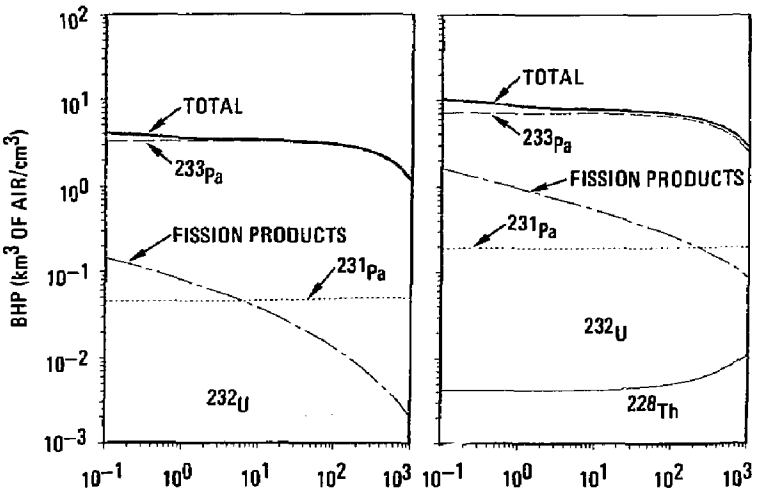

Fig. V.B.5 BHP versus time after shutdown for two irradiation times and enrichments.

decay results in a reduction of their BHP to a level substantially below that of the actinides within hours of shutdown. Other than from the higher level of BHP attained in achieving a higher enrichment, no additional safety differences are observed for the two enrichment levels. A maximum enrichment of 1.6% based upon criticality considerations is discussed in Section II.C.

The impact of higher enrichment on the decay afterheat is apparent upon analysis of the results shown in Figure V.B.6. The increase in decay afterheat is due mainly to the fission-products. In the event of loss of cooling capability to a blanket module, the decay afterheat in the first wall and fuel pebbles will initiate a rise in temperature in the module structures. The importance of minimizing the afterheat rate was evaluated and is presented in Section V.D.2. That section presents the thermal response of the blanket for a range of first wall afterheat levels.

To establish a measure of the time available in which to restore cooling, a preliminary assessment of the time to creep-rupture failure at a given stress level was evaluated for temperatures in the range of 700° to 925°C. The material data are presented in Table V.B.1. The maximum stress level in the first wall structure from lithiostatic pressure was calculated to be ~2000 psia. This result was coupled with the data of Table V.B.1, and a maximum temperature of 700° to 750°C at stress was established as a safe limit at which a module experiencing these temperatures could be reused. Above 900°C, structural failure can be presumed to occur.

The safety systems for the Fusion Breeder Reactor (FBR) were selected to ensure that the safety of the public, as well as the capital investment, was adequately protected. This was accomplished by factoring in the characteristics of the reference blanket with conventional safety system criteria. These latter criteria are presented below.

- Single Failure Criteria -- The need for safety system was determined by methodically going through the entire reactor design in a Failure Mode and Effects Analysis (FMEA) and assuming that each component had failed in a mechanistically credible, but worst case, not expected way. The response of the system to this postulated initiating event was considered and then the impact of an additional random single failure,

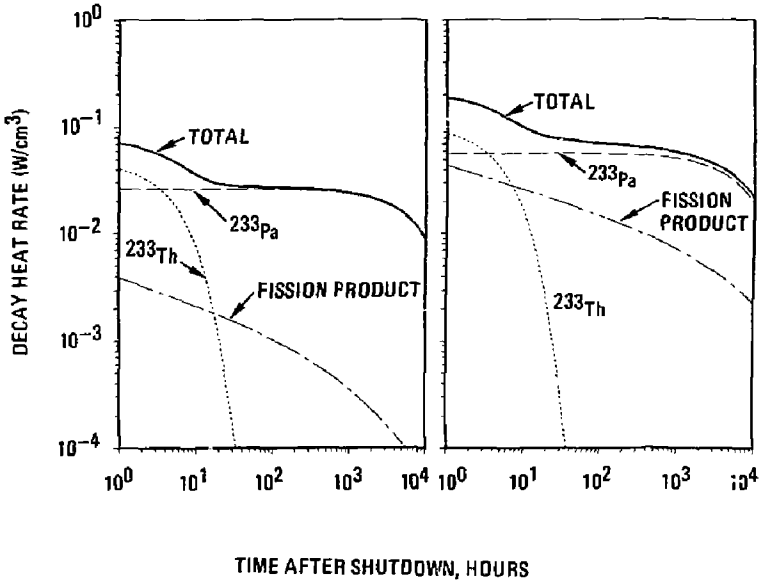

a) 20 DAY IRRADIATION, 0.4% ENRICHMENT

b) 80 DAY IRRADIATION, 1.4% ENRICHMENT

Fig. V.8.6 Decay afterheat rate versus time after shutdown for two irradiation times and enrichments.

TABLE V.B.1. The Time to Creep Rupture Failure at Stress Versus Temperature for HT-9 and 2-1/4-Cr-1Mo.

Temperature, °C	Stress level (psi)	Time-to-failure at stress (hours)
700	4000	1000 (2-1/4CR-1Mo)
750	1500 - 2000	<100 (2-1/4Cr-1Mo)
	1500	2000 (HT-9)
	2000	250 (HT-9)
925	1500 - 2000	~1/2 (HT-9)

unrelated to the initiating event, was considered. Safety equipment was specified to ensure continued cooling of the blanket and containment of hazardous materials in the event of this additional single failure.

- *Redundancy -- In order to ensure that the public and the reactor* are adequately protected, each of the functions needed to maintain cooling and containment must be redundantly protected. That is, protection must be provided in parallel so that failure of a given component results in its function being carried by the parallel components. The selected safety system incorporates redundancy, and excess capacity per component is intentionally included.

- Diversity -- In addition to providing additional capacity to accommodate failures, some of that capacity must be provided in a way that is fundamentally different so that common mode failures are avoided. This *is accomplished in the present system by using the fuel handling heat* removal circuit as a backup to the primary cooling system.

- Common Mode Failures -- A common mode failure is one in which a single fault or a single generic defect in safety equipment results in the failure of all the parallel, redundant systems. This is protected against by providing equipment that accomplish the same function by a different means, that is, by providing diversity.

- Safety Grade Equipment -- All equipment that is relied upon to protect the public following the postulated initiating events must be safety grade equipment built to ASME Section 3 Class 1 requirements. This means that it is designed to withstand the design basis earthquake with no degradation of performance.

- Probabilistic Risk Analysis -- PRA is expected to be a necessary requirement of licensing the fusion breeder. Such analysis verifies that not only are the above criteria met, but also that there is an acceptably low probability of multiple failures (beyond the initiating event and single postulated failure) that could endanger the public. This analysis has not yet been performed. When such analyses were done for the LMFBR and Gas Cooled Fast Reactor (GCFR) systems, the result generally was the requirement for additional safety systems to reduce the total risk (consequence of an accident times probability of the accident) to allowed levels. This

optimization depends strongly on the system being considered and especially on the stored energy available to break containment barriers and on the hazard inventory.

- Cost -- The cost of safety systems has become a major factor in fission reactor design. We have tried to minimize cost by making maximum use of systems needed for other purposes (such as the primary heat transfer system and the fuel changeout system) to also serve safety tasks.

References, Section V.B

1) K. R. Schultz et al., "Hybrid Reactor Safety Study, Second Annual Report," General Atomic Report GA-A16185, December 1980; also, I. Maya et al., "Safety Evaluations of Hybrid Blanket Concepts," Fourth ANS Topical Meeting on the Technology of Controlled Nuclear Fusion, CONF-801011, 1980, and General Atomic Report Ga-A16101, September 1980.
2) J. D. Lee et al., "Feasibility Study of a Fission-Suppressed Tandem Mirror Hybrid Reactor," Lawrence Livermore National Laboratory Report UCID-19327, April 1982; also, I. Maya et al., "Safety Considerations in the Tandem Mirror Hybrid Reactor Study," ANS Transactions, v. 39, 1981.

V.C SELECTION OF REFERENCE SAFETY SYSTEMS

This section presents the selection of the safety system components and configuration that are required to ensure the safety of the general public and to prevent damage to the reactor during both normal and off-normal events. The reference systems presented here focus on those safety systems which would have significant impact at the conceptual design stage due to their uniqueness (requiring special design effort), interface requirements (impacting parallel system design efforts), or cost. The key uncertainties in designing the safety systems are also identified, and the required supporting analyses noted.

V.C.1 Approach

The major safety concerns in the reference fusion breeder and other hybrid reactors have been identified in numerous reports (e.g., References 1 through 5). In summary, the major concern is the release of radioactivity as a result of loss of cooling conditions to either the first wall/blanket region or the bred fuel handling equipment. In systems containing liquid metals, another conceivable mechanism for volatilization of radioactivity is presented by the potential for a liquid metal fire. To prevent or otherwise minimize the release of radioactivity, safety is incorporated by a number of techniques.

1. Eliminating hazards to the greatest extent possible.
2. Providing redundancy by proper design and system configuration.
3. Incorporating mitigating barriers to the propagation of accident sequences.
4. Using dedicated safety systems.

These techniques are discussed briefly below, and in more detail in other sections.

The radioactive hazard and afterheat levels in the reference blanket have been minimized by adopting the fission-suppressed concept. The listed references have shown that a fertile-dilute fission-suppressed blanket offers significant reduction in the biological hazard and afterheat relative to earlier fast-fissioning blankets.

Advantageous use of a redundant design configuration can result in a safer reactor. A simple example of a redundant configuration would be the use of two or more pumps for each module, either one of which would be adequate to safely cool the module in the decay heat mode. The integration of safety and reliability into the selection of the reference safety systems is described in Section V.C.2.

As the design of the fusion breeder plant develops, specific hazards, failure modes, and hazard pathways have been and will continue to be identified and quantified. This permits the erection of mitigating barriers to interrupt accident progressions. The safety analysis and design, performed integrally with the mechanical, thermal-hydraulic, and materials systems design efforts results in beneficial safety feedback. The safety analysis is presented in Section V.D.

The guiding philosophy in the design of dedicated safety systems for the fusion breeder is to employ passive safety systems to the greatest extent possible. Examples of passive and semi-passive systems are those relying purely on natural properties and characteristics of materials for fail-safe operation, such as gravity, high-heat capacity, natural convection, natural circulation, buoyancy, etc. A number of examples of safety system options are listed in Table V.C.1 and discussed in Section V.D. With proper redundancy, semi-passive and active safety systems are also acceptable, and examples of these are also listed in Table V.C.1. Many of these tecnniques are presently being used in conjunction with the liquid-metal fast breeder program. Therefore, a sound data base for their adaptation to the fusion breeder can be provided.

V.C.2 Reference Safety Systems

For the purposes of the present work, the large body of systems required to ensure safety was functionally divided into the primary reactor protection systems (which include decay heat removal and liquid metal and radioactivity containment) and the secondary systems (which include piping and valving, leak detection, plasma shutdown, instrumentation and control,

TABLE V.C.1. Some safety system design options for the FBR

Passive

- Inert gas environment in reactor building
- Steel-lined concrete chambers
- Sacrificial material between steel liner and concrete
- Deep, narrow sumps in reactor building floor
- Sloped surfaces to sumps
- Steel balls and hollow graphite microspheres in spillage areas
- Natural circulation in the liquid lithium coolant circuit

Semi-passive

- Passively-cooled dump tank (natural convection or heat pipes to heat sink)
- High heat capacity thermal exchange (i.e., pebbles or fluid)

Active

- Pump reactor building cover gas through plasma chamber
- Reduced primary loop coolant pressure
- Dump coolant system (e.g., STARFIRE/DEMO)
- Pool surface cooling
- Inert gas makeup or recirculation
- Chemical fire fighting methods
- Forced injection of hollow graphite microspheres

filters, etc.). It is expected that the secondary systems, though forming an integral and necessary part of the overall safety system, can be designed on the basis of present-day technology and/or a reasonable application of sound engineering principles. Thus, emphasis was placed on the primary safety systems. Specifically addressed in the present work are the components and configuration of the primary coolant and decay afterheat removal systems, the module safety coolant system, and the safety dump system.

The primary coolant safety systems are described first. These are followed in turn by a brief discussion of reliability analysis, and the considerations entering into the selection of the primary coolant system components and configurations. Considerations of the valving arrangements are discussed in Section V.D.

Reliability analysis has become an increasingly important part of the design process of nuclear reactors. This increased attention to reliability stems from two major concerns. First, from a safety point of view, reliability analysis is useful in formally classifying the importance of various reactor accidents to assure that all major accident types are being addressed. Particularly in reference to the heat removal and transport systems, the primary coolant system can be considered as the first level of safety. A highly reliable primary coolant system is less likely to call on the plant safety systems. Second, from an economic point of view, increased reliability increases plant availability. Since decay afterheat removal under normal conditions can be accomplished with much reduced capability of the primary coolant system, the corresponding incremental benefit to overall safety from a given increase in the reliability of the primary coolant system may be small. However, the economic benefit from increased operational reliability can be significant. For example, the payback required on a $6 billion capital investment at 18% carrying charge and a 75% availability is such that system improvements that result in a 1% improvement in overall availability may cost over $14 million per year, corresponding to an $80 million capital investment. Thus, emphasis was placed on high reliability, as well as satisfying the single failure criterion.

The primary coolant system is also addressed in the safety section because it serves to provide the first level of safety and also serves as

the decay afterheat removal system during normal shutdown and off-normal events. Its principal safety function is to remove decay heat from the primary sources, the first wall and blanket structure and the fertile fuel. The primary coolant system also serves as the primary driving force for pebble removal during normal fuel changeout and emergency fuel dump (discussed in Chapter IV). Its principal components are five lithium coolant pumps, six Li-to-Na heat exchangers, the hot outlet manifold, the cold inlet manifold, the heat exchanger common plenum manifold, and associated valving and piping. The configuration selected is shown in Figure V.A.1 and is very similar to that selected for the primary coolant loop of the Standard Mirror Hybrid Reactor described in Reference 4. The design bases and descriptions of the major components are discussed in Sections I.C and II.B of this report. The reliability and redundancy considerations of the configuration are discussed below.

Of the components comprising the primary coolant system, the liquid metal pumps are expected to dominate the reliability of the system since relatively, they will require the most development and are considered active components. They will also be high cost items. In comparison, the other high cost components, the Li-to-Na heat exchangers, are more passive in nature, and will thus have lower failure probabilities. Reliability as a function of component failure probability and the number of required and backup components is given by the expression (7):

$$R = \sum_{i=k}^{N} \frac{N!}{i!(N-i)!} r^i (1-r)^{N-i} \quad ,$$

where N is the total number of parallel identically reliable components of reliability r, only k of which are required for success. The individual component reliability is related to the random failure probability rate, λ, (obtained from historical data or predicted using techniques such as fault tree analysis, etc.) by:

$$r = e^{-\lambda t} \quad ,$$

where it is the time interval within which the reliability is to be calculated. Common cause or dependent failure effects are not included in the above expressions and would tend to lower the system reliability. Thus, nuclear piping greater than 6 in. in size, with a failure rate of 10^{-5} to 10^{-3} per plant year[8], has a reliability over one year of 0.99999 to 0.999. The U.S. Nuclear Regulatory experience with coolant pumps is that they have an observed failure rate of 3×10^{-2} per year, resulting in a reliability of 0.97. The assessed median failure rate for all pumps (including non-nuclear related experience) is 0.3 per year, with a reliability of 0.74. In general, for 0.9 and 0.7 reliability components (the expected range applicable to the pumps), the overall reliability of various system configurations incorporating combinations of required and backup components is presented in Table V.C.2. The table shows that the accumulated reliability increases with the number of backup components for a fixed number of required components, and decreases with increasing number of required components. The table also shows that for 0.9 reliable pumps, diminishing incremental increases in reliability are experienced after two backups have been incorporated into the system. For 0.7 reliability pumps, a minimum of two backup pumps are required for adequate reliability. Table V.C.2 shows the advantage of reducing the number of required components, which implies use of as large components as possible in order to maximize reliability.

An additional consideration in the selection of a configuration is the observation that components that are working at partial loading have lower failure probabilities than those that are operating at peak capacity. These considerations, plus the consideration of available components sizes, helped to guide the selection of the number of pumps and heat exchangers. It also points to the design approach of using common manifolds for the pumps and heat exchangers so that maximum sharing of redundant components can occur.

The above simple analysis and its design guidance do not account for common-mode failure mechanisms. Though these can potentially contribute significantly to a decrease in reliability and the methodology is available with which to address them (9), two points argue in favor of the present analysis. The first is that common-mode failures can be minimized

TABLE V.C.2. Overall Reliability as a Function of Various Combinations of Required and Backup Components

Number of Components Required for Operation	Number of Backup Components Available		
	0	1	2
1	0.9/0.7[1]	0.99/0.91	0.999/0.97
3	0.73/0.34	0.95/0.65	0.99/0.84
5	0.59/0.17	0.89/0.42	0.97/0.65

[1]Corresponding to component reliability = 0.9/0.7.

significantly by precautions taken during detailed design, construction, and operational levels from both managerial and technical perspectives (10). The second is that given the uncertainty in the present desig, a common-mode analysis would provide highly uncertain and possibly misleading conclusions.

Auxiliary decay heat removal during scheduled shutdowns is accomplished by the primary coolant system. Under certain failure modes described in the safety analysis of Section V.D, e.g., isolated single failures of primary coolant pumps or primary heat exchangers, continued full power operation may be possible after a programmed reduction in power to allow the load to be redistributed among the operating components. During forced shutdown, the redundancy incorporated in the primary system design and the manifolding arrangement of Figure V.A.1 provides the required decay heat removal and affords protection against component failures. Additional backup auxiliary coolins is provided by the module coolant system via the fuel changeout circuit. This latter circuit and the fuel and liquid metal containment system are described in Section IV.B.

The other primary reactor protection system addressed in this study is the safety dump and coolant system. The functions of the safety dump system are to reduce the heat load requirement on the primary decay heat removal system during certain routine and accident conditions, to minimize the quantity of uncontained liquid metal during accident conditions, and to provide an additional barrier to the release of radioactivity. The system used to accomplish this function is the fuel handling circuit described in Chapter IV. This circuit also provides the redundant and diverse system required to achieve module cooling in the event of a malfunction of the primary coolant system. In addition to the features dictated by fuel management concerns, system safety features include the potential for the utilization of natural circulation as described in Section V.D, sloped surfaces beneath the reactor to direct spills into designated areas, and an inert cover gas environment to prevent combustion.

The safety analyses performed in support of the above design selections is presented in the following section. It describes the Failure Modes and Effects Analysis (FMEA) and thermal analyses performed to resolve the key uncertainties.

References, Section V.C

1) J. D. Lee et al., "Feasibility Study of a Fission-Suppressed Tandem Mirror Hybrid Reactor," to be published, 1982; also, I. Maya et al., "Safety Considerations in the Tandem Mirror Hybrid Reactor Study," ANS Transactions, v. 39, 1981.

2) K. R. Schultz et al., "Hybrid Reactor Safety Study, Second Annual Report," General Atomic Report GA-A16185, December 1980; also, I. Maya et al., "Safety Evaluations of Hybrid Blanket Concepts," Fourth ANS Topical Meeting on the Technology of Controlled Nuclear Fusion, CONF-801011, 1980, and General Atomic Report GA-A16101, September 1980; also, K. R. Schultz et al., "Hybrid Reactor Safety Study, Annual Report," General Atomic Report, GA-A15578, December 1979.

3) W. E. Kastenberg et al., "Some Safety Studies for Conceptual Fusion-Fission Hybrid Reactors," EPRI, ER-548, July 1978.

4) D. J. Bender et al., "Reference Design for the Standard Mirror Hybrid Reactor," joint Lawrence Livermore National Laboratory and General Atomic Report UCRL-52478 and GA-A14796, May 1978, pp. 466-513.

5) R. P. Rose et al., "Fusion-Driven Breeder Reactor Design Study," Westinghouse Report, WFPS-TME-043, May 1977, Chapter 7.

6) C. C. Baker et al., "STARFIRE - A Commercial Tokamak Fusion Power Plant Study," Argonne National Laboratory Report ANL/FPP-80-1, September 1980, Chapter 10; also, "STARFIRE/DEMO - A Demonstration Tokamak Power Plant Study," Draft Interim Report, Chapter 4, January 1982.

7) D. D. Orvis et al., "Guidebook for Reliability, Availability, and Maintainability of NWTS Repository Equipment," General Atomic Report GA-A16191, vol. 2, April 1982, pp. B-14, 15.

8) US NRC, "Reactor Safety Study, Appendix III, Failure Data," WASH-1400, October 1975.

9) K. N. Fleming, "A Reliability Model for Common Mode Failures in Redundant Safety Systems," Sixth Littsburg Conf. on Modeling and Simulation, and General Atomic Report GA-A13284, April 1975; also, Project Staff, "HTGR Accident Initiation and Progression Analysis Status Report, Volume II, AIPA Risk Assessment Methodology," General Atomic Report GA-A13617, October 1975.

10) A. J. Bourne et al., "Defenses Against Common-Mode Faiures in Redundance Systems - A Guide for Management, Designers and Operators," UKAEA Safety and Reliability Directorate Report SRD R 196, January 1981.

V.D SAFETY ANALYSIS OF REFERENCE SYSTEM

This section presents the safety analyses performed in support of the reference safety systems described in the preceeding section. A failure modes and effects analysis (FMEA) of the primary coolant system is presented in Section V.D.1. It was performed to formalize the safety methodology being used to analyze the fusion breeder reactor, and to systematically identify and categorize the failure modes requiring design attention. The FMEA is followed by the thermal analyses in Section V.D.2. These were performed to determine the effect of particular event sequences identified by the FMEA. Finally, the results of a preliminary analyses of a passive safety systems is presented in Section V.D.3.

V.D.1 Failure Mode and Effects Analysis

A failure mode and effects analysis is a structured, logical analysis tool that is used to identify all failure modes of a system and analyze their resultant effects on the system. The process of performing a FMEA results in a qualitative evaluation of a system's ability to perform its function. It also results in an extensive, structured compilation of information and knowledge about failure mechanisms, the causes of degraded or unacceptable performance, and alternative courses of corrective action.

The main advantages of a FMEA are that it is simple to apply and it provides an orderly examination of the hazard conditions in the system. It also provides a convenient starting point for many of the other safety and reliability analysis methods, such as a fault tree analysis. A disadvantage is that, typically, the FMEA considers only single failure events and the effects of each failure alone. Common-cause failures can be addressed, except that the number of combinations requiring analysis can become large for complex systems.

Another technique often used in safety assessments is event tree analysis. This technique is used to obtain a quantitative evaluation of the consequence-probability distribution (i.e., the risk profile) of a given

system and thus identifies the major risk contributors for subsequent design attention. This technique can also be used to evaluate and compare design alternatives in order to achieve minimum risk. Event trees can be constructed, and the accompanying analysis carried out at either the system or component level. Event tree analysis of the fusion-fission hybrid at the system level has been performed in the past (1,2), and has identified the failure of the heat removal system as a primary contribution to overall risk. To further develop the risk profile, or to evaluate the removal system design alternatives, event trees at the component level are required. Since adequate design details are not available for the fusion breeder to permit either construction of significantly improved event trees or to lower the uncertainty in the failure rate data, the FMEA was chosen as the analysis tool for the present effort. In addition, as mentioned above, in conjunction with increasing definition of the heat removal systems, the FMEA can serve as the starting point for the construction of fault trees. The fault trees could then be used to generate the failure probability data which would be required in the event trees for the items with insufficient historical data to permit a confident estimate of the failure rate.

A simplified schematic diagram of the primary coolant system was presented in Figure V.A.1 and described in Section V.C. The system components and interfaces are shown in Table V.D.1.

In brief, the system works as follows. Lithium is transported from a common "cold" manifold to the modules via dual inlet pipes leading to the module inlet lithium distribution plenum. In each module, the lithium circulates past the first wall, through the fertile fuel ball region, and into outlet pipes leading to the module lithium outlet plenum. The lithium from all the modules is then directed to a common "hot" manifold, which in turn distributes the coolant to the primary pumps. From the pumps, the lithium travels to a common manifold which distributes the coolant to the primary heat exchangers. On exit from the heat exchangers, the cooled lithium then completes its circuit by arriving at the common cold manifold. Valves are located as appropriate and are discussed below in more detail.

TABLE V.D.1 Primary Coolant System Components and Interfaces

System Components

- Cold manifold
- Inlet piping
- Inlet distribution plena
- Modules
- Module outlet piping
- Module outlet plena
- Outlet piping
- Hot manifold
- Primary coolant pumps
- Common manifold
- Primary Li-to-Na heat exchangers
- Piping to and from pumps and heat exchangers
- Valves

System Interfaces

- Fuel changeout system
- Electric power system
- Secondary heat removal system
- Control room via detection and instrumentation systems
- Maintenance

The results of the FMEA for the primary circuit major failures are presented in Table V.D.2. The analysis was performed at the component level, commensurate with the level of the design. Failures considered include active component malfunction, primary coolant outer boundary, and first wall structural failure, and failures of interface system such as the power supply and secondary heat removal. Detection and instrumentation, leaky valves, and maintenance errors were not considered due to insufficient definition, but the results of the FMEA can serve to guide the formation of specifications covering these systems.

In general, the failure modes can be divided into three categories related to their effect on the system. The categories are failure modes that lead to:

- Loss of coolant flow
- Partial loss of coolant
- Complete loss of coolant

These main categories are further subdivided into accidents with and without the fertile fuel in place within the module.

Transient thermal analyses (described in Section V.D.2) were used to determine the most suitable course of action to follow subsequent to the initial failure. Some of the results of the analyses were very sensitive to the assumed parameters governing the heat transfer. In summary, using the best estimates for the present configuration, module structural failure ensues only for initiating events which lead to partial or complete loss of lithium with the fertile fuel pellets in place. These results guided the decision-making as to which accident scenarios require fuel dumping.

The initiating events which would lead to uncovered fertile fuel were determined to be rupture or leakage of the piping leading to or from the first wall, and mechanistic failure of the first wall. These events require dumping, since a short-circuit path may occur which may preclude coolant from reaching the fuel. Failure to dump the fuel (i.e., due to dump valve failure) would then lead to loss of the module. Although the probability of such a sequence of events is thought to be very low, it is recommended that the adjacent modules be dumped in order to limit failure propagation and minimize accident consequences in the event the dump of the failed module is for some reason not successful.

TABLE V.D.2 Primary Circuit Major Failure Mode and Effects Analysis

Component	Failure Mode	Failure Effect	Corrective Action
Primary Coolant Pump	A. Rupture, leakage, single pump stopping, or other local loss.	Partial loss-of-flow; Inadequate pumping capacity will lead to increase in module temperatures; possible lithium spill to guard vessel.	I. *Reactor shutdown with decay* heat removal by remaining pumps, failed pump is isolated; or II. For minor failures, programmed power reduction to permit remaining pumps to pickup load, failed pump is isolated.
	B. Major loss of pumping capacity due to loss of power.	Complete loss of pumping; will lead to failure of all modules without corrective action.	I. Diversity in power supply circuitry must be specified to preclude this event; or II. Backup power supply will supply power for decay heat removal; or III. Backup residual heat removal system with diverse power supply is activated; or IV. Redirect coolant circuitry and de-energize magnets to make use of natural circulation for afterheat power removal

TABLE V.D.2 Primary Circuit Major Failure Mode and Effects Analysis (Continued)

Component	Failure Mode	Failure Effect	Corrective Action
Primary Heat Exchanger	A. Rupture or leakage	Inadequate heat removal; will lead to increase in module temperatures; possible liquid metal spill to guard vessel.	I. Reactor shutdown until heat exchanger repaired; or failed unit isolated; fire prevention alert.
	B. Local loss of secondary Na flow	Inadequate heat removal will lead to increase in module temperatures.	I. Reactor shutdown until secondary system restored; or II. Redundancy in secondary may permit continued operation.
	C. Major loss of secondary system	Complete loss of heat removal capability; will lead to failure of all modules without corrective action.	I. Reactor shutdown. Redundancy must be specified in secondary to assure decay heat removal capability; or II. Reactor shutdown and backup residual heat removal system in the primary circuit activated.

TABLE V.D.2 Primary Circuit Major Failure Mode and Effects Analysis (Continued)

Component	Failure Mode	Failure Effect	Corrective Action
Piping to or from Primary Coolant Pumps	Rupture or leakage	Loss of feed to one coolant pump (see above); lithium spill to outer pipe.	I. Reactor shutdown with decay heat removal by operative pumps, affected pump is isolated; or II. For minor failures, programmed shutdown to permit isolation of affected pump and for remaining units to pick up load.
Section of Common Manifold between Coolant Pumps and Heat Exchanger	Rupture or leakage	Partial loss of configurational redundancy; lithium spill.	I. Reactor shutdown with decay heat removal by unaffected portion; or II. For minor failures, programmed shutdown to isolate failed section, then renew operation.
Piping to or from Primary Heat Exchangers	Rupture or leakage	Loss of affected heat exchanger (see above); lithium spill to outer pipe.	I. Reactor shutdown with decay heat removed by operative heat exchangers, affected heat exchanger is isolated; or II. For minor failures, programmed shutdown to permit isolation of affected heat exchanger and for remaining units to pick up load.

TABLE V.D.2 Primary Circuit Major Failure Mode and Effects Analysis (Continued)

Component	Failure Mode	Failure Effect	Corrective Action
Section of Cold or Hot Manifold	Rupture or leakage	Minimum-partial loss of configurational redundancy; maximum-loss of primary coolant flow to affected modules; lithium spill.	I. Reactor shutdown with decay heat removal by either unaffected portion of primary system or backup residual heat removal system. II. For maximum case, reactor is shutdown, and unisolated modules are dumped and cooled with backup residual heat removal system.
Inlet/Outlet Piping to Module Inlet/ Outlet Manifolds	Rupture or leakage	Loss of coolant (flow) to affected module; lithium spill to outer pipe (for concentric double-walled piping).	I. Reactor shutdown, module is isolated, then dumped. Cooling is accomplished by backup residual heat removal system.
Module Inlet/ Outlet Ring Manifolds or Piping Leading to First Wall	Rupture or leakage	Loss-of-coolant to affected module; lithium spill to steel-lined, sloped floor; lithium spill to outer pipe (for concentric double-walled piping).	I. Reactor and magnet shutdown, module is isolated then dumped. Adjacent modules also dumped.

TABLE V.D.2 Primary Circuit Major Failure Mode and Effects Analysis (Continued)

Component	Failure Mode	Failure Effect	Corrective Action
First Wall	Rupture or leakage	Loss-of-coolant to affected module; lithium spill to plasma chamber.	I. Reactor and magnet shutdown; module is isolated, then dumped. Adjacent modules also dumped.

The optimum number and location of valves throughout the primary coolant system are best determined from an integrated analysis of reliability, availability, maintenance, and safety. From the point of view of the single failure criterion, in order to not place overly stringent requirements on the backup module safety coolant system, valves are required in every stretch of piping such that a failed section can be isolated without losing primary heat removal capability. However, from the point of view of probabilistic analyses, historical data indicates that valve failures have a higher probability than passive pipe failures. At this level of design definition, it is thus not clear how to attain optimum system configuration while satisfying the spirit of regulation and the single failure criterion. A general and more detailed discussion of the dichotomy is presented in Ref. 3. From a practical point of view, 1 meter diameter manifolds will require valves approximately 1 meter in length. The hot and cold manifolds are sectioned off by the inlet/outlet pipes from the modules at 4-meter intervals. In addition, piping from the heat exchanger and pumps will create many shorter length sections. The net effect is that standard valving arrangements satisfying the single failure criterion may not be practical.

For the above reasons, three-way valves with total shutoff capability are specified at the inlet and outlet piping from the primary coolant pumps and heat exchangers only. Positive shutoff stop valves are located in the inlet/outlet piping from each module. Then, to completely satisfy single failure criteria, the hot and cold manifolds are assumed to be double-walled and sectioned to limit the quantity of lithium that will be lost in the event of inner-wall failure. As a backup, freeze valves, which can be much thinner than standard valves, can be incorporated. This piping and valve arrangement, without freeze valves, provides the results described in the FMEA of Table V.D.2.

V.D.2 Thermal Analysis

The ultimate effect of coolant system failures and the need for corrective action is established by the temporal behavior of the blanket module temperature distribution. To provide guidance to the design and

analysis of the safety systems, the transient thermal analyses of the fuel and structures in loss of coolant and flow situations were performed using the Systems Improved Numerical Differencing Analyzer (SINDA) code (4). One dimensional models described below were used to analyze the following four accident situations:

1. Loss of coolant flow with fuel in place,
2. Loss of coolant flow with fuel removed,
3. Loss of coolant with fuel in place, and
4. Loss of coolant with fuel removed.

The reactor plasma was assumed to be shutdown immediately in all cases. The results for cases 1 and 2 indicate that the reactor temperatures will remain within safe limits in loss of coolant flow accidents. Safe limits of 750°C for re-use of the module and 900°C for structural failure were chosen for this study, as discussed in more detail in Section V.B. Loss of coolant with irradiated thorium fuel remaining in the reactor (case 3) will cause rapid heating, severely damaging the reactor in 50 minutes to 4 hours. For case 4, uncertainties in both the emissivity and afterheat levels yield results that span the safe temperature range. Using the best estimates for these parameters for the present configuration, it is expected that the first wall temperature can be maintained below the limit for failure.

V.D.2.a Description of Thermal Model. The one-dimensional cylindrical model consists of nine zones as pictured in Fig. V.D.1. The first wall, perforated intermediate wall, and perforated inter-zone dividers are modeled as single temperature nodes. The intermediate wall and inter-zone dividers are 80% steel and 20% holes. In the loss of flow cases (1 and 2), the lithium and lithium/fuel zones were broken into nodes as shown in Fig. V.D.1. In case 3 (loss of Coolant with fuel in place), the same nodes were taken in the fuel zones, with the lithium inlet and outlet regions becoming radiation paths. In the loss of coolant without fuel (case 4), the lithium and fuel regions are all radiation paths. Radial structural members were neglected because of their small conduction areas and long conduction paths. The shield was assumed to be cooled, and is modeled as a constant temperature node. An initial temperature of 500°C was taken in all the

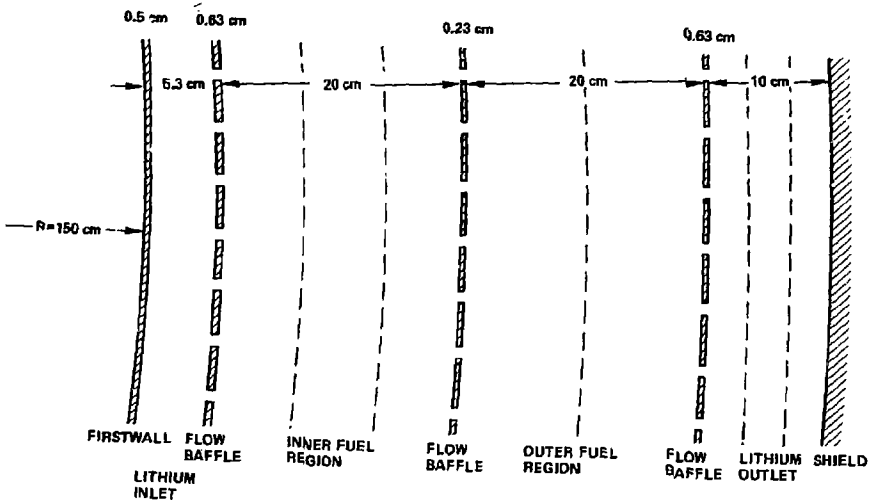

Fig. V.D.1 One dimensional thermal model.

cases for all nodes except the shield. Materials properties used are given in Table V.D.3. Emissivity values are discussed below in case 4.

Afterheat in the thorium fuel was calculated for the reference blanket design (5). Three sources of afterheat were considered: fission products, ^{233}Th, and ^{233}Pa. The afterheat magnitude in each of 4 zones (10 cm each) and the time dependence is given in Table V.D.4.

Afterheat in the steel is less defined, so upper and lower bounds were estimated. For HT-9 (0.3V, 0.5Ni, 1Mo, 12Cr, 86.2Fe), afterheat is dominated by the decay of ^{56}Mn with a half-life of 2.58 hours (6). Based on previous studies (4,5), the initial HT-9 shutdown afterheat value was estimated to be between 1.0 and 1.5 W/cm^3. Afterheat variation with radial position and time was calculated with the following equation:

$$\dot{q}''' = \dot{q}_o''' \exp[-11.5\ (r - r_0)][0.15 + 0.85 \exp(-7.46 \times 10^{-4} t)] \quad , \quad (1)$$

where:

$\dot{q}'''$ = afterheat at radius r and time t in W/cm^3,
$\dot{q}_o'''$ = afterheat at radius r_0 and time zero (reactor shutdown) in W/cm^3,
r_0 = the first wall radius (1.5 m), and
t = time after shutdown in seconds.

V.D.2.b Thermal Modeling Results.

Case 1, Loss of Lithium Collant Flow with Fuel in Place. The thermal conductivities, thermal capacities, and heat generation rates in the fuel zone were calculated by volume averaging and time dependent heat transfer by conduction was modeled. Results are shown in Figs. V.D.2 and V.D.3. Even for the high afterheat value, only a peak temperature of 570°C is reached in 35 minutes with the shield maintained at 100°C and a peak of 668°C in 4.7 hours with the shield at 500°C. Thus, if shield cooling is maintained, reactor temperatures can be kept within reasonable limits in loss of coolant flow conditions.

Case 2, Loss of Lithium Coolant Flow with Fuel Removed. Case 2 is similar to case 1 without the extra heat generated by the irradiated thorium

TABLE V.D.3. Thermal Properties.

Material	Conductivity (W/m K)	Heat Capacity (J/kg K)	Density (kg/m^3)
Lithium	38.1	4174	441
Berrylium[a]	65.0	3065	1850
HT-9	29.0	1234	7539

[a] 80% dense.

TABLE V.D.4. Breeding Fuel Afterheat.

	Magnitude, W/cm^3				Time Dependence
	Inner Fuel Zones		Outer Fuel Zones		(t in secs)
Fission	0.203	0.109	0.073	0.022	$(t + 1)^{-0.2}$
Thorium	0.111	0.079	0.046	0.024	exp(-5.2 E-4*t)
Protactinium	0.060	0.042	0.024	0.013	exp(-0.3 E-7*t)

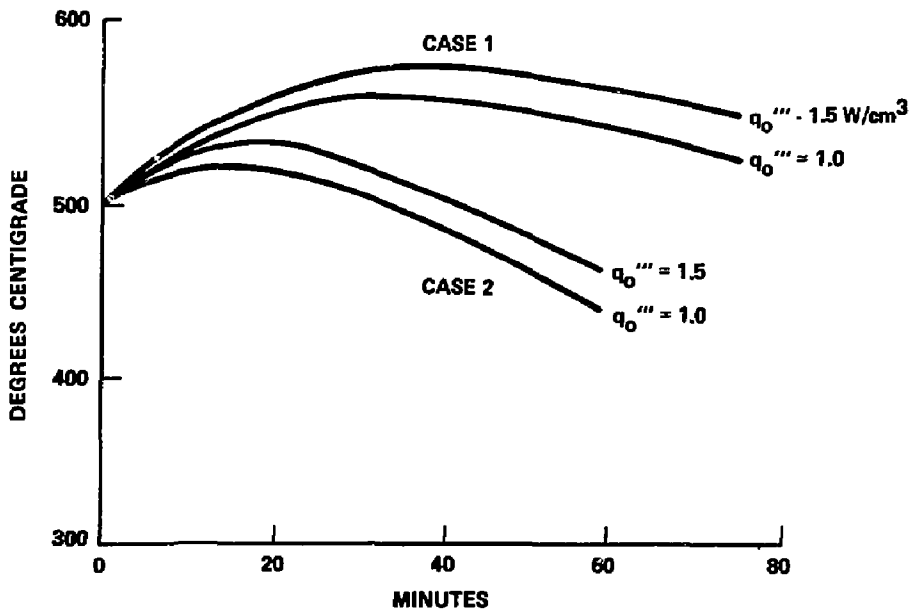

Fig. V.D.2 First wall temperatures for cases 1 and 2, loss of coolant flow with 100°C shield temperature.

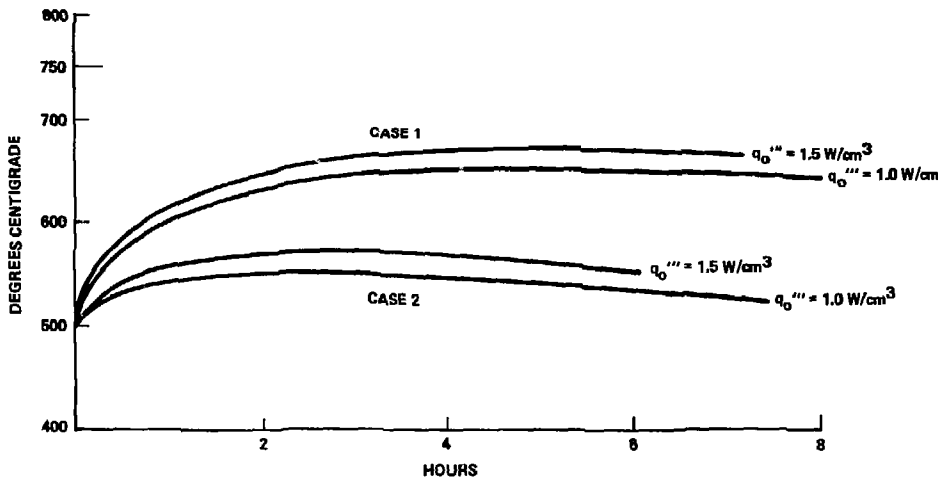

Fig. V.D.3 First wall temperatures for cases 1 and 2, loss of coolant flow with 500°C shield temperature.

fuel. As can be seen in Figs. V.D.2 and V.D.3, reactor afterheat temperatures are easily controlled with shield cooling.

Case 3, Loss of Lithium Coolant with Fuel in Place. In case 3, heat transfer is dominated by radiation across the lithium inlet and outlet and by contact conduction between the beryllium spheres in the fuel zone. Analysis shows that less than 6% of the volumetrically generated heat could be removed from the first wall by natural convection in a one atmosphere helium cover gas. Convection has therefore been neglected. Conduction dominates heat transfer in the fuel zones if good thermal contact between the spheres is assumed. Assuming optimistic values for the first wall afterheat, emissivity (1.0), and contact area between spheres (0.1, or 10% of the solid area), and a 100°C shield temperature, the first wall temperature rises to 900°C in 4 hours and 10 minutes (see Fig. V.D.4). This is intended as an upper bound on the response time to take corrective action in a loss of coolant accident with fuel in place. A lower bound of 50 minutes is obtained from the curve shown in Fig. V.D.4 for adiabatic first wall afterheat conditions at the higher afterheat value. This indicates that the loss of coolant condition with fuel in place cannot be tolerated for more than a few hours without risking damage to the first wall.

Case 4, Loss of Lithium Coolant with Fuel Removed. Case 4 is radiation dominated. As for case 3, less than 6% of the first wall afterheat can be removed by natural convection because of the low density of the one atmosphere cover-gas. Long conduction paths and small conduction areas allow very little heat transfer through radial structural members. As shown in Figs. V.D.5 and V.D.6, temperatures span a wide range depending upon afterheat rates and emissivity. At the higher afterheat value, ($\dot{q}''' = 1.5$ w/cm^3), an emissivity of at least 0.4 is needed to keep the first wall below 750°C. With lower afterheat ($\dot{q}''' = 1.0$ w/cm^3), an emissivity greater than 0.2 will keep the hottest point below 750°C. The actual emissivity of HT-9 after exposure to lithium in a high heat flux environment is unknown, but probably lies between 0.1 and 0.6.

Steel emissivity is affected by initial surface treatment, liquid metal corrosion, liquid metal remaining on the surface, impurities (oxygen in the cover gas) and temperature. Corrosion may be sufficient to remove any

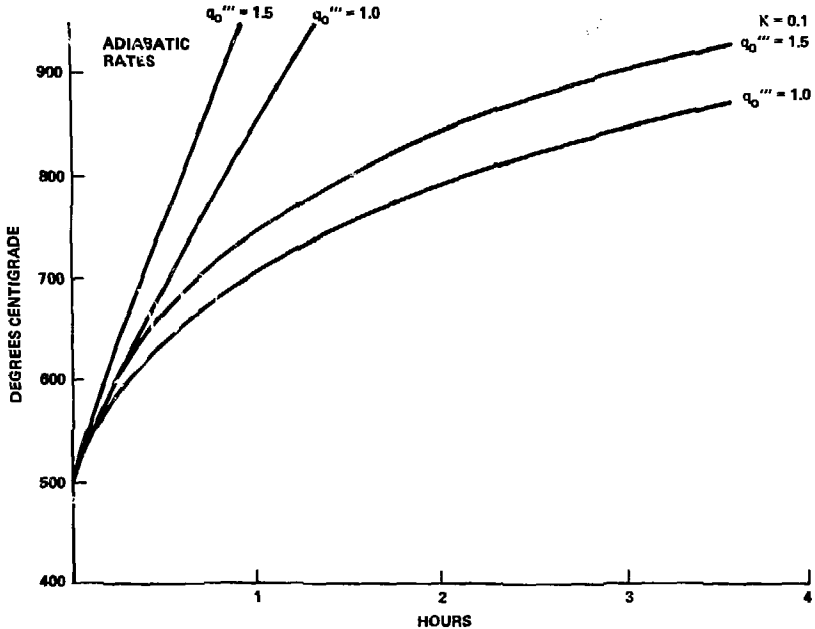

Fig. V.D.4 First wall temperatures for case 3, loss of coolant with fuel in place. Adiabatic rates and conduction dominated rates with 50% contact area (k = 0.1) and 100°C shield temperature.

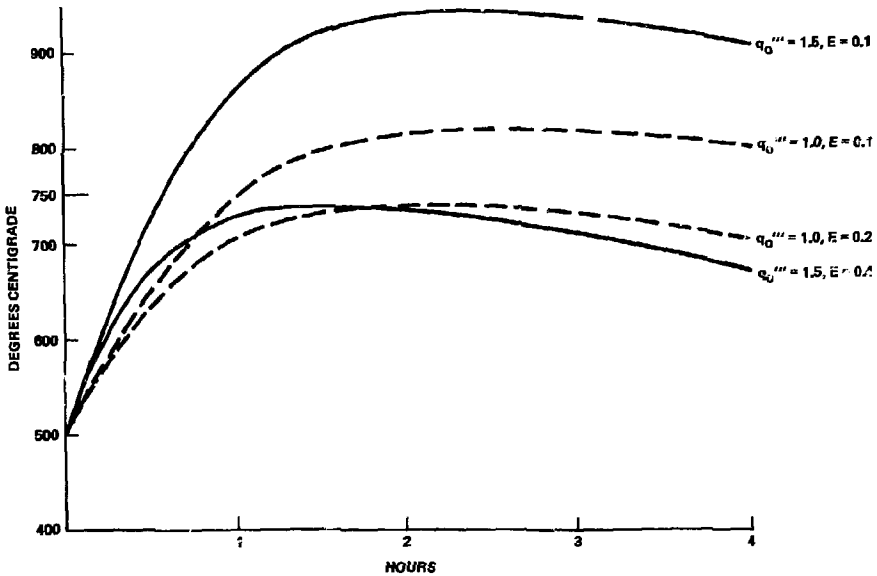

Fig. V.D.5 First wall temperatures for case 4, loss of coolant and fuel at various first wall heat generation rates ($\dot{q}_0'''$) and emissivities (E), with a 100°C shield temperature.

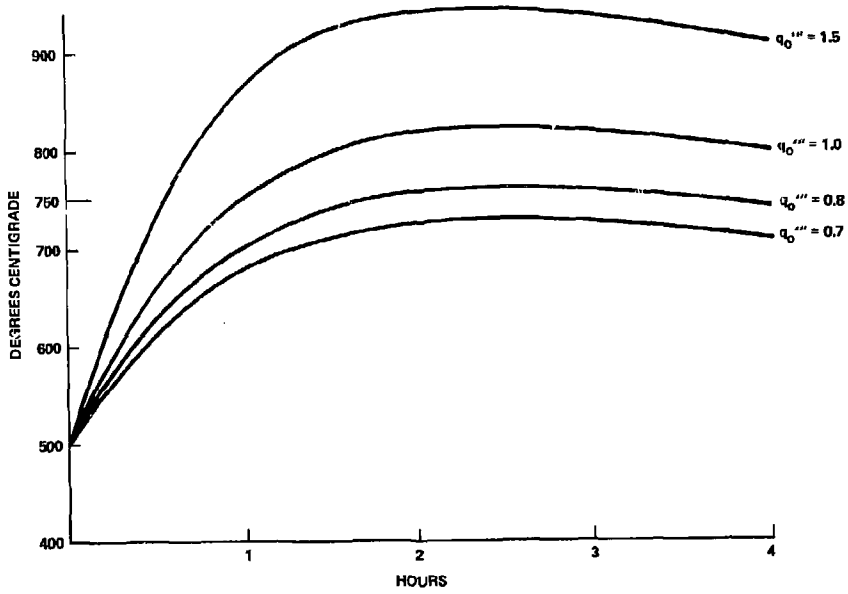

Fig. V.D.6 First wall temperatures for case 4, loss of coolant and fuel at various first wall heat generation rates ($\dot{q}_0'''$) an emmissivity of 0.1, and 100°C shield temperature.

dependence on the initial surface treatment. Hot liquid metal corrosion could raise or lower emissivity; lithium corrosion will simultaneously polish and deposit particles on the hot structural reactor surfaces. The effect of this combined process is unknown. Small amounts of oxygen in the cover gas may rapidly oxidize exposed metallic surfaces, increasing emissivity. Emmissivity values for steels with differing histories (Table V.D.5) give an indication of the range of possible emissivities of reactor structures. Using the steel values shown, values between 0.18 and 0.42 would be expected at 500°C.

Lithium emissivity may be important depending on the amount of lithium adhering to the steel surfaces. Lithium adhesion will depend on surface roughness and lithium viscosity, which depends on temperature. Lithium emissivity in applicable temperature ranges is unknown. Sodium emissivity under conditions somewhat similar to those expected in a fusion blanket* has been measured (9) at 0.55 to 0.92 at 450°C.

Most liquid metal cooled fusion reactor designs rely on radiation for cooling in loss of coolant accidents. Some relatively simple experiments using existing liquid metal loops could alleviate much uncertainty.

V.D.3 Passive Safety Systems

Natural circulation of the lithium coolant was investigated during this study as a passive safety system potentially capable of handling the decay afterheat levels of the fusion breeder. The temperature differential that will exist in both the primary and backup heat removal systems due to the decay heat source in the fuel and structural material will create a gradient in the lithium densities in each loop. This density gradient can be used to establish natural circulation currents in the loops and allow the generated thermal power to be deposited in a heat sink outside of the blanket. By proper design of the coolant column heights and orientation, this natural

*Emissivity of sodium wetted 304 stainless steel at 450°C in argon with 10,000 and with 50 vppm oxygen was measured.

TABLE V.D.5. Emissivities of Steels.[a]

	Temperature (°C)	Total Emmissivity
Steel, polished	100	0.13 - 0.21
	500	0.18 - 0.26
	1000	0.55 - 0.80
Steel, clean	100	0.21 - 0.38
	500	0.25 - 0.42
	1000	0.50 - 0.77
Stainless steel, oxidized	400	0.80 - 0.87
	600	0.84 - 0.91
	800	0.89 - 0.95
Stainless steel, after red heat in air for 30 min	400	0.17 - 0.30
	600	0.23 - 0.37
	800	0.30 - 0.44

[a]Data from Ref. 8.

circulation may be sufficient to remove the afterheat from the first wall so that its temperature can be maintained below the prescribed level of 750°C to 900°C, without any operating, active components. In fact, the results of the analysis presented below show that, in the absence of magnetic field, the height of the reactor module volume is itself sufficient to produce the minimum flow velocity necessary to limit the maximum first-wall temperature to much less than 700°C by using either the primary coolant circuit or the backup heat removal circuit. This is a very encouraging result which can independently prevent damage to the equipment during loss-of-flow events. With a magnetic field present in the blanket, the required height is in the range of thousands of meters, making natural circulation impractical. Thus, active magnet dump capability is required in order to allow the passive natural circulation system to operate.

The analysis, summarized below, was carried out with and without the magnetic field using the correlation for liquid metal flow between parallel plates. In the absence of a magnetic field, the Nusselt number is given by (10):

$$Nu = 5.8 + 0.02\ Pe^{0.8} \quad , \tag{1a}$$

where Pe is the Peclet number, the product of the Reynolds and Prandtl numbers. In the presence of a magnetic field, the Nusselt number is given in Reference 11, as

$$Nu = 12 \quad , \tag{1b}$$

These correlations for the heat transfer coefficient were used with the convective equation for heat transfer across the first wall given by,

$$\frac{\dot{q}'''V}{A} = h\ (T_{max} - T_{out}) \quad , \tag{2}$$

where $\dot{q}'''$, V, A, and T_{max} are the first wall volumetric heat generation rate, volume, heat transfer area, and maximum temperature, T_{out} is the

coolant outlet temperature, and h is the heat transfer coefficient. The equation for the total heat removed by the flowing coolant is given by

$$\dot{q}'''V = \dot{m}\, Cp\, (T_{out} - T_{in}) \quad , \tag{3}$$

where $\dot{m}$, Cp, and T_{in} refer to the coolant mass flow rate, heat capacity, and inlet temperature. An equation relating the pressure differential that will be required to overcome the frictional pressure drop and turning losses through the blanket is

$$\Delta p = H\Delta\rho g = \frac{L}{D} f \frac{\rho v^2}{2} + n \frac{1}{2} \rho v^2 \quad . \tag{4}$$

where H is the necessary coolant height in which a density differential of $\Delta\rho$ has been established, L, D, f, and n are the length, hydraulic diameter friction factors and number of turns in the module, ρ is the coolant density, and v is the coolant velocity.

In a magnetic field, Eq. 4 has an additional MHD pressure drop term given by $\sigma B^2 Lv$, where σ is the lithium electrical conductivity, and B is the magnetic field strength.

Assuming a coolant inlet temperature of 340°C (its value during routine opertion, and a value for T_{out}) equations 1 through 4 can be solved self-consistently for v, H, and h. The results are that without a magnetic field, a heat transfer coefficient of 8470 W/m^2-K and a lithium outlet temperature of 345°C will require a coolant velocity of 0.39 m/sec. This flow rate can be established by the height of 20 m. The film drop temperature at this heat transfer coefficient is less than 1°C. This result indicates the feasibility of using natural circulation for afterheat removal and the flexibility of locating the heat sink above the reactor.

With a magnetic field, the heat transfer coefficient is ~1000 W/m^2-K, and the lithium outlet temperature can be as high as 680°C in order to reduce the flow rate to 0.6 cm/sec. However, due to the MHD pressure drop through the module, the coolant column height required to establish the

heat transfer conditions is impractical (8740 m at a magnetic field strength of 4.24 T). These results indicate that natural circulation at zero B field should definitely be considered as a method of afterheat removal. In the presence of a magnetic field, natural circulation is not adequate. Therefore, safety analyses must clearly identify the situations in which natural circulation will be required to ensure module integrity in order to minimize the number of emergency magnet shutdowns.

References, Section V.D

1) J. D. Lee et al., "Feasibility Study of a Fission-Suppressed Tandem Mirror Hybrid Reactor," Lawrence Livermoe National Laboratory Report, UCID-19327, April 1982; also, Maya, I., et al., "Safety Considerations in the Tandem Mirror Hybrid Reactor Design," ANS Transactions 39, November 1981, pp. 257-58.
2) K. R. Schultz et al., "Hybrid Reactor Safety Study - Second Annual Report," General Atomic Report, GA-A16185, December 1980; also, I. Maya et al., "Safety Evaluation of Hybrid Blanket Concepts," Fourth Topical on the Technology of Fusion, October 1980, and General Atomic Report, GA-A16101, September 1980.
3) W. W. Weaver, "Deterministic Criteria versus Probabilistic Analyses: Examining the Single Failure and Separation Criteria," Nuclear Technology 47, February 1980, pp. 234-243.
4) J. D. Gaski, L. C. Fink, and T. Ishimoto, "Systems Improved Numerical Differencing Analyzer Users Manual," TRW Systems Report 11027-6003-RO-00 (1970).
5) R. Whitley, Memo to Isaac Maya, TRW-FWP-82-075, July 15, 1982.
6) B. Badger, "WITAMIR-I, A University of Wisconsin Tandem Mirror Reactor Design," University of Wisconsin Report UWFDM-400 (1980).
7) J. K. Garner, TRW Internal Communication (1982).
8) C. J. Smithells, "Metal Reference Book," Butterworths and Co. (1978).

9) N. L. Haines, R. E. Craig, D. R. Forsythe, and E. H. Novendstern, International Conference of Liquid Metal Technology for Energy Systems, Richland, Washington, April 20, 1980.

10) El-Wakil, M. M., Nuclear Heat Transport, International Textbook Company, Scranton, Pennsylvania, 1971, p. 269.

11) Hoffman, Myron A., "Magnetic Field Effects on the Heat Transfer of Potential Fusion Reactor Coolants," Lawrence Radiation Laboratory Report, UCRL-73993, June 1972, Table 2, p. 32.

CHAPTER VI
FUSION BREEDER PLANT CONCEPT

VI.A INTRODUCTION

Although the fusion breeder program has emphasized the design of breeding blankets and associated technologies, there has also been an attempt to describe and cost the entire power plant. There are three reasons why such an exercise is required:

- A more complete definition of the surrounding plant provides additional confidence in the reference blanket concept by demonstrating its reasonableness in the overall plant context
- A format is provided whereby plant related issues which are not directly associated with the blanket design can be brought forward
- An integrated description of the plant cost and performance can be used to generate trade and optimization studies and to provide a best estimate of the ultimate commercial merit of the fusion breeder application.

The plant design information developed in this chapter is used to generate the systems and economics analysis described in Chapter VIII.

The remainder of this chapter is broken into four principal sections. Section VI.B is a description of the central cell layout and thermal power conversion system adopted for use with the reference fusion breeder blanket. The selected thermal power conversion system draws heavily upon LMFBR design experience, but also makes provision for the attainment of fusion breeder safety and reliability goals. A geometric layout of the reactor central cell (with emphasis on the arrangement of piping, pumps, and heat exchangers) is provided. The central cell operation and maintenance scheme was discussed in Section II.E.

Section VI.C provides a description of the end cell layout with brief descriptions of the cost and performance basis for various fusion subsystems. In most cases these subsystems were modeled using the TRW Tandem Mirror Reactor Design Code (TMRDC)(1). TMRDC utilizes an internal modeling data base and input from the LLNL Tandem Mirror Physics Code (TMPC)(2) to size and cost

the various subsystems. TMPC provides estimates of the fusion and injected power flow given the fusion power, central cell length, magnetic field profile, neutral beam and radio frequency heating system characteristics, etc.

Sections VI.D and VI.E provide an integrated model of the plant power flow and a detailed breakout of the plant direct cost. These quantities are later (Chapter VIII) used in the TRW PERFEC code to predict the symbiotic cost of electricity and the cost of fissile fuel(3).

References, Section VI.A

1) Original code as described in D.L. Chapin, et.al., "Preliminary Feasibility Assessment of Fusion Fission Hybrids", WFPS-TME-81-003, Westinghouse Fusion Power Systems Department (1981). Current version of the code is maintained at TRW.

2) Original code developed as described in G.A. Carlson, et.al., "Comparative End Plug Study for Tandem Mirror Reactors", UCID-19271, Lawrence Livermore National Laboratory (1981). Current version of the code is maintained at LLNL.

3) Original code developed as described in D.H. Berwald, et.al., "An Economics Method for Fusion-Fission Electricity Generation Systems", Nucl. Tech./Fusion, 1, 128 (1981).

VI.B THERMAL POWER CONVERSION AND CENTRAL CELL LAYOUT

VI.B.1 Thermal Power Conversion

The thermal power conversion system permits the thermal energy deposited in the blanket to be converted into electricity. We have chosen a conventional Rankine cycle using water as the secondary coolant for this system, relying heavily on previous designs for fast-fission reactors. The design, however, is optimized for the Fusion Breeder Reactor. The design approach used and the description of the resulting design are discussed here.

VI.B.1.a Design Approach. In this section, the design approach for the selection of the thermal power conversion system is presented. Three subjects will be discussed; the design guidelines of the power conversion system, a comparison of the near-term or existing power conversion systems for LMFBRs (Liquid Metal Fast Breeder Reactor) and the system proposed for the HYLIFE (High Yield Lithium Injection Fusion Energy Converter) fusion reactor; and a discussion on the method of selecting the number of key components such as the primary liquid metal pumps and the heat exchangers for the reference reactor. The primary circuit piping sizes are presented in the next section.

The guidelines that we used to select the thermal power conversion system are the following:

- A safe and highly reliable design is required to operate at full power at the end of blanket life when the blanket energy multiplication is at a maximum.
- The selection of components for the power conversion system is based upon either near-term or state-of-the-art designs.
- The selected design minimizes the fluid pressure experienced upon the first wall.

In order to satisfy the guideline to minimize the coolant pressure seen by the first wall, the primary coolant pump was placed at the exit of the blanket coolant. This will help ease the blanket mechanical design

requirements, thus enhancing the neutronics performance by minimizing the blanket structural material volume fraction. This will, however, require the development of lithium pumps capable of operating at the relatively high temperature of 490°C (rather than 340°C).

In order to base the power conversion system design on near-term or state-of-the-art components, liquid sodium cooled fast-fission reactor designs were reviewed. The power conversion system proposed for HYLIFE (1), an electricity producing laser fusion reactor utilizing a liquid-lithium primary coolant, a sodium secondary coolant, and a steam power conversion cycle was also considered. The reference HYLIFE reactor, designed during 1978-80, is most similar to our reference design. A brief description of the LMFBR designs which were reviewed is listed below:

CRBRP - The Clinch River Breeder Reactor Plant (2), a 375 MW(e) prototype LMFBR which is completely designed and scheduled for critical operatin in 1987, pending funding support from the U.S. Federal government.

PLBR - A conceptual U.S. Government and EPRI (Electrical Power Research Institute) funded Prototype Large Liquid Metal Breeder Reactor design study (3), completed in 1977.

SUPER PHENIX - The only commercial scale LMFBR under construction, a 1200 MW(e) fast breeder reactor under construction in France.

CDFR - A United Kingdom 1320 MW(e) Commercial Demonstration Fast Reactor, scheduled for critical operation in ~1990.

Except HYLIFE, all the above reactors are sodium cooled for both the primary and secondary power conversion circuits. We have used these reactors as references to guide the selection of sizes and types of critical power conversion components for the reference design of the Fusion Breeder Reactor. The characteristics of some of the key components of the power conversion systems of the above reactors are listed in Table VI.B.1 with those of the fusion breeder.

As discussed in Chapter V (Safety Systems), we have given strong priority in the power conversion system design to reliability. We believe

TABLE VI.B.1 Power Conversion System Characteristics of Reference Liquid Metal-Cooled Reactors

	Fusion Breeder Reactor	HYLIFE[a]	CRBRP[b]	PLBR[c]	Super Phenix[b]	CDFR[b]
P_{th}, MW	4710	3216	975	2550	3000	3300
P_e, MW	1880	1254	375	1000	1200	1320
Coolant						
Primary/Secondary	Li/Na	Li/Na	Na/Na	Na/Na	Na/Na	Na/Na
Primary						
Pump type	Centrifugal	Centrifugal	Centrifugal	Centri-fugal	Centrifugal	Centrifugal
Pump position	Hot	Hot	Hot	Hot	Cold	Cold
Number of pumps	5[d]	16	3	3	4	6
Flow rate/pump, kg/s	2511	3917	1733	4584	4225	3750
, GPM	85,000	128,000	31,000	82,000	75,663	67,157
T_{in}/T_{out}, °C	340/490	340/500	388/535	341/508	395/545	370/540
Number of IHX	6[e]	4	3	3	8	8
Load/IHX, MW(t)	788	794	325	857	375	412
Secondary						
Number of pumps	8[d]	4	3	4	4	4
Pump type	Centrifugal	Centrifugal	Centrifugal	Centri-fugal	Centrifugal	Centrifugal

TABLE VI.B.1 (Continued)

	Fusion Breeder Reactor	HYLIFE[a]	CRBRP[b]	PLBR[c]	Super Phenix[b]	CDFR[b]
Flow rate/pump, kg/s	4669	4184	1620	3958	3300	3600
, GPM	90,700	81,300	31,500	82,000	64,000	70,000
T_{in}/T_{out}, °C	316/472	316/482	344/502	312/482	345/525	335/510
Steam Generator						
Number of steam generators	15	I2	2	3	I	NA[f]
Type	Hockey stick	Hockey stick	Hockey stick	NA[f]	Integral helical coil	Integral helical coil
Turbine						
Type/Number	Superheated/2	Superheated/1	Recirculate tandem compound/1	NA[f]	Condensing/2	Tandem compound/2
T_{in}	447	457	482	457	490	486

[a]Reference 1.
[b]Reference 2.
[c]Reference 3.
[d]Required number + 2.
[e]Required number + 1.
[f]Not available.

that it will be difficult or impossible for the plasma to operate for extended periods of time at partial power if a component in the power conversion system fails. Thus, to satisfy safety and cost considerations, we require that a sufficient number of power conversion system components be provided to assure 100% capacity with a high degree of reliability. In order to achieve a system reliability of 99.9% using multiple components with an individual component reliability of 90%, the number of parallel components needed must exceed the minimum required to achieve 100% capacity by two.

By assuming that the equipment cost is proportional to (equipment size)$^{0.6}$, a component total cost function can be written as,

$$f(x) = \left(\frac{1}{x}\right)^{0.6} (x + 2) \quad . \quad . \quad . \qquad (1)$$

where x is the number of components used (not including redundant components). Equation (1) is plotted in Fig. VI.B.1, which shows a minimum of the total cost function at x = 3. Based upon this information, the required capacity of the centrifugal liquid metal pumps was calculated and compared with existing or projected pump sizes. It was found that, for a selection of three pumps and two backups, each pump needs to be able to handle 85,000 GPM, within the design capacity range of sodium pumps as indicated in Table VI.B.1. Lithium centrifugal pumps of this capacity will need further development, but since sodium pumps of the required size exist, the development should be straightforward. The same is true for the lithium metal valves. MHD pumps are also likely candidates for the Fusion Breeder Reactor, although MHD pumps of the required capacity have not been demonstrated. Pump designers believe that as the MHD pump capacity increases, the pump efficiency will also increase, to be comparable to that of mechanical pumps. The simplicity and lack of moving parts in MHD pumps is a major incentive to their use.

The primary liquid-metal heat exchanger is a more passive component than the centrifugal pump, and a higher degree of unit reliability can be assigned. To minimize the total capital cost, only one backup heat

FROM RELIABILITY CONSIDERATION
NUMBER SELECTED = NUMBER REQUIRED + 2
LET: EQUIPMENT COST α (EQUIPMENT SIZE)$^{0.6}$
THEREFORE: COST FUNCTION F(X) = $(1/X)^{0.6}(X+2)$

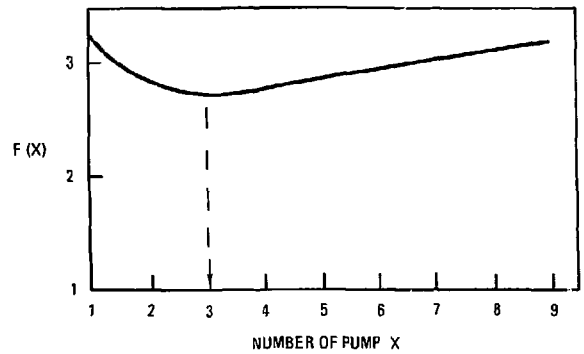

NUMBER OF PUMP SELECTED = 3 + 2 = 5

Fig. VI.B.1 Reliability and equipment size trade off.

exchanger is recommended to support the minimum requirement of five heat exchangers while the reactor is operating at full power at the end of blanket life.

VI.B.1.b Thermal Power Conversion System Design. The selected power conversion cycle for the reference design, as listed in Table VI.B.2, is presented in this section and illustrated in Fig. VI.B.2. With this design, the thermal power conversion efficiency is calculated to be 36.7%.

Figure VI.B.3 illustrates the piping arrangement of the lithium primary circuit with consideration of the reference reactor operating characteristics and illustration of the common manifolds. The piping sizes are also indicated, with the design criteria of lithium flow speed not to exceed 6.1 m/s (20 ft/s).

TABLE VI.B.2 Power Conversion System Summary

Reactor thermal power, maximum	4711 MW
Gross power conversion efficiency	40%
Electrical power	1881 MW
Auxiliary electrical power[a]	154 MW
Net blanket power conversion efficiency	36.7%

[a]The auxiliary electrical power requirement includes all pumping and clean-up equipment for the primary loop, all heat and tritium removal machinery, and miscellaneous in-plant equipment.

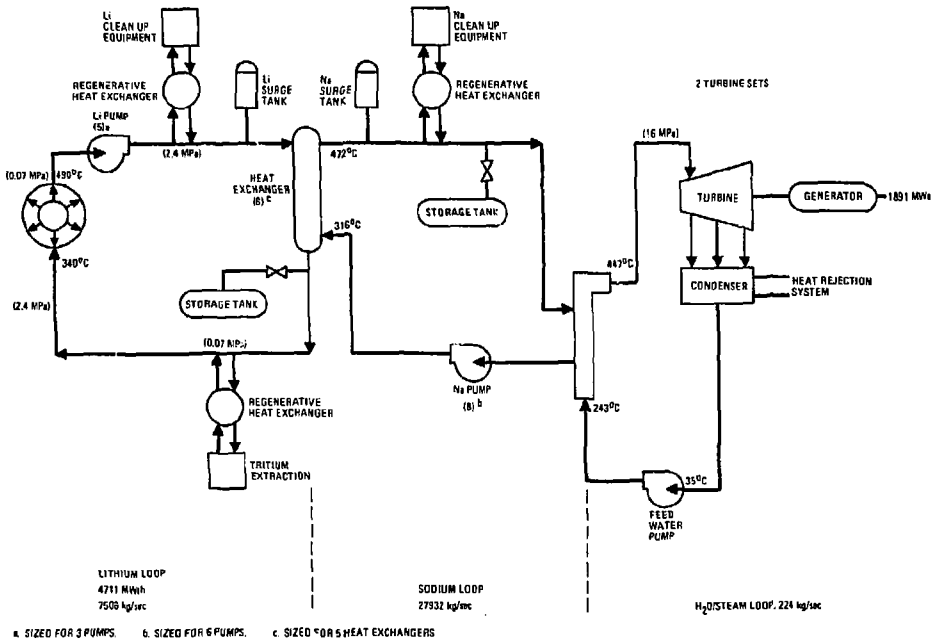

Fig. VI.8.2 Power conversion cycle schematic

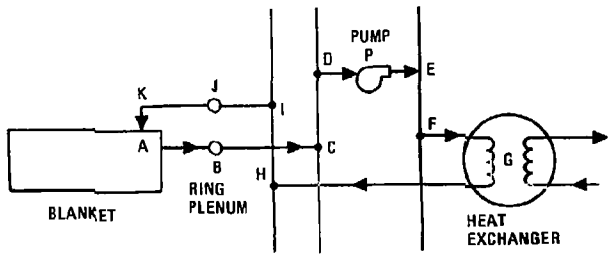

PIPE	AB	BC	DP	PE	FG	GH	IJ	JK
DIAMETER (m)	0.5	0.38	1.1	1.0	0.73	0.72	0.25	0.1
COMMON MANIFOLDS	CD	EF	HI					
DIAMETER (m)	1.1	1.1	1.1					
RING MANIFOLDS	J	B						
DIAMETER (m)	0.75	0.6						

Fig. VI.B.3 Primary circuit piping arrangement and sizes.

VI.B.2 Central Cell Layout

The main reactor building will contain the 200 m long central cell section and will terminate at the walls adjoining the end plug regions at both ends of the central cell. The building inner wall interfaces with the first and last blanket module and the outer walls with the end cells. The blanket central cell containing 50 modules and a typical section with its piping are shown in Figure VI.B.4. The piping into and out of the modules is not included, except at the "typical" group of 10 modules at the right end of the central cell. The central cell contains 5 of these 10 module groups. This "typical" group is enlarged in Figure VI.B.5. As shown, the lithium coolant is discharged from each module outlet torus to a common outlet header. Effectively the flow from ten modules enters an 85,000 gpm pump and discharges into a common header which feeds the intermediate heat exchanger (IHX). Each set of pumps and heat exchangers is piped into a parallel circuit. There are 5 pumps (2 redundant) and 6 IHXs (1 redundant) and normally all are in service. The pumps therefore will not all be operating at full flow capacity, but in the event of a failure the speed and flow on the remaining active pumps can be increased without having to undergo a startup from shutdown condition. This will minimize any perturbation in the coolant flow through the modules. As a minimum, a check valve would have to be installed in each pump inlet line to prevent back flow through the blanket. In the event of a heat exchanger failure it would be valved off and isolated from the circuit. The total valving arrangement for isolation of the pumps, heat exchangers and modules is discussed in Chapter V.

An elevation view of the component arrangement inside the reactor building is shown in Figure VI.B.6. The figure shows the relative size of the components and piping as well as the crossover pipes to secondary headers on the module opposite from the main headers, pumps and IHXs. Some of the central cell features and the pump design features are tabulated in Tables VI.B.3 and VI.B.4 respectively.

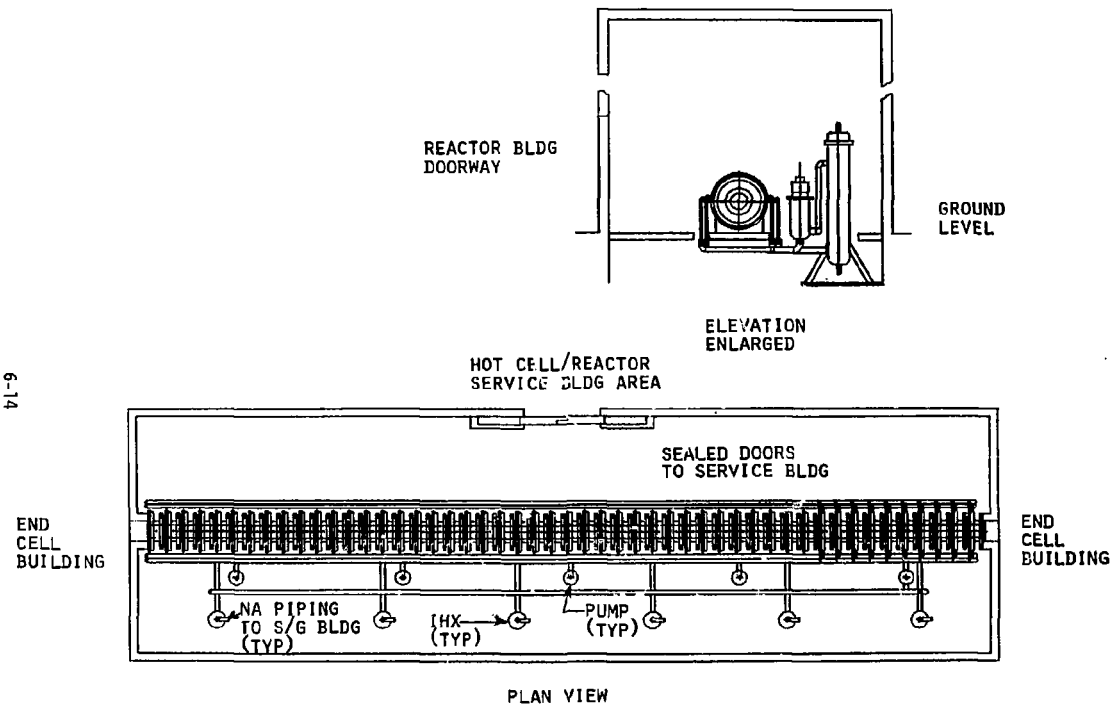

FIG. VI.B.4. Fusion Breeder Reactor reactor building showing central cell, piping and component arrangement.

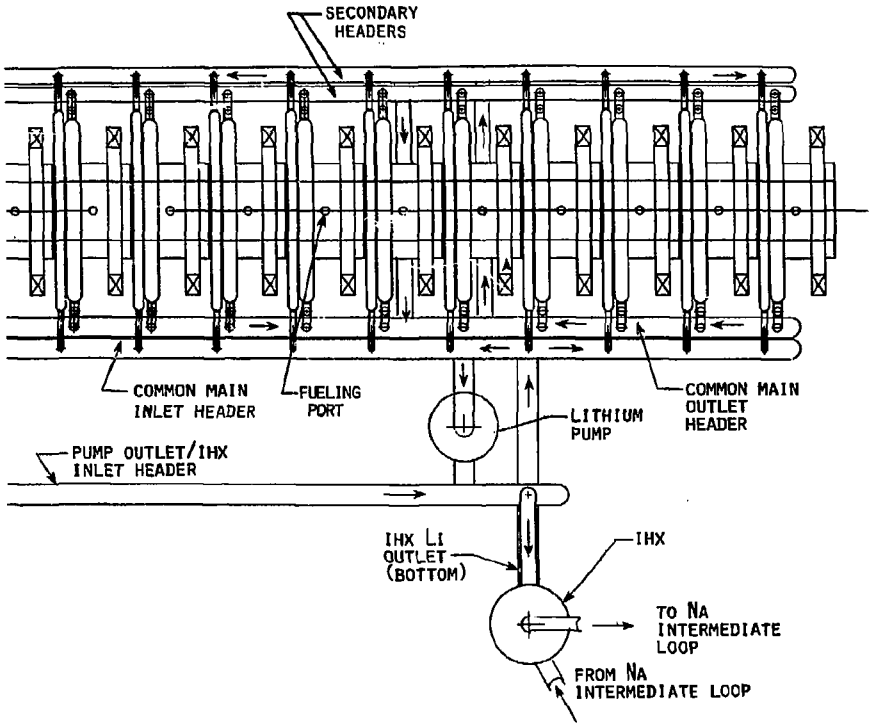

FIG. VI.B.5. Typical 10 module group of Fusion Breeder Reactor central cell assembly.

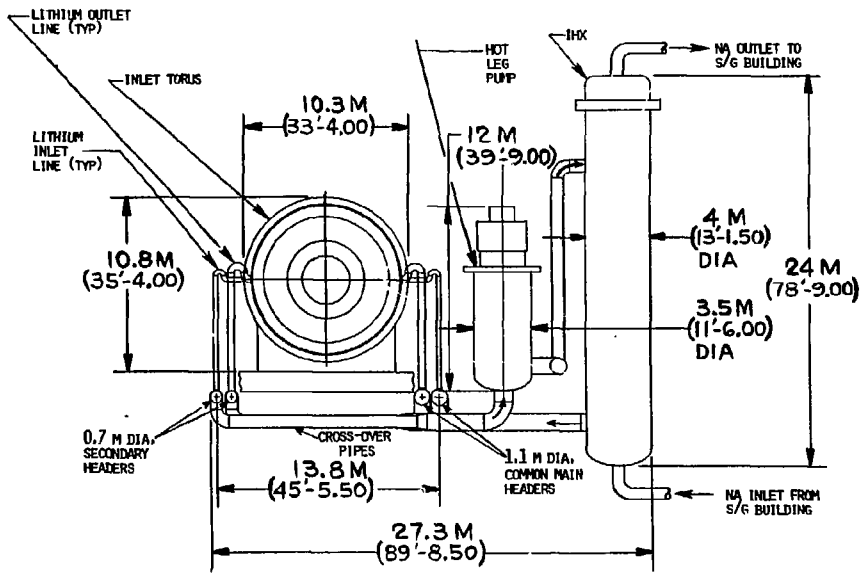

FIG. VI.B.6. Central cell and component arrangement within the Fusion Breeder Reactor building.

TABLE VI.B.3. Reactor building central cell features.

Number of Modules	50
Number of Loops	10
Number of Intermediate Heat Exchangers (One Redundant)	6
Number of Primary Coolant Pumps (Two Redundant)	5
Flow Rate per Module	5100 gpm (0.32 m^3/sec)
Common Hot Leg Manifold Pipe Diameter	1.1 m
Coolant Velocity	<3 m/s
Common Cold Leg Manifold Pipe Diameter	1.1 m
Coolant Velocity	<3 m/s
Approximate Heat Exchanger Size (Est)	
Diameter	4.0 m
Height	24 m

TABLE VI.B.4. Fusion breeder reactor lithium coolant pump design features.

Flow Rate	85,000 gpm (~5 m^3/s)
Discharge Head	350 psi
Net Positive Suction Head	10 psig
Impeller Diameter	1.5 m est.
Pump Tank Diameter	3.5 m est.
Total Length	12 m est.
Speed	909 rpm
Pump Power Consumption	~15.7 mw
Pump Inlet Nozzle	1.1 m
Coolant Velocity	5.6 m/s
Pump Outlet Nozzle	1 m
Coolant Velocity	6.8 m/s

Note that only 3 pumps are required to supply the approximately 250,000 gpm of coolant for the complete central cell.

The reactor building component arrangement was influenced by the following factors. The components are located on one side of the cell to permit module removal without having interference with the pumps and heat exchangers. In addition, this arrangement permits the IHXs to be connected to the sodium intermediate leg piping with a minimum number of pipes crossing the central cell. Both of these considerations make remote maintenance of the central cell less complicated. The pumps are located in the hot leg of the primary heat transport system close to the module coolant outlet. This arrangement minimizes the pressure drop across the first wall because many of the pressure drops in the primary heat transport system occur before the coolant reaches the first wall.

VI.B.3 Key Central Cell Cost Components

Key central cell direct cost contributors include the following four components: the central cell magnets, the blanket/shield modules, the heat transport system, and the reactor building. These costs are described below. In all cases, these direct costs were developed using the TRW tandem mirror reactor design code(4).

VI.B.3.a Central Cell Magnet Costs

The design code calculates the central cell magnet direct costs (for 50 magnets) based upon an estimate of the various component costs including the conductor cost (25 \$/Kg), the dewar cost (18 \$/Kg), the vacuum case cost (18 \$/Kg), the cost of insulation (14 \$/Kg of conductor), the liquid nitrogen shield cost (1500 $\$/m^2$ surface), the magnet power supply cost (200 \$/kW), and the refrigeration plant cost (40 \$M for both central cell and end cell magnet heat loads). A detailed structural model of the coils was used to derive the quantities of the above materials based upon geometric constraints implied by the blanket/shield and end cell and physics design requirements. These include the magnet pitch, inner bore, required field on axis, allowed field ripple, allowed width, heat load, etc.).

The overall direct cost of the 50 4.2 Tesla central cell magnets is estimated to be 554 \$M. Of this, 55% of the cost is associated with the conductor, 15% of the cost is associated with the insulation, and 17% of the cost is associated with winding the insulation. The cost per magnet is about 11 \$M.

VI.B.3.b Blanket/Shield Costs

The design code calculates the blanket/shield direct cost based upon estimates of the cost per unit volume and volume of the various blanket constituents by region. The estimated volumes and masses of blanket/shield materials are shown in Table VI.B.5.

As shown, the blanket shield system cost is 492 \$/M. Of this, about 60% is associated with the beryllium inventory, about 18% is associated with depleted lithium, and about 18% is associated with the steel structure. The beryllium cost estimate is based upon a raw material cost of 330 \$/Kg (see Section VII.B.). The lithium cost estimate is based upon a depleted lithium

TABLE VI.B.5 Summary of Blanket/Shield Costing

Blanket/Shield Material	Volume (m^3)	Mass (MT)	Unit Cost ($M/$m^3$)	Direct Cost ($M)
HT-9 Ferritic Steel	360	2770	0.245	88
Depleted Lithium[a]	1326	703	0.066	87
Natural Lithium[b]	292	155	0.020	5.8
Beryllium	480	885	0.610	292
Thorium	25	293	0.703	18
Borated Concrete	2340	8190	0.00044	1.0
				492 $/M

a) 0.2 a/o ^{6}Li (125 $/Kg @ 20 $/Ky SWU separation cost)

b) used to cool shield only

cost of 125 $/Kg (see Section VII.E). The steel cost is based upon PNL estimates(5) for complex stainless steel first wall components (31.8 $/Kg including escalation to 1982). This cost estimate is considered to be quite conservative since HT-9 has a low nickel content and because most blanket structural components are relatively simple in comparison with the first wall.

VI.B.3.C Reactor Building Costs

The reactor containment building cost is estimated by the design code to be 171 $M based upon a floor area of 5570 m^2 and a volume of $0.38 \cdot 10^6$ m^3. The building cost model assumes that the reactor building will be similar to an LWR containment building. Other buildings associated with reactor service, auxiliary, and maintenance functions are estimated cost an additional 146 $M.

References, Section VI.B.

1) "Laser Program", Annual Reports, 1978, 1979, 1980, Lawrence Livermore National Laboratory Reports, UCRL-50021-78, -79, and -80.

2) A.E. Waltar, "Fast Breeder Reactors", Pergamon Press, 1981.

3) "ERDA-EPRI LMFBR Design Projects - Phase II, Final Report", TID-27690, June 1977.

4) Original code as described in D.L. Chapin, et.al., "Preliminary Feasibility Assessment of Fusion-Fission Hybrids", WFPS-TME-81-003, Westinghouse Fusion Power Systems Department (1981). Current version of the code is maintained at TRW.

5) S.C. Schulte, et.al., "Fusion Reactor Design Studies - Standard Unit Costs and Cost Scaling Rules", PNL-2987, Battelle Pacific Northwest Laboratory (1979).

VI.C. END CELL CONFIGURATION AND COMPONENT SUBSYSTEM DESCRIPTION

In this section we provide an overview of the tandem mirror hybrid reactor end cell configuration and describe cost and performance basis for the key end cell components. The components within the two end cells (or end plugs) provide the principal mechanisms for plasma containment via the use of applied magnetic and electro-static fields. The end cells also contain the direct converter, the cryogenic vacuum systems, and the plasma and beam dumps. It is anticipated that each end cell and the central cell will be housed within a separate building which can be individually isolated by the closure of two large gate valves located in the transition region between the barrier field coils and the first blanket module. The ability to isolate the end cell and the central cell components is important from a safety point of view since the central cell contains liquid lithium and no water while the end cell components (including the direct converter grids) are water cooled.

VI.C.1 End Cell Layout

The end cell is shown in Figure VI.C.1. Its total length is about 55 meters including the distance from the last central cell module to the outside of the Yin-Yang coils (~ 33 m) plus the length of the direct converter (~ 22 m). The left end cell does not have a direct converter, but rather an electron dump which is somewhat smaller. The combined floor areas of both end cell buildings is estimated to be 3360 m^2 and the combined volume is estimated to be $1.88 \cdot 10^5$ m^3 (56 m height).

The axicell section of the end plug consists of two high field, circular coils of 13 and 15 tesla field strength on axis (0.38 and 0.35 m bore, respectively). Each barrier coil consists of a Nb-Sn superconducting coil to 12 T and a copper insert coil to provide the additional field on axis. These coils are each about 0.8 m in width and are separated to provide about 1.2 m of free axis between the coils.

Following the axicell coils are the transition coils. These non-circular coils re-shape the magnetic flux lines to enter the Yin-Yang region and assist in promoting radial particle transport for impurity pumping and MHD stability. MHD stability is primarily provided by the "positive curvature" obtained when ions sample the quadrapole field in the Yin-Yangs.

Figure VI.C.1

FUSION BREEDER AXI-CELL CONFIGURATION

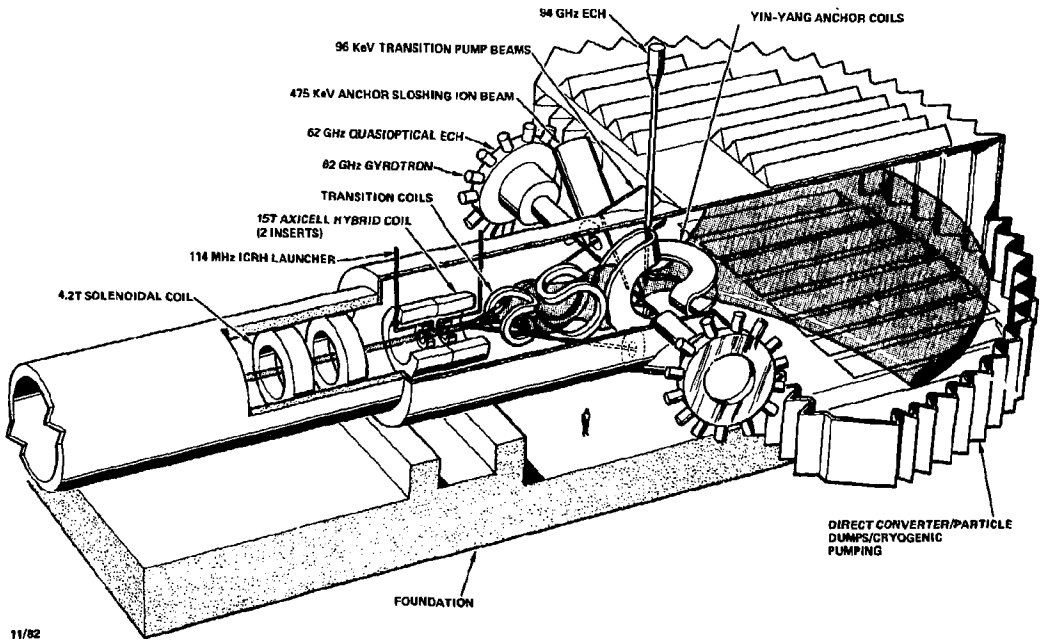

Various other functions are also provided in the end cells to create electro-static potential barriers and to provide microstability. Anchor sloshing ion neutral beams (475 KeV) are injected into the Yin-Yang (anchor) region while charge exchange pump beams (96 KeV) are injected into the transition coil region. Two frequencies of electron cyclotron resonance heating (62 GHz and 93 GHz) are injected into the anchor region and ion cyclotron resonance heating is injected between the barrier coils in the axicell. D-T fuel pellets (ice) are injected into the central cell near the axicell.

The cryogenic vacuum systems and plasma dumps associatied with the halo plasma (detail not shown) are located in the direct converter region. The direct converter grid is cooled with hot water (~ 300°C) and an energy conversion loop to recover about half of the thermal power on the grids is implied (but not yet designed).

The physics basis for the components described about is defined in Chapter I. The associated cost and power flow data are presented in Sections VI.C.2 and VI.D.

VI.C.2 Cost Performance Basis for Key End Cell Components

The estimated performance and cost of a tandem mirror reactor (regardless of the blanket application) is largely dependent upon assumptions concerning several key fusion subsystems: neutral beams, radio frequency (rf) heating, magnets, and direct energy conversion systems. In this section we discuss the fusion component performance and cost estimates used in our analysis and discuss the modeling techniques used to develop such data(1,2).

The estimates reflect the expected performance and present dollar (1982 $) cost of fusion technologies to be used in a 10th of a kind facility which might operate during the 2030 timeframe. The cost estimates do not include a 20% contingency factor which is later applied to all plant components. The reader is referred to Chapter VIII for a more complete discussion of the sensitivities in overall performance to uncertainties in the cost and performance of the various subsystems.

VI.C.2.a Plasma Heating Systems

A summary of the power flow, cost, and electrical efficiency data as it applies to the five plasma heating systems is provided in Table VI.C.1. As shown, a total of 322 MW is injected into the plasma and 307 MW is absorbed. Averaged over all five component heating systems, the net wall plug efficiency is 66.4%. Therefore, 476 MW (307/.645) of electricity is required to operate heating systems.

Among these, the 475 keV sloshing ion beams are expected to reepresent the most difficult technology. These are modeled by the tandem mirror reactor design code assuming the use of the following component technologies(3)

- self extraction negation ion source
- advanced R.F. or D.C. accelerator
- laser photo-detachment neutralizer
- direct recovery of un-neutralized species which are bent out of the beam

On this basis, the sloshing ion beam direct cost is about 38 $M (1.8 $/W). The new cost estimate is similar to our previous estimate(4) of about 1.7 $/W (converted from 1.5 $/W in 1980 dollars to 1.73 $/W in 1982 dollars by 1.10 x 1.05 = 1.155 factor). The estimated wall plug to injected energy efficiency is 70%, but the net efficiency to trapped energy is only 37%.

The charge exchange pump beams require the largest source of wall plug power (288 MWe), but are similar to the sloshing ion beams in most other respects (source, neutralizer, beam lines). At the lower energy required for charge exchange pumping (96 versus 475 keV for sloshing ions), more conventional D.C. accelerators can be used. We estimate the direct cost of these beams as 235 $M (1.52 $/W) - a slightly lower unit cost than the high energy beam, but the highest total cost among the plasma heating systems.

The 114 MW, 62 GHz, RF heating system is estimated to cost 108 $M at 0.95 $/W. This system is modeled by the tandem mirror reactor design code assuming the use of the following component technologies(3):

- Graetz bridge based power supply
- 1 MW gyrotron tubes with depressed collectors
- quasi-optical microwave transmission system and launcher

TABLE VI.C.1 Plasma Heating System Power Flow, Cost, and Electrical Efficiency Data

OVERALL PLASMA HEATING SYSTEM POWER FLOW SUMMARY	
Fusion Power	3000 MW
Total Power Injected into the Plasma	322 MW
Total Power Trapped (Absorbed) in the Plasma	307 MW
Net Trapping Efficiency	95.3%
Net Injector Beam Generation Efficiency	69.5%
Net Trapped Energy to Wall Plug Efficiency	66.4%
SLOSHING ION NEUTRAL BEAMS	
Beam Energy (Negative Ion)	475 KeV
Total Injected Power	20.9 MW
Total Trapped Power	11.1 MW
Trapping Efficiency	53.0%
Beam Generation Efficiency	69.6%
Net Trapped Energy to Wall Plug Efficiency	36.9%
Direct Cost per Unit power Injected	1.8 $/W
Total Direct Cost	37.6 $M
CHARGE EXCHANGE PUMP NEUTRAL BEAMS	
Beam Energy (Negative Ion)	96 KeV
Total Injected Power	155 MW
Total Trapped Power	154 MW
Trapping Efficiency	99.3%
Beam Generation Efficiency	68.0%
Net Trapped Energy to Wall Plug Efficiency	67.6%
Direct Cost per Unit Power Injected	1.52 $/W
Total Direct Cost	235 $M

TABLE VI.C.1 (Continued)

AXICELL ION CYCLOTRON RF HEATING	
Frequency	114 MHz
Total Injected Power	23.5 MW
Total Trapped Power	20.0 MW
Trapping Efficiency	85.0%
RF Generation Efficiency	48.0%
Net Trapped Energy to Wall Plug Efficiency	40.8%
Direct Cost per Unit Power Injected	1.2 $/W
Total Direct Cost	28.2 $M
ANCHOR ELECTRON CYCLOTRON RF HEATING	
1) Lower Frequency System	
Frequency	62 GHz
Total Injected Power	114 MW
Total Trapped Power	114 MW
Trapping Efficiency	100%
RF Generation Efficiency	74.2%
Net Trapped Energy to Wall Plug Efficiency	74.2%
Direct Cost per Unit Power Injected	0.95 $/W
Total Direct Cost	108 $M
2) Higher Frequency System	
Frequency	94 GHz
Total Injected Power	8.7 MW
Total Trapped Power	8.7 MW
Trapping Efficiency	100%
RF Generation Efficiency	50.9%
Net Trapped Energy to Wall Plug Efficiency	50.9%
Direct Cost per Unit Power Injected	2.3 $/W
Total Direct Cost	20.0 $M

On this basis, the 62 GHz RF system cost estimate is about 70% lower than our previous estimate(4) of about 3.45 $/W (adjusted to 1982 dollars). The cost savings is largely attributed to the efficient use of large power supplies and the assumed development of gyrotron tubes of five times the power rating of these that a currently available (200 kW each). Since the ECRH power is efficiency trapped by the plasma, a high net wall plug efficiency of 74% is estimated.

The higher frequency ECRH system (94 GHz, 8.7 MW) is estimated to be less efficient (about 51%) and more costly than the lower frequency ECRH system (on a per watt basis). The higher cost estimate of 2.3 $/W results because of the lower power of this system which results in a less cost efficient use of the power supplies and redundant gyrotron tubes (which are provided to assume high availability of this RF system). The current unit cost is 35% below the previous estimate(4) of about 3.45 $/W.

The fifth heating system, the 114 MHz ICRH system, is estimated to cost about 28 $M, or 1.2 $/W. Although the ICRH launcher will require some development(3), ICRH sources are state-of-the-art components and the indicated cost estimate reflects a higher degree of confidence than those associated with ther heating systems. The estimated wall plug to injected energy efficiency of this system is about 48%, but the net efficiency to trapped energy (about 41%) is lower.

VI.C.2.b End Cell Magnets

The key characteristics and costs of the six end cell magnets (twelve considering both end cells), as modeled using the tandem mirror reactor design code, are shown in Table VI.C.2.

Beginning with the barrier coils, the cost and power consumption estimates are based upon interpolations between point designs(3) for similar coils of somewhat higher magnetic field (i.e., 20-28 T). Since these coils required copper inserts for operation with a Nb-Sn superconductor, some power is consumed. The design code estimates that these coils will cost about $64 M and will require about 76 MWe of input power.

TABLE VI.C.2 Key Characteristics and Costs of End Cell Magnets

MAGNET TYPE[a]	FIEL ON AXIS	RESISTIVE POWER CONSUMPTION	MINOR RADIUS	MAJOR RADIUS	WIDTH	SWEEP	COST
INSIDE BARRIER COILS	13T	23.8 x 2 = 47.6 MWe	0.38 M	CIRCULAR COIL	0.8 M	CIRCULAR COIL	16.9 x 2 = 33.8 $M
OUTSIDE BARRIER COILS	15T	14.3 x 2 = 28.6 MWe	0.35 M	CIRCULAR COIL	0.8 M	CIRCULAR COIL	15.0 x 2 = 30.0 $M
TRANSITION COILS	1.6T	SUPER-CONDUCTING	0.68 M	2.1 M	0.5 M	90°	9.5 x 4 = 38.0 $M
YIN COILS	2.2T	SUPER-CONDUCTING	0.68 M	2.1 M	1.8 M	90°	8.3 x 2 = 16.6 $M
YANG COILS	2.2T	SUPER-CONDUCTING	0.68 M	2.1 M	1.9 M	73°	10.5 x 2 = 21.0 $M
TOTAL		76.2 MWe					140 $M

a) 2 OF EACH MAGNET TYPE

The transition and Yin-Yang coils are entirely superconducting and are modeled based upon correlations between the inductance, total stored energy, mass per unit stored energy, and cost per unit mass. The models used to provide the cost estimates for these magnets (about 76 $M) have been checked against the MFTF-B magnet design cost(5) and the estimated TMNS magnet design cost(6). Relatively good agreement is provided.

VI.C.2.c Direct Converter and Beam Dump Systems

Other key end cell systems include the direct converter, electron dump, and halo plasma dump. Together, these systems handle

$$P_f \times (0.2 + 1/(Q_p \eta_t)) - P_{bd} = 3000 \times (0.2 + 1/(9.76 \times 9.55)) - 14.4 = 907 \text{ MW}$$

of charged particle power where P_f is the fusion power, Q_p is the plasma gain, η_t is the net trapping efficiency, for power injected into the plasma and P_{bd} is the heating power absorbed on beam dumps. Of the 907 MW input, 438 MWe (48%) is directly converted to electricity, 235 MW_t (36%) of useful power is transferred to the thermal conversion system, and 235 MW_t (26%) of the low grade power is lost to the waste heat sinks.

The direct cost of the direct converter, cryogenic pumping, and other particle dump systems (including electron dump and halo dump) is estimated to be 131 $M. This cost (not including buildings) is broken out as follows:

Component	Cost
Direct Converter Grids	7.4
Electron Dump	25.0
Halo Plasma Dump	10.0
Structural Components	50.0
Power Conditioning	30.6
Cryopanels	8.4
	131.4

References, Section VI.C.

1) Original code developed as described in G.A. Carlson, et.al., "Comparative End Plug Study for Tandem Mirror Reactors", UCID-19271, Lawrence Livermore National Laboratory (1981). Current version of the code is maintained at LLNL.

2) Original code developed as described in D.L. Chapin, et.al., "Preliminary Feasibility Assessment of Fusion-Fission Hybrids", WFPS-TME-81-003, Westinghouse Fusion Power Systems Department (1981). Current version of the code is maintained at TRW.

3) B.G. Logan, et al., "Mirror Advanced Reactor Study - Interim Design Report", in preparation to be released January, 1983, Lawrence Livermore National Laboratory.

4) J.D. Lee, et al., "Feasibility Study of a Fission-Suppressed Tandem-Mirror Hybrid Reactor" UCID-19327, Lawrence Livermore National Laboratory (1982).

5) K.I. Thomassen and V.N. Karpenko, "Tandem Mirror Fusion Test Facility (MFTF-B) - Conceptual Design Report and Project Proposal", LLNL-Prop-163, Rev. 1, (1980).

6) R.E. Tatro and R.W. Baldi, "Design Scoping Study of the 12 T Yin-Yang Magnet System for the Tandem Mirror Next Step (TMNS), General Dynamics Report (1981).

VI.D. INTEGRATED POWER FLOW

The integrated power flow associated with the reference fusion breeder design concept is shown in Figure VI.D.1. In this figure, the heating systems discussed in Section VI.C. are lumped into one system designated "driver". As shown, the driver systems require a total of 463 MWe of recirculating power. Other plant systems (magnets, pumps, cryo systems, BOP) are estimated to require an additional 256 MWe of recirculating power for a total recirculating power requirements of about 720 MWe.

The blanket output of 4728 MW_t is thermal converted to electricity at 40% (gross) yielding 1891 MWe. The other 262 MW_t of thermal power (mostly from particle dumps) are assumed to be thermal converted at 20% efficiency yielding a total electrical output of 1891 + 52 = 1943 MWe due to thermal conversion. The corresponding lumped thermal conversion efficiency is 1943/(4728 + 262) = .389.

It should be noted, however, that the blanket energy multiplication shown (1.97) is a maximum end-of-cycle (EOC) value. The average blanket energy multiplication is 1.61. This corresponds to an average blanket thermal output of 3864 MW_t. In this case, the total thermal conversion cycle output is 1546 + 52 = 1598 MWe, or 20% lower than the maximum. The minimum total thermal conversion cycle output (corresponding to a beginning-of-cycle blanket energy multiplication of 1.25) is 1252 MWe.

Adding the direct converter electricity output of 438 MWe and subtracting the recirculating power requirement of 719 MWe yields BOC, average, and EOC total net electricity generation values of 971, 1317, and 1662 MWe. The overall power swing, summarized in Table VI.D.1, is ±26%. This power swing could be reduced by axial fuel zoning or adjustments in the fusion power level (decreasing it to match the BOC to EOC blanket energy multiplication evolution). Neither option is adopted for reasons discussed in Chapter IV.

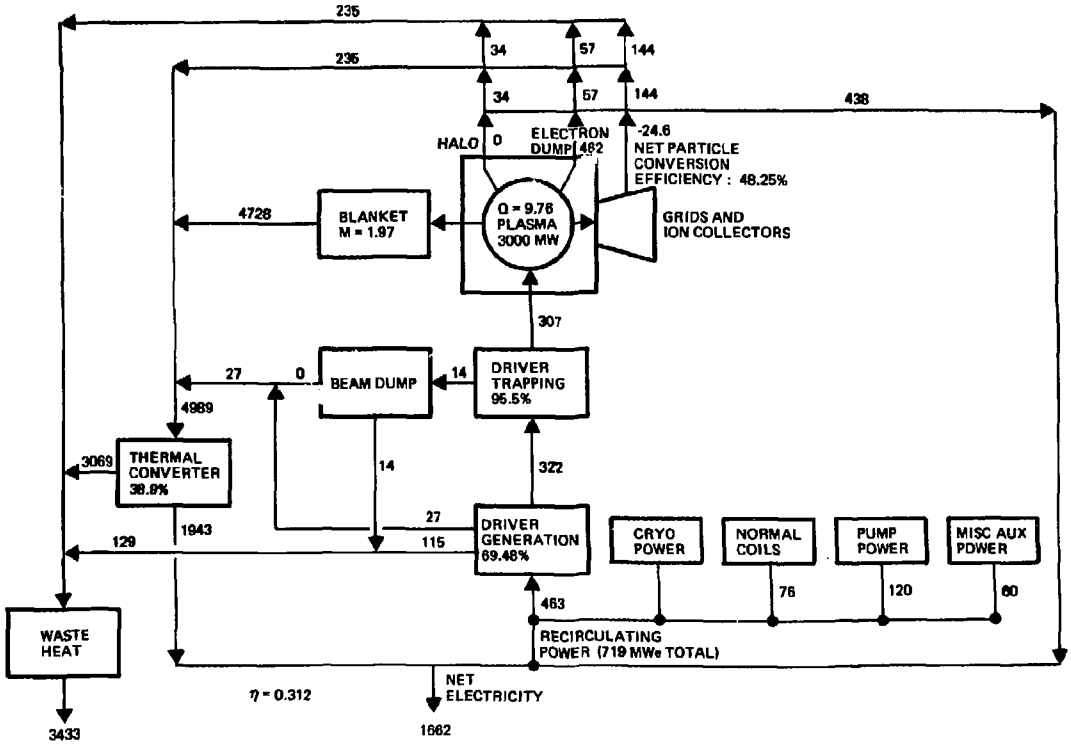

Fig. VI.D.1 Integrated Power Flow for Reference Fusion Breeder

Table VI.D.1 Power Swing Summary

	BOC	AVERAGE	EOC
Blanket M	1.25	1.61	1.97
Blanket Thermal Power	3000 MW_t	3864 MW_t	4728 MW_t
Electricity from Blanket Thermal[a]	1200 MWe	1546 MWe	1891 MWe
Electricity from Other Thermal	52 MWe	52 MWe	52 MWe
Electricity from Direct Conversion	438 MWe	438 MWe	438 MWe
Gross Electricity	1690 MWe	2036 MWe	2381 MWe
Recirculating Power Requirement	719 MWe	719 MWe	719 MWe
Net Electrical Output	971 MWe	1317 MWe	1662 MWe
Relative Power Swing	- 26%	0	+ 26%
Net Electrical Efficiency[b]	0.269	0.295	0.311

a) *low grade heat converted to electricity at 20% efficiency*

b) defined as (net electrical output)/(fusion power x [0.8 x blanket energy multiplication + 0.2]).

VI.E PLANT COST SUMMARY

In this section the overall direct and operating costs of the reference system are described. These costs are used in the systems analysis described in Chapter VIII.

VI.E.1 Direct Cost Summary

The plant direct costs, as tabulated by the design code(1), are summarized in Table VI.E.1. Among the costs shown, several contributions to the various subsystem costs not included in the code models were also estimated. These contributions, totaling about 335 $M (or 9% of the total cost estimate) are listed in Table VI.E.2. The total direct cost estimate of 3744 $M includes fuel reprocessing plant direct costs totalling 307 $M.

It is important to note that the costs developed in Table VI.E.1 relate to direct costs only. The total cost including field indirect costs, the architect/engineer/constructors, home office costs, the owners engineering cost, the time value of money during construction, and a 20% contingency factor is estimated to be 7770 $M (1982 dollars), or 2.178 times the direct cost. This factor is developed in more detail in Chapter VII.

VI.E.2 Plant Annual Operating Costs

The plant operating costs are broken into three categories: fuel cycle costs, miscellaneous operation and maintenance costs, and blanket structure replacement costs. These are described below:

VI.E.2.a Fuel Cycle Costs

The annual fuel cycle costs include contributions due to five major activities: fuel reprocessing, thorium fabrication, beryllium fabrication, beryllium material losses, and product transfer and radioactive waste transfer. It should be noted that the costs described below are non-capital related costs. In particular, the capital costs associated with the fuel reprocessing plant, beryllium pebble fabrication plant, and thorium snap-ring fabrication plant are included in the plant direct cost developed in the previous section.

TABLE VI.E.1 Reference Fusion Breeding Direct Cost Breakout by Cost Account Number (1982 dollars)

ACCOUNT NUMBER				ACCOUNT TITLE	DIRECT COST ($M)
20				*Land and land rights*	6
21				Buildings and structures	569
	21.1			Site improvements and facilities	14
	21.2			Reactor containment building	171
	21.3			Turbine generator building	56
	21.4			Cooling system structure	9
	21.5			Other plant buildings	319
		21.6.1		Reactor auxiliary building, R	68
		21.6.2		Reactor auxiliary building, NR	16
		21.6.3		Reactor service building	62
		21.6.4		Steam generator building	51
		21.6.5		Control building	23
		21.6.6		End cell buildings	85
		21.6.7		Misc. structures	14
22				Reactor plant equipment	2694
	22.1			Fusion reactor equipment	1375
		22.1.1		Magnets	674
			22.1.1.1	End cell magnets	140
			22.1.1.2	Central cell magnets	554
		22.1.2		Plasma heating systems	429
			22.1.2.1	Neutral beams	273
			22.1.2.2	RF heating	156
		22.1.3		Direct converter and beam dump	131
		22.1.4		Vacuum vessels	15
		22.1.5		Cryogenics plant	35
		22.1.6		Intermodule Structure	5
	22.2			Nuclear plant and fuel cycle equipment	1319
		22.2.1		Blanket/shield	492
		22.2.2		Remote maintenance equipment	75
		22.2.3		Heat transport system	390
		22.2.4		Fuel management equipment	15
		22.2.5		Dump tank and coolant	40
		22.2.6		Beryllium Fabrication Plant	50
		22.2.7		Thorium Fabrication Plant	15
		22.2.8		THOREX Reprocessing Plant	307

Table VI.E.1 (Continued)

23		Turbine plant equipment	304
	23.1	Turbine generators	158
	23.2	Main steam system	14
	23.3	Heat rejection system	41
	23.4	Condensing system	29
	23.5	Feed heating system	39
	23.6	Other equipment	23
24		Electric Plant Equipment	157
	24.1-24.3	Switch gear and related equipment	8
	24.4	Protective equipment	3
	24.5-24.6	Electrical bulks	140
	24.7	Electrical lighting	6
25		Misc. plant equipment	14
90	TOTAL PLANT DIRECT CAPITAL COST		3744

TABLE VI.E.2 Direct Cost Estimates for Component Costs Not Modeled in the Design Code

- Direct Converter and Beam Dump Components - 85 $M[a]
  - Electron Dump - 25 $M
  - Halo Plasma Dump - 10 $M
  - Structural Components - 50 $M
- Cryogenics Plant - 35 $M
- Remote Maintenance Equipment 75 $M
- Fuel Management/Dump Tank Circuit - 68 $M
  - Fuel Management Equipment - 15 $M
  - Dump Tank and Coolant Loop - 53 $M
- Beryllium Fabrication Plant - 32 $M
- Thorium Fabrication Plant - 15 $M
- End Cell Vacuum Vessel - 15 $M
- Intermodule Structure - 10 $M

a) total cost of these systems is 131 $M (of which 46 $M results from design code modeling).

The THOREX fuel reprocessing plant required for the reference fusion breeder must have an average throughput of 604 MT/yr (5646 Kg/yr ^{233}U at 0.934% average enrichment). As discussed in section VII.C, the annual operating costs is estimated to be

$$57 \text{ \$M/yr} \times \left(\frac{604}{1030}\right)^{.57} = 42 \text{ \$M/yr}$$

or about 70 \$/Kg of thorium.

We expect that the operating cost to fabricate simple thorium snap-rings will be less than 25¢ per pin. Each pin weighs 8 grams, so the cost per unit of throughput is 31 \$/Kg, or 19 \$M/yr for 604 MT/yr.

For a two year beryllium pebble life, the pebble re-manufacture rate would be $18 \cdot 10^6$ pebbles/yr. Assuming a 25¢ per pebble handling charge, the overall operating cost of the beryllium manufacturing equipment (see Section VII.B) is estimated to be about 4.5 \$M/yr.

In the beryllium manufacturing process, about 7% of the beryllium material which is cycled will be lost. Thus, about 29.3 MT/yr of beryllium will have to be replaced. At a cost of 330 \$/Kg (Section VII.B), the annual cost is estimated to be about 9.7 \$M/yr. A 0.6 \$M/yr cost is added to account for operating the equipment to fabricate this makeup material.

The cost of product and radioactive waste transfer and other miscellaneous fuel cycle charges are estimated to be 9 \$M/yr.

VI.E.2.b Miscellaneous Operation and Maintenance Charges

The miscellaneous operation and maintenance charges include the following annual costs:

- Salaries of Plant Personnel
- Miscellaneous Supplies and Equipment
- Outside Support Services
- General and Administrative Costs
- Coolant Makeup
- Miscellaneous Process Materials
- Fuel Handling Costs
- Other Miscellaneous Costs

As recommended by PNL, we have estimated these costs as 2% of the direct plus indirect plant cost not including the time value of money during construction (see Chapter VIII). Applying this factor as described above results in a large miscellaneous operating cost estimate of 137 $M/yr.

VI.E.2.c Blanket Structure Replacement Costs

When blanket modules are replaced, the blanket structure and piping is replaced, but the shield, magnet, lithium coolant, and beryllium multiplier are saved for reuse. The latter components represent the majority of the blanket/shield cost and, as a general observation, the loss of availability due to blanket changeout (Section II.E and Chapter IV) is a much greater consideration then the cost of materials. In particular, the capital charges associated with lost availability are about 3.5 $M/day. In contrast, for a ten year blanket lifetime (Section III.B), the annual cost of replacing one-tenth of the blanket structure is estimated to be only about 2 $M.

VI.E.2.d Summary of Plant Annual Operating Costs

The operating costs are summarized in Table IV.E.3. As shown, the total annual operating cost is estimated to be 223 $M/yr. As will be discussed in Chapter VIII, the plant annual operation costs are about 15% of the plant annual capital costs. However, since the operating costs are expected to increase annually (with general inflation) while the capital cost is fixed, their contribution to the overall annual cost over the 30 year life of the plant will be larger than 15%.

Table VI.E.3 Summary of Plant Annual Operating Costs

• Fuel Cycle Costs:	
• Fuel Reprocessing Plant Operating Cost	42 $M/yr
• Thorium Fabrication Plant Operating Cost	19 $M/yr
• Beryllium Fabrication Plant Operating Cost	4.5 $M/yr
• Beryllium Material Losses	10 $M/yr
• Product and Waste Transfer	9 $M/yr
• Blanket Structure Replacement Cost	2 $M/yr
• Miscellaneous Operation and Maintenance Cost	137 $M/yr
Total	223 $M/yr

References, Section VI.E.

1) Original code developed as described in D.L. Chapin, et al., "Preliminary Feasibility Assessment of Fusion-Fission Hybrids", WFPS-TME-81-003, Westinghouse Fusion Power Systems Department (1981). Current version of the code is maintained at TRW.

CHAPTER VII

FUEL CYCLE TECHNOLOGIES

VII.A OVERVIEW OF FUEL CYCLES

VII.A.1 Introduction

The principal role of the fusion breeder reactor is to provide an external source of fissile fuel to support a fission power reactor economy composed of light water reactors (LWRs) or other fission reactors. In this role, the fusion breeder is operationally similar to a fissile enrichment plant which requires no fissile feed stream and is an electricity producer rather than a consumer. In contrast with fission breeder reactors (i.e., liquid metal fast breeder reactor (LMRBR) and light water breeder reactor (LWBR)), the neutron rich fusion breeder is a subcritical assembly, produces an order of magnitude more net excess fuel per unit of thermal power, and is not subject to the neutron balance constraints of conventional fission reactors. As a result, a wide variety of fuel cycles and fuel forms are possible. In general, the fusion breeders may produce either ^{233}U or ^{239}Pu using metal, oxide, carbide, molten salt or other fertile fuel forms.

After the bred fissile material is recovered from the fertile fuel, it may be used to provide initial inventories or fissile makeup to fuel conventional light water reactor (LWR) clients operating on one of several possible fuel cycles. Alternatively, the bred fuel could be used to fuel advanced fission converter reactors such as the high temperature gas cooled reactor (HTGR) or the Canadian heavy water reactor (CANDU). If desired, the fusion breeder might also breed fuel to provide initial fissile inventories for liquid metal breeder reactors (LMFBR).

Fuel cycle related issues will, in general, depend upon the particular breeding blanket design, the choice of a fertile fuel form, and the choices of a client reactor type and its associated fuel cycle. These issues can have a potentially large impact on the cost of bred fuel, the cost of electricity generation, and overall feasibility of the fusion breeder.

In this chapter we first review several candidate fuel cycle options for fusion breeders and LWRs. This review is followed by more detailed discussions relating to the reference fusion breeder considered during this study (Section VII.A). A process description and cost estimate for beryllium pebble manufacture/recycling is provided in Section VII.B. Conceptual plant designs and costing analysis relating to PUREX/THOREX and pyro-chemical fuel reprocessing facilities for the fusion breeder discharge fuel are presented in Section VII.C and D. These reprocessing technologies are considered to be key elements in the symbiotic electricity generation system and Section VII.E compares the relative economics of the various options. Cost estimates for other fuel cycle operations (e.g., tritium removal from lithium) are also provided.

Additional information which applies to the following related subjects may be found elsewhere in this report:

- Section II.C - Nuclear Design
- Section II.E - Operation and Maintenance
- Section III.C - Beryllium/Thorium Fuel Forms and Lifetime Estimates
- Chapter IV - Fuel Management Systems and Analysis
- Chapter V - Safety Systems Design
- Section VI.E - Plant Cost Estimates
- Chapter VIII - Systems and Economics Analysis.

VII.A.2 Fuel Cycle Options and Issues

A general schematic of the fusion breeder/fission burner reactor fuel cycle is shown in Figure VII.A.1. Although this schematic does not address any specific fuel form, several features are deserving of note. Most importantly, the overall fuel cycle is separated into two distinct fuel cycles which are coupled by the flow of bred fissile material from the fusion breeder to the fission converters. With the exception of issues which bear upon the type of converter fuel fabrication plant required (e.g., the amount of ^{232}U in the bred ^{233}U), the breeder and burner fuel cycles are entirely separable.

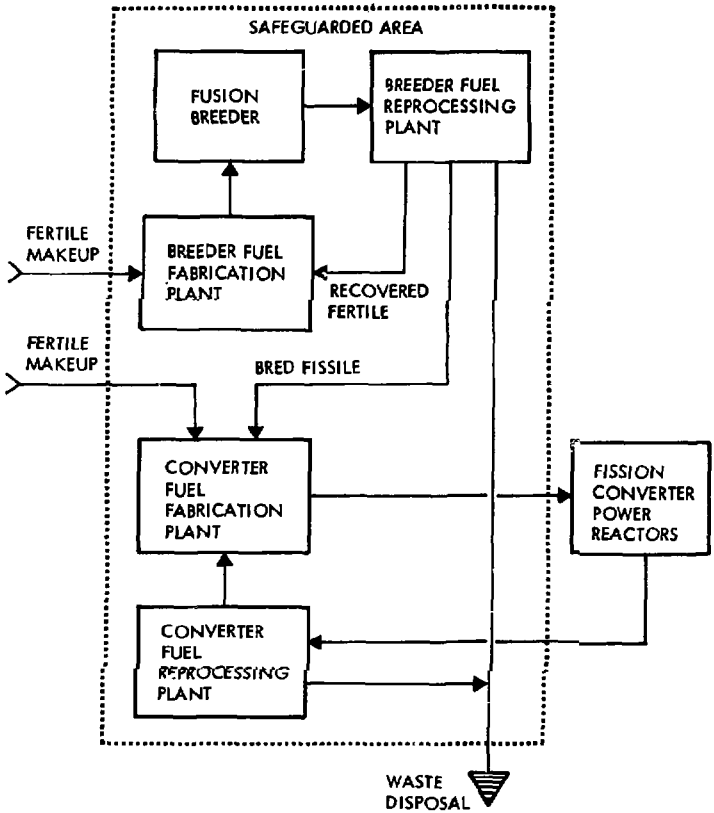

Fig. VII.A.1 General Schematic of the Fusion Breeder/Fission Burner Reactor Fuel Cycle

Also, both the fusion breeder and fission client fuel cycles are closed by reprocessing and recovery of fissile materials. Although direct enrichment (or "refresh") fuel cycles which do not employ reprocessing have been examined in the past(1,2), these lead to inefficient fissile production in the fusion breeder as well as the disposal and loss of large quantities of valuable fissile resources. Our results indicate that, like the LMFBR, the fusion breeder requires a closed fuel cycle to achieve adequate economic performance. The fusion breeder and LMFBR fuel cycles are also similar in that only small quantities of fertile materials are required for makeup, mining requirements are minimal, and isotopic enrichment capabilities are not required.

VII.A.2.a Overview of Fusion Breeder Fuel Cycles and Issues

In developing the reference fusion breeder concept we have considered two alternative fuel reprocessing technologies. The first of these, a THOREX, aqueous chemistry, fuel reprocessing plant to extract ^{233}U from thorium metal fuel was first investigated for fusion breeder applications in 1980(3), but was revisited and compared with the PUREX technology (aqueous reprocessing for uranium/plutonium fuels) as part of this study (see Section VII.C).

A principal concern regarding the aqueous reprocessing technologies is cost. In particular, the suppressed fission fusion breeder fuel cycle is unique in the respect that fissile fuel is discharged at very low fission burnup (~ 800 MWD/MTHM) and at very low concentration (~ 1.2% fissile material in thorium). This leads to an advantage and a disadvantage when the reference blanket is compared with fast fission blankets which have been investigated in the past(4). Lower burnup, an advantage, leads to lower radioactivity in the discharged fuel with favorable impact on fuel reprocessing and fabrication processes. Conversely, low discharge concentration, can be expected to lead to higher unit costs (i.e., $/gm) to recover the bred fuel. This situation is illustrated in Figure VII.A.2 which shows the allowable reprocessing cost to obtain a fixed contribution to the overall cost of bred fuel as a function of the fissile discharge concentration. For instance, in the case of ~ 1% discharge enrichment, a 30 $/gm impact on the cost of bred fissile fuel would

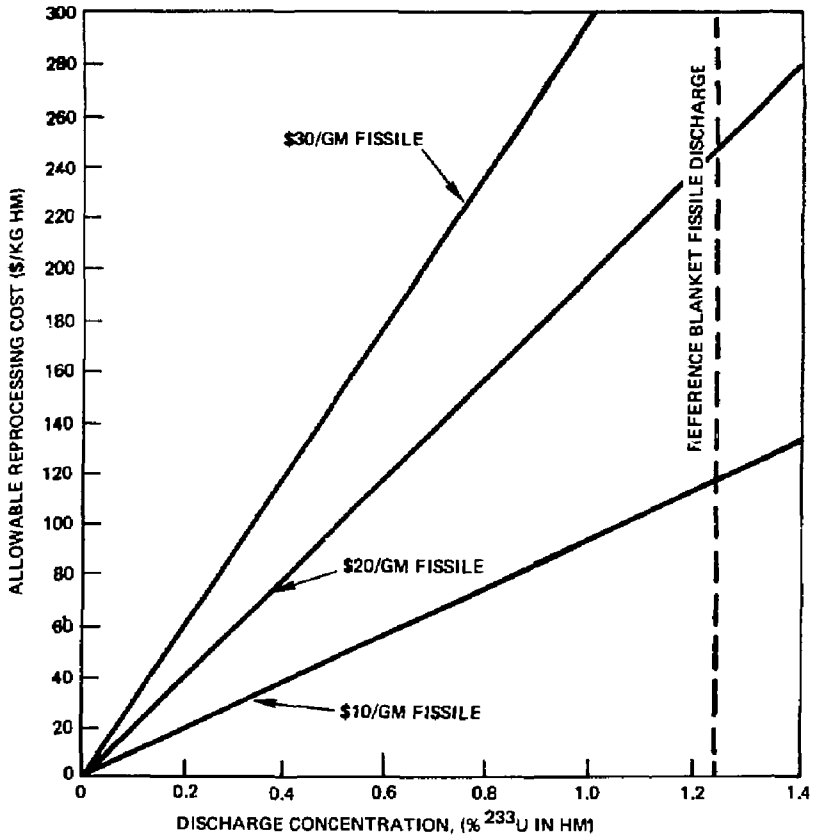

Figure VII.A.2. Allowable Reprocessing Cost to Obtain a Fixed Contribution to the Overall Cost of Bred Fuel

require a reprocessing cost of ~ 300 $/KgHM. This compares with the cost estimates(4) for THOREX reprocessing of high burnup (~ 33,000 MWD/MTHM) thorium oxide fuels for LWRs which are as high as 550 $/KgHM (1982 dollars).

Obviously, a major parameter to be optimized in the suppressed fission blanket is the discharge fissile enrichment. As the fissile enrichment builds up, so does the power density and radioactive inventory. The maximum discharge enrichment is constrained by the maximum allowable power density, the design limits of the safety and cooling systems, and the maximum tolerable high level radioactive waste inventory. The constraints on fission power density are quite low in order to limit the MHD pressure drop and capitalize on the improved safety features of suppressed fission blankets. While it is desirable to remove the bred fissile fuel at as low an enrichment as possible, it is more economical to reprocess at higher enrichments. This optimization is discussed in more detail in Chapters IV and V.

In comparison with the aqueous fuel reprocessing technologies, the pyrochemical fuel reprocessing technology for thorium metal fuels (Section VII.D) is expected to be quite inexpensive and is expected to result in a nearly insignificant contribution to the cost of bred fissile fuel. However, the development program required to assure the feasibility of this technology is a concern. The pyrochemical reprocessing technology, when adapted to the low burnup thorium metal fuel discharged by fusion breeder, is a simplification when compared to the technology requirements for fission reactors which utilize ceramic fuel forms. In particular, a simple magnesium dissolution reprocessing scheme is preferred. The magnesium dissolation technology has potential to eliminate several of the more difficult separation processes.

In addition to fuel reprocessing, a technology to manufacture and recycle the beryllium pebbles is a key to the successful development of the reference fusion breeder. In this respect, the average expected lifetime of the pebbles (estimated in Section III.C. to exceed two years) is the critical parameter which determines the required manufacture/recycle rate and associated process cost. A plant to perform this function is described in Section VII.B.

VII.A.2.b Overview of LWR Fuel Cycles and Issues

Light water power reactors are expected to dominate nuclear power production in the 2020 timeframe when the fusion breeder reactor could become commercially available. Consequently, the LWR is considered as the principal type of fission client reactor in the symbiotic electricity generation system. The cores of these reactors would be modified to accomodate new types of oxide fuels, but studies suggest that the modified cores might not differ substantially in design or operational characteristics when compared with the current generation of LWRs(5,6). The fuel cycle facilities required for modified LWR clients do, in some cases, require further development, but are not generically different than those that would be required to support other fission reactor options which require a close fuel cycle (e.g., LMFBR).

If the fuel bred in the fusion breeder is ^{233}U, three fuel cycle options are available:

- The thorium fuel cycle (typically 3.4% ^{233}U, 96.6% ^{232}Th)
- The denatured thorium fuel cycle (typically 3.3% ^{233}U, 18% ^{238}U, 78.7% ^{232}Th)
- The denatured uranium fuel cycle (typically 2.4% ^{233}U, 97.6% ^{238}U)

Among these, the thorium fuel cycle is most efficient with respect to fissile feed requirements, but the denatured fuel cycles provide some isotopic dilution and have improved intrinsic proliferation resistance.

Both the thorium and denatured thorium LWR fuel cycles will require the THOREX fuel reprocessing plant technology as well as a remote and shielded fuel fabrication technology. These technologies have not yet been developed to commercial scale and, although technically straightforward, both processes are expected to result in comparatively high costs per unit of heavy metal throughput. The denatured uranium fuel cycle requires 28% more fissile feed than the denatured thorium fuel cycle, but is compatible with the more developed PUREX reprocessing plant technology.

If the fuel bred in the fusion breeder is fissile plutonium, denatured fuel cycles are not possible and a mixture of plutonium and ^{238}U (typically 4.9% Pu_f, 95.1% ^{238}U) would be used. This fuel cycle is less efficient than

the denatured uranium fuel cycle and is also less efficient than the denatured thorium fuel cycle, but entirely circumvents both THOREX and the highly shielded ^{233}U fuel fabrication technology. It is important to note that some plutonium burners might be used even if ^{233}U is bred in the fusion breeder. That is, both the denatured thorium fuel cycle and the denatured uranium fuel cycle produce appreciable quanitites of plutonium in the ^{233}U fueled LWRs(5,6). This is a result of neutron absorption in ^{238}U with subsequent conversion to fissile plutonium. The "secondary" fissile plutonium would, most likely, be recovered and recycled in "secondary" plutonium burning LWRs which might be located with the fusion breeders within the safeguarded fuel cycle centers.

The LWR fuel cycle performance data used in the analysis provided in Section VII.A.3 and in Chapter VIII is summarized in Table VII.A.1(4,5). In this table, six LWR fuel cycles are presented. The first, for a plutonium burner with full recycle (i.e., reprocessing) interfaces to a fusion breeder which breeds fissile plutonium form fertile uranium, but also applies to the LWRs which would be used to burn excess plutonium produced in ^{233}U burners which use ^{238}U as fertile material. The second and third fuel cycles, described earlier, would each produce some excess plutonium. The fourth fuel cycle is a combination of the first and second case, (74% ^{233}U burners, 26% Pu burners) such that all fissile material is recycled. The fifth fuel cycle combines the first and third fuel cycles similarly (88% ^{233}U burners, 12% Pu burners).

Finally, the sixth fuel cycle applies to an LWR which uses natural uranium and recycles both the remaining uranium at end-of-cycle and the bred plutonium. This case was used to compare the cost of electricity for symbiotic fusion/fission system (e.g., fifth fuel cycle in Table VII.A.1) and a conventionally fueled LWR with mined uranium at near-current cost (55 $/Kg) and reprocessing. Such an analysis is presented in Chapter VIII.

Table VII.A.1 LWR Fuel Cycle Performance Data

	LWR FUEL CYCLE TYPE					
	Pu Burner	Denatured Uranium (DU)	Denatured Thorium (DT)	DU + Pu (a)	DT + Pu (b)	^{235}U Burner
Net Fissile Requirement, g/KW-yr (c)	0.200	0.205	0.144	0.153	0.126	0.194
Excess Plutonium Production, g/KW_t-yr(c)	none-recycled	0.068	0.028	none-recycled	none-recycled	none-recycled
Fuel Burnup, MWD/MTHM	30,400	33,000	33,400	32,300	33,000	30,400
Equilibrium Fissile Enrichment, atom %	4.9	2.4	3.3	3.1	3.5	3.2
Core Power Density, kW_t/KgHM	37.1	37.2	40.2	37.2	39.8	38.4
Equilibrium Fissile Inventory, g/KW_t	1.83	0.68	1.09	1.07	1.29	1.14
Net Thermal-to-Electric Efficiency, %	33.4	33.4	33.4	33.4	33.4	33.4

a) mixed system includes 74% denatured uranium fuel cycle LWRs and 26% plutonium fuel cycle LWRs

b) mixed system includes 88% denatured thorium fuel cycle LWRs and 12% plutonium fuel cycle LWRs

c) at 100% plant capacity factor

VII.A.3 Fuel Cycle Summary for Reference Fusion Breeder

In this section, important global parameters relating to fuel cycle data for the reference fusion breeder plant are presented. Overall fuel cycle parameters for both the fusion breeder and its client LWRs are also presented.

VII.A.3.a Fusion Breeder Plant Fuel Cycle Summary

A summary of fuel cycle data for the reference fusion breeder is shown in Table VII.A.2. The reference fusion breeder operates in a batch fuel reprocessing mode in which the first fuel zone is discharged at relatively frequent intervals after about 80 days of exposure when the combined (^{233}U plus ^{233}Pa) fissile concentration in thorium reaches about 1.4%. The second, or rear, zone is irradiated for twice this period such that its combined fissile concentration at discharge is 0.93%. Considering both zones altogether, the net average fissile discharge concentration is $(2 \times 1.4 + 0.93)/3 \approx 1.24$ atom percent in the thorium. A more detailed description of the fuel management mode is provided in Chapter IV.

As discussed in Section II.C and shown in Table VII.A.2, 5464 Kg/yr of fissile fuel is produced annually if the plant capacity factor is 70%. The amount of fissile material in-core (i.e., the blanket) and ex-core (i.e., the reprocessing loop) is important from the economics perspective. That is, this quantity (3816 Kg total) determines the period of time (about 0.7 year) required before the fusion breeder is able to derive revenues from the sale of its principal product - fuel. Prior to this time, the breeder sells only electricity and accumulates a negative cash flow. The magnitude of this penalty may be put into perspective by assuming that the fusion breeder does not wait the required period before fissile production, but borrows enough fuel to initially operate in steady state on an equilibrium cycle. In this hypothetical case, there is no delay, but the fusion breeder operator would be expected to carry the borrowed resource as a non-depreciating asset and pay an annual carrying over charge over the life of the plant.

Assuming typical values for bred ^{233}U of 75 \$/gm (see Chapter VIII) and a carrying charge of 8.6%/yr, the 3816 Kg inventory associated with the beryllium/thorium oxide blanket would result in a $25 \cdot 10^6$ \$/yr operating cost. Typically, over a 30 year plant lifetime, this charge would be about 2% of the overall cost of the fusion breeder plant capital.

Table VII.A.2 Fuel Cycle Summary for the Reference Fusion Breeder Plant

Thorium Inventory, MT	293
Fissile Inventories, Kg	
^{233}U + ^{233}Pa In-core[a]	1032
^{233}U + ^{233}Pa Ex-core[b]	2784
Fuel Management Mode[c]	Batch
Zone 1 Fuel Residence Time[c], yr	0.21
Zone 2 Fuel Residence Time[c], yr	0.42
Net Fissile Production[d], Kg/yr ^{233}U	5646
Average Blanket Discharge Concentrations in Thorium[a], atom %	
^{233}U	0.81
^{233}Pa	0.42
Fission Products	0.081
^{228}Th	$2.92 \cdot 10^{-7}$
^{232}U	$3.21 \cdot 10^{-4}$
Reprocessing Plant Thorium Throughput[d], MT/yr	604
Reprocessing Plant Discharge Product Concentrations[b], atom %	
^{232}U in ^{233}U	0.026
^{228}Th in Thorium	$1.7 \cdot 10^{-6}$
Beryllium Inventory, MT	885
Number of Be Pebbles	$36 \cdot 10^{6}$
Estimated Pebble Lifetime[d], yr	2
Estimated Pebble Throughput, yr^{-1}	$18 \cdot 10^{6}$
Required Be Makeup[e], MT/yr	29

a) average over fuel cycle and fuel zones
b) 0.5 yr ^{233}Pa decay to ^{233}U included
c) see Chapter IV for details
d) 70% average plant capacity factor included
e) 7% loss assumed

The larger fraction of the total fissile inventory associated with this blanket is the ex-core inventory. This quantity is based upon a six month delay prior to reprocessing to allow the fuel to cool and to allow for 99% of the ^{233}Pa to decay ($T^{1/2}$ = 27d) to ^{233}U prior to reprocessing. The smaller in-core fissile inventory results from the fertile dilute nature of the blanket (only 293 MT thorium in-core).

Concerning the thorium oxide reprocessing facility, the thorium oxide throughput for a single fusion breeder will be 604 MT/yr. This size is less than half that of typical commerical fuel reprocessing plant designs, but is equivalent to the heavy metal throughput rate of about twenty 1 GWe LWRs. Such comparisons illustrate the importance of reprocessing technologies for suppressed fission hybrid blanket concepts.

The isotopic content of fuel discharged from the reprocessing plant is important with regard to fabrication of the product ^{233}U into LWR fuel elements and recycle of the recovered ^{232}Th. In general, ^{232}U will be produced with the product ^{233}U and will decay to ^{228}Th. The daughter, ^{228}Th ($T^{1/2}$ = 1.9/yr), will lead to the generation of ^{208}Tl, which emits a 2.6 MeV gamma 36% of the time. As a result, unless fuel fabrication can be accomplished within days after reprocessing, the LWR fuel fabrication facility will require full shielding and remote operation. We have assumed that this is the case.

Similarly, ^{228}Th activity in the recovered thorium leads to a requirement for remote operation and additional shielding or, alternately, an ~ 15 year cool-off prior to hands-on refabrication. For the purpose of this study, we have assumed that a remotely maintained and fully shielded facility will be employed. If the 15 year cool-off is selected, The value of 15 years thorium throughput (or 9060 MT) at 20 $/Kg thorium, is 181 $M. Using an 18%/yr carrying charge (see Chapter VIII), the annual cost would be 32 $M/yr, or about 2% of the overall cost of the fusion breeder plant capital.

VII.A.3.b Symbiotic Electricity Generation Systems

It is of interest to define the minimum size and characteristics of a fuel cycle center which contains fusion breeders, their fuel cycle facilities, and the fuel cycle facilities associated with a self-consistent number of

client LWRs. The size of such a fuel cycle center will be determined by two constraints:

- All fuel cycle facilities should be large enough to benefit from economies of scale
- The total number of fuel cycle centers should be small (perhaps 5-10 in the U.S.)

In Figure VII.A.3, a fuel cycle center concept for the reference fusion breeder with LWR denatured thorium (and plutonium) fuel cycle clients is shown. In this configuration, three fusion breeders supply 16,900 Kg/yr of ^{233}U (70% capacity factor) to support sixty four 1 GWe LWR clients for a total electrical output of 68 GWe. The plutonium produced by 56 of the LWRs is sufficient to support an additional eight 1 GWe LWRs (or, alternatively, it could be stockpiled for LMFBR inventories). The fusion breeders each have a dedicated beryllium recycle plant and, together share a single fuel reprocessing plant of 1812 MT/yr capacity. The mixed oxide LWR reprocessing/-fabrication throughput is about 1300 MT/yr. Of this, about 70 MT/yr is asociated with the plutonium burners (i.e., PUREX) and about 1200 MT/yr is associated with the ^{233}U burners, (i.e., THOREX).

All facilities are large enough to benefit from economies of scale with the possible exception of the fuel fabrication facilities for the plutonium burners. If several such fuel cycle centers were to exist, economies of scale for the plutonium burner fuel cycle facilities could be achieved by concentrating such facilities in only one of four or five fuel cycle centers.

It is anticipated that low level wastes generated in the reprocessing and fuel fabrication facilities would be disposed on-site, but that high level wastes would be shipped elsewhere for permanent disposal. Although not shown, the facility described above would require on the order of 220 MT of mined thorium per year for makeup (8% losses assumed).

A similar fuel cycle center concept where LWR denatured uranium fuel cycle clients are utilized instead of denatured thorium fuel cycle clients has also been considered and is shown in Figure VII.A.4. In this case a smaller total of about 54 LWRs can be supported (including about 14 plutonium burners), but since none of the LWR fuel is thorium oxide based, the need for THOREX reprocessing of LWR fuel is eliminated and PUREX reprocessing (1350

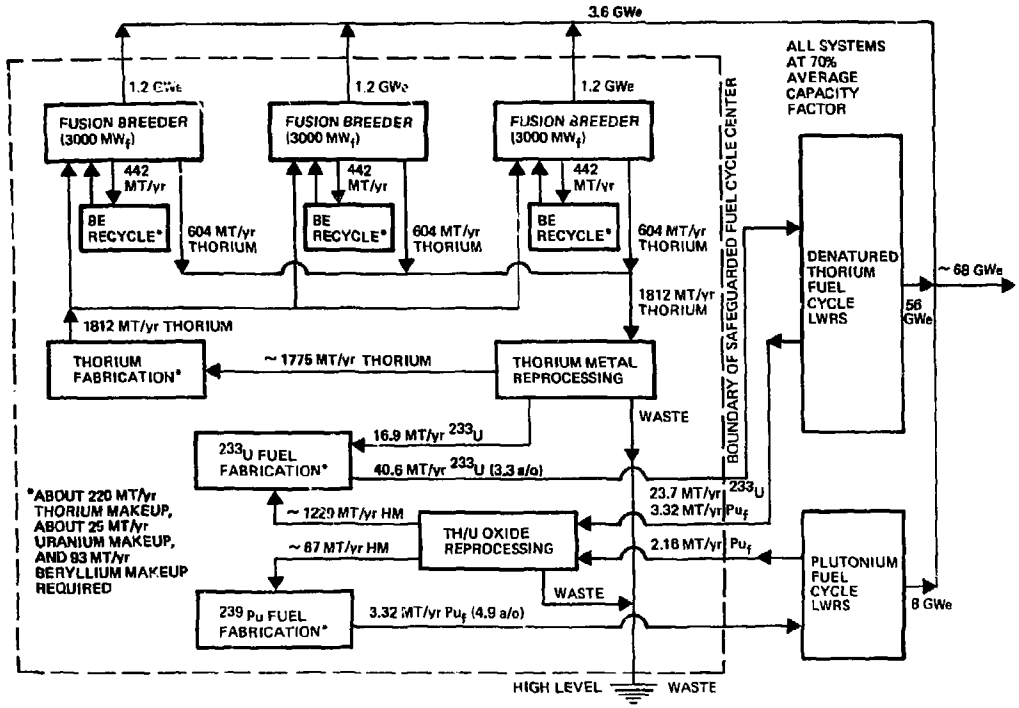

Figure VII.A.3. Symbiotic Electricity Generation System Based Upon Reference Fusion Breeder Denatured Thorium Fuel Cycle

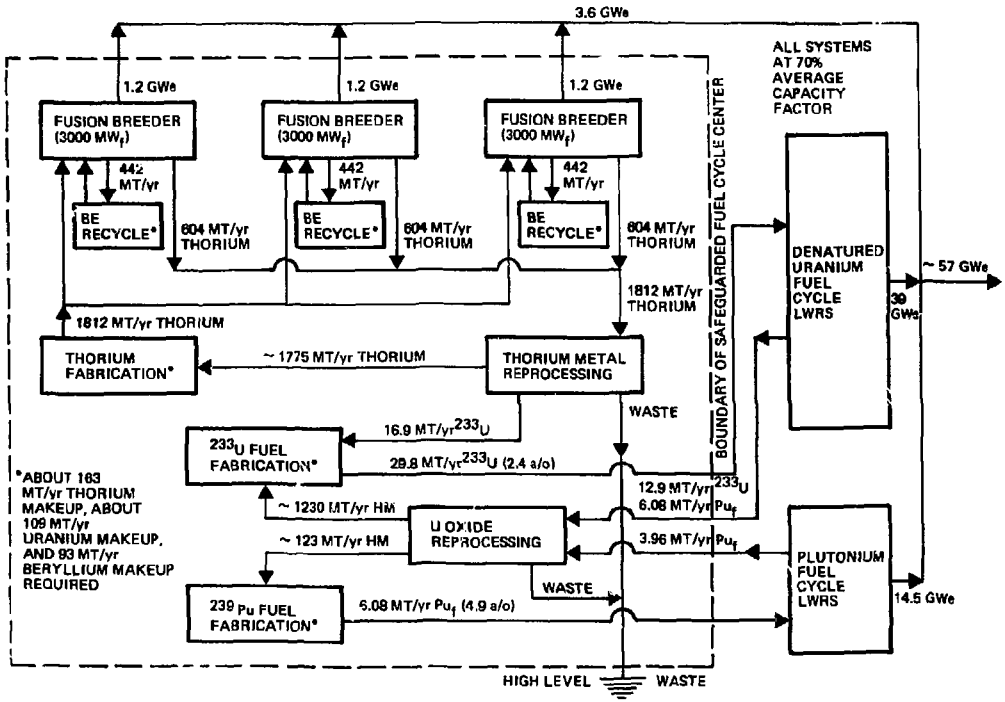

Figure VII.A.4. Symbiotic Electricity Generation System Based Upon Reference Fusion Breeder and Denatured Uranium Fuel Cycle

MT/yr uranium) can be used exclusively for these fuels. In comparison with THOREX, the PUREX process is considered to be closer to commercial viability and less expensive. The net electrical output for this three fusion breeder driven system would be 57 GWe.

References, Section VII.A

1) R.W. Conn, et al., "SOLASE-H: A Laser Fusion Hybrid Study", UWFDM-270, University of Wisconsin (1979).

2) K.R. Schultz, et al., "Preliminary Evaluation of the ^{233}U Refresh Cycle Hybrid Power System Concept", Proc. Third Topical Meeting Technology of Controlled Nuclear Fusion, Santa Fe, New Mexico, May 9-11, 1978, also see, GA-A14940, General Atomic (1978).

3) J.A. Maniscalco, et al., "Laser Fusion Breeder Design Study", DOE Contract DE-AC08-79DP40-111; TRW (1980).

4) S.L. Bogart, editor, "Proc. Section Fusion-Fission Energy Systems Review Meeting", Conf-771155, Washington, D.C., November 1977.

5) Nonproliferation Alternative Systems Assessment Program (NASAP), DOE/NE-0001, U.S. DOE (1980).

6) Y.I. Chang, et al., "Alternative Fuel Cycle Options: Performance Characteristics and Impact on Nuclear Power Growth Potential", ANL-77-70, Argonne National Laboratory (1977).

VII.B BERYLLIUM PEBBLE FABRICATION TECHNOLOGIES

In this section, the technology required to produce and recycle beryllium pebbles for the reference blanket is described. Beryllium availability is reviewed, a production process is proposed, its cost is estimated, and process development issues are discussed. The beryllium pebble design and lifetime considerations were discussed in Section III.C. The lifetime of the beryllium pebbles is presently quite uncertain (two years assumed in this analysis), but is, to a large extent, dependent upon the fabricated properties described below.

VII.B.1 Requirements

As described in Section III.C., each beryllium pebble is a solid sphere of 3 cm diameter with provision for a thorium snap ring which fits in a narrow groove on the outside circumference. The pebbles occupy two fuel zones of 20 cm each outside of the intermediate wall (See Section II.B). The volume of these two zones, for a 200 in reference central cell length, is 845 m^3. For an ~ 60% pebble packing fraction, the pebble volume is 507 m^3. Therefore, 35.9×10^6 pebbles will be required for the initial inventory. Of the total pebble volume, about 25 m^3 represents the thorium snap rings, so the net beryllium volume is about 480 m^3 or about 885 MT (1.84 g/cm^3). For a conservatively assumed average pebble lifetime of two calendar years (see Section III.C) the annual throughput through the hot beryllium fabrication plant will be $18 \cdot 10^6$ pebbles/yr or 442 MT/yr. The above quantities are summarized in Table VII.B.1.

VII.B.2 Beryllium Availability

Our FY81 assessment of long term beryllium availability(1) indicated that the amount of beryllium required for the reference blanket would represent about 3.5%. of the known beryllium reserves in the U.S. (Bureau of Mines estimate). Similarly, the same 885 MT requirement represents about 1.2% of the total estimated U.S. beryllium resource, about 0.2% of the known world beryllium reserves, and about 0.08% of the total estimated world beryllium resource.

TABLE VII.B.1 BERYLLIUM REQUIREMENTS FOR THE REFERENCE BLANKET

Total Fuel Zone Volume[a]	845 m^3
Pebble Volume[b]	507 m^3
Pebble Quantity[c]	$35.9 \cdot 10^6$
Beryllium Volume[d]	480 m^3
Thorium Volume[d]	25 m^3
Beryllium Mass[e]	885 MT
Average Beryllium Lifetime[f]	~ 2 yr
Annual Pebble Throughput	$18 \cdot 10^6$ yr^{-1}
Annual Beryllium Mass Throughput	442 MT/year

a) 200 m central cell
b) ~ 60% packing
c) 3 cm diameter pebbles
d) 2.9% of fuel zone volume is thorium
e) 1.84 g/cm^3 product density
f) conservative assumption

Our energy growth projections of the same study(1) indicated that on the order of 40 fusion breeders might eventually be built prior to 2050. On this basis we conclude that the U.S. beryllium resource will be marginally adequate for this application without a definitive requirement for imported beryllium.

Currently, the only source of Be metal in the free world is Brush Wellman. They produce $Be(OH)_2$ at a mill in Delta, Utah. The Be source is Bertrandite ore which contains ~ 4 lbs of Be/ton. Their mill produces approximately 270 MT of Be/yr. They are planning to increase production by about 60% using Chinese ore (40-50 lb of Be/ton) to satisfy their projected needs for BeO and Cu Be alloys.

Brush Wellman converts ~ 27 MT/yr of the Be from the mill in Delta to Be metal in a plant at Elmore, Ohio. They estimate the maximum capacity of the metal production capability of the plant to be ~ 115 MT/yr.

Recognizing the current production capability, it is of interest to consider Brush's capability to expand capacity. To produce one entire beryllium inventory during a four year period (i.e., for the first commercial sized fusion breeder), a beryllium requirement of 220 MT/yr would require Brush to expand operations as follows:

1. Develop a source of high grade ore (perhaps Chinese)
2. Expand the mill at Delta by 50%
3. Double the metal production capability at Elmore.

It is quite clear that the beryllium production capacity would have to be carefully coordinated with fusion breeder development to assure that a supply bottleneck does not occur.

VII.B.3 Fabrication Process

The selected pebble fabrication process involves the development of an automated line which will cold press pebbles, vacuum sinter them, hot forge them to full density, and vacuum anneal them. Brush currently uses the first three steps of this process to produce aircraft brake segments - the only difference is that the process is manually operated because current Be powder is not free flowing and amenable to automated operations. In order to automate this process, a free flowing Be powder is required.

The brake parts produced by Brush have properties as good or better than S-200-E.

Ultimate tensile strength	40 ksi
Yield strength	30 ksi
Elongation (%)	1
Density	1.84 g/cc

We do not expect a free flowing powder to degrade these mechanical properties. In fact, using some of the manufacturing processing currently being discussed with Brush, both the tensile strength and elongation would be expected to increase.

The equipment needed for production is simple: mechanical presses and powder feeders to make cold pressed compacts, automated vacuum sintering furnaces for pressureless sintering, mechanical presses for hot sizing the sintered compacts, an automated vacuum furnace for annealing the forged compact and an automated mill to machine the fuel snap ring groove to final dimensions.

For fabrication of pebbles too damaged to reinsert into the blanket after an irradiation period, we would vacuum melt the hot pebbles and use an automated atomization process (modeled after the Brush Wellman process) to first re-manufacture the beryllium powder prior to the cold press step. The entire process will require provision for shielding and remote maintainability. In addition, hooding requirements as per OSHA limits (2 μ g/m^3) must be maintained to limit airborne contaimination. A beryllium decontamination step (e.g., electro-refining) is not assumed, but might simplify the shielding and remoting requirements.

Given a two year beryllium lifetime, and assuming an automated plant which operates 24 hours/day, 7 days/week, and is operating 85% of the time with no rejects, the production rate will be 240 balls per minute. While this is a very high production rate for Be parts, it is very low for some powder metal industries (e.g., Ta capacitor manufacturers produce thousands of parts/minute). The beryllium reprocessing line is estimated to lose 7-10% of the beryllium throughput, so a small feedstream is required.

As an alternative, lower density parts can be made by cold pressing and sintering. If the parts are sintered to 90% of the theoretical density they are predicted to have 70-80% of their full density conductivity. Some 90% dense Be parts made in this manner are currently being tested at LLNL. These will be characterized with respect to mechanical properties, porosity, etc. It is possible that the lower density parts will have lower swelling and, consequently, longer life.

VII.B.4 Process Cost Estimate

The process components and their estimated cost are listed below:

	Process Components	Cost
8	Presses with feeders	3.2
4	Sintering furances	1.6
4	Sizing Presses	1.6
4	Annealing Furnaces	1.6
4	Milling Machines	1.6
	Transfer line	2.4
	Air handling, filters, etc.	4.0
	Subtotal	16.0
	Remoting (100%)	16.0
	TOTAL	$32.0 M

The above equipment is sufficient to produce or recycle the entire beryllium inventory in two years. The cost attributed to remoting the process is a guess.

There will also be an operating cost associated with operation of the above equipment. This cost is, we believe, conservatively estimated to be about $0.25 per pebble ($9 M for the initial inventory, $4.5 M/year for refabrication).

Finally, the cost of fine commercial grade beryllium is estimated to be 330 $/Kg ($292 M for the initial inventory, $10 M/year to make up for the 7% loss and two year average lifetime).

VII.B.5 Development Issues

The only special equipment needed for the process line is the air handling system needed to contain the Be powder. The die life should be comparable to other powder metallurgy products (500,000 - 1,000,000 parts/die with punches redressed every ~ 50,000 parts).

Production of a free flowing Be powder suitable for automated operations requires further development. This might be achieved by a new powder manufacturing technique at Brush Wellman (spherical powder) or the use of binders which can be totally removed during a bake-out prior to sintering.

Development of a pressing technique which produces a uniform dense sphere with a groove on the outside which can be pressureless sintered to 90-95% of theoretical density is also required. The pressed sphere must be strong enough to permit automated handling.

References, Section VII.B

1) J.D. Lee, et. al., "Feasibility Study of a Fission Suppressed Tandem Mirror Hybrid Reactor", UCID-19327, Lawrence Livermore National Laboratory (1982).

VII.C URANIUM REPROCESSING PLANT

Although the reference blanket utilizes a thorium metal fuel form to breed ^{233}U, this design could be modified to breed ^{239}Pu from uranium carbide. As such, we have investigated the possible fuel cycle applications of such a choice with concentration on the most important fuel cycle technology -- breeder fuel reprocessing. In this section we present a conceptual design and costing estimate for a PUREX reprocessing plant which would be dedicated to the recovery of plutonium from low burnup fuels discharged from a fusion breeder. This study complements a THOREX reprocessing plant study for thorium metal fuels performed during 1980 and some comparisons are drawn.

In the PUREX assessment, the design basis plant was sized to allow processing of 1030 metric tons per year of uranium in the form of carbide at an instantaneous rate of 4 MT/day. The economic scaling factor for larger and smaller plants was also estimated. The fusion breeder reactor, reprocessing plant, and uranium carbide fabrication plant were assumed to be colocated on-site. The fission reactor fuel fabrication plant is optionally on- or off-site.

The purposes of the PUREX reprocessing plant in the suppressed fission/fusion breeder system are to recover the fissile ^{239}Pu from the irradiated uranium carbide blanket; to transfer the purified plutonium product to either an onsite or offsite fission reactor fuel fabricator; to transfer the uranyl nitrate product to uranium carbide blanket refabrication; and to treat, solidify, and package the high-level waste stream for repository disposal. The U/Pu fuel cycle is shown in Fig. VII.C.1 and the basic functions of the reprocessing plant and their inter-relations is shown in Fig. VII.C.2.

VII.C.1 Reprocessing Plant Design Basis

VII.C.1.a Battery Limits. The irradiated fuel storage facilities at the site are not part of the reprocessing plant. Rather, facilities to provide four months of cooling between reactor discharge and chemical processing

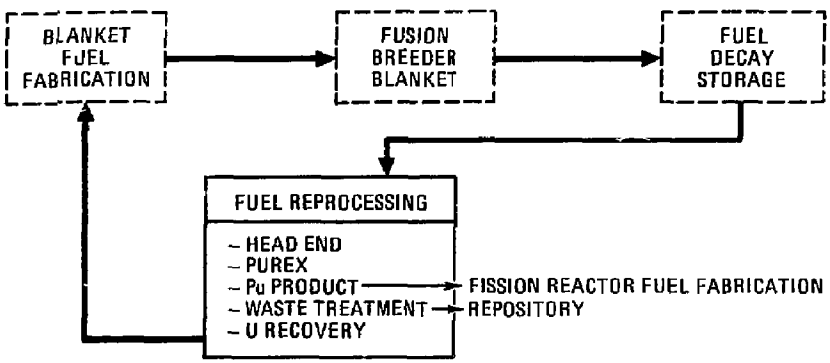

Fig. VII.C.1 U/Pu fuel cycle.

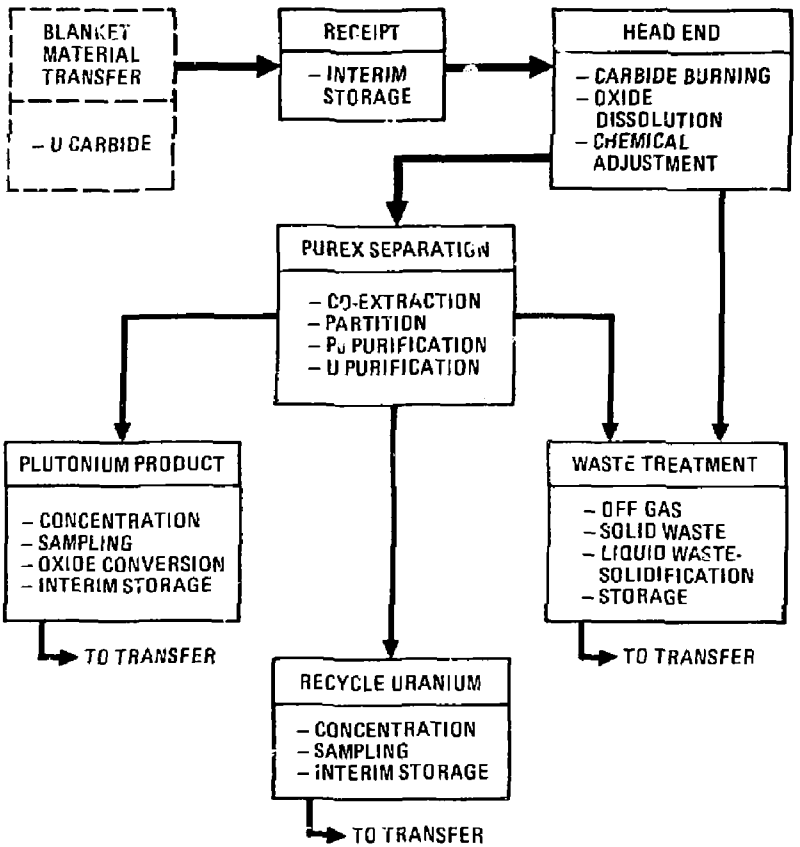

Fig. VII.C.2. Purex reprocessing.

are part of the reactor design. Transfer of the irradiated fuel to the reprocessing plant will be done in a batch operation.

The high-level and intermediate-level liquid waste produced in the reprocessing plant will be concentrated, stored for five years, and solidified prior to shipment to a Federal repository. Radioactive solid-waste (e.g., spent-filters, resin-beds, failed-equipment) and low-level liquid waste will be transferred to a waste management facility which services the entire complex.

The recovered uranium will be transferred to the on-site uranium carbide fabrication plant as a concentrated uranyl nitrate solution via a double-walled pipeline. The recovered plutonium will also be transferred to the on-site fission reactor fuel fabrication plant as a ion-concentrated nitrate solution via a double-wall pipeline. An option for producing plutonium dioxide for off-site shipment is included.

VII.C.1.b Reference Plant and Flowsheet. Several plant designs and flowsheets were surveyed and a composite reference was selected. To the extent compatible, the fission-fusion hybrid reprocessing plant design, the flowsheet, the equipment, and the operating mode will parallel that described in Ref. 1 and is based upon the Barnwell Nuclear Fuel Plant (BNFP) design (2).

Table VII.C.1 lists the design constraints for the fission-fusion hybrid reprocessing plant. These design bases are related to the throughput, irradiated fuel characteristics, product specifications, effluent limits, allowable personnel exposures, and structural design criteria. Of the product specifications shown in Table VII.C.1, the recovery factors have little impact on cost. Relaxation of the uranium and plutonium product specifications to give products requiring remote refabrication and having a factor of 10 increase in cross contamination would lower the plant cost but the lower cost could probably not justify the remote refabrication costs. This would be especially true if glovebox fabrication of low exposure plutonium becomes possible in the near future.

VII.C.1.c Operation and Maintenance. The hybrid fuel reprocessing plant is envisioned to employ a combination of maintenance philosophies similar to

TABLE VII.C.1 Plant Design Basis

Operating period	255 days/year
Throughput:	
Overall	1030 MTHM/year
Head-end	4 MTHM/day
Solvent extraction	
Coextraction	4 MTHM/day
Plutonium purification	44 kg HM/day
Feed characteristics	
Physical and chemical	Uranium carbide cylinders
	0.7 cm diameter
	Containing 1.08% Pu
	0.038% Np
	Burnup 0.096%
Plutonium product isotopic composition:	
Pu-236	0.00028%
Pu-238	0.068%
Pu-239	98.2%
Pu-240	1.6%
Pu-241	0.15%
Minimum cooling time	120 days
Product specifications:	
Recovery factors	99% of uranium
	99% of plutonium
Uranium product	<10 ppb plutonium
	10^7 FP DF[a]
Plutonium product	<1000 ppm uranium
	10^6 FP DF[a]

TABLE VII.C.1 (Continued)

Effluent limits	
Liquid	No discharge of radioactive liquids
Gas	Volatile FPs separated from uranium carbide burner off-gas krypton released
Solid	High-level waste to be converted to boro silicate glass within three years after separation.

[a]FP DF = fission product decontamination factor.

those used in recently constructed or designed LWR reprocessing plants (1,2,3). This consists of placing all equipment associated with high levels of gamma radiation in fully remote cells. Equipment exposed to intermediate levels of gamma radiation is located in semi-remote cells where both remote and some contact maintenance work can be performed. Contact maintenance is utilized where no or low radiation levels are present or where radioactive materials are well confined and shielded (e.g., storage areas).

Due to the radioactivity associated with the uranium and plutonium, remote operation is used throughout the plant in the conceptual design. However, detailed calculations of dose rate should be made for the plutonium isotopes to determine if the added cost is warranted for the plutonium nitrate to oxide conversion line. All instrument readout and control locations will be separated and shielded from the process equipment.

Proliferation deterrence for this reprocessing plant is provided by hardened physical protection (guards, double-fenced site, remote sensing equipment, etc.) and material accountability systems. The plutonium is partitioned from the uranium. This allows smaller and cheaper plutonium purification and conversion systems. Processing plutonium products mixed with uranium does not improve proliferation resistance of plutonium other than by increasing the weight. Physical protection is considered the only satisfactory way to safeguard this material.

VII.C.1.d Plant Description. The process flowsheet is shown in Fig. VII.C.3 and a description of the various streams is provided in Table VII.C.2. In addition to the systems detailed in Fig. VII.C.3, the plant also contains the following systems: off-gas treatment solvent recovery, acid and water recovery and make-up, waste treatment, ventilation, process cooling and heating, and waste storage facilities. Complete material balances were not calculated, however, the flowsheet was derived from previously determined flowsheets (2,3) so that the range of flowrates and conditions could be estimated to specify equipment and facility size, layout, and cost.

The lithium wetted uranium carbide cylinders are loaded from the reactor storage compartments into cylindrical tubes and transferred to interim dry storage in the reprocessing plant (1). All transfer operations

TABLE VII.C.2 Process Flowsheet Streams Identification

Stream Number	Identification	Description
1	Uranium carbide cylinder transfer	Unclean lithium contaminated spheres
2	Oxygen	--
3	U_3O_8 dissolver feed	Oxidized uranium carbide
4	Dissolver chemicals	~5 M HNO_3
5	Dissolver solution	~1.3 M uranyl nitrate
6	Clarified dissolver solution	--
7	Chemical adjustment	Water or acid
8	High activity feed	U, Pu, FPs in ~1 M HNO_3
9	Nitric acid scrub with neptunium reagent	~2 M HNO_3-sulfanic acid
10	Organic solvent from waste recovery column	30% Tributyl phosphate in hydrocarbon diluent
11	Centrifuged solids	--
12	Clean organic solvent	30% Tributyl phosphate in hydrocarbon diluent
13	Loaded organic solvent	Uranium plus plutonium
14	High-level waste	FPs in HNO_3
15	Plutonium-reducing strip	Hydroxylamine nitrate or ferrous sulfanate in 0.1 M HNO_3
16	Clean organic solvent	30% TBP
17	Loaded organic	Uranium only (plutonium removal)
18	Plutonium nitrate stream	Plutonium III nitrate
19	Uranium strip solution	0.01 M HNO_3
20	Organic raffinate	30% TBP
21	Uranyl nitrate solution	--
22	IC concentrator overheads	--
23	Concentrated uranyl nitrate	~2 M HNO_3
24	Nitric acid scrub with plutronium-reducing reagent	~0.5 M HNO_3 hydrorylamine

TABLE VII.C.2 (Continued)

Stream Number	Identification	Description
25	Clean organic solvent	30% TBP
26	2D column waste to recycle reagent to kill plutonium reducing agent in 24	--
27	Loaded organic uranium only	--
28	Uranium strip solution	0.01 M HNO_3
29	Uranyl nitrate solution	--
30	Recycle organic	30% TBP
31	Uranium product concentrator overheads	0.01 M HNO_3
32	Uranium product	~2 M UNH
33	Clean solvent	30% TBP
34	Nitrous acid	--
35	Plutonium IV nitrate feed to 2A column	--
36	HNO_3 scrub	~2 M HNO_3
37	Plutonium loaded solvent	--
38	2A column raffinate	--
40	Plutonium strip solution	0.3 M HNO_3
41	Recycle organic	30% TBP
42	Plutonium nitrate product (uranium free)	--
43	Concentrated plutonium nitrate product	~1 M plutonium nitrate
44	Oxalic acid solution	--
45	Filter wash water	--
46	Plutonium oxalate filtrate	--
47	Oxidizer solution	--
48	Oxalate-free filtrate	--
49	Plutonium oxalate cake	--
50	Plutonium oxide	
51	1R column feed (combined aqueous wastes)	
52	Clean solvent	30% TBP
53	1R column raffinate	

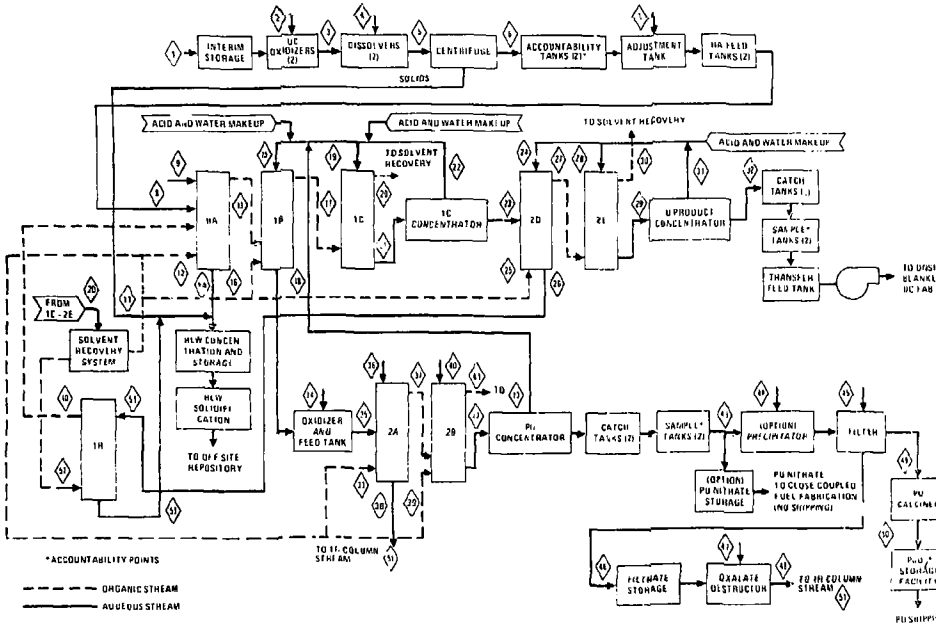

Fig. VII.C.3 Process flow sheet

are carried out in a dry inert atmosphere to prevent lithium and uranium carbide reactions. The cylinders are removed from dry storage and placed in the rotary kiln oxidizer where the lithium metal and uranium carbide are converted to the oxides. The oxygen addition <2> and temperature are controlled to regulate the oxidation rate. The resultant oxides <3> are metered to a continuous dissolver to which is fed 5 M HNO_3 acid <4>. The dissolver solution <5> overflows through a continuous centrifuge. The centrifuged solution <6> overflows to accountability tanks. The solids are transferred back to the dissolver. Occasionally, washed, solids will be transferred to the high level waste when insolubles build up to an intolerable level for recycle. From the accountability tanks, the solution is transferred to the feed adjustment tank where acid and water is added to give consistent feed composition for the solvent extraction separation. The solvent extraction feed <8> is metered to the first extraction cycle (HA) pulse column centerline where the uranium and plutonium are extracted into an organic phase <12> [30% tri-n-butyl phosphate (TBP) in normal parafin hydrocarbon (NPH) diluent]. The majority of the fission products (FPs) and other impurities remain in the aqueous raffinate stream <14> and are routed to the high-level waste (HLW) concentrator. The organic phase passes through the scrub section where a dilute acid stream <9> removes most of the extracted fission products. The uranium and plutonium-loaded solvent <13> overflows to a centerfeed on the partition (1B) pulse column where a dilute acid stream with a chemical reducing agent added <15> reduces and strips the plutonium from the solvent. (AGNS Plant substitutes electrolysis for the chemical-reducing agent.) A low flow 30% TBP stream <16> extracts most of the uranium stripped with the plutonium. The solvent stream <17> loaded with uranium is stripped in the 1C column with very dilute acid <19> and concentrated <21> to make feed for the final uranium cycle <23>. The condensate from the reprocessing plant concentrators is recycled back through catch tanks to various process streams to lower or eliminate aqueous effluents from the plant.

The final uranium cycle (2D-2E columns) repeats the first extraction, scrub strip sequence to further purify the uranum. Here the chemical reducing agent is added to the scrub stream <24> to lower the plutonium content

of the uranium to allow direct handling refabrication of the uranyl nitrate to blanket uranium carbide.

The plutonium solution from the first cycle <18> is mixed in a critically safe tank with an oxidant to allow re-extraction of the plutonium. The plutonium then goes through another extraction-scrub-strip cycle (2A-2B columns) which removes the fission products to a low enough level for glove box fabrication of the fission reactor fuel elements. Additional uranium separation can be gained, if desired, by adding plutonium-reducing agent to stream <40> and back extracting the uranium with 30% TBP <39>.

The plutonium product is concentrated, sampled for accountability, and goes to storage for transfer to an on-site fission reactor fuel fabrication plant or as an option <43> converted to plutonium oxide using the standard oxalate precepitation, calciration process. The plutonium nitrate is mixed with oxalic acid <44>, filtered, and washed <45>. The moist cake is transferred to a calciner where it is converted to the dioxide which is sampled for accountability and stored prior to shipment. All aqueous waste solutions are back cycled to the waste recovery (1R) pulse column. The 30% TBP stream which extracts the residual uranium and plutonium is then routed back to the first cycle extraction (HA) column.

In addition to the process described above, the plant will also include systems for off-gas treatment, solvent recovery, acid and water recovery, high-level waste concentration, storage and solidification, building ventilation, and process heating and cooling. A detailed description of these systems is not provided, since they are similar to systems in previous fuel reprocessing plant designs (2). The decreased burn-up of these fuels may allow some reduction in the size of the HLW solidification system and decrease the requirements of the off-gas system, but the size of most auxiliaries will be dictated by plant capacity and not radiation levels.

VII.C.1.e Process Equipment and Facilities. The equipment required for the reprocessing flowsheet described in the previous section is similar to that of the Barnwell Nuclear Fuel Plant (2).

The equipment will be fabricated from 304 stainless steel with the exception of the plutonium nitrate concentrator which will be fabricated of

titanium. A brief description of the major components in each major system of the reprocessing plant is provided in Table VII.C.3.

The layout of the blanket reprocessing facility is shown in Fig. VII.C.4. The materials are reinforced concrete with stainless steel liners inside the cell so the cells can be completely decontaminated. The cell wall thicknesses shown in Fig. VII.C.4 are for low burnup fuel. The concentrated high level waste solution is the controlling factor in the cell wall thickness. The 4 ft wall between cells will permit contact maintenance in one cell without decontamination of the neighboring remote cells being necessary. Higher burnup fuels would required walls up to 6 to 7 ft thick.

The remote process cell contains the interim dry storage, the uranium carbide oxidizer and its dedicated off-gas system, the dissolver system, and the centrifuge. All operations and maintenance in this cell are performed remotely.

The high-level cell contains the feed accountability tanks, adjustment tanks, and transfer tanks. The cell is designed for remote operation and contact maintenance after process fluid removal and decontamination of the equipment.

The waste process cell contains the first cycle extraction (HA) column, the waste concentrator, the waste liquid transfer system to and from underground storage, the waste calciner, the glass melter, the canned waste glass storage and its transfer system for shipment. This cell is remotely operated and maintained.

The intermediate level cell houses the partition (1B), uranium strip (1C) and waste recovery (1R) columns, the uranium intercycle concentrator, and their associated piping and auxiliary equipment. This cell also contains the balance-of-plant off-gas treatment and solvent recovery system. The cell is remotely operated and contact maintained.

The uranium process cell contains the second column uranium extraction and strip (2D and 2E) columns, and the uranium product concentrator. This cell is also remotely operated and contact maintained.

The plutonium process cell contains the plutonium oxidizer tank, the second cycle plutonium extraction and strip (2A and 2B) columns, and the plutonium product concentrator. This cell is remotely operated and contact

TABLE VII.C.3 Reprocessing Plant Components

Component	Description
1. Head End	
Fuel receiving	Batch transfer: cylindrical can with removable sealed fittings.
Interim storage	Dry inert gas.
Accountability	Can count-check against reactor accountability.
Uranium carbide oxidizer	Rotary kiln (ORNL voloxidizer design starting point) (off-gas collects semi-volatiles, tritium, and krypton released).
2. Feed Preparation	
Dissolution	Feed hoppers - continuous dissolver (BNFP).
Centrifuge	Continuous-vertical-solids recycle to dissolver.
Accountability	Tanks with weight, gamma, and neutron interrogation with wet chemical backup.
Feed adjustment	Tank
Solvent extraction feed	Two tanks with instrumented liquid level.
3. Solvent Extraction	
Pulse columns and associated equipment	(1) Large coextraction column (1) Large partition column (1) Large uranium stripping column (2) Large uranium purification columns (2) Small plutonium purification columns (1) Medium recovery column (1) Uranium intercycle concentrator
4. Uranium Product Concentration Concentration and Sampling	(1) Uranium product concentrator (2) Uranium product catch tank (1) Uranium produce sample accountability tanks (1) Transfer system

TABLE VII.C.3 (Continued)

Component	Description
5. Plutonium Product Concentration	
Concentration and sampling	(1) Plutonium product concentrator (2) Plutonium product catch tank (1) Plutonium product sample accountability tank (3) Plutonium product storage tanks (1) Plutonium product transfer system
6. Plutonium Product Oxide conversion	
Precipitation, calcination, rework	(1) Oxalate precipitator (1) Filter system (1) Plutonium oxalate calciner (1) plutonium oxide storage area (1) Oxalate kill tank
7. Off-Gas Treatment	
UC oxidizer off-gas (BOG)	Particulate, tritium, ruthenium, cesium iodine
Dissolver off-gas (DOG)	Nitrogen oxides and iodine
Vessel-off-gas (VOG)	HEPA filtration
8. Acid Recovery	
Capture, treatment, and make up	Concentrator, fractionator, and catch tanks
9. Solvent Recovery Treatment and Makeup	Filtration wash column catch and feed tanks
10. High-Level Waste Treatment	
Concentration storage and solidification	- Waste feed tanks, concentrator - Underground storage tanks - Calciner and glass melter
11. Low-Level Waste Treatment	
Collection and transfer	Compactor, transfer system, etc.

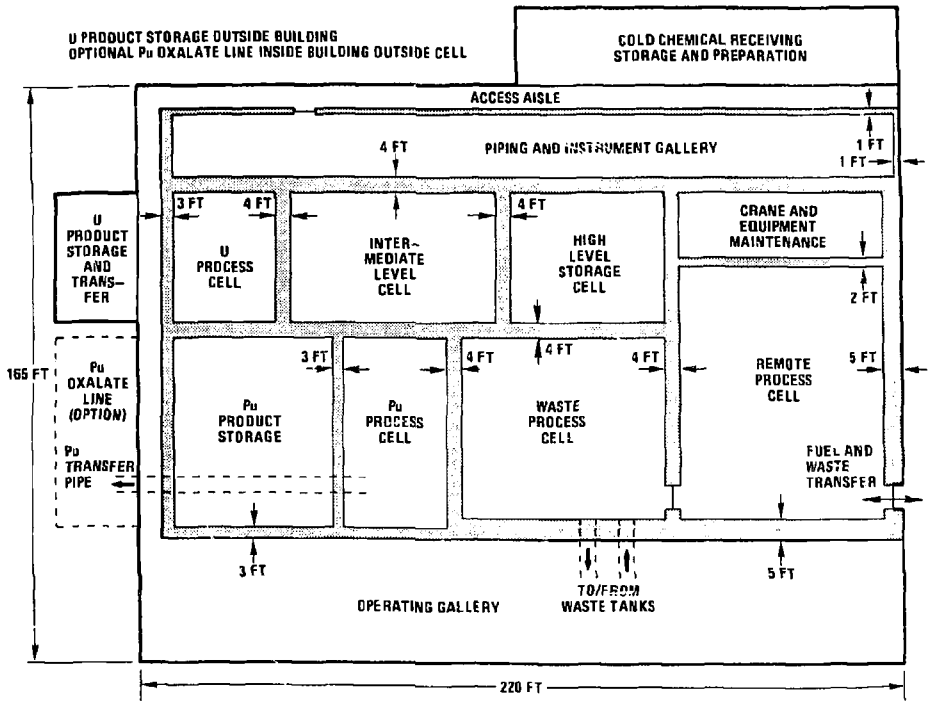

Figure VII.C.4 PUREX Facility Layout

maintained with special double containment features in selected areas to improve plutonium containment.

The plutonium product-storage cell contains either racks for PuO_2 storage or slab tanks for plutonium nitrate storage, depending upon product option selected. This cell is remotely operated and contact maintained. Special safeguard systems are employed. The plutonium oxide conversion is a special glove box line, outside the shielded cells which are partially remotely operated, but contact maintained. This area also has special safeguard systems.

The uranium nitrate storage tanks are outside the cell. This solution storage and transfer area is directly operated and contact maintained.

VII.C.2 Cost

The total equipment, facility, and operating costs for the reprocessing facility were estimated. These costs were estimated on a modular basis in a manner similar to that described in Ref. 1. The capital and operating costs are estimated for 1982 dollars (and of the first quarter). These capital costs include direct material costs, field labor costs, field distributable costs, engineering services costs, and a 20% contingency, but do not include cost of capital or site land. The annual operating costs include labor, consumables, utilities, equipment replacement, and waste disposal, but do not include taxes or the eventual cost of plant decommissioning.

Table VII.C.4 provides a breakdown of the capital cost by Equipment Section and includes the conversion factor for plant size. Table VII.C.5 provides the breakdown of the annual operating cost and the conversion factor for plant size.

Not utilizing the plutonium oxide conversion option will lower the capital cost of the 1030 MTHM/year facility by 35 million and lower the annual operating cost by 2 million.

VII.C.3 Development Requirements

The only major development effort required prior to design and construction of the U/Pu blanket reprocessing facility would be complete

Table VII.C.4 Uranium Carbide Blanket Reprocessing Plant Equipment and Facility Cost (1030 MTHM/year)

Equipment Section	Cost 1982 Dollars (Millions)[a]
Receiving and storage	84
Uranium carbide oxidizers and off-gas	70
Dissolvers and centrifuge (includes feed storage)	56
Solvent extraction (includes solvent washing and intercycle uranium concentration	50
Acid and water recovery	20
High-level waste treatment, storage, and shipping capability	120
Uranium product concentration and storage	11
Plutonium product concentration and storage	14
Δ plutonium product oxide conversion (optional)	35
Balance-of-plant	280
Total equipment and facility	740[b]

[a]End of first quarter

[b]Equipment facility total for 515 MTHM/year plant = 475

1545 MTHM/year plant = 960

or (size factor) $^{0.64}$ = cost factor.

TABLE VII.C.5 Reprocessing Plant Uranium Carbide Blanket Annual Operating Cost (1030 MTHM/Year)

Cost Component	Cost 1982 Dollars (Millions)[a]
Labor (400 @ 55K/year)	22
Consumables	6
Utilities	9
Equipment replacement	8
Waste disposal	12
Total annual operating cost	57[b]

[a]End of first quarter.
[b]Annual operating cost total for
515 MTHM/year = 38
1545 MTHM/year = 72
or (size factor)$^{0.57}$ = cost factor.

The annual operating costs have a slightly lower power function than the equipment and facility costs because of the small change in labor force with plant size.

prototypic demonstration of the uranium carbide oxidizer and off-gas system. Questions concerning operability, heating, and cooling of a rotary kiln burning uranium carbide cylinder need to be answered. The considerable development effort expended at ORNL on the UO_2 voloxidizer would be used as a starting point in this development activity (4).

The uranium carbide oxidizers will not be required if uranium dioxide is used as the target material. Some savings in capital and operating costs could be achieved if the oxidizers were not required. This savings would be about 7% of total costs.

The centrifuge can be removed from this facility design if clean dissolution of oxidized irradiated uranium carbide fertile materials can be demonstrated.

VII.C.4 Comparisons with Thorium Blanket Reprocessing

The capital and operating costs were estimated earlier for aqueous reprocessing of thorium metal spheres to recover the fissile uranium-233 isotope (5).

The cost estimate for the thorium blanket agrees fairly well with this current estimate with the following differences:

1. The thorium reprocessing estimate assumed that the throughput of auxiliary systems would be greatly reduced due to the lower burnup of thorium targets when compared to LWR fuel reprocessing (page 8-17 of Ref. 5). In the current U/Pu estimate it was assumed the auxiliaries' throughput was controlled by plant heavy metal throughput, except for the volume of concentrated and solidified high-level waste.

2. The centrifuge was not remotely maintained in the thorium case and is the U/Pu case. Historically, attempts to contact and maintain centrifuges has met with great difficulty. The Idaho Chemical Plant experience has shown that centrifuges must be remotely maintained.

3. Thorium underwent only one solvent extraction cycle in the thorium case-study. Meeting the 99.5% recovery of uranium would be difficult without a second thorium cycle which has uranium separation capabilities built into it. Uranium thorium partitioning at startup is difficult and considerable rework would be required to meet an average 99.5% uranium recovery

without backup partitioning capability (6). Both uranium and plutonium solvent extraction have two cycles in solvent extraction.

4. The thorium study listed the feed adjustment system as a tank. However, it is actually a high-temperature (135°C) concentrator system which should be remotely maintained.

5. The cost estimate for uranium/plutonium waste treatment is considerably higher than that in the earlier thorium reprocessing case. The reason for the apparently low estimate for the thorium/uranium waste treatment is unknown. All the necessary equipment was included in the equipment list.

VII.C.5 Isotope Considerations

The 2.8 ppm ^{236}Pu at reactor discharge will cause buildup in gamma activity of the plutonium product with time after separation from the uranium and thorium daughters in the reprocessing plant. The buildup of the ^{236}Pu daughter ^{232}U in the depleted uranium recycled to the blanket will in time require that some of the uranium be diverted to other uses such as fission reactor fuel systems to allow continued hands-on refabrication of both blanket and fuel materials.

The estimates for dose rates for 1 kg of material as a function of time are shown in Table VII.C.6. It can be seen from these estimates that it is important to operate the fusion blanket in a manner which will maintain low ^{236}Pu content in the bred plutonium.

TABLE VII.C.6 Estimated Dose Rates for Separated Plutonium and Uranium Products[a]

Time After Separation (Days)	Dose Rate at 1 ft for 1 kg of Product[b] (mr/hour)	
	Plutonium	Uranium
10	0.02	--
35	0.7	--
180	4	0.01
365	20	0.08
3650	230	0.2

[a]120-day cooling before separation; 2.8 ppm Pu^{236} at reactor discharge.
[b]No self shielding assumed; dose rate from 2.6 MeV gamma Tl^{208}.

References, Section VII.C

1) "*The Economics of Reprocessing* Alternative Nuclear Fuels," Exxon Nuclear Company, Inc., ORNL/Sub-7501/4, Oak Ridge National Laboratory 1979.
2) "Barnwell Nuclear Fuel Plant Final Safety Analysis Report," Allied-General Nuclear Services, Docket #50-332 (1973)
3) "Barnwell Nuclear Fuels Plant Applicability Study," U.S. Department of Energy, DOE/ET/0043/3, Washington, D.C. (1978).
4) Private communication, M.E. Whatley, ORNL, July 8, 1982.
5) "Laser Fusion Driven Breeder Design Study," Final Report, TRW (December 1980).
6) R.R. Jackson and R.L. Walser, ed., "Purex Process Operation and Performance - 1970 Thoria Campaign," ARH 2127, Atlantic Richfield Hanford Company (1977).

VII.D PYROCHEMICAL REPROCESSING

VII.D.1 Introduction

One of the options presently being considered for utilization of the neutrons obtained from D-T fusion is absorption of slow neutrons (after multiplication and moderation in a beryllium lattice) in a blanket of fertile thorium metal. Since the fission cross-section of ^{232}Th is negligibly low below the fission threshold of approximately 0.4 MeV, the amount of fission products present in such a breeding blanket are a direct function of the level of ^{233}U that is allowed to build up in the blanket. If a simple, inexpensive uranium recovery process can be achieved, the uranium concentration, and hence the level of fission in the blanket, can be held to a very low value. Although the presence of even small quantities of young fission products in the material to be processed dictates that the processing must be performed by remote means, it is possible to recover the uranium fraction without performing a specific chemical separation to remove fission products first.

We have carefully evaluated several processes that might be suitable for uranium recovery from thorium metal, and have chosen two that hold great promise. Both are simple non-aqueous methods that can readily be performed by remote means, and both require only a few simple process steps.

Our first choice for uranium recovery is a process that exploits the high solubility of thorium, and the low solubility of uranium, in molten magnesium. Uranium metal is essentially insoluble in both pure magnesium and magnesium-thorium alloys while thorium is quite soluble (see Figures VII.D-1 to VII.D-4). We propose to utilize thorium metal directly from the blanket, which may contain from 0.5 to 1.5% uranium-233 plus a small quantity of fission products, and dissolve it in a bath of molten magnesium. The uranium contained in the original blanket will be essentially insoluble in the melt at 950 K (677°C) and exist as β-uranium metal. At 950 K the solubility of uranium in 33 wt% th-67 wt% Mg alloy is 1.6×10^{-5} moles/mole solvent[1,2,3,4], or 0.032 wt% of the thorium in the solvent. If we assume 0.94 wt% ^{233}U build-up in the alloy, the uranium remaining dissolved in the solvent would be 3.4% of the initial uranium present. Essentially all of this ^{233}U can be recovered by scavenging the solvent alloy with an equal mass of ^{238}U, thereby diluting the isotopic purity to 50% ^{233}U. As safeguards regulations will probably require isotopic dilution prior to shipment of

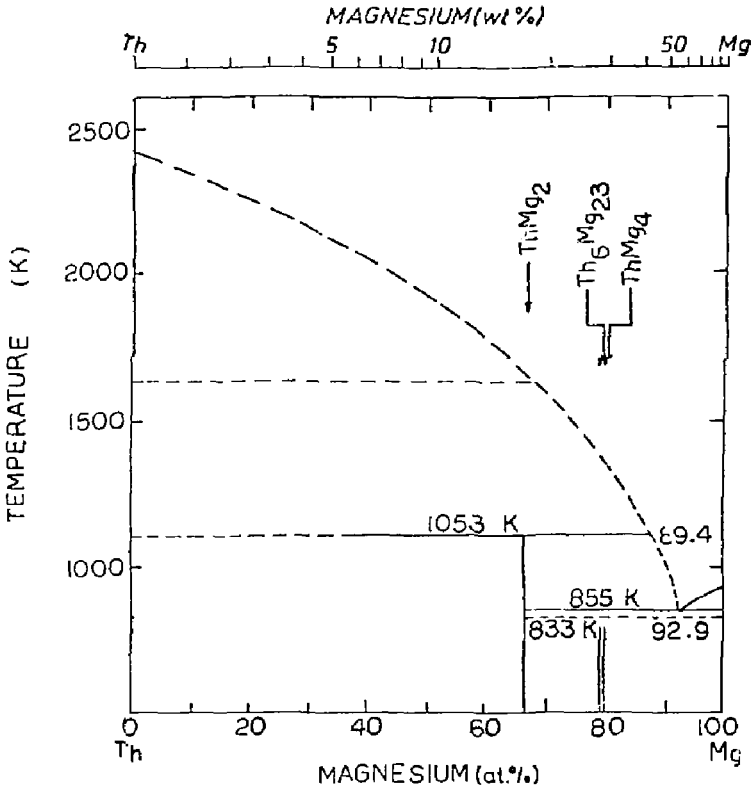

Phase diagram of the system thorium-magnesium.

Figure VII.D-1

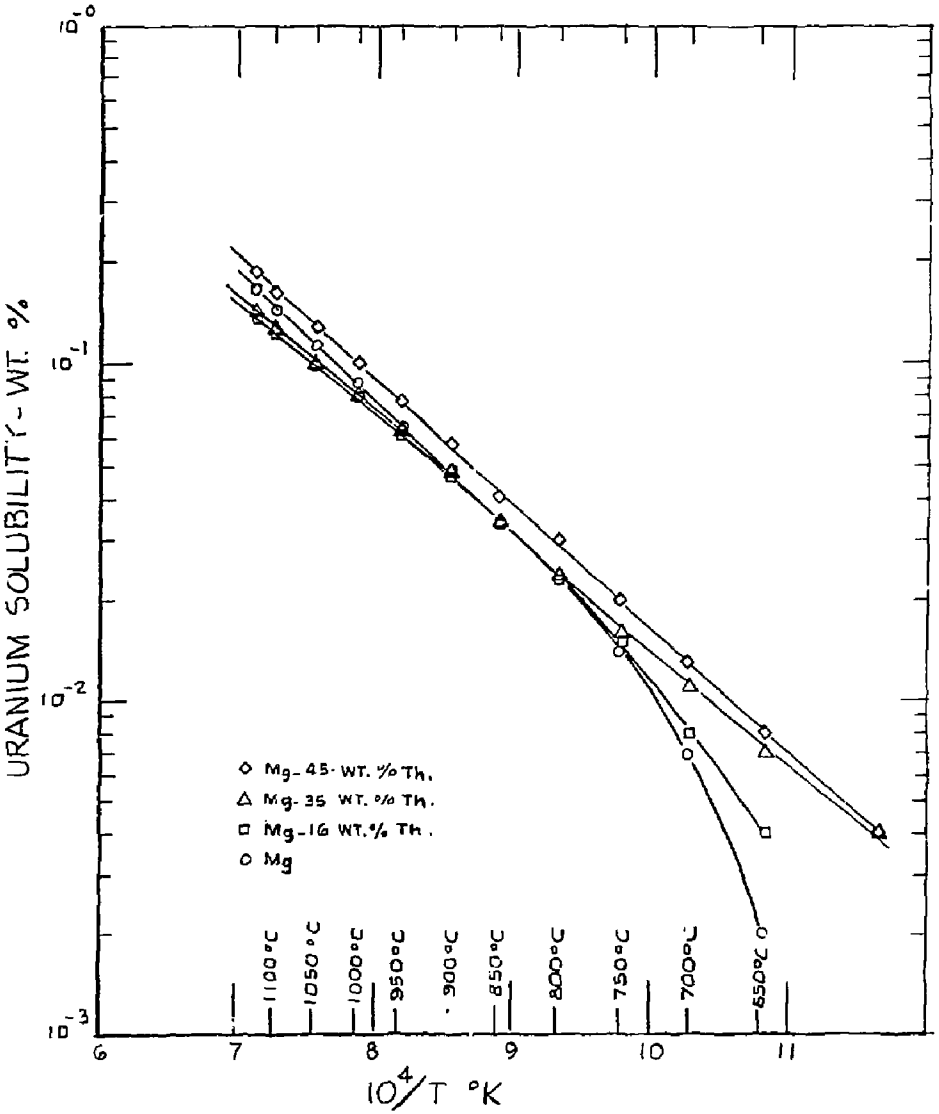

Figure VII.D-2 DATA BY CHIOTTI AND VOIGT
IND. ENG CHEM VOL. 50 PP 137-140 (1958)

Temperature		U solubility (atom fraction) in indicated solvent	
(^{o}C)	$10^4/T(^{o}K)$	Mg	Mg-33 wt% Th
600	11.45	- -	7.1×10^{-6}
650	10.83	5.9×10^{-6}	1.3×10^{-5}
700	10.28	1.1×10^{-5}	- - -
750	9.78	1.68×10^{-5}	2.75×10^{-5}
800	9.32	2.73×10^{-5}	4.22×10^{-5}
800	9.32	2.38×10^{-5}	
850	8.90	4.04×10^{-5}	5.07×10^{-5}

Figure VII.D-3 Solubility of Uranium in Pure Magesium and Mg-33 wt% Th Between 600 and 850^{o}C*

*Reference: Unpublished Work, Fred J. Smith, October 6, 1982, Oak Ridge National Laboratory. Sponsored by Division of Chemical Sciences, Office of Basic Energy Sciences, D.O.E.

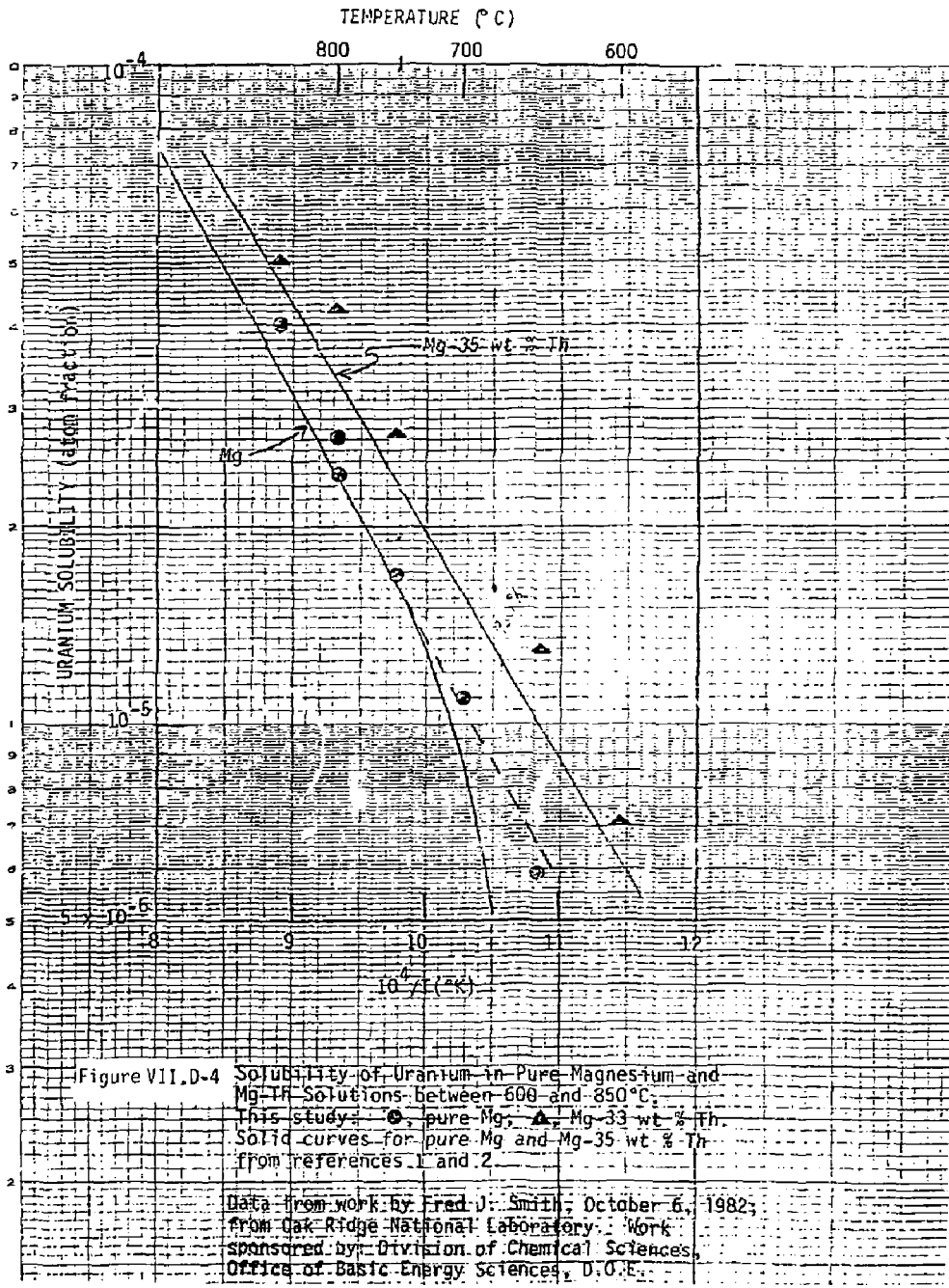

Figure VII.D-4 Solubility of Uranium in Pure Magnesium and Mg-Th Solutions between 600 and 850°C. This study: ●, pure Mg; ▲, Mg-33 wt % Th. Solid curves for pure Mg and Mg-35 wt % Th from references 1 and 2.

Data from work by Fred J. Smith, October 6, 1982, from Oak Ridge National Laboratory. Work sponsored by: Division of Chemical Sciences, Office of Basic Energy Sciences, D.O.E.

recovered ^{233}U anyhow, it is possible to protect the product in process by diluting the ^{233}U by a factor of five with ^{238}U at dissolution and eliminate the scavenging step after initial precipitation; this would lead to trace amounts of ^{239}Pu being formed during irradiation of the recovered thorium fraction.

The thorium is recovered from the magnesium alloy by simply distilling the volatile magnesium fraction away from the residual thorium and fission products. This distillation can be easily performed at 950 K under about one torr vacuum. The recovered magnesium will be used for dissolution of the next batch of blanket feed. The residual thorium and FP fraction can be refabricated into suitable metallic shapes for return to the breeder blanket assembly. Most of the fission products will remain in the thorium metal and decay away during the next irradiation sequence. After many blanket cycles the stable fission product concentrations may require removal, or alternatively, a replacement thorium blanket. The highly contaminated thorium blanket can simply be treated as fission product waste.

Our alternative method utilizes selective extraction of uranium from a molten thorium-uranium-copper-magnesium alloy into molten magnesium chloride salt at 1000 K. The feed (donor) alloy is formed by dissolving the thorium-uranium-FP blanket in a small amount of copper-magnesium diluent. The uranium can be extracted from this alloy as the chemical activity of uranium in copper-magnesium alloy is very high.

The uranium is then back extracted from the magnesium chloride molten salt by a small quantity of magnesium-zinc (acceptor) alloy. Uranium metal is recovered from the alloy by distilling off the volatile metal fraction (under vacuum). This process is a variant of the general family of molten salt extraction schemes known as "Salt Transport Processes". The basic utility of these processes was carefully studied by Argonne National Lab in the period 1965-1970, and the basic technology is fully understood and thoroughly documented[5,6]. Pilot-plant scale operations of this type have been performed with radioactive feed stocks and perform as predicted.

VII.D.2 Magnesium Precipitation Process

For design purposes we shall assume that the concentration of uranium-233 in the blanket thorium metal will be one percent by weight, and the mass of thorium blanket that must be processed will be 600 tons per year. Criticality

considerations will limit ^{233}U batches to approximately 10 kilograms each. In order to keep the operating temperature of the process as low as practicable, the concentration of magnesium must be maintained above 58% by weight; as a practical compromise we have chosen to use 33% Th-67% Mg as a design alloy. The solubility of uranium in this alloy is well documented[1-4].

The volume of Mg-33Th alloy needed to contain one ton of thorium is 1235 liters or 326 gallons; this can be contained in a cylindrical tank 48 inches in diameter by 48" tall (376 gallon capacity). The specific volume of 10 kilograms of uranium metal is 0.524 liters in solid form; as a finely divided powder a reasonable estimate would be 1.0 to 1.5 liters. The separation of one liter of fine powder from 1200 liters of molten alloy at 675°C is a formidable task.

We propose to circumvent this problem by utilizing the known property of uranium to wet and adhere to the surface of either tungsten or tantalum sheet to form a thin deposit of uranium metal on the substrate surface. This thin deposit can be formed by suspending tungsten foil in the thorium-magnesium alloy to collect uranium metal that will be precipitated from the melt. The uranium can then be either oxidized to UO_2 or hydrided to UH_3 to form a crystalline powder that can be mechanically removed from the foil collector. If hydriding is chosen, it can be converted back to metal by dehydriding under vacuum, and cast into ingot metal.

An alternative recovery method that has been used in similiar circumstances is centrifugal collection of the uranium powder by use of a rotating bowl that is suspended in the liquid alloy. The bowl shape is designed to pump liquid through the bowl during rotation, while collecting high density uranium powder in outer region of the spinning bowl. The assembly is suspended in the melt from a rotating shaft positioned above the tank of molten alloy, and stirs the tank contents by its pumping action while collecting precipitate by centrifugal separation. Removal of the product from the tungsten or tantalum bowl would be by oxidation or hydriding as described above.

Three dissolver tanks 4 ft. in diameter and 4 ft. tall would be required to accommodate 600 tons of thorium metal feed per year. After uranium removal by one of the above methods, the thorium would be reclaimed as metal sponge by distilling off the solvent magnesium (to be saved for use in later operations). The vapor pressure of magnesium is about 2 torr at 900 K and has a heat of

vaporization of 1.34 KCal/gram. Approximately 4 MW-hrs of electrical energy is required to cycle 2 tons of magnesium from room temperature through vaporization. If we assume 30% process efficiency, the 1200 tons of magnesium required to dissolve 600 tons of thorium per year will require 8 GW-hrs of electrical energy per year to melt and distill off the magnesium for process recycle. At 8¢ per KWH, the cost would be approximately $650K per year for this basic process step. Additional energy will be required for consolidation and refabrication of the recovered thorium metal. Electron beam heating has been successfully used to make high density thorium ingot from sponge metal, and produces a very high purity product. The steps leading from magnesium-thorium eutectic to high quality metal have been successfully demonstrated as an industrial process[7].

The equipment needed for the dissolver tanks, stills, and uranium recovery equipment would necessarily be fabricated from either tantalum lined steel components or other refractory metal alloy. The atmosphere within the process facility will need to be truly inert to utilize such process vessels. High purity argon gas is expected to be satisfactory for this purpose.

VII.D.3 Shielded Containment Facility

We propose to use the existing argon-atmosphere Hot-Cell Facility at the EBR-II site at Idaho National Engineering Laboratory (HFEF-N)* as a prototype cell that would be suitable to contain all irradiated process materials and hardware needed to perform uranium recovery from irradiated blanket feedstock. This facility includes a 30 ft wide by 70 ft long fully-inert (argon) shielded cell with 15 master-slave operated work stations and viewing windows. The cell is shielded with 48 inches of high density concrete (220 lbs/cu ft) up to a height of 16 ft above the operating floor. The ceiling clearance within the cell is 25 ft, and the cell is constructed with a 10-foot-deep, readily accessable sub-cell below the normal operating floor (remotely removable floor plates). An air atmosphere support cell 30 ft x 20 ft adjoins the inert cell and is used to decontaminate process equipment prior to service or disposal.

According to Melvin Feldman, the engineer responsible for the design and construction of the existing facility, the entire operating facility could be

*Hot Fuels Examination Facility - North

duplicated today for $65M (1983 dollars)[8]. A basic facility layout is included in the appedix for engineering information.

A duplicate HFEF-N should provide adequate space to contain dissolver tanks, magnesium stills, electron beam consolidation furnaces, casting capabilities, and extrusion presses for refabrication of new breeder blanket targets. A cursory equipment layout indicates that the uranium recovery chemical equipment could be placed along one inner wall (7 work stations) and the refabrication equipment along the opposite wall (7 work stations). Such an arrangement should be able to process the proposed 600 tons of blanket feed per year. We can only guess at the cost of the fully outfitted facility, but $35M seems ample to cover the cost of the basic in-cell equipment, as much of the refabrication hardware is commercially available for industrial use. We have not identified the metallurgical process that would be needed to re-fabricate the recovered thorium to suitable metallic shapes.

In light of the above information, it appears practical at this time to propose that pyrochemical processing as a possible alternative method for uranium recovery from thorium blanket feeds. Estimates of the support facility capital costs to perform such a process are expected to be in the $100M range, based on FY'83 projections.

VII.D.4 Salt Transport Alternative Process

Figure VII.D-5 shows a conceptual salt transport process for recovery of uranium from the thorium blanket. Because the reactor blanket is fission suppressed the concentration of fission products is held to a very low level. The major objective of this flow sheet is to separate uranium from thorium; no special provisions have been made to remove fission products. However, because of the nature of the salt transport process, significant separation of uranium from FP-1 and FP-2* fission products will occur. Partial removal of FP-3 elements will also occur. The flow sheet shows a thorium metal blanket feed and either an oxide or uranium metal product.

In the salt transport process, a molten salt is circulated between a donor alloy and an acceptor alloy. At the donor, uranium is oxidized by

*FP-1 Fission products are the volatile elements at 800°C,
FP-2 Elements are the refractory and noble metals,
FP-3 Elements are the rare-earth family of elements.

CONCEPTUAL SALT TRANSPORT FLOW SHEET FOR PROCESSING THORIUM BLANKET

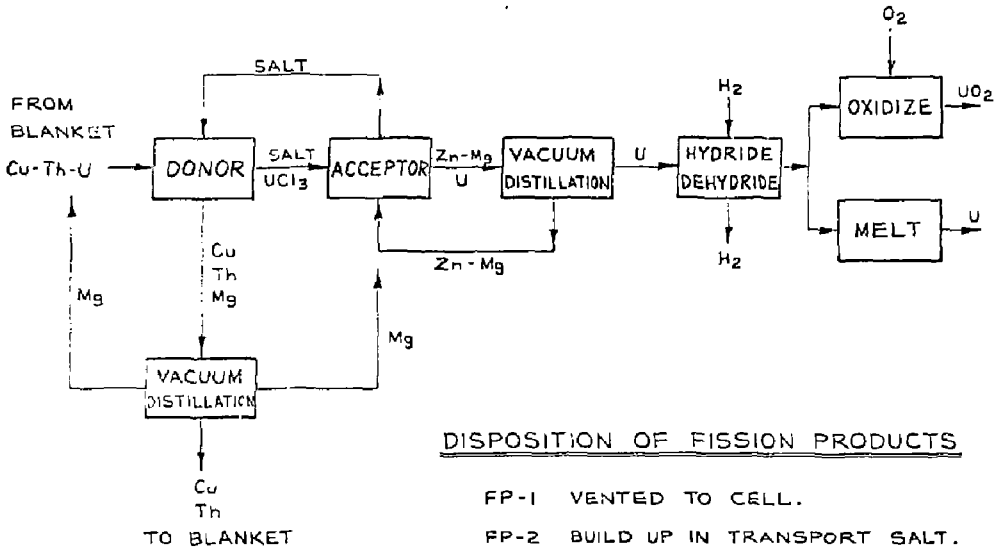

DISPOSITION OF FISSION PRODUCTS

FP-1	VENTED TO CELL.
FP-2	BUILD UP IN TRANSPORT SALT.
FP-3	BUILD UP IN TRANSPORT SALT AND ACCEPTOR ALLOY.
FP-4	FOLLOW THORIUM, WILL FOLLOW COPPER IF THORIUM-COPPER SEPARATION IS MADE.

Figure VII.D-5

$MgCl_2$ by the reaction:

$$U^o + 3/2\ MgCl_2 \rightarrow UCl_3 + 3/2\ Mg^o$$

At the acceptor, uranium chloride is reduced by magnesium by the reaction:

$$UCl_3 + 3/2\ Mg^o \rightarrow U^o + 3/2\ MgCl_2$$

The acceptor reaction is the reverse of the donor reaction, i.e., the $MgCl_2$ consumed at the donor is regenerated at the acceptor. The $MgCl_2$ enters into the overall reaction, but is not consumed and may be reused indefinitely. The overall reaction is therefore uranium transfer from the donor to the acceptor, and the reverse transfer of magnesium needed to keep the chemical reaction balanced:

$$U_{(donor)} + 3/2\ Mg_{(acceptor)} \rightarrow U_{(acceptor)} + 3/2\ Mg_{(donor)}$$

For every mole of uranium transferred from the donor to the acceptor, there is the reverse transfer of 1.5 moles of magnesium from the acceptor to the donor. The driving force for this overall reaction is the difference between the uranium and magnesium activity in the donor and acceptor alloys.

Up to the present time no thorium based alloys have been identified as uranium donor alloys. The donor alloy must be liquid at the temperature needed to melt the transport salt, and should have the least possible magnesium content. Because of the very high melting point of thorium (1750°C), pure thorium metal can not be used as a donor alloy. However, the addition of 8 wt% copper to the alloy causes a very dramatic decrease of melting point to 940°C (Figure VII.D-6). Both thorium and copper form alloy systems with magnesium. The addition of small amounts of magnesium to the 92 wt% Th - 8 wt% Cu eutectic should further lower the melting point and form a uranium donor alloy. In the absence of experimental data, an alloy composition of 89 wt% Th, 8 wt% Cu, 3 wt% Mg is assumed as the uranium donor alloy. (It is interesting to note that regions of immiscibility exist in the three binary alloys Th-U, Cu-U, and Mg-U, which suggest that the uranium activity coefficient will be greater than unity in this proposed donor alloy.)

In the acceptor reaction uranium metal will be formed at the salt-metal interface; this uranium metal is taken up by the acceptor alloy. All zinc-magnesium alloys ranging from about 98 wt% Zn - 2 wt% Mg to about 95 wt% Mg - 5 wt% Zn are uranium acceptor alloys. The 80 wt% Mg - 20 wt% Zn alloy was selected as the uranium acceptor for the following reasons: (1) uranium metal is the equilibrium solid phase and no solvent metal is combined with

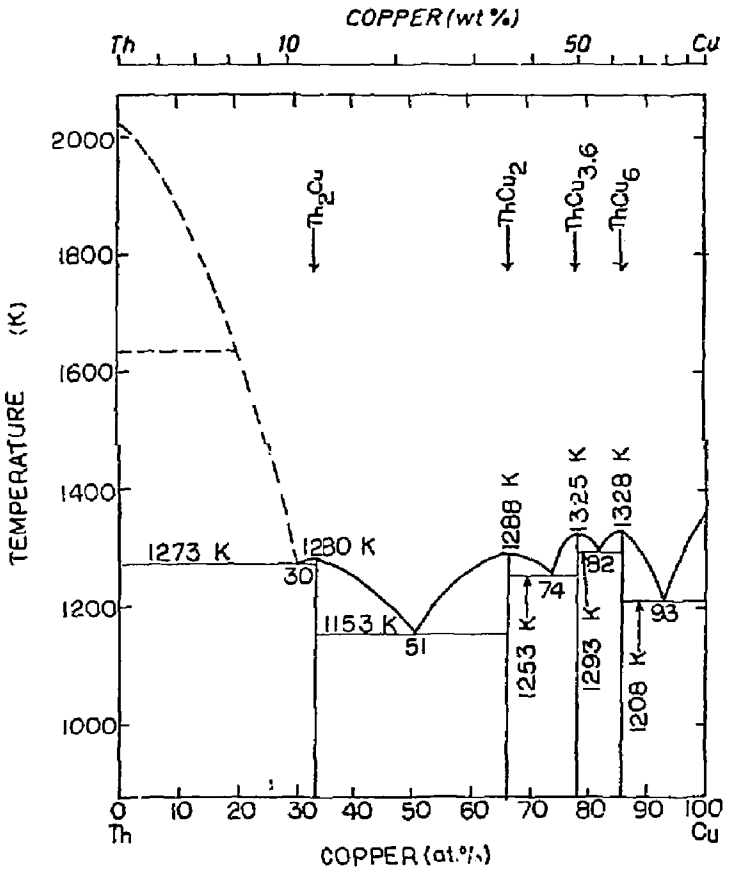

Phase diagram of the system thorium-copper.

Figure VII.D-6

uranium, (2) the alloy density is greater than the density of $MgCl_2$ (a density inversion is avoided), (3) the uranium solubility of 5×10^{-2} wt% at 800°C is very low, (4) the bulk of the acceptor alloy can be easily removed from the precipitated uranium, (5) the volume of the acceptor alloy is very small, and (6) the amount of volatile metals to be removed by distillation is held to an absolute minimum.

Magnesium chloride containing one percent thorium chloride is the preferred transport salt. 99% $MgCl_2$-1% $ThCl_4$ will give the largest value for the uranium distribution coefficient at the donor alloy, while minimizing build-up of magnesium in the donor as uranium is transported to the acceptor alloy phase. To drive the rate of uranium mass transfer between the donor and acceptor alloys, each salt-alloy system must be mixed, and the common salt phase circulated between the two alloys. Entrainment of metal in the salt must be avoided.

Although this process is not specifically designed for uranium-fission product separation, the very nature of the process will provide significant fission product decontamination of the recovered uranium fraction.

Transfer of uranium from the donor alloy to the acceptor alloy will be equilibrium limited. The following conditions are used to estimate the potential of the salt transport process to separate and recover uranium:

Donor -

U Kd = 5 (estimated value)

U solubility = 1 (all uranium is assumed to be in solution in the donor alloy)

Acceptor -

U Kd = 2.5×10^{-1} (known for $MgCl_2$)

U solubility = 5×10^{-2} wt% (known)

Transport Salt -

99% $MgCl_2$-1% $ThCl_4$

The acceptor alloy salt equilibrium determines the equilibrium conditions at the donor.

The maximum uranium content in the transport salt in equilibrium with the acceptor is the product of the distribution coefficient and the uranium solubility in the acceptor.

$$\text{Maximum U in salt} = \text{Kd} \times \text{solubility}$$
$$= 1.25 \times 10^{-2} \text{ wt\% U}$$

Mass transfer will stop when the salt in equilibrium with the donor has a similar uranium content of 1.25×10^{-2} wt% U. The uranium content in the donor at equilibrium will therefore be:

$$\text{wt\% U in metal} = \frac{\text{wt\% U in Salt}}{\text{U Kd (donor)}} = \frac{1.25 \times 10^{-2}}{5} = 2.5 \times 10^{-3} \text{ wt\% U}$$

The uranium content of the thorium blanket is assumed to be about 0.9 wt%. The total uranium transferred out of the donor may therefore be approximated by:

$$\text{\% U transferred out of donor} = \frac{0.9 - .0025}{0.9} \times 100 = 99.5\%$$

Attainment of equilibrium conditions may take a considerable period of time as the transfer rate will decrease markedly as the uranium content of the donor is lowered. Uranium content of the transport salt will be 1.25×10^{-2} wt% U at equilibrium and the actual amount in the salt will be dependent up to the amount of molten $MgCl_2$ present in the system. This uranium in the salt does not represent a loss, just an in-process inventory.

The salt transport process is dependent upon the utilization of a uranium donor alloy. The proposed donor alloy uses copper and magnesium as alloying agents to obtain donor properties at 800°C. The magnesium may be removed from the depleted donor alloy by vacuum melting. Other processes for separation of copper and FP-4 elements from thorium would be required if thorium is to be recycled back to the breeder blanket. The economics of remote fabrcation of the thorium for recycle may dictate a once through cycle for thorium.

Figure VII.D-7 shows a conceptual mode of operation for the salt transport process.

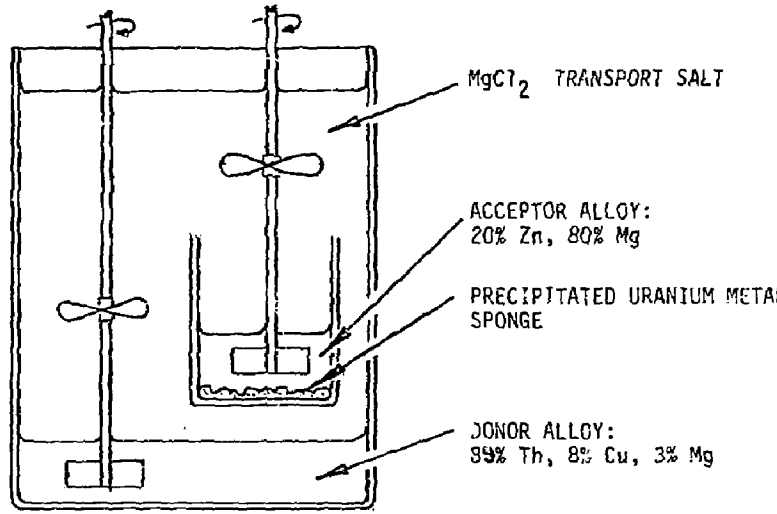

1. Donor and acceptor alloys are in mutual contact with salt.

2. Mixing of alloy phases is done by submerged mixers to avoid metal entrainment in salt.

3. Salt is mixed by propeller mixer to push salt down to the metal surface and to circulate the salt between the donor and acceptor alloys.

4. After uranium transport is completed, the acceptor crucible is removed from the salt bath. The salt and acceptor alloy are removed from the crucible, leaving the uranium metal precipitate and a small amount of acceptor alloy in the bottom of the crucible.

5. The volatile acceptor alloy and any salt associated with the crucible are separated by vacuum distillation, leaving a metallic uranium product in the crucible.

6. The uranium is hydrided to form a free flowing powder which falls from the inverted crucible.

7. The UH_3 may be oxidized to form UO_2 orthe UH_3 may be dehydrided and melted to form a uranium metal ingot.

Figure VII.D-7

References

1. P. Chiotti and H. E. Shoemaker, Ind. Eng. Chem. 50, 137 (1958).

2. Reactor Handbook, Vol. II, Fuel Reprocessing, S. M. Stoller and R. B. Richards, eds., Interscience, 1961, p. 323.

3. L. M. Ferris, J. C. Mailen, J. J. Lawrence, F. J. Smith and E. D. Nogueira, J. Inorg., Nucl. Chem. 32, 2019 (1970).

4. Private communication, L. M. Ferris, 10/6/82.

5. *R. K. Steunenberg, R. D. Pierce, and* L. Burris. Argonne National Laboratory in: "Progress in Nuclear Energy", Series III, Process Chemistry; Editors C. E. Stevenson, E. A. Mason. Pergammon Press, Inc., 1970. p.p. 461-504.

6. J. [illegible] Knighton, I. Johnson, and R. K. Steunenberg "Uranium and Plutonium Purification by the Salt Transport Method" Symposium on Reprocessing of Nuclear Fuels, Ames, Iowa, Conf-690801. p.p. 337-362.

7. "Thorium: Preparation and Properties", J. F. Smith, O. N. Carlson, D. T. Peterson, T. E. Scott, the Iowa State University Press/Ames, Iowa 1975. Chapter 1.

8. Private communication with Melvin Feldman, Consolidated Fuel Reprocessing Facility, Oak Ridge National Laboratory, Nov. 1982.

VII.E COMPARISON OF REPROCESSING COSTS

During the past three years, the following four studies of reprocessing plant technologies have been conducted to estimate the cost to recover fuel produced in a fusion breeder:

- a pre-conceptual design and cost estimate for a PUREX fuel reprocessing plant for uranium-plutonium fuels. (Section VII.C of this report).
- a pre-conceptual design and cost estimate for a THOREX fuel reprocessing plant for thorium-uranium fuels(1).
- a conceptual description and rough cost estimate for a pyro-chemical fuel reprocessing plant for thorium metal fuels. (Section VII.D of this report).
- a pre-conceptual design and cost estimate for a molten salt fuel reprocessing plant for molten thorium-uranium fluoride salt fuels(2).

Importantly, the first of the above studies also provided a critical review of the second, and the THOREX cost estimate was revised upwards as shown in Table VII.E.1. The total capital cost of 1076 $M for the THOREX plant compares with an estimated cost of 1006 $M for a PUREX plant to handle the same throughput - in this case uranium metal instead of thorium metal. The operating costs for these facilities are expected to be similar - about 63 $M/yr in both cases. If we use the suggested cost versus throughput scaling exponents (0.64 for the capital cost, 0.57 for the operating cost), then the capital cost estimate for a THOREX reprocessing plant to process the 604 MT/yr annual throughput of the reference fusion breeder would be 685 $M. The operating cost estimate is 42 $M/yr.

Conversely, if the blanket were designed to breed plutonium from uranium carbide (which is compatable with liquid lithium), the capital and operating cost estimates for a PUREX plant would be 641 $M and 42 $M/yr, respectively. Since uranium metal and uranium oxide are not chemically compatable with liquid lithium, we would not propose their use in a design similar to the reference blanket. Nevertheless, these fuel forms may be appropriate for alternate concepts and we estimate an ~ 6% reprocessing cost savings relative to the carbide because the carbide oxidizers can be eliminated (see Section VII.C).

Table VII.E.1 Revised Thorium Metal Reprocessing Plant (THOREX)
Equipment and Facility Cost Estimate

(**Basis:** 1222 MT/yr throughput)
(1982 $)

Component	Cost ($ Million)
Headend[a]	233
Solvent Extraction[a]	84
Waste Treatment[a]	205
Balance of Plant[a]	308
Total Equipment and Facility[a]	830
Owners Cost and Other Charges during Construction[b]	246
Total Capital Cost[c]	1076 $M
Total Operating Cost[d,e]	62.8 $M/yr

a) Values include direct material cost, field labor, field distributable cost, engineering services cost, and a 20% contingency

b) Factor of 1.296 = 1.10 (owners cost) x 1.178 (cost of money). See Table VIII.C.3

c) Capital cost scaling: Capital cost = 1076 (size/1222)$^{0.64}$

d) Includes labor, consumables, utilities, equipment replacement, waste disposal

e) Operating cost scaling: Operating cost = 57 (size/1222)$^{0.57}$

Regarding the pyro-chemical reprocessing plant described in Section VII.D, only a rough cost estimate is available at this time. If we assume, based upon the greatly reduced volume of the facility and other considerations, that the total capital cost is about 1/4 that of the aquious processes, then a total capital cost estimate of 150 $M appears to be reasonable. The operating cost is expected to be less than 10 $M/yr.

Although the molten salt reprocessing plant described in reference 2 is attractive and provides a very low reprocessing cost (~ 2-5 $/gm fissile recovered), it is not suitable for adaptation to the reference blanket and is not discussed in this chapter.

In summary, the THOREX reprocessing cost estimates are compared with cost estimates for PUREX and pyro-chemical reprocessing in Table VII.E.2. In all cases, a 604 MT/yr throughput and 1.24% fissile atom fraction in thorium are assumed since these correspond to the reference case (see Table VII.A.2). The cost estimates for aqueous reprocessing are quite similar despite the fuel form, but the pyro-chemical reprocessing technology has potential to reduce the reprocessing cost about four-fold.

It should be noted that the unit reprocessing costs shown are lower than those obtained in previous studies(1,2) due to the higher discharge enrichment which is achieved in the present design. Since the overall cost of bred fissile fuel is expected to be about 195 $/g during the first year of operation, the impact of aquious reprocessing would only be about 11%.

Also, it should be noted that the above THOREX cost relates to thorium metal reprocessing rather than thorium oxide (thoria). The cost to reprocess the later has been suggested to be substantially higher(3).

Under these conditions, there are three possible incentives for pyro-chemical reprocessing. First, the 11% cost impact discussed about might be reduced to about 2.5%. Second, if safety, environmental, or other economic conditions warrant it, the discharge enrichment could be decreased to about 0.5% without a significant deleterious impact on product cost. Finally, since the cost of aqueous reprocessing is somewhat uncertain, pyro-chemical reprocessing can provide an effective backup which is relatively insensitive to cost uncertainties.

Table VII.E.2 Reprocessing Cost Comparison

PROCESS	THOREX	PUREX	PUREX	PYRO-CHEMICAL
Fuel Type	thorium metal	uranium carbide	uranium metal or oxide	thorium metal
Throughput,[a] MTHM/yr	604	604	604	604
Fissile Discharge Assay,[a] atom %	1.24	1.24	1.24	1.24
Plant Capital Cost, $M	685	641	602	150
Cost of Capital,[b] $M/yr	124	115	109	27.1
Plant Operating Cost, $M/yr	42	42	39	10
Total Annual Cost, $M/yr	166	157	148	37.1
Reprocessing Cost,[c] $/KgHM	274	260	245	61.4
Unit Cost,[c] $/g fissile	22.2	21.0	19.8	4.95

a) based upon reference fuel cycle as described in Section VII.A.

b) 18.04% carrying charge (see Chapter VIII)

c) Current dollar cost referenced to 1982 dollars

References, Section VII.E

1) J.A. Maniscalco, et al., "Laser Fusion Breeder Design Study - Final Report", DOE Contract DE-AC08-79P040-11, TRW (1980).

2) J.D. Lee, et al., "Feasibility Study of a Fission-Suppressed Tandem Mirror Hybrid Reactor, UCID-19327, Lawrence Livermore National Laboratory, (1982).

3) Exxon Nuclear Co., Inc., "The Economics of Reprocessing Alternative Nuclear Fuels", ORNL/Sub-7501/4, Oak Ridge National Laboratory (1979).

VII.F TRITIUM PROCESSING

VII.F.1 Overview and Material Choice

The reference blanket breeds all of the tritium required for reactor operation from the lithium coolant. The lithium is depleted to 0.2% ^{6}Li in order to enhance the tritium producing reaction in the ^{7}Li and to limit the overall tritium breeding. The lithium is continuously circulated in a heat transport loop, as described in the previous section. As the lithium is circulated, it is processed to recover the bred tritium and helium that is also produced.

Although tritium safety and environmental considerations such as permeation through structural barriers have not been adequately addressed in this study, we have adopted two general approaches to address this concern. First, the use of liquid lithium, which has a high solubility for tritium, is expected to result in very low normal releases when compared with a low solubility carrier such as lead-lithium. Second, an important consideration in the design of the lithium processing system has been to limit the blanket tritium inventory less than ~1 Kg so that the tritium inventories in the plasma fueling and vacuum systems will be expected to dominate the overall tritium concerns. The ability to maintain a small blanket tritium inventory will depend largely on the lithium processing rate and on the capability of the extraction process to recover the tritium from the lithium at fairly low concentrations. Third, it is important to recognize that, in accident situations. the biological hazard potential associated with tritium will be orders of magnitude lower than that of any of the other major contributors (activated structure, actinides, fission products)(1). Therefore, our philosophy in designing the fusion breeder has not emphasized the accidental release of tritium from the blanket, but has emphasized overall safety (including lithium fires) in the context of achieving acceptably low normal releases and good overall safety in a remotely sited facility. Our work in this area is described in Chapter V.

VII.F.2 Tritium Processing and Inventory Analysis

A model for the tritium inventory of the reactor and the performance and cost of a molten salt extraction process for liquid lithium systems is given below(2,3). This model is based upon work performed at Argonne National

Laboratory. As a function of the total tritium inventory desired, the lithium inventory, and the tritium production rate, the model calculates the lithium flow rate to the extraction system required to maintain the given tritium inventory or concentration. The lithium flow rate determines the number of extractor units required. The cost and the power requirements of the extraction system are directly proportional to the number of extractor units.

The fraction of the total lithium inventory that must be circulated through the tritium extraction system per unit time is given by

$$X = \frac{R_g}{I_{ss}} \cdot \frac{(\varepsilon D_v \eta)+1}{\varepsilon D_v \eta}$$

where

R_g = tritium generation rate which may include unburned as well as bred tritium

I_{ss} = steady-state tritium inventory

ε = efficiency of tritium recovery from the salt

D_v = volumetric distribution coefficient of tritium between the lithium and the salt

η = efficiency factor that accounts for non-equilibrium tritium distribution during contacting.

Typical values for ε, D_v, and η are 0.9, 2.0, and 0.3, respectively.

The lithium flow rate to the tritium extraction system is then

$$F = XI_L/\rho_L \qquad cm^3/s$$

where

I_L = lithium inventory, g

ρ_L = lithium density, g/cm^3

The number of extractor units required in parallel for a single stage operation is

$$N = F/3200$$

where F is in cm^3/s. This is based on a capacity per extractor unit of 23 m^3/hr (lithium plus salt) used in a process where equal volumes of salt and lithium are contacted. Each extractor draws 3.73 kW_e for continuous operation and costs on the order of one million dollars.

A summary of key parameters related to the blanket lithium and tritium inventories is shown in Table VII.F.1 for a fusion power of 3000 MW. As the table shows, at 3000 MW of fusion power the tritium production rate is 484 g/day, and the blanket Li inventory is ~ 1100 MT. For this system, a total tritium inventory of 1 kg may be achieved for a lithium processing rate of about 100 m^3/hr. The nine required extractor units cycle the entire lithium inventory in about 21 hours. The direct cost of the tritium extractor units is about ten million dollars and they are expected to consume a negligible amount of electrical power. Since the extraction process has been demonstrated at tritium concentrations on the order of 1 wppm, a 1 kg tritium inventory seems quite reasonable.

As noted previously, the lithium used in the blanket design is depleted to 0.2% ^6Li, whereas natural lithium is composed of 7.5% ^6Li. As shown in Table VII.F.1, the lithium inventory for 3000 MW of fusion power is ~ 1.1×10^6 kg. A possible concern with this design might then be the cost for this depleted lithium. A study by McGrath(4) estimated the amount of separative work required to isotopically separate lithium, but it was difficult to calculate the actual cost because the cost of a unit of separative work was not known. By doing a parametric study, it was estimated that the cost for the lithium depleted to 0.2% ^6Li might be in the range of 100-150/kg ($125/kg reference value). Hence, the capital cost for the blanket lithium inventory for 3000 MW of fusion power would be in the range of 140$M. While this is not a prohibitive cost, it would be desirable to perform future studies to attempt to more accurately estimate the cost of highly depleted lithium.

TABLE VII.F.1 Key Parameters Related to the Lithium and Tritium Inventories for the Lithium-Molten Salt Blanket

; ɔion Power, MW	3000
Neutron Wall Loading, MW/m^2	1.27
Total Li Inventory, kg	$1110 \cdot 10^3$
T Production Rate, g/day	484
T Inventory in Lithium, g	1000
T Concentration in Li, wppm	0.90
Li Processing Rate, m^3/hr	104
Time to Circulate Entire Li Inventory, hr	20.7
Number of Extractors Required	9

References, Section VII.F

1) J.D. Lee, et al., "Feasibility Study of a Fission Suppressed Tandem-Mirror Hybrid Reactor, UCID-19327, Lawrence Livermore National Laboratory (1982).

2) W.F. Calaway, "Electrochemical Extraction of Hydrogen from Molten LiF-LiCl-LiBr and Its Application to Liquid Lithium Fusion Reactor Blanket Processing", Nucl. Tech., 39, 63. (1978).

3) V.A. Maroni, et al., "Some Preliminary Consideration of a Molten Salt Process to Remove Tritium from Liquid Lithium Fusion Reactor Blankets", Nucl. Tech., 25, 83, (1975).

4) R.T. McGrath, "Conceptual Design and Neutronics Analysis of a Flowing Lithium/Molten Salt Blanket Fusion Hybrid Breeder Reactor", Ph.D. Thesis, University of Michigan, (1980).

CHAPTER VIII

SYSTEMS AND ECONOMIC ANALYSIS

VIII.A INTRODUCTION AND OVERVIEW

VIII.A.1 Introduction

The economic incentives for a fusion breeder reactor can be best understood and evaluated in the context of a symbiotic fusion fuel factor-fission burner electricity generation system. In this concept, the fusion fuel factory is typically incorporated into a remotely sited and safeguarded fuel cycle complex along with fuel reprocessing plants, fuel fabrication facilities and possibly a waste disposal facility. The fissile fuel produced in the fusion fuel factory is recovered by reprocessing, mixed with fertile fuel, fabricated into fuel rods and shipped to the fission burner reactors. The spent fuel from the burner reactors is shipped back to the safeguarded fuel cycle complex where the remaining fissile fuel is separated from radioactive waste material and the latter is processed for disposal. Typical fuel cycle complex configurations are discussed in more detail in Section VII.A.

As shown earlier, four such fuel cycle complexes, containing three fusion breeders each, could provide makeup fissile material to support about 250 GWe of LWR capacity. Only about 15 GWe would be produced by the fusion breeders themselves (~ 1250 MWe per fusion breeder).

The basic analytical capability used to generate the results presented in this chapter is provided by three computer codes developed over the course of the past several years and implemented on the Magnetic Fusion Energy Computing Network: the LLNL Tandem Mirror Physics Code (TMPC)(1), the TRW Tandem Mirror Reactor Design Code (TMRDC)(2), and the TRW economics analysis code (PERFEC)(3). As shown in Figure VIII.A.1, each of these codes has a distinct function. TMPC is used to estimate plasma engineering parameters associated with the fusion driver configuration and power flow (see Chapters I and VI). TMRDC is used to integrate these quantities into a reactor design and estimate the net TMHR power flow, fissile production, and direct cost (see Chapter VI). PERFEC combines the TMRDC output with fission reactor, fission fuel cycle, and financial accounting data to estimate the economic performance of

Figure VIII.A.1 Fusion Breeder/LWR Systems Modeling Code Capabilities

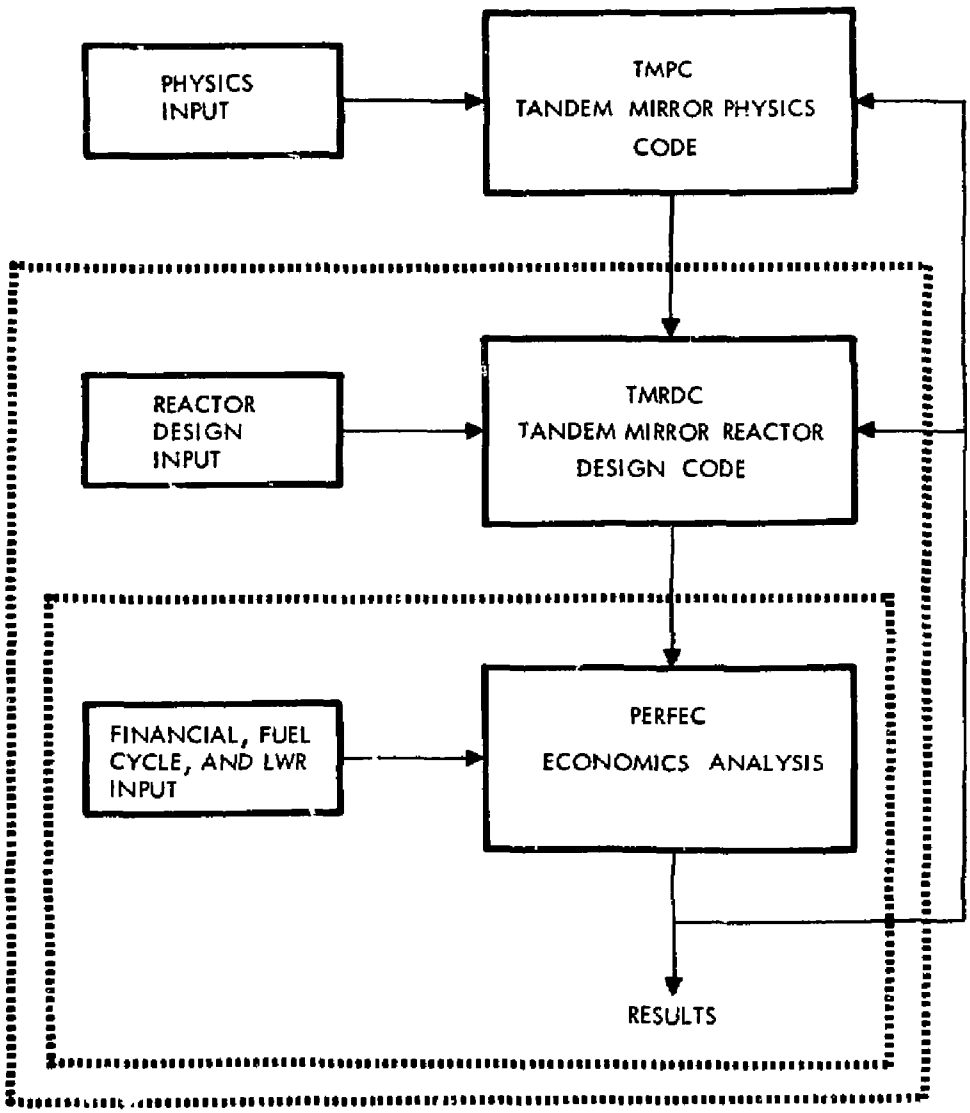

the entire symbiotic electricity generation system. In performing the systems and economic analysis, the capital and operating costs of the entire symbiotic electricity generation system are used to estimate the costs of the production of one net product, electricity.

Each of the three codes may be utilized in a stand-alone mode or may be interfaced to the adjoining code. For instance, given a fixed set of inputs from TMRDC, PERFEC can be used to estimate the effects of parametric variations in the financial, fission fuel cycle, and/or LWR client data. In another mode, changes in plasma physics assumptions can be modeled using TMPC and the new results can be used to generate new TMRDC and PERFEC results. This capability provides a logical and straightforward mechanism to perform trade and optimization studies similar to those which have been performed in the past.

VIII.A.2 Overview

Chapter VIII is broken into four principal subsections. Section VIII.B is a description of the economics method which is utilized in the later sections. This method is uniquely suited to estimate the symbiotic electricity cost for a generation system consisting of a fusion breeder and its client fission burner power reactors.

In Section VIII.C, this method is applied to the baseline fusion breeder described in the previous chapters. In this section we first provide a detailed description of global cost, performance and fuel cycle data which is required to develop the economics analysis. The economic results, focusing upon the cost of electricity for the symbiotic system as compared with the electricity generation cost for a conventionally fueled LWR (mined U_3O_8 at 55 $/Kg with full reprocessing and recycle), are presented next.

Section VIII.D describes optimizations of the fusion breeder about the reference case which can provide a lower symbiotic cost of electricity. Three cases are considered. In the first case, an improved fusion driver and fuel management operating point is developed based upon the optimization scheme discussed in Section IV.C. In the second case, we consider the cost advantages associated with the use of pyrochemical reprocessing instead of aqueous

(THOREX) reprocessing (Chapter VII). In the third case we consider the economics of switching from the denatured thorium to denatured uranium fuel cycle on the LWR burner side of the system.

Section VIII.E addresses the sensitivity of the system electricity cost to plant component cost and performance uncertainties. In particular, electricity cost sensitivities associated with power flow and capital cost uncertainties are considered. The cost of electricity as a function of achievable plasma energy gain (i.e., Q_p) is compared with consistently derived results for a fusion electric plant.

References, Section VIII.A

1) Original code developed as described in G.A. Carlson, et al., "Comparative End Plug Study for Tandem Mirror Reactors", UCID-19271, Lawrence Livermore National Laboratory (1981). Current version of the code is maintained at LLNL.

2) Original code as described in D.L. Chapin, et al., "Preliminary Feasibility Assessment of Fusion-Fission Hybrids", WFPS-TME-81-003, Westinghouse Fusion Power Systems Department (1981). Current version of the code is maintained at TRW.

3) Original code as described in D.H. Berwald and J.A. Maniscalco, "An Economics Method for Fusion-Fission Electricity Generation Systems", Nucl. Tech./Fusion, January 1981. Current version of the code is maintained at TRW.

4) D.H. Berwald, and J.A. Maniscalco, "Performance and Economics Analysis of Several Laser Fusion Breeder Fueled Electricity Generation Systems", Nucl. Tech./Fusion, January 1981.

5) J.A. Maniscalco, et al., "Recent Progress in Fusion-Fission Hybrid Reactor Design Studies", Nucl. Tech/Fusion, October 1981.

6) J.D. Lee, et al., "Feasibility Study of a Fission Suppressed Tandem Mirror Hybrid Reactor", UCID-19327, Lawrence Livermore National Laboratory (1982).

VIII.B AN ECONOMICS METHOD FOR SYMBIOTIC FUSION-FISSION ELECTRICITY GENERATION SYSTEMS

VIII.B.1 Introduction

In this section, a self-consistent analytical methodology for evaluating the economic incentives for symbiotic electricity generation systems that consist of fusion breeder reactors and supported fission converter reactors is developed. This methodology employs a discounted cash flow analysis of breeder and converter direct operating costs and indirect capital costs, as well as a novel treatment of fissile inventory charges. Three figures of merit are emphasized:

1) *The cost of electricity generated by the symbiotic system*

2) The cost of fuel exchanged by the fusion breeder and fission converter reactors in the system

3) The cost of electricity for the same fission converter when it is fueled using mined uranium at a specified cost.

The reference fusion breeder with LWR clients is provided as a relevant example in Section VIII.C.

In its general application, the proposed model can be used to compute the cost of electricity and fissile fuel for a fusion breeder (i.e., hybrid) reactor or a spallation neutron source (i.e., accelerator breeder) which produces power and/or fuel as a primary product. It can be used to address the economic implications of several important questions:

1) Should fusion breeders be optimized towards fuel or power production?

2) Are fusion breeders most attractive when they fuel light water reactors (LWRs) or more fuel efficient, but more expensive, advanced converter reactors?

3) Can fusion breeders that cost several times more than LWRs compete in the energy economy with other advanced concepts?

4) Can fusion breeders compete with the cost of conventionally mined uranium to fuel fission reactors?

5) Are the increased costs of proposed proliferation resistant fuel cycles (e.g., refresh or denatured uranium) justified?

6) What are the effects of performance and cost uncertainties on system economics?

When such a model is incorporated into a small digital computer code, it can provide a flexible tool for both point and parametric studies of the performance and economics of symbiotic electricity generation systems. This code, PERTEC, has been used to generate the results shown in Sections VIII.C, VIII.D, and VIII.E.

It is important to recognize that the method described applies to the less general "free expansion" case of fusion breeders that supply only the makeup fuel requirements of a consistent number of client fission converter reactors. The more general "bound expansion" case of fusion breeders which must also produce fissile fuel to supply the initial fissile inventory requirements of an expanding system of fission reactors is not discussed in this chapter.

VIII.B.2 Defining the Model

The basic premise that is applied in this model is best illustrated in Figure VII.A.1, a typical system schematic diagram. In this schematic diagram, fusion breeders within a safeguarded fuel cycle center provide fissile fuel to light water power reactors. Referring to the right side of the figure, we note that the only net product of the combined fusion breeder-fission converter system is electricity. Also, considering the hyrid breeder and a consistent number of supported fission reactors, we note that the closed energy system shown is entirely self-sufficient in fissile fuel such that the net fuel production of the entire system is zero. Thus, the sale of fissile fuel by the breeder operator can, for the moment, be treated as an internal transfer. However, the system does utilize a considerable fissile inventory and fissile inventory carrying charges contibute significantly to operating expenses. These charges will be discussed in later sections.

In this case it is reasonable and appropriate to define the most important system parameter, the system electricity cost in year n, S_n [mill/kW(electric)h], as

$$S_n = 1000\ C_{op,n}^{Tot}/E^{Tot} \qquad (1)$$

where

$C^{Tot}_{op,n}$ = total cost of operating the closed electricity generation system in year n (including all capital related costs, fuel inventory costs, fuel cycle processing costs, operation and maintenance costs, taxes and profit ($/yr))

E^{Tot} = net total electrical output of the closed electricity generation system [kW(electric)h/yr].

We will show that, given S_n, it is possible to consistently define the value of a gram of exchanged fuel in year n. Thus, the proposed method describes a solution to the system economics problem such that the breeder and converter reactor operators will sell and buy fuel at the same price when their electricity also sells for the same price. Profit considerations can also be addressed since the profit is explicitly included in the determination of $C^{Tot}_{op,n}$.

In practice, $C^{Tot}_{op,n}$, is expanded as the sum of two quantities, i.e.,

$$C^{Tot}_{op,n} = C^{B}_{op,n} + C^{C}_{op,n}, \qquad (2)$$

where

$C^{B}_{op,n}$ = total fusion breeder operating cost in year n ($/yr)

$C^{C}_{op,n}$ = total operating cost of all client converter reactors in year n ($/yr)

and the symbols B and C represent breeder and converter, respectively. For useful results these terms must be further expanded to include several contributions

$$C^{B,C}_{op,n} = p^{B,C} C^{B,C}_{kWt,n} = (C^{B,C}_{1} + C^{B,C}_{d,n} + C^{B,C}_{inv,n})\, p^{B,C}, \qquad (3)$$

where

$P^{B,C}$ = total installed thermal power generate capacity of the breeder or supported client converter reactors [kW(thermal)]

$C^{B,C}_{kWt,n}$ = total year n cost per kW(thermal) of installed plant capacity [$/kW(thermally)yr]

$C^{B,C}_{i}$ = total fixed (indirect) cost of plant capital [$/kW(thermal)yr]

$C^{B,C}_{d,n}$ = total variable (direct) cost of plant operation in year n [$/kW(thermal)yr]

$C^{B,C}_{inv,n}$ = total cost of fissile inventory carrying charges in year n [$/kW(thermal)yr]

In the above expressions n ranges from 1, the first year of operation to N, the last year of operation. The term "year zero" designates the initial date of plant operation. The fixed costs, $C^{B,C}_{i}$ do not vary over time.

VIII.B.3 Expanding the Fixed and Variable Cost Terms

Returning to Eq. (3), the fixed, or indirect cost term can be further expanded as

$$C^{B,C}_{i} = f^{B,C}_{tot}\, C^{B,C}_{cap} = (f^{B,C}_{cap} + f^{B,C}_{tax} + f^{B,C}_{p,of} + f^{B,C}_{misc})C^{B,C}_{cap} \qquad (4)$$

where

$C^{B,C}_{cap}$ = total present investment per kW(thermal) in year zero including direct and time related costs, working capital, and the present value of future salvage or decommissioning (but not including the cost of the initial fissile inventory or the salvage value of such fuel) [$/kW(thermal) installed]

$f^{B,C}_{tot}$ = total fixed charge rate of capital (yr^{-1})

$f^{B,C}_{cap}$ = capital recovery factor (interest and amortization) (yr^{-1})

$f^{B,C}_{tax}$ = income and property tax factor (yr^{-1})

$f^{B,C}_{prof}$ = profit factor (profit greater than normally returned on equity and debt) (yr^{-1})

$f^{B,C}_{misc}$ = recovery factor for other miscellaneous charges such as insurance and decomissioning (yr^{-1}).

Of particular interest is the capital recovery factor. This is typically given by

$$f^{B,C}_{cap} = \frac{d(1+d)^N}{(1+d)^N - 1} \qquad (5)$$

where d (yr^{-1}) is the reactor operators discount rate (cost of financing equity and debt including inflation.

Similarly, the variable, direct, or cost term from Eq. (3) can be expanded as

$$C^{B,C}_{d,n} = T^{B,C}\,(C^{B,C}_{r,n} + C^{B,C}_{f,n} + C^{B,C}_{t,n} + C^{B,C}_{b,n} + C^{B,C}_{e,n}) + C^{B,C}_{o+m,n} + C^{B,C}_{str,n} \qquad (6)$$

where

$T^{B,C}$ = heavy metal throughput [kgHm/kW(thermal)yr]

$C^{B,C}_{r,n}$ = fuel reprocessing cost in year n ($/kgHM)

$C^{B,C}_{f,n}$ = fuel fabrication cost in year n ($/kgHM)

$C^{B,C}_{t,n}$ = fuel transportation cost in year n ($/kgHM)

$C^{B,C}_{b,n}$ = back end fuel cycle cost (waste storage and disposal) in year n ($/kgHM)

$C^{B,C}_{e,n}$ = front end fissile enrichment cost in year n (if any) ($/kgHM)

$C^{B,C}_{o+m,n}$ = operation and maintenance costs (including spare parts) in year n [$/kW(thermal)yr]

$C^{B,C}_{str,n}$ = reactor structure (e.g., first wall replacement cost in year n [$/kW(thermal)yr].

For the fusion breeder, the quantity T^B is given by

$$T^B = \frac{\gamma^B F^B}{1000\ \varepsilon^B_d} \qquad (7)$$

where

F^B = net breeder fissile production at full plant capacity [g/kW(thermal)yr]

$\gamma^{B,C}$ = overall plant capacity factor (e.g., $\gamma^B = 0.75$ means that the fusion breeder operates such that it produces 75% of its full rated output)

ε^B_d = net fissile discharge enrichment of breeder (e.g., 1% ≡ 0.01)

For the fission converters, the quantity T^B is given by

$$T^B = \frac{365.25\ \gamma^C}{B^C} \qquad (8)$$

where

B^C = average discharge fuel burnup [kW(thermal)day/kgHM]

VIII.B.4 Inventory Charges

It is assumed that the symbiotic system begins equilibrium operation at time zero, and the entire system is assumed to have a constant and fixed fissile inventory at any given time. The total inventory (including the out-of-core inventory) is considered to be nondepreciating resource purchased at the beginning of a year of operation and sold at the end of the year. A fixed carrying charge is paid each year against the value of fissile fuel in that year to account for the above transaction. Thus, the fissile inventory carrying charge term from Eq. (3) is given in more detail by

$$C^{B,C}_{inv,n} = bC^{B,C}_{fiss,n}\left(I^{B,C}_{int} + I^{B,C}_{BOC} + I^{B,C}_{EOC}\right) = bC^{B,C}_{fiss,n}\ I^{B,C}_{tot}\ , \qquad (9)$$

where

b = fixed charge rate on fissile inventory (yr^{-1})

$C^{B,C}_{fiss,n}$ = value of fissile fuel discharged by the breeder and/or charged to the converter in year n

$I^{B,C}_{int}$ = specific (in-core) fissile inventory averaged over the breeder fuel cycle [g/kW(thermal)]

$I^{B,C}_{BOC}$ = average specific (out-of-core) fissile inventory associated with processing steps during period between the end of fuel reprocessing and the charge of fabricated fuel to reactor [g/kW(thermal)]

$I^{B,C}_{EOC}$ = average total specific fissile inventory [g/kW(thermal)].

In Eq. (9), the specific inventory terms for converter reactor batch fuel cycles can be modeled linearly as

$$I^C_{int} = \frac{1000\ \varepsilon^C_o}{D^C} - \left[\frac{F^C\ (B^C/365)}{(M^C)^2\ D^C}\right] \sum_{m=1}^{M^C} \left(m - \frac{1}{2}\right), \qquad (10)$$

$$I^C_{BOC} = \tau^C_{BOC}\ (1000\ \varepsilon^C_o/D^C)[\gamma^C\ D^{\beta,C}/(B^C/365)], \qquad (11)$$

$$I^C_{EOC} = \tau^C_{EOC}\ \{I^C_{int} - [F^C(B^C/365)/2D^C M^C]\} \times [\gamma^C D^C/(B^C/365)], \qquad (12)$$

where

M^C = number of in-core fuel batches (e.g., three for an LWR)

ε^C_o = equilibrium enrichment (assay) of fresh fissile charged to the converter reactor

F^C = net converter fissile consumption at full plant capacity [g/kW(thermal)yr]

D^C = average specific power density in fission region [kW(thermal)/kgHM]

τ^C_{BOC} = time period between reprocessing discharge [or front end fissile procurement and reactor charge (yr)]

τ^C_{EOC} = time period between reactor discharge and reprocessing discharge (yr).

Note that the term F^C can be adjusted to include fuel losses (e.g., reprocessing losses or fabrication losses), if significant.

VIII.B.5 Year-by-Year Fissile and Electricity Costs

The inventory carrying charges from Eq. (9) are unique in this analysis because they depend upon the value of fissile fuel in the symbiotic system. This quantity is not explicitly determined but, rather, is determined year-by-year as the solution to a system of equations which require a balanced year-by-year cash flow for both the fusion breeder and its fission converter clients.

$$8.76\ \eta^{B}_{net}\ \gamma^{B}\ S^{B}_{n} + C^{B}_{fiss,n}\ \gamma^{B} F^{B} = C^{B}_{i} + C^{B}_{d,n} + C^{B}_{fiss,n}\ b\ I^{B}_{tot} \qquad (13)$$

$$8.76\ \eta^{C}_{net}\ \gamma^{C}\ S^{C}_{n} - C^{C}_{fiss,n}\ \gamma^{C}\ F^{C} = C^{C}_{i} + C^{C}_{d,n} + C^{C}_{fiss,n}\ b\ I^{C}_{tot} \qquad (14)$$

where

$\eta^{B,C}_{net}$ = net thermal-to-electric conversion efficiency

S^{B}_{n} = cost of electricity in year n [mil/kW(electric)hr]

If we impose the reasonable constraints that

$$S_{n} = S^{B}_{n} = S^{C}_{n} \qquad (15)$$

$$C_{fiss,n} = C^{B}_{fiss,n} = C^{C}_{fiss,n} \qquad (16)$$

then the above system of equations can be solved in each of N years of operation as

$$S_{n} = \frac{(C^{B}_{i} + R\ C^{C}_{i}) + (C^{B}_{d,n} + R\ C^{C}_{d,n})}{8.76(\eta^{B}_{net}\ \gamma^{B} + R\ \eta^{C}_{net}\ \gamma^{C})} \qquad (17)$$

$$C_{fiss,n} = \frac{(C^{B}_{i} - \eta_{rel}\ C^{C}_{i}) + (C^{B}_{d,n} - \eta_{rel}\ C^{C}_{d,n})}{(\gamma^{B} F^{B} + \eta_{rel}\ \gamma^{C} F_{C}) - b\ (I^{B}_{tot} - \eta_{rel} I^{C}_{tot})} \qquad (18)$$

where

$$R = \frac{\gamma^B F^B - b\, I^B_{tot}}{\gamma^C F^C + b\, I^C_{tot}} \tag{19}$$

$$\eta_{rel} = \frac{\eta^B_{net}\, \gamma^B}{\eta^C_{net}\, \gamma^C} \tag{20}$$

In equation 19, R represents the usual thermal support ratio when the inventory terms are zero and a financial support ratio when these terms exist. In equation 20, η_{rel} represents the relative e ectricity generation efficiency of the breeder and its clients.

If we further assume that the direct cost components in eqs. (17) and (18) would increase annually by the general inflation rate, i, then the electricity cost and fissile cost in year n can be easily determined as:

$$S_n = \frac{(C^B_i + RC^C_i) + (1+i)^n (C^B_{d,o} + R\, C^C_{d,o})}{8.76\ (\eta^B_{net}\, \gamma^B + R\, \eta^C_{net}\, \gamma^C)} \tag{21}$$

$$C_{fiss,n} = \frac{(C^B_i - \eta_{rel}\, C^C_i) + (1+i)^n\ (C^B_{d,o} - \eta_{rel}\, C^C_{d,o})}{(\gamma^B F^B + \eta_{rel}\, \gamma^C F_C) - b\ (I^B_{tot} - \eta_{rel} I^C_{tot})} \tag{22}$$

where $C_{d,o}$ is the direct cost in year zero, etc.

VIII.B.6 Average Present Value of Fissile and Electricity Costs

Although the year-by-year fissile and electricity cost are easily calculated using eqs. (21) and (22), lumped, or averaged values over the plant life are of interest. Two useful lumped parameters are the average present values given by

$$S_{PV} = \frac{1}{N} \sum_{n=0}^{N-1} \frac{S_n}{(1+i)^n} \tag{23}$$

$$C_{fiss,PV} = \frac{1}{N} \sum_{n=0}^{N-1} \frac{C_{fiss,n}}{(1+i)^n} \qquad (24)$$

These represent the effective average costs of electricity and fuel in year zero dolllars. Two other useful lumped parameters are the leveled values defined in previous work(1,2).

VIII.B.7 Cost of Electricity For Same Converter Using Mined Uranium

As a point of comparison it is often of interest to estimate the cost of electricity for the same fission converter operating on an alternate fuel cycle which utilizes mined uranium as a feed material rather than uranium produced in a fusion breeder.

To begin, in analogy to Eq. (14), the year-by-year cost of electricity for the converter reactor operating on the alternative fuel cycle (denoted by symbol C1) is related to the fuel and operating cost as

$$8.76\ \eta_{net}^{C1}\ \gamma^{C1}\ S_n^{C1} - C_{fiss,n}^{C1}\ (\gamma^{C1} F^{C1} + bI_{tot}^{C1}) = C_i^{C1} + C_{d,n}^{C1} \qquad (25)$$

Since the alternative fuel cycle converter is, presumably, fueled via an external source (e.g., mined uranium), Eq. (25) can be solved directly for S_n^{C1}

$$S_n^{C1} = \frac{C_i^{C1} + C_{d,n}^{C1} + C_{fiss,n}^{C1}\ (\gamma^{C1} F^{C1} + b\ I_{tot}^{C1})}{8.76\ \eta_{net}^{C1}\ \gamma^{C1}} \qquad (26)$$

If the alternatively fueled reactor is the same type as the previously considered client converter reactor, and its overall performance is similar, then we make the following simplifying assumptions:

$$\gamma^{C1} = \gamma^{C}, \qquad (27)$$

$$\eta_{het}^{C1} = \eta_{het}^{C}, \tag{28}$$

$$C_{i,o}^{C1} = C_{i,o}^{C}, \tag{29}$$

Also, if the alternate fuel is enriched ^{235}U derived from mined U_3O_8, then we can expand the equivalent fissile cost as follows:

$$C_{fiss,n}^{C1} = \frac{0.166}{\eta_{enr}} C_{U_3O_8,n} \tag{30}$$

where

$C_{U_3O_8,n}$ = the cost of mined and converted yellowcake in year n ($/kg)

η_{enr} = ratio of ^{235}U atoms in final product to ^{235}U atoms in U_3O_8 feed.

The factor 0.166 in the above represents the number of kilograms of U_3O_8 per gram of ^{235}U. In general, for isotopic enrichment processes, η_{enr} is given by

$$\eta_{enr} = \left(\frac{x_p}{x_f}\right)\left(\frac{X_f - X_T}{X_p - X_T}\right) \tag{31}$$

where

X_T = uranium tails assay (typically 0.002)

X_f = uranium tails assay (typically 0.0071)

X_p = uranium product assay (typically 0.032)

Therefore, by substituting eqs. (27), (28), (29), (30), and (31) into equation (26) we can express the cost of electricity for the alternatively fueled converter as

$$S_n^{Cl} = \frac{(C_i^C + C_{d,n}^{Cl} + 0.0166\ (\frac{X_f}{X_p})(\frac{X_p - X_T}{X_f - X_T})\ C_{U_3O_8,n}(\gamma^C F^{Cl} + b\ I_{tot}^{Cl})}{8.76\ \eta_{net}^C\ \gamma^C} \qquad (32)$$

In the above equation, any expected mined uranium cost profile can be input.

Note that the cost of enrichment (separative work) must be included in the direct cost term, $C_{d,n}^{Cl}$. This is given by

$$C_{e,n}^{Cl} = \Omega(X_p, X_o, X_f, X_t)C_{SWU}, \qquad (33)$$

with

$$\Omega = [V(X_p) - V(X_o)] - \frac{X_p - X_o}{X_f - X_t}[V(X_f) - V(X_T)], \qquad (34)$$

where

Ω = units of separative work per kilogram enriched product (kg SWU/kgHM)

C_{SWU} = cost of separative work ($/kg SWU)

X_p = final assay of enriched product

X_o = starting assay of enriched product

$V(x)$ = value of assay fissile X.

In the above, the value function is given by

$$(V(X) = (2X - 1)\ln\ (\frac{X}{1 - X}). \qquad (35)$$

If we further assume that the direct cost increases by a factor (1+i) each year and that the U_3O_8 cost increases by a factor (i+e) each year (where e might be slightly higher than i the cost of electricity for mined fuel can be expressed as

$$S_n^{Cl} = \frac{C_i^C + (1+i)^n C_{d,o}^{Cl} + 0.166\ (1+e)^n \left(\frac{X_f}{X_p}\right)\left(\frac{X_p - X_T}{X_f - X_T}\right) C_{U_3O_8,n}(\gamma^C F^{Cl} + b\ I_{tot}^{Cl})}{8.76\ \eta_{net}^C\ \gamma^C} \quad (33)$$

In analogy to equation (23), the average present value of electricity for the alternate (conventional) fuel cycle is

$$S_{PV}^{Cl} = \frac{1}{N} \sum_{n=0}^{N-1} \frac{S_n^{Cl}}{(1+i)^n} \quad (36)$$

When $S_{PV}^{Cl} > S_{PV}$ from Eq. (23), the average present value of electricity for the symbiotic system is less than that of the same converter using convetional mined fuel and the following net benefit over the N year lifetime is indicated

$$B = 8.76\ N\ (S_{PV}^{Cl} - S_{PV})\ (\eta_{net}^B\ \gamma^B + (\frac{F^B \gamma^B}{F^C \gamma^C})\ \eta_{net}^C\ \gamma^C), \quad (37)$$

The units of B are year zero dollars per kilowatt (thermal) of installed fusion breeder capacity.

References, Section VIII.B

1) Original code as described in D.H. Berwald and J.A. Maniscalco, "An Economics Method for Fusion-Fission Electricity Generation Systems", Nucl. Tech./Fusion, January 1981. Current version of the code is maintained at TRW.

2) J.D. Lee, et al., "Feasibility Study of a Fission Suppressed Tandem Mirror Hybrid Reactor", UCID-19327, Lawrence Livermore National Laboratory (1982).

VIII.C BASELINE ECONOMICS ANALYSIS

VIII.C.1 Overview of Baseline Analysis

In this section we develop an economics data base for an electricity generation system consisting of reference fusion breeder described in earlier chapters and its client LWRs. The economics model described in the previous section is applied to this data base and detailed year-by-year electricity and fuel costs are estimated.

A knowledge of the following quantities for both fusion breeder and the client fission burners is required to estimate the system electricity cost:

- Fixed capital cost
- Variable operating costs
- Fissile fuel production and consumption
- Fissile fuel inventories
- Net thermal-to-electric conversion efficiencies

These quantities are described in sections VIII.C.2 and VIII.C.3.

Given the above data, the PERFEC computer code(1) may be used to estimate the average present value of the cost of electricity over the fixed operating lifetime of the fusion breeder and its fission reactor clients. The PERFEC method is applied to the reference case in Section VIII.C.4.

VIII.C.2 Reference Fusion Breeder Description

The cost and performance data provided in this section are described in more detail in Chapters VI and VII.

VIII.C.2.a Reference Fusion Breeder Performance Parameters

The reference fusion breeder performance data required for input to the PERFEC code is listed in Table VIII.C.1. As shown, all values input to PERFEC are normalized to the nuclear power of the fusion breeder. This quantity, which is similar to the thermal power of most nuclear systems (including fusion reactors which do not utilize direct conversion), is defined as

TABLE VIII.C.1 Reference Fusion Breeder Performance Parameters

Fusion Power, MW_f	3000
Average Blanket Energy Multiplication, (M)[a]	1.61
Average Total Nuclear Power, MW_n[a]	4464
Average Net Electrical Power, MW_e[a]	1317
Average Net Nuclear-to-Electrical Efficiency[a]	0.295
Net Fissile Fuel Production Rate, Kg/yr[b]	5646
Net Specific Fissile Fuel Production Rate, Kg/MW_n-yr[c]	1 81
In-Core Fissile Inventory, Kg	1032
Ex-Core Fissile Inventory, Kg[b]	2874
Total Fissile Inventory, Kg[b]	3816
Specific Fissile Inventory, Kg/MW_n	0.854
Average Fissile Discharge Enrichment, %[a]	1.24
Heavy Metal Throughput, MT/yr thorium[b]	604
Average Plant Capacity Factor, %	70

a) Average over blanket operation

b) At 70% capacity factor

c) Value for full power operation

$$P_{nuclear} \equiv P_{fusion} \times (0.8\ M + 0.2)$$

where M is the blanket energy multiplication and P_{fusion} is the fusion power. Since, in a tandem mirror, 20% of the fusion power is converted to electricity in the direct converter rather than the thermal cycle, the nuclear power is a more easily defined measure of the total available power than the thermal power. The average nuclear power in the reference case is 4464 MW_n.

VIII.C.2.b Reference Fusion Breeder Cost Parameters

The fusion breeder cost characteristics are described by two types of charges: fixed (indirect) charges associated with plant capital and variable (direct) charges associated with fuel cycle and operation and maintenance. These are presented separately. All costs are given in 1982 dollars.

Annual Fixed (Indirect) Charges.

The breeder fixed charges are given by the product of the total breeder capital cost at the beginning of plant operation and the total fixed charge rate. The latter consists of the various components shown in Table VIII.C.2. Note that the total fixed charge rate of 18.04% includes 7% inflation. This fixed charge rate is typical of private utility financing and is also applied to LWR capital costs.

The total breeder capital cost is computed as shown in Table VIII.C.3. To obtain the total cost in 1982 dollars, the breeder direct cost is multiplied by a factor of 2.178 (2.052 for LWR)(2). The direct capital cost of the reference fusion breeder design discussed above was computed using the tandem-mirror reactor design code (TMRDC) as described in Chapter VI.

The fixed charges associated with this design are summarized in Table VIII.C.4. These charges will be compared with similar charges for an LWR in Section VIII.C.3.

Breeder variable (Direct) Charges.

Breeder variable charges consist of both fuel cycle charges and operation and maintenance charges. These are computed for the first year of operation (i.e., year zero = 1982 dollars) and are assumed to escalate in subsequent

Table VIII.C.2 Fixed Charge Rate Components

COMPONENT	CHARGE RATE, %
Capital recovery[a]	11.74
Income and property tax[b]	5.80
Salvage Cost[c]	0.25
Miscellaneous and Insurance	0.25
Total Fixed Charge Rate	18.04

a) Plant Lifetime = 30 years, bond fraction = 55%, bond return = 10%, stock return = 13%, inflation = 7%.

b) Income tax rate = 50%, property tax rate = 1.5%, depreciation rate = 3.3%/yr (straight-line)

c) Decommissioning cost = 5% of original plant cost (1982 dollars)

Table VIII.C.3 Total Plant Capital Cost Components

	BREEDER COST MULTIPLIERS	LWR COST MULTIPLIERS
Total Direct Cost[a]	1.00	1.00
Total Indirect Cost[b]	1.849	1.742
Time Value of Money[c]	1.178	1.178
Total	2.178	2.052

a) 1982 dollars

b) Field indirect cost multiplier = 1.2, home office cost multiplier = 1.2, contingency factor = 1.2 (hybrid) or 1.10 (LWR), owners cost factor = 1.07 (hybrid) or 1.10 (LWR).

c) Inflation = 7%, escalation = 7%, construction period = 10 years.

Table VIII.C.4 Summary of Fusion Breeder Fixed (Indirect) Charges

Direct Cost, $M	3744
Indirect Cost, $M	3179
Time-related cost, $M	1232
Total Capital Cost, $M (1982 $)	8155
Specific Cost, $/kW$_n$	1826
Total Annual Charge at 18.04%/yr $/kW$_n$-yr	329

years according to general inflation rate (7%/yr in this analysis). The year zero variable charges for the reference fusion breeder are shown in Table VIII.C.5.

Note that the capital cost of a THOREX reprocessing plant (670 $M total cost) is included in the total cost of Table VIII.C.4. This facility is considered to be an integral part of the plant. The total cost might be reduced by about 500 $M if the pyrochemical reprocessing technology described in Chapter VII were adopted for the baseline instead of the conventional THOREX process. A first-order comparison of the cost to reprocess thorium metal fuels based on the same fissile throughput and average in-blanket ^{233}U concentration in thorium was presented in Section VII.F. A comparison of the reprocessing cost impact of the two types of fuel reprocessing on the overall economics will be given in Section VIII.D.

Although not included in this section, fissile inventory carrying charges are calculated implicity, by PERFEC, using the self-consistent method discussed in Section VIII.B to determine the value of fissile material in the fusion-fission electricity generation system. Fissile inventory carrying charges are given by the product of the fissile inventory (units: g/kW_t), the value of fissile material in the sytem (units: $/g), and the fissile inventory carrying charge (units: yr^{-1}). The latter quantity, 8.16%/yr in this analysis, reflects the assumption that the fissile inventory carrying charge is given by the difference between the cost of carrying fissile fuel (15.16%/yr) and the increased value of such fuel (7%/yr = general inflation rate). Fissile fuel is amortized over a one year period and is treated as a non-depreciating asset.

VIII.C.2.c LWR Performance and Cost Characteristics

The performance characteristics of the mixed (or synthesized) LWR reactor systems, which couple to the reference fusion breeder, were provided in Table VII.A.1. These data, as well as the LWR economics data, have been derived from various sources including the EPRI's "Technical Assessment Guide", the DOE's NASAP reports, fuel cycle studies generated at ANL, fuel reprocessing

Table VIII.C.5 Summary of Fusion Breeder Variable (Direct) Charges in Year Zero

Fuel Cycle Operating Cost, $M/yr[a]	89
Blanket Structure Replacement Cost, $M/yr	2
Miscellaneous Operation and Maintenance cost, $M/yr	132
Total Variable (Direct) Charge in Year Zero, $M/yr	223
Specific Variable (Direct) Charge in Year Zero, $/KW$_n$-yr	50.0

a) see further breakdown in Section VI.E.

studies performed by Exxon Nuclear Company, and information provided by Bechtel(3,4,5,6,2). However, in many cases, it has been necessary to revise, blend, renormalize, or cost escalate the source data to provide for a consistent treatment in this analysis.

The economic characteristics of the LWRs modeled in this section and later sections are given in Table VIII.C.6 and VIII.C.7. Table VIII.C.6 is a summary of LWR fixed charges (analogous to Table VIII.C.4 for the breeder). A comparison of Tables VIII.C.4 and VIII.C.6 indicates that on a unit thermal power basis, the reference fusion breeder considered in this analysis is 3.4 times as costly as an LWR. Table VIII.C.7 is a summary of the year zero LWR variable charges (analogous to Table VIII.C.5 for the breeder). The denatured throium fuel cycle fuel reprocessing costs listed refer to the blending of both uranium oxide and thorium oxide fuels to satisfy the requirements of the mixtures of ^{233}U burners and plutonium burners as described in Section VII.A (e.g., 12% Pu burners and 88% ^{233}U burners in denatured throum fuel cycle). The reason for the higher thorium oxide reprocessing costs is a more expensive head-end. The high fuel fabrication costs for both fuel cycles reflect the expected need for fully remote fabrication of both ^{233}U and plutonium oxide fuels. In comparison with the breeders, on a unit nuclear (or thermal) power basis, the year zero, LWR variable costs are ~ 45% of the breeder costs. After year zero, LWR variable costs are assumed to escalate to the general inflation rate, 7%/yr.

VIII.C.3 Results of Baseline Analysis

The economic performance of the baseline fusion breeder design was calculated for a symbiotic system consisting of the fusion breeder and LWRs operating on the denatured thorium fuel cycle (with plutonium recycle). This analysis followed the economics method developed in Section VIII.B and utilized the data base provided in Section VIII.C.

In Table VIII.C.8 we list the year-by-year symbiotic cost of electricity and cost of the bred fissile fuel. A 30 year plant life for both the breeder and its supported fission converters is assumed. The year-by-year discounted cost of electricity and the discounted cost of fissile fuel are also listed. Since the entire system is heavily capitalized, the cost of electricity in the

Table VIII.C.6 Summary of LWR Fixed (Indirect) Charges

Direct Cost, $M	789
Indirect Cost, $M	585
Time-related Cost, $M	245
Total Capital Cost, $M (1982 dollars)[a]	1620
Specific Cost, $/kW$_t$	540
Total Annual Charge at 18.04%/yr, $/kW$_t$-yr	97

a) **Basis:** informal Ebasco cost estimate for 1000 MW$_e$ (3000 MW$_t$) LWR; 1982 dollars

Table VIII.C.7 Summary of LWR Variable (Direct) Charges in Year Zero

	FUEL CYCLE[a]	
	Denatured Thorium	Denatured Uranium
Annual Fuel Processing charge, $/kW$_t$-yr	12.36	12.02
Fuel Reprocessing Cost, $/kgHM	600	558
Fuel Fabrication Cost, $/kgHM	865	865
Fuel Transportation cost, $/kgHM	22	22
Back End Fuel Cycle Cost, $/kgHM	75	75
Total Unit Processing Cost, $/kgHM	1562	1520
Fuel Throughput, kgHM/kW$_t$-yr[b]	0.0077	0.0079
Operation and Maintenance Charge, $/kW$_t$-yr	9.16	9.16
Total Year Zero Variable Charge, $/kW$_t$-yr[b]	21.5	21.2

a) See also Table VII.A.2

b) Includes 70% capacity factor

Table VIII.C.8 Summary of Year-by-Year Symbiotic Cost of Electricity and Fuel

End of Year	Symbiotic Cost of Electricity (Current dollars) (mil/KW_e-H)	Present Value of Symbiotic Cost of Electricity (1982 dollars) (mil/kW_e-H)	Cost of Bred Fuel (Current dollars) ($/g)	Present Value of Cost of Fuel (1982 dollars) ($/g)
1	77.14	72.09	199.07	186.04
2	78.04	68.17	200.45	175.08
3	79.02	64.50	201.94	164.84
4	80.05	61.07	203.53	155.27
5	81.17	57.87	205.23	146.33
6	82.36	54.88	207.05	137.96
7	83.63	52.08	208.99	130.15
8	84.99	49.46	211.08	122.85
9	86.45	47.02	213.31	116.02
10	88.01	44.74	215.69	109.65
11	89.67	42.60	218.24	103.69
12	91.46	40.61	220.97	98.11
13	93.37	38.74	223.89	92.91
14	95.41	37.00	227.02	88.04
15	97.60	35.37	230.36	83.49
16	99.94	33.85	233.94	79.24
17	102.44	32.43	237.77	75.27
18	105.12	31.10	241.87	71.56
19	107.99	29.86	246.25	68.09
20	111.05	28.70	250.94	64.85
21	114.34	27.61	255.96	61.82
22	117.85	26.60	261.33	58.99
23	121.60	25.65	267.08	56.34
24	125.62	24.77	273.23	53.87
25	129.93	23.94	279.81	51.55
26	134.53	23.17	286.85	49.39
27	139.45	22.44	294.38	47.37
28	144.72	21.77	302.44	45.49
29	150.36	21.14	311.06	43.72
30	156.40	20.55	320.29	42.08
Ave.	N/A	38.7	N/A	92.7

30th year (in year 30 dollars) is only twice the year zero cost (despite an increase in the plant variable costs by 7.6 fold during this period). The present value electricity costs for this capital dominated system decrease dramatically over the plant life and the average of the thirty present values is 38.7 mil/kW_e-H.

This symbiotic cost of electricity is compared with the year-by-year cost of electricity for the same LWR fueled with conventional mined uranium in Table VIII.C.9. In this case, the LWR fuel cycle includes full recycle of both uranium and plutonium. Information analogous to that of Tables VIII.C.7 for the conventional fuel cycle is shown in Table VIII.C.10. The fuel cycle performance for this fuel cycle was provided in Table VII.A.2.

Table VIII.C.9 also shows the assumed year-by-year cost of U_3O_8. This cost is assumed to increase from its year zero value of 55 $/kg by 3%/yr above the general inflation rate of 7%/yr. For this assumed U_3O_8 escalation rate, the cost of electricity through the twenty third year of operation is less than the symbiotic cost of electricity (see Table VIII.C.9).

The results of the economics analysis for the baseline case are summarized in Table VIII.C.11. The average present value of the cost of electricity for the same LWR using mined U_3O_8 at an intital cost (25 $/lb) near todays cost is 34.8 mils/KWe-H. These results indicate that the fusion breeder can cap the cost of LWR electricity at a level which is only about 11% above currently achievable costs.

The fusion breeder will be optimized for still lower system electricity cost in Section VIII.D.

Table VIII.C.9 Comparison of Symbiotic (Fusion Breeder) and Conventional (Mined U_3O_8 Fueled) LWR Cost of Electricity

End of Year	Symbiotic Cost of Electricity (Current dollars) (mil/kW_e-H)	Cost of U_3O_8 (Current dollars) ($/Kg)	Cost of Conventional Electricity (mil/kW_e-H)
1	77.14	60.62	62.87
2	78.04	66.80	63.99
3	79.02	73.63	65.18
4	80.05	81.14	66.46
5	81.17	89.43	67.84
6	82.36	98.56	69.33
7	83.63	108.62	70.92
8	84.99	119.71	72.63
9	86.45	131.93	74.48
10	88.01	145.40	76.46
11	89.67	160.25	78.59
12	91.46	176.61	80.88
13	93.37	194.64	83.35
14	95.41	214.51	86.00
15	97.60	236.42	88.86
16	99.94	260.55	91.93
17	102.44	287.16	95.24
18	105.12	316.48	98.80
19	107.99	348.79	102.64
20	111.05	384.40	106.76
21	114.34	423.65	111.21
22	117.85	466.90	116.00
23	121.60	514.57	121.16
24	125.62	567.11	126.72
25	129.93	625.01	132.71
26	134.53	688.82	139.17
27	139.45	759.15	146.13
28	144.72	836.66	153.64
29	150.36	922.09	161.73
30	156.40	1016.23	170.46

Table VIII.C.10 Summary of LWR Variable Charges in Year Zero for the Mined Uranium Fuel Cycle

Annual Fuel Processing Charge, $/kW$_t$-yr	15.24
Fuel Enrichment Cost,[a] $/KgHM	605
Fuel Reprocessing Cost, $/KgHM	558
Fuel Fabrication Cost, $/KgHM	554
Fuel Transportation Cost, $/KgHM	22
Fuel Disposal cost, $/KgHM	75
Total Unit Processing cost, $/KgHM	1674
Fuel Throughput, KgHM/KW$_t$-yr[b]	0.0084
Operation and Maintenance Cost, $/KW$_t$-yr	9.16
Total Year Zero Variable Charge, $/KW$_t$-yr[b]	24.40

a) 130 $/Kg Separative work cost, 0.2% tails assay

b) Includes 70% plant capacity factor

Table VIII.C.11 Summary of Results for Baseline Economics Analysis

Year Zero Bred Fissile Fuel Cost[a]	198 $/g
Ave. Present Value of Bred Fissile Fuel	93 $/g
Year Zero Symbiotic Electricity Cost	76.3 mil/KW_eH
Ave. Present Value of Symbiotic Electricity Cost	38.7 mil/KW_eH
Year Zero Conventional Electricity Cost	61.8
Ave. Present Value of Conventional Electricity Cost	34.8
Symbiotic/Conventional Cost of Electricity[b]	1.11

a) All costs in 1982 dollars

b) Basis: average present value

References, Section VIII.C

1) Original code as described in D.H. Berwald and J.A. Maniscalco, "An Economics Method for Fusion-Fission Electricity Generation Systems", Nucl. Tech./Fusion, January 1981. Current version of the code is maintained at TRW.

2) J.A. Maniscalco, et al., "Laser Fusion Driven Breeder Design Study, Final Report", Contract DE-AC08-79PD40-11, TRW Systems and Energy for the U.S. Department of Energy (1980).

3) "Technical Assessment Guide", EPRI-PS-1201-SR, Electric Power Research Institute (1979).

4) "Nuclear Proliferation and Civilian Nuclear Power: Report of the Nonproliferation Alternative Systems Assessment Program", DOE/NE-0001, U.S. Department of Energy (1979).

5) Y.I. Chang, et al., "Alternative Fuel Cycle Options: Performance Characteristics and Impact on Nuclear Growth", ANL-77-70, Argonne National Laboratory (1979).

6) R.E. Tomlinson, et al., "The Economics of Reprocessing Alternative Nuclear Fuels", ORNL/Sub-7501/4, Exxon Nuclear Company for Oak Ridge National Laboratory (1979).

VIII.D DEVELOPMENT OF AN OPTIMIZED CASE

VIII.D.1 Overview

The baseline fusion breeder economics discussed in Section VIII.C relate to the reference fusion breeder as designed and described in the previous chapters. However, in Section IV.C, we describe variations about the reference fusion driver design and fuel management mode which lead to a lower symbiotic cost of electricity and the definition of an optimized fusion breeder. In this section we review and summarize the important results of Section IV.C, and also consider two alternative paths which have not yet been factored into the analysis. The first is substitution of the less expensive pyrochemical reprocessing technology for THOREX reprocessing of the fusion breeder discharge fuel (see Chapter VII for descriptions of these technologies). The second alternate path is the use of the denatured uranium LWR fuel cycle instead of the denatured thorium fuel cycle. In the later case, fuel cycle and inventory charges are reduced, but the number of LWRs which are supported by the fusion breeder is also reduced.

VIII.D.2 Driver/Fuel Cycle Optimization

In Section IV.C, the reference driver and fuel cycle were reconfigured and optimized subject to several constraints:

- fixed central cell fusion power of 3000 MW
- fixed end-of-cycle MHD pressure drop obtained by requiring that the product of the neutron wall loading, maximum blanket energy multiplication, and and the square of center cell field strength is the same as the reference case (i.e., $\Gamma M B^2 \approx \Gamma_o M_o B_o^2 \approx 1.27 \times 1.97 \times 4.2^2 = 44.1$ in all cases).
- fixed wall loading over the entire fuel cycle period such that the fusion power is constant and the blanket thermal power increases with time
- maximum central cell length of 200 m and minimum neutron wall loading of 1.27
- fixed first wall radius of 1.5 m

- no axial variation of blanket module maturity (i.e., enrichment)
- two radial fuel zones with an inner-to-outer reprocessing frequency of 2-to-1.
- maximum axicell magnet field strength of 20 tesla
- 70% overall plant capacity factor

The motivating rationale for these constraints is discussed in more detail in Chapter IV, but is related to a desire to limit the overall facility size and power level while maintaining relevancy of the blanket design point, maximizing the use of the expensive fusion driver, and simplifying the impact of fuel management on plant operations.

In Table VIII.D.1 (see also Table IV.D.2) we summarize important differences in the optimized and reference (baseline) cases as they relate to the fusion breeder design, cost, and the resulting symbiotic electricity generation system results. Importantly, the optimized plant, which costs about 2.7 times as much as an LWR on a per thermal power basis, provides about the same fissile fuel production and about 30% higher average electricity production at a capital cost which is about 8% lower than that of the reference system. This results in a 26% decrease in the cost of fissile fuel and a 6% decrease in the symbiotic cost of electricity (to only about 5% above the cost of electricity for a conventionally fueled LWR). As shown in Chapter IV, the scheduled maintenance period is also increased by about 50% in the optimized case.

VIII.D.3 Pyrochemical Reprocessing Economics

In Chapter VII, pyrochemical reprocessing is suggested as a less expensive alternative to aquious THOREX reprocessing. In this section we consider the economic effect of its use in the context of a further improvement to the optimized case presented in Section VIII.D.2.

In general, the cost of a pyrochemical reprocessing plant is expected to be about 1/4 the cost of an aquious plant of the same capacity. Therefore, we estimate that the total cost of a facility to reprocess the discharge fuel in the optimized case (674 MT/yr) would be on the order of 1/4 x 600 = 150 $M. The operating cost for such a facility is estimated to be on the order of 5-10 $M/yr.

Table VIII.D.1 Comparison of Reference and Optimized Fusion Breeders

	Reference System	Optimized System
Fusion Power, MW	3000	3000
Maximum End Cell B Field, Tesla	15	20
Central Cell Length, m	200	193
Central Cell B Field, Tesla	4.20	3.66
Fusion Power Gain ($N_{trap}Q$)[a]	14.6	16.6
Neutron Wall Loading, MW/m^2	1.27	1.32
BOC Blanket Energy Multiplication	1.25	1.25
EOC Blanket Energy Multiplication	1.97	2.50
Average Blanket Energy Multiplication	1.61	1.885
EOC Net Electrical Production, MW	1662	2256
Average Net Electricity Production, MW	1317	1720
Annual Fissile Fuel Production,[b] Kg	5646	5590
Discharge Fissile Enrichment, %	1.24	1.10
Direct Capital Cost, $	3744	3439
Average Present Value Cost of Electricity, mil/KWeH	38.7	36.5
Average present Value Cost of Fissile Fuel, $/g	92.7	68.7
Cost of Electricity Relative to LWR with Reprocessing and 55 $/Kg Mined U_3O_8	1.11	1.05

a) $N_{trap}Q$ is the ratio of fusion power to injected power

b) at 70% capacity factor

Our analysis indicates that, for the optimized case, a switch to pyrochemical reprocessing would be equivalent to an overall capital cost savings of about 951 $M (or 13%) and could decrease the symbiotic electricity cost by about 0.55 mil/kWe (about 1.5%).

Although the cost of electricity would decrease only marginally, the average present value of the cost of reprocessing fissile fuel would decrease by about 14 $/g to 55 $/g (20% decrease). This comparison is summarized in Table VIII.D.2.

It is important to note that the sensitivity to reprocessing costs would be much larger were the fissile discharge concentration lower than the optimized value (1.1% ^{233}U + ^{233}Pa in thorium metal). Earlier suppressed fission blankets which wer designed to about 0.6% discharge concentration are about twice as sensitive to the cost of reprocessing such that an ~ 30 $/g impact of pyroprocessing would be implied.

VIII.D.4 Denatured Uranium Fuel Cycle Economics

During the first part of the study, a systems analysis was performed to investigate the economic incentives for ^{233}U versus ^{239}Pu production in a suppressed fission type fusion breeder. As discussed in the interim report(1), there is considerable incentive for ^{233}U breeding. The economic effect of operating on the denatured uranium fuel cycle instead of the denatured thorium fuel cycle was considered later in the study. As discussed in Section VII.A, the latter fuel cycle provides a 21% larger number of LWR clients, but the fissile inventory cost and fuel reprocessing cost (to a lesser extent) are lower for the depleted uranium fuel cycle. As a result, the calculated difference in the electricity cost (a decrease of 0.15 mil/-KWe-H) is insignificant and the two fuel cycles are equally attractive from an economics perspective.

A choice between these must derive from non-economic considerations such as the larger LWR support and a smaller fraction of plutonium burners for the denatured thorium fuel cycle (see Chapter VII). The denatured uranium fuel cycle preserves PUREX reprocessing on the LWR side of the system and minimizes the LWR fissile inventory per unit electrical power generation.

Table VIII.D.2 Economic Impact of Pyrochemical Reprocessing

	THOREX	PYRO
Throughput, MTHM/yr	674	674
Total Reprocessing Plant Capital Cost, $M	600	150
Annual Operating Cost, $M/yr	45	5
Symbiotic Cost of Electricity,[a,b] mil/KWeH	36.45	35.90
Cost of Fissile Fuel,[a] $/g	69	55

a) average present value of 30 year operation

b) based upon equivalent capital cost savings of 450 + ([45-5]/0.1804) x 2.26 = 951 $M where 0.1804 is the fixed charge rate (yr^{-1}) and the weighting factor 2.25 is the conversion from the average present value of a dollar of operating cost to the average present value of a dollar of fixed charge.

References, Section VIII.D

1) R.W. Moir, et al., "Fusion Breeder Program Interim Report: December 1981 - February 1982", UCID-19406-1, Lawrence Livermore National Laboratory (1982).

VIII.E SENSITIVITY STUDIES AND COMPARISON WITH FUSION ELECTRIC

In this section we present sensitivity studies which indicate the change in the present value of the symbiotic cost of electricity as a function of the uncertainties in the cost of the fusion breeder, the recirculating power requirement, and the fusion power gain (Q). In all cases we have selected the optimized design described in Section VIII.D.2 as the reference point.

In Figure VIII.E.1, the sensitivity in the electricity cost is plotted as a function of the plant direct capital cost. The reference point, at 3.44 $B corresponds to a fusion breeder which cost 2.7 times as much as an LWR on a unit thermal power basis. The figure shows that a ± 50% change in the capital cost of the breeder corresponds to a ± 13.6% change in the system cost of electricity, or a low sensitivity coefficient of 0.27 (i.e., 13.6%/50%).

This sensitivity is compared in the same figure with a similar analysis for a pure fusion electric tandem mirror which was modeled consistently using the same physics, design, and economics codes(1,2,3). In the latter case, a 50% change in the capital cost corresponds to a 49% change in the cost of electricity, or a high sensitivity coefficient of 1.0. Therefore, the fusion electric case is at a disadvantage with respect to both the reference cost of electricity (71% higher than the symbiotic system) and its sensitivity to cost uncertainties.

Interestingly, if the cost of the fusion breeder decreased to about 500 $\$/Kw_t$ (~ 2 times the LWR cost), then the 30 year average present value of the cost of symbiotic electricity would be similar to that of the conventionally fueled LWR with the current (55 $/Kg) U_3O_8 cost. The fusion electric direct capital cost would have to decrease to about 300 $\$/KW_t$ (~ 1.2 times the LWR cost) to achieve the same breakeven.

In Figure VIII.E.2 we show similar sensitivities to uncertainties in the recirculating power requirement of the fusion breeder. Our optimized case, with a fusion gain of 16.6, assumes that a very efficient fusion plant will be available. This result is consistent with current theoretical projections (see Chapter I), but any number of factors could increase the recirculating power. The figure indicates that, on a power flow basis alone, such uncertainties are not highly important for this application. In particular, a 50% increase in the recirculating power from 500 to 750 MW_e (such as would be

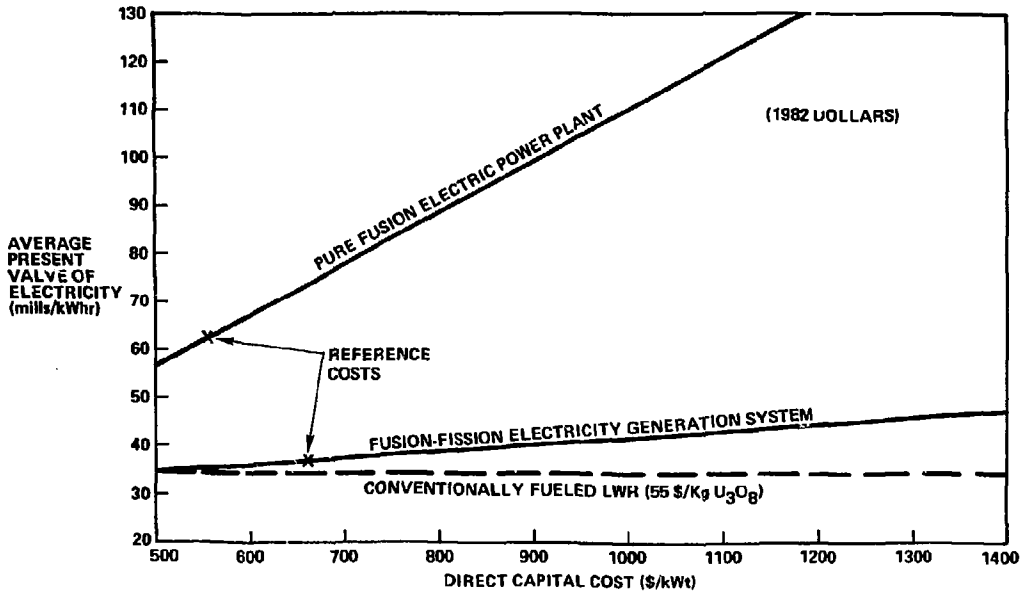

Figure VIII.E.1. The Cost of Electricity for Fusion-Fission Electricity Generation and Fusion Electric Versus the Capital Cost of the Plant

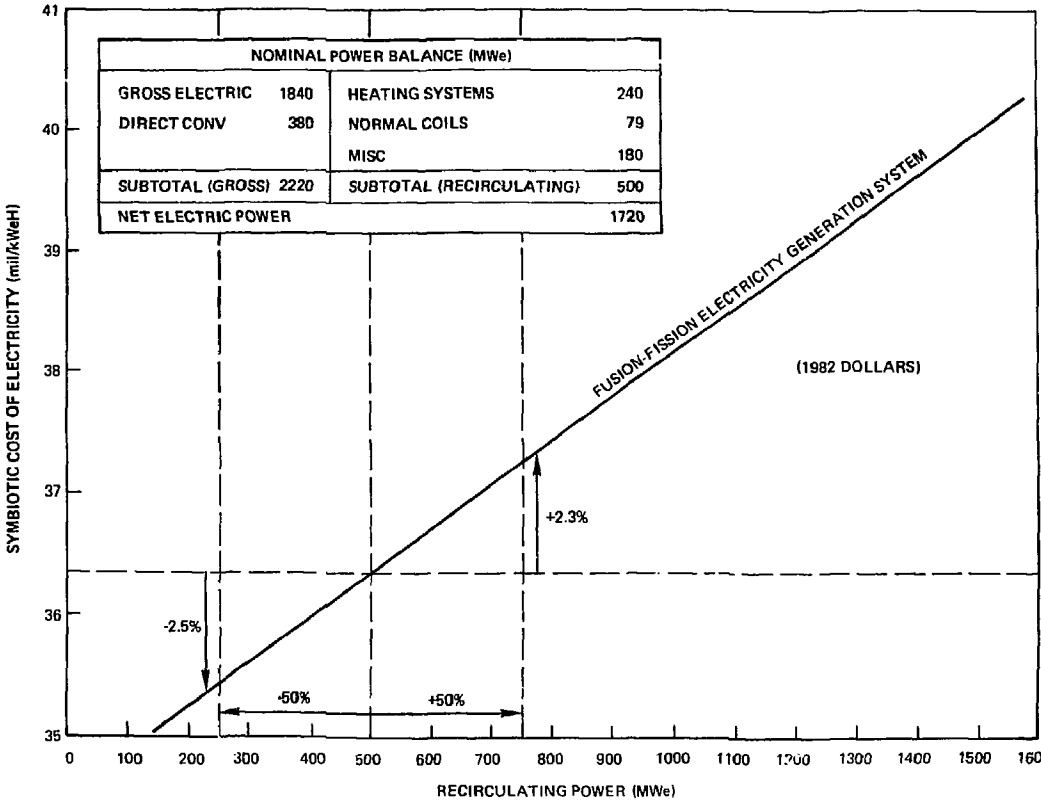

Figure VIII.E.2. Cost of Symbiotic Electricity as a Function of Total Recirculating Power for the Optimized Fusion Breeder Case

obtained by halving the heating system efficiencies or by halving the fusion gain) results in only a 2.3% increase of the cost of symbiotic electricity.

In fact, the largest uncertainty, the fusion gain ($n_{trap}Q$) does not affect the recirculating power requirement alone, but also affects the size and cost of the plasma heating systems. In Figure VII.E.3 we show the affect of fusion gain uncertainties for both the fusion breeder and fusion electric cases.* As shown, the symbiotic cost of electricity is insensitive to fusion gains below about 10 and does not increase significantly until the gain falls to about 5 - three fold below the predicted value. Conversely, for fusion electric generation, the range of insensitivity is above 30 and very substantial increases in the cost of electricity occur for gains below about 15.

---

* It is important to note that the cases shown in Figure VIII.E.3 do not represent optimized plant costs versus plasma gain, but are developed by assuming that the heating system cost and recirculating power are each inversely proportional to the plasma gain.

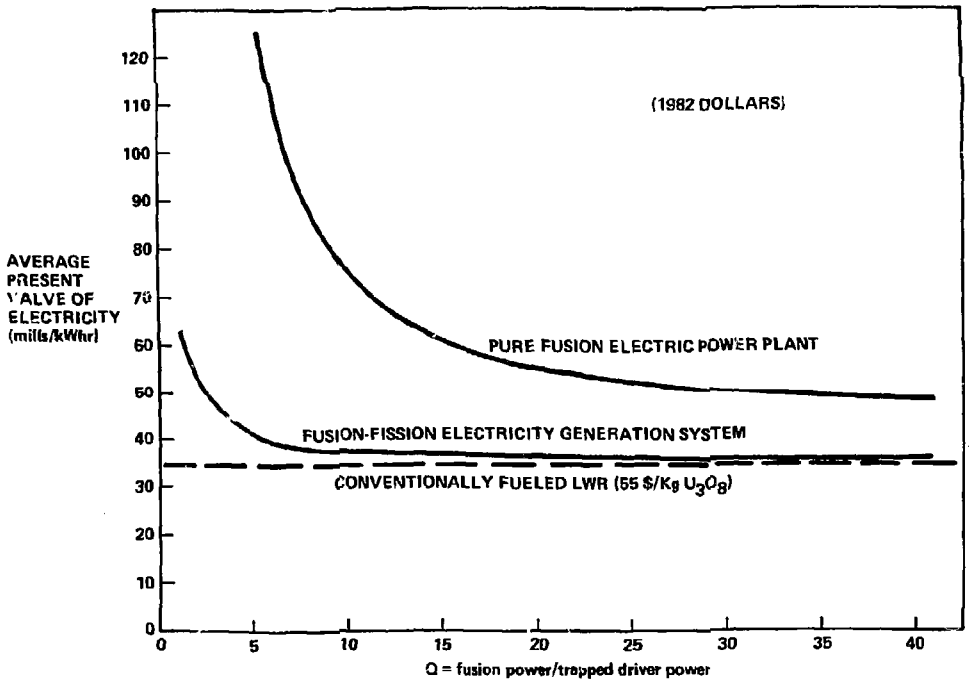

Figure VIII.E.3. The Cost of Electricity for Fusion-Fission Electricity Generation and Fusion Electric Versus the Fusion Gain

References, Section VIII.E

1) Original code developed as described in G.A. Garlson, et al., "Comparative End Plug Study for Tandem Mirror Reactors", UCID-19271, Lawrence Livermore National Laboratory (1981). Current version of the code is maintained at LLNL.

2) Original code as described in D.L. Chapin, et al., "Preliminary Feasibility Assessment of Fusion-Fission Hybrids", WFPS-TME-81-003, Westinghouse Fusion Power Systems Department (1981). Current version of the code is maintained at TRW.

3) Original code as described in D.H. Berwald and J.A. Maniscalco, "An Economics Method for Fusion-Fission Electricity Generation Systems", Nucl. Tech./Fusion, January 1981. Current version of the code is maintained at TRW.

GPO 888-753/9441